

New π -Conjugated Materials for Optoelectronic Applications

A thesis submitted to the
Savitribai Phule Pune University
for the degree of
DOCTOR OF PHILOSOPHY

in

CHEMISTRY

by

RUPALI RAMKRISHNA JADHAV

Research Guide

Dr. Prakash P. Wadgaonkar

Polymers and Advanced Materials Laboratory,
Polymer Science and Engineering Division,
CSIR-National Chemical Laboratory,
Pune 411 008
India

Research Co-guide

PD Dr. Daniel A. M. Egbe

Institute of Polymeric Materials and Testing
Johannes Kepler University
Linz
Austria

July 2019



*To My Dear Father,
Late Ramkrishna Rajaram Jadhav,
My Dear Mother Geetanjali,
and My Grandparents*

DECLARATION BY THE CANDIDATE

I hereby declare that the research work embodied in this thesis entitled, “**New π -Conjugated Materials for Optoelectronic Applications**” submitted to the Savitribai Phule Pune University for the award of the Degree of **Doctor of Philosophy (Ph.D.)** is the outcome of experimental investigations carried out by me at the Polymer Science and Engineering Division of CSIR-National Chemical Laboratory, Pune, India, and at Linz Institute of Organic Solar Cells, Johannes Kepler University, Linz, Austria, under the supervision of **Dr. Prakash P. Wadgaonkar**, at CSIR-National Chemical Laboratory, Pune, and **Dr. Daniel A. M. Egbe**, at Johannes Kepler University, Linz, Austria. I further affirm that to the best of my knowledge, the work incorporated is original, and has not been submitted to any other Academy, University and Institute for the award of any degree.

Ms. Rupali Jadhav

(Research Student)

July, 2019

Polymer Science and Engineering Division

CSIR-National Chemical Laboratory

Pune-411008

Acknowledgement

I express sincere heartfelt gratitude towards the Almighty for giving me the courage and strength to endure when faced with hardships. I take this moment to fondly remember and thank my late father for instilling in me discipline, hard-work and an undying love for science....my PhD thesis would not exist without his moulding influence. Also, I remember and thank my mother (Geetanjali), brother (Rohit), sisters (Anjali and Sonali) and brother in law (Mr. Deepak More) for their care, understanding and wisdom; who would be happiest to see me complete my PhD journey, from up above. Thanks are due to my beloved husband (Mr. Sagar B. Chavan), my in-laws (Mr. Balkrishna M. Chavan and Mrs. Nanda B. Chavan) and family, for supporting me, in every step of the way. Special thanks to my little princess Aaradhya for her wonderful presence and support through the tough journey.

It takes intense pleasure in thanking my supervisor, Dr. Prakash P. Wadgaonkar, for giving me the opportunity to do research and providing invaluable guidance, support, encouragement and intellectual stimulation throughout my PhD tenure. His astute observations and comments helped me to establish the overall direction of my research. He taught me how to understand a scientific problem and logically arrive at a solution through scientific enquiry. His invaluable guidance has helped in making me a better person and professional. When it comes down to my PhD thesis: I owe it all to him! My sincere thanks to Dr. Harald Hoppe and Ass. Prof. Daniel A. M. Egbe for introducing me to the world of organic photovoltaics and giving me opportunity to work with them. Special thanks

to Prof. Niyazi Serdar Sariciftci for allowing me to perform part of this thesis work in his lab in Linz, Austria.

I am extremely grateful to the Council of Scientific and Industrial Research (CSIR) for providing me research fellowship and financial support. I extend my gratitude to Prof Ashwinikumar Nangia (Director, CSIR-NCL), Dr. Vijayamohanan Pillai (Former Director, CSIR-NCL), Dr. Sourav Pal (Former Director, CSIR-NCL) and Dr. S. Sivaram (Former Director, CSIR-NCL) for allowing me to pursue research in CSIR-NCL. I greatly appreciate Dr. U. K. Kharul (Chair, PSE Division) and Dr. Ashish Lele (Former Chair, PSE Division), for giving me the opportunity to work in Polymer Science and Engineering Division and providing the instrumental facilities and infrastructure to perform my research work. I owe my sincere thanks to Dr. C. V. Avadhani, Mr. S. K. Menon, Mr. Anandrao Patil and Dr. Ashootosh Ambade for their kind support and help throughout my PhD tenure.

I would also like to thank my research progress monitoring committee members: Dr. U. P. Mulik (C-MET, Pune), Dr. Milind Kulkarni (C-MET, Pune), and Dr. Asha S. K. (CSIR-NCL, Pune) for their insightful comments.

My special thanks are due to Mr. Stefan Türk (TU Chemnitz, Germany) for his initial help in synthesis and Mr. Shahidul Alam (FSU Jena, Germany), for helping me to accomplish solar cell device fabrication and characterisation. I am especially indebted to Ass. Prof. Prashant Sonar (QUT, Australia) for the useful scientific discussions. Special thanks are due to Dr. K. Krishnamoorthy (CSIR-NCL, Pune), Dr. Satej Dharmapurikar, Dr. Rajashri, Chithiravel S. and Dr. Chayanika Das for their help with DPP synthesis, electrochemical characterisations and charge carrier mobility measurements.

I would like to express my sincere thanks to Mrs. Deepa Dhoble, Mrs. Poorvi Purohit and Dr. B. Santhakumari for providing analytical facilities. Many special thanks to Dr. P. R. Rajamohanam, and the entire NMR facility for helping me in NMR characterisations. I deeply appreciate Student Academic Office (SAO) Chairman Dr. M. S. Shashidhar and other staff members including Mrs. P. Kolhe and Shri S. Iyer for their continual cooperation and support.

I am deeply indebted to my past colleagues in our group: Dr. Rahul Shingte, Dr. Anjana Sarkar, Dr. Pandurang Honkhambe, Dr. Dnyaneshwar Palaskar, Dr. Nagendra, Dr. Snehalata Bapat, Dr. Arvind More, Dr. Arun Kulkarni, Dr. Prakash Sane, Dr. Nilakshi Sadavarte, Dr. Savita Kumari, Dr. Mahesh Biyani, Dr. Sharad Pasale, Dr. Kishor Kumbhar, Dr. Nagendra Kalva, Dr. Naganath Patil, Dr. Bhausheeb Tawade, Dr. Indravadan Parmar, Dr. Sachin Patil, Dr. Sachin Kuhire, Jagdish Salunke, Dr. Vikas Kumar, Dr. Kavita Garg, Dr. Ravindra Patil, Dr. Renji, Dr. Ikhlas Gadwal, Dr. Namdev Ghule, Dr. Shraddha Chhatre, Dr. Sayali Shaligram, Dr. Samadhan Nagane, Dr. Bharat Shrimant, Dr. Deepshikha Chatterjee, Dr. Durgaparasad Shinde, Sachin Basutkar, Nitin Valsange, as well as present members: Deepak, Nitin Basutkar, Geethika, Ashwini, Uday, Amol, Shakeb, Yogesh Neware, Ketan, Pravin, Swami, Dr. Prakash Babu and Dr. Shivshankar Mane. All of them made my life in the lab easier and more enjoyable.

At this special moment, I cannot forget to thank my university professor- Late Dr. Arun Vaidya, Late Dr. Chitale, Dr. Konde-Deshmukh; my project guides- Dr. A. J. Varma (Former Chair, PSE Division), Dr. M. G. Kulkarni (Former Chair, PSE Division), Dr. GVN Rathna and my friends- Mr. Vikas Paliwale, Mr. Nilesh Bangale, Dr. Sangram Gore, Dr. Prerana Patil, Dr. Sunita Satav, Dr. Anupa Menjoge, Dr. Aarti Shedge, Mr. P. R.

Suresha, Dr. Santosh Hire and Dr. Mahesh Gore for their valuable guidance.

Finally, I thank all the other people in CSIR-NCL, who cannot be named due to space constraints for their valuable helping hands.

Ms. Rupali Jadhav

July, 2019

Table of Contents

	Description	Page No.
	● Abstract	i
	● Abbreviations	v
	● List of Tables	vii
	● List of Schemes	ix
	● List of Figures	xi
<hr/> <hr/>		
Chapter 1	Introduction and Literature Survey	
<hr/> <hr/>		
1.1	Introduction	1
1.1.1	Energy crisis and renewable energy resources	1
1.1.2	Solar energy technology	2
1.2	Photovoltaics	4
1.3	Organic Solar Cells (Organic Photovoltaics)	9
1.3.1	Inorganic Photovoltaics vs. Organic Photovoltaics	9
1.3.2	Small molecular semiconductors vs. Polymeric semiconductors	10
1.3.3	Organic solar cells device structure and working principle	11
1.3.3.1	Organic solar cell device structure-	11
1.3.3.2	Working principle-	13
1.3.3.3	Organic Solar Cell Architectures	14
1.3.3.4	Characterisation of solar cells	16
1.3.3.5	Low band-gap materials in organic solar cells	17
1.3.3.6	Strategies for band-gap engineering of conjugated materials	19
1.3.4	Approaches for the design of high-performance conjugated polymers	22
1.3.4.1	Low band gap donor-acceptor copolymers	22
1.3.4.2	Two-dimensional (2-D) conjugated systems	22
1.3.4.3	Terpolymer approach	26
1.3.4.4	Incorporation of non-covalent interactions	29
1.3.4.5	Flexible Linker strategy	30
1.4	Summary	31

References	32	
Chapter 2	Scope and Objectives	42
Chapter 3a	Anthracene Containing PAE-PV Polymers: Influence of π - π Stacking Distance on the Morphology and Performance of Solar Cells	
3a.1	Introduction	50
3a.2	Experimental	52
3a.2.1	Materials	52
3a.2.2	Characterisation and techniques	52
3a.2.3	Fabrication and characterization of the photovoltaic cells	54
3a.3	Synthesis	55
3a.3.1	Synthesis of anthracene-containing dialdehydes	55
3a.3.1.1	Synthesis of 9,10-bis[(4-formyl-2,5-dioctyloxy)phenyl ethynyl]anthracene (6a)	55
3a.3.1.1.1	Synthesis of 2,5-dibromo-hydroquinone (1a)	55
3a.3.1.1.2	Synthesis of 1,4-dibromo-2,5-bis(octyloxy) benzene (2a)	55
3a.3.1.1.3	Synthesis of 4-bromo-2,5-bis(octyloxy) benzaldehyde (3a)	55
3a.3.1.1.4	Synthesis of 2,5-bis(octyloxy)-4-[(trimethylsilyl)ethynyl]benzaldehyde (4a)	56
3a.3.1.1.5	Synthesis of 4-ethynyl-2,5-bis(octyloxy)benzaldehyde (5a)	57
3a.3.1.1.6	Synthesis of 9,10-bis[(4-formyl-2,5-dioctyloxy)phenylethynyl] anthracene (6a)	57
3a.3.1.2	9,10-Bis{[2,5-di(2-ethylhexyloxy)-4-formyl]phenyl}-ethynyl}anthracene (6b)	58
3a.3.1.2.1	Synthesis of 2,5-bis(2-ethylhexyloxy)-4-ethynylbenzaldehyde (5b) (a precursor in the synthesis of 6b)	58
3a.3.1.2.2	Synthesis of 9,10-bis{[2,5-di(2-ethylhexyloxy)-4-formyl]phenyl}-ethynyl} anthracene (6b)	58

3a.3.1.3	Synthesis of 9,10-bis[(4-formyl-2-(2'-ethylhexyloxy)-5-methoxy)phenylethynyl]anthracene (6c)	59
3a.3.1.3.1	Synthesis of 5-(2-ethylhexyloxy)-4-ethynyl-2-methoxybenzaldehyde (5c) (a precursor in the synthesis of 6c)	59
3a.3.1.3.2	Synthesis of 9,10-bis[(4-formyl-2-(2'-ethylhexyloxy)-5-methoxy)phenylethynyl]anthracene (6c)	60
3a.3.2	Synthesis of bisphosphonates	60
3a.3.2.1	Synthesis of 2,5-bis((2-ethylhexyloxy)-p-xylylene-bis(diethylphosphonate) (14b)	60
3a.3.2.1.1	Synthesis of 1,4-bis(2-ethylhexyloxy)benzene (12b)	60
3a.3.2.1.2	Synthesis of 1,4-bis-bromomethyl-2,5-bis-(2-ethylhexyloxy)-benzene (13b)	61
3a.3.2.1.3	Synthesis of 2,5-bis((2-ethylhexyl)oxy)-p-xylylene-bis(diethylphosphonate) (14b)	61
3a.3.2.2	Synthesis of 2,5-dioctyloxy-p-xylylene-bis(diethyl phosphonate) (14a)	62
3a.3.2.2.1	Synthesis of 1,4-dioctyloxybenzene (12a)	62
3a.3.2.2.2	Synthesis of 1,4-bis(bromomethyl)-2,5-dioctyloxybenzene (13a)	62
3a.3.2.2.3	Synthesis of 2,5-dioctyloxy-p-xylylene-bis(diethylphosphonate) (14a)	62
3a.3.2.3	Synthesis of 2,5-didecyloxy-p-xylylene-bis(diethylphosphonate) (14d)	62
3a.3.2.3.1	Synthesis of 1,4-didecyloxybenzene (12d)	63
3a.3.2.3.2	Synthesis of 1,4-bis(bromomethyl)-2,5-didecyloxybenzene (13d)	63
3a.3.2.3.3	Synthesis of 2,5-didecyloxy-p-xylylene-bis(diethylphosphonate) (14d)	63
3a.3.2.4	Synthesis of 5-(2-ethylhexyloxy)-2-methoxy-p-xylylenebis(diethylphosphonate) (14c)	63
3a.3.2.4.1	Synthesis of 1-(2-ethylhexyloxy)-4-methoxybenzene (7)	63
3a.3.2.4.2	1,4-Bis(bromomethyl)-5-(2-ethylhexyloxy)-2-methoxybenzene (13c)	64

3a.3.2.4.3	Synthesis of 5-(2-ethylhexyloxy)-2-methoxy-p-xylylenebis (diethylphosphonate) (14c)	64
3a.3.3	Synthesis of AnE-PV polymers	65
3a.3.3.1	Synthesis of polymer AnE-PVab:	65
3a.3.3.2	Synthesis of polymer AnE-PVad:	66
3a.3.3.3	Synthesis of polymer AnE-PVba:	66
3a.3.3.4	Synthesis of polymer AnE-PVbb:	66
3a.3.3.5	Synthesis of polymer AnE-PVcc:	67
3a.4	Results and Discussion	67
3a.4.1	Synthesis of dialdehydes	67
3a.4.1.1	Synthesis of dialdehydes bearing symmetric side chains on phenyl rings (6a, 6b)	67
3a.4.1.2	Synthesis of dialdehydes bearing asymmetric side chains on phenyl rings (6c)	70
3a.4.2	Synthesis of bisphosphonates (14)	71
3a.4.3	Synthesis of AnE-PV polymers	72
3a.4.4	Thermal properties of AnE-PV polymers	75
3a.4.5	Wide-Angle X-ray Scattering Analysis	77
3a.4.6	Photophysical Study	80
3a.4.7	Electrochemical Study	85
3a.4.8	Charge carrier mobility measurements:	86
3a.4.9	Morphological Studies	87
3a.4.10	Photovoltaic Studies	88
3a.5	Conclusions	92
	References	93

Chapter 3b Donor-Acceptor Low Band Gap Small Molecule Containing Anthracene Based Donor Unit and Diketopyrrolopyrrole, Benzothiadazole as Acceptor Units

3b.1	Introduction	103
3b.2	Experimental	104
3b.2.1	Materials	104
3b.2.2	Characterisation and techniques	105
3b.2.3		106

	Fabrication and characterization of the organic field effect transistor devices (OFET)	
3b.3	Synthesis	106
3b.3.1	Synthesis of 9,10-bis((2,5-bis(octyloxy)-4-vinylphenyl)ethynyl)anthracene (15)	106
3b.3.2	Synthesis of 3,6-bis(5-bromothiophen-2-yl)-2,5-bis(2-ethylhexyl)-2,5-dihydropyrrolo[3,4-c]pyrrole-1,4-dione (3)	107
3b.3.2.1	Synthesis of 3,6-di(thiophen-2-yl)-2,5-dihydropyrrolo[3,4-c]pyrrole-1,4-dione (1)	107
3b.3.2.2	Synthesis of 2,5-bis(2-ethylhexyl)-3,6-di(thiophen-2-yl)-2,5-dihydropyrrolo[3,4-c]pyrrole-1,4-dione (2)	107
3b.3.2.3	Synthesis of 3,6-bis(5-bromothiophen-2-yl)-2,5-bis(2-ethylhexyl)-2,5-dihydropyrrolo[3,4-c]pyrrole-1,4-dione (3)	108
3b.3.3	Synthesis of AnPPE-Th-DPP(EH)	108
3b.3.4	Synthesis of AnPPE-Th-BTDA	109
3b.4	Results and Discussion	109
3b.4.1	Synthesis of donor unit 9,10-bis((2,5-bis(octyloxy)-4-vinylphenyl)ethynyl)anthracene (AnPPE) (15)	109
3b.4.2	Synthesis of acceptor unit 3,6-bis(5-bromothiophen-2-yl)-2,5-bis(2-ethylhexyl)-2,5-dihydropyrrolo[3,4-c]pyrrole-1,4-dione (3, DPP(EH))	111
3b.4.3	Synthesis of AnPPE-Th-DPP(EH)	112
3b.4.4	Synthesis of AnPPE-Th-BTDA	114
3b.4.5	Photophysical Study	116
3b.4.6	Electrochemical Study	119
3b.4.7	Charge carrier mobility measurements	121
3b.5	Conclusions	123
	References	123

Chapter 4 Bi(thienylene-vinylene)thiophene Containing PAE-PV: Modulation of Charge Carrier Mobility by Side Chain Engineering

4.1	Introduction	127
4.2	Experimental	128
4.2.1	Materials	128

4.2.2	Characterisation and techniques	129
4.2.3	Charge carrier mobility measurements by Time of Flight (TOF) experiments	130
4.2.4	Fabrication and Characterization of the Photovoltaic Cells	130
4.3	Synthesis	131
4.3.1	Synthesis of bi(thienylenevinylene)thiophene containing dialdehydes	131
4.3.1.1	2,5-Bis{[(2,5-dioctyloxy-4-formyl)phenyl]ethynyl}-3-(2-{5-[2-(5-dodecyl)thiophenyl] vinyl}thiophenyl)vinyl-thiophene (3a)	131
4.3.1.2	2,5-Bis({[2,5-di(2-ethyl)hexyloxy-4-formyl]phenyl}ethynyl)-3-(2-{5-[2-(5-dodecyl)thiophenyl] vinyl}thiophenyl)vinyl-thiophene (3b)	131
4.3.2	Synthesis of bi(thienylenevinylene)thiophene containing PPE-PPV polymers	132
4.3.2.1	Synthesis of polymer BTE-PVab (General procedure)	132
4.3.2.2	Synthesis of polymer BTE-PVaa	133
4.3.2.3	Synthesis of polymer BTE-PVbb	133
4.3.2.4	Synthesis of Polymer BTE-PVba	133
4.4	Results and Discussion	134
4.4.1	Synthesis of bi(thienylenevinylene)thiophene-containing dialdehydes	134
4.4.2	Synthesis of bi(thienylenevinylene)thiophene-containing PPE-PPV polymers	136
4.4.3	Photophysical Study	139
4.4.4	Charge carrier mobility measurements:	141
4.4.5	X-Ray Diffraction studies	143
4.4.6	Photovoltaic studies	144
4.5	Conclusions	148
	References	149

Chapter 5 Benzo[1,2-c:4,5-c']dithiophene-4,8-dione Containing Copolymers and Terpolymers: Implications of Active Layer Morphology on Photovoltaic Performance

5.1	Introduction	156
-----	--------------	-----

5.2	Experimental	171
5.2.1	Materials	171
5.2.2	Characterisation and techniques	172
5.2.3	Fabrication and Characterization of the Photovoltaic Cells	173
5.3	Synthesis	174
5.3.1	Synthesis of 1,3-bis(5-bromothiophen-2-yl)-5,7-bis(2-ethylhexyl)-benzo[1,2-c:4,5-c']dithiophene-4,8-dione (BDD monomer)	174
5.3.1.1	Synthesis of 2-(2-ethylhexyl)thiophene (1)	174
5.3.1.2	Synthesis of 2-ethyl-1-(5-(2-ethylhexyl)thiophen-2-yl)hexan-1-one (2)	174
5.3.1.3	Synthesis of 2,5-bis(2-ethylhexyl)thiophene (3)	175
5.3.1.4	Synthesis of 2,5-dibromothiophene-3,4-dicarboxylic acid (4)	175
5.3.1.5	Synthesis of 1,3-dibromo-5,7-bis(2-ethylhexyl)-4H,8H-benzo[1,2-c:4,5-c']dithiophene-4,8-dione (5)	176
5.3.1.6	Synthesis of 1,3-bis(2-ethylhexyl)-5,7-di(thiophen-2-yl)benzo[1,2-c:4,5-c']-dithiophene-4,8-dione (6)	177
5.3.1.7	Synthesis of 1,3-bis(5-bromothiophen-2-yl)-5,7-bis(2-ethylhexyl)-benzo[1,2-c:4,5-c']dithiophene-4,8-dione (BDD monomer)	177
5.3.2	Synthesis of 3,6-bis(5-bromothiophen-2-yl)-2,5-bis(2-hexyldecyl)-2,5-dihydropyrrolo[3,4-c]pyrrole-1,4-dione (DPP(HD) monomer)	178
5.3.2.1	Synthesis of 2,5-bis(2-hexyldecyl)-3,6-di(thiophen-2-yl)-2,5-dihydropyrrolo[3,4-c]pyrrole-1,4-dione (7)	178
5.3.2.2	Synthesis of 3,6-bis(5-bromothiophen-2-yl)-2,5-bis(2-hexyldecyl)pyrrolo[3,4-c]pyrrole-1,4(2H,5H)-dione (DPP(HD) monomer)	178
5.3.3	Synthesis of 2,6-bis(trimethyltin)-4,8-bis(2-ethylhexyl)benzo[1,2-b:4,5-b']dithiophene (BDT monomer)	178
5.3.3.1	Synthesis of thiophene-3-carbonyl chloride (8)	178
5.3.3.2	Synthesis of N,N-diethylthiophene-3-carboxamide (9)	179
5.3.3.3	Synthesis of 4,8-dihydrobenzo[1,2-b:4,5-b']dithiophen-4,8-dione (10)	179
5.3.3.4	Synthesis of 4,8-bis((2-ethylhexyl)oxy)benzo[1,2-b:4,5-b']dithiophene (11)	180
5.3.3.5	Synthesis of 2,6-dibromo-4,8-bis(2-ethylhexyl)benzo[1,2-b:4,5-b']dithiophene (12)	180

5.3.3.6	Synthesis of 2,6-bis(trimethyltin)-4,8-bis(2-ethylhexyl)benzo[1,2-b:4,5-b']dithiophene (BDT monomer)	180
5.3.4	Synthesis of (4,4-bis(2-ethylhexyl)-4H-cyclopenta[2,1-b:3,4-b']dithiophene-2,6-diyl)bis(trimethylstannane) (CPDT monomer)	181
5.3.4.1	Synthesis of 4,4-bis(2-ethylhexyl)-4H-cyclopenta[2,1-b:3,4-b']dithiophene (13)	181
5.3.4.2	Synthesis of (4,4-bis(2-ethylhexyl)-4H-cyclopenta[2,1-b:3,4-b']dithiophene-2,6-diyl)bis(trimethylstannane) (CPDT monomer)	182
5.3.5	Synthesis of copolymers and terpolymers	182
5.3.5.1	Synthesis of CPDT-BDD copolymer: Typical procedure	182
5.3.5.2	Synthesis of BT-BDD copolymer	183
5.3.5.3	Synthesis of BDT-DPP(EH)-BDD terpolymer: Typical procedure	183
5.3.5.4	Synthesis of BDT-DPP(HD)-BDD terpolymer	184
5.3.5.5	Synthesis of BT-DPP(EH)-BDD terpolymer	184
5.3.5.6	Synthesis of BT-DPP(HD)-BDD terpolymer	185
5.4	Results and Discussion	185
5.4.1	Synthesis of 1,3-bis(5-bromothiophen-2-yl)-5,7-bis(2-ethylhexyl)-benzo[1,2-c:4,5-c']dithiophene-4,8-dione (BDD monomer)	185
5.4.2	Synthesis of 3,6-bis(5-bromothiophen-2-yl)-2,5-bis(2-hexyldecyl)pyrrolo[3,4-c]pyrrole-1,4(2H,5H)-dione (DPP(HD) monomer)	189
5.4.3	Synthesis of 2,6-bis(trimethyltin)-4,8-bis(2-ethylhexyl)benzo[1,2-b:4,5-b']dithiophene (BDT monomer)	192
5.4.4	Synthesis of (4,4-bis(2-ethylhexyl)-4H-cyclopenta[2,1-b:3,4-b']dithiophene-2,6-diyl)bis(trimethylstannane) (CPDT monomer)	193
5.4.5	Synthesis of BDD based copolymers	195
5.4.6	Synthesis of BDD based random terpolymers	197
5.4.6.1	Synthesis of BDD based random terpolymers comprising benzo[1,2-b:4,5-b']dithiophene (BDT) as donor unit	197
5.4.6.2	Synthesis of BDD based random terpolymers comprising bithiophene (BT) as donor unit	200
5.4.7	Photophysical Study	204
5.4.8	Electrochemical Study	210
5.4.9	Photovoltaic Studies	211

5.5	Conclusions	213
	References	214
<hr/>		
Chapter 6	DPP-Based Spacer Polymers Functionalized with Urethane Linker Containing Alkyl Side chains: Study of Self-assembly Behaviour	
<hr/>		
6.1	Introduction	229
6.2	Experimental	232
6.2.1	Materials	232
6.2.2	Characterisation and techniques	232
6.3	Synthesis	233
6.3.1	Synthesis of 3,6-bis(5-bromothiophen-2-yl)-2,5-bis(2-octyldodecyl)-2,5-dihydropyrrolo[3,4-c]pyrrole-1,4-dione (DPP(OD) monomer)	233
6.3.1.1	Synthesis of 9-(iodomethyl) nonadecane	234
6.3.1.2	Synthesis of 2,5-bis(2-octyldodecyl)-3,6-di(thiophen-2-yl)-2,5-dihydropyrrolo[3,4-c]pyrrole-1,4-dione	234
6.3.1.3	Synthesis of 3,6-bis(5-bromothiophen-2-yl)-2,5-bis(2-octyldodecyl)pyrrolo [3,4-c]pyrrole-1,4(2H,5H)-dione (DPP(OD) monomer)	235
6.3.2	Synthesis of DPP monomer with urethane linkage containing side chain (DPPurethane monomer)	235
6.3.2.1	Synthesis of 2-octyldodecyl (10-bromodecyl)carbamate (urethane linkage containing side chain) (compound 2)	235
6.3.2.2	Synthesis of DPPurethane (compound 3)	236
6.3.2.3	Synthesis of DPPurethane monomer (compound 4)	237
6.3.3	Synthesis of 1,4-bis(5-(trimethylstannyl)thiophen-2-yl)butane (spacer monomer)	237
6.3.3.1	Synthesis of 1,4-di(thiophen-2-yl)butane	238
6.3.3.2	Synthesis of 1,4-bis(5-(trimethylstannyl)thiophen-2-yl)butane (spacer monomer)	238
6.3.4	Synthesis of spacer polymers	239
6.3.4.1	Synthesis of DPPurethane spacer polymer: Typical procedure	239
6.3.4.2	Synthesis of DPPalkyl spacer polymer (DPPalkyl-Th-C4-Th polymer)	239
6.4	Results and Discussion	240
6.4.1	Synthesis of spacer polymers	240

6.4.1.1	Synthesis of DPPurethane monomer	240
6.4.1.2	Synthesis of 1,4-bis(5-(trimethylstannyl)thiophen-2-yl)butane (spacer monomer)	244
6.4.1.3	Synthesis of polymers- DPPurethane-Th-C4-Th polymer and DPPalkyl-Th-C4-Th polymer	245
6.4.2	Optical and Electrochemical studies:	250
6.4.3	Self-assembly in methyl cyclohexane	252
6.5	Conclusions	255
	References	255

Chapter 7 Summary and Conclusions

7.1	Summary and Conclusions	262
7.2	Future Perspectives	266
	Synopsis	268
	List of publications	277

Abstract

Renewable energy sources hold promise as environmentally benign sources of energy for the sustainability of our ecosystem, since the utilisation of traditional sources such as fossil fuels has damaged our planet by releasing toxic by-products and are dwindling. Solar energy is one of this kind which is abundantly available and has potential to replace the conventional energy sources. Silicon solar cells/ inorganic photovoltaics, invented in 1950s, were initially used in space programs. Later the field has rapidly grown due to the increased efficiencies, reliability and substantial decrease in the fabrication costs. Nevertheless, the solar electricity still remains expensive than the electricity from electrical grid.

Organic electronics or organic photovoltaics, in particular are of great importance in this context due to the possibility of processing organic semiconductors (light absorbing conjugated polymers or small molecules) from solution at low temperature and for large area devices with substantially reduced cost. Moreover, they can be deposited on flexible plastic substrates and can find convenient applications in products such as organic solar cells (OSCs), organic field effect transistors (OFETs), and organic light emitting diodes (OLEDs); with lower cost, flexibility and lighter weight. The most interesting feature of organic electronics is the fine tuning of final properties of device by slight variation in the molecular structure of organic semiconductors. The past four decades have been marked by intensive research in the field of OSCs. A number of interesting conjugated polymeric materials, exhibiting band gap energies around and below 2 eV have been designed and synthesized for organic solar cell applications. High power conversion efficiencies have been reported by various research groups using different conjugated polymers as donor materials in conjunction with fullerene derivatives (PC₆₁BM or PC₇₁BM) as acceptors in a bulk hetero-junction construct.

The present research work deals with the design, synthesis, characterization and evaluation of various conjugated polymers with anticipated solar light absorption and with appropriate band-gap engineering. The structure-property relationship was established. The new polymers were investigated for their performance in devices such as organic solar cells and organic field effect transistors. In yet another approach of the present work, non-covalent interactions, such as hydrogen-bonding were introduced in the polymer structure

to guide polymer self-assembly and its influence on optoelectronic properties was studied. The chapter-wise contents are presented below in brief.

Chapter 1 presents a brief account of different types of π -conjugated polymers utilised in devices such as OSC and OFET. Their structure-property relationship is discussed along with the relevant literature search. The working principle and fabrication of organic solar cell device is discussed.

Chapter 2 enumerates the scope and objectives of the present work.

Chapter 3 has been divided into two sections.

Chapter 3a describes the synthesis of anthracene-containing poly(*p*-arylene-ethynylene)-*alt*-poly(*p*-arylene-vinylene)s (PAE-PAV) polymers and provides a study of the influence of π - π stacking distance on the morphology and performance of solar cells. The side chains on the polymers were systematically varied between linear, branched and asymmetric substitution. Photo-physical and electrochemical characterizations revealed typical band-gap energies of 2 eV (optical) and 1.8 eV (electrochemical), respectively. Structure investigation in the bulk and in filaments yielded information about crystallinity and order with respect to the interlayer distance and the π - π stacking distance. Polymers with linear side chains on PAE unit showed improved ordering during and after annealing at 80-100°C. Relatively high open circuit voltage values (0.9 V) were achieved due to lower LUMO levels of the polymers. Solar cell efficiencies up to 3.1 % were achieved.

Chapter 3b describes the synthesis of donor-acceptor low band gap small molecules comprising anthracene-containing (*p*-phenylene ethynylene) (AnPPE) as a donor unit; and diketopyrrolopyrrole (DPP) or benzothiadiazole (BTDA) as acceptor units, respectively by Pd-catalyzed Heck reaction. The small molecules were characterized by ¹H-NMR and UV-Visible spectroscopy. UV-Visible absorption spectra of AnPPE-Th-DPP(EH) and AnPPE-Th-BTDA showed absorption maximum at 676 nm and 535 nm, respectively. Electrochemical band-gap energies of AnPPE-Th-DPP(EH) and AnPPE-Th-BTDA were 1.29 eV and 1.55 eV, respectively. AnPPE-Th-DPP(EH) showed hole mobility value of $4.19 \times 10^{-6} \text{ cm}^2 \text{ V}^{-1} \text{ s}^{-1}$ in OFET devices.

Chapter 4 describes the synthesis of bi(thienylene-vinylene)thiophene based PAE-PV polymers (BTE-PVs) and provided the study on the modulation of charge carrier mobility by side-chain engineering. The four polymers differ in the side-chain nature

(linear/branched). The drift mobility of holes in polymer BTE-PV ba , reached a quite impressive value of $10^{-2} \text{ cm}^2 \text{ V}^{-1} \text{ s}^{-1}$ among the amorphous polymers. Polymers having linear side chains (BTE-PV aa , BTE-PV ab) at BTE unit showed higher efficiencies in solar cells. The highest efficiency of 2.0 % was obtained for polymer BTE-PV ab bearing linear side chains at PAE unit and branched side chain at PV unit. This result correlates well with previous results reported for AnE-PPV polymers.

Chapter 5 describes the synthesis of benzo[1,2- c :4,5- c']dithiophene-4,8-dione-containing copolymers and terpolymers. Two copolymers and four terpolymers comprising cyclopentadithiophene (CPDT), bithiophene (BT), benzo[1,2- b :4,5- b']dithiophene (BDT) as electron donor units and diketopyrrolopyrrole (DPP), benzo[1,2- c :4,5- c']dithiophene-4,8-dione (BDD) as electron acceptor units were synthesized and characterized by ^1H and ^{13}C -NMR spectroscopy. Terpolymers showed much broader absorption in visible and near IR region of solar spectrum and improved solubility in organic solvents as compared to copolymers. CPDT-BDD copolymer was used as donor material in active layer of bulk hetero-junction solar cells. It showed maximum power conversion efficiency of 1.63 % and 1.39 % in inverted and conventional device architecture, respectively. Terpolymers-BDT-DPP(EH)-BDD and BDT-DPP(HD)-BDD exhibited temperature dependent UV-Vis absorption spectra, which indicated aggregation behaviour of these polymers. This property can be utilised to manipulate morphology of active layer during the fabrication of solar cell devices. The terpolymer BDT-DPP(EH)-BDD exhibited power conversion efficiency of 1.57 % in conventional device. The longer side chain analogue- BDT-DPP(HD)-BDD exhibited negligible power conversion efficiency. The high side chain density in BDT-DPP(HD)-BDD was found to cause steric hinderance, and disrupts planarity of molecule. The unfavorable morphology (as demonstrated by AFM studies) of this polymer when blended with PC $_{70}$ BM, hampered the exciton dissociation due to the reduced donor-acceptor interfacial area and hence the inferior photovoltaic performance. The absence of PL quenching in the blend film further supported the observed results.

Chapter 6 describes the synthesis and characterization of DPP-based spacer polymers functionalised with urethane linker containing side chain. Their self-assembly in solution was studied. Two diketopyrrolopyrrole (DPP) based polymers with either alkyl chain or urethane linkage containing alkyl chain on DPP unit, namely- DPP-alkyl-Th-C4-

Th and DPP-urethane-Th-C4-Th, were synthesized and characterized by ^1H and ^{13}C -NMR spectroscopy. These polymers were completely soluble in chloroform but insoluble in cyclohexane and methyl cyclohexane at room temperature. At higher temperature (80°C), they were found to dissolve in both of the solvents as confirmed by ^1H -NMR spectroscopy. This indicated that the polymers form self-assembly in cyclohexane or methyl cyclohexane at room temperature. Variable temperature ^1H -NMR spectra demonstrated the presence of hydrogen-bonding and self-assembled behavior in these polymers. These supramolecular interactions have been known to modify the thin film morphology and potentially affect the charge transport in the solid state.

Chapter 7 summarises the results and describes salient conclusions along with future prospects of the investigations reported in this thesis.

List of Abbreviations

A	Ampere
AFM	Atomic Force Microscopy
BDD	1,3-Bis(thiophen-2-yl)-5,7-bis(2-ethylhexyl)benzo-[1,2c:4,5c'] dithiophene-4,8-dione
BDT	Benzodithiophene
BTDA	2,1,3-Benzothiadiazole
BT	Bithiophene
CV	Cyclic Voltammetry
Cd	Candela
CuI	Copper Iodide
CPDT	Cyclopentadithiophene
CELIV	Charge Extraction by Linearly Increasing Voltage
DMF	N, N-Dimethylformamide
DMSO	Dimethyl sulfoxide
DPP	Diketopyrrolopyrrole
DSC	Differential Scanning Calorimetry
ϵ_{\max}	Absorption coefficient at the maximum wavelength
eV	Electron volt
Φ_f	Fluorescence Quantum Yield
FWHM	Full-Width-at- Half-Maximum
GPC	Gel Permeation Chromatography
Hz	Hertz
IPCE	Incident Photon to Converted Electron
IR	Infrared
ITO	Indium tin oxide
λ_a	Absorption maximum
λ_e	Emission maximum
$\lambda_{\text{exc.}}$	Excitation wavelength
LED	Light Emitting Diode
MALDI	Matrix-Assisted Laser Desorption Ionisation
MHz	Megahertz
MS	Mass Spectroscopy

M_n	Number-average molecular-weight
M_w	Weight-average molecular-weight
NBS	N-Bromosuccinimide
NMR	Nuclear Magnetic Resonance
<i>t</i> -BuOK	Potassium <i>tert</i> -butoxide
K_2CO_3	Potassium carbonate
<i>n</i> -BuLi	N-Butyllithium
OFET	Organic field-effect transistor
OLED	Organic light emitting diode
OPV	Organic photovoltaic cell
OSC	Organic solar cell
PSC	Polymer solar cells
PCBM	Phenyl C61 butyric acid methyl ester
Ph_3PCH_3Br	Methyltriphenylphosphonium bromide
$Pd(OAc)_2$	Palladium (II) acetate
$P(o\text{-tolyl})_3$	Tri(<i>o</i> -tolyl)phosphine
$Pd(PPh_3)_2Cl_2$	Bis(triphenylphosphine)palladium(II) dichloride
PEDOT	Poly(3,4-ethylenedioxythiophene)
PPE	Poly(- <i>p</i> -phenylene-ethynylene)
PPV	Poly(- <i>p</i> -phenylene-vinylene)
PSS	Poly(styrenesulfonate)
SAXS	Small Angle X-Ray Scattering
T_g	Glass transition temperature
TBAB	Tetrabutylammonium bromide
THF	Tetrahydrofuran
V	Volt
WAXS	Wide angle X-ray scattering
ITIC	2,2'-[[6,6,12,12-Tetrakis(4-hexylphenyl)-6,12 dihydrodithieno[2,3- <i>d</i> :2',3'- <i>d'</i>]-s-indaceno[1,2- <i>b</i> :5,6 <i>b'</i>]dithiophene-2,8-diyl]bis[methyldiylidene(3-oxo-1 <i>H</i> -indene 2,1(3 <i>H</i>)-diylidene)]]bis[propanedinitrile]
IC ₆₀ BA	Indene-C ₆₀ bisadduct

List of Tables

Table No.	Description	Page No.
1.1	Photovoltaic properties of reported 2-D-conjugated polymers	25
1.2	Photovoltaic properties of representative D-D-A type terpolymers	27
1.3	Photovoltaic properties of representative D-A-A terpolymers	28
3a.1	Data obtained from GPC and TGA studies	75
3a.2	Transitions temperatures determined from the peak maxima of the DSC thermograms	76
3a.3	Interlayer distance and π - π stacking distance from WAXS analysis	80
3a.4	Photophysical data of AnE-PV polymers in solution and on thin films	83
3a.5	Electrochemical data for polymer films spin-coated from chlorobenzene solution	86
3a.6	Hole mobilities (μ_{hole}) of polymers	87
3a.7	Photovoltaic parameters for polymer solar cells	90
3b.1	Data obtained from GPC and MALDI study	115
3b.2	Photophysical data of D-A small molecules in solution	119
3b.3	Electrochemical data for small molecules films spin-coated from chlorobenzene	120
3b.4	The OFET parameters of device prepared from AnPPE-Th-DPP(EH)	122
4.1	Data obtained from GPC and TGA studies	139
4.2	Photophysical data in dilute chloroform solution and thin film	141
4.3	Hole (μ_{h}) and electron (μ_{e}) mobilities of polymers for an electric field of $8 \times 10^4 \text{ Vcm}^{-1}$	143
4.4	Photovoltaic parameters of solar cells made of BTE-PVs as donors and PC ₆₁ BM as acceptor	147
5.1	BDD-based copolymers reported in the literature.	158
5.2	Data obtained from GPC and TGA studies	204
5.3	Photophysical data of BDD based polymers in solution and on thin films	208
5.4	Electrochemical data for polymer films spin-coated from chlorobenzene solution	211
5.5	Photovoltaic parameters for polymer solar cells	212

6.1	Data obtained from GPC and TGA studies	249
6.2	Photophysical and electrochemical data of polymers	251

List of Schemes

Scheme No.	Description	Page No.
3a.1	Synthesis of dialdehydes bearing symmetric side chains on phenyl rings (6a and 6b)	68
3a.2	Synthesis of dialdehydes bearing asymmetric side chains on phenyl rings (6c)	70
3a.3	Synthesis of bisphosphonates	71
3a.4	Synthesis of AnE-PV polymers	73
3b.1	Synthesis of 9,10-bis((2,5-bis(octyloxy)-4-vinylphenyl)ethynyl)anthracene (15, AnPPE)	110
3b.2	Synthesis of 3,6-bis(5-bromothiophen-2-yl)-2,5-bis(2-ethylhexyl)-2,5-dihydropyrrolo[3,4-c]pyrrole-1,4-dione (3, DPP(EH))	111
3b.3	Synthesis of AnPPE-Th-DPP(EH)	113
3b.4	Synthesis of AnPPE-Th-BTDA	114
4.1	Synthesis of bi(thienylenevinylene)thiophene-containing dialdehydes (3a and 3b)	134
4.2	Synthesis of bi(thienylenevinylene)thiophene-containing polymers BTE-PV _{aa} , BTE-PV _{ab} , BTE-PV _{ba} and BTE-PV _{bb}	137
5.1	Synthesis of 1,3-bis(5-bromothiophen-2-yl)-5,7-bis(2-ethylhexyl)benzo[1,2-c:4,5-c']dithiophene-4,8-dione (BDD monomer)	187
5.2	Synthesis of 3,6-bis(5-bromothiophen-2-yl)-2,5-bis(2-hexyldecyl)pyrrolo[3,4-c]pyrrole-1,4(2H,5H)-dione (DPP(HD) monomer)	190
5.3	Synthesis of 2,6-bis(trimethyltin)-4,8-bis(2-ethylhexyl)benzo[1,2-b:4,5-b']dithiophene (BDT monomer)	192
5.4	Synthesis of (4,4-bis(2-ethylhexyl)-4H-cyclopenta[2,1-b:3,4-b']dithiophene-2,6-diyl)bis(trimethylstannane) (CPDT monomer)	194
5.5	Synthesis of BDD based copolymers- 1) CPDT-BDD and 2) BT-BDD	195
5.6	Synthesis of BDD based random terpolymers comprising BDT as donor unit- 3) BDT-DPP(EH)-BDD and 4) BDT-DPP(HD)-BDD	198
5.7	Synthesis of BDD based random terpolymers comprising BT as donor unit- 5) BT-DPP(EH)-BDD and 6) BT-DPP(HD)-BDD	201
6.1	Synthetic scheme of DPP _{urethane} monomer (4)	241
6.2	Synthesis of 1,4-bis(5-(trimethylstannyl)thiophen-2-yl)butane (spacer monomer)	244
6.3	Synthesis of spacer polymers A) DPP _{urethane} -Th-C ₄ -Th polymer B)	246

DPP_{alkyl}-Th-C₄-Th polymer

List of Figures

Figure No.	Description	Page No.
1.1	Percent usage of different energy resources	1
1.2	An overview of renewable energy resources	2
1.3	Classification of solar cell technologies	3
1.4	Schematic representation of the components of DSSC	5
1.5	Crystal structure of the hybrid perovskite $\text{CH}_3\text{NH}_3\text{PbI}_{3-x}\text{Cl}_x$	7
1.6	Architectures of perovskite solar cells- a) Hybrid perovskite solar cell on mesoporous TiO_2 , b) Planar hybrid perovskite solar cell	7
1.7	Brief history of solar cells ²⁵	8
1.8	a) Schematic diagram of OSC device, b) energy level diagram for a donor-acceptor heterojunction in OSC device and c) picture of typical OSC device on lab scale	12
1.9	Operating mechanism of D–A type organic/ polymer solar cells	14
1.10	Various architectures of organic solar cell device	16
1.11	<i>J-V</i> curve and various device parameters for the characterization of solar cells	17
1.12	a) Energy level diagram for device operation b) Solar photon flux	18
1.13	Various strategies for band-gap engineering	20
1.14	Structures of representative 2-D conjugated polymers	25
1.15	Structures of representative D-D-A type terpolymers	27
1.16	Structures of representative D-A-A type terpolymers	28
1.17	The structures of representative polymers comprising flexible linkers.	31
2.1	The theme of the thesis	43
3a.1	$^1\text{H-NMR}$ spectrum (CDCl_3) of 9,10-bis[(4-formyl-2,5-dioctyloxy)phenylethynyl]anthracene (6a)	69
3a.2	$^{13}\text{C-NMR}$ spectrum (CDCl_3) of 9,10-bis[(4-formyl-2,5-dioctyloxy)phenylethynyl]anthracene (6a)	69
3a.3	$^1\text{H-NMR}$ spectrum (CDCl_3) of 2,5-bis(2-ethylhexyloxy)-p-xylylene-bis(diethylphosphonate) (14b)	72
3a.4	$^1\text{H-NMR}$ spectrum (CDCl_3) of polymer AnE-PVab.	73
3a.5	TG curves of polymers	75
3a.6	DSC thermograms (heat flow dH/dt as a function of temperature T)	76

	obtained during the first heating run.	
3a.7	WAXS results for powder samples after different annealing steps	78
3a.8	A sketch of the layered structure of AnE-PV polymers	79
3a.9	The absorption and emission spectra of AnE-PV polymers in dilute chloroform solution	81
3a.10	Temperature-dependent absorption spectra of AnE-PV _{ad} in toluene	82
3a.11	Thin film absorption and emission spectra of polymers and polymer:PCBM (1:1) blends	84
3a.12	Tapping mode AFM images (area 2.5 x 2.5 μm ²) for polymers	88
3a.13	<i>J-V</i> curves of solar cells incorporating polymer:PCBM active layers (with weight ratios 1:1 and 1:2)	89
3a.14	Comparison of light <i>J-V</i> curves of AnE-PV _{cc} :PCBM (1:1) blends cast from chlorobenzene (black) and mixture of chlorobenzene-chloroform (1:1, v/v)	91
SI 3a.1	¹ H-NMR spectrum (DMSO- <i>d</i> ₆) of 2,5-dibromo-hydroquinone (1a)	97
SI 3a.2	¹ H-NMR spectrum (CDCl ₃) of 1,4-dibromo-2,5-bis(octyloxy)benzene (2a)	97
SI 3a.3	¹³ C-NMR-DEPT spectrum (CDCl ₃) of 4-bromo-2,5-bis(octyloxy)benzaldehyde (3a)	98
SI 3a.4	¹ H-NMR spectrum (CDCl ₃) of 2,5-bis(octyloxy)-4-[(trimethylsilyl)ethynyl]benzaldehyde (4a)	99
SI 3a.5	¹ H-NMR spectrum (CDCl ₃) of 4-ethynyl-2,5-bis(octyloxy)benzaldehyde (5a)	100
SI 3a.6	¹ H-NMR spectrum (CDCl ₃) of 1,4-bis((2-ethylhexyl)oxy)benzene (12b)	100
SI 3a.7	¹ H-NMR spectrum (CDCl ₃) of 1,4-bis-bromomethyl-2,5-bis-(2-ethylhexyloxy)-benzene (13b)	101
SI 3a.8	Cyclic voltammograms of AnE-PV polymers	101
SI 3a.9	CELIV study of AnE-PV polymers	102
3b.1	¹ H-NMR spectrum (CDCl ₃) of 9,10-bis((2,5-bis(octyloxy)-4-vinylphenyl)ethynyl)anthracene (15, AnPPE)	110
3b.2	¹ H-NMR spectrum (CDCl ₃) of 3,6-bis(5-bromothiophen-2-yl)-2,5-bis(2-ethylhexyl)-2,5-dihydropyrrolo[3,4- <i>c</i>]pyrrole-1,4-dione (3, DPP(EH))	112
3b.3	¹ H-NMR spectrum (CDCl ₃) of AnPPE-Th-DPP(EH)	113
3b.4	MALDI-TOF spectrum of AnPPE-Th-DPP(EH)	116
3b.5	Predicted structure of AnPPE-Th-DPP(EH)	116
3b.6	The absorption spectra of AnPPE, DPP(EH) and AnPPE-Th-	117

	DPP(EH) in dilute chloroform solution	
3b.7	Absorption spectra of AnPPE, BTDA and AnPPE-Th-BTDA in dilute chlorobenzene solution	118
3b.8	The photoluminescence spectra of AnPPE, DPP(EH) and AnPPE-Th-DPP(EH) in dilute chloroform solution	118
3b.9	The photoluminescence spectra of AnPPE, BTDA and AnPPE-Th-BTDA in dilute chlorobenzene solution	119
3b.10	Cyclic voltammograms of a) AnPPE-Th-DPP(EH) and, b) AnPPE-Th-BTDA	120
3b.11	Output and Transfer characteristics of OFETs based on AnPPE-Th-DPP(EH) at room temperature	122
3b.12	Output and Transfer characteristics of OFETs based on AnPPE-Th-DPP(EH) after thermal annealing at 100 °C	122
SI 3b.1	¹ H-NMR spectrum of AnE-Th-DPP(EH)	126
4.1	¹ H-NMR spectrum (CDCl ₃) of 2,5-Bis{[(2,5-dioctyloxy-4-formyl)phenyl]ethynyl}-3-(2-{5-[2-(5-dodecyl)thiophenyl]vinyl}thiophenyl)vinyl- thiophene (3a)	135
4.2	¹ H-NMR spectrum (CDCl ₃) of 2,5-bis{[(2,5-di-ethylhexyloxy-4-formyl)phenyl]ethynyl}-3-(2-{5-[2-(5-dodecyl)thiophenyl]vinyl}thiophenyl)vinyl- thiophene (3b)	136
4.3	¹ H-NMR spectrum (CDCl ₃) of the polymer BTE-PV _{ab}	138
4.4	The absorption and emission spectra of AnE-PV polymers in dilute chloroform solution	140
4.5	The absorption and emission spectra of AnE-PV polymers in thin films	140
4.6	Hole mobility (a) and electron mobility (b) as a function of the square root of the electric field for BTE-PVs.	142
4.7	XRD patterns of polymer films drop-casted onto zero-background quartz substrate	144
4.8	AFM height images (5 μm × 5 μm) of BTE-PV _{ab} : PC ₆₁ BM blends	146
4.9	(a) <i>J-V</i> curves for the best performing solar cells obtained under simulated AM1.5 illumination and (b) corresponding EQE spectra	147
SI 4.1	¹ H-NMR spectrum (CDCl ₃) of polymers- 1) BTE-PV _{aa} , 2) BTE-PV _{bb} and 3) BTE-PV _{ba}	153
SI 4.2	TG curves of BTE-PV polymers	153
SI 4.3	Luminescence decay curves in dilute chloroform solution and thin film	154
SI 4.4	Typical TOF signals for positive (black lines) and negative charge carriers (gray lines) in log-log scales	154

SI 4.5	AFM height images (20 μm x 20 μm) of BTE-PVba: PC ₆₁ BM blends	155
5.1	¹ H-NMR spectrum (CDCl ₃) of 1,3-bis(5-bromothiophen-2-yl)-5,7-bis(2-ethylhexyl)-benzo[1,2-c:4,5-c']dithiophene-4,8-dione (BDD monomer)	188
5.2	¹³ C-NMR spectrum (CDCl ₃) of 1,3-bis(5-bromothiophen-2-yl)-5,7-bis(2-ethylhexyl)-benzo[1,2-c:4,5-c']dithiophene-4,8-dione (BDD monomer)	189
5.3	a) ¹ H-NMR and b) ¹³ C-NMR spectrum (CDCl ₃) of 3,6-bis(5-bromothiophen-2-yl)-2,5-bis(2-hexyldecyl)pyrrolo[3,4-c]pyrrole-1,4(2H,5H)-dione (DPP(HD) monomer)	191
5.4	¹ H-NMR spectrum (CDCl ₃) of 2,6-bis(trimethyltin)-4,8-bis(2-ethylhexyl)benzo[1,2-b:4,5-b']dithiophene	193
5.5	¹ H-NMR spectrum (CDCl ₃) of (4,4-bis(2-ethylhexyl)-4H-cyclopenta[2,1-b:3,4-b']dithiophene-2,6-diyl)bis(trimethylstannane) (CPDT monomer)	194
5.6	¹ H-NMR spectrum (CDCl ₃) of copolymer CPDT-BDD	196
5.7	¹ H-NMR spectrum (CDCl ₃) of copolymer BT-BDD	197
5.8	¹ H-NMR spectrum (TCE-d ₂) of terpolymer BDT-DPP(EH)-BDD	199
5.9	¹ H-NMR spectrum (TCE-d ₂) of terpolymer BDT-DPP(HD)-BDD	200
5.10	¹ H-NMR spectrum (CDCl ₃) of terpolymer BT-DPP(EH)-BDD	202
5.11	¹ H-NMR spectrum (TCE-d ₂) of terpolymer BT-DPP(HD)-BDD	203
5.12	The absorption and photoluminescence spectra of copolymer and terpolymers comprising bithiophene (BT) as donor unit in dilute chloroform solution	205
5.13	The absorption and photoluminescence spectra of terpolymers comprising benzo[1,2-b:4,5-b']dithiophene (BDT) as donor unit in dilute chloroform solution	206
5.14	The absorption and photoluminescence spectra of thin films of copolymer and terpolymers solution comprising bithiophene (BT) as donor unit, spin coated from their chlorobenzene solution.	207
5.15	The absorption and photoluminescence spectra of thin films of terpolymers comprising BDT as donor unit, spin coated from chlorobenzene solution	207
5.16	Thin film absorption and photoluminescence spectra of polymers and their 1:1 blends with PC ₇₀ BM	209
5.17	The temperature dependent absorption spectrum of BDT-DPP(EH)-BDD and BDT-DPP(HD)-BDD in chlorobenzene solution	210
5.18	<i>J-V</i> curves of solar cells incorporating polymer: PC ₇₀ BM active layers of 1) CPDT-BDD 2) BDT-DPP(EH)-BDD	212

5.19	AFM image of active layer (polymer:PC ₇₀ BM blend film) of polymer BDT-DPP(EH)-BDD and BDT-DPP(HD)-BDD	213
SI 5.1	¹ H-NMR spectrum (CDCl ₃) of 2-(2-ethylhexyl)thiophene (1)	219
SI 5.2	¹ H-NMR spectrum (CDCl ₃) of 2-ethyl-1-(5-(2-ethylhexyl)thiophen-2-yl)hexan-1-one (2)	219
SI 5.3	¹³ C-NMR spectrum (CDCl ₃) of 2-ethyl-1-(5-(2-ethylhexyl)thiophen-2-yl)hexan-1-one (2)	220
SI 5.4	¹ H-NMR spectrum (CDCl ₃) of 2,5-bis(2-ethylhexyl)thiophene (3)	220
SI 5.5	¹³ C-NMR spectrum (CDCl ₃) of 2,5-bis(2-ethylhexyl)thiophene (3)	221
SI 5.6	¹ H-NMR spectrum (Acetone-d ₆) of 2,5-dibromothiophene-3,4-dicarboxylic acid (4)	221
SI 5.7	¹³ C-NMR spectrum (Acetone-d ₆) of 2,5-dibromothiophene-3,4-dicarboxylic acid (4)	222
SI 5.8	¹ H-NMR spectrum (CDCl ₃) of 1,3-dibromo-5,7-bis(2-ethylhexyl)-4H,8H-benzo[1,2-c:4,5-c']dithiophene-4,8-dione (5)	222
SI 5.9	¹³ C-NMR spectrum (CDCl ₃) of 1,3-dibromo-5,7-bis(2-ethylhexyl)-4H,8H-benzo[1,2-c:4,5-c']dithiophene-4,8-dione (5)	223
SI 5.10	¹ H-NMR spectrum (CDCl ₃) of 1,3-bis(2-ethylhexyl)-5,7-di(thiophen-2-yl)benzo[1,2-c:4,5-c']-dithiophene-4,8-dione (6)	223
SI 5.11	¹³ C-DEPT-NMR spectrum (CDCl ₃) of 1,3-bis(5-bromothiophen-2-yl)-5,7-bis(2-ethylhexyl)-benzo[1,2-c:4,5-c']dithiophene-4,8-dione (BDD monomer)	224
SI 5.12	¹ H-NMR spectrum (CDCl ₃) of N,N-diethylthiophene-3-carboxamide (9)	224
SI 5.13	a) ¹ H-NMR spectrum and b) ¹³ C-NMR spectrum (CDCl ₃) of 4,8-dihydrobenzo[1,2-b:4,5-b']dithiophen-4,8-dione (10)	225
SI 5.14	¹ H-NMR spectrum (CDCl ₃) of 4,8-bis((2-ethylhexyl)oxy)benzo[1,2-b:4,5-b']dithiophene (11)	226
SI 5.15	1) ¹ H-NMR spectrum and 2) ¹³ C-NMR spectrum (CDCl ₃) of 4,4-bis(2-ethylhexyl)-4H-cyclopenta[2,1-b:3,4-b']dithiophene (13)	227
SI 5.16	TG curves of BDD based copolymers and terpolymers	228
SI 5.17	CV curves for BDD based copolymers and terpolymers	229
6.1	¹ H-NMR spectrum (CDCl ₃) of 2-octyldodecyl (10-bromodecyl)carbamate (urethane linkage containing side chain) (2)	242
6.2	¹ H-NMR spectrum (CDCl ₃) of DPP _{urethane} (3)	243
6.3	¹ H-NMR spectrum (CDCl ₃) of DPP _{urethane} monomer (4)	244
6.4	¹ H-NMR spectrum (CDCl ₃) of 1,4-bis(5-(trimethylstannyl)thiophen-2-yl)butane (spacer monomer)	245
6.5	¹ H-NMR spectrum (CDCl ₃) of DPP _{urethane} -Th-C ₄ -Th polymer	247

6.6	$^1\text{H-NMR}$ spectrum (CDCl_3) of $\text{DPP}_{\text{alkyl}}\text{-Th-C}_4\text{-Th}$ polymer	248
6.7	TG curves for the spacer polymers	249
6.8	Variable temperature $^1\text{H-NMR}$ spectrum of $\text{DPP}_{\text{urethane}}\text{-Th-C}_4\text{-Th}$ polymer	250
6.9	Thin-film cyclic voltammogram of spacer polymers	251
6.10	The absorption spectra of spacer polymers in dilute chloroform (CHCl_3) solution and dilute methylcyclohexane (MCH) solution	252
6.11	The absorption and emission spectra of spacer polymers on thin films prepared from their dilute chloroform and methylcyclohexane (MCH) solution	252
6.12	$^1\text{H-NMR}$ spectra of spacer polymers in tetrachloroethane- D_2 at RT and at 80°C	253
6.13	$^1\text{H-NMR}$ spectra of spacer polymers in cyclohexane- D_{12} at RT and at 80°C	254
SI 6.1	$^1\text{H-NMR}$ spectrum (CDCl_3) of 1,4-di(thiophen-2-yl)butane	260
SI 6.2	$^{13}\text{C-NMR}$ spectrum (CDCl_3) of $\text{DPP}_{\text{urethane}}$	260
SI 6.3	$^{13}\text{C-NMR}$ spectrum (CDCl_3) of $\text{DPP}_{\text{urethane}}$ monomer	261
SI 6.4	GPC traces for spacer polymers	261

CHAPTER 1

Introduction and Literature Survey

1.1 Introduction

1.1.1 Energy crisis and renewable energy resources

Energy remains a critical issue for the survival and prosperity of human civilization. Since the beginning of journey of human development, the energy consumption has been increasing and it is projected to increase with population and economic growth in the world. Currently, the energy consumption mainly originates from fossil resources (e.g., petroleum, coal and natural gas). In 2016, worldwide energy consumption was 18 TW and 80 % of that energy came from fossil fuel such as coal, oil and natural gas. The predicted energy consumption for 2050 will amount to as much as 28-35 TW. So, the main issue of fossil resources is sustainability, especially with the continuous increase of the demand for energy. **Figure 1.1** represents percent usage of different energy resources.

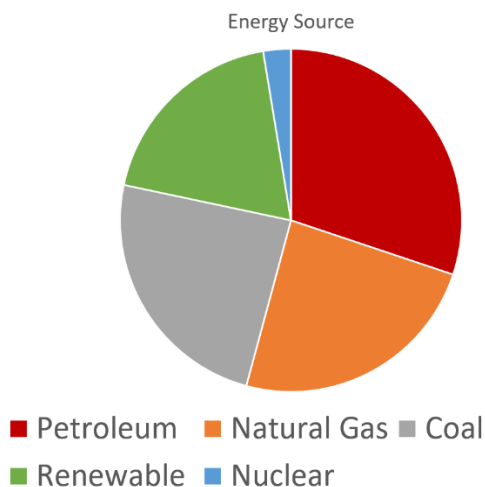


Figure 1.1 Percent usage of different energy resources

After 1950, the CO₂ emission due to fossil fuel has been increased rapidly and after 2000, the CO₂ emission has crossed 10000 million tons. Thus, fossil fuel usage has a detrimental effect on environment causing greenhouse gas emission, air pollution, water and soil contamination and recent climate change. In addition to the environmental and climate impacts (e.g., environmental pollutions and global warming) caused by the production and combustion of fossil fuels, these non-renewable resources are also becoming increasingly shorter in supply. Due to this reason, worldwide there is a fear of the exhaustion of conventional sources of energy. Thus, the energy crisis is the concern that the world's demands on the limited natural resources that are used to power industrial

society are diminishing as the demand rises. To avoid an energy crisis, secure, clean and renewable energy sources are believed to be the eventual solution for sustainable energy. Renewable energies are energy sources that are continually replenished by nature.¹ These include- solar energy (thermal, photo-chemical, and photo-electric), wind energy, tidal energy, hydro energy, geothermal energy and bioenergy (photosynthetic energy stored in biomass). Renewable energy technologies turn these natural energy sources into usable forms of energy i.e. electricity, heat and fuels. Renewable energy provides the dual goals of reducing greenhouse gas emissions, thereby limiting future extreme weather and climate conditions, and at the same time, ensures reliable and cost-efficient supply of energy. **Figure 1.2** provides an overview of renewable energy sources.²

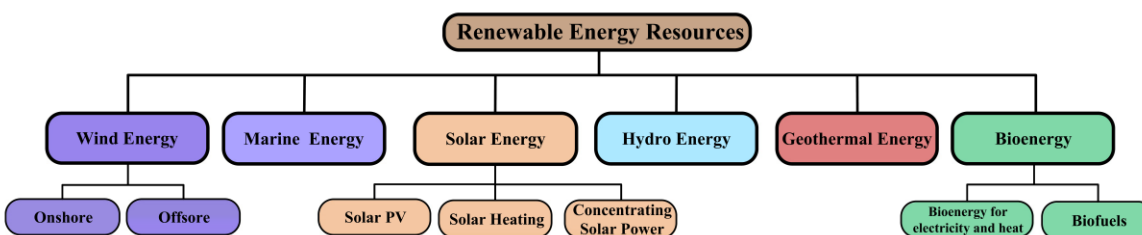


Figure 1.2 An overview of renewable energy sources²

1.1.2 Solar energy technology

Among above mentioned renewable energy resources, only three renewable energy sources (i.e., biomass, geothermal, and solar) can be utilized to yield sufficient heat energy for power generation. Out of these three, solar energy exhibits the highest global potential, since- i) The geothermal sources are limited to a few locations and ii) the supply of biomass is not ubiquitous in nature. The intensity of the solar influx that passes through Earth's atmosphere varies with number of factors such as- latitude, diurnal variation, climate, and geographic variation. The average amount of solar energy received at Earth's atmosphere is around 342 W m^{-2} , of which ca. 30% is scattered or reflected back to space, leaving ca. 70% (239 W m^{-2}) available for harvesting and capture. The annual effective solar irradiance varies from 60 to 250 W m^{-2} worldwide. The whole solar energy concept is regarded as the harvesting and utilization of light and/or heat energy generated by the Sun and technologies (passive and active) involved in it. A classification of present solar energy technologies is shown in **Figure 1.3**.

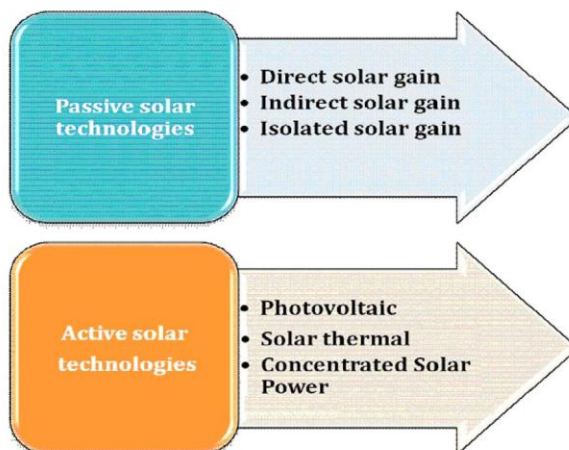


Figure 1.3 Classification of solar cell technologies³

1. Passive solar technology: Passive solar technology involves the accumulation of solar energy without transforming thermal or light energy into any other form. Solar energy collection, storage, and distribution in the form of heat for the heating of homes during the winter season, can be considered as a form of passive solar technology.

2. Active solar technology: Active solar system collects solar radiation and uses mechanical and electrical equipment (e.g., pumps and fans) for the conversion of solar energy into heat and electric power. The most well-known application of this system is the solar water heater system.

In general, active solar energy technology can be further grouped into two categories: (i) photovoltaic technology and (ii) solar thermal technology. In recent years, photovoltaic technology which involves the use of semiconductors to convert sunlight directly into electrical energy has become potential option. The intense research in this field has resulted into an improved efficiency of photovoltaic technology; for example, a promising achievement in hybrid perovskite solar cells ($(\text{CH}_3\text{NH}_3)\text{PbI}_3$), (an efficiency of about 18 %) has been reported.⁴ Apart from this, the photovoltaic technology involving wafer-based cells (traditional crystalline silicon or gallium arsenide), commercial thin-film cells (cadmium telluride, amorphous silicon, copper indium gallium diselenide), and new thin-film technologies (perovskites, organic materials, quantum dots) are also progressing as a result of intense R & D efforts.⁵

In solar thermal technology, solar energy is harnessed into thermal energy for domestic and/or commercial applications such as drying, heating, cooling, cooking, etc.

However, on the industrial scale, concentrated solar thermal (CST) technologies are used to fulfill heating requirements and concentrated solar power (CSP) technologies are used to generate electricity. CSP technology involves the use of high-magnification mirrors to concentrate solar energy prior to converting it into heat energy to power a steam turbine. Four types of CSP technologies are currently available in the market: (i) parabolic troughs (these concentrate sunlight onto a receiver tube containing a working liquid); (ii) Fresnel mirrors (use multiple flat mirrors to concentrate solar sunlight onto a receiver tube); (iii) power towers (an array of thousands of sun-tracking reflecting mirrors positioned in a field to concentrate solar radiation to a single point), and (iv) solar dish collectors (concentrate power by focusing solar energy onto a single point situated above a reflector dish). Presently, a number of CSP projects are coming online and are under progress in both developed and developing countries, although the system is more expensive than PV technology. PV technologies for the time being may continue to be the primary source of solar power generation.

1.2 Photovoltaics

Photovoltaics technology can convert solar energy into electricity by using photovoltaic cells (solar cells) constructed with semiconducting materials. The first practical solar cell based on a Si (silicon) p-n junction was fabricated by Daryl Chapin et al. in 1954 at Bell Laboratories. This solar cell exhibited a power conversion efficiency of ~ 6%. Since then, solar cell technology has been rapidly developing in both academia and industry. Unfortunately, this solar cell was very much expensive and its initial applications were restricted to space programs (space laboratories, communication satellites and orbiting astronomical observatories). Thus, due to cost related issues, these solar cells had less potential for terrestrial applications. The thrust to search affordable alternatives gave rise to the development of thin-film solar cells mostly incorporating inorganic materials. The thin-film technologies included amorphous Si (a-Si),⁶ cadmium telluride (CdTe),⁷ and copper indium gallium diselenide (CIGS)⁸ which benefited in terms of reduction in material consumption and elimination of the use of expensive wafers. These solar cells have been successfully applied in power supplies for remote locations, for example for lighting, communications, weather monitoring systems, water pumping systems used in developing countries and in consumer products such as, electronic calculators and garden

lights. Although these thin film technologies reduced the manufacturing cost to some extent, it still required high-temperature processes and high-cost vacuum evaporation techniques. These drawbacks resulted into further evolution of solution-processed thin-film solar cells, as described below, which significantly lowered the production cost by high material utilization and use of techniques such as roll-to-roll processing, and spin casting. These solution-processed solar cells include-

1. Organic solar cells

Organic solar cells will be discussed in details in upcoming sections.

2. Dye-sensitized solar cells (DSSCs),

The concept and architecture of dye sensitized solar cell (DSSC) was first discovered by Grätzel *et al.* in 1991.⁹ DSSCs are considered as potential alternative to the silicon based solar cells on account of their facile processing techniques, attractive performance to cost ratio, applicability under diffused light and possibility of their functioning even on flexible substrates. The four major components present in DSSC include: semiconducting electrode, dye sensitizer, redox mediator and counter electrode (Figure 4c.9).¹⁰

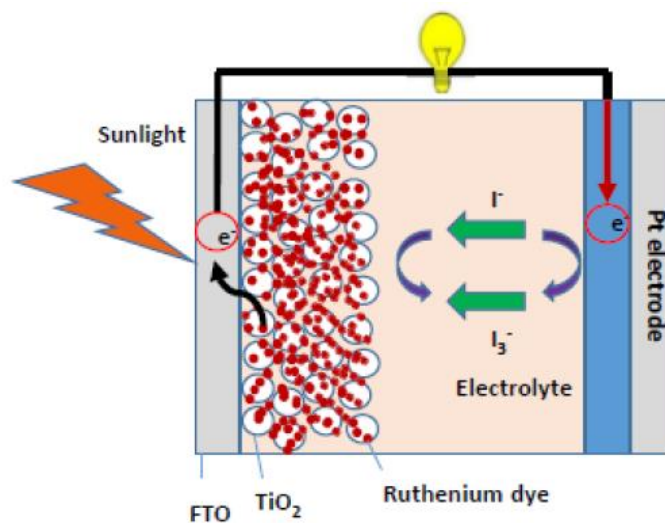
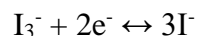
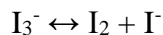


Figure 1.4 Schematic representation of the components of DSSC

The redox electrolyte is one of the important components of DSSCs and is very crucial for the performance and long-term stability of DSSCs. The redox reactions involved for commonly used iodide/tri-iodide redox couple are:





This redox couple is generally prepared by dissolving iodine and lithium iodide in a suitable solvent. The liquid nature of the redox electrolyte ensures intimate contact of TiO₂/dye and electrolyte forming a good interface which facilitates the dye regeneration process.¹¹ The fabrication and sealing procedure of DSSCs involves tedious task of injecting liquid redox electrolyte in DSSC assembly followed by sealing the hole from where the liquid electrolyte was injected. The liquid nature of redox electrolyte is unsuitable due to its evaporation and leakage issues, over a period of time.^{12,13} Thus, despite the fact that liquid electrolytes form good interface, DSSCs suffer from drawbacks in terms of long-term use and practicality. To address these issues, efforts have made towards replacing liquid electrolyte with solid state electrolytes such as p-type semiconductors,¹⁴ hole-conductors,¹⁵ and polymeric materials incorporating the redox couple I₃⁻/I⁻.^{16–18} However, the power conversion efficiencies of DSSCs involving these types of electrolytes are still lower due to poor TiO₂/dye/electrolyte interface and lower ionic mobility.

3. Hybrid perovskite solar cells (PSCs),

Perovskite solar cells based on hybrid organic–inorganic metal halides as the light absorber are considered promising material in thin film photovoltaic technology due to their high efficiency, cost effective fabrication techniques, and low material cost.¹⁹ Perovskite-based photovoltaic technology is a potential alternative to the technologies such as organic photovoltaics and dye-sensitized solar cells due to rapid improvement in its device performance which is attributed to the unique characteristics such as a broad spectral absorption range, very high absorption coefficient, high carrier mobility, longer diffusion length, and longer carrier lifetime.

Perovskites, named after the mineral CaTiO₃, have a generic chemical formula ABX₃ and a cubic structure. The A and B sites can accommodate inorganic cations of various valency and ionic radius. Alternatively, suitable organic species can replace cation A and create organic–inorganic hybrid materials (**Figure 1.5**).

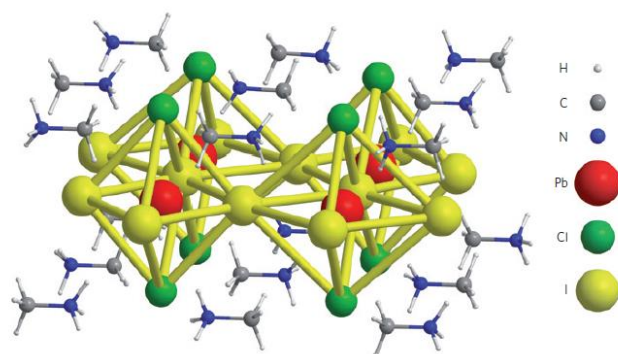


Figure 1.5 Crystal structure of the hybrid perovskite $\text{CH}_3\text{NH}_3\text{PbI}_{3-x}\text{Cl}_x$.²⁰

Recently, organic–inorganic hybrid perovskites (in particular $\text{CH}_3\text{NH}_3\text{PbX}_3$, where $X = \text{I}, \text{Cl}, \text{Br}$) have been intensively investigated as result of their high performance in converting solar light into electrical power, with power conversion efficiencies (PCE) exceeding 20 %.^{21–23} This result is even more impressive considering that the first perovskite solar cells were only reported in 2009, and displayed PCE values as low as 3.8 %.²⁴ These initial prototypes were based on the classical architecture of dye-sensitized solar cells, with the organic–inorganic compounds deposited on top of a mesoporous TiO_2 structure (**Figure 1.6 a**). More recent works demonstrated that a simpler geometry- a perovskite layer sandwiched between a compact thin film of TiO_2 and a hole-conducting organic compound (**Figure 1.6 b**)- is also able to convert light with efficiencies higher than 10 %, provided that a uniform and dense morphology is achieved in the deposited layer. However, the understanding of the mechanisms underlying such exceptional performance has not grown at the same pace.

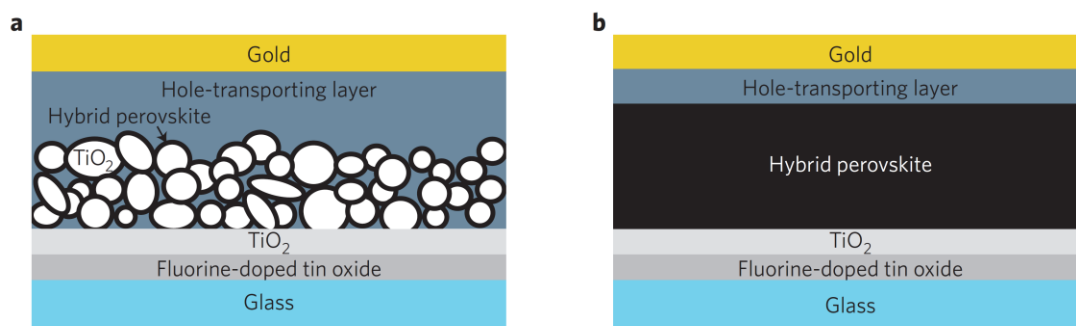


Figure 1.6 Architectures of perovskite solar cells- a) Hybrid perovskite solar cell on mesoporous TiO_2 , b) Planar hybrid perovskite solar cell.²⁰

Perovskite solar cells are the fastest-advancing solar technology to date, with the potential of achieving even higher efficiencies and very low production costs, perovskite solar cells have become commercially attractive.

Figure 1.7 depicts the brief history (evolution) of solar cell.

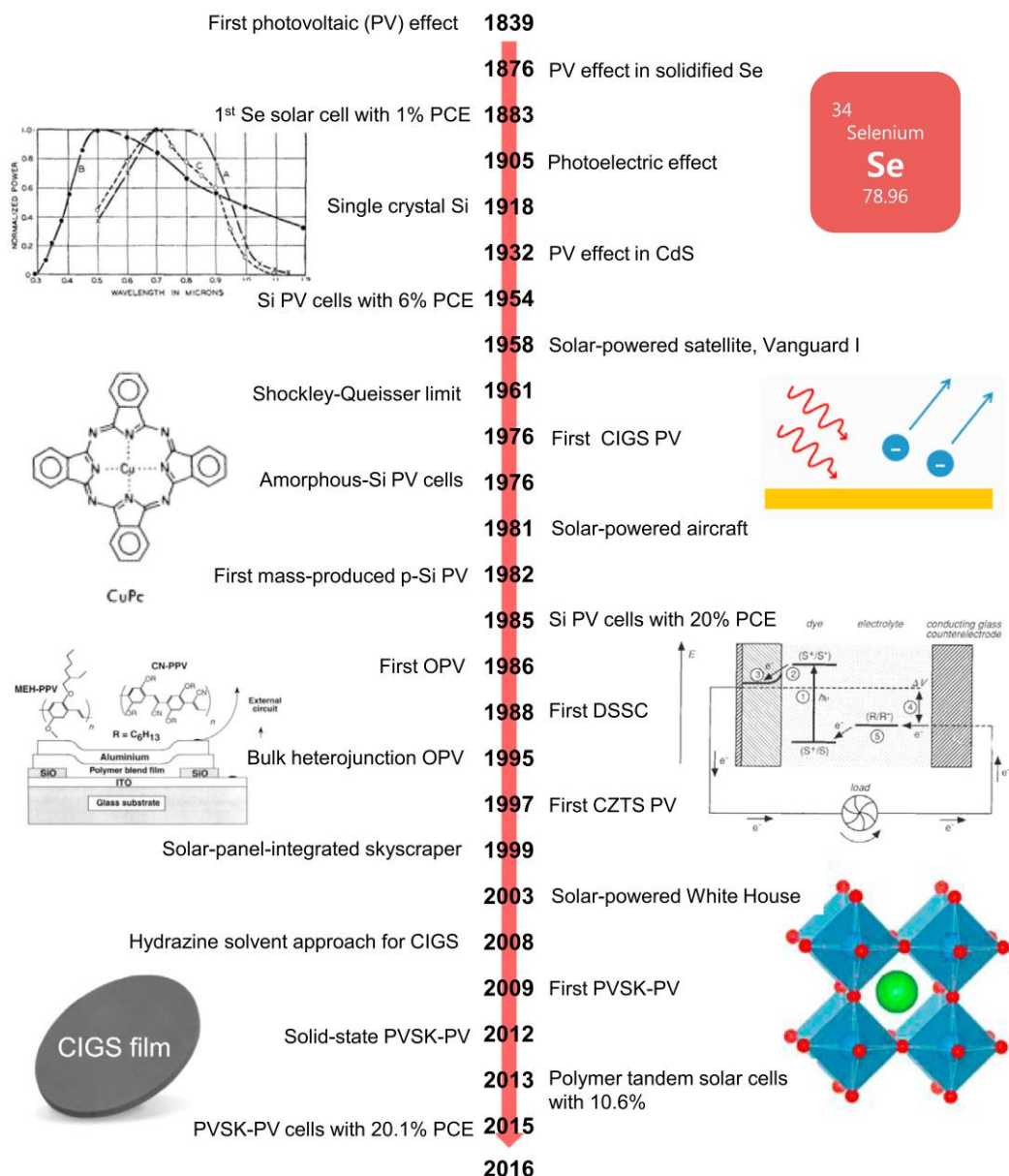


Figure 1.7 Brief history of solar cells²⁵

The present thesis mostly deals with the organic solar cells (OSC). Hence, in the section, we will focus mostly on materials and strategies utilized in the development of OSC.

1.3 Organic Solar Cells (Organic Photovoltaics)

1.3.1 Inorganic Photovoltaics vs. Organic Photovoltaics

Organic solar cells (OSC), utilising organic semiconductors have recently attracted extensive attention due to the possibility of processing organic semiconductors from solution, at low temperature and for large area devices with low cost. Moreover, organic semiconductors can be deposited on various substrates including flexible plastic substrates, which opens the way for their applications in products with lower cost, optical transparency, flexibility and light weights. The most useful feature of organic semiconductors is the structural versatility. Their properties can be tuned by slight change (incorporation of functionalities) in molecular design which in turn result in tuning the targeted device properties. These properties of organic semiconductor are hard to achieve for inorganic semiconductors. This superiority of organic semiconductors has led to the enormous growth in the field of organic electronics in particular in organic photovoltaics.

The electronic structure of organic semiconductors constitute alternation of single (σ -bonds) and double (one σ -bond and one π -bond) bonds to form a π -conjugated system. The π -electrons are much more mobile than the σ -electrons. In a conjugated system, π orbitals overlap mutually along the conjugation path, which causes the wave functions to delocalize over the conjugated backbone. The π -bands are either empty (referred as the Lowest Unoccupied Molecular Orbital - LUMO) or filled with electrons (referred as the Highest Occupied Molecular Orbital - HOMO). The energy difference between the HOMO and LUMO determines the band-gap of these materials. This π -electron system has all the essential electronic features of organic materials, such as, light absorption and emission, charge generation and transport.

Some of the limitations of organic semiconductors include-

- i) the charge carrier mobility of organic materials²⁶ is significantly lower than the mobility of inorganic materials since the intermolecular charge transport in organic materials is much difficult and normally limited by charge hopping from one molecule to the other.

ii) organic materials after photoexcitation, form tightly bound excitons (electron–hole pairs) with short lifetime due to their low dielectric constant.²⁷ The exciton binding energy is much higher than the kinetic energy of electrons and holes at room temperature limiting the dissociation of the excitons into free charges.

Nonetheless, there are several advantages of organic semiconductors over inorganic semiconductors which include-

- i) high absorption coefficient,²⁸ which require a very thin layer of the material to fully absorb the incident photons, for their application in photovoltaics and photodetectors.
- ii) high photoluminescence quantum efficiency (less rate of nonradiative decay) for light emitting diode applications.
- iii) the small band-gap allows easy charge injection of electrons into LUMO and/or holes into HOMO
- iv) enables effective charge transport of both negative and positive charges as a result of strong molecular polarity. Thus, the materials exhibit p-type and n-type charge transport and show great promise for ambipolar field effect transistors.

1.3.2 Small molecular semiconductors vs. Polymeric semiconductors

Organic semiconductors are broadly classified into two categories, viz.-1) small molecular semiconductors and, 2) polymeric semiconductors.

Small molecular semiconductors have well-defined molecular structure, definite molecular weight, and high purity without batch-to-batch variations. Small molecules also exhibit a greater tendency to form ordered domains, affording higher charge carrier mobilities.

Polymer semiconductors possess following superior properties than small molecular semiconductors.

1. Thin films of polymeric materials are generally very smooth and uniform which enables a great control over the structural and morphological characteristics of film, on large scale. Printing requires good control of the solution rheological properties. These properties can be effectively tuned for polymer-based solutions.
2. Polymer crystalline domains are typically much smaller than the length scale of several optoelectronic devices resulting in isotropic transport characteristics. This allows low

- device-to-device performance variability, which is important requirement for thin film transistor (TFT) integration into circuits.
3. Fabrication of multilayers from solution deposition processes requires that each stacked layer is inert to the solvents and processing temperatures, that it is subsequently exposed to, during deposition of the next layer. The reduced solubility parameter window of polymers, and their large bulk viscosity, typically increases the options to find orthogonal solvents for solution deposition on top of polymer layers, thus expanding the choice of materials that can be used in the devices.
 4. Polymers do not vaporize before decomposition and thus have negligible vapor pressure. Hence, they are not susceptible to interlayer diffusion during the typical device-fabrication thermal cycles. They exhibit robust mechanical properties, due to which the nanometer-thick semiconductor films are compatible with roll-to-roll fabrication on flexible substrates.

Organic solar cells (OSCs) are generally referred as polymer solar cells (PSCs) due to enhanced use of polymeric materials as an active layer material in solar cell device.

1.3.3 Organic solar cells device structure and working principle

1.3.3.1 Organic solar cell device structure-

Photoactive layer (donor-acceptor blend layer) is sandwiched between an indium tin oxide (ITO), a positive electrode (anode) and a metal negative electrode (cathode). Organic and/or inorganic interlayers are also used to improve hole collection to the anode and electron collection to the cathode. Poly(3,4-ethylenedioxythiophene) poly(styrenesulfonate) (PEDOT:PSS) is a buffer layer, which improves the electrical contact between an active layer and an indium tin oxide (ITO) electrode and therefore makes hole extraction easier. Lithium fluoride (LiF) layer facilitates the electron collecting to the cathode. **Figure 1.8 a** depicts the typical device structure of organic solar cell (OSC).

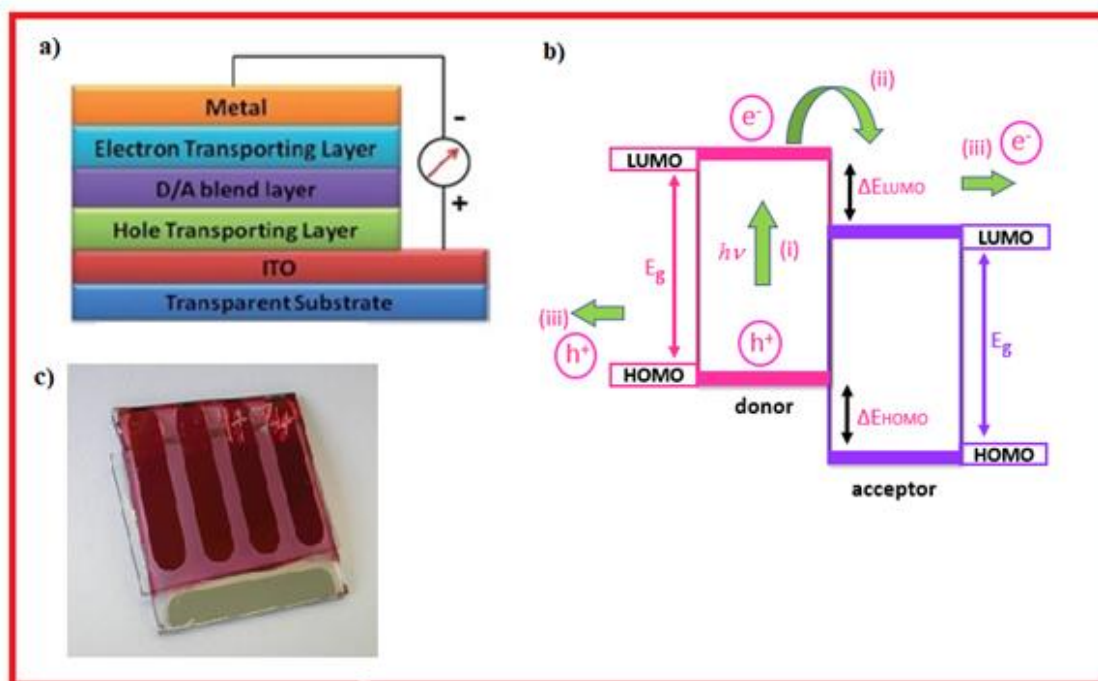


Figure 1.8 a) Schematic diagram of OSC device, b) energy level diagram for a donor-acceptor heterojunction in OSC device and c) picture of typical OSC device on lab scale.

In a typical solar cell, a low band gap conjugated polymer donor and a soluble molecular acceptor are used. Typical acceptors are soluble fullerene derivatives such as [6,6]-phenyl-C₆₁-butyric acid methyl ester (PC₆₁BM). As a component in the active layer, a conjugated polymer donor serves as the main absorber to solar photon flux, as well as the hole transporting phase. Therefore, wide optical absorption to match the solar spectrum and large hole (bulk) mobility are basic requirements to design an ideal polymer donor.

Fullerene derivatives have been demonstrated as the most effective acceptor materials due to several advantages listed below-

1. Fullerenes (C₆₀) can stabilize negative charges very well because of their low-lying triply degenerate LUMO energy levels.²⁹
2. Photoinduced electron transfer from a donor polymer to a fullerene in a BHJ blend film occurs in femtoseconds. It is much faster than the other competing relaxation processes such as photoluminescence (~1 nanosecond).

3. Fullerene derivatives usually exhibit high electron mobility. For example, C₆₀ showed a mobility of about 1.0 cm² V⁻¹ s⁻¹ in an organic field effect transistor.³⁰

Some of the drawbacks of fullerene which obviously can be overcome are-

1. Fullerene tend to crystallise and shows poor solubility in organic solvents which hamper their application in solution processable devices. After functionalization of C₆₀ and C₇₀ with solubilising groups, [6,6]-phenyl-C₆₁ (or C₇₁)-butyric acid methyl esters (PC₆₁BM_s/ PC₇₁BM_s) have been extensively used as acceptor materials in solar cells.
2. Fullerenes absorb less in the visible region due to their structural symmetry which forbids low-energy transitions. The efficiency of BHJ devices can be improved by replacing acceptor PC₆₀BM with its higher fullerene analogue PC₇₁BM³¹ and indene fullerene bisadduct (ICBA)³² which has lower symmetry and higher absorption in visible region.

1.3.3.2 Working principle-

The π - conjugated materials (organic semiconductors) used in OSC, possess small energy gap between highest occupied molecular orbital (HOMO) and the lowest unoccupied molecular orbital (LUMO) as a result of alternate single bond and double bond character in the material. Thus, absorption of light by these materials causes electrons in the HOMO level to photo-excite to LUMO level, leaving behind the hole in HOMO. Thus, photo-excitation of organic semiconductors produces bound electron-hole pairs, also known as excitons. These excitons have a large binding energy (typically 0.2–1.0 eV) that drives the electron and hole to recombine after photoexcitation.³³ The pioneering work by Tang *et al* in 1986,³⁴ provided the solution to this problem which involves combining two organic semiconductors with slightly offset HOMO and LUMO energy levels, such that the photoexcited electron in the first material (donor) is transferred to the second material (acceptor), allowing the charges to be separated at the junction between these two materials.

The general operating mechanism of D–A type organic solar cells is shown in **Figure 1.9**.

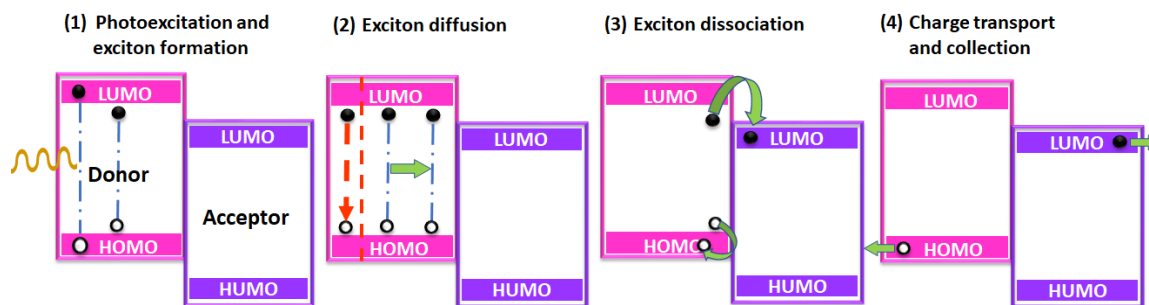


Figure 1.9 Operating mechanism of D–A type organic/ polymer solar cells

The process of conversion of light into electricity by an OSC is as follows:

1. Absorption of a photon leading to the formation of exciton (coulombically bound electron-hole pair)
2. Exciton diffusion to the donor-acceptor interface
3. Exciton dissociation into free charge carriers at the donor-acceptor interface
4. Transport of fully dissociated charge carriers to the respective electrodes with the aid of internal electric field; consequently, generating photocurrent and photovoltage.

1.3.3.3 Organic Solar Cell Architectures

Figure 1.10 depicts various architectures of organic solar cell device

1. Single layer devices-

Active layer is sandwiched between two dissimilar electrodes with different work functions. In this case, the built-in potential is derived either from the difference in work function of the electrodes or from a Schottky-type potential barrier at one of the metal/organic contacts. The major drawback for the single layer device is that the photovoltaic properties are strongly dependent on the nature of the electrodes or the interface contact between the electrode and organic layer, which leads to a very low fill factor and low power conversion efficiency.

2. Double layer (bilayer) devices-

In bilayer heterojunction architecture, the donor and acceptor materials are deposited successively layer by layer on the ITO coated glass substrate, then the metal anode is finally deposited on top of the acceptor layer. The introduction of the donor–acceptor heterojunction interface in the active layer facilitates the efficient charge separation into electrons and holes after excitation by incident light, and then the free

electrons and holes transfer to the metal anodes and ITO cathodes with the help of an internal electrical field, and finally form output voltage. However, the performance of OPV based on such bilayer device structure is limited by the short exciton diffusion length in organic materials (typically 10-20 nm).²⁸ Since exciton dissociation process is confined to the D/A interfacial zone, only excitons produced at a distance shorter than their diffusion length have a good probability to reach the interfacial zone and generate free charge carriers. So, the exciton diffusion length limits the maximum thickness of the active layer consequently lowering the absorption of light resulting in reduced power conversion efficiency.

3. Bulk-heterojunction devices

Bulk-heterojunction device (BHJ) is the most successful architecture for organic photovoltaic cells. BHJ architecture uses a blend of donor and acceptor materials forming bi-continuous and interpenetrating network in a bulk volume. In donor-acceptor BHJ blend, an interpenetrating network with nanoscale phase separation can be formed throughout the bulk which enables a greater degree of interfacial contact between the donor and the acceptor. The enhanced interfacial contact ensures efficient exciton dissociation leading to the generation of free electrons and holes. Bi-continuous and interpenetrating network connecting to the two electrodes allows the dissociated free electrons and holes to efficiently move to the respective electrodes (efficient charge transport) resulting in efficient charge generation.

4. Tandem Devices

In the tandem architecture two or even four solar cells with different absorption characteristics are linked together in series or in parallel. Tandem structure resolves two limiting factors existing intrinsically among organic semiconductors viz.-i) poor charge carrier mobility and, ii) narrow absorption range.

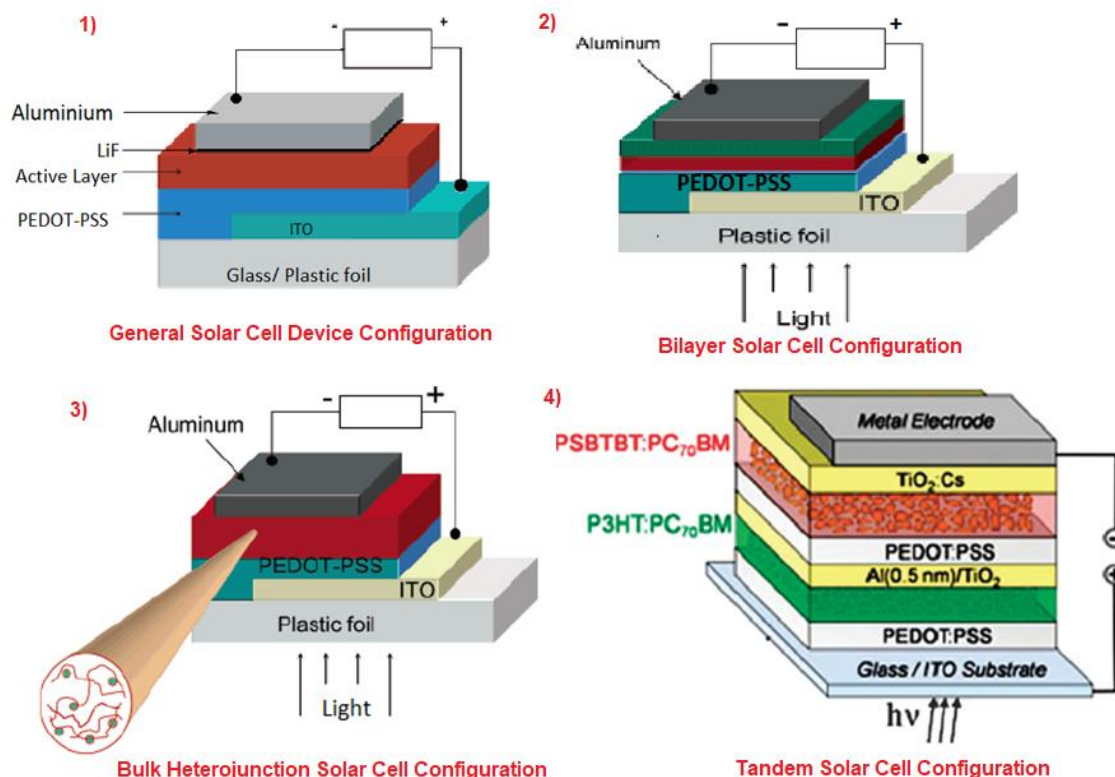


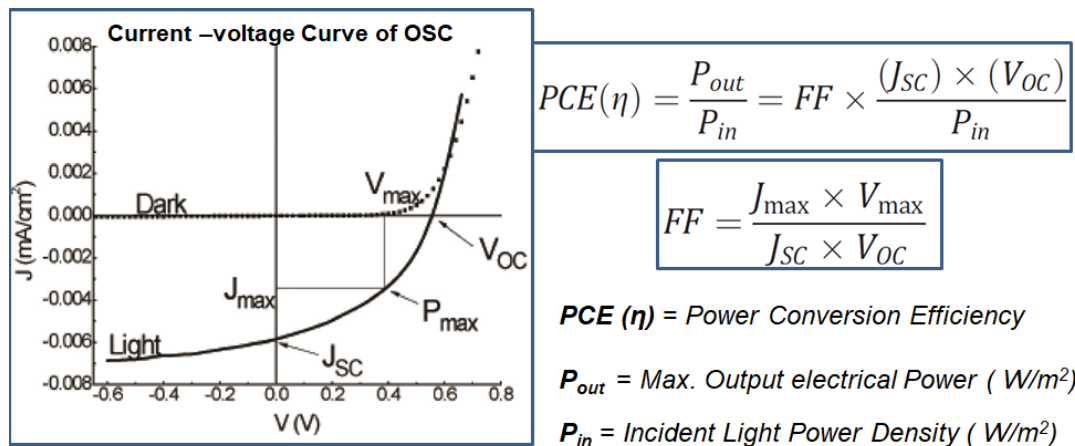
Figure 1.10 Various architectures of organic solar cell device (adapted from reference³⁵)

1.3.3.4 Characterisation of solar cells

Figure 1.11 depicts J - V curve and various device parameters for the characterisation of solar cells. From the current density-voltage curve, it is possible to derive the ability of the solar cells to convert photons to electrons under irradiation with certain wavelengths and intensities. The important performance parameters such as power conversion efficiency (PCE or η) and the open circuit voltage (V_{oc}) can be extracted from the solar cell J - V curves measured under the simulated AM1.5 solar light. Thus, the overall PCE is calculated according to the following equations:

$$PCE(\eta) = \frac{P_{out}}{P_{in}} = FF \times \frac{J_{sc}}{P_{in}} \times (V_{oc})$$

$$FF = \frac{J_{max} \times V_{max}}{J_{sc} \times V_{oc}}$$



V_{OC} = Open Circuit Voltage (V)

J_{SC} = Short Circuit Current Density (mA/cm^2)

FF = Fill Factor

J_{max} and V_{max} = Current Density and Voltage at which device's electric power output is maximum

Figure 1.11 J - V curve and various device parameters for the characterisation of solar cells.

Where P_{out} is the maximum output electrical power (in W/m^2) of the device under illumination, P_{in} (in W/m^2) is the light intensity incident on the device and V_{oc} is the open circuit voltage. Other important parameters which can be extracted from the photocurrent-photovoltage plots are the short circuit current density (J_{sc}) and the fill factor (FF). J_{sc} is the current extracted from the device under illumination when no bias is applied. The parameter FF is defined as the voltage (V_{max}) and current (J_{max}) at the maximum power point in the J - V curve, respectively. Thus, an ideal device would have a rectangular shaped J - V curve and therefore a fill factor (FF) value approaching unity.

1.3.3.5 Low band-gap materials in organic solar cells

The overall efficiency is an important parameter for evaluating the performance of the device. It is important to note that besides experimentally characterizing the performance of the organic solar cells, a key parameter, the V_{oc} , can be estimated from electrochemical measurements and given by the difference between the donor HOMO level and the acceptor LUMO level. It is now well-accepted that for a given acceptor V_{oc} correlates linearly with the donor HOMO level and vice versa. To achieve an organic BHJ-solar cell with large power conversion efficiency and stability, the materials have to be designed carefully to fulfill key parameters such as HOMO/LUMO energy levels, solar

light absorption, and blend morphology/ microstructure to maximize light absorption, charge separation, and charge transport/collection.

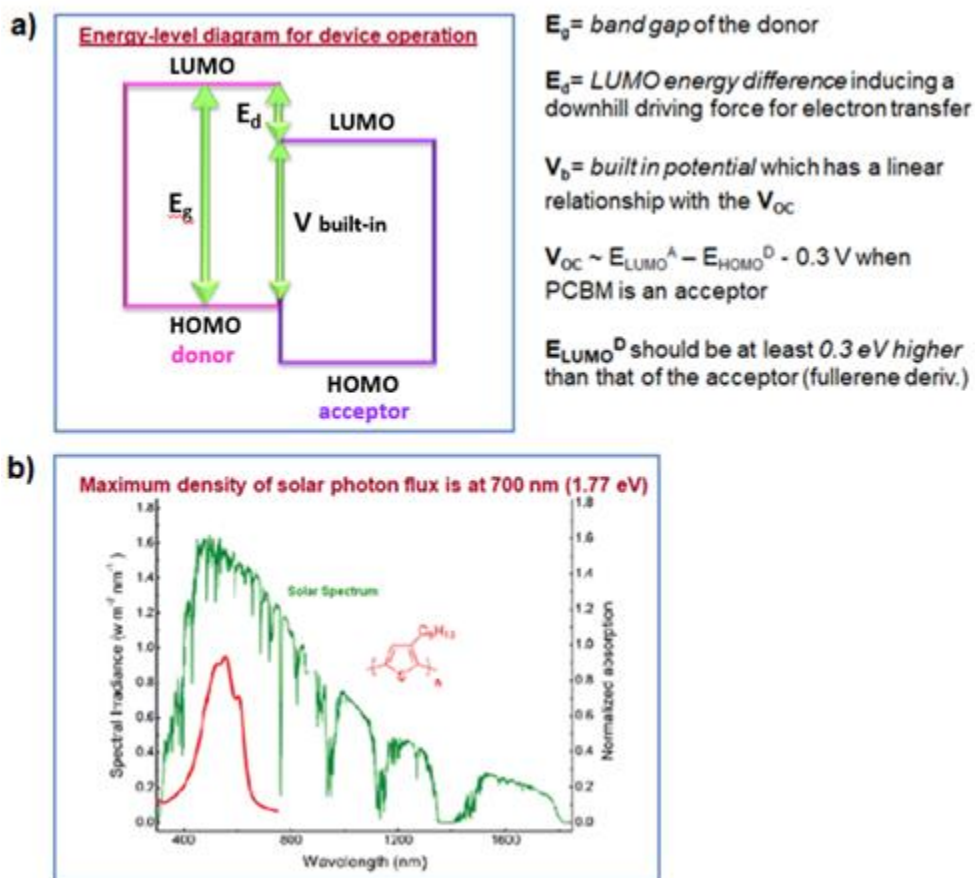


Figure 1.12 a) Energy level diagram for device operation b) Solar photon flux

A proper driving force for electron transfer should be higher than the coulombic binding energy of the exciton and can be compensated for, by utilizing the energy offset between the LUMO levels of the donor and acceptor. It is reported that the LUMO level of the donor should be at least 0.3 eV higher than that of the acceptor.³⁶ As discussed above, V_{oc} is correlated with the difference between the HOMO energy level of the donor and the LUMO energy level of the acceptor. Narrowing the band-gap of the donor polymer while trying to maintain the driving force for charge separation (**Figure 1.12a**) leads to reduction of the theoretically achievable maximum value of V_{oc} . Therefore, it is crucial to engineer the energy levels of the donor conjugated polymers to achieve a balance between pursuing the narrow band-gap of the donor and matching HOMO/LUMO energy levels to that of

acceptor with minimizing a loss in V_{oc} . All of these processes and parameters must be synergistically optimized to maximize the efficiency of polymer/fullerene BHJ solar cell.

The solar photon flux (**Figure 1.12b**) distributes over a wavelength range from 280 nm to 4000 nm and its maximum density is located at about 700 nm. In order to effectively harvest the solar energy, optical absorption of the active layer in polymer BHJ solar cells must be optimally matched with the region of maximum photon flux. Thus, it is essential to develop low/narrow band-gap polymers with high absorption coefficients in the red to near-infrared regions. For effective absorption of light, the overall extinction coefficients of the polymers should be high and should not be sacrificed as the optical band gaps become smaller. The low band gap conjugated polymers have been intensely studied for more than two decades to realize the ultimate goal of developing organic semiconducting materials.^{37–47}

1.3.3.6 Strategies for band-gap engineering of conjugated materials

Figure 1.13 depicts various strategies for band-gap engineering of conjugated polymers.

1. Increasing quinoid form of aromatic moieties in the backbone

Compared to the aromatic form, the quinoid form is energetically less stable and hence has a smaller band gap because adopting a quinoid structure requires destruction of the aromaticity and a loss in the stabilization energy. A reduction in aromaticity of the aromatic units in the conjugated main chain allows a greater tendency to adopt the quinoid form through π -electron delocalization.

The ratio of the aromatic to quinoid population in a polyaromatic conjugated system can be correlated and represented by a geometrical parameter, i.e., bond length alternation (BLA). The more the aromatic form prevails in the ground state, the larger the BLA value obtained. Overall, the HOMO-LUMO band gap decreases linearly as a function of the increasing quinoid character with concomitant decrease in BLA value.

The perfect example to increase the quinoid character of polythiophene is given by constructing the polymer polyisothianaphthene (PITN).⁴⁸ The main chain of PITN tends to favor the quinoid form by selectively maintaining the benzene aromaticity. PITN the first conjugated polymer with a narrow band gap energy of 1 eV.

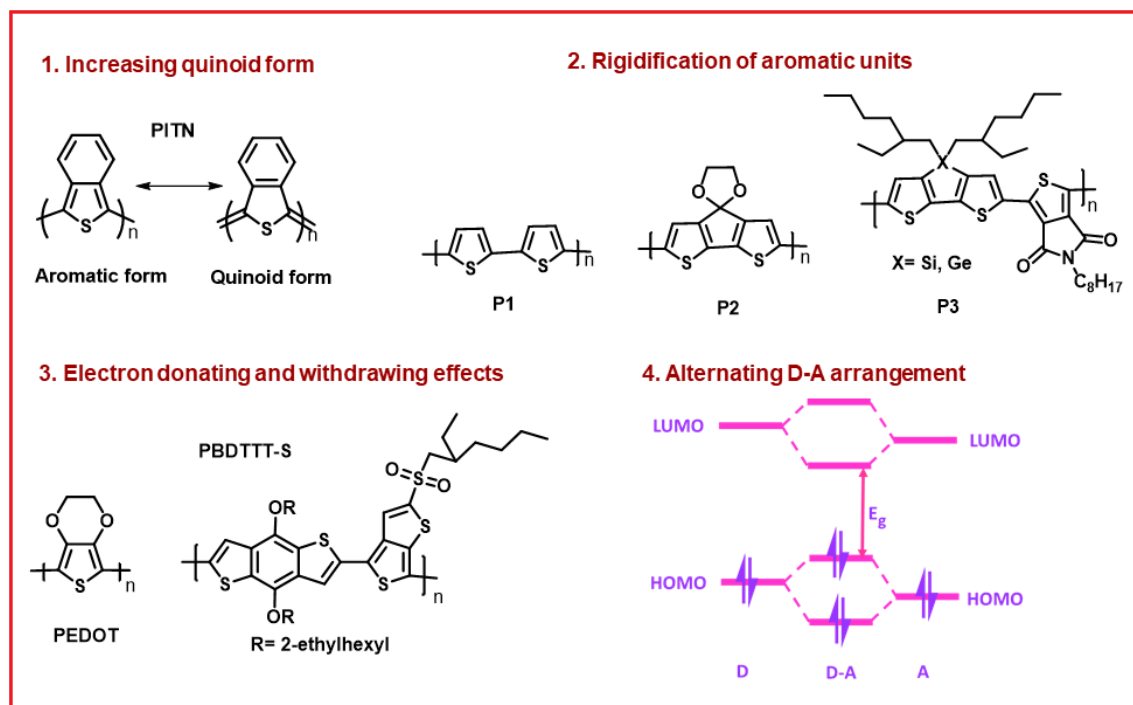


Figure 1.13 Various strategies for band-gap engineering

2. Chemical rigidification:

Planar arrangement of adjacent aromatic units results in improved p-orbital interactions with extended conjugation and thus facilitates the electron delocalization. This leads to a decrease in the BLA and reduction of the band-gap. Thus, to minimize the rotational disorder due to steric hindrance it is important to tie the two adjacent aromatic units through covalent chemical bonding and making the structure rigid. For example, bithiophene polymer was converted into a rigid polymer P1, by tying the two thiophene units with the sp^3 carbon bridging with the ketal group.⁴⁹ The band-gap is lowered to 1.2 eV.

The effect of bridging atom was also studied. It was demonstrated that adjacent rings bridged by Si or Ge generate more ordered structures of polymer chains than their carbon analogs, due to the longer covalent bond and orbital interactions of Si or Ge with the two aromatic rings.^{50,51}

3. Electron donating and electron withdrawing effects:

The incorporation of electron-donating or electron-withdrawing substituents directly onto the aromatic unit in the main chain represents another effective way of

perturbing the molecular orbitals. In general, electron-donating groups raise the HOMO energy, while electron-withdrawing groups lower the LUMO energy, resulting in a decreased band gap. For example, in case of poly(ethylenedioxy)thiophene (PEDOT), attachment of electron-donating alkoxy groups to the parent polythiophenes leads to the reduction of the band-gap to 1.5 eV, which is about 0.5 eV lower than that of polythiophene.⁵²

Hou et al. incorporated a strong electron-withdrawing sulfonyl group on the thienothiophene (TT) unit of PBDTTT polymer to obtain a new copolymer PBDTTT-S which shows a narrow bandgap of 1.65 eV, lower HOMO energy levels at -5.12 eV and high V_{oc} of 0.76 V.⁵³ The polymer demonstrated a PCE of 6.22% with fullerene acceptor.

4. Alternating D-A arrangement:

The most successful strategy in designing low band gap conjugated polymers is to alternate a conjugated electron rich donor (D) unit and a conjugated electron-deficient acceptor (A) unit in the same polymer backbone. Through the introduction of push-pull driving forces to facilitate electron delocalization and the formation of quinoid mesomeric structures over the conjugated main chain, the BLA can be significantly reduced.

The principle of band gap and energy level manipulation by ICT interaction in push-pull conjugated polymers can be easily understood by molecular orbital theory. As depicted in **Figure 1.13**, the HOMO of the donor segment will interact with that of the acceptor segment to generate two new occupied molecular orbitals after covalent bond connection of two different moieties, one of them is higher and the other one is lower than the two initial HOMOs before molecular orbital hybridization. Two new unoccupied molecular orbitals would also be generated in a similar manner after molecular orbital hybridization, where one is lower and the other is higher than the two initial LUMOs of the two moieties. Hence the overall effect of this redistribution of frontier molecular orbitals is the formation of a higher-positioned HOMO and a lower-positioned LUMO in the whole conjugated main chain, and this accordingly leads to the narrowing of the band gap.

1.3.4 Approaches for the design of high-performance conjugated polymers

The following sections describe various approaches for the design of high-performance conjugated polymers for organic/ polymer solar cells (OSCs/PSCs) applications.

1.3.4.1 Low band gap donor-acceptor copolymers

As described above, low band gap donor-acceptor copolymers are widely studied materials for photovoltaic applications. This topic is thoroughly covered in the excellent reviews by various authors.⁵⁴⁻⁶¹

Several other novel aspects such as- 1) two-dimensional (2-D) conjugation, 2) design of terpolymeric systems, 3) introduction of non-covalent interactions and 4) incorporation of flexible linker (aliphatic spacer) are important in the design of highly efficient polymeric systems for their practical applications in organic solar cells. These aspects are described in the following sections.

1.3.4.2 Two-dimensional (2-D) conjugated systems

The variety of LBG polymers synthesised in the past decade suffer from a major drawback- i.e. their capacity to absorb solar radiations. Most of the LBG polymers absorb near-IR to IR-region of solar spectrum, lacking the absorption in visible region. This has seriously limited short circuit current density (J_{sc}) achievable from these materials which has resulted in lower photovoltaic performance in many cases. So, there is a need to develop conjugated polymers having strong and broad absorption through-out the solar spectrum to maximise photon harvesting which leads to improved J_{sc} and consequent enhancement in power conversion efficiency.

Most of conjugated polymers are designed with a conventional linear structure having π -conjugation along the backbone. However, the extension of the conjugation in the lateral direction to form two-dimensionally conjugated systems or side chain conjugated system are expected to have a considerable impact on electronic properties of these polymers. The charge carrier mobility of conjugated system constitutes an important factor for their applications in organic electronic devices, such as OSCs, OLEDs and OFETs. Both intramolecular and intermolecular charge transport of conjugated polymers are found to be crucial to achieve high charge carrier mobilities. Among these,

intermolecular charge transport in conjugated polymers is known to occur by hopping mechanism wherein π -electrons tend to hop between the overlapping π -electron orbits of adjacent conjugated chain. Thus, in order to improve intermolecular charge transport, it is highly desirable to enhance the conjugation of backbone to increase the probability of formation of effective interchain π - π overlaps. With additional lateral conjugation, 2-D conjugated polymeric systems are known to fulfill this criterion. **Figure 1.14** depicts the structures of reported 2-D conjugated polymers which have shown significant performance in OSC devices. The various solar cell device parameters for 2-D-conjugated polymers are summarized in **Table 1.1**.

Li et al. first utilised the strategy of attaching a conjugated side group to the main polymeric chain to improve the degree of electronic interaction in the solid state. They synthesised various polythiophene derivatives with different conjugated side chains, which show a broad absorption in the visible region and a high field effect mobility.^{62,63} In order to further improve the visible absorption and intensify the absorbance, Li *et al* synthesized polythiophene derivatives with conjugated bi(thienylenevinylene) side chains (biTV-PT) which display a strong and broad absorption plateau in the visible region from 350 nm to 650 nm. In addition, the HOMO energy level of the PTs with bi(thienylenevinylene) conjugated side chains is dropped by about 0.2 eV in comparison with that of P3HT without the conjugated side chains. The polymer exhibits maximum power conversion efficiency of 3.18 %.⁶⁴ Further attempts have been reported to improve intermolecular electronic interaction by linking polymeric chains either by conjugated bridges⁶⁵ or by using tetrafunctional branching agent.⁶⁶

Wei et al. synthesised a series of regioregular 3-hexylthiophene-based copolymers incorporating octylphenanthrenyl-imidazole moiety (P₃HT-co-T_{ph-Im}) directly conjugated with the main thiophene chain.⁶⁷ Electron withdrawing nature of this particular moiety facilitates intramolecular charge transfer from donor thiophene main chain to the conjugated acceptor side chain. High short-circuit current density of 13.7 mA/cm² and power conversion efficiency of 3.45 % was observed for the copolymer with 90 mol % incorporation of octylphenanthrenyl-imidazole moieties.

Recently, benzo[1,2-b:4,5-b']dithiophene (BDT) containing D-A low band gap polymers are extensively studied.^{68,69} BDT unit has large planer structure which promotes

cofacial π - π stacking which in turn result into high charge carrier mobility in the copolymers involving BDT unit as donor component. Two alkyl⁷⁰ or alkoxy side chain were incorporated into 4 and 8 positions of the BDT ring to improve solubility of BDT containing polymers.^{68,71} Based on two-dimensional conjugation concept, Huo et. al. designed a new BDT monomer containing two 2-alkylthienyl conjugated side chains, (BDT-T) and copolymerised with various other acceptor units to form highly efficient copolymers, namely- PBDTTBT, PBDTTTZ and PBDTDTQ_x-T. The research group further demonstrated that the copolymers based on 2-alkylthienyl substituted BDT units exhibit better thermal stabilities, slightly red shifted absorption spectra, higher hole mobilities and significantly improved photovoltaic properties, in comparison with their corresponding alkoxy substituted analogues.⁷²

Yang et al. synthesised 2-D-conjugated polymer PBDTDPP-T containing alkylthienyl substituted BDT as donor unit and DPP as acceptor unit. In this polymer, HOMO has been lowered to -5.30 eV as compared to the analogous polymer with alkoxy substitution on BDT (-5.16 eV) and exhibited superior photovoltaic performance (η = 6.6 %).⁷³ Changing the substituent on BDT, from alkyl thienyl to *p*-alkylphenyl in a polymer PBDTDTBT-P resulted in lowering of HOMO and power conversion efficiency (PCE) of 8.07 % was achieved for this polymer by Hou et al. The position of alkoxy chain on side chain also affected molecular energy levels and thus photovoltaic performance. For example, Hou et al. used *meta*-alkoxyl-phenyl substituted BDT in a polymer PBT-OP with much reduced HOMO (-5.17 eV) and enhanced PCE of 7.5 %.⁷⁴ Molecular energy levels of D-A conjugated polymers can also be tuned by introduction of fluorine atom into the structure. The V_{oc} of the polymer solar cell based on trifluorinated polymer, PBT-3F was 0.22V higher than the nonfluorinated analogue and exhibited efficiency of 8.6 %.⁷⁵ More linear backbone structure is found to be helpful in improving photovoltaic properties of the polymer as observed in the polymer PDT-S-T (η = 7.79%).⁷⁶ Recently, Yang et al. synthesized alkylthienyl substituted asymmetric 2D polymer, PBDT_{Th}DT_{ff}BT with PCE=9.2 % taking advantage of different types of side chains which simultaneously improved J_{sc} and V_{oc} .⁷⁷

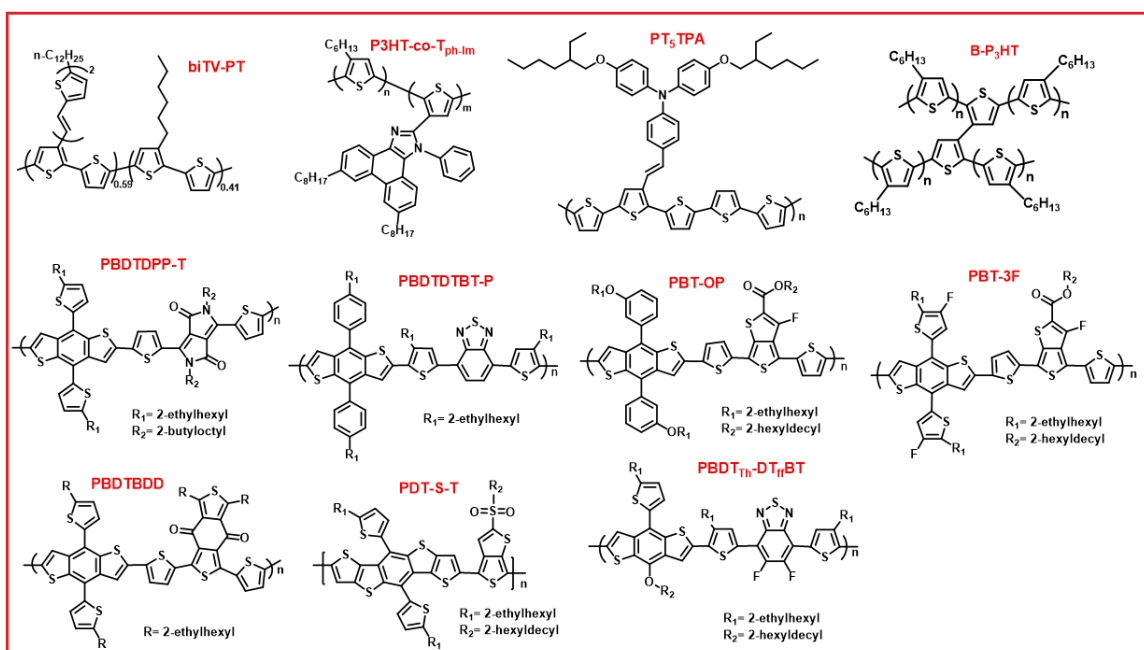


Figure 1.14 Structures of representative 2-D conjugated polymers

Table 1.1 Photovoltaic properties of reported 2-D-conjugated polymers

Polymer	Acceptor	HOMO (eV)	LUMO (eV)	E_g (eV)	J_{sc} (mA/cm ²)	V_{oc} (V)	FF	η (%)	Ref
biTV-PT	PC ₆₁ BM	-4.93	-2.96	1.97	10.3	0.72	43	3.18	64
P ₃ HT-co-T _{ph} -Im	PC ₆₁ BM	-	-	1.80	13.7	0.68	37	3.45	67
PT ₅ TPA	PC ₆₁ BM	-5.15	-3.10	2.05	-	0.55	47	2.01	63
B-P ₃ HT	IC ₆₀ BA	-5.10	-3.08	2.02	6.55	0.94	58	3.60	66
PBDDTDP-T	PC ₇₁ BM	-5.30	-3.86	1.44	14.0	0.73	65	6.6	73
PBDDTDTBT-P	PC ₇₁ BM	-5.35	-3.65	1.70	12.94	0.88	70.9	8.07	78
PBT-OP	PC ₇₁ BM	-5.17	-3.47	1.70	13.4	0.78	71.8	7.5	74
PBT-3F	PC ₇₁ BM	-5.20	-3.56	1.64	15.2	0.78	72.4	8.6	75
PBDDTBD	PC ₆₁ BM	-	-	-	10.68	0.86	72.3	6.67	79
PDT-S-T	PC ₇₁ BM	-5.21	-1.08	1.59	16.63	0.73	64.1	7.79	76
PBDDT _{1n} DT _n BT	PC ₇₁ BM	-5.37	-3.47	1.76	15.66	0.87	70.4	9.22	77

IC₆₀BA- Indene-C₆₀ bisadduct

Thus, the available literature reports emphasised that the polymers with conjugated side-groups exhibit a higher hole-mobility and a broader absorption spectrum, due to an improved degree of electronic interaction between polymer chains in the solid state

provided by the two-dimensional conjugated system. Consequently, they exhibited enhanced photovoltaic performance.

1.3.4.3 Terpolymer approach

Although donor-acceptor polymers (or low band-gap polymers) have been successfully employed as a donor material in the bulk heterojunction solar cells, their power conversion efficiency is mainly limited by smaller current densities (J_{sc} values). This is because, most of the D-A polymers absorb strongly in near IR region but they exhibit very low absorption in the visible region. In the present scenario, designing and synthesizing novel structures of D and A units for new, more efficient D-A copolymers requires tedious and lengthy synthetic procedures along with the time required for their optimisation and development for photovoltaic applications. Thus, development of new D-A polymers has now become limited, and non-economic.⁸⁰ In this regards, design of terpolymers based on the knowledge of existing D-A polymers is considered as important approach in the development of new materials with improved photovoltaic performance in polymer solar cells.

In this regard, terpolymers, which consist of three different units in the polymer backbone, are promising candidates. The incorporation of a third component (donor D or acceptor A) into D-A copolymers affords either D-A-A or D-D-A type terpolymeric system.⁸¹⁻⁸⁴ With added new D or A unit, there exists a possibility of tuning solar absorption, solubility, HOMO-LUMO energy levels and π - π stacking of terpolymers.⁸³⁻⁸⁸ In general, terpolymers show a broader absorption range compared to their corresponding D-A copolymers. The extended light absorption favours more photon harvesting, resulting in more exciton generation which mainly contribute to high photocurrent.^{85,89} Interestingly, side chains on the new D or A unit, apart from enhancing solubility, also play important role in manipulating π - π stacking and thus the molecular packing.^{87,88,90} Furthermore, in random terpolymers, the ratio of monomers can be carefully optimised to get large current densities⁹¹ and desired crystallinity with superior performance in PSCs.⁹² Therefore, the design of terpolymers based on knowledge of existing promising D-A copolymers, is found to be attractive strategy for tailoring polymers with superior opto-electronic properties by proper selection of the third component.

Figure 1.15 summarizes the structures and **Table 1.2** summarizes the various solar cell device parameters for some representative D-D-A type terpolymers.

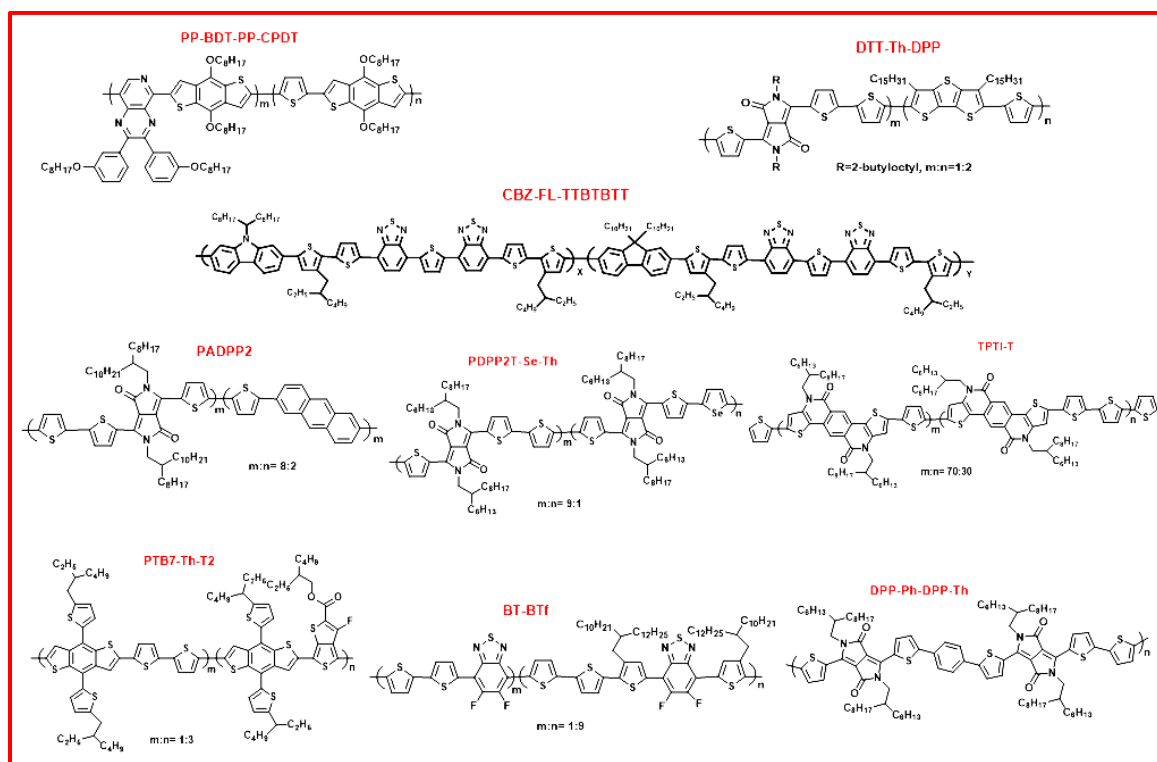


Figure 1.15 Structures of representative D-D-A type terpolymers

Table 1.2 Photovoltaic properties of representative D-D-A type terpolymers

Polymer	Acceptor	HOMO (eV)	LUMO (eV)	E_g (eV)	J_{sc} (mA/cm ²)	V_{oc} (V)	FF	η (%)	Ref
PP-BDT-PP-CPDT	PC ₇₀ BM	-5.20	-3.28	1.60	6.41	0.71	52	2.35	93
DTT-Th-DPP	PC ₇₁ BM	-5.14	-3.77	1.37	12.76	0.58	67	5.02	94
CBZ-FL-TTBTBTT	PC ₇₀ BM	-5.56	-3.89	1.65	13.5	0.79	63	6.70	95
PADPP2	PC ₇₁ BM	-5.28	-3.29	1.36	15.50	0.61	66	6.24	96
PDPP2T-Se-Th	PC ₆₀ BM	-5.22	-3.53	1.33	16.22	0.67	66	7.20	92
TPTI-T	PC ₇₁ BM	-5.44	-2.79	1.85	18.3	0.83	71	9.91	97
PTB7-Th-T2	PC ₇₁ BM	-5.28	-3.67	1.61	15.40	0.79	67	8.19	98
BT-BTf	PC ₇₁ BM	-5.42	-3.80	1.62	18.92	0.74	73	10.31	99
DPP-Ph-DPP-Th	PC ₇₀ BM	-5.16	-3.73	1.43	15.9	0.75	67	8.00	100

Figure 1.16 summarizes the structures and **Table 1.3** summarizes the various solar cell device parameters for some representative D-D-A type terpolymers.

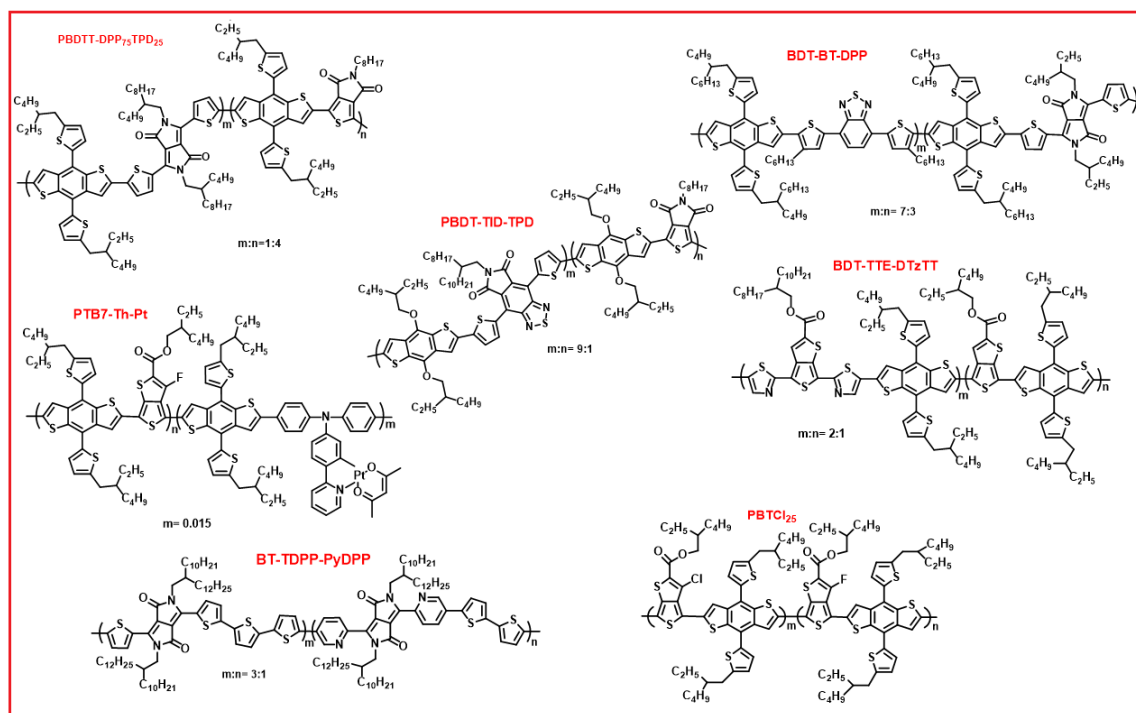


Figure 1.16 Structures of representative D-A-A type terpolymers

Table 1.3 Photovoltaic properties of representative D-A-A terpolymers

Polymer	Acceptor	HOMO (eV)	LUMO (eV)	E _g (eV)	J _{sc} (mA/cm ²)	V _{oc} (V)	FF	η (%)	Ref
PBDTT-DPP-TPD	PC ₇₁ BM	-5.35	-3.51	1.40	13.99	0.74	54	5.61	101
PBDT-TID-TPD	PC ₇₁ BM	-5.59	-3.96	1.52	13.86	0.81	65	7.30	102
BDT-BT-DPP	PC ₇₁ BM	-5.28	-3.00	1.52	18.45	0.73	67	9.01	103
PBTCl ₂₅	PC ₇₁ BM	-5.36	-3.71	1.57	15.31	0.82	66	8.31	104
PTB7-Th-Pt	PC ₇₁ BM	-5.28	-3.43	1.54	16.21	0.80	65	8.45	105
BT-TDPP-PyDPP	PC ₇₁ BM	-5.30	-3.93	1.37	16.44	0.69	71	8.11	106
BDT-TTE-DTzTT	PC ₇₁ BM	-5.36	-3.69	1.67	15.98	0.78	73	9.09	107

Recently, several research groups demonstrated that conjugated terpolymers with one donor and two acceptor units (D-A-A) is an effective strategy for designing high-performance solar cell materials as compared to that of D-D-A terpolymers.^{85,102,108}

1.3.4.4 Incorporation of non-covalent interactions

Yet another strategy for rational design of conjugated polymers with improved electronic properties includes incorporation of non-covalent interactions apart from usual π - π and hydrogen bonding interactions. These non-covalent interactions comprise interactions between sulfur-oxygen, sulfur-nitrogen, fluorine-hydrogen, nitrogen-hydrogen etc.¹⁰⁹⁻¹¹¹ These interactions induce intramolecular locks which help in improving polymer backbone planarity, π -delocalization and thus charge carrier mobility in OFETs. Hydrogen bonds have also known to influence polymer self-assembly and the solid-state morphology of conjugated materials.¹¹²⁻¹²¹ Recently, Zhang et al. reported DPP-quarterthiophene conjugated polymers in which part of branching alkyl chains were replaced by urea containing alkyl chains.¹²² Incorporation of urea groups in the side chains promoted hydrogen bonding and induced inter-chain interactions in the polymer resulting in improved photovoltaic performance (Power Conversion Efficiency = 6.8 %) in solar cell devices and an outstanding value of hole mobility ($13.1 \text{ cm}^2 \text{ s}^{-1} \text{ V}^{-1}$) in Field Effect Transistor (FET) devices. The same research group further synthesized new thiazole-flanked DPP-based polymers with urea containing linear side-chains.¹²³ Ambipolar semiconducting properties of thin films of these polymers, including the hole and electron mobilities were enhanced compared to those of the polymer without urea groups. In 2018, Rondeau-Gagné et al. synthesized DPP based conjugated polymers with amide group containing alkyl side chains.¹²⁴ They demonstrated that the intermolecular hydrogen bonds formed between adjacent amide moieties affected the lamellar packing of the polymer and aggregation, but the π -conjugation remained unaffected. The charge carrier mobility in organic field-effect transistor (OFET) devices using these materials achieved a maximum value of $2.46 \text{ cm}^2 \text{ s}^{-1} \text{ V}^{-1}$ for 5 mol % of amide containing polymer. They further demonstrated that the introduction of hydrogen bonding influenced the mechanical properties of this class of DPP-polymers. It improves their stretching ability, reduces the elastic modulus of the polymers and facilitates the molecular alignment after stretch.

1.3.4.5 Flexible Linker strategy

In bulk heterojunction solar cells, the inherent thermodynamic immiscibility of the donor and acceptor phases promotes phase separation and thus decreases device performance. Crystallization of donor phase is found to be another driving force for blend separation. Thus, the improvement of morphological stability of BHJ film for longer time is one of the major challenges in the photovoltaics. Various strategies such as, volatile additives like diiodooctane, non-volatile nucleation promoters, or insulating polymers have been employed to address the issue. But these approaches were unsuccessful to offer the control over donor crystallization or the stability of blend morphology. Introduction of a “flexible linker” or “conjugation break spacer” in which conjugated segments are covalently linked with flexible aliphatic chains in a polymer, was found to be an interesting approach to overcome above mentioned problems.^{125–127}

Since the non-conjugated spacer interrupts the continuous conjugation typical of most semiconducting polymers, the spacers are often referred to as “conjugation-break spacers.” Alternatively, since the spacers also add a degree of conformational freedom to the otherwise rigid conjugated backbone, they have also been referred to as “flexible linkers.” Apparently, the incorporation of non-conjugated linkers along the polymer backbone could be expected to disrupt intramolecular charge carrier transport and create a high degree disorder in the material in the solid state. Even though, this may be thought to only negatively impact the optoelectronic properties, recent demonstrations have highlighted the usefulness of this approach in easing backbone rigidity to enhance processability, and offering unique self-assembly motifs for efficient device performance.^{128,129}

Nonetheless, this strategy is already known to modulate molecular arrangement in solid state and resulting opto-electronic properties of small organic materials;^{130–132} and poly phenylene-vinylene (PPV) based polymers.¹³³ The incorporation of flexible aliphatic linkers/spacers in the conjugated backbone provides unique control over solution processability of semiconducting polymers,^{134,135} morphology,¹²⁹ thermal stability,^{136,137} and mechanical properties^{128,138,139} of solution processed polymer thin films without negatively affecting charge transport properties. The superior mechanical properties of this class of conjugated systems possessing flexible linkers in their backbone make them potential candidates for stretchable electronics applications.^{139–141}

Figure 1.17 summarises the structures of representative polymers comprising flexible linkers.

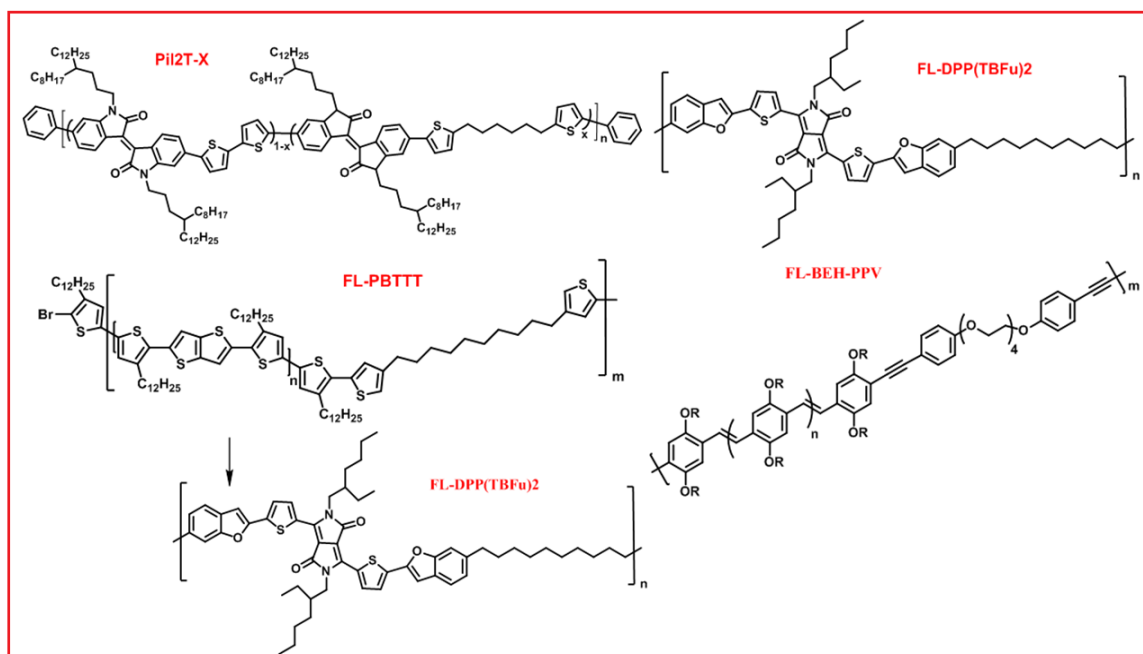


Figure 1.17 The structures of representative polymers comprising flexible linkers.

1.4 Summary

The tremendous progress has been achieved for conjugated polymer-based solar cells in last three decades. The power conversion efficiency (η) has reached $\sim 14\%$ in academic labs, making polymer solar cells a viable counterpart of amorphous silicon solar cells ($\sim 13\%$). This triumph is a result of synergistic efforts among chemists, physicists, and engineers, a true testimony to the necessity of having interdisciplinary approaches to tackle complex problems. A polymer solar cell, typically consisting of a polymer:fullerene blend in a bulk heterojunction (BHJ) configuration for converting light into electricity, is a complex system. Though the material properties of the active layer (i.e., optoelectronic properties of polymers and fullerenes) determine the efficiency of photovoltaic device, many other factors need to be optimized and function synergistically to maximize the device characteristics (i.e., short circuit current, J_{sc} ; open circuit voltage, V_{oc} ; and the fill factor, FF). The intrinsic complexity of BHJ solar cells thus requires a variety of expertise in synthesis, morphology, and device physics.

Design and synthesis of materials has primarily focused on the polymers, given that there is a limited amount of functionalization one can apply to the synthesis of fullerenes. Still, there are numerous factors to be considered in the synthetic design of these polymers. From a molecular engineering point of view, choosing the right conjugated repeating unit decides the energy levels and the band gap; selecting the appropriate side chains largely determines the solubility in the processing solvent; both conjugated backbone and the side chains have a significant impact on the aggregation and intermolecular interactions in the active layer. From a polymer engineering point of view, one needs to carefully balance the molecular weight, dispersity, solubility in the processing solvents, and viscosity of the resulting solution (i.e., the “active ink”). The polymer:fullerene blend in a processing solvent, the “active ink”, then goes through one of several solution-processing methods (e.g., spin coating, slot-die, doctor-blading, etc.), to become a thin film (i.e., the active layer) that has the optimal morphology to maximize the device output. Given the significance of the morphology, a variety of methods have been applied to control the morphology of the active layer, including weight ratio of polymer vs fullerene, processing additives, solvent annealing, and thermal annealing. The device efficiency of polymer:fullerene bulk heterojunction solar cells has recently surpassed 14 %, as a result of synergistic efforts among chemists, physicists, and engineers. Since the conjugated polymers are unequivocally the “heart” of this emerging technology, their design and synthesis have consistently played the key role in the device efficiency enhancement. Thus, it is crucial to elucidate the fundamental, underlying principles that govern the device characteristics and to establish structure-property correlations. Such correlations are crucial to the design and synthesis of next generation materials to further improve the device efficiency.

REFERENCES

- 1 O. Ellabban, H. Abu-Rub and F. Blaabjerg, *Renew. Sustain. Energy Rev.*, 2014, **39**, 748–764.
- 2 S. R. Bull, *Proc. IEEE*, 2001, **89**, 1216–1226.
- 3 E. Kabir, P. Kumar, S. Kumar, A. A. Adelodun and K.-H. Kim, *Renew. Sustain. Energy Rev.*, 2018, **82**, 894–900.

- 4 M. A. Green, A. Ho-Baillie and H. J. Snaith, *Nat. Photonics*, 2014, **8**, 506–514.
- 5 F. H. Alharbi and S. Kais, *Renew. Sustain. Energy Rev.*, 2015, **43**, 1073–1089.
- 6 D. E. Carlson and C. R. Wronski, *Appl. Phys. Lett.*, 1976, **28**, 671–673.
- 7 T. L. Chu, S. S. Chu, S. T. Ang and M. K. Mantravadi, *Sol. Cells*, 1987, **21**, 73–80.
- 8 J. Ramanujam and U. P. Singh, *Energy Environ. Sci.*, 2017, **10**, 1306–1319.
- 9 B. O'Regan and M. Grätzel, *Nature*, 1991, **353**, 737–740.
- 10 J. Wang, K. Liu, L. Ma and X. Zhan, *Chem. Rev.*, 2016, **116**, 14675–14725.
- 11 J. Wu, Z. Lan, J. Lin, M. Huang, Y. Huang, L. Fan and G. Luo, *Chem. Rev.*, 2015, **115**, 2136–2173.
- 12 Z. Yu, N. Vlachopoulos, M. Gorlov and L. Kloo, *Dalt. Trans.*, 2011, **40**, 10289–10303.
- 13 M. Wang, C. Grätzel, S. M. Zakeeruddin and M. Grätzel, *Energy Environ. Sci.*, 2012, **5**, 9394–9405.
- 14 G. R. R. . Kumara, A. Konno, G. K. R. Senadeera, P. V. V Jayaweera, D. B. R. . De Silva and K. Tennakone, *Sol. Energy Mater. Sol. Cells*, 2001, **69**, 195–199.
- 15 U. Bach, D. Lupo, P. Comte, J. E. Moser, F. Weissörtel, J. Salbeck, H. Spreitzer and M. Grätzel, *Nature*, 1998, **395**, 583–585.
- 16 M. A. K. L. Dissanayake, L. R. A. K. Bandara, R. S. P. Bokalawala, P. A. R. D. Jayathilaka, O. A. Ileperuma and S. Somasundaram, *Mater. Res. Bull.*, 2002, **37**, 867–874.
- 17 O. A. Ileperuma, M. A. K. . Dissanayake and S. Somasundaram, *Electrochim. Acta*, 2002, **47**, 2801–2807.
- 18 P. Wang, S. M. Zakeeruddin, I. Exnar and M. Grätzel, *Chem. Commun.*, 2002, 2972–2973.
- 19 L. N. Quan, B. P. Rand, R. H. Friend, S. G. Mhaisalkar, T.-W. Lee and E. H. Sargent, *Chem. Rev.*, 2019, **119**, 7444–7477.
- 20 M. Antonietta Loi and J. C. Hummelen, *Nat. Mater.*, 2013, **12**, 1087–1089.
- 21 M. Liu, M. B. Johnston and H. J. Snaith, *Nature*, 2013, **501**, 395.
- 22 J. Burschka, N. Pellet, S.-J. Moon, R. Humphry-Baker, P. Gao, M. K. Nazeeruddin and M. Grätzel, *Nature*, 2013, **499**, 316.
- 23 J. S. Manser, J. A. Christians and P. V Kamat, *Chem. Rev.*, 2016, **116**, 12956–

- 13008.
- 24 A. Kojima, K. Teshima, Y. Shirai and T. Miyasaka, *J. Am. Chem. Soc.*, 2009, **131**, 6050–6051.
- 25 S.-H. Bae, H. Zhao, Y.-T. Hsieh, L. Zuo, N. De Marco, Y. S. Rim, G. Li and Y. Yang, *Chem*, 2016, **1**, 197–219.
- 26 A. F. Nogueira, I. Montanari, J. Nelson, J. R. Durrant, C. Winder, N. S. Sariciftci and C. Brabec, *J. Phys. Chem. B*, 2003, **107**, 1567–1573.
- 27 C. Deibel and V. Dyakonov, *Reports Prog. Phys.*, 2010, **73**, 96401.
- 28 J.-M. Nunzi, *Comptes Rendus Phys.*, 2002, **3**, 523–542.
- 29 P. M. Allemand, A. Koch, F. Wudl, Y. Rubin, F. Diederich, M. M. Alvarez, S. J. Anz and R. L. Whetten, *J. Am. Chem. Soc.*, 1991, **113**, 1050–1051.
- 30 T. B. Singh, N. Marjanović, G. J. Matt, S. Günes, N. S. Sariciftci, A. Montaigne Ramil, A. Andreev, H. Sitter, R. Schwödiauer and S. Bauer, *Org. Electron.*, 2005, **6**, 105–110.
- 31 M. M. Wienk, J. M. Kroon, W. J. H. Verhees, J. Knol, J. C. Hummelen, P. A. van Hal and R. A. J. Janssen, *Angew. Chemie Int. Ed.*, 2003, **42**, 3371–3375.
- 32 Y. He, H.-Y. Chen, J. Hou and Y. Li, *J. Am. Chem. Soc.*, 2010, **132**, 1377–1382.
- 33 L. J. A. Koster, V. D. Mihailetschi and P. W. M. Blom, *Appl. Phys. Lett.*, 2006, **88**, 93511.
- 34 C. W. Tang, *Appl. Phys. Lett.*, 1986, **48**, 183–185.
- 35 H. Zhou, L. Yang and W. You, *Macromolecules*, 2012, **45**, 607–632.
- 36 C. J. Brabec, C. Winder, N. S. Sariciftci, J. C. Hummelen, A. Dhanabalan, P. A. van Hal and R. A. J. Janssen, *Adv. Funct. Mater.*, 2002, **12**, 709–712.
- 37 C. Gu, Q. Zhu, X. Bao, S. Wen, M. Qiu, L. Han, W. Huang, D. Zhu and R. Yang, *Polym. Chem.*, 2015, **6**, 6219–6226.
- 38 L. Han, X. Bao, T. Hu, Z. Du, W. Chen, D. Zhu, Q. Liu, M. Sun and R. Yang, *Macromol. Rapid Commun.*, 2014, **35**, 1153–1157.
- 39 M. Zhang, X. Guo, X. Wang, H. Wang and Y. Li, *Chem. Mater.*, 2011, **23**, 4264–4270.
- 40 D. Mühlbacher, M. Scharber, M. Morana, Z. Zhu, D. Waller, R. Gaudiana and C. Brabec, *Adv. Mater.*, 2006, **18**, 2884–2889.

- 41 A. J. Moulé, A. Tsami, T. W. Bünnagel, M. Forster, N. M. Kronenberg, M. Scharber, M. Koppe, M. Morana, C. J. Brabec, K. Meerholz and U. Scherf, *Chem. Mater.*, 2008, **20**, 4045–4050.
- 42 S. Albrecht, S. Janietz, W. Schindler, J. Frisch, J. Kurpiers, J. Kniepert, S. Inal, P. Pingel, K. Fostiropoulos, N. Koch and D. Neher, *J. Am. Chem. Soc.*, 2012, **134**, 14932–14944.
- 43 C. Liu, K. Wang, X. Gong and A. J. Heeger, *Chem. Soc. Rev.*, 2016, **45**, 4825–4846.
- 44 Y.-C. Chen, C.-Y. Yu, Y.-L. Fan, L.-I. Hung, C.-P. Chen and C. Ting, *Chem. Commun.*, 2010, **46**, 6503–6505.
- 45 E. Perzon, F. Zhang, M. Andersson, W. Mammo, O. Inganäs and M. R. Andersson, *Adv. Mater.*, 2007, **19**, 3308–3311.
- 46 J. Qi, J. Han, X. Zhou, D. Yang, J. Zhang, W. Qiao, D. Ma and Z. Y. Wang, *Macromolecules*, 2015, **48**, 3941–3948.
- 47 C. Kitamura, S. Tanaka and Y. Yamashita, *Chem. Mater.*, 1996, **8**, 570–578.
- 48 F. Wudl, M. Kobayashi and A. J. Heeger, *J. Org. Chem.*, 1984, **49**, 3382–3384.
- 49 H. Brisset, C. Thobie-Gautier, A. Gorgues, M. Jubault and J. Roncali, *J. Chem. Soc., Chem. Commun.*, 1994, 1305–1306.
- 50 H. Y. Chen, J. Hou, A. E. Hayden, H. Yang, K. N. Houk and Y. Yang, *Adv. Mater.*, 2010, **22**, 371–375.
- 51 C. M. Amb, S. Chen, K. R. Graham, J. Subbiah, C. E. Small, F. So and J. R. Reynolds, *J. Am. Chem. Soc.*, 2011, **133**, 10062–10065.
- 52 Q. Pei, G. Zuccarello, M. Ahlskog and O. Inganäs, *Polymer (Guildf.)*, 1994, **35**, 1347–1351.
- 53 Y. Huang, L. Huo, S. Zhang, X. Guo, C. C. Han, Y. Li and J. Hou, *Chem. Commun.*, 2011, **47**, 8904–8906.
- 54 L. Dou, Y. Liu, Z. Hong, G. Li and Y. Yang, *Chem. Rev.*, 2015, **115**, 12633–12665.
- 55 Y.-J. Cheng, S.-H. Yang and C.-S. Hsu, *Chem. Rev.*, 2009, **109**, 5868–5923.
- 56 S. Holliday, Y. Li and C. K. Luscombe, *Prog. Polym. Sci.*, 2017, **70**, 34–51.
- 57 J. W. Jung, J. W. Jo, E. H. Jung and W. H. Jo, *Org. Electron.*, 2016, **31**, 149–170.

- 58 J. Chen and Y. Cao, *Acc. Chem. Res.*, 2009, **42**, 1709–1718.
- 59 Y. Li, *Acc. Chem. Res.*, 2012, **45**, 723–733.
- 60 X. Guo, M. Baumgarten and K. Müllen, *Prog. Polym. Sci.*, 2013, **38**, 1832–1908.
- 61 C. Duan, F. Huang and Y. Cao, *J. Mater. Chem.*, 2012, **22**, 10416–10434.
- 62 Y. Li and Y. Zou, *Adv. Mater.*, 2008, **20**, 2952–2958.
- 63 Z.-G. Zhang, S. Zhang, J. Min, C. Chui, J. Zhang, M. Zhang and Y. Li, *Macromolecules*, 2012, **45**, 113–118.
- 64 J. Hou, Z. Tan, Y. Yan, Y. He, C. Yang and Y. Li, *J. Am. Chem. Soc.*, 2006, **128**, 4911–4916.
- 65 E. Zhou, Z. Tan, C. Yang and Y. Li, *Macromol. Rapid Commun.*, 2006, **27**, 793–798.
- 66 G. Tu, A. Bilge, S. Adamczyk, M. Forster, R. Heiderhoff, L. J. Balk, D. Mühlbacher, M. Morana, M. Koppe, M. C. Scharber, S. A. Choulis, C. J. Brabec and U. Scherf, *Macromol. Rapid Commun.*, 2007, **28**, 1781–1785.
- 67 Y.-T. Chang, S.-L. Hsu, G.-Y. Chen, M.-H. Su, T. A. Singh, E. W.-G. Diao and K.-H. Wei, *Adv. Funct. Mater.*, 2008, **18**, 2356–2365.
- 68 J. Hou, M.-H. Park, S. Zhang, Y. Yao, L.-M. Chen, J.-H. Li and Y. Yang, *Macromolecules*, 2008, **41**, 6012–6018.
- 69 L. Huo and J. Hou, *Polym. Chem.*, 2011, **2**, 2453–2461.
- 70 H. Pan, Y. Li, Y. Wu, P. Liu, B. S. Ong, S. Zhu and G. Xu, *Chem. Mater.*, 2006, **18**, 3237–3241.
- 71 S. C. Price, A. C. Stuart, L. Yang, H. Zhou and W. You, *J. Am. Chem. Soc.*, 2011, **133**, 4625–4631.
- 72 L. Huo, S. Zhang, X. Guo, F. Xu, Y. Li and J. Hou, *Angew. Chemie Int. Ed.*, 2011, **50**, 9697–9702.
- 73 L. Dou, J. Gao, E. Richard, J. You, C.-C. Chen, K. C. Cha, Y. He, G. Li and Y. Yang, *J. Am. Chem. Soc.*, 2012, **134**, 10071–10079.
- 74 M. Zhang, X. Guo, W. Ma, S. Zhang, L. Huo, H. Ade and J. Hou, *Adv. Mater.*, 2014, **26**, 2089–2095.
- 75 M. Zhang, X. Guo, S. Zhang and J. Hou, *Adv. Mater.*, 2014, **26**, 1118–1123.
- 76 Y. Wu, Z. Li, W. Ma, Y. Huang, L. Huo, X. Guo, M. Zhang, H. Ade and J. Hou,

- Adv. Mater.*, 2013, **25**, 3449–3455.
- 77 C. Gu, D. Liu, J. Wang, Q. Niu, C. Gu, B. Shahid, B. Yu, H. Cong and R. Yang, *J. Mater. Chem. A*, 2018, **6**, 2371–2378.
- 78 M. Zhang, Y. Gu, X. Guo, F. Liu, S. Zhang, L. Huo, T. P. Russell and J. Hou, *Adv. Mater.*, 2013, **25**, 4944–4949.
- 79 D. Qian, L. Ye, M. Zhang, Y. Liang, L. Li, Y. Huang, X. Guo, S. Zhang, Z. Tan and J. Hou, *Macromolecules*, 2012, **45**, 9611–9617.
- 80 D. Dang, D. Yu and E. Wang, *Adv. Mater.*, 2019, **31**, 1807019.
- 81 X. Huang, G. Zhang, C. Zhou, L. Liu, Y. Jin, S. Liu, L. Ying, F. Huang and Y. Cao, *Polym. Chem.*, 2015, **6**, 4154–4161.
- 82 D. Dang, W. Chen, R. Yang, W. Zhu, W. Mammo and E. Wang, *Chem. Commun.*, 2013, **49**, 9335.
- 83 T. Qin, W. Zajaczkowski, W. Pisula, M. Baumgarten, M. Chen, M. Gao, G. Wilson, C. D. Easton, K. Müllen and S. E. Watkins, *J. Am. Chem. Soc.*, 2014, **136**, 6049–6055.
- 84 J. Zhou, S. Xie, E. F. Amond and M. L. Becker, *Macromolecules*, 2013, **46**, 3391–3394.
- 85 Q. Tao, Y. Xia, X. Xu, S. Hedström, O. Bäcke, D. I. James, P. Persson, E. Olsson, O. Inganäs, L. Hou, W. Zhu and E. Wang, *Macromolecules*, 2015, **48**, 1009–1016.
- 86 B. Fan, X. Xue, X. Meng, X. Sun, L. Huo, W. Ma and Y. Sun, *J. Mater. Chem. A*, 2016, **4**, 13930–13937.
- 87 L. Fang, Y. Zhou, Y.-X. Yao, Y. Diao, W.-Y. Lee, A. L. Appleton, R. Allen, J. Reinspach, S. C. B. Mannsfeld and Z. Bao, *Chem. Mater.*, 2013, **25**, 4874–4880.
- 88 W.-H. Chang, J. Gao, L. Dou, C.-C. Chen, Y. Liu and Y. Yang, *Adv. Energy Mater.*, 2014, **4**, 1300864.
- 89 B. Fan, X. Xue, X. Meng, X. Sun, L. Huo, W. Ma and Y. Sun, *J. Mater. Chem. A*, 2016, **4**, 13930–13937.
- 90 L. Huo, X. Xue, T. Liu, W. Xiong, F. Qi, B. Fan, D. Xie, F. Liu, C. Yang and Y. Sun, *Chem. Mater.*, 2018, **30**, 3294–3300.
- 91 B. Burkhart, P. P. Khlyabich and B. C. Thompson, *ACS Macro Lett.*, 2012, **1**, 660–666.

- 92 K.-H. Kim, S. Park, H. Yu, H. Kang, I. Song, J. H. Oh and B. J. Kim, *Chem. Mater.*, 2014, **26**, 6963–6970.
- 93 M.-C. Yuan, M.-Y. Chiu, C.-M. Chiang and K.-H. Wei, *Macromolecules*, 2010, **43**, 6270–6277.
- 94 J. Li, K.-H. Ong, S.-L. Lim, G.-M. Ng, H.-S. Tan and Z.-K. Chen, *Chem. Commun.*, 2011, **47**, 9480–9482.
- 95 I. E. Kuznetsov, A. V. Akkuratow, D. K. Susarova, D. V. Anokhin, Y. L. Moskvina, M. V. Kluyev, A. S. Peregodov and P. A. Troshin, *Chem. Commun.*, 2015, **51**, 7562–7564.
- 96 H. Ju, Y. Yang, Z. Wang, S. Yang, Z. Liu, G. Zhang and D. Zhang, *Polym. Chem.*, 2016, **7**, 6798–6804.
- 97 H. J. Cho, Y. J. Kim, S. Chen, J. Lee, T. J. Shin, C. E. Park and C. Yang, *Nano Energy*, 2017, **39**, 229–237.
- 98 T. Jiang, J. Yang, Y. Tao, C. Fan, L. Xue, Z. Zhang, H. Li, Y. Li and W. Huang, *Polym. Chem.*, 2016, **7**, 926–932.
- 99 I. Shin, H. ju Ahn, J. H. Yun, J. W. Jo, S. Park, S. Joe, J. Bang and H. J. Son, *Adv. Energy Mater.*, 2018, **8**, 1870028.
- 100 H. K. H., H. G. H. L., G. V. S., W. M. M. and J. R. A. J., *Angew. Chemie Int. Ed.*, 2013, **52**, 8341–8344.
- 101 T. E. Kang, H.-H. Cho, H. jun Kim, W. Lee, H. Kang and B. J. Kim, *Macromolecules*, 2013, **46**, 6806–6813.
- 102 S. Beaupré, S. Shaker-Sepasgozar, A. Najari and M. Leclerc, *J. Mater. Chem. A*, 2017, **5**, 6638–6647.
- 103 X. Xu, G. Zhang, Y. Zhao, J. Liu, Y. Li and Q. Peng, *Chinese J. Polym. Sci.*, 2017, **35**, 249–260.
- 104 S. Qu, H. Wang, D. Mo, P. Chao, Z. Yang, L. Li, L. Tian, W. Chen and F. He, *Macromolecules*, 2017, **50**, 4962–4971.
- 105 Z. Wan, J. Yang, Y. Liu, S. Wang, Y. Zhong, C. Li, Z. Zhang, G. Xing, S. Huettner, Y. Tao, Y. Li and W. Huang, *Polym. Chem.*, 2017, **8**, 4729–4737.
- 106 J. W. Lee, H. Ahn and W. H. Jo, *Macromolecules*, 2015, **48**, 7836–7842.
- 107 Q. Wang, Y. Wang, W. Zheng, B. Shahid, M. Qiu, D. Wang, D. Zhu and R. Yang,

- ACS Appl. Mater. Interfaces*, 2017, **9**, 32126–32134.
- 108 W. Sun, Z. Ma, D. Dang, W. Zhu, M. R. Andersson, F. Zhang and E. Wang, *J. Mater. Chem. A*, 2013, **1**, 11141.
- 109 N. E. Jackson, B. M. Savoie, K. L. Kohlstedt, M. Olvera de la Cruz, G. C. Schatz, L. X. Chen and M. A. Ratner, *J. Am. Chem. Soc.*, 2013, **135**, 10475–10483.
- 110 Y. Cheng, Y. Qi, Y. Tang, C. Zheng, Y. Wan, W. Huang and R. Chen, *J. Phys. Chem. Lett.*, 2016, **7**, 3609–3615.
- 111 M. E. Ziffer, S. B. Jo, Y. Liu, H. Zhong, J. C. Mohammed, J. S. Harrison, A. K.-Y. Jen and D. S. Ginger, *J. Phys. Chem. C*, 2018, **122**, 18860–18869.
- 112 A. P. H. J. Schenning and E. W. Meijer, *Chem. Commun.*, 2005, 3245.
- 113 S.-L. Hsu, C.-M. Chen, Y.-H. Cheng and K.-H. Wei, *J. Polym. Sci. Part A Polym. Chem.*, 2011, **49**, 603–611.
- 114 F. Li, K. G. Yager, N. M. Dawson, J. Yang, K. J. Malloy and Y. Qin, *Macromolecules*, 2013, **46**, 9021–9031.
- 115 S. J. Ananthakrishnan, B. S. Kumar, N. Somanathan and A. B. Mandal, *RSC Adv.*, 2013, **3**, 8331.
- 116 J. Huang, B. Peng, W. Wang, H. Ji, L. Li, K. Xi, W. Lai, X. Zhang and X. Jia, *Adv. Funct. Mater.*, 2016, **26**, 1646–1655.
- 117 F. Li, K. G. Yager, N. M. Dawson, Y. Jiang, K. J. Malloy and Y. Qin, *Polym. Chem.*, 2015, **6**, 721–731.
- 118 Y. Lin, J. A. Lim, Q. Wei, S. C. B. Mannsfeld, A. L. Briseno and J. J. Watkins, *Chem. Mater.*, 2012, **24**, 622–632.
- 119 C. Liu, S. Dong, P. Cai, P. Liu, S. Liu, J. Chen, F. Liu, L. Ying, T. P. Russell, F. Huang and Y. Cao, *ACS Appl. Mater. Interfaces*, 2015, **7**, 9038–9051.
- 120 B. Adhikari, X. Lin, M. Yamauchi, H. Ouchi, K. Aratsu and S. Yagai, *Chem. Commun.*, 2017, **53**, 9663–9683.
- 121 H. Cui, X. Chen, Y. Wang, D. Wei, F. Qiu and J. Peng, *Soft Matter*, 2018, **14**, 5906–5912.
- 122 J. Yao, C. Yu, Z. Liu, H. Luo, Y. Yang, G. Zhang and D. Zhang, *J. Am. Chem. Soc.*, 2016, **138**, 173–185.
- 123 J. Ma, Z. Liu, J. Yao, Z. Wang, G. Zhang, X. Zhang and D. Zhang,

- Macromolecules*, 2018, **51**, 6003–6010.
- 124 M. U. Ocheje, B. P. Charron, Y.-H. Cheng, C.-H. Chuang, A. Soldera, Y.-C. Chiu and S. Rondeau-Gagné, *Macromolecules*, 2018, **51**, 1336–1344.
- 125 H.-J. Li, J.-T. Wang, C.-Y. Mei and W.-S. Li, *Chem. Commun.*, 2014, **50**, 7720–7722.
- 126 A. Gasperini, S. Bivaud and K. Sivula, *Chem. Sci.*, 2014, **5**, 4922–4927.
- 127 Y. Zhao, X. Zhao, Y. Zang, C. Di, Y. Diao and J. Mei, *Macromolecules*, 2015, **48**, 2048–2053.
- 128 E. L. Melenbrink, K. M. Hilby, K. Choudhary, S. Samal, N. Kazerouni, J. L. McConn, D. J. Lipomi and B. C. Thompson, *ACS Appl. Polym. Mater.*, 2019, **1**, 1107–1117.
- 129 W.-J. Xiao, J. Wang, H.-J. Li, L. Liang, X. Xiang, X.-Q. Chen, J. Li, Z. Lu and W.-S. Li, *RSC Adv.*, 2018, **8**, 23546–23554.
- 130 Z. Liang, R. A. Cormier, A. M. Nardes and B. A. Gregg, *Synth. Met.*, 2011, **161**, 1014–1021.
- 131 L. Ding, H.-B. Li, T. Lei, H.-Z. Ying, R.-B. Wang, Y. Zhou, Z.-M. Su and J. Pei, *Chem. Mater.*, 2012, **24**, 1944–1949.
- 132 X. Lin, M. Hirono, T. Seki, H. Kurata, T. Karatsu, A. Kitamura, D. Kuzuhara, H. Yamada, T. Ohba, A. Saeki, S. Seki and S. Yagai, *Chem. - A Eur. J.*, 2013, **19**, 6561–6565.
- 133 X. Zhu, M. C. Traub, D. A. Vanden Bout and K. N. Plunkett, *Macromolecules*, 2012, **45**, 5051–5057.
- 134 G.-J. N. Wang, F. Molina-Lopez, H. Zhang, J. Xu, H.-C. Wu, J. Lopez, L. Shaw, J. Mun, Q. Zhang, S. Wang, A. Ehrlich and Z. Bao, *Macromolecules*, 2018, **51**, 4976–4985.
- 135 Y. Zhao, X. Zhao, M. Roders, G. Qu, Y. Diao, A. L. Ayzner and J. Mei, *Chem. Mater.*, 2015, **27**, 7164–7170.
- 136 A. Gasperini, X. A. Jeanbourquin, A. Rahmanudin, X. Yu and K. Sivula, *Adv. Mater.*, 2015, **27**, 5541–5546.
- 137 X. A. Jeanbourquin, A. Rahmanudin, A. Gasperini, E. Ripaud, X. Yu, M. Johnson, N. Guijarro and K. Sivula, *J. Mater. Chem. A*, 2017, **5**, 10526–10536.

-
- 138 J. Mun, G.-J. N. Wang, J. Y. Oh, T. Katsumata, F. L. Lee, J. Kang, H.-C. Wu, F. Lissel, S. Rondeau-Gagné, J. B. H. Tok and Z. Bao, *Adv. Funct. Mater.*, 2018, **28**, 1804222.
- 139 B. C. Schroeder, Y.-C. Chiu, X. Gu, Y. Zhou, J. Xu, J. Lopez, C. Lu, M. F. Toney and Z. Bao, *Adv. Electron. Mater.*, 2016, **2**, 1600104.
- 140 E. L. Melenbrink, K. M. Hilby, M. A. Alkhadra, S. Samal, D. J. Lipomi and B. C. Thompson, *ACS Appl. Mater. Interfaces*, 2018, **10**, 32426–32434.
- 141 Y.-C. Chiang, H.-C. Wu, H.-F. Wen, C.-C. Hung, C.-W. Hong, C.-C. Kuo, T. Higashihara and W.-C. Chen, *Macromolecules*, 2019, **52**, 4396–4404.

CHAPTER 2

Scope and Objectives

2.1 SCOPE AND OBJECTIVES

The increasing demand of various types of energy, particularly electrical energy, in a civilized world has put tremendous pressure on non-renewable energy sources such as fossil fuels along with the possibility of their exhaustion in near future. The pressing need for alternative renewable energy sources ushered the world of photovoltaics (PV). The traditional inorganic photovoltaics is based on silicon and silicon dioxide which require high processing temperatures. Due to this reason, this technology became much expensive. Also, the modules made with inorganic semiconductors are relatively heavy and brittle. Organic photovoltaics (OPV) which employ organic semiconductors (light absorbing small molecules or polymers) to generate electricity from light, have emerged as a complementary alternative to silicon/ inorganic photovoltaics. Since polymeric materials can be melt or solution processed, OPV utilises low-temperature, solution processed fabrication techniques such as roll-to-roll and ink-jet printing which tremendously reduces their manufacturing cost. Moreover, the potential for large-area, light weight and mechanically flexible modules, with options for semi-transparent and coloured films provide novel opportunities in building-integrated photovoltaics.^{1,2} Another fascinating feature of OPVs is the fine tuning of the device properties by the slight change in the structure of the organic semiconductor.³ Furthermore, OPVs give better operation at low light levels i.e. indoor applications, which is an important advantage over inorganic PV.⁴⁻⁶ The OPV technology has enormously evolved in last few decades, with frequent reports delivering power conversion efficiency values $> 10\%$. Majority of this progress can be attributed to the development of new π -conjugated organic semiconductors.

The π -conjugated organic semiconductors are basically grouped into two classes- i) small molecular semiconductors and ii) polymeric semiconductors. Small molecular semiconductors for OPVs exhibit advantages over their polymer counterparts which include well-defined molecular structure, definite molecular weight, and high purity without batch-to-batch variations, resulting in improved reproducibility of fabrication.⁷ They show greater tendency to form ordered domains leading to high charge carrier mobilities.⁸ Thus, small molecular semiconductors have attracted considerable attention as a promising alternative to polymeric semiconductors.⁹⁻¹⁴ Nonetheless, excluding few exceptions of solution processible molecular semiconductors, most of them require high

temperature vacuum deposition techniques for their integration into a device which is a limiting parameter for molecular semiconductors. Polymeric semiconductors, on the other hand, exhibit isotropic charge transport, great control over large scale of the film structural and morphological characteristics (solution rheological properties) which is a prerequisite for printing technique. Moreover, polymers are not susceptible to interlayer diffusion during the typical device-fabrication and exhibit robust mechanical properties, making nanometer-thick semiconductor films potentially compatible with roll-to-roll fabrication on flexible substrates. With all these favourable parameters, on certain accounts, polymers are considered far more superior than small molecules in organic electronics. This has led to intensive research in the development of π -conjugated polymers for their applications in various organic electronic devices such as- organic photovoltaic cells (OPVs),^{15,16} organic light emitting diodes (OLEDs),¹⁷ organic field-effect transistors (OFETs),^{18,19} organic lasers,²⁰ and memory cells.²¹

The overall objective of the present work was to synthesize π -conjugated materials for organic solar cell applications using various synthetic strategies and study their structure-property relationship. **Figure 2.1** suitably illustrates the theme of the thesis.

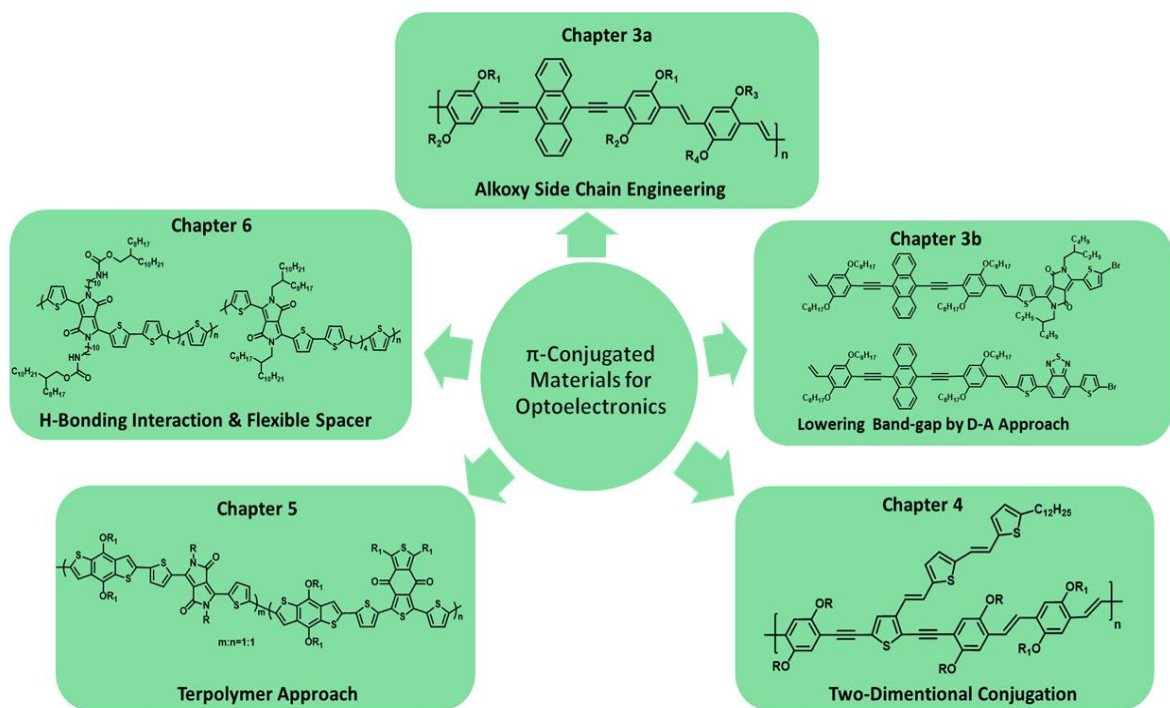


Figure 2.1 The theme of the thesis.

1) **Synthesis of anthracene containing PAE-PV polymers and to study the influence of π - π stacking distance on the morphology and performance of solar cells**

Poly(*p*-arylene-ethynylene)-*alt*-poly(*p*-arylene-vinylene)s (PAE-PAVs) are known to combine the interesting intrinsic properties of both of their constituents (PAE and PAV) within a single polymeric backbone and in addition exhibit novel promising structure-specific properties.²² Incorporation of anthracene moiety into PAE-PAV polymers, lowered the band-gap of polymer and improved the film absorption coefficient. Considering interesting properties of anthracene, following objectives were chosen for the study:

- i) To synthesize anthracene-containing dialdehydes and bisphosphonates.
- iii) To synthesize anthracene-containing PAE-PV copolymers by Horner-Wadsworth-Emmons olefination reaction of corresponding dialdehydes with bisphosphonates. The side chains on PAE and PAV units were systematically varied between linear, branched and asymmetric substitution.
- iv) To study photo-physical and electrochemical properties of polymers. Structural investigations were performed on powder and on filaments by wide-angle X-ray scattering analysis (WAXS) to obtain information about crystallinity and order with respect to the interlayer distance and the π - π stacking distance.
- v) To study charge carrier mobility by Charge Extraction by Linearly Increasing Voltage (CELIV) method. To investigate thin film morphology of polymer films and polymer blends with PCBM by atomic force microscopy experiments (AFM).
- vi) To fabricate solar cell devices and establish a correlation between the ability to form π - π -stacking, the absorption behavior, the charge carrier mobility, the active layer nanoscale morphology, and the photovoltaic performance.

2. **Synthesis of donor-acceptor low band gap small molecules containing anthracene-based donor unit and diketopyrrolopyrrole and benzothiadiazole as acceptor units and investigation of charge carrier mobility by OFET devices**

Low (narrow) band gap (LBG) conjugated polymers/small molecules which absorb in near IR region are interesting candidates for optoelectronic applications due to possibility of obtaining higher open circuit voltage values and efficient charge separation

in solar cell devices.²³ Combining donor unit with acceptor unit to form donor-acceptor kind of systems is an important approach to design high performance low band-gap materials. The objectives of the present work are as follows-

- i) Synthesis of anthracene-containing (*p*-phenylene ethynylene) (AnPPE) monomer, diketopyrrolopyrrole (DPP) monomer and benzothiadiazole (BTDA) monomer.
- ii) Synthesis of low band gap donor-acceptor small molecules by palladium-catalysed Heck coupling reaction.
- iii) To study photophysical and electrochemical properties for the determination of band-gap energy and HOMO-LUMO energy levels of the small molecules.
- iv) To investigate charge carrier mobility of the small molecules in OFET devices.

3. Synthesis of bi(thienylenevinylene)thiophene-containing PPE-PPVs and investigation of the influence of side-chain engineering on modulation of charge carrier mobility and photovoltaic performance

Two-dimensional conjugated polymeric systems comprising of the conjugated main chain along with conjugated side chain have emerged as an attractive approach for the design of conjugated polymers with improved optoelectronic properties.²⁴ The two-dimensional conjugated polymeric systems exhibit broad absorption and deep-lying HOMO levels beneficial for high photovoltaic performance. The objectives of the present work are as follows-

- i) Synthesis of bi(thienylenevinylene)thiophene-containing dialdehydes and bisphosphonates.
- ii) Synthesis of bi(thienylenevinylene)thiophene-containing PPE-PPVs by Horner-Wadsworth-Emmons olefination reaction of corresponding dialdehydes with bisphosphonates.
- iii) To study photophysical and electrochemical properties of the polymers to evaluate band-gap energy and HOMO-LUMO energy levels of the polymers.
- iv) To investigate charge carrier mobility by time of flight measurements.
- v) To fabricate solar cell devices for determination of photovoltaic performance.

4. Synthesis of benzo[1,2-c:4,5-c']dithiophene-4,8-dione containing copolymers and terpolymers; and an investigation of implications of active layer morphology on photovoltaic performance

The design of terpolymers by proper selection of the third component, based on knowledge of existing D-A copolymers, is found to be promising strategy for finely tailoring polymers with superior optoelectronic properties.²⁵ In general, terpolymers show a broader absorption range and higher photocurrent compared to their corresponding D-A copolymers.²⁶ Recently a new acceptor viz., 1,3-bis(thiophen-2-yl)-5,7-bis(2-ethylhexyl)benzo-[1,2-c:4,5c']dithiophene-4,8-dione (BDD)²⁷⁻²⁹ was evolved as a promising unit for the synthesis of high performance D-A copolymers with impressive photovoltaic properties. Inspired by excellent properties of BDD molecule, the following objectives were chosen.

- i) To synthesize BDD monomer, diketopyrrolopyrrole monomer with 2-ethylhexyl side chain (DPP (EH)), diketopyrrolopyrrole monomer with 2-hexyldecyl side chain (DPP (HD)), cyclopentadithiophene (CPDT) monomer, bithiophene (BT) monomer, and benzodithiophene (BDT) monomer.
- ii) Synthesis of random copolymers and D-A-A type terpolymers involving CPDT, BT and BDT as donor units; and DPP and BDD as acceptor units.
- iii) To study photophysical and electrochemical properties of the polymers to determine band-gap energy and HOMO, LUMO energy levels of the polymers.
- iv) To study active layer morphology by atomic force microscopy experiments.
- v) To investigate solar cell performance of the copolymers and terpolymers.

5. DPP-based spacer polymers functionalized with urethane linker containing alkyl side chains: Study of self-assembly behaviour

The incorporation of non-covalent interactions in the polymer chains is known to create intramolecular conformational locks which help to improve polymer backbone planarity, π -delocalization and thus charge carrier mobility in OFETs.³⁰ Hydrogen bonds have also known to influence polymer self-assembly and the solid-state morphology of conjugated materials. Urethane linkage is an interesting moiety to incorporate non-covalent interactions in the polymers.

The objectives of the present work are as follows-

- i) To synthesize urethane linker containing alkyl side chain, urethane linker containing DPP monomer (DPP_{urethane}), DPP_{alkyl} monomer and spacer monomer.
- ii) Synthesis of random copolymers of DPP_{urethane} and DPP_{alkyl} with C₄ alkyl spacer monomer.
- iii) To study photophysical and electrochemical properties of the polymers to determine band-gap energy and HOMO, LUMO energy levels of the polymers.
- iv) To study hydrogen-bonding interactions by variable temperature ¹H-NMR spectroscopy and UV-Vis spectroscopy. Further, to study self-assembly in cyclohexane by high temperature ¹H-NMR spectroscopy.

REFERENCES

- 1 C.-C. Chen, L. Dou, R. Zhu, C.-H. Chung, T.-B. Song, Y. B. Zheng, S. Hawks, G. Li, P. S. Weiss and Y. Yang, *ACS Nano*, 2012, **6**, 7185–7190.
- 2 A. Colsmann, A. Puetz, A. Bauer, J. Hanisch, E. Ahlswede and U. Lemmer, *Adv. Energy Mater.*, 2011, **1**, 599–603.
- 3 L. Huo, X. Xue, T. Liu, W. Xiong, F. Qi, B. Fan, D. Xie, F. Liu, C. Yang and Y. Sun, *Chem. Mater.*, 2018, **30**, 3294–3300.
- 4 H. K. H. Lee, J. Wu, J. Barbé, S. M. Jain, S. Wood, E. M. Speller, Z. Li, F. A. Castro, J. R. Durrant and W. C. Tsoi, *J. Mater. Chem. A*, 2018, **6**, 5618–5626.
- 5 R. Steim, T. Ameri, P. Schilinsky, C. Waldauf, G. Dennler, M. Scharber and C. J. Brabec, *Sol. Energy Mater. Sol. Cells*, 2011, **95**, 3256–3261.
- 6 C. L. Cutting, M. Bag and D. Venkataraman, *J. Mater. Chem. C*, 2016, **4**, 10367–10370.
- 7 X.-H. Zhu, J. Peng, Y. Cao and J. Roncali, *Chem. Soc. Rev.*, 2011, **40**, 3509–3524.
- 8 H. Dong, C. Wang and W. Hu, *Chem. Commun.*, 2010, **46**, 5211.
- 9 V. Steinmann, N. M. Kronenberg, M. R. Lenze, S. M. Graf, D. Hertel, K. Meerholz, H. Bürckstümmer, E. V Tulyakova and F. Würthner, *Adv. Energy Mater.*, 2011, **1**, 888–893.
- 10 Z. Li, G. He, X. Wan, Y. Liu, J. Zhou, G. Long, Y. Zuo, M. Zhang and Y. Chen, *Adv. Energy Mater.*, 2012, **2**, 74–77.

- 11 G. Feng, Y. Xu, J. Zhang, Z. Wang, Y. Zhou, Y. Li, Z. Wei, C. Li and W. Li, *J. Mater. Chem. A*, 2016, **4**, 6056–6063.
- 12 J. Roncali, *Acc. Chem. Res.*, 2009, **42**, 1719–1730.
- 13 B. Walker, C. Kim and T.-Q. Nguyen, *Chem. Mater.*, 2011, **23**, 470–482.
- 14 Y. Zou, Y. Dong, C. Sun, Y. Wu, H. Yang, C. Cui and Y. Li, *Chem. Mater.*, 2019, **31**, 4222–4227.
- 15 J. W. Jung, J. W. Jo, E. H. Jung and W. H. Jo, *Org. Electron.*, 2016, **31**, 149–170.
- 16 B. Kippelen and J.-L. Brédas, *Energy Environ. Sci.*, 2009, **2**, 251–261.
- 17 A. C. Grimsdale, K. Leok Chan, R. E. Martin, P. G. Jokisz and A. B. Holmes, *Chem. Rev.*, 2009, **109**, 897–1091.
- 18 T. Sekitani and T. Someya, *Adv. Mater.*, 2010, **22**, 2228–2246.
- 19 C. Wang, H. Dong, W. Hu, Y. Liu and D. Zhu, *Chem. Rev.*, 2012, **112**, 2208–2267.
- 20 S. Chénais and S. Forget, *Polym. Int.*, 2012, **61**, 390–406.
- 21 J. Ouyang, C.-W. Chu, D. Sieves and Y. Yang, *Appl. Phys. Lett.*, 2005, **86**, 123507.
- 22 D. A. M. Egbe, B. Carbonnier, E. Birckner and U. W. Grummt, *Prog. Polym. Sci.*, 2009, **34**, 1023–1067.
- 23 C. Liu, K. Wang, X. Gong and A. J. Heeger, *Chem. Soc. Rev.*, 2016, **45**, 4825–4846.
- 24 L. Huo, S. Zhang, X. Guo, F. Xu, Y. Li and J. Hou, *Angew. Chemie Int. Ed.*, 2011, **50**, 9697–9702.
- 25 B. Fan, X. Xue, X. Meng, X. Sun, L. Huo, W. Ma and Y. Sun, *J. Mater. Chem. A*, 2016, **4**, 13930–13937.
- 26 K. H. Hendriks, G. H. L. Heintges, M. M. Wienk and R. A. J. Janssen, *J. Mater. Chem. A*, 2014, **2**, 17899–17905.
- 27 W. Zhao, S. Li, H. Yao, S. Zhang, Y. Zhang, B. Yang and J. Hou, *J. Am. Chem. Soc.*, 2017, **139**, 7148–7151.
- 28 B. Huang, L. Hu, L. Chen, S. Chen, M. Hu, Y. Zhou, Y. Zhang, C. Yang and Y. Chen, *J. Mater. Chem. A*, 2019, **7**, 4847–4854.
- 29 T. Liu, X. Pan, X. Meng, Y. Liu, D. Wei, W. Ma, L. Huo, X. Sun, T. H. Lee, M.

- Huang, H. Choi, J. Y. Kim, W. C. H. Choy and Y. Sun, *Adv. Mater.*, 2017, **29**, 1604251.
- 30 M. U. Ocheje, B. P. Charron, Y.-H. Cheng, C.-H. Chuang, A. Soldera, Y.-C. Chiu and S. Rondeau-Gagné, *Macromolecules*, 2018, **51**, 1336–1344.

CHAPTER 3a

Anthracene Containing Poly(-*p*-arylene-ethynylene)-*alt*-poly(-*p*-arylene-vinylene) (AnE-PV): Influence of π – π Stacking Distance on the Morphology and Performance of Solar Cells

3a.1 INTRODUCTION

The interest in π -conjugated polymers as active materials in organic electronic devices has increased over the years from the time of discovery of electrical conductivity in the doped polyacetylene by Shirakawa et al in 1977.^{1,2} Since then, tremendous progress has been made in the design, synthesis and application of π -conjugated polymers in various organic electronic devices such as chemical sensors,^{3,4} light emitting diodes,^{5,6} field effect transistors⁷ and photovoltaics.⁸ π -Conjugated polymers have advantages like solution processability, transparency, flexibility, lower cost and fabrication of large area devices (spin coating, doctor blade techniques), over traditional inorganic semiconductors. As a result, considerable research has been devoted in designing and studying structure- property relationship of various conjugated polymeric systems.

Electroluminescence in conjugated polymers was first discovered in the polymer poly(1,4-phenylene vinylene) (PPV) by Cavendish group.⁹ The focus on PPV polymer was much enhanced after the discovery of ultrafast (femtosecond) photoinduced charge transfer from alkoxy-substituted PPV to the Buckminsterfullerene by Sariciftci and Heeger.¹⁰ PPV type materials are predominantly hole-conducting materials with high-lying lowest unoccupied molecular orbital (LUMO). The unbalanced charge carrier transport properties and the relative high barrier for electron injection from electrode metals such as aluminium lead to low efficiency mono-layered LED devices.^{6,9,11} In contrast, (phenylene-ethynylene)s (PPEs) have comparatively lower-lying LUMO due to enhanced electron affinity, which is ascribed to the electron-withdrawing nature of triple bonds ($-C\equiv C-$). PPEs moreover exhibit a highly rigid conjugated system with differences in polarization, molar extinction coefficients, and especially higher fluorescence quantum yields in dilute medium.^{12,13}

Several approaches have been explored to improve the electron affinity of PPVs. One approach is to attach electron-withdrawing groups either on vinylene position, like in CN-substituted PPVs,¹⁴ or onto the phenyl ring, like in halogen-(Cl-, Br-) substituted PPVs,¹⁵ and in CF₃-substituted PPVs.¹⁶ Another approach is to insert electron-deficient aromatic rings in the polymer backbone, like in oxadiazole-,^{17,18} quinoline-,¹⁹ quinoxaline-²⁰ or pyridine-containing poly-(arylene vinylene)s (PAVs).²¹ Inserting weak

electron-withdrawing triple bonds ($-C\equiv C-$) within PPV-backbone leading to hybrid PPE-PPVs, is regarded as important approach of enhancing the electron affinity of PPVs. Poly(-p-arylene-ethynylene)-alt-poly(-p-arylene-vinylene)s (PAE-PAVs) are conjugated systems, which combine the interesting intrinsic properties of both of their constituents within a single polymeric backbone and in addition exhibit novel promising structure-specific properties. Bunz *et al* developed alkyl-substituted PPE-PPV hybrid polymers of general chemical formula: $(-C\equiv C-Ph-CH=CH-Ph-)_n$, which were synthesized by $Mo(CO)_6$ -catalyzed acyclic diyne metathesis.²² The work by Egbe *et al* constitute solely alkoxy-substituted as well as mixed alkyl- and alkoxy-substituted PPE-PPVs of various conjugated patterns.²³⁻²⁵ The appended alkyl and/or alkoxy chains on the polymeric backbone not only fulfill the function of solubilising agents and enabling the processability of the polymers into thin films for various applications, but also lead to dramatic changes in the optical, electronic and transport properties in their primary molecular structure.²⁶ For example, the absorption spectra of alkyl-substituted polymers are hypsochromically shifted compared to their corresponding alkoxy-substituted counterparts due to less electron-donating nature of alkyl groups and strong steric hindrances.

Thin film morphology of active layer is an important parameter in the design of high-performance polymer-fullerene bulk heterojunction solar cells. The optimized nanoscale morphology of active layer provides good contact between donor and acceptor phases and provide efficient percolating path for both electrons and holes to the corresponding electrodes. Various approaches to improve the solar cell performance by tuning the morphology of the active layer include the use of specific solvents or solvent mixtures for film deposition,²⁷ annealing²⁸ and changing the drying conditions of the active layers as well as the use of additives.²⁹ On the basis of poly(arylene-ethynylene)-alt-poly(arylenevinylene)s PAE-PAV,³⁰ Egbe *et al* were able to demonstrate that the solubilizing alkoxy side chains are a further significant aspect to be considered in the control of the active layer nanomorphology as a result of their hydrophobic nature.^{31,32} High side chain density is disadvantageous in the construct of solar cells, since it dilutes the concentration of the absorbing conjugated species per volume unit and also reduces the interfacial area between donor and acceptor components leading to strong phase

separation and concomitant poor photovoltaic performance. On the other hand, the nature (linear or branched) and length of the alkoxy side chains can be useful in the control of the π - π -stacking of rigid conjugated polymers and their photoluminescent behavior.²³

This chapter is dedicated to a series of anthracene-containing PAE-PAV copolymers. The side chains of these polymers were systematically varied among only linear, only branched and mixed linear and branched in order to tune π - π stacking ability of materials. Polymers with strong tendency to π - π stacking showed well resolved thin film absorption peak, stronger phase separation and better photovoltaic performance than the polymers with less or no intrinsic stacking ability. Thus, a correlation was established between the ability to form π - π stacking, the absorption behaviour, the charge carrier mobility, the active layer nanoscale morphology and the photovoltaic performance.

3a.2 EXPERIMENTAL

3a.2.1 Materials:

Bromine, n-butyllithium solution (2.7 M in n-heptane), ethynyl trimethyl silane, bis (triphenylphosphine) palladium (II)dichloride ($\text{Pd}(\text{PPh}_3)_2\text{Cl}_2$), tetrakis(triphenylphosphine)palladium(0) ($\text{Pd}(\text{PPh}_3)_4$), copper iodide (CuI), diisopropyl amine, potassium *tert*-butoxide, 1-octyl bromide, 2-ethylhexyl bromide and 1-decyl bromide (Aldrich Chemicals) were purchased and were used as received. Potassium hydroxide powder, paraformaldehyde, sodium bromide, potassium fluoride, glacial acetic acid, triethyl phosphite, benzyl bromide, hydroquinone and benzaldehyde (Merck) were purchased and were used as received.

N,N-Dimethylformamide (DMF), dimethyl sulphoxide (DMSO), diethyl ether, tetrahydrofuran (THF) and toluene (Aldrich Chemicals) were purchased and were dried and distilled according to standard procedures and stored under argon.³³ Methanol, chloroform, n-hexane and ethyl acetate (Merck) were purchased and were used as received. If not otherwise specified, solvents or solution were degassed by bubbling with nitrogen 1 h prior to use.

3a.2.2 Characterisation and techniques

Different techniques were used for characterization of monomers and polymers and are listed below.

NMR Spectroscopy: ^1H and ^{13}C NMR spectra of monomers and polymers were recorded using a Bruker-AV spectrometer at operating frequency of 200 MHz, 400 MHz and 500 MHz in CDCl_3 or $\text{DMSO}-d_6$ with tetramethylsilane as an internal standard.

Gel permeation chromatography (GPC): Molecular weights and dispersity values of polymers were determined on Knauer make GPC using chloroform as an eluent at a flow rate of 1 mL min^{-1} at 25°C . Sample concentration was 2 mg mL^{-1} and narrow dispersity polystyrenes were used as calibration standards.

Differential scanning calorimetry (DSC): DSC measurements were carried out on a Mettler DSC 30 with a cell purged with nitrogen. Calibration for temperature and enthalpy changes was performed using an Indium standard. The temperature was varied between 0 and 250°C with a heating/cooling rate of 10 K/min . In total two heating-cooling cycles were performed on each sample.

Thermogravimetric analysis (TGA): TGA was performed on a Mettler TA-300-thermal analyzer operating under nitrogen atmosphere. The samples were heated from 0 to 700°C with a heating rate of 10 K/min .

Wide-angle X-ray scattering (WAXS): WAXS experiments were performed on Bruker HI-STAR, 1024×1024 pixels. The WAXS measurements were performed on the powder samples as well as on aligned fiber samples as described in literature.²⁵

Absorption and emission spectroscopy: The absorption spectra were recorded in dilute chloroform solution ($c \approx 10^{-6} \text{ mol l}^{-1}$) on a Perkin–Elmer UV/VIS-NIR Spectrometer Lambda 19. The absorption spectra of thin films spin coated from chlorobenzene solution were recorded on Varian UV/Vis spectrophotometer and the corresponding emission spectra were recorded on a home-built photoluminescence setup. Thin films were spin coated on glass substrates using chlorobenzene solution (0.6-0.8 wt %).

Cyclic voltammetry (CV): CV was performed with a PA4 polarographic analyzer (Laboratory Instruments, Prague, CZ) with a three-electrode cell. Platinum (Pt) wire electrodes were used both as working and counter electrodes, and a non-aqueous Ag/Ag^+ electrode (Ag in 0.1 M AgNO_3 solution) was used as the reference electrode. CV measurements were made in solutions of 0.1 M tetrabutylammonium hexafluorophosphate (TBAPF6) in acetonitrile under nitrogen atmosphere. Typical scan rates were 20 , 50 and 100 mVs^{-1} , respectively. Polymer thin films were prepared onto Pt

wire electrodes from chlorobenzene solution. All measurements and film preparations were performed in a nitrogen atmosphere within a glove box.

Charge Extraction by Linearly Increasing Voltage (CELIV): The CELIV method was used for the measurement of charge carrier mobility.³⁴ The charge carriers were photogenerated with laser pulse. After delay time of 100 ns, the applied triangle-shaped rising voltage pulse extracts the photogenerated charge carriers toward back electrode and CELIV current transients were measured for all polymers. The carrier mobility was estimated from the extraction maxima.

Atomic Force Microscopy: The surface morphology of the samples was studied by Atomic Force Microscopy (AFM). The AFM images were obtained by means of a Digital Instruments Dimension 3100 microscope working in tapping mode. The samples were prepared by spin-coating from chlorobenzene solution.

3a.2.3 Fabrication and characterization of the photovoltaic cells

Anthracene-containing poly(-p-arylene-ethynylene)-alt-poly(-p-arylene-vinylene) (AnE-PV) as donor and phenyl C61 butyric acid methyl ester (PCBM, Solenne 99.5%) as an acceptor were used. AnE-PV was blended with PCBM in chlorobenzene and stirred at 40 °C for 24-48 h. The donor: acceptor (D: A) ratio was varied from 1:1 to 1:2 (w/w) and total concentrations of (D+A) in chlorobenzene solution was ~10 mg/mL. Indium tin oxide (ITO) coated glass (Merck KgaA, Darmstadt) was used as substrate for device fabrication. A part of ITO layer on glass was etched using aqua regia for selective contacting of back electrode. These glass substrates were thoroughly cleaned by subjecting them to ultrasonication in soap, deionized water, acetone and in isopropyl alcohol. The substrates were then dried for several hours in an oven at 120 °C. A hole transporting layer- PEDOT:PSS (Baytron/Clevios PH H.C. Starck) was spin coated at 3000 rpm for 60 sec. Then the photoactive layer was spin coated with polymer: PCBM blend solution at 4000 rpm for 60 sec. The final thickness of each active layer film was 100~110 nm. Finally, aluminum (~100 nm) was thermally deposited under high vacuum (~10⁻⁷ torr). The active area of solar cells was 0.5 cm² for all the devices. The photovoltaic performance of the devices was measured using a solar spectrum simulator with an air-mass (AM) 1.5 G filter. The intensity of the solar simulator was carefully

calibrated using an AIST-certified silicon photodiode. The current-voltage behavior was measured using a Keithley 2400 SMU.

3a.3 SYNTHESIS

3a.3.1 Synthesis of anthracene-containing dialdehydes

3a.3.1.1 Synthesis of 9,10-bis[(4-formyl-2,5-dioctyloxy)phenylethynyl]anthracene (6a)

3a.3.1.1.1 Synthesis of 2,5-dibromo-hydroquinone (1a)

Into a 250 mL single-necked round bottom flask equipped with an addition funnel and a magnetic stir bar were added hydroquinone (50 g, 0.454 mol) and glacial acetic acid to form a suspension. Bromine (47 mL, 0.454 mol) dissolved in acetic acid (60 mL) was added dropwise into the suspension. The colour of reaction mixture became greenish yellow. The reaction mixture was stirred overnight at room temperature. It was then filtered, washed with water several times and dried to obtain off-white coloured crystals.

Yield: 65.2 g, (54 %)

¹H-NMR (200 MHz, DMSO-*d*₆, δ/ppm): 9.88 (-OH), 7.04 (Ar-H).

3a.3.1.1.2 Synthesis of 1,4-dibromo-2,5-bis(octyloxy)benzene (2a)

Into a 500 mL three-necked round bottom flask equipped with a nitrogen gas inlet and a magnetic stir bar were added KOH (39.76 g, 0.708 mol) and dimethyl sulphoxide (200 mL) to form a suspension. This suspension was degassed for 30 min. To it 2,5-dibromo hydroquinone (20 g, 0.0746 mol) was added and stirred for about 15 minutes. Then octyl bromide (50.4 g, 0.2612 mol) was added and reaction mixture was stirred overnight. Next day the oily suspension was filtered and washed several times with water and allowed to dry. The crude product was recrystallised from acetone.

Yield: 16.40 g (80.1 %)

¹H-NMR (200 MHz, CDCl₃, δ/ppm): 7.09 (s, 2H, Ar-H), 3.95 (t, 4H, -O CH₂-), 1.8 (quintet, 4H, -OCH₂-CH₂-(CH₂)₅-CH₃), 1.48 (m, 4H, -OCH₂-CH₂-CH₂-(CH₂)₄-CH₃), 1.33-1.17 (m, 16H, -OCH₂-CH₂-(CH₂)₅-CH₃), 0.95-0.83 (t, 6H, -CH₃).

3a.3.1.1.3 Synthesis of 4-bromo-2,5-bis(octyloxy)benzaldehyde (3a)

Into a 500 mL three-necked round bottom flask equipped with a nitrogen gas inlet and a magnetic stir bar were added 1,4-dibromo-2,5-bis(octyloxy)benzene (9.8 g, 20

mmol) and dry diethyl ether (300 mL). The solution was degassed under nitrogen and cooled to 0 °C. The solution of butyllithium (2.7 M in heptane, 7.5 mL, 20 mmol) was added dropwise into it. After 15 min, DMF (1.92 mL, 25 mmol) was added dropwise to the mixture. Then the temperature was allowed to rise to 10 °C. The clear solution was kept between 0-10 °C and was stirred for 2 h. Subsequently, a 10% aqueous HCl solution (100 mL) was added to the mixture, and the phases were separated. The organic phase was washed with NaHCO₃ solution, dried over Na₂SO₄ and concentrated on rotary evaporator. The residue was recrystallized from methanol. The pure product was obtained as light-yellow crystals.

Yield: 5.4 g (61 %)

Melting point: 62-63 °C

¹H-NMR (200 MHz, CDCl₃, δ/ppm): 10.42 (s, 1H), 7.32 (s, 1H, Ar-H), 7.23 (s, 1H, Ar-H), 4.08-3.95 (t, 4H, -OCH₂-), 1.90-1.74 (quintet, 4H, -CH₂-), 1.50-1.22 (m, 20H, -CH₂), 0.92 (t, 6 H, -CH₃).

¹³C-NMR (200 MHz, CDCl₃, δ/ppm): 188.92 (-CHO), 155.79 and 149.91 (Ar-OR), 124.36 (Ar-CHO), 120.98 (Ar-Br), 118.53 and 110.72 (Ar-H), 69.90 and 69.53 (-CH₂O-), 31.78, 29.25, 29.20, 29.04, 26.00, 22.64, 14.07 (-(CH₂)₆CH₃).

3a.3.1.1.4 Synthesis of 2,5-bis(octyloxy)-4-[(trimethylsilyl)ethynyl]benzaldehyde (4a)

Into a 250 mL three-necked round bottom flask equipped with a nitrogen gas inlet and a magnetic stir bar was added diisopropylamine (100 mL) and was degassed for 1 h under nitrogen atmosphere. To it 4-bromo-2,5-dioctyloxybenzaldehyde (4 g, 9.06 mmol), Pd(PPh₃)₂Cl₂ (140 mg, 0.199 mmol), and CuI (42.4 mg, 0.213 mmol) were added and reaction mixture was further degassed for 50 min. Trimethylsilylacetylene (893 mg (1.3 mL), 9.09 mmol) was added dropwise to the vigorously stirred suspension. The reaction mixture was then refluxed for 8 h. After cooling, 20 mL toluene was added and the white precipitate of diisopropyl ammonium bromide was filtered off. The solvent was removed under reduced pressure. The residue was purified by column chromatography over silica gel with toluene as an eluent to yield a dark yellow oil.

Yield: 3.2 g (76 %)

¹H-NMR (200 MHz, CDCl₃, δ/ppm): 10.23 (s, 1H, -CHO), 7.07 (s, 1H, Ar-H), 6.85 (s, 1H, Ar-H), 3.88-3.76 (-OCH₂-), 1.69-1.54 (quintet, 4H, -CH₂-), 1.25-0.99 (m, 20 H, -CH₂-), 0.74-0.65 (t, 6 H, -CH₃), 0.01-0.18 (-Si(CH₃)₃).

3a.3.1.1.5 Synthesis of 4-ethynyl-2,5-bis(octyloxy)benzaldehyde (5a)

Into a 250 mL three-necked round bottom flask equipped with a nitrogen gas inlet and a magnetic stir bar were added 2,5-bis(octyloxy)-4-[(trimethylsilyl)ethynyl]benzaldehyde (2.27 g, 4.9 mmol), methanol (28 mL), tetrahydrofuran (55 mL) and degassed under nitrogen for 1 h. Potassium Fluoride (1.14 g, 19.6 mmol) was added at room temperature to the above solution. The reaction mixture was protected from light and was stirred at room temperature for 3 h. The solvent was removed under reduced pressure, residue was dissolved in toluene and washed with water (3 x 50 mL). The organic layer was dried over Na₂SO₄, concentrated under reduced pressure and the residue was purified by column chromatography using toluene:hexane (1:1, v/v) mixture as an eluent to yield orange crystals.

Yield 1.42 g (74 %)

Melting Point: 116-117 °C

IR (KBr, cm⁻¹): 3346 (w, -C≡C-H), 2924 and 2853 (vs, -CH₂- and -CH₃), 2760 (w, -CHO), 1683 (vs, -CHO), 1600 (s, phenyl ring), 1218 (Ar-OR).

¹H-NMR (400 MHz, CDCl₃, δ/ppm): 10.45 (s, 1H, -CHO), 7.31 (s, 1H, Ar-H), 7.09 (s, 1H, Ar-H), 4.03 (t, 4H, -OCH₂-), 3.46 (s, 1H, -C≡C-H), 1.86-1.78 (quintet, 4H, -CH₂-), 1.43-1.15 (m, 20H, -CH₂-), 0.91-0.87 (t, 6 H, -CH₃).

3a.3.1.1.6 Synthesis of 9,10-bis[(4-formyl-2,5-dioctyloxy)phenylethynyl] anthracene (6a)

Into a 250 mL three-necked round bottom flask equipped with a nitrogen gas inlet, a reflux condenser and a magnetic stir bar were added 9,10-dibromoanthracene (618 mg, 1.84 mmol), 4-ethynyl-2,5-dioctyloxybenzaldehyde (1.42 g, 3.7 mmol), toluene (100 mL), diisopropylamine (50 mL) and degassed for 0.5 h in nitrogen atmosphere. Pd(PPh₃)₄ (85.5 mg, 7.4 x 10⁻² mmol, 4 mol %) and CuI (14.5 mg, 7.4 x 10⁻² mmol, 4 mol %) were added into the reaction mixture and degassed for 0.5 h. Then the reaction mixture was refluxed (80 °C) for 24 h in an argon atmosphere. After cooling to room temperature, the precipitated diisopropylammonium bromide was filtered off and the solvent was distilled

off under reduced pressure. The residue was subjected to column chromatography using toluene: hexane (1:1, v/v) mixture as an eluent to yield red colored pure product.

Yield: 1.13 g (65 %)

Melting point: 138-142 °C.

MS (70 eV ESI with H₂O): m/z = 947 (M⁺⁺ + 1, 100%), 835 (10%), 535 (5%), 158 (30%).

IR (KBr, cm⁻¹): 3056 (w, C_{aryl}-H), 2929 and 2856 (vs, CH₂ and CH₃), 2756 (w, CHO), 2188 (w, disubst -C≡C-), 1682 (s, CHO), 1600 (s, -C=C_{aryl}-), 1219 (vs, C_{aryl}-OR).

¹H-NMR (400 MHz, CDCl₃, δ/ppm): 10.51 (s, 2H, CHO), 8.81 (d, 4H, C_{anthracenyl}-H), 7.66 (d, 4H, C_{anthracenyl}-H), 7.42 (s, 2H, Ar-H), 7.31 (s, 2H, Ar-H), 4.17 (t, 8H, -OCH₂-), 2.0-1.87 (m, 8H, -CH₂-), 1.30-1.20 (m, 40H, -CH₂-), 0.95- 0.87 (m, 12H, -CH₃).

¹³C-NMR (200 MHz, CDCl₃, δ/ppm): 189.11 (-CHO), 155.60 and 154.01 (C_{aryl}-OR), 127.44 (C_{anthracenyl}-C=), 132.25 and 126.92 (C_{anthracenyl}-H), 125.15 (C_{aryl}-CHO), 120.21 (C_{anthracenyl}-C≡C-), 118.88 (C_{aryl}-C≡C-), 117.04 and 109.36 (C_{aryl}), 99.04 and 94.61 (-C≡C-), 69.47 and 69.35 (-OCH₂-), 31.79, 31.76, 29.52, 29.42, 29.33, 29.22, 26.10, 26.04, 22.64, 22.59, (-(CH₂)₆-), 14.07 (-CH₃).

3a.3.1.2 9,10-Bis{[2,5-di(2-ethylhexyloxy)-4-formyl]phenyl}-ethynyl}anthracene (6b)

3a.3.1.2.1 Synthesis of 2,5-bis(2-ethylhexyloxy)-4-ethynylbenzaldehyde (5b) (a precursor in the synthesis of 6b)

2,5-Bis(2-ethylhexyloxy)-4-ethynylbenzaldehyde was synthesized by using the procedure described in section 3a.3.1.1.5, starting with hydroquinone, following the same sequence of reactions- bromination, alkylation, mono-formylation, ethynylation and desilylation.

Yield: (4.2 g, 79 %)

¹H-NMR (400 MHz, CDCl₃, δ/ppm): 10.45 (s, 1H -CHO), 7.30 (s, 1H, Ar-H), 7.10 (s, 1H, Ar-H), 3.90 (m, 4H, -OCH₂), 3.46 (s, 1H, -C≡CH), 1.90 – 1.65 (m, 2H, -CH₂), 1.58 – 1.11 (m, 16H, -CH₂), 1.05 – 0.78 (m, 12H).

¹³C-NMR (100 MHz, CDCl₃, δ/ppm): 189.0 (CHO); 155.33, 155.21 (C_{aryl}-OR), 125.59, 118.65, 118.10, 109.81 (C_{aryl}), 80.90, 79.67 (-C≡C-), 71.92, 71.46 (-OCH₂-), 39.20 (-CH-), 30.55, 29.02, 23.01, 22.97 (-CH₂-), 14.08, 14.04 (CH₃-hexyl), 11.14 (CH₃-ethyl).

3a.3.1.2.2 Synthesis of 9,10-bis{[2,5-di(2-ethylhexyloxy)-4-formyl]phenyl}-ethynyl}anthracene (6b)

The synthesis of 9,10-bis{[2,5-di(2-ethylhexyloxy)-4-formyl]phenyl}-ethynyl}anthracene (**6b**) was carried out under the same reaction conditions as described in the section 3a.3.1.1 by using 2,5-bis(2-ethylhexyloxy)-4-ethynylbenzaldehyde (**5b**).

Yield: (1.6 g, 78 %)

IR (KBr, cm^{-1}): 3059 (w, $\text{C}_{\text{aryl}}\text{-H}$), 2957, 2925 and 2857 (vs, $\text{-CH}_2\text{-}$ and -CH_3), 2190 (w, disubst. $\text{-C}\equiv\text{C-}$), 1676 (vs, -CHO), 1600 (vs, $\text{-C}=\text{C}_{\text{aryl}}\text{-}$), 1382 (vs, -CH_3), 1281 and 1207 (vs, $\text{C}_{\text{aryl}}\text{-OR}$).

$^1\text{H-NMR}$ (400 MHz, CDCl_3 , δ/ppm): 10.52 (s, 2H, CHO), 8.82 (d, 4H, $\text{C}_{\text{anthracenyl}}\text{-H}$), 7.67 (d, 4H, $\text{C}_{\text{anthracenyl}}\text{-H}$), 7.43 (s, 2H, $\text{C}_{\text{aryl}}\text{-H}$), 7.32 (s, 2H, $\text{C}_{\text{aryl}}\text{-H}$), 4.07 (t, 8H, $\text{-OCH}_2\text{-}$), 2.04- 1.85 (m, 4H, $\text{-CH}_2\text{-}$), 1.32-1.22 (m, 32H, $\text{-CH}_2\text{-}$), 0.95- 0.88 (m, 24H, -CH_3).

$^{13}\text{C-NMR}$ (100 MHz, CDCl_3 , δ/ppm): 189.09 (-CHO), 155.67 and 153.99 ($\text{C}_{\text{aryl}}\text{-OR}$), 127.44 ($\text{C}_{\text{anthracenyl}}\text{-C=}$), 132.18 and 126.95 ($\text{C}_{\text{anthracenyl}}\text{-H}$), 125.07 ($\text{C}_{\text{aryl}}\text{-CHO}$), 120.16 ($\text{C}_{\text{anthracenyl}}\text{-C}\equiv\text{C-}$), 118.88 ($\text{C}_{\text{aryl}}\text{-C}\equiv\text{C-}$), 117.11 and 109.29 (C_{aryl}), 98.98 and 94.32 ($\text{-C}\equiv\text{C-}$), 71.57 and 71.52 ($\text{-OCH}_2\text{-}$), 39.54, 39.41 (-CH-); 30.64, 30.24, 29.11, 28.95, 24.00, 23.67, 23.00 ($\text{-CH}_2\text{-}$), 14.08, 13.99 ($\text{-CH}_3\text{-hexyl}$), 11.24, 10.90 ($\text{-CH}_3\text{-ethyl}$).

3a.3.1.3 Synthesis of 9,10-bis[(4-formyl-2-(2'-ethylhexyloxy)-5-methoxy)phenylethynyl]anthracene (**6c**)

3a.3.1.3.1 Synthesis of 5-(2-ethylhexyloxy)-4-ethynyl-2-methoxybenzaldehyde (**5c**) (a precursor in the synthesis of **6c**)

5-(2-Ethylhexyloxy)-4-ethynyl-2-methoxybenzaldehyde was synthesized by using the procedure described in the section 3a.3.1.1, starting with 4-methoxy phenol, following the same sequence of reactions- iodination, alkylation, mono-formylation, ethynylation and de-silylation.

Yield: 8.0 g (98 %).

$^1\text{H-NMR}$ (400 MHz, CDCl_3 , δ/ppm): 10.41 (s, 1H, CHO), 7.30 (s, 1H, Ar-H), 7.07 (s, 1H, Ar-H), 3.90 (d, 2H, $\text{-OCH}_2\text{-}$), 3.89 (s, 3H, -OCH_3), 3.45 (s, 1H, $\text{-C}\equiv\text{CH}$), 1.76 (m, 1H, -CH-), 1.58-1.32 (m, 8H, $\text{-CH}_2\text{-}$), 0.93 (t, 6H, -CH_3).

$^{13}\text{C-NMR}$ (100 MHz, CDCl_3 , δ/ppm): 188.72 (CHO), 155.20, 154.35 (Ar-OR), 124.82, 118.73, 116.93, 109.79 (Ar), 84.32, 79.01 ($\text{C}\equiv\text{C}$), 71.58 ($\text{-OCH}_2\text{-}$), 56.88 (-OCH_3), 38.96 (-CH-), 30.15, 28.71, 23.58, 22.70 ($\text{-CH}_2\text{-}$), 13.73 (-CH_3 ethyl), 10.83 (-CH_3 hexyl).

3a.3.1.3.2 Synthesis of 9,10-bis[(4-formyl-2-(2'-ethylhexyloxy)-5-methoxy)phenylethynyl]anthracene (6c)

The synthesis of 9,10-bis[(4-formyl-2-(2'-ethylhexyloxy)-5-methoxy)phenylethynyl]anthracene was carried out under the same reaction conditions as described in the section 3a.3.1.1 by using 5-(2-ethylhexyloxy)-4-ethynyl-2-methoxybenzaldehyde (5c).

Yield: 1.52 g (74 %).

¹H-NMR (200 MHz, CDCl₃, δ/ppm): 10.49 (s, 2H, CHO), 8.83-8.76 (m, 4H, C_{anthracenyl}-H), 7.70 - 7.63 (m, 4H, C_{anthracenyl}-H), 7.43 (s, 2H, C_{aryl}-H), 7.32 (s, 2H, C_{aryl}-H), 4.06 (d, 4H, -OCH₂-), 4.02 (s, 6H, -OCH₃), 1.97 (m, 2H, -CH-), 1.78 - 1.18 (m, 16H, -CH₂-), 0.95 (t, 6H, -CH₃-ethyl), 0.82 (t, 6H, -CH₃-hexyl).

¹³C-NMR (100 MHz, CDCl₃, δ/ppm): 189.01 (CHO), 155.81, 154.23 (C_{aryl}-OR), 132.22, 127.41, 126.98, 125.02, 120.16, 118.83, 116.34, 109.69 (C_{aryl}), 98.95, 94.39 (C≡C), 71.70 (-OCH₂), 56.39 (-OCH₃), 39.49 (-CH-), 30.30, 28.99, 23.74, 23.01 (-CH₂-), 13.97 (-CH₃-ethyl), 10.93 (-CH₃-hexyl).

3a.3.2 Synthesis of bisphosphonates

Typical synthetic procedure of bisphosphonates is exemplified by synthesizing 2,5-bis((2-ethylhexyloxy)-p-xylylene-bis(diethylphosphonate) (14b). The synthesis involves 3 steps starting with hydroquinone as follows-

3a.3.2.1 Synthesis of 2,5-bis((2-ethylhexyloxy)-p-xylylene-bis(diethylphosphonate) (14b)

3a.3.2.1.1 Synthesis of 1,4-bis(2-ethylhexyloxy)benzene (12b)

Into a 250 mL three-necked round bottom flask equipped with a nitrogen gas inlet and a magnetic stir bar were added KOH powder (20.4 g, 0.36 mol) and dry DMSO (100 mL) to form a suspension which was degassed for 1 h. Hydroquinone (10.00 g, 0.09 mol) and 2-ethylhexyl bromide (36.9 g, 0.18 mol) were then added into the suspension. The reaction mixture was stirred for 3 h at room temperature and finally poured into 500 mL ice water. The organic layer was collected and the aqueous layer was extracted with hexane (3 x200 mL). The combined organic layers were dried over Na₂SO₄, and the solvent was evaporated to give a yellow oil. The impure oily product was then purified by vacuum distillation to yield a colourless liquid.

Yield: 24.0 g, (78 %).

Boiling point: 165 °C (0.05 Torr)

¹H-NMR (400 MHz, CDCl₃, δ/ppm): 6.89 (4H, s, Ar-H), 3.86 (4H, d, -OCH₂-), 1.76 (2H, m, -CH-), 1.54-1.34 (16H, m, -CH₂-), 0.98 (12H, t, -CH₃).

3a.3.2.1.2 Synthesis of 1,4-bis-bromomethyl-2,5-bis-(2-ethylhexyloxy)-benzene (13b)

Into a 250 mL three-necked round bottom flask equipped with a reflux condenser, an addition funnel and a magnetic stir bar were added 1,4-bis((2-ethylhexyl)oxy)benzene (12 g, 0.036 mol), paraformaldehyde (15.14 g, 0.504 mol), NaBr (18.52 g, 0.18 mol) and glacial acetic acid (100 mL) to form a suspension. The reaction mixture was heated at 80 °C for 30 min to get homogenous mixture. Then, a mixture of concentrated sulfuric acid (18 mL) and glacial acetic acid (18 mL) was added dropwise and the reaction mixture was stirred at 80 °C for 4 h. After the reaction was cooled, the precipitate was filtered off, washed several times with water, and recrystallized from hexane to obtain white crystalline solid product.

Yield: 13.3 g (91 %).

Melting point: 63-64 °C.

¹H-NMR (200 MHz, CDCl₃, δ/ppm): 6.86 (2H, s, Ar-H), 4.53 (4H, s, Ar-CH₂-Br), 3.90 (4H, d, -OCH₂-), 1.76 (2H, m, -CH-), 1.56-1.32 (16H, m, -CH₂-), 0.95 (12H, t, -CH₃).

3a.3.2.1.3 Synthesis of 2,5-bis((2-ethylhexyl)oxy)-p-xylylene-bis(diethylphosphonate) (14b)

Into a 50 mL single-necked round bottom flask equipped with distillation condenser and a magnetic stir bar were added triethyl phosphite (12.41 g, 74.7 mmol) and 1,4-bis-bromomethyl-2,5-bis-(2-ethyl-hexyloxy)-benzene (13 g, 24.9 mmol). The reaction mixture was allowed to heat slowly to 160 °C, and the evolving ethyl bromide was distilled off simultaneously. After 5 h, vacuum was applied for 1 h at 180 °C to remove the remaining triethyl phosphite. The resulting oil was dried under vacuum.

Yield: 15.7 g (99 %).

Melting point: 18-20°C.

¹H-NMR (200 MHz, CDCl₃, δ/ppm): 6.94 (2H, s, Ar-H), 3.95 (8H, m, -OCH₂- on phosphonate group), 3.81 (4H, d, -OCH₂- on ethylhexyl side chain), 3.22 (4H, d, Ar-CH₂-

P), 1.75-1.21 (18H, m, -CH₂- and -CH-), 1.16 (12H, -CH₃ on phosphonate group), 0.87 (12H, -CH₃ on ethylhexyl side chain).

3a.3.2.2 Synthesis of 2,5-dioctyloxy-p-xylylene-bis(diethylphosphonate) (14a)

3a.3.2.2.1 Synthesis of 1,4-dioctyloxybenzene (12a)

The synthesis of 1,4-dioctyloxybenzene was carried out under the same reaction conditions as described in the section 3a.3.2.1.1 by using hydroquinone and 1-bromooctane.

Yield: 50.0 g (76 %).

Melting point: 48-51 °C.

¹H-NMR (400 MHz, CDCl₃, δ/ppm): 6.80 (4H, s, Ar-H), 3.86 (4H, t, -OCH₂-), 1.76 (4H, m, -CH₂-), 1.54-1.34 (20H, m, -CH₂-), 0.96 (6H, t, -CH₃).

3a.3.2.2.2 Synthesis of 1,4-bis(bromomethyl)-2,5-dioctyloxybenzene (13a)

The synthesis of 1,4-bis(bromomethyl)-2,5-dioctyloxybenzene was carried out under the same reaction conditions as described in the section 3a.3.2.1.2 by using 1,4-dioctyloxybenzene.

Yield: 26 g (85 %),

Melting point: 83-84 °C.

¹H-NMR (200 MHz, CDCl₃, δ/ppm): 6.77 (2H, s, Ar-H), 4.50 (4H, s, Ar-CH₂-Br), 3.97 (4H, t, -OCH₂-), 1.76 (4H, m, -CH₂-), 1.46-1.29 (20H, m, -CH₂-), 0.92 (6H, t, -CH₃).

3a.3.2.2.3 Synthesis of 2,5-dioctyloxy-p-xylylene-bis(diethylphosphonate) (14a)

The synthesis of 2,5-dioctyloxy-p-xylylene-bis(diethylphosphonate) was carried out under the same reaction conditions as described in the section 3a.3.2.1.3 by using 1,4-bis(bromomethyl)-2,5-dioctyloxybenzene. The product was purified by recrystallisation with diethyl ether.

Yield: 25 g (76 %).

Melting point: 50-52 °C.

¹H-NMR (200 MHz, CDCl₃, δ/ppm): 6.84 (2H, s, Ar-H), 3.95 (8H, m, -OCH₂- on phosphonate group), 3.84 (4H, t, -OCH₂- on octyl side chain), 3.15 (4H, d, Ar-CH₂-P), 1.21-1.75 (24H, m, -CH₂-), 1.16 (12H, -CH₃ on phosphonate group), 0.87 (6H, -CH₃ on octyl side chain).

3a.3.2.3 Synthesis of 2,5-didecyloxy-p-xylylene-bis(diethylphosphonate) (14d)

3a.3.2.3.1 Synthesis of 1,4-didecyloxybenzene (12d)

The synthesis of 1,4-didecyloxybenzene was carried out under the same reaction conditions as described in the section 3a.3.2.1.1 by using 1-bromodecane.

Yield: 51.5 g, (90 %).

Boiling point: 64-66 °C.

¹H-NMR (200 MHz, CDCl₃, δ/ppm): 6.81 (4H, s, Ar-H), 3.88 (4H, t, -OCH₂-), 1.76 (4H, m, -CH₂-), 1.54-1.16 (28H, m, -CH₂-), 0.90 (6H, t, -CH₃).

3a.3.2.3.2 Synthesis of 1,4-bis(bromomethyl)-2,5-didecyloxybenzene (13d)

The synthesis of 1,4-bis(bromomethyl)-2,5-didecyloxybenzene was carried out under the same reaction conditions as described in the section 3a.3.2.1.2 by using 1,4-didecyloxybenzene.

Yield: 12.1 g, (85 %).

Boiling point: 90-92 °C.

¹H-NMR (200 MHz, CDCl₃, δ/ppm): 6.80 (2H, s, Ar-H), 4.51 (4H, s, Ar-CH₂-Br), 3.96 (4H, t, -OCH₂-), 1.75 (4H, m, -CH₂-), 1.52-1.21 (28H, m, -CH₂-), 0.88 (6H, t, -CH₃).

3a.3.2.3.3 Synthesis of 2,5-didecyloxy-p-xylylene-bis(diethylphosphonate) (14d)

The synthesis of 2,5-didecyloxy-p-xylylene-bis(diethylphosphonate) was carried out under the same reaction conditions as described in the section 3a.3.2.1.3 by using 1,4-bis(bromomethyl)-2,5-didecyloxybenzene. The product was purified by recrystallisation from diethyl ether.

Yield: 6.94 g (97 %).

Melting point: 54-55 °C.

¹H-NMR (200 MHz, CDCl₃, δ/ppm): 6.88 (2H, s, Ar-H), 3.99 (8H, m, -OCH₂- on phosphonate group), 3.88 (4H, t, -OCH₂- on decyl side chain), 3.19 (4H, d, Ar-CH₂-P), 1.78-1.18 (32 H, m, -CH₂-), 1.16 (12H, -CH₃ on phosphonate group), 0.87 (6H, -CH₃ on decyl side chain).

3a.3.2.4 Synthesis of 5-(2-ethylhexyloxy)-2-methoxy-p-xylylenebis(diethylphosphonate) (14c)**3a.3.2.4.1 Synthesis of 1-(2-ethylhexyloxy)-4-methoxybenzene (7)**

Into a 250 mL three-necked round bottom flask equipped with a nitrogen gas inlet and a magnetic stir bar were added KOH powder (44.89 g, 800 mmol) and dry DMSO

(300 mL) to form a suspension which was degassed for 1 h. 4-Methoxyphenol (20.0 g, 161 mmol) was added in one portion and 2-ethylhexylbromide (42 mL, 243.6 mmol) was added dropwise over a period of 30 min to the solution. The reaction mixture was stirred at room temperature for 60 h and finally poured into ice water (1000 mL). The organic layer was collected and the aqueous layer was extracted with hexane. The combined organic layers were dried over Na₂SO₄ and the solvent was evaporated to give an orange oil. Distillation under reduced pressure yielded a colorless liquid.

Yield: (34.97 g, 92 %).

¹H-NMR (200 MHz, CDCl₃, δ/ppm): 6.86 (s, 2H, Ar-H), 6.87 (s, 2H, Ar-H), 3.81 (d, 2H, -OCH₂), 3.82 (s, 3H, -OCH₃), 1.74 (heptet, 1H, -CH), 1.62–1.33 (m, 8H, -CH₂), 0.96 (t, 6H, -CH₃).

3a.3.2.4.2 1,4-Bis(bromomethyl)-5-(2-ethylhexyloxy)-2-methoxybenzene (13c)

Into a 250 mL three-necked round bottom flask equipped with a nitrogen gas inlet, a reflux condenser and a magnetic stir bar were added 1-(2-ethylhexyloxy)-4-methoxybenzene (25 g, 0.105 mol), paraformaldehyde (15 g, 0.5 mol), acetic acid (50 mL), and 30% HBr in acetic acid (50 mL). The reaction mixture was degassed under nitrogen for 30 min and then was heated at 80 °C for 4 h. After cooling to room temperature, the reaction mixture was diluted with chloroform (100 mL), washed with water and aqueous NaHCO₃. The chloroform extract was dried over Na₂SO₄ and concentrated under reduced pressure. The product was purified by recrystallisation from hexane.

Yield: 35.5 g (80 %),

Melting point: 81-82 °C.

¹H-NMR (200 MHz, CDCl₃, δ/ppm): 6.86 (s, 2H, Ar-H), 4.53 (s, 4H, Ar-CH₂-Br), 3.86 (s, 5H, -OCH₂, -OCH₃), 1.8-0.8 (m, 15H, CH₃).

¹³C-NMR (200 MHz, CDCl₃, δ/ppm): 151.09, 151.04, 127.54, 127.40, 114.37, 113.85, 71.02, 56.32, 39.68, 30.72, 29.19, 28.76, 28.70, 24.10, 23.12, 14.17, 11.33.

3a.3.2.4.3 Synthesis of 5-(2-ethylhexyloxy)-2-methoxy-p-xylylenebis(diethylphosphonate) (14c)

The synthesis of 14c was carried out under the same reaction conditions as described in the section 3a.3.2.1.3 by using 13c.

Yield: 5.60 g (90 %).

¹H-NMR (200 MHz, CDCl₃, δ/ppm): 6.87 (2H, s, Ar-H), 3.95 (8H, m, -OCH₂- on phosphonate group), 3.84 (4H, t, -OCH₂, -OCH₃), 3.19 (4H, d, Ar-CH₂-P), 1.77-1.19 (8H, m, -CH₂-), 1.16 (12H, -CH₃ on phosphonate group), 0.87 (6H, -CH₃ on 2-ethylhexyl chain).

3a.3.3 Synthesis of AnE-PV polymers

3a.3.3.1 Synthesis of polymer AnE-PV_{ab}: Typical procedure

Into a 100 mL three-necked round bottom flask equipped with a nitrogen gas inlet, a reflux condenser and a magnetic stir bar were added 9,10-bis[(4-formyl-2,5-dioctyloxy)phenylethynyl]anthracene (400 mg, 0.42 mmol), 1,4-bis-bromomethyl-2,5-bis-(2-ethylhexyloxy)-benzene (240 mg, 0.42 mmol) and dry toluene (40 mL). The reaction mixture was stirred vigorously under nitrogen atmosphere and was heated to reflux and then potassium-*tert*-butoxide (188 mg, 1.68 mmol) was added into it. After the addition of potassium-*tert*-butoxide the solution became successively darker and thicker. The reaction mixture was allowed to stir vigorously under reflux in nitrogen atmosphere for 3 h. Then the reaction mixture was cooled down, 15 mL toluene was added, and the reaction was quenched with 5 % aqueous HCl. The organic phase was separated and washed several times with distilled water until the aqueous phase became neutral. The remaining water was removed by heating using a Dean-Stark apparatus. The resulting toluene solution was filtered, evaporated under vacuum to small amount, and precipitated in methanol. The polymer was filtered and Soxhlet extracted with methanol/diethyl ether for 10 h, dissolved in small amount of toluene, reprecipitated in methanol, and dried under vacuum. Polymer was obtained as a purple-red solid.

Yield: 559 mg (85 %).

IR (KBr, cm⁻¹): 3057 (w, Ar-H), 2923 and 2852 (s, CH₃ and -CH₂-), 2184 (w, disubstituted -C≡C-), 1597 (w, aryl-C=C-), 1203 (s, Ar-OR), 971 (m, trans -CH=CH-).

¹H-NMR (200 MHz, CDCl₃, δ/ppm): 8.84, 7.60-7.51, 7.19 and 6.91-6.84 (18H, -arylene and vinylene protons), 4.20-3.62 (12H, m, -OCH₂-), 2.05-0.84 (90H, m, -CH₂- and -CH₃).

¹³C-NMR (200 MHz, CDCl₃, δ/ppm): 154.56, 150.54, 132.07, 127.59, 126.47, 116.95 (arylene and vinylene C's), 99.45 (-C≡C-), 69.71, 69.55, 69.35 (-OCH₂-), 39.21 (-CH-), 31.89, 31.87, 29.70, 29.53, 29.47, 29.34, 29.29, 26.22, 22.66, 14.07(-CH₂- and -CH₃).

3a.3.3.2 Synthesis of polymer AnE-PVad:

The synthesis of AnE-PVad was carried out under the same reaction conditions as described in the section 3a.3.3.1 by using 9,10-bis[(4-formyl-2,5-dioctyloxy)phenylethynyl]anthracene (6a) and 2,5-didecyloxy-p-xylylene-bis(diethylphosphonate) (14d).

Yield: 300 mg, 90 %.

IR (KBr, cm^{-1}): 3057 (w, Ar-H), 2921, 2852 (s, $-\text{CH}_2-$ and $-\text{CH}_3$), 2186 (w, disubstituted $\text{C}\equiv\text{C}-$), 1595 (w, aryl- $\text{C}=\text{C}-$), 1200 (vs, Ar-OR), 967 (s, trans $-\text{CH}=\text{CH}-$).

^1H NMR (200 MHz, CDCl_3 , δ/ppm): 8.87, 7.64-7.58 and 6.87 (18H, arylene and vinylene H's); 4.12-3.70 (12H, m, $-\text{OCH}_2-$), 1.92-0.85 (98H, m, $-\text{CH}_2-$ and $-\text{CH}_3$).

3a.3.3.3 Synthesis of polymer AnE-PVba:

The synthesis of AnE-PVba was carried out under the same reaction conditions as described in the section 3a.3.3.1 by using 9,10-bis[(4-formyl-2,5-bis(2-ethylhexyloxy)phenylethynyl]anthracene (6b) and 2,5-dioctyloxy-p-xylylene-bis(diethylphosphonate) (14a).

Yield: 710 mg (53 %).

IR (KBr, cm^{-1}): 3058 (w, Ar-H), 2955, 2923 and 2856 (s, $-\text{CH}_2-$ and $-\text{CH}_3$), 2185 (w, disubst.- $\text{C}\equiv\text{C}-$), 1620 and 1598 (w, aryl- $\text{C}=\text{C}-$), 1200 (s, Ar-OR), 968 (s, trans $-\text{CH}=\text{CH}-$).

^1H -NMR (200 MHz, CDCl_3 , δ/ppm): 8.83, 7.58-7.53, 7.18 and 6.86-6.80 (18H, arylene and vinylene H's); 4.05-3.62 (12H, m, $-\text{OCH}_2-$); 1.82-0.89 (90H, m, $-\text{CH}_2-$ and $-\text{CH}_3$).

^{13}C -NMR (200 MHz, CDCl_3 , δ/ppm): 154.11, 150.56, 150.09, 131.57, 128.65, 126.02, 118.35, 116.43, 111.96, 109.08 (arylene and vinylene carbons), 99.48 ($-\text{C}\equiv\text{C}-$), 71.41, 71.20, 70.96, 68.94, 68.84 68.63 ($-\text{OCH}_2-$), 39.16 ($-\text{CH}-$), 30.47, 30.19, 29.95, 29.17, 28.71, 28.59, 28.34 25.71, 23.56, 23.31, 22.68, 22.52, 21.58 ($-\text{CH}_2-$), 13.65, 13.47, 11.63($-\text{CH}_3$).

3a.3.3.4 Synthesis of polymer AnE-PVbb:

The synthesis of AnE-PVbb was carried out under the same reaction conditions as described in the section 3a.3.3.1 by using 9,10-bis{[2,5-di(2-ethylhexyloxy)-4-formyl]phenyl}-ethynyl}anthracene (6b) and 2,5-di(2-ethylhexyloxy)-p-xylylene-bis(diethylphosphonate) (14b)

Yield: 635 mg (94 %).

IR (KBr, cm^{-1}): 3058 (w, Ar-H), 2956, 2923, 2870 and 2857 (s, $-\text{CH}_2-$ and $-\text{CH}_3$), 2186 (w, disubstituted- $\text{C}\equiv\text{C}-$), 1620 and 1598 (w, aryl- $\text{C}=\text{C}-$), 1200 (vs, Ar-OR), 967 (s, trans- $\text{CH}=\text{CH}-$).

$^1\text{H-NMR}$ (200 MHz, CDCl_3 , δ/ppm): 8.86-8.82, 7.63-7.56 and 6.85-6.81 (18H, arylene and vinylene H's), 4.05-3.63 (12H, $-\text{OCH}_2-$), 2.05-0.84 (90H, $-\text{CH}_2-$ and $-\text{CH}_3$).

3a.3.3.5 Synthesis of polymer AnE-PVcc:

The synthesis of AnE-PVcc was carried out under the same reaction conditions as described in the section 3a.3.3.1 by using 9,10-bis[(4-formyl-2-(2'-ethylhexyloxy)-5-methoxy)phenylethynyl]anthracene (6c) and 5-(2-ethylhexyloxy)-2-methoxy-p-xylylenebis (diethylphosphonate) (14c)

Yield: 860 mg (86 %).

IR (KBr, cm^{-1}): 3056 (w, Ar-H), 2954, 2924 and 2857 (s, $-\text{CH}_2-$ and $-\text{CH}_3$), 2186 (w, disubstituted $-\text{C}\equiv\text{C}-$), 1594 (w, aryl- $\text{C}=\text{C}-$), 1200 (vs, Ar-OR), 965 (s, trans- $\text{CH}=\text{CH}-$).

$^1\text{H-NMR}$ (200 MHz, CDCl_3 , δ/ppm): 8.84 and 7.64 (8H, $\text{C}_{\text{anthracene-H}}$); 6.93-6.79 (8H, phenylene and vinylene H's); 4.01 (6H, $-\text{OCH}_2-$); 3.59-3.54 (9H, $-\text{OCH}_3$), 2.00-0.85 (45H, $-\text{CH}_2-$ and $-\text{CH}_3$).

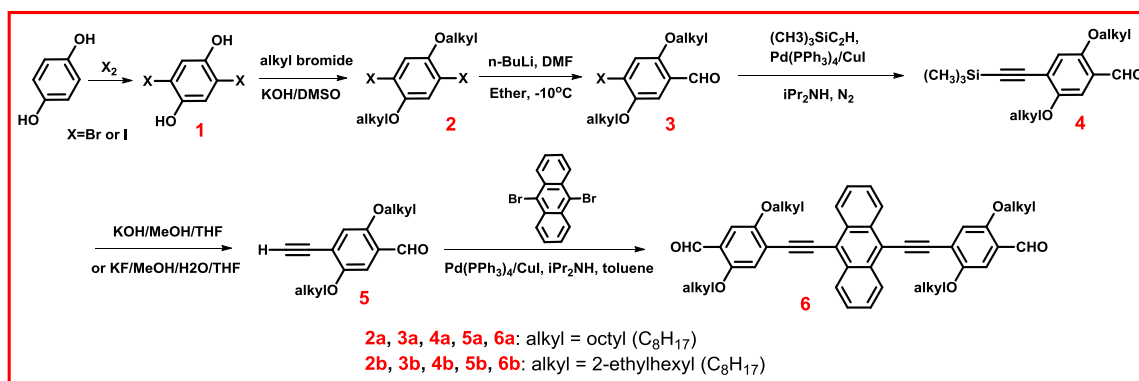
3a.4 RESULTS AND DISCUSSION

3a.4.1 Synthesis of dialdehydes

3a.4.1.1 Synthesis of dialdehydes bearing symmetric side chains on phenyl rings (6a, 6b)

The six-step route for the synthesis of symmetric anthracene-containing dialdehydes (6) from hydroquinone is depicted in **Scheme 3a.1**. Hydroquinone was first brominated with bromine in acetic acid to yield compound **1** which on alkylation with corresponding alkyl bromide under basic conditions gave compound **2**. Compound **2** underwent Bouveault formylation^{35,36} in the presence of n-butyllithium and N,N-dimethylformamide in ether to yield monoformylated compound **3**. Small amount of bisformylated product was separated by flash column chromatography using toluene:hexane (1:1, v/v) mixture as an eluent. Compound **4** was obtained by reaction of **3** with trimethylsilylacetylene in diisopropylamine, in the presence of catalysts

$\text{Pd}(\text{PPh}_3)_2\text{Cl}_2$ and CuI . Subsequent desilylation of **4** with KF in THF: methanol mixture afforded compound **5** along with Glaser coupling product (diyne) which was separated by column chromatography using toluene:hexane (1:1, v/v) mixture as an eluent. The target monomer i.e. anthracene-containing dialdehyde (**6**) was obtained by Heck–Cassar–Sonogashira–Hagihara Pd-catalysed cross coupling reaction^{37,38} of compound **5** with 9,10-dibromoanthracene. The dialdehyde was purified by column chromatography using toluene:hexane (1:1, v/v) mixture as an eluent. The chemical structures of all the intermediates were confirmed by IR, ^1H and ^{13}C NMR spectroscopy and HR-MS analysis.



Scheme 3a.1 Synthesis of dialdehydes bearing symmetric side chains on phenyl rings.

^1H -NMR spectrum of dialdehyde **6a** is presented in **Figure 3a.1**. The peak due to aldehyde group was observed at 10.51 δ ppm. The presence of anthracene protons was confirmed by the appearance of two doublets at 8.81 δ ppm and 7.66 δ ppm. The aromatic protons on phenyl ring were observed as singlets at 7.42 δ ppm and 7.31 δ ppm. The CH_2 proton, adjacent to O, on octyloxy side chain was observed as a triplet at 4.17 δ ppm. The remaining CH_2 protons appeared in the range 1.15–2.04 δ ppm. Methyl protons appeared at 0.91 δ ppm.

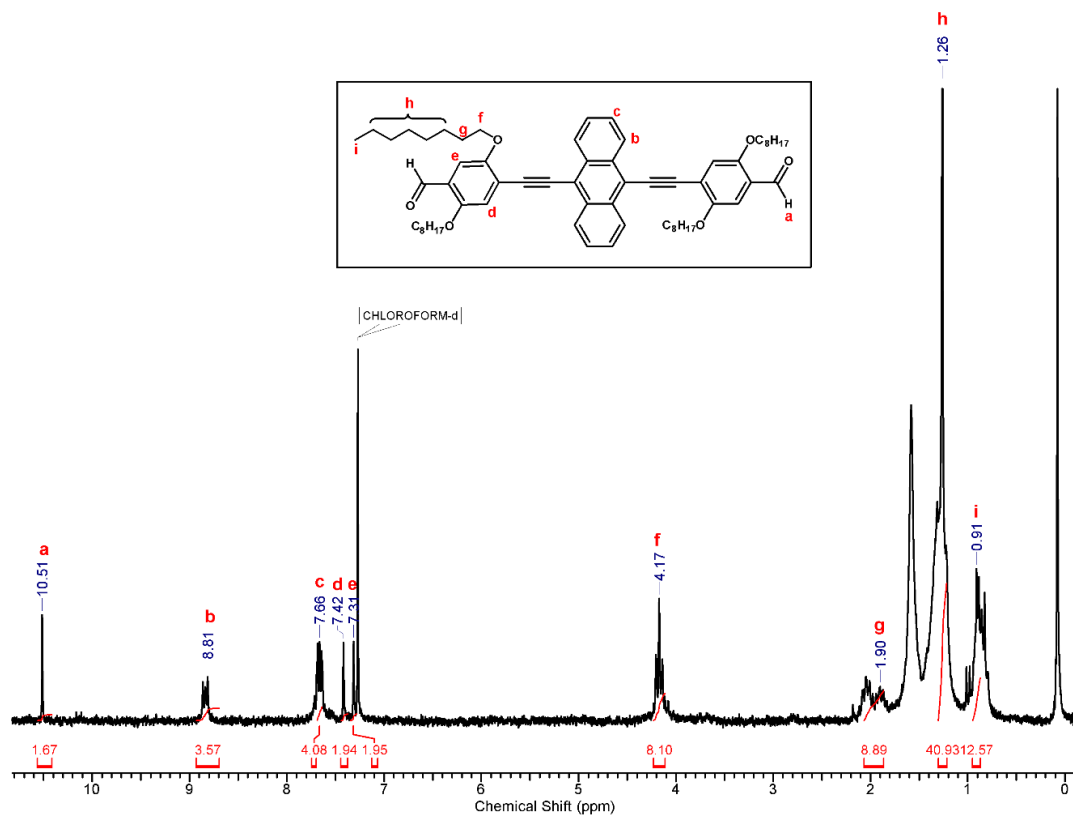


Figure 3a.1 ¹H-NMR spectrum (CDCl₃) of 9,10-bis[4-formyl-2,5-dioctyloxy)phenylethynyl]anthracene (6a).

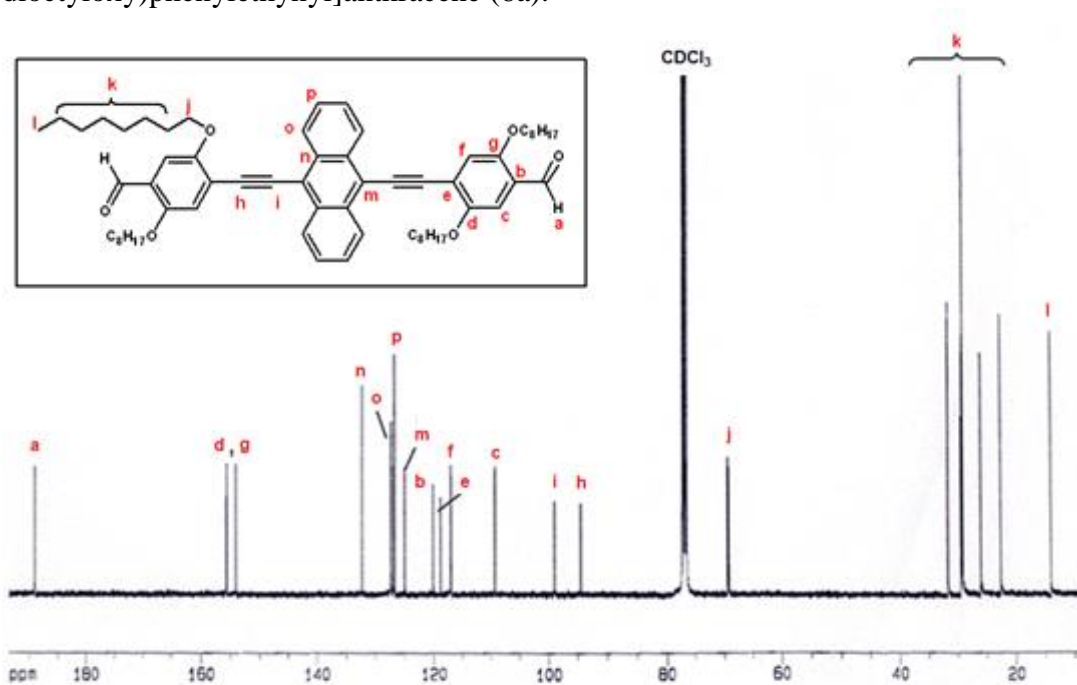
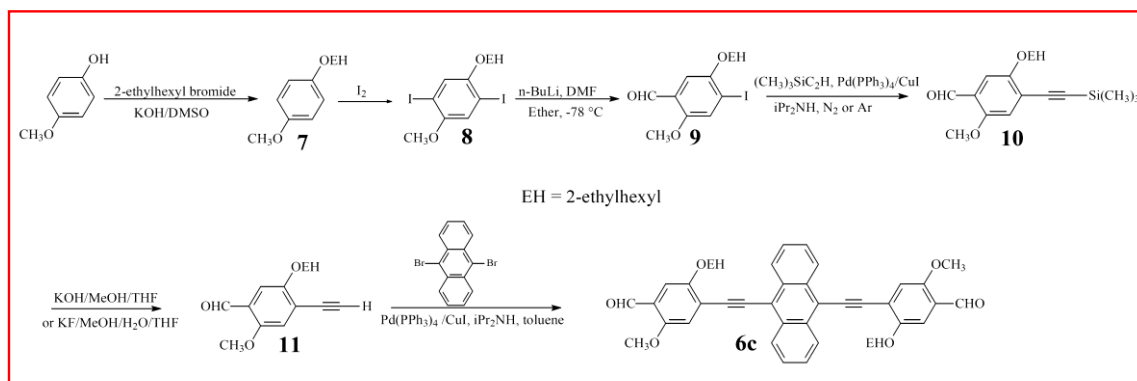


Figure 3a.2 ¹³C-NMR spectrum (CDCl₃) of 9,10-bis[4-formyl-2,5-dioctyloxy)phenylethynyl]anthracene (6a).

^{13}C -NMR spectrum of dialdehyde **6a** is presented in **Figure 3a.2**. The carbonyl carbon of aldehyde group was observed at 189.11 δ ppm. The carbon atoms on phenyl ring which are directly attached to oxygen atom of alkoxy chain were observed at 155.60 δ ppm and 154.01 δ ppm and those which are directly attached to 'CHO' appeared at 125 δ ppm. The carbon atoms on anthracene appeared in the range of 120.21-132.25 δ ppm. The carbon atoms on phenyl ring which are attached to 'C \equiv C' resonated at 118.88 δ ppm. Remaining phenyl carbon atoms were observed at 117.04 δ ppm and 109.36 δ ppm. The acetylene carbon atoms appeared at 99.04 δ ppm and 94.61 δ ppm. The methylene carbon atoms adjacent to oxygen atom alkoxy chain appeared at 69.47 δ ppm and 69.35 δ ppm. The methylene and methyl carbon atoms on side chains appeared in the range 31.79-14.07 δ ppm.

3a.4.1.2 Synthesis of dialdehydes bearing asymmetric side chains on phenyl rings (6c)

The six-step route for the synthesis of dialdehydes bearing asymmetric side chains on phenyl rings (6c) starting from 4-methoxy phenol is depicted in **Scheme 3a.2**. The synthetic procedure is similar to that of dialdehydes bearing symmetric side chains except first two steps.³⁹ In the first step, 4-methoxy phenol was alkylated with 2-ethylhexyl to form **7** which on subsequent iodination yielded diiodo derivative **8**. Compound **8** then underwent same reaction sequence as that described in 3a.4.1 to give final dialdehyde **6c**.



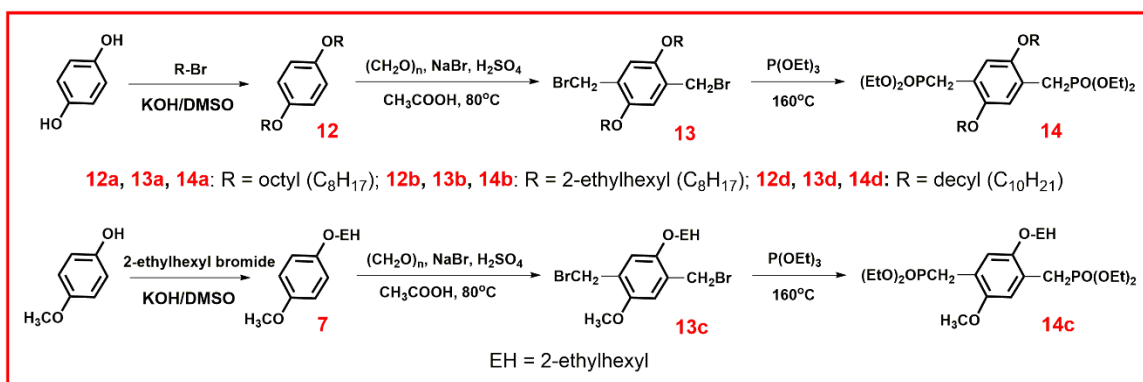
Scheme 3a.2 Synthesis of dialdehydes bearing asymmetric side chains on phenyl rings (6c).

^1H -NMR and ^{13}C -NMR spectra of dialdehyde **6c** (asymmetric side chains) is similar to that of dialdehyde **6b** (symmetric side chains), except one extra peak due to

methoxy group (-OCH₃) at 4.02 δ ppm in ¹H-NMR spectrum and at 56.39 δ ppm in ¹³C-NMR spectrum.

3a.4.2 Synthesis of bisphosphonates (14)

The three-step route for the synthesis of symmetric bisphosphonates (**14**) from hydroquinone and asymmetric bisphosphonate (**14c**) from 4-methoxy phenol is depicted in **Scheme 3a.3**. Hydroquinone /4-methoxy phenol was first alkylated with corresponding alkyl bromide to obtain the alkyloxy derivatives **12** or **7**, respectively. In the second step, **12** and **7** were bromomethylated using NaBr/H₂SO₄ and paraformaldehyde to yield **13** and **13c**, respectively. Finally, the bis(bromomethyl) derivatives **13** and **13c** were converted to corresponding bisphosphonate esters **14** and **14c** by the Michealis-Arbuzov reaction.⁴⁰



Scheme 3a.3 Synthesis of bisphosphonates.

¹H-NMR spectrum of bisphosphonate **14b** is presented in **Figure 3a.3**. The aromatic protons appeared as singlet at 6.94 δ ppm. Methylene protons on phosphonate group which are directly attached to oxygen atom resonated at 3.95 δ ppm. Methylene protons on 2-ethylhexyl chain which are directly attached to oxygen atom appeared at 3.81 δ ppm. Methylene protons which are attached to phosphonate group (Ar-CH₂-P) appeared as doublet at 3.22 δ ppm. The remaining methylene protons (-CH₂-) and -CH- protons observed in the range of 1.75-1.21 δ ppm. Methyl protons on phosphonate group appeared as triplet at 1.16 δ ppm. Methyl protons on 2-ethylhexyl chain appeared at 0.87 δ ppm.

¹H-NMR spectra of intermediates produced during the synthesis of bisphosphonate **14b** is provided in supporting information.

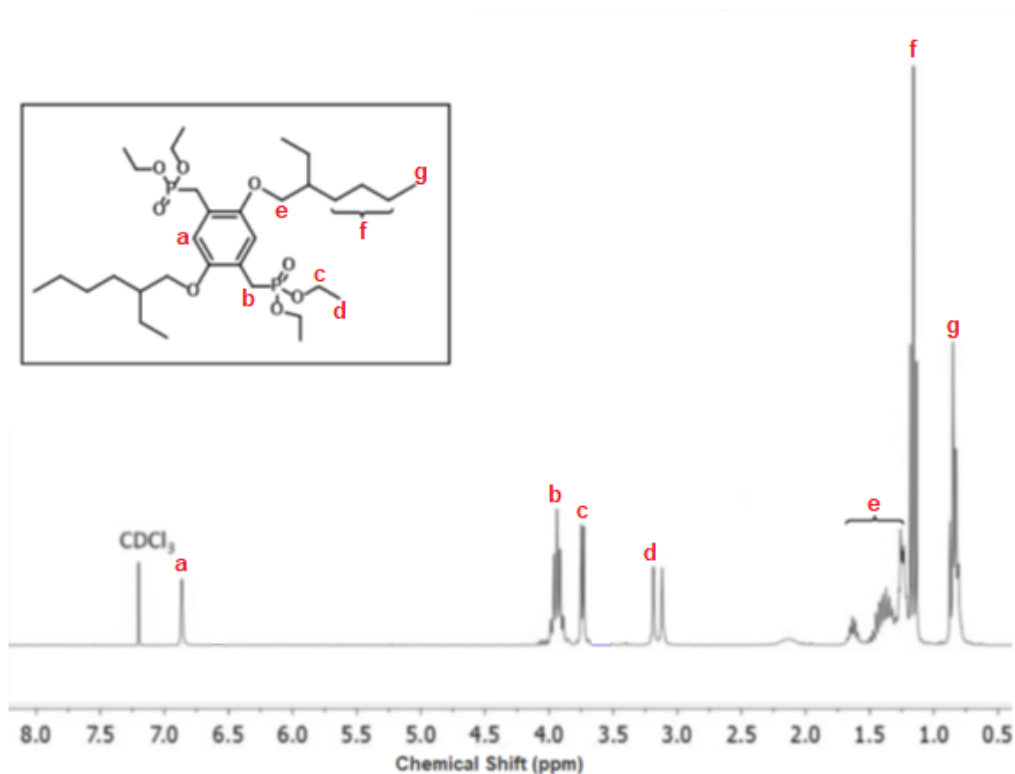
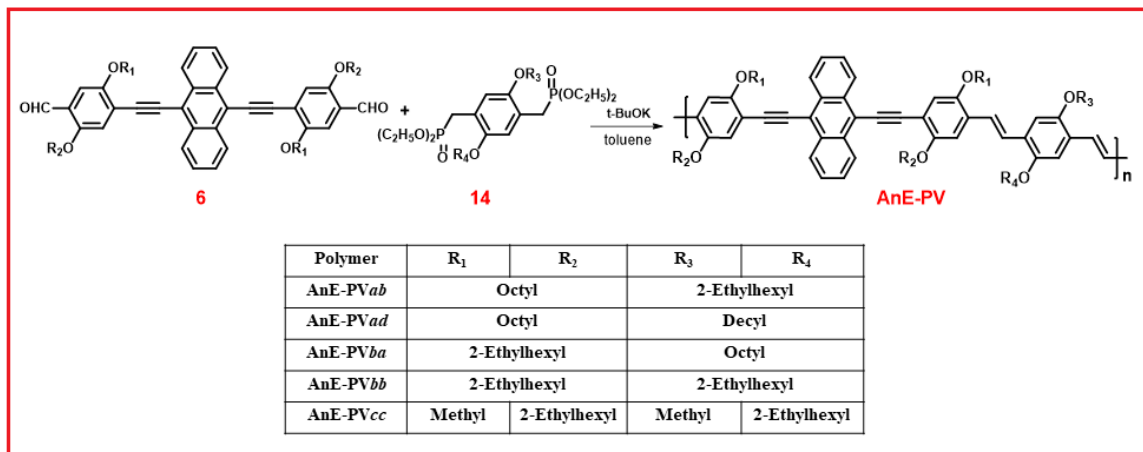


Figure 3a.3 $^1\text{H-NMR}$ spectrum (CDCl_3) of 2,5-bis(2-ethylhexyloxy)-*p*-xylylene-bis(diethylphosphonate) (14b).

3a.4.3 Synthesis of AnE-PV polymers

The AnE-PPV polymers were synthesized by Horner-Wadsworth-Emmons (HWE) polycondensation reaction of dialdehydes 6a-b with bisphosphonates 14a-d in toluene, in the presence of an excess of potassium tert-butoxide. The synthesis is depicted in **Scheme 3a.4**. This method was first introduced by Hörhold *et al.*,⁴¹ and is particularly advantageous because it provides defect-free polymers and the newly formed double bonds have *all-trans* (E) configuration. Horner-Wadsworth-Emmons polycondensation method shows very high reactivity, consequently, high molecular weight polymers are formed in relatively short reaction time.



Scheme 3a.4 Synthesis of AnE-PV polymers.

FT-IR spectrum of polymer AnE-PVab showed medium intensity absorption band at 917 cm^{-1} due to newly formed trans double bond which confirmed formation of polymer. The two weak bands at 2184 cm^{-1} and 1597 cm^{-1} corresponds to disubstituted $\text{C}\equiv\text{C}$ - and aryl- $\text{C}=\text{C}$ - stretching frequency, respectively. Strong band at 1203 cm^{-1} is due to aromatic C-O stretch which confirmed the presence of alkoxy chains. Weak band at 3057 cm^{-1} and strong bands at 2923 cm^{-1} , 2852 cm^{-1} correspond to aromatic and aliphatic C-H stretch, respectively.

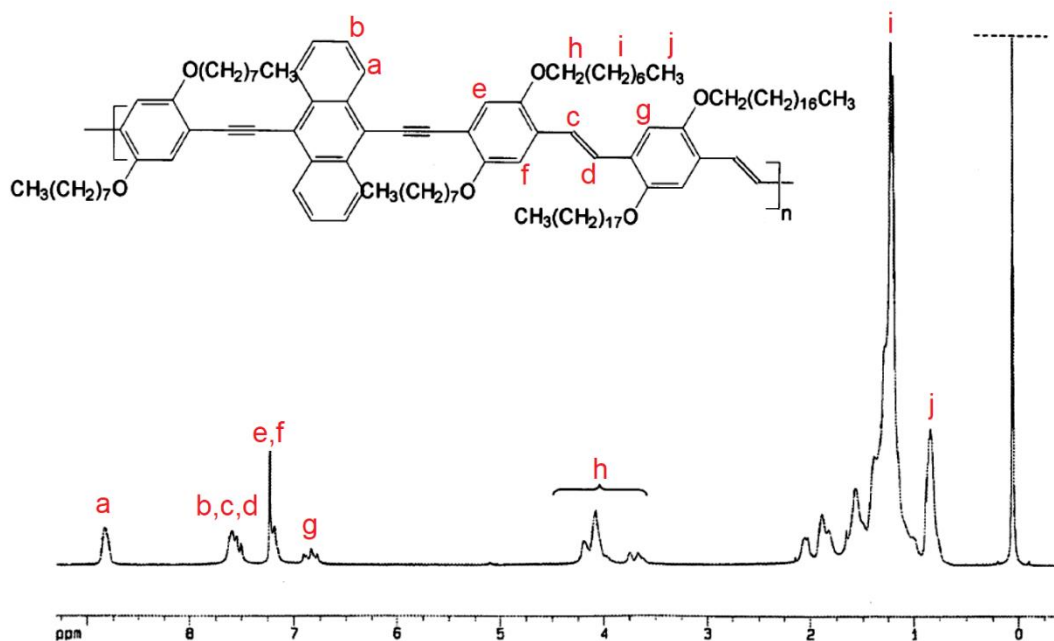


Figure 3a.4 $^1\text{H-NMR}$ spectrum (CDCl_3) of polymer AnE-PVab.

¹H-NMR spectrum of polymer AnE-PV ab is presented in **Figure 3a.4**. The peak at 8.84 δ ppm was observed for four anthracene protons. Remaining four anthracene protons and vinylene protons appeared in the range of 7.60-7.51 δ ppm. The other aromatic protons appeared in the range of 6.84-7.19 δ ppm. Methylene protons on side chains which are attached to oxygen atom appeared in the range of 4.20-3.62 δ ppm. Remaining methylene and methyl protons appeared in the range of 2.05-0.88 δ ppm.

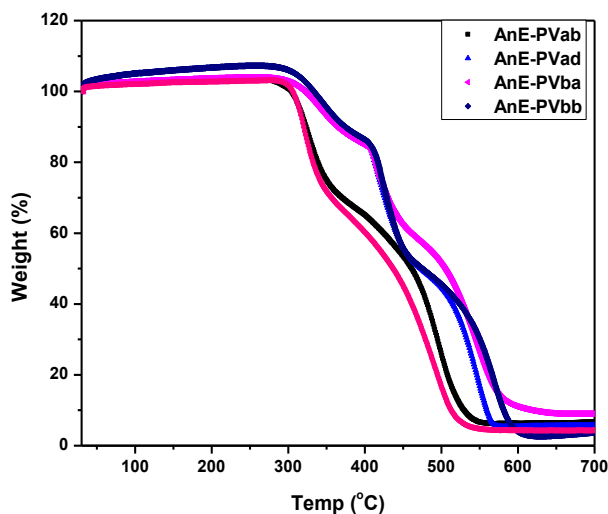
Five different anthracene-containing poly(*p*-phenylene-ethynylene)-alt-poly(*p*-phenylene-vinylene) (PPE-PPV) copolymers denoted as AnE-PV were synthesized and characterized. The copolymers differ in the nature (linear/branched) and length of the side chains appended on the polymer backbone. The side chains were systematically varied as- solely linear (AnE-PV aa , - ad), solely branched (AnE-PV bb) and mixed linear and branched (AnE-PV ab , - ba , - cc) alkoxy side chains. In the polymer AnE-PV cc , the side chain density was reduced compared to the polymers AnE-PV ab and - bb by partly replacing the branched side chains by methyl groups. All the polymers were found to be soluble in organic solvents such as chloroform, dichloromethane, tetrahydrofuran, toluene and chlorobenzene at room temperature. Soluble polymers were obtained with the yields in the range 53 % and 94 %.

Molecular weights of polymers were determined by gel permeation chromatography (GPC) in chloroform using polystyrene as the standard. The data obtained from GPC and thermogravimetric analysis (TGA) is summarised in **Table 3a.1**. Number average molecular weights were in the range 15.8- 47.5 kg/mol. Dispersities were in the range of 1.9– 3.5. **Figure 3a.5** shows TGA curves for various polymers. Thermal degradation under air at 10% weight loss ($T_{10\%}$) were recorded between 317 and 351 °C

Table 3a.1 Data obtained from GPC and TGA studies.

Polymer	M _n (kg/mol) ^a	M _w (kg/mol) ^b	Dispersity (M _w /M _n)	T _{10%} /°C ^c
AnE-PVab	40.0	141.6	3.5	317
AnE-PVad	19.3	54.0	2.8	351
AnE-PVba	25.5	77.8	3.0	348
AnE-PVbb	15.8	47.2	2.9	346
AnE-PVcc	47.5	91.9	1.9	317

a: M_n= number-average molecular weight, b: M_w= weight-average molecular weight, c: T_{10%}=decomposition temperatures at 10% weight loss

**Figure 3a.5** TG curves of polymers.

3a.4.4 Thermal properties of AnE-PV polymers

DSC measurements were carried out to study the transitions occurring in the polymers as a function of temperature. The temperature was varied from 0 to 250 °C with a heating/cooling rate of 10 K/min. Two heating-cooling cycles were performed on each

sample. The DSC thermograms obtained during the first heating run and a summary of the transition temperatures are provided in **Figure 3a.6** and **Table 3a.2**, respectively.

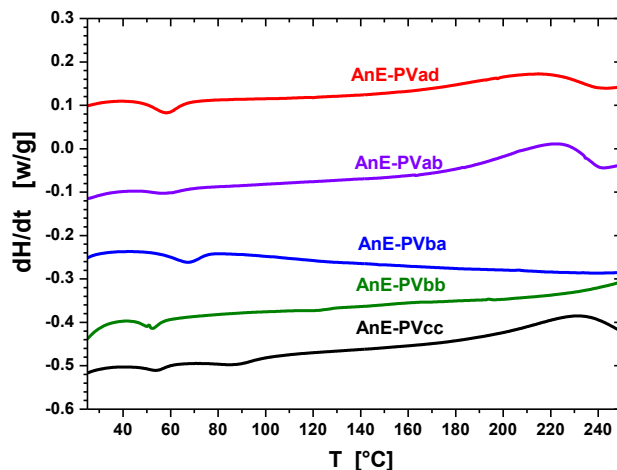


Figure 3a.6 DSC thermograms (heat flow dH/dt as a function of temperature T) obtained during the first heating run. Data graphs are shifted along the y-axis for better visibility.

Table 3a.2 Transitions temperatures determined from the peak maxima of the DSC thermograms.

Polymer	1 st T/°C	2 nd T/°C	3 rd T/°C
AnE-PVad	59	—	215
AnE-PVab	58	—	221
AnE-PVba	67	—	—
AnE-PVbb	53	—	—
AnE-PVcc	54	88	231

In the first heating cycle, the as synthesized polymer samples (powders) showed an endothermic transition at low temperature (53°C-67°C) and a broad exothermic transition at temperatures between 170°C and 250°C. No transitions were visible in the subsequent heating and cooling cycles. These solid-solid phase transitions were presumed to originate from melting of the side chains (low temperature transition) and from backbone-reorganization/crystallization (high temperature transition), respectively. Since these transitions were not seen in the subsequent DSC cooling and heating runs they

might result from non-equilibrium structures, frozen in during the preparation process. The low-temperature transitions were absent in the subsequent runs, indicating that, the side chains are most likely amorphous in the equilibrium structure. The transitions at high temperatures leads to an improved interlayer stacking which is preserved during cooling the sample back to room temperature and therefore can be presumed to be the equilibrium structure. These results are further supported by the X-ray scattering experiments.

3a.4.5 Wide-Angle X-ray Scattering Analysis

WAXS experiments were performed on the powder samples as well as on aligned fiber samples. The determination of the π - π stacking distance ($d_{\pi-\pi}$) was done as per the literature.²⁵ WAXS experiments were performed on the powdered samples at different temperatures in order to study the effect of annealing on the structural properties. Measurements were done at room temperature, (1), at 100 °C that is above the side chain melting temperature, (2), and at 210 °C where the polymers are known to undergo backbone reorganization, (4). The samples were cooled down back to room temperature and measured again after each annealing step (3) and (5). **Figure 3a.7** depicts WAXS spectra taken at different steps of the annealing for powdered samples of various polymers.

The WAXS experiments (combination of powder and filament experiments) reveal that the polymers AnE-PVad, -ab bearing linear octyl side chains at R₁ and R₂ on the more rigid part of the conjugated backbone (AnE segment), arrange in a stacked structure. This layered structure comprises π - π -stacks of the backbones ($d_{\pi-\pi}$) which are separated by interlayers (d_{inter}) built by the side chains. A sketch of the layered structure of the non-amorphous AnE-PV polymers is provided in **Figure 3a.8**. The first sharp Bragg peak originates from interlayer stacking (**Figure 3a.7**). The interlayer distance (d_{inter}) can be obtained from the positions of the Bragg-peaks. The peak intensity as well as the widths of the Bragg-peaks can be taken as a measure of the degree of order.²⁵ Correlations along the backbone direction, contributions from the (amorphous) side chains as well as from π - π -stacking all appear as broad peaks in the same q region- 10 nm⁻¹- 18 nm⁻¹.

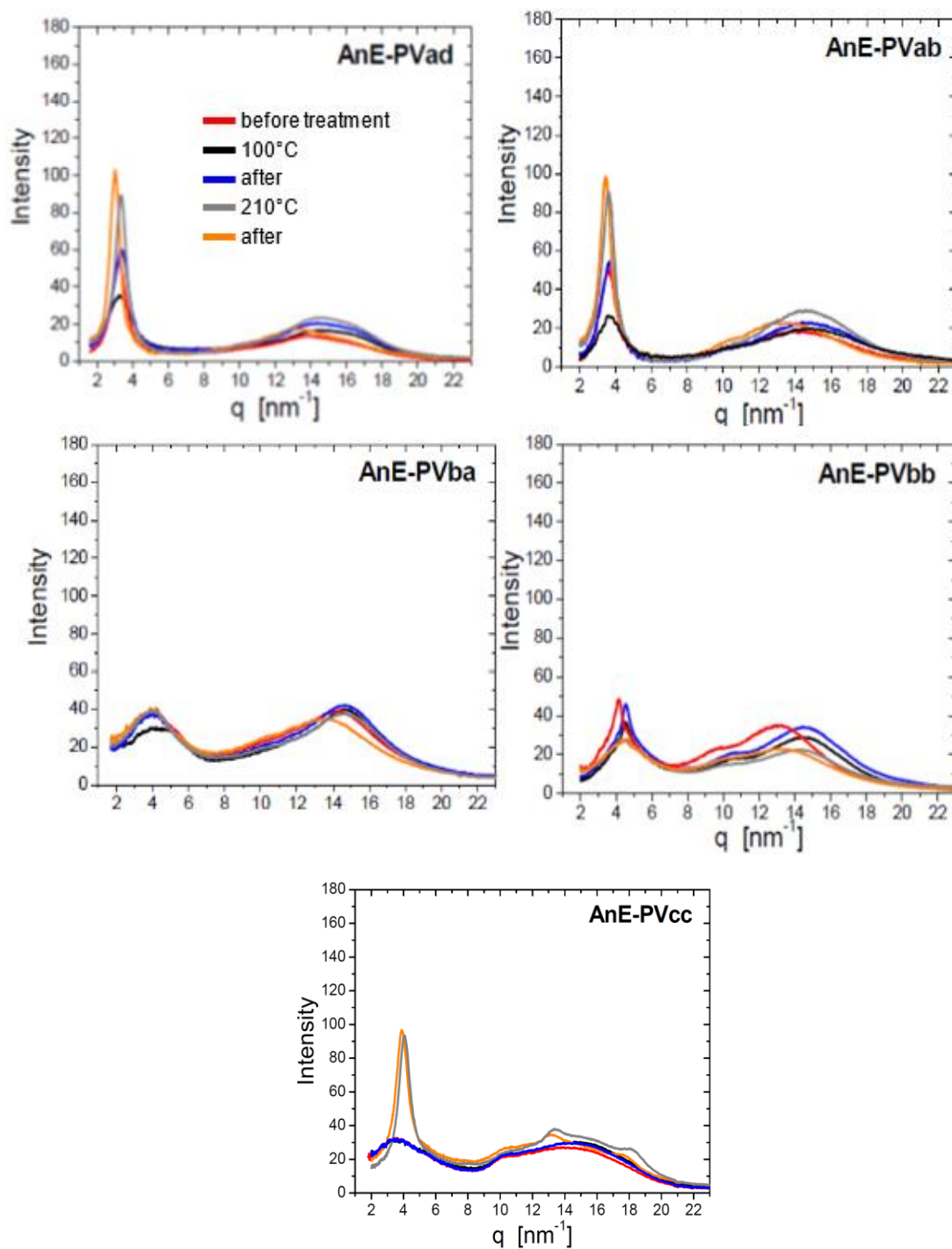


Figure 3a.7 WAXS results for powder samples after different annealing steps.

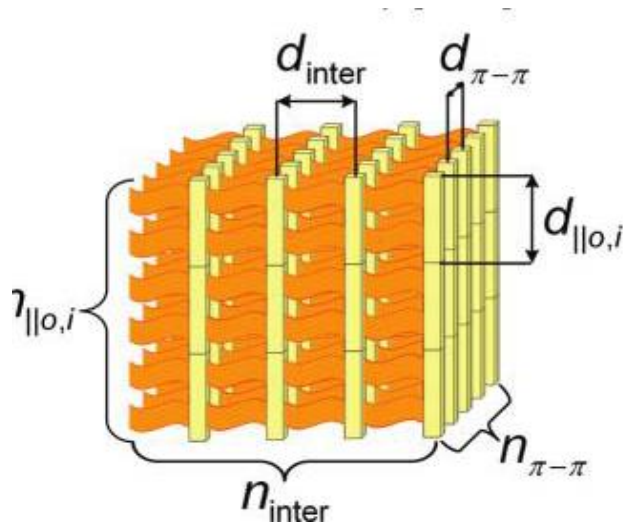


Figure 3a.8 A sketch of the layered structure of AnE-PV polymers.

The degree of order increases when the samples are annealed at temperatures above the side chain melting temperature and backbone reorganization temperature. An enhanced order can be preserved if the sample is cooled back to room temperature (Figure 3a.6). For the polymers with all linear substitution (AnE-PV ad) annealing results in an increase in the degree of order. The samples AnE-PV ab containing bulky 2-ethylhexyl side chains exhibit a smaller improvement of the order at room temperature in response to annealing. The polymers AnE-PV ba and AnE-PV bb with bulky, branched 2-ethylhexyl attached to the arylene-ethynylene segment exhibit only two broad peaks indicating no long-range order. The asymmetric substituted polymer AnE-PV cc ($R_1=R_3=2$ -ethylhexyl and $R_2=R_4$ =methyl), shows a distinct behavior. It is amorphous at temperatures up to about 100 °C. However, when the sample is annealed up to the backbone recrystallization temperature it reorganizes into a stacked structure. The degree of order can be preserved when the sample is cooled back to room temperature.

Table 3a.3 summarizes the interlayer distances (d_{inter}) and π - π -stacking distances ($d_{\pi-\pi}$), obtained for the non-amorphous samples from the WAXS fiber spectra.

Table 3a.3 Interlayer distance and π - π stacking distance from WAXS analysis

Polymer	R ₁	R ₂	R ₃	R ₄	Aligned at [°C]	Interlayer distance [nm]		π - π stacking distance [nm]
						100°C	210°C	
AnE-PVad	Octyl		Decyl		120	1.88 ±0.01		0.38
AnE-PVab	Octyl		2-Ethylhexyl		120	1.74 ±0.01		0.39
AnE-PVba	2-Ethylhexyl		Octyl		-	1.57	1.61	-
AnE-PVbb	2-Ethylhexyl		2-Ethylhexyl		-	1.37 ±0.01		-
AnE-PVcc	2-EH	Methyl	2-EH	Methyl	190	-	1.55	0.38, 0.34

For polymers bearing only linear side chains, AnE-PVad, the π - π -stacking distance was determined to be 0.38 nm. The presence of bulky, branched 2-ethylhexyl at R₃ and R₄ in AnE-PVab widened the stacking distance to 0.39 nm. This widening leads to better photovoltaic performance as reported in photovoltaic studies in this chapter. For the asymmetric substituted polymer AnE-PVcc two peaks were observed in the WAXS spectra which correspond to π - π -stacking distances of about 0.38 nm (as for the polymer AnE-PVad) and 0.34 nm, respectively. The appearance of two peaks might be due to the presence of two polymorphs. As the polymers AnE-PVba and AnE-PVbb were completely amorphous, they didn't show any stacking.

3a.4.6 Photophysical Study

The photophysical data of polymers was measured in chloroform solution as well as on thin films spin coated from chloroform and chlorobenzene, respectively. **Table 3a.4** summarizes photophysical data which include wavelength at absorption maximum (λ_a), wavelength at which 10% of the absorption maximum is reached on the lower energy side ($\lambda_{a10\%}$), the optical band gap energy⁴² (E_g^{opt}) calculated using $1240/\lambda_{a10\%}$, the wavelength at the emission maximum, λ_f . The absorption and emission spectra in dilute chloroform solution are depicted in **Figure 3a.9**.

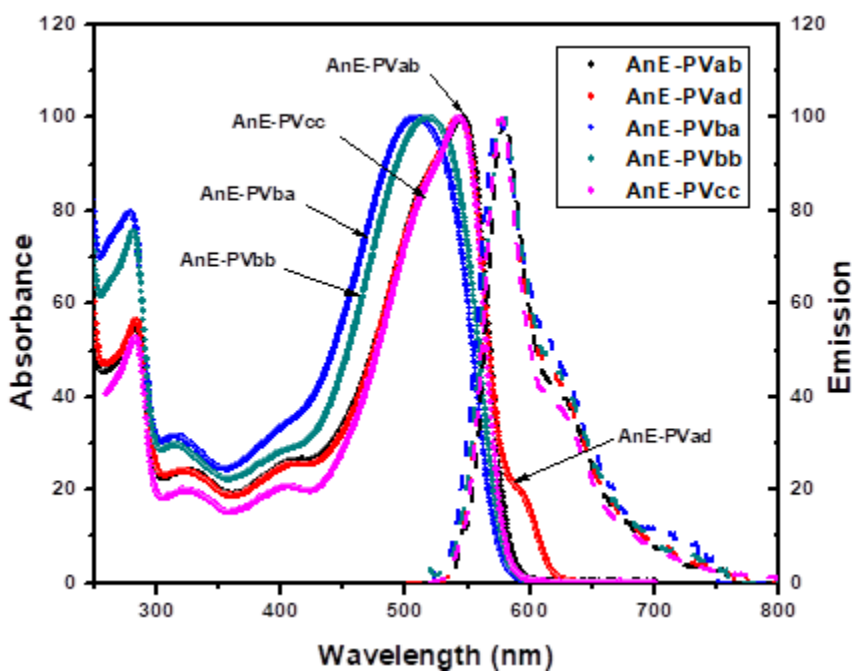


Figure 3a.9 The absorption and emission spectra of AnE-PV polymers in dilute chloroform solution

In solution, polymers bearing only linear side chains, AnE-PVad, and those incorporating branched 2-ethylhexyl, AnE-PVi ($i = ab, ba, bb, \text{ and } cc$) showed distinct behavior. The absorption spectra of AnE-PVad exhibited a shoulder at around 600 nm, which is ascribed to the formation of aggregates already in dilute solution. This aggregate formation was confirmed by recording temperature-dependent absorption spectra of AnE-PVad in toluene (**Figure 3a.10**). Upon increasing the temperature from 20 to 80 °C, the shoulder band gradually disappeared with simultaneous blue shift of the absorption peak from 540 to 528 nm. Subsequent cooling from 80 to 20 °C resulted in an increase of the intensity and a red shift ($\lambda_a = 544$ nm) of the main absorption peak. Moreover, the shoulder band was finally transformed into a real peak centered at 596 nm with enhanced intensity. This study demonstrated that the heating and cooling process induced an enhanced backbone planarization and stronger intermolecular interactions (aggregate formation) in polymer solution. Thus, this heating and cooling process might be useful to induce preorganization of polymers prior to the spin-coating step during solar cell preparation.

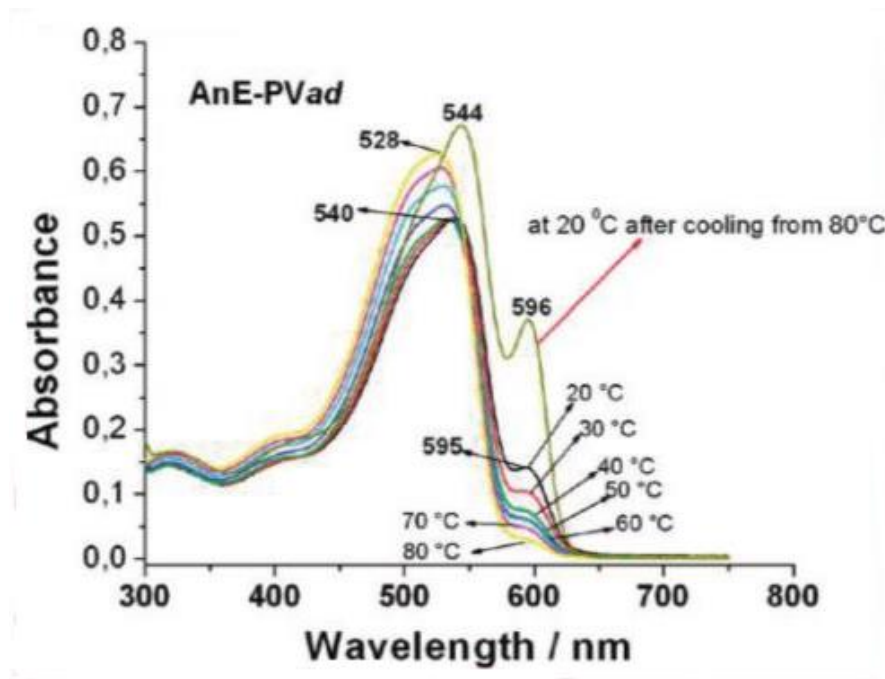


Figure 3a.10 Temperature-dependent absorption spectra of AnE-PVad in toluene

The absorption peak of the polymers AnE-PVba ($\lambda_a=510$ nm) and AnE-PVbb ($\lambda_a=519$ nm) bearing bulky 2-ethylhexyl at R₁ and R₂, i.e. close to the AnE unit, was blue-shifted relative to that $\lambda_a \sim 545$ nm of the polymers AnE-PVi ($i = ad, ab$) bearing linear side chains (R₁=R₂=octyl) and the asymmetric substituted polymer AnE-PVcc (R₁=2-ethylhexyl, R₂=methyl) (Please refer **Table 3a.4**). This hypsochromic shift was due to the high sensitivity of the anthracene moiety to steric hindrances in its neighborhood.^{39,43,44} In the polymer AnE-PVcc the small methyl group obviously compensates for steric crowding induced by the bulky 2-ethylhexyl group at R₂.

Irrespective of the differences in the solution absorptive behavior, the optical band gap energies of all the polymers were found to be between 2.0 and 2.1 eV. The main emission peak for all polymers in solution was centered around $\lambda_f=580$ nm.

Table 3a.4 Photophysical data of AnE-PV polymers in solution and on thin films

Polymers	λ_a [nm]	$\lambda_{10\%}$ [nm]	E_g^{opt} [eV]	λ_f [nm]
AnE-PVab	546	584	2.12	579
AnE-PVab ^{a)}	<u>541</u> , 570	622	1.99	622
AnE-PVab ^{b)}	<u>508</u> , <u>583</u>	687	1.80	624
AnE-PVad	545	608	2.03	578
AnE-PVad ^{a)}	544, <u>583</u>	624	1.98	<u>623</u> , 673
AnE-PVad ^{b)}	552, 590	650	1.91	<u>621</u>
AnE-PVba	510	575	2.15	576
AnE-PVba ^{a)}	507	596	2.08	602
AnE-PVba ^{b)}	504	636	1.95	605
AnE-PVbb	519	578	2.14	580
AnE-PVbb ^{a)}	521	610	2.03	598
AnE-PVbb ^{b)}	527	613	2.02	600
AnE-PVcc	544	580	2.13	578
AnE-PVcc ^{a)}	540, 578	628	1.97	617
AnE-PVcc ^{b)}	532, 580	674	1.84	617

Thin film spin coated from ^{a)} chloroform solution and ^{b)} chlorobenzene solution

The absorption and emission spectra of the pristine polymer thin films of AnE-PVad, ab, ba, and cc and of the corresponding polymer-PCBM blend layers (weight ratio 1:1) are depicted in **Figure 3a.11**. The films were spin-coated from chlorobenzene. It was observed that, there is substantial quenching of photoluminescence in the blend due to photoinduced charge transfer from the polymer to PCBM.^{8,45-49}

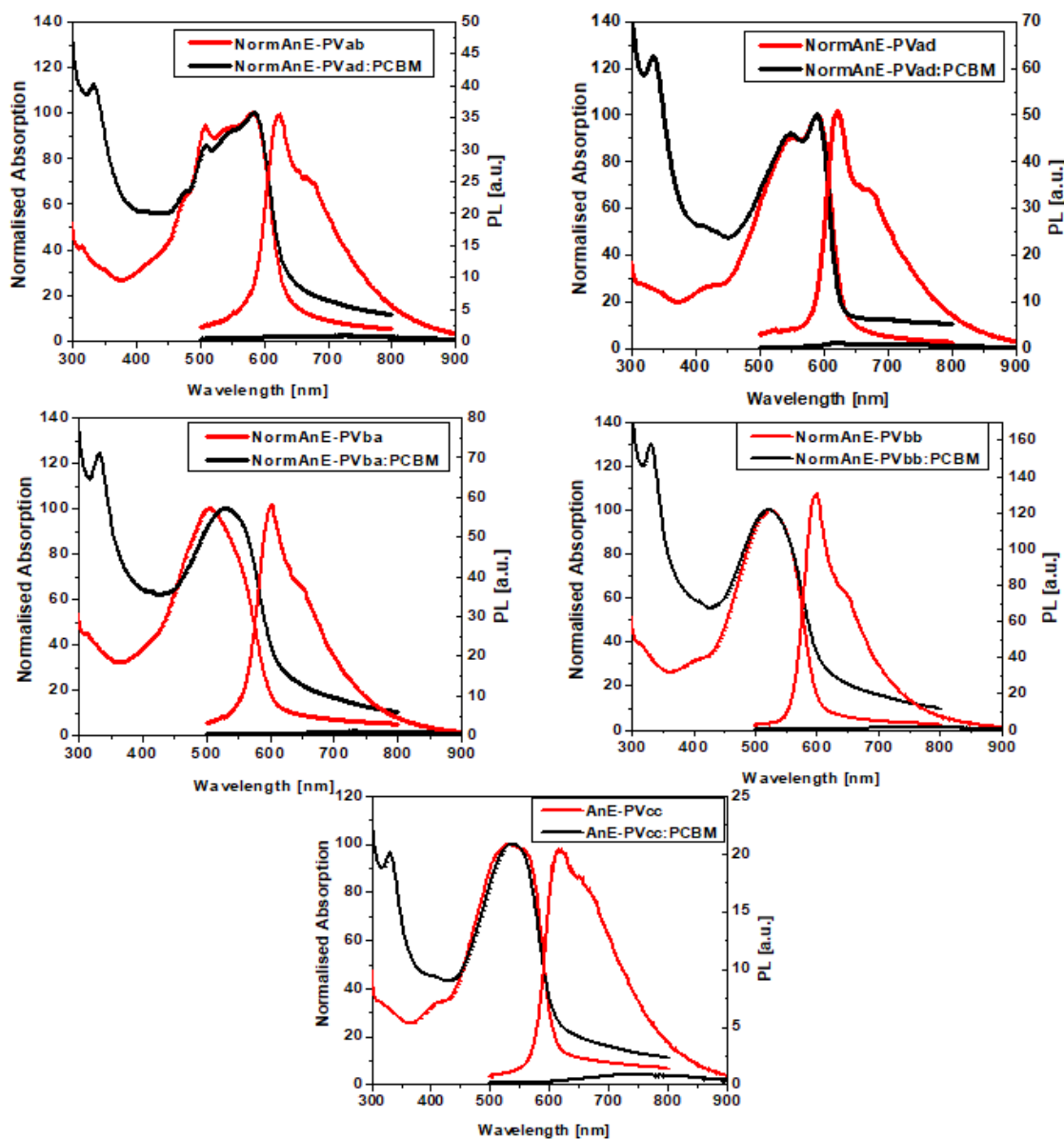


Figure 3a.11 Thin film absorption and emission spectra of polymers and polymer:PCBM (1:1) blends.

From the absorption spectra, polymers can be divided into two main groups: (1) polymers bearing linear side chains close to the AnE units (i.e., $R_1 = R_2 = \text{octyl}$), AnE-PV i ($i = ad, ab$) and (2) polymers bearing bulky branched 2-ethylhexyl chain at R_1 and R_2 , AnE-PV i ($i = ba, bb$). The first group showed well resolved absorption spectra, with main absorption bands consisting of two peaks at around 540 and 580 nm. The appearance of two peaks is indicative of improved ordering as confirmed by X-ray scattering

experiments from which the intermolecular π - π -stacking distance ($d_{\pi-\pi}$) and interlayer stacking distance (d_{inter}) were determined. In contrast, the second group showed featureless peak (π - π^* transition band). These results were consistent with the X-ray results which revealed that these polymers are amorphous in nature, showed no π - π -stacking signal and no interlayer ordering. The absorption peak of these polymers was located around 505 and 520 nm for AnE-PVba and AnE-PVbb, respectively. The polymer AnE-PVcc bearing a small methyl- as well as a branched 2-ethylhexyl group close to AnE showed an intermediate behavior. The absorption band of AnE-PVcc was slightly structured in the pristine form, but becomes featureless in the blend.

The data in **Table 3a.4** showed that the optical band gap energies (E_g^{opt}), were lower for thin films as compared to the solutions due to enhanced planarization and intermolecular interaction in the films. Optical band gap values were in the range of 1.8 and 2.0 eV, the lower end being similar to the electrochemical ones (**Table 3a.5**). This variation of E_g^{opt} values might be related to differences in backbone coplanarity and film thickness.⁵⁰

3a.4.7 Electrochemical Study

Electrochemical experiments were performed on thin polymer films spin coated from chlorobenzene solutions under inert condition by using cyclic voltammetry technique (CV).³⁹ The ionization potential (HOMO), E_{IP} , and electron affinity (LUMO), E_A , were estimated from oxidation and reduction onset potentials on the basis of the reference energy level of ferrocene (4.8 eV below the vacuum level) using the equation $E_{IP} (E_A) = -(E_0 - E_{ferr}) - 4.8$ eV, where E_{ferr} is the value for ferrocene vs the Ag/Ag⁺ electrode. E_0 values were obtained averaging the anodic and cathodic peak potentials, $E_0 = (E_{pa} + E_{pc})/2$. The E_{IP} and E_A values were evaluated from the first oxidation and reduction peaks of the cyclic voltamograms measured at scan rates of 20 and 50 mV/s. The CV curves are shown in the Supporting Information (**Figure SI 3a.8**) and the electronic data are summarized in **Table 3a.5** (values for E_g^{opt} were included from **Table 3a.4** for comparison). The electrochemical band gap energy, E_g^{elc} for all polymers was around 1.80 eV.

Table 3a.5 Electrochemical data for polymer films spin-coated from chlorobenzene solution

Polymer	HOMO (eV)	LUMO (eV)	E_g^{elc} (eV)	E_g^{opt} (eV)
AnE-PVad	5.15	3.38	1.77	1.91
AnE-PVab	5.17	3.37	1.80	1.80
AnE-PVba	5.16	3.37	1.79	1.95
AnE-PVbb	5.19	3.40	1.79	2.02
AnE-PVcc	5.15	3.34	1.81	1.84

3a.4.8 Charge carrier mobility measurements:

Charge Extraction by Linearly Increasing Voltage (CELIV) method was used for charge carrier mobility studies. The CELIV method has been used successfully to study the charge transport in various disordered organic and inorganic semiconducting films.³⁴ The main advantages of this method over time-of-flight (TOF) is that it allows to study films with various conductivities as well as with rather dispersive charge transport.⁵¹ In general, the planar organic field effect transistor (OFET) geometry provides information about the charge transport in parallel direction to the substrate plane.⁵² On contrary to this, CELIV measures charge transport in perpendicular direction to substrate plane.⁵³ A laser pulse was used to photogenerate the charge carriers. After delay time of 100 ns, the applied triangle-shaped rising voltage pulse extracts the photogenerated charge carriers toward back electrode and the carrier mobility is determined from the extraction maxima. The CELIV current transients are shown in **Figure SI 3a.9**.

Since the laser pulse was illuminating the positive electrode during the measurements, the photocurrent due to mobile holes was recorded and mobility of photogenerated holes was calculated from current transients. The hole mobility values are summarized in **Table 3a.6**. The values range from $1.5 \times 10^{-5} \text{ cm}^2\text{V}^{-1}\text{s}^{-1}$ (AnE-PVad) to $4.5 \times 10^{-4} \text{ cm}^2\text{V}^{-1}\text{s}^{-1}$ (AnE-PVba). The amorphous polymers (AnE-PVbb, -ba), i.e. polymers bearing 2-ethylhexyl close to the AnE unit exhibited higher charge carrier mobilities than those with higher stacking tendency (AnE-PVad, -ab). This would suggest that π - π stacking might be detrimental to charge carrier mobility for this class of

polymers. Similar trends were previously observed in photoconductivity studies on PPE-PPV materials. Higher photoconductivity values at lower threshold voltages were obtained for materials with less aggregation tendency. Decreasing aggregation tendency were achieved by incorporation of either very long linear octadecyl or bulky branched 2-ethylhexyl side chains to the conjugated backbones.²³

Table 3a.6 Hole mobilities (μ_{hole}) of polymers

Polymer	μ_{hole} ($\text{cm}^2\text{V}^{-1}\text{s}^{-1}$)
AnE-PVad	1.69×10^{-5}
AnE-PVab	2.57×10^{-5}
AnE-PVba	4.52×10^{-4}
AnE-PVbb	1.53×10^{-4}
AnE-PVcc	9.22×10^{-5}

3a.4.9 Morphological Studies

Tapping-mode atomic force microscopy (AFM) technique was used to investigate the kind and scale of phase separation present in the photoactive layers. For the study, polymer:PCBM (1:1) blends were spin-cast from chlorobenzene solution on glass slides and their topography was investigated by AFM. The AFM images are presented in **Figure 3a.12**.

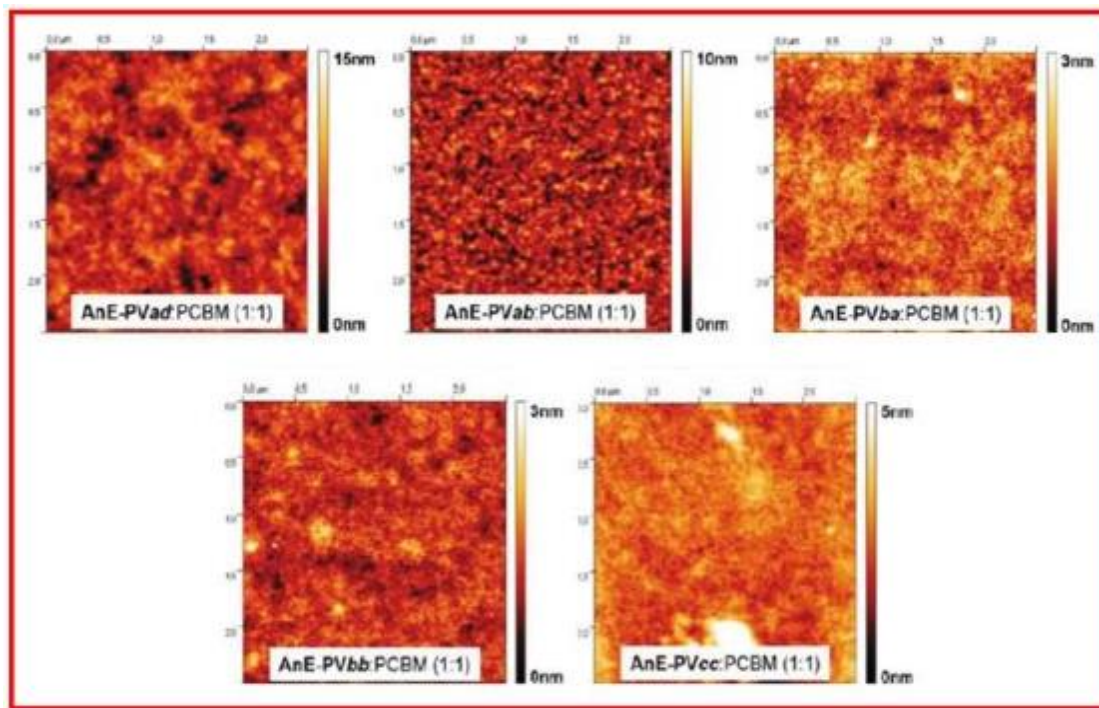


Figure 3a.12 Tapping mode AFM images (area $2.5 \times 2.5 \mu\text{m}^2$) for polymers.

Polymers with linear side chains near the AnE unit (AnE-PVad, -ab) showed more coarse scale morphologies which is reflected by peak-to-valley variations between 10 and 20 nm and by features indicating the formation of polymeric aggregates. On the other hand, polymers bearing branched side chains near the AnE unit (AnE-PVbb, -ba) exhibited fine scale morphologies resulting in rather flat topographies varying within only 3 nm. The asymmetrically substituted polymer AnEPVcc showed similar thin film morphologies as that for AnE-PVbb, -ba due to reduced side chain density. It was assumed that the higher crystallization tendency of the polymers AnE-PVad, -ab, resulted in more coarse scale thin film morphologies in polymer: PCBM blends. It is demonstrated in further discussion (in section 3a.4.8) that these more coarse grained film morphologies resulted in improved photovoltaic behavior by providing improved percolation paths and better charge transport for both type of charge carriers.

3a.4.10 Photovoltaic Studies

The solar cells were prepared by the configuration: glass substrate/ITO/PEDOT:PSS/active layer/Al. Photovoltaic devices based on polymer:PCBM active layers with weight ratios of 1:1 and 1:2 were prepared and optimized by variation of solution concentration and film thickness. **Figure 3a.13** depicts the current-voltage (*IV*)

curves of the solar cells based on polymer:PCBM (with weight ratios 1:1 and 1:2) active layers. A solar simulator (AM1.5, class A) was used for illumination.

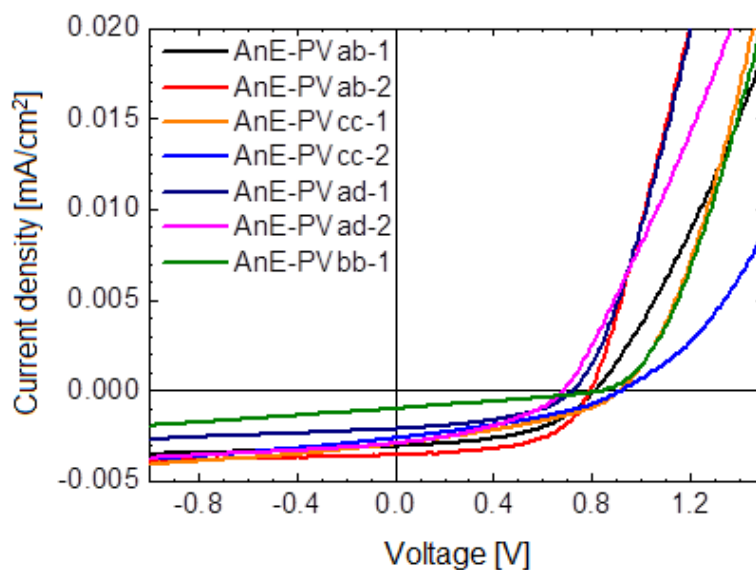


Figure 3a.13 J - V curves of solar cells incorporating polymer:PCBM active layers (with weight ratios 1:1 and 1:2).

In **Table 3a.7**, are summarized the photovoltaic parameters obtained from current-voltage (J - V) measurements for all polymer:PCBM blends. These include the short circuit current, (J_{sc}) the open circuit voltage (V_{oc}), the fill factor (FF), the series and parallel resistance (R_s and R_p). In general, solar cells with active layers having higher fullerene contents yielded higher power conversion efficiencies (η). The power conversion efficiencies range from $\eta = 0.34\%$ to 3.14% . The lower power conversion efficiencies were obtained for amorphous polymers AnE-PV ba and $-bb$, irrespective of their high mobilities. For these polymers, high miscibility of the active layer components resulted in insufficient percolation paths for the photogenerated charges and hence lower power conversion efficiencies.

Polymer AnE-PV ab exhibiting a good percolation path due to its more coarse-grained thin film nanomorphology, showed the highest power conversion efficiency. This polymer also showed the highest π - π -stacking distance ($d_{\pi-\pi} = 0.386$ nm) of all polymers in this series. Higher side chain density in AnE-PV ad hindered the charge transfer between donor and acceptor, resulting in lower photovoltages and fill factors and thus lower photovoltaic performance as compared to AnE-PV ab . In general, for PPE-PPV

based polymers, it has been observed that the open circuit voltage (V_{OC}) increases with decreasing side chain density.³¹ For instance, in the case of polymer:PCBM (1:1) blends, polymers bearing longer decyloxy side chains (AnE-PVad) leads to low V_{OC} values around 0.68 V. Polymers bearing octyloxy and/or 2-ethylhexyloxy chains, AnE-PVab, -bb, -ba, yielded V_{OC} values of about 0.80 V. Whereas AnE-PVcc having the lowest side chain density demonstrated the highest V_{OC} (0.93 V).

Table 3a.7 Photovoltaic parameters for polymer solar cells^a

Polymer:PCBM (Blend Ratio)	J_{sc} (mA/cm ²)	V_{oc} (V)	FF (%)	η (%)	R_s (Ω)	R_p (Ω)
AnE-PVab:PCBM (1:1)	6.13	0.81	49.08	2.44	22.2	1480
AnE-PVab:PCBM (1:2)	7.14	0.79	55.65	3.14	14.3	2227
AnE-PVad:PCBM (1:1)	4.24	0.72	44.6	1.36	11.3	1361
AnE-PVad:PCBM (1:2)	5.85	0.68	39.31	1.56	21.8	700
AnE-PVba:PCBM (1:1)	1.59	0.77	27.38	0.34	18.6	1081
AnE-PVba:PCBM (1:2)	3.44	0.93	34.67	1.11	31.2	942
AnE-PVbb:PCBM (1:1)	1.99	0.84	29.23	0.49	16	1012
AnE-PVbb:PCBM (1:2)	4.22	0.83	34.8	1.22	26.6	740
AnE-PVcc:PCBM (1:1)	3.66	0.93	29.98	1.02	36.3	657
AnE-PVcc:PCBM (1:2)	5.65	0.91	36.89	1.9	19.1	606
AnE-PVcc:PCBM (1:1) ^b	5.86	0.91	37.5	2.00	12.8	625

^a The active layer (area of 0.5 cm²) was spin-cast from chlorobenzene solution, ^b Active layer spin-cast from a mixture of chloroform and chlorobenzene.

The relatively low fill factors (FF), and high series resistances (R_s), in all blends indicated a non-balanced charge transport. Further optimization could be done by increasing the fullerene content in the blend. The solar cells based on polymers AnE-PVad, -ab, and -cc reached reasonable values of short circuit currents, J_{sc} i.e between 5 and 7 mA/cm². Polymer AnE-PVbb showed inferior currents, which may indicate incomplete or hindered charge separation efficiency after transfer. Furthermore, the larger current densities of AnE-PVab as compared to AnE-PVbb may be related to a better ordering caused by π - π -stacking, leading to improved charge transport properties. The high photocurrent densities of photovoltaic devices based on AnE-PVcc may be related to a lower side-chain density as compared to AnE-PVbb. In general, smaller parallel resistances, R_p , resulted in smaller fill factors in case of AnE-PVbb and AnE-PVcc, while the large photocurrents in case of AnE-PVab and AnE-PVcc promote relatively high-power conversion efficiencies of $\eta \geq 2\%$.

The use of mixture of solvents for blend solution preparation as a possible way for polymer solar cell optimization was carried out on polymer AnE-PVcc. Changing the solvent from chlorobenzene to a chlorobenzene:chloroform mixture (1:1 v/v) for active layer deposition resulted in a 2-fold increase in the power conversion efficiency. **Figure 3a.14** compares the J-V-curves obtained for the solar cells based on polymer AnE-PVcc active layers deposited from chlorobenzene and a mixture of chlorobenzene:chloroform, respectively.

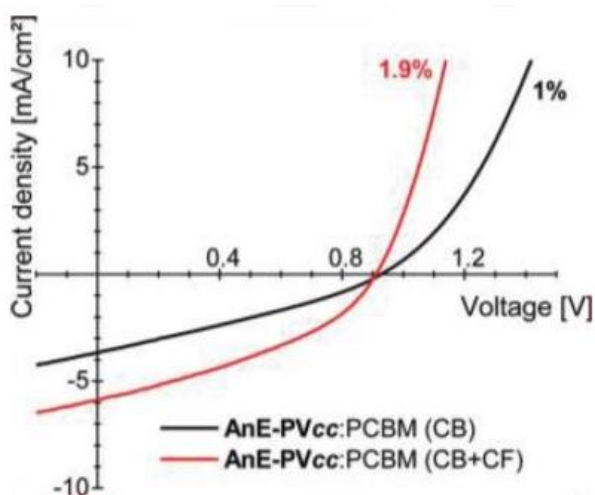


Figure 3a.14 Comparison of light J - V curves of AnE-PVcc:PCBM (1:1) blends cast from chlorobenzene (black) and mixture of chlorobenzene-chloroform (1:1, v/v) (red)

The energy generation mechanism in organic solar cells demands interpenetrating nanoscale phase separated domains of donors and acceptors for exciton dissociation and charge separation.⁵⁴ At the same time, well-organized arrangement in the individual donor and acceptor domains is a prerequisite for providing hassle free pathways to the charge transport. As different solvents have different intrinsic abilities to dissolve the polymer component, use of solvent mixture influences crystallinity and phase separation in blend domains. Thus, the application of combination of different solvents provides a possibility to gain precise control over the interconnected percolated nanoscale phase separated domains of donor and acceptor. The increased efficiency in above case, might be due to optimum solubility of the blend leading to efficient crystallization and enhanced photon absorption by the active layer, also due to optimum morphology leading to fine separation between the phases for charge generation and transport.^{55,56}

3a.5 CONCLUSIONS

Five anthracene-containing PPE-PPV copolymers bearing different side chain lengths and nature were synthesized and characterized. A correlation between the ability to form π - π -stacking, the absorption behavior, the charge carrier mobility, the active layer nanoscale morphology, and the photovoltaic performance was established. The π - π -stacking ability was controlled through incorporation of linear and/or branched alkoxy side chains. Polymer with octyloxy substitution close to the AnE units (AnE-PV ab , - ad) arrange in a stacked structure. Whereas asymmetric (AnE-PV cc) or branched side chain substitution (AnE-PV bb , - ba) near the AnE unit yielded less organized or even amorphous polymers. Polymers with strong tendency of stacking exhibited well resolved thin film absorption peaks. The polymers with less or no intrinsic stacking ability exhibited featureless absorption peaks. Although these polymers (AnE-PV bb , - ba , - cc) exhibited higher hole mobilities as compared to their ordered counterparts, insufficient donor-acceptor phase separation in their blends with PCBM, hindered efficient charge separation and thus resulted in poor photovoltaic performance. The polymers having inclination to stack, exhibited stronger phase separation and better photovoltaic performance. The best performance was achieved for polymer AnE-PV ab , which on one hand, showed ability to stack and on the other hand exhibited the highest $d_{\pi-\pi}$ value. Solar

cell devices fabricated using above polymer thin films, showed power conversion efficiencies ranging from 0.34 to 3.14 %. Thus, it was concluded that the alkoxy chains appended on the polymer backbone, not only improve polymer solubility, but also play a significant role in controlling active layer nano-morphology and hence the solar cell performance.

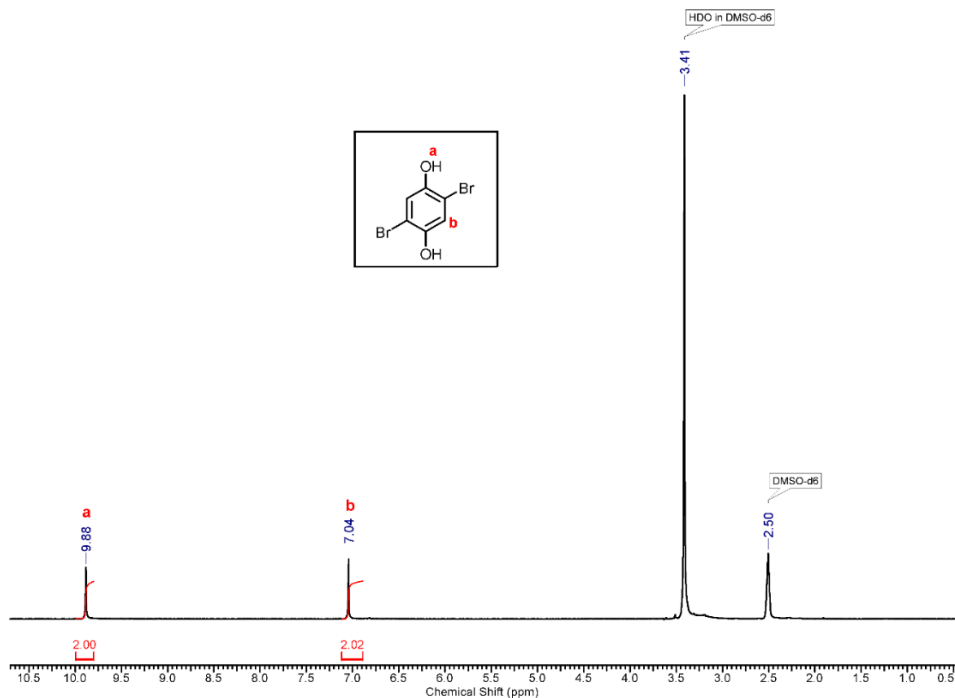
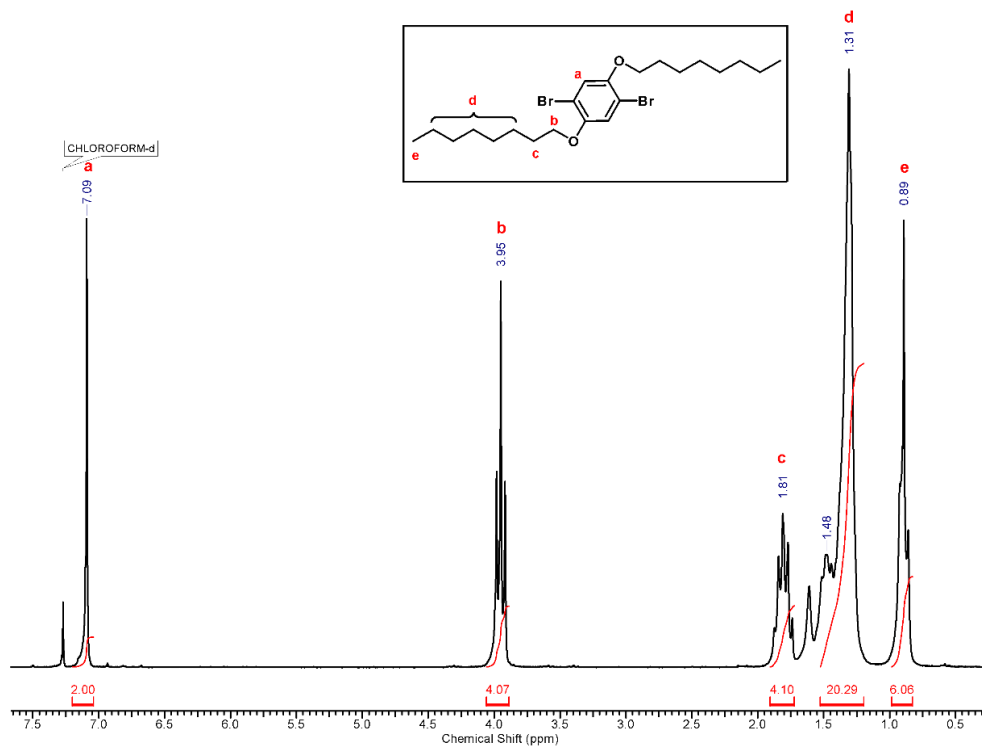
REFERENCES

- 1 H. Shirakawa, E. Louis, A. MacDiarmid, C. Chiang and J. Heeger, *J.C.S Chem. Comm*, 1977, **13**, 578–580.
- 2 C. K. Chiang, M. A. Druy, S. C. Gau, A. J. Heeger, E. J. Louis, A. G. MacDiarmid, Y. W. Park and H. Shirakawa, *J. Am. Chem. Soc.*, 1978, **100**, 1013–1015.
- 3 M. Leclerc, *Adv. Mater.*, 1999, **11**, 1491–1498.
- 4 D. Tyler McQuade, A. E. Pullen and T. M. Swager, *Chem. Rev.*, 2000, **100**, 2537–2574.
- 5 R. H. Friend, R. W. Gymer, A. B. Holmes, J. H. Burroughes, R. N. Marks, C. Taliani, D. D. C. Bradley, D. A. Dos Santos, J. L. Brédas, M. Lögdlund and W. R. Salaneck, *Nature*, 1999, **397**, 121–128.
- 6 A. Kraft, A. C. Grimsdale and A. B. Holmes, *Angew. Chemie Int. Ed.*, 1998, **37**, 402–428.
- 7 C. R. Newman, C. D. Frisbie, D. A. da Silva Filho, J.-L. Brédas, P. C. Ewbank and K. R. Mann, *Chem. Mater.*, 2004, **16**, 4436–4451.
- 8 C. J. Brabec, N. S. Sariciftci and J. C. Hummelen, *Adv. Funct. Mater.*, 2001, **11**, 15–26.
- 9 J. H. Burroughes, D. D. C. Bradley, A. R. Brown, R. N. Marks, K. Mackay, R. H. Friend, P. L. Burns and A. B. Holmes, *Nature*, 1990, **347**, 539–541.
- 10 N. S. Sariciftci, L. Smilowitz, A. J. Heeger and F. Wudl, *Science*, 1992, **258**, 1474–1476.
- 11 N. C. Greenham, S. C. Moratti, D. D. C. Bradley, R. H. Friend and A. B. Holmes, *Nature*, 1993, **365**, 628–630.
- 12 T. M. Swager, C. J. Gil and M. S. Wrighton, *J. Phys. Chem.*, 1995, **99**, 4886–4893.

- 13 C. Weder and M. S. Wrighton, *Macromolecules*, 1996, **29**, 5157–5165.
- 14 M. R. Pinto, B. Hu, F. E. Karasz and L. Akcelrud, *Polymer*, 2000, **41**, 2603–2611.
- 15 R. M. Gurge, A. Sarker, P. M. Lahti, B. Hu and F. E. Karasz, *Macromolecules*, 1996, **29**, 4287–4292.
- 16 A. Lux, A. B. Holmes, R. Cervini, J. E. Davies, S. C. Moratti, J. Grüner, F. Cacialli and R. H. Friend, *Synth. Met.*, 1997, **84**, 293–294.
- 17 J. A. Mikroyannidis, I. K. Spiliopoulos, T. S. Kasimis, A. P. Kulkarni and S. A. Jenekhe, *Macromolecules*, 2003, **36**, 9295–9302.
- 18 Z. Peng, Z. Bao and M. E. Galvin, *Adv. Mater.*, 1998, **10**, 680–684.
- 19 X. Zhan, Y. Liu, X. Wu, S. Wang and D. Zhu, *Macromolecules*, 2002, **35**, 2529–2537.
- 20 M. Jonforsen, T. Johansson, O. Inganäs and M. R. Andersson, *Macromolecules*, 2002, **35**, 1638–1643.
- 21 M. J. Marsella, D. - K Fu and T. M. Swager, *Adv. Mater.*, 1995, **7**, 145–147.
- 22 L. Kloppenburg, D. Song and U. H. F. Bunz, *J. Am. Chem. Soc.*, 1998, **120**, 7973–7974.
- 23 D. A. M. Egbe, C. P. Roll, E. Birckner, U.-W. Grummt, R. Stockmann and E. Klemm, *Macromolecules*, 2002, **35**, 3825–3837.
- 24 D. A. M. Egbe, C. Bader, E. Klemm, L. Ding, F. E. Karasz, U. Grummt and E. Birckner, *Macromolecules*, 2003, **36**, 9303–9312.
- 25 S. Rathgeber, D. Bastos de Toledo, E. Birckner, H. Hoppe and D. A. M. Egbe, *Macromolecules*, 2010, **43**, 306–315.
- 26 F. Cacialli, P. Samorì and C. Silva, *Mater. Today*, 2004, **7**, 24–32.
- 27 H. Hoppe and N. S. Sariciftci, *J. Mater. Chem.*, 2006, **16**, 45–61.
- 28 G. Li, V. Shrotriya, J. Huang, Y. Yao, T. Moriarty, K. Emery and Y. Yang, *Nat. Mater.*, 2005, **4**, 864–868.
- 29 J. Peet, J. Y. Kim, N. E. Coates, W. L. Ma, D. Moses, A. J. Heeger and G. C. Bazan, *Nat. Mater.*, 2007, **6**, 497–500.
- 30 D. A. M. Egbe, H. Tillmann, E. Birckner and E. Klemm, *Macromol. Chem. Phys.*, 2001, **202**, 2712–2726.
- 31 D. A. M. Egbe, L. H. Nguyen, H. Hoppe, D. Mühlbacher and N. S. Sariciftci,

- Macromol. Rapid Commun.*, 2005, **26**, 1389–1394.
- 32 D. A. M. Egbe, B. Carbonnier, E. Birckner and U. W. Grummt, *Prog. Polym. Sci.*, 2009, **34**, 1023–1067.
- 33 D. D. Armarego, K. N., Perrin, in *Purification of Laboratory Chemicals*, Butterworth-Heinemann, Oxford, 4th Edition, Butterworth Heinemann, 1996.
- 34 R. Österbacka, A. Pivrikas, G. Juška, K. Genevičius, K. Arlauskas and H. Stubb, *Curr. Appl. Phys.*, 2004, **4**, 534–538.
- 35 J. Sicé, *J. Am. Chem. Soc.*, 1953, **75**, 3697–3700.
- 36 L. I. Smith and M. Bayliss, *J. Org. Chem.*, 1941, **06**, 437–442.
- 37 K. Sonogashira, Y. Tohda and N. Hagihara, *Tetrahedron Lett.*, 1975, **16**, 4467–4470.
- 38 M. Schilz and H. Plenio, *J. Org. Chem.*, 2012, **77**, 2798–2807.
- 39 A. Wild, D. A. M. Egbe, E. Birckner, V. Cimrová, R. Baumann, U.-W. Grummt and U. S. Schubert, *J. Polym. Sci. Part A Polym. Chem.*, 2009, **47**, 2243–2261.
- 40 B. A. Arbusow, *Pure Appl. Chem.*, 2008, **9**, 307–336.
- 41 V. H.-H. Hörhold and J. Opfermann, *Die Makromol. Chemie*, 1970, **131**, 105–132.
- 42 D. A. M. Egbe, B. Cornelia, J. Nowotny, W. Günther and E. Klemm, *Macromolecules*, 2003, **36**, 5459–5469.
- 43 R. O. Garay, H. Naarmann and K. Muellen, *Macromolecules*, 1994, **27**, 1922–1927.
- 44 J. A. Mikroyannidis, M. M. Stylianakis, P. Balraju, P. Suresh and G. D. Sharma, *ACS Appl. Mater. Interfaces*, 2009, **1**, 1711–1718.
- 45 P. Schilinsky, U. Asawapirom, U. Scherf, M. Biele and C. J. Brabec, *Chem. Mater.*, 2005, **17**, 2175–2180.
- 46 F. C. Krebs, *Sol. Energy Mater. Sol. Cells*, 2009, **93**, 394–412.
- 47 H. Hoppe and N. S. Sariciftci, *J. Mater. Res.*, 2004, **19**, 1924–1945.
- 48 C. Winder and N. S. Sariciftci, *J. Mater. Chem.*, 2004, **14**, 1077.
- 49 Y. Cheng, S. Yang and C. Hsu, *Chem. Rev.*, 2009, **109**, 5868–5923.
- 50 D. Ayuk Mbi Egbe, L. H. Nguyen, K. Schmidtke, A. Wild, C. Sieber, S. Guenes and N. Serdar Sariciftci, *J. Polym. Sci. Part A Polym. Chem.*, 2007, **45**, 1619–1631.

- 51 T. Tiedje and A. Rose, *Solid State Commun.*, 1981, **37**, 49–52.
- 52 H. Klauk, G. Schmid, W. Radlik, W. Weber, L. Zhou, C. D. Sheraw, J. A. Nichols and T. N. Jackson, *Solid. State. Electron.*, 2003, **47**, 297–301.
- 53 G. Horowitz, *Adv. Mater.*, 1998, **10**, 365–377.
- 54 H. Hoppe, M. Niggemann, C. Winder, J. Kraut, R. Hiesgen, A. Hinsch, D. Meissner and N. S. Sariciftci, *Adv. Funct. Mater.*, 2004, **14**, 1005–1011.
- 55 Y. Yao, J. Hou, Z. Xu, G. Li and Y. Yang, *Adv. Funct. Mater.*, 2008, **18**, 1783–1789.
- 56 S. S. Nair, D. Kumar and A. Majumdar, *Polym. Eng. Sci.*, 2015, **55**, 1382–1388.

Supporting Information**Figure SI 3a.1** $^1\text{H-NMR}$ spectrum ($\text{DMSO-}d_6$) of 2,5-dibromo-1,4-dihydroquinone (1a)**Figure SI 3a.2** $^1\text{H-NMR}$ spectrum (CDCl_3) of 1,4-dibromo-2,5-bis(octyloxy)benzene (2a)

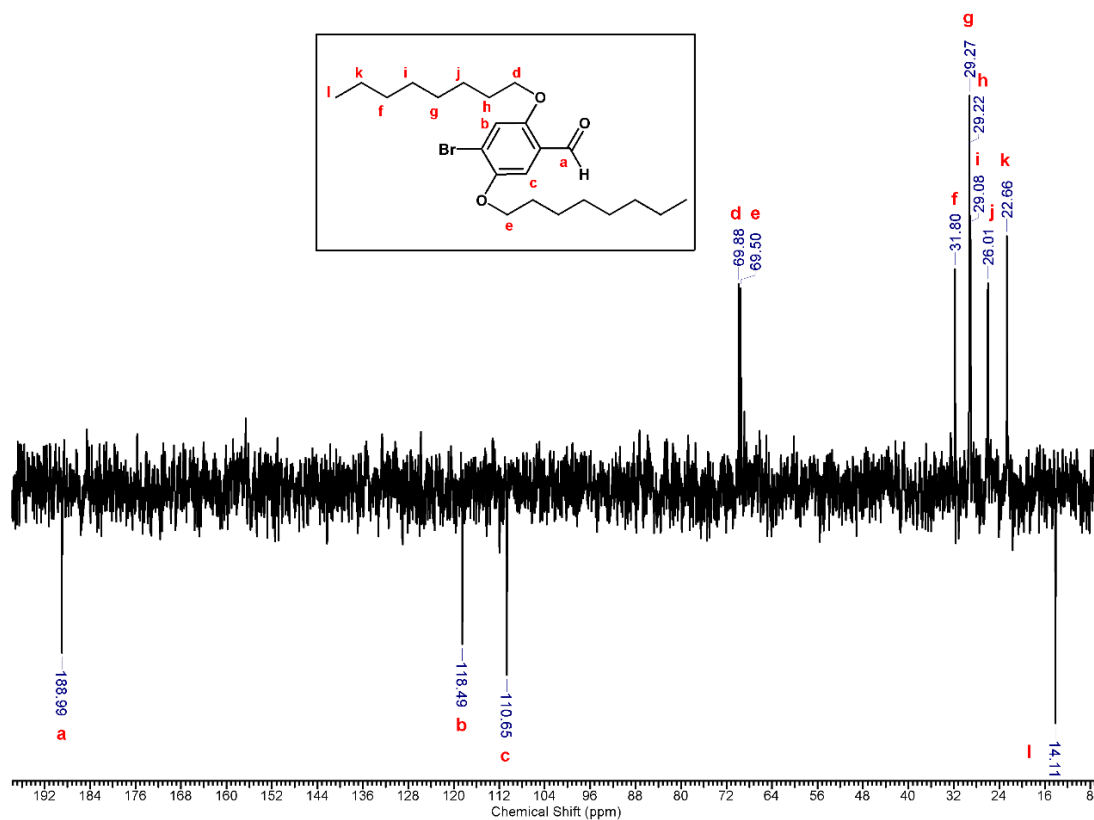


Figure SI 3a.3 ^{13}C -NMR-DEPT spectrum (CDCl_3) of 4-bromo-2,5-bis(octyloxy)benzaldehyde (3a)

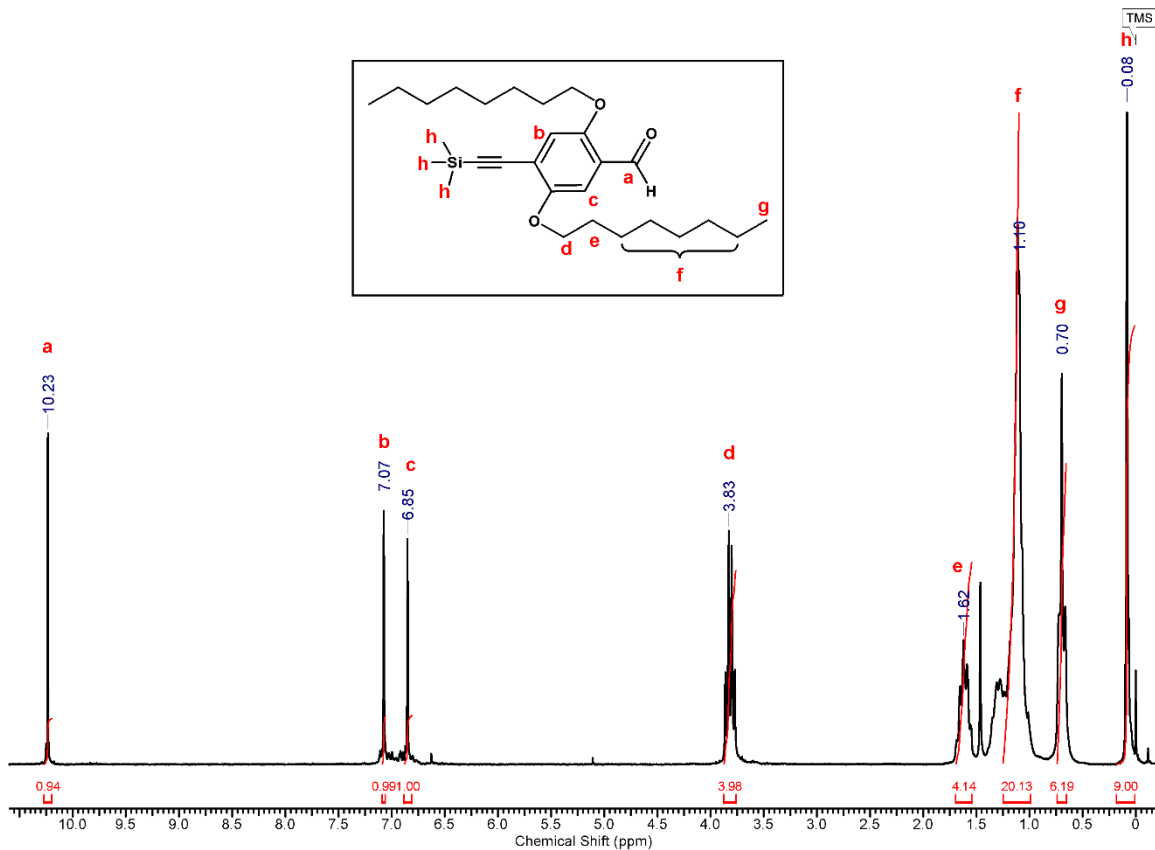


Figure SI 3a.4 ¹H-NMR spectrum (CDCl₃) of 2,5-bis(octyloxy)-4-[(trimethylsilyl)ethynyl]benzaldehyde (4a)

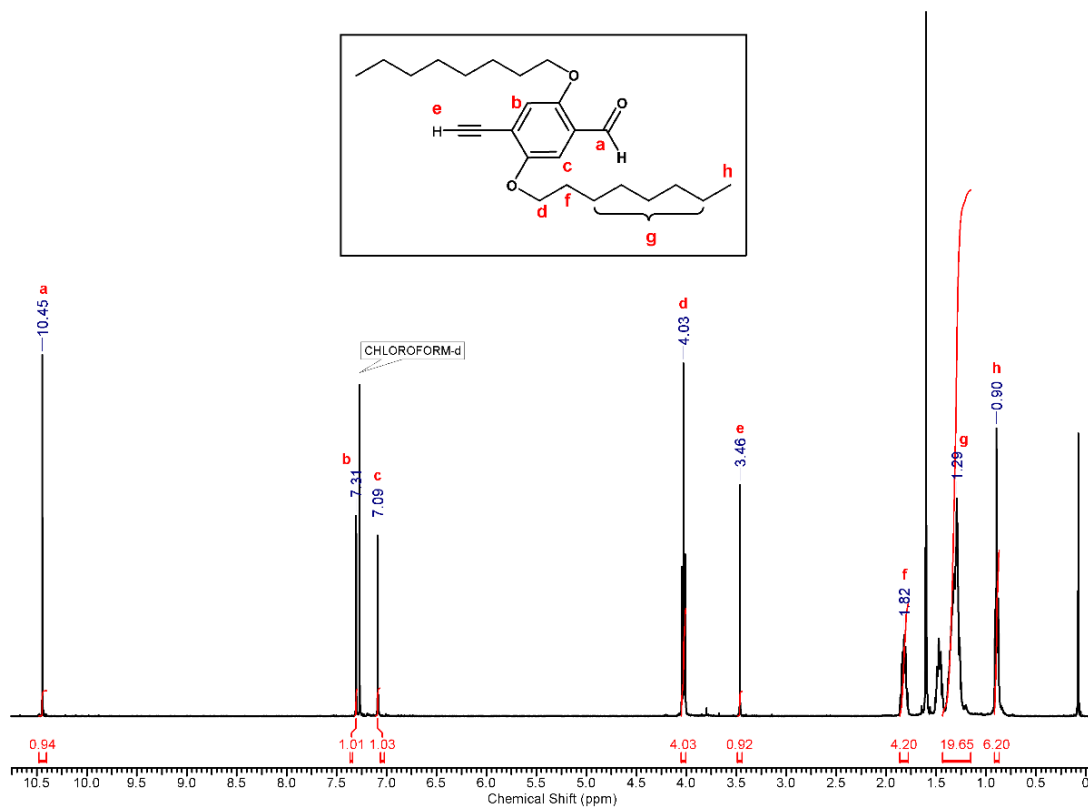


Figure SI 3a.5 $^1\text{H-NMR}$ spectrum (CDCl₃) of 4-ethynyl-2,5-bis(octyloxy)benzaldehyde (5a)

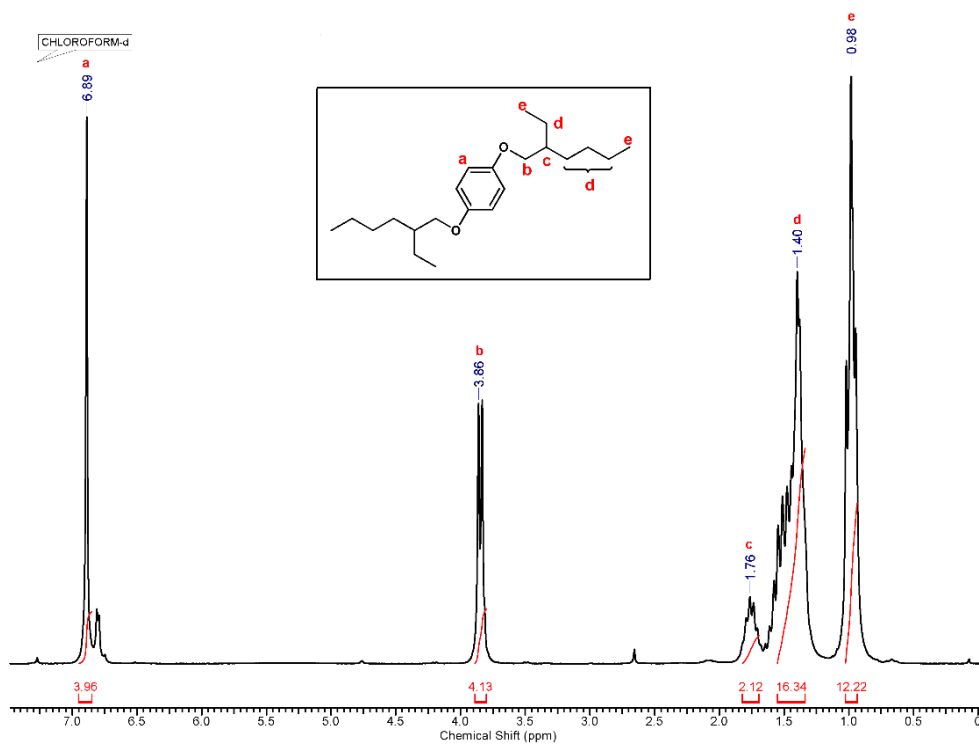


Figure SI 3a.6 $^1\text{H-NMR}$ spectrum (CDCl₃) of 1,4-bis((2-ethylhexyl)oxy)benzene (12b)

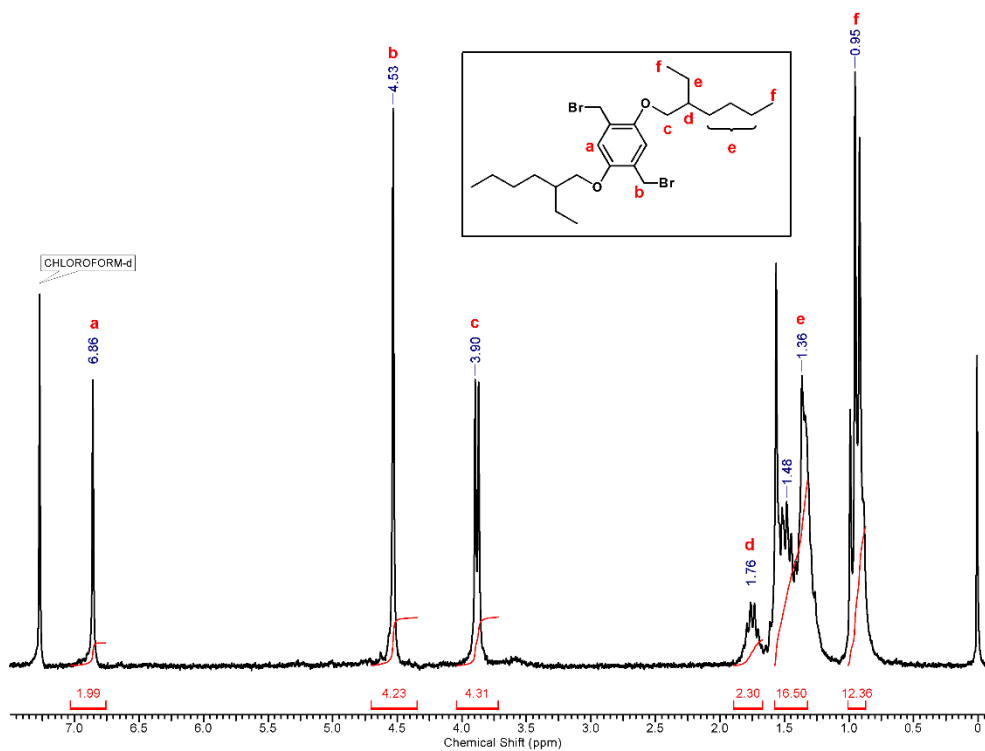


Figure SI 3a.7 $^1\text{H-NMR}$ spectrum (CDCl_3) of 1,4-bis-bromomethyl-2,5-bis-(2-ethylhexyloxy)-benzene (13b)

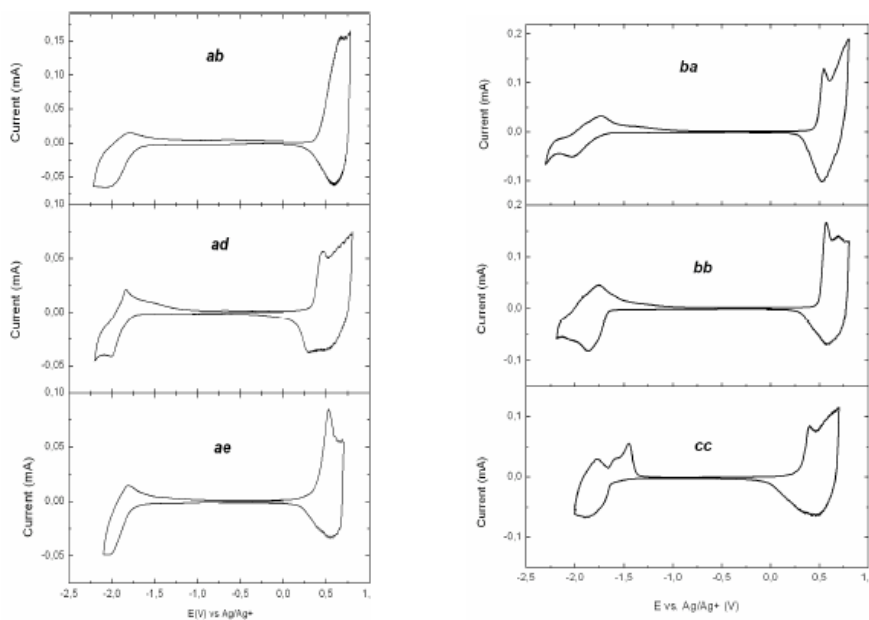


Figure SI 3a.8 Cyclic voltammograms of AnE-PV polymers

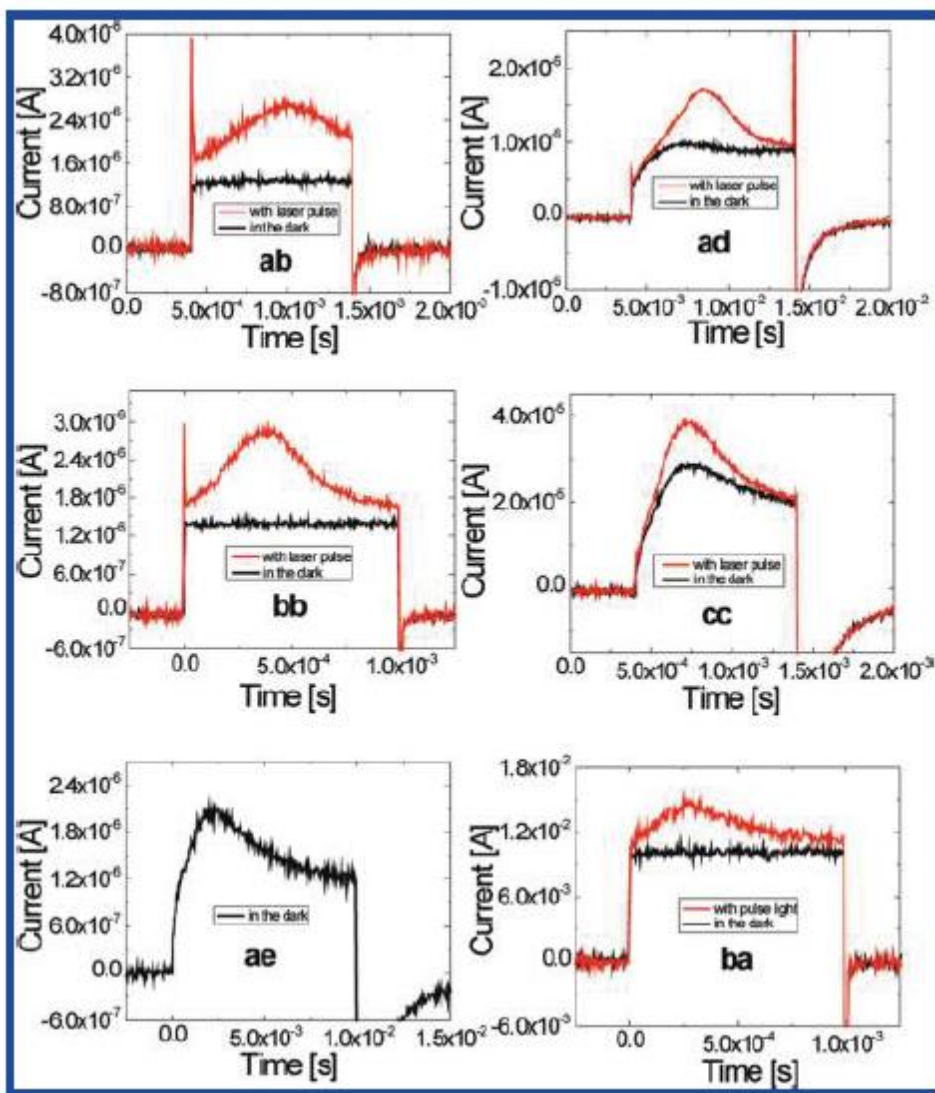


Figure SI 3a.9 CELIV study of AnE-PV polymers

CHAPTER 3b

Donor-Acceptor Low Band Gap Small Molecule Containing Anthracene Based Donor Unit and Diketopyrrolopyrrole, Benzothiadazole as Acceptor Units

3b.1 INTRODUCTION

The conjugated polymers/semiconducting polymers due to their tunable electronic and optical properties, lower cost, high flexibility and synthetic versatility, have garnered much attention as promising candidates in the future organic electronics market. The growing field of organic photovoltaics (OPVs)/ Organic solar cells (OSCs) has led to the astonishing developments in the design and synthesis of several new conjugated polymers.¹⁻³ For high performance in any particular device, semiconducting materials should possess narrow optical band-gaps, tunable HOMO-LUMO energy levels, high charge carrier mobilities and optimum morphology.

Low (narrow) band-gap (LBG) conjugated polymers/small molecules which absorb in near IR region and possess a band-gap less than 1.6 eV are particularly attractive in optoelectronic applications such as organic solar cells and photodetectors. LBG materials possess following interesting physical properties- i) their open circuit voltage (V_{oc}) values are closer to band-gap values than wide band-gap materials. This may be due to their electronic orbitals are more closely overlapping and the electrons are more delocalized;⁴ ii) charge separation in such materials is more efficient due to their larger dielectric constant, stronger dipole moment, and lower exciton binding energy.⁵ Therefore, LBG materials experienced rapid growth in the family of organic semiconductor materials and have experienced significant breakthroughs in the field of OPV towards the commercialization of solar cells.⁶⁻⁸

Various strategies to lower the band-gap of conjugated polymers include-1) increasing quinoid form of aromatic moieties in the backbone, 2) chemical rigidification, 3) inductive and mesomeric effects, 4) bridging the adjacent aromatic rings 5) alternating donor-acceptor unit, and 6) two-dimensional conjugation. Copolymerization of donor and acceptor units (D-A copolymer) is one of the most important strategies to broaden the absorption and lowering the band-gap of the conjugated polymers. In a copolymer, frontier molecular orbitals of donor and acceptor units interact with each other to form two new HOMOs and two new LUMOs. After the electrons redistribute from their original noninteracting orbitals to the new hybridized orbitals of the polymer, higher HOMO and lower LUMO energy levels are generated, leading to a narrowing of the optical band-gap.^{9,10}

The last decade has been marked by the intensive research on diketopyrrolopyrrole (DPP)-containing conjugated polymers which show promising optoelectronic characteristics such as brilliant red color, high photoluminescent and electroluminescent properties¹¹ and also possess exceptional electrochemical stability. DPP is a bicyclic heteroaromatic compound with two lactam units due to which it exhibits strong electron deficiency and can be used as acceptor unit in D-A conjugated copolymers. DPP shows efficient charge transport due to conjugated and highly planar structure with strong π - π interaction. Owing to all these favorable properties, DPP based polymers have been successfully employed in a variety of optoelectronic devices such as organic solar cells, transistors, light emitting diodes, chemo-sensors, two-photon absorption, and solid-state dye lasers.¹²⁻¹⁴ 2,1,3-Benzothiadiazole (BTDA) unit is another efficient electron acceptor building block for the synthesis of low band-gap D-A copolymers. Although BT has low solubility and relatively high-lying LUMO energy level, BTDA-based polymers have been considered as promising candidates for high performance OPVs.¹⁵⁻¹⁷

In this chapter, we attempted to synthesize two low band gap polymers using anthracene containing (*p*-phenylene-ethynylene) (AnPPE) as donor unit and either DPP or BTDA as acceptor units by Heck polymerization reaction. However, the polymer formation did not take place. Instead, the Heck reaction between the corresponding donor and acceptor units resulted in the formation of two donor-acceptor small molecules. Thus, in this chapter, synthesis and characterization of two low band gap D-A small molecules namely- AnPPE-Th-DPP(EH) and AnPPE-Th-BTDA is reported. The band-gap energy was considerably reduced for molecule AnPPE-Th-DPP(EH) (1.35 eV) as compared to molecule AnPPE-Th-BTDA (1.55 eV).

3b.2 EXPERIMENTAL

3b.2.1 Materials:

9,10-Bis[(4-formyl-2,5-dioctyloxy)phenylethynyl]anthracene (6a) was synthesised as described in Chapter 3a. *n*-Butyllithium solution (1.6 M in hexane), methyltriphenylphosphonium bromide ($\text{Ph}_3\text{PCH}_3\text{Br}$) 98%, palladium (II) acetate ($\text{Pd}(\text{OAc})_2$), tri(*o*-tolyl)phosphine ($\text{P}(\text{o-tolyl})_3$) (Aldrich Chemicals) and 4,7-bis(5-

bromothiophen-2-yl)benzo[c][1,2,5]thiadiazole (BTDA) (TCI Chemicals) were purchased and used as received. Triethylamine (SD Fine Chemicals) was purchased and was dried and distilled according to standard procedure.¹⁸

N,N-Dimethylformamide (DMF) and tetrahydrofuran (THF) were purchased and were dried and distilled according to standard procedures and stored under argon. Methanol, chloroform, *n*-hexane, toluene, diethyl ether and ethyl acetate (Merck) were purchased and used as received. If not otherwise specified, solvents or solution were degassed by bubbling with argon 1 h prior to use.

3b.2.2 Characterisation and techniques

Different techniques used for characterization of small molecules are described below-

NMR Spectroscopy: ¹H and ¹³C NMR spectra of donor, acceptor units and small molecules were recorded using a Bruker-AV spectrometer at operating frequency of 200 MHz, 400 MHz or 500 MHz in CDCl₃ or DMSO-*d*₆ with tetramethylsilane as an internal standard.

Gel permeation chromatography (GPC): Molecular weights and dispersity values of oligomers were determined on Thermo-Finnigan make GPC using tetrahydrofuran as an eluent at a flow rate of 1 mL min⁻¹ at 25 °C. Sample concentration was 2 mg mL⁻¹ and narrow dispersity polystyrenes were used as calibration standards.

Matrix assisted laser desorption/ionization time-of-flight (MALDI-TOF): MALDI-TOF spectra were obtained on a Bruker Autoflex TOF/TOF instrument using dithranol as a matrix.

Absorption and emission spectroscopy: The absorption spectra were recorded in dilute chloroform solution ($c \approx 10^{-6}$ mol l⁻¹) on a Perkin–Elmer UV/VIS-NIR Spectrometer Lambda 19. The absorption spectra of thin film from chlorobenzene solution were recorded on Varian UV/Vis-spectrophotometer and the corresponding emission spectra were recorded on a home-built photoluminescence setup. Thin films were spin coated on glass substrates using chlorobenzene solutions (0.6-0.8 wt %).

Cyclic voltammetry (CV): CV was performed with a PA4 polarographic analyzer (Laboratory Instruments, Prague, CZ) with a three-electrode cell. Platinum (Pt) wire electrodes were used both as working and counter electrodes, and a non-aqueous Ag/Ag⁺ electrode (Ag in 0.1 M AgNO₃ solution) was used as the reference electrode. CV

measurements were made in solutions of 0.1 M tetrabutylammonium hexafluorophosphate (TBAPF6) in acetonitrile under nitrogen atmosphere. Typical scan rates were 20, 50 and 100 mVs⁻¹, respectively. Thin films of small molecules were prepared onto Pt wire electrodes from chlorobenzene solution. All measurements and film preparations were performed in a nitrogen atmosphere within a glove box.

3b.2.3 Fabrication and characterization of the organic field effect transistor devices (OFET)

Charge carrier mobility was measured in field effect transistor device by using the bottom gate and bottom contact device architecture.^{19,20} OFET device was fabricated using commercially available FET substrate. The N-doped silicon was used as a gate electrode and silicon dioxide (SiO₂) layer was used as a gate dielectric. The thickness of silicon oxide was 240 nm. The source and drain electrodes were patterned on the top of dielectric layer. First, device was cleaned by sonicating in acetone and then in 2-propanol. The device was then dried using a hot air gun and kept in an argon atmosphere. Then, the device was surface modified by self-assembled monolayer of hexamethyldisilane (HMDS).^{21,22} The monolayer was prepared by the dipping the device in a 0.1 M solution of HMDS in chloroform for 12 h. The device was dried before casting the active layer. The active layer was cast by spin coating the solution (10 mg/mL of small molecule in 1,2-dichlorobenzene). Agilent 4156 semiconductor probe analyzer and semiprobe station were used for OFET measurements. Charge carrier mobility of oligomer was measured at room temperature. In order to study the impact of thermal annealing, the devices were annealed at 100°C under an argon atmosphere for 10 min and charge carrier mobility of annealed device was measured.

3b.3 SYNTHESIS

3b.3.1 Synthesis of 9,10-bis((2,5-bis(octyloxy)-4-vinylphenyl)ethynyl)anthracene (15)

AnPPE (15) was synthesised from 9,10-bis[(4-formyl-2,5-dioctyloxy)phenylethynyl]anthracene (6a). The synthesis of 6a is described in Chapter 3a (section 3a.4.1.1.1)

Into a 250 mL three-necked round bottom flask equipped with nitrogen gas inlet and a magnetic stir bar were added methyltriphenylphosphonium bromide (0.514 g, 1.44

mmol) and dry THF (30 mL) and the suspension was cooled to 0 °C. Then solution of *n*-butyllithium (1.6 M in hexane, 0.9 mL, 1.44 mmol) was added dropwise into it and the reaction mixture was stirred for 10 min. The solution of 6a (0.68 g, 0.72 mmol) in 40 mL THF was added dropwise into the reaction mixture. It was then allowed to attain room temperature and was stirred for 24 h. The reaction mixture was added into water (100 mL) and stirred for 10 min and then the product was extracted with diethyl ether (3 × 100 mL). The combined organic solutions were dried over Na₂SO₄, filtered and concentrated under reduced pressure. The residue was purified by column chromatography over silica gel with toluene: hexane (1:1, v/v) as eluent to yield orange colored solid.

Yield: 0.58 g, (86%)

¹H-NMR (200 MHz, CDCl₃, δ/ppm): 8.79 (d, 4H, anthracene H), 7.57 (m, 4H, anthracene H), 7.20 (s, 2H, Ar-H), 7.13-7.0 (m, 4H, Ar-H and vinyl protons), 5.87 (d, 2H, vinyl protons), 5.39 (d, 2H, vinyl protons), 4.21-4.02 (m, 8H, -OCH₂-), 1.96-1.76 (m, 8H, -OCH₂-CH₂-(CH₂)₅-CH₃), 1.31-1.21 (m, 40H, -CH₂-), 0.91 (t, 12H, -CH₃).

3b.3.2 Synthesis of 3,6-bis(5-bromothiophen-2-yl)-2,5-bis(2-ethylhexyl)-2,5-dihydropyrrolo[3,4-c]pyrrole-1,4-dione (3)

3b.3.2.1 Synthesis of 3,6-di(thiophen-2-yl)-2,5-dihydropyrrolo[3,4-c]pyrrole-1,4-dione (1)

Compound 1 was synthesised from 2-thiophene carbonitrile and dimethyl succinate by following the literature procedures.^{23,24}

3b.3.2.2 Synthesis of 2,5-bis(2-ethylhexyl)-3,6-di(thiophen-2-yl)-2,5-dihydropyrrolo[3,4-c]pyrrole-1,4-dione (2)

Into a 250 mL three-necked round bottom flask equipped with a nitrogen gas inlet and a magnetic stir bar were added compound 1 (13.5 g, 45.0 mmol), anhydrous potassium carbonate (25 g, 180 mmol) and dry DMF (250 mL). The reaction mixture was heated at 140°C under inert atmosphere. 2-Ethylhexyl bromide (38.6 g, 200 mmol) was added dropwise. Then the reaction mixture was heated at 140°C for 24 h. Then it was cooled, poured into 500 mL of ice-cold water, stirred for 1 h and extracted with chloroform (3 x 200 mL). The organic layer was dried over Na₂SO₄, filtered and concentrated. The residue was purified by column chromatography using dichloromethane to afford purple-black powder.

Yield= 16.5 g (70 %).

¹H-NMR (400 MHz, CDCl₃, δ/ppm): 8.94 (d, 2H, thiophene H), 7.61 (d, 2H, thiophene H), 7.28 (d, 2H, thiophene H), 4.02 (m, 4H, -OCH₂-), 1.85 (m, 2H, -CH-), 1.35-1.22 (m, 16H, -CH₂-), 0.84 (m, 12H, -CH₃).

3b.3.2.3 Synthesis of 3,6-bis(5-bromothiophen-2-yl)-2,5-bis(2-ethylhexyl)-2,5-dihydropyrrolo[3,4-c]pyrrole-1,4-dione (3)

Into a 250 mL three-necked round bottom flask equipped with an argon gas inlet and a magnetic stir bar were added compound 2 (4.19 g, 8.0 mmol) and 300 mL chloroform. The solution was protected from light and was kept under argon protection. N-Bromosuccinimide (2.91 g, 16.33 mmol) was added portion-wise, and the reaction mixture was stirred at room temperature for 40 h. Then reaction mixture was poured into water, and the organic phase was separated and washed by water. The organic layer was dried over Na₂SO₄ and concentrated by rotary evaporation. The crude reaction mixture was purified by column chromatography on silica gel using chloroform: hexane (1:1, v/v) solvent mixture as an eluent, to yield dark-purple solid as pure product.

Yield: 16.0 g (76%).

¹H-NMR (400 MHz, CDCl₃, δ/ppm): 8.64 (d, 2H, thiophene H), 7.24 (d, 2H, thiophene H), 3.92 (m, 4H, -OCH₂-), 1.84 (m, 2H, -CH-), 1.4-1.2 (br, 16H, -CH₂-), 0.89 (m, 12H, -CH₃).

3b.3.3 Synthesis of AnPPE-Th-DPP(EH)

Into a 100 mL Schlenk tube equipped with an argon gas inlet and a magnetic stir bar were added compound 15 (100 mg, 0.11 mmol), compound 3 (72.41 mg, 0.11 mmol) and DMF (3 mL) and toluene (3 mL) (1: 1 ratio). To this reaction mixture, triethyl amine (0.2 ml) was added and the reaction mixture was degassed under argon for 1 h. Then, Pd(OAc)₂ (2.5 mg, 0.011 mmol) and P(o-tolyl)₃ (16.7 mg, 0.055 mmol) were added into the reaction mixture. The reaction mixture was stirred at 80 °C under inert atmosphere for 24 h. After cooling to room temperature, the reaction mixture was added into methanol and precipitated compound was filtered and dried. The product was purified by Soxhlet extraction with methanol and hexane for 24 h. Then the compound was dried under vacuum to yield an indigo coloured solid.

Yield: 98 mg (63 %).

¹H-NMR (200 MHz, CDCl₃, δ/ppm): 9.06-8.87 (multiple peaks, 6H, anthracene and thiophene protons), 7.70-7.29 (multiple peaks, 8H, 4 anthracene protons and 4 newly formed vinylene protons), 7.26-6.97 (multiple peaks, 6H, 2 thiophene and 4 phenylene protons), 4.10-3.95 (12H, m, -OCH₂-), 2.08-1.80 (10H, m, -OCH₂-CH₂- of octyl chain and -OCH₂-CH₂- of ethylhexyl chain), 1.35-1.20 (m, 56H, -CH₂-), 0.91-0.86 (t, 24H, -CH₃).

3b.3.4 Synthesis of AnPPE-Th-BTDA

The synthesis of AnPPE-Th-BTDA was carried out under the same reaction conditions as described in section 3a.3.3 by using compound 15 (90 mg) and 4,7-bis(5-bromothiophen-2-yl)benzo[c][1,2,5]thiadiazole (BTDA) (47 mg) Pd(OAc)₂ (2.4 mg, mmol), P(o-tolyl)₃ (15.3 mg, mmol) and triethyl amine (2 mL).

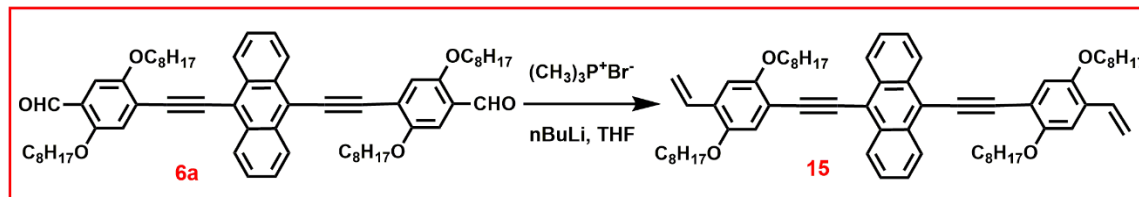
Yield: 72 mg (51 %).

¹H-NMR spectrum was not obtained for this compound, as it remained mostly insoluble in organic solvents such as chloroform, dimethyl sulphoxide. It was partially soluble in dichloromethane and chlorobenzene at high temperature.

3b.4 RESULTS AND DISCUSSION

3b.4.1 Synthesis of donor unit 9,10-bis((2,5-bis(octyloxy)-4-vinylphenyl)ethynyl)anthracene (AnPPE) (15)

The precursor- 9,10-bis[(4-formyl-2,5-dioctyloxy)phenylethynyl]anthracene (6a) was synthesised by following the six-step synthetic protocol as described in Chapter 3a in section 3a.4.1.1.1. The target compound (donor unit) 9,10-bis((2,5-bis(octyloxy)-4-vinylphenyl)ethynyl)anthracene (15) was synthesised from 6a, as depicted in **Scheme 3b.1**. Compound 15 was synthesised from 6a by Wittig olefination reaction using methyltriphenylphosphonium bromide (Ph₃PCH₃Br) in presence of n-butyllithium, at room temperature. This synthetic route was particularly advantageous due to facile separation of desired product (divinyl derivative, 15) from the monoaldehyde impurities, resulting from incomplete conversion. Strong polarity difference of reactant and product facilitates chromatographic purification of the product.²⁵



Scheme 3b.1 Synthesis of 9,10-bis((2,5-bis(octyloxy)-4-vinylphenyl)ethynyl)anthracene (**15**, AnPPE).

$^1\text{H-NMR}$ spectrum of divinyl derivative **15** is presented in **Figure 3b.1**. The peaks due to anthracene protons were observed at 8.79 and 7.57 ppm. Multiple peaks due to protons on phenyl ring and vicinal double bond protons were observed in the range 7.22-7.03 δ ppm. The presence of newly formed double bonds was confirmed by the appearance of two doublets at 5.87 ppm and 5.39 ppm due to geminal protons on double bond. The $-\text{CH}_2$ protons on octyloxy side chain which are adjacent to oxygen, were observed in the range of 4.02-4.21 ppm. The remaining CH_2 protons were in the range 1.96-1.22 ppm. Methyl protons appeared at 0.91 ppm.

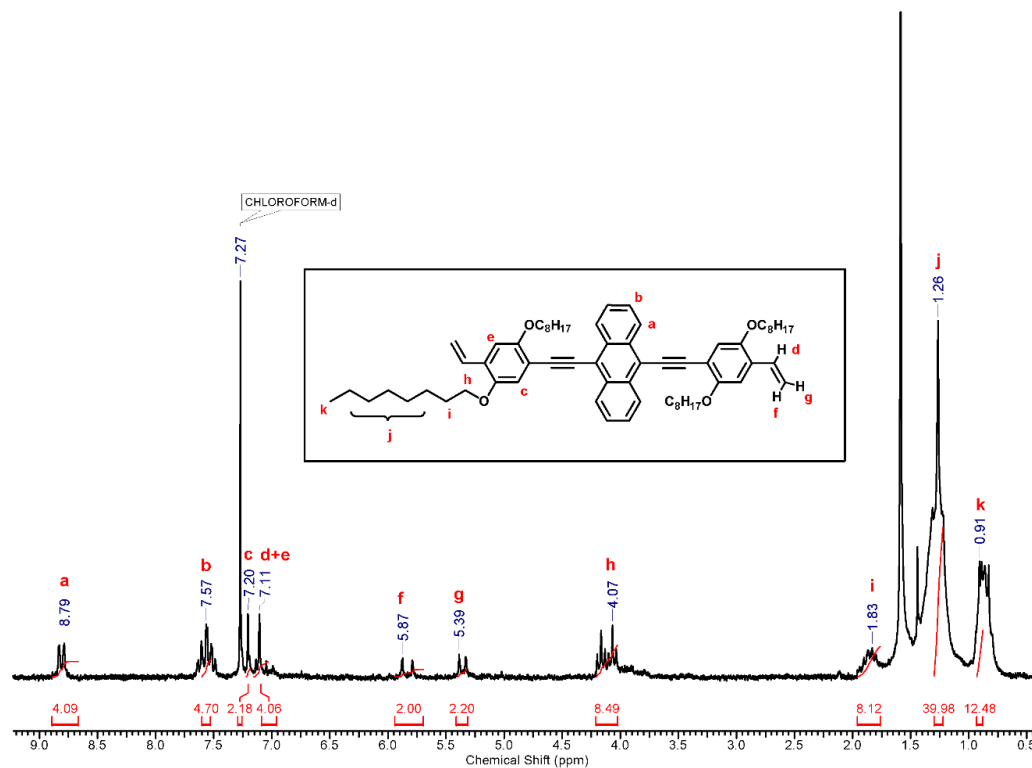
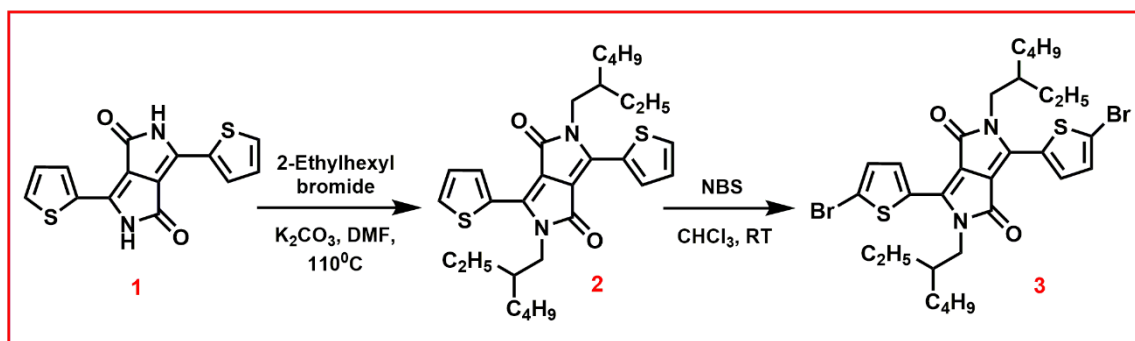


Figure 3b.1 $^1\text{H-NMR}$ spectrum (CDCl_3) of 9,10-bis((2,5-bis(octyloxy)-4-vinylphenyl)ethynyl)anthracene (**15**, AnPPE).

3b.4.2 Synthesis of acceptor unit 3,6-bis(5-bromothiophen-2-yl)-2,5-bis(2-ethylhexyl)-2,5-dihydropyrrolo[3,4-c]pyrrole-1,4-dione (3, DPP(EH))

The two step synthesis of 3 from 3,6-di(thiophen-2-yl)-2,5-dihydropyrrolo[3,4-c]pyrrole-1,4-dione (1) is depicted in **Scheme 3a.1**. Compound 1 was synthesised by condensation of 2-thiophene carbonitrile and dimethyl succinate in *tert*-amyl alcohol using potassium *tert*-butoxide as a base.^{23,26} Compound 1 was then N-alkylated using 2-ethylhexyl bromide and potassium carbonate to yield 2,5-bis(2-ethylhexyl)-3,6-di(thiophen-2-yl)-2,5-dihydropyrrolo[3,4-c]pyrrole-1,4-dione (2). The subsequent bromination of N-alkylated derivative 2 with N-bromosuccinimide in chloroform afforded the desired product- DPP(EH) (3).



Scheme 3b.2 Synthesis of 3,6-bis(5-bromothiophen-2-yl)-2,5-bis(2-ethylhexyl)-2,5-dihydropyrrolo[3,4-c]pyrrole-1,4-dione (3, DPP(EH)).

¹H-NMR spectrum of DPP(EH) (3) is presented in **Figure 3b.2**. The protons on thiophene ring appeared as doublets at 8.64 and 7.24 δ ppm. The CH₂ protons on ethylhexyl side chain which are adjacent to nitrogen atom of lactum ring, were observed as a doublet at 3.92 δ ppm. The two protons at branch position of ethylhexyl side chain were observed as multiplet in the range 1.89-1.60 δ ppm. The remaining CH₂ protons on ethylhexyl side chain were observed in the range 1.20-1.35 δ ppm. The peak due to CH₃ protons appeared as a triplet at 0.89 δ ppm.

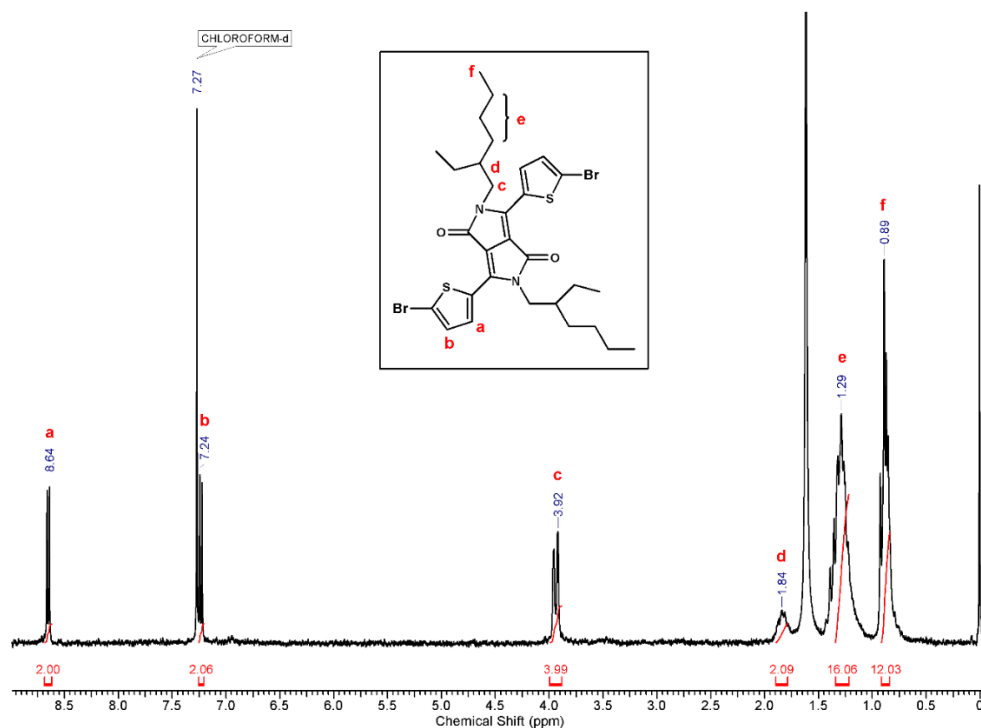
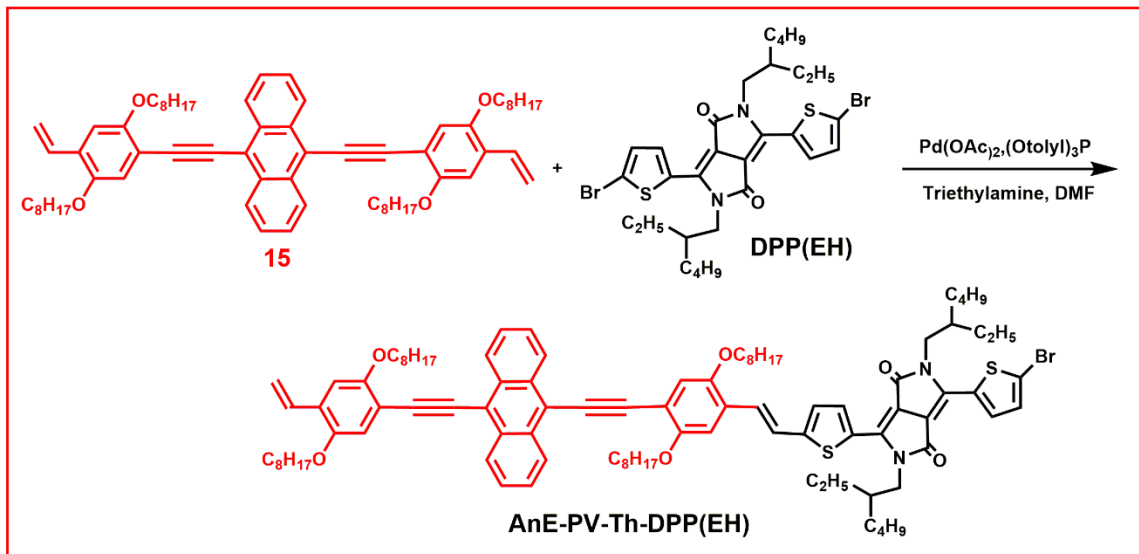


Figure 3b.2 ¹H-NMR spectrum (CDCl₃) of 3,6-bis(5-bromothiophen-2-yl)-2,5-bis(2-ethylhexyl)-2,5-dihydropyrrolo[3,4-c]pyrrole-1,4-dione (3, DPP(EH)).

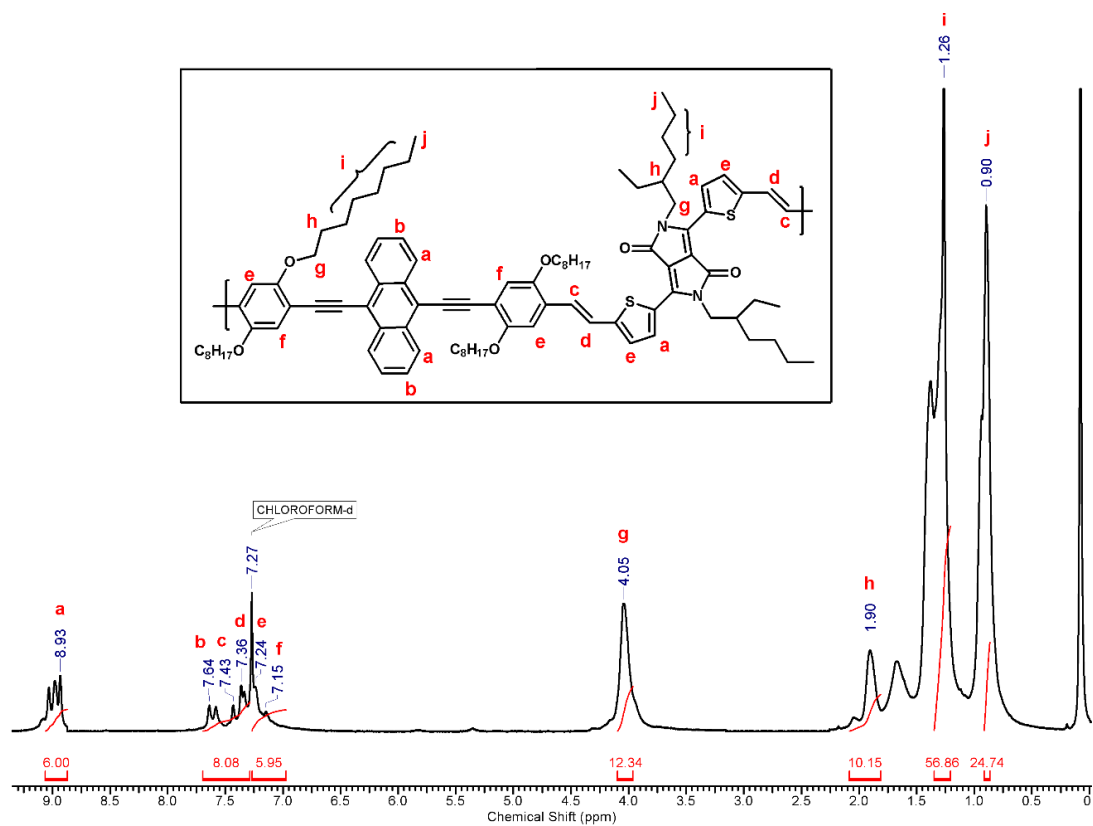
3b.4.3 Synthesis of AnPPE-Th-DPP(EH)

AnPPE-Th-DPP(EH) was synthesised by Heck coupling reaction^{27,28} of 9,10-bis((2,5-bis(octyloxy)-4-vinylphenyl)ethynyl)anthracene (15) with 3,6-bis(5-bromothiophen-2-yl)-2,5-bis(2-ethylhexyl)-2,5-dihydropyrrolo[3,4-c]pyrrole-1,4-dione (3) in the presence of palladium (II) acetate (Pd(OAc)₂) as catalyst, tri(o-tolyl)phosphine (P(o-tolyl)₃) as ligand and triethyl amine as a base. Synthesis of AnPPE-Th-DPP(EH) is depicted in **Scheme 3b.3**.

¹H-NMR spectrum of AnPPE-Th-DPP(EH) is presented in **Figure 3b.3**. Anthracene and thiophene protons were appeared as multiple peaks in the range 9.06-8.87 ppm. Multiple peaks observed in the range 7.70-7.29 ppm were due to anthracene and newly formed double bond protons. Two peaks appeared in the range 7.26-6.97 ppm were due to thiophene and phenylene protons. Methylene protons attached to oxygen atom of alkoxy side chain and nitrogen atom of lactam ring of DPP were observed in the range 4.10-3.95 ppm. Remaining methylene protons of side chains were appeared in the range 2.08-1.20 ppm. Methyl protons were observed as triplet at 0.9 ppm.

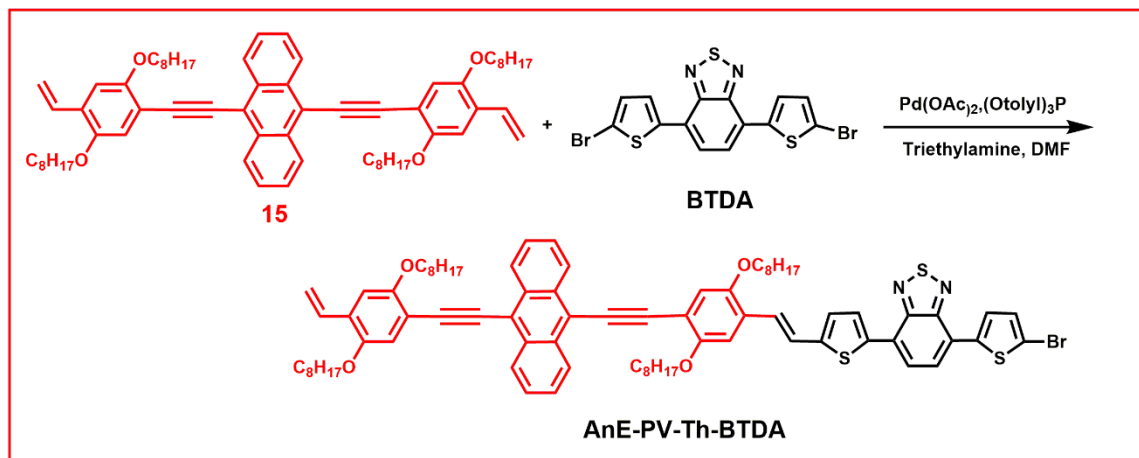


Scheme 3b.3 Synthesis of AnPPE-Th-DPP(EH)

Figure 3b.3 ¹H-NMR spectrum (CDCl₃) of AnPPE-Th-DPP(EH).

3b.4.4 Synthesis of AnPPE-Th-BTDA

AnPPE-Th-BTDA was synthesised by Heck coupling reaction of 9,10-bis((2,5-bis(octyloxy)-4-vinylphenyl)ethynyl)anthracene (15) with 4,7-bis(5-bromothiophen-2-yl)benzo[c][1,2,5]thiadiazole (BTDA) as depicted in **Scheme 3b.4**



Scheme 3b.4 Synthesis of AnPPE-Th-BTDA.

Two different kind of anthracene containing donor-acceptor small molecules namely- AnPPE-Th-DPP(EH) and AnPPE-Th-BTDA were synthesized by Pd-catalyzed Heck reaction. These small molecules consist of anthracene containing (*p*-phenylene-ethynylene) (AnPPE) as a donor unit and either diketopyrrolopyrrole (DPP) or benzothiadazole (BTDA) as acceptor units.

AnPPE-Th-DPP(EH) was soluble in organic solvents such as chloroform, dichloromethane, tetrahydrofuran, toluene and chlorobenzene at room temperature. AnPPE-Th-BTDA was partly soluble in dichloromethane and chlorobenzene at high temperature (90°C). The data obtained from GPC and Matrix assisted laser desorption ionisation (MALDI-TOF) experiment are summarised in **Table 3b.1**.

Table 3b.1. Data obtained from GPC and MALDI study

Small molecule	Molecular Weight by GPC			Mass by MALDI-TOF
	M _n	M _w	Dispersity	
AnPPE-Th-DPP(EH)	1380	2300	1.7	1570
AnPPE-Th-BTDA*	-	-	-	-

* Molecular weight determination by GPC and mass determination by MALDI-TOF was not possible for AnPPE-Th-BTDA due to solubility issue

Number average molecular weight of AnPPE-Th-DPP(EH) by GPC was found to be 1380 g/mol. MALDI-TOF of AnPPE-Th-DPP(EH) was recorded using dithranol as a matrix and the spectrum is shown in **Figure 3b.4**. MALDI-TOF spectrum showed signal at 1569.51 corresponding to $[M+Na]^+$ of AnPPE-Th-DPP(EH) (calcd. for $[M+Na]^+$ for $C_{96}H_{123}BrN_2O_6S_2Na = 1568.80$). From GPC and MALDI-TOF results, it was concluded that AnPPE-Th-DPP(EH) formed as a donor-acceptor monomeric unit, as shown in the **Figure 3b.5**. Repeated batches for synthesis of AnPPE-Th-DPP(EH), result in similar molecular weight material. The obtained results, demonstrated that polymer chain is not growing. Similar result was obtained by Jung *et al*²⁹ for similar system which they attributed to inherent low reactivity of Heck coupling reaction.³⁰ One more possibility may be the steric crowd of donor unit (AnPPE) which might hinder the reaction site for polymerization.

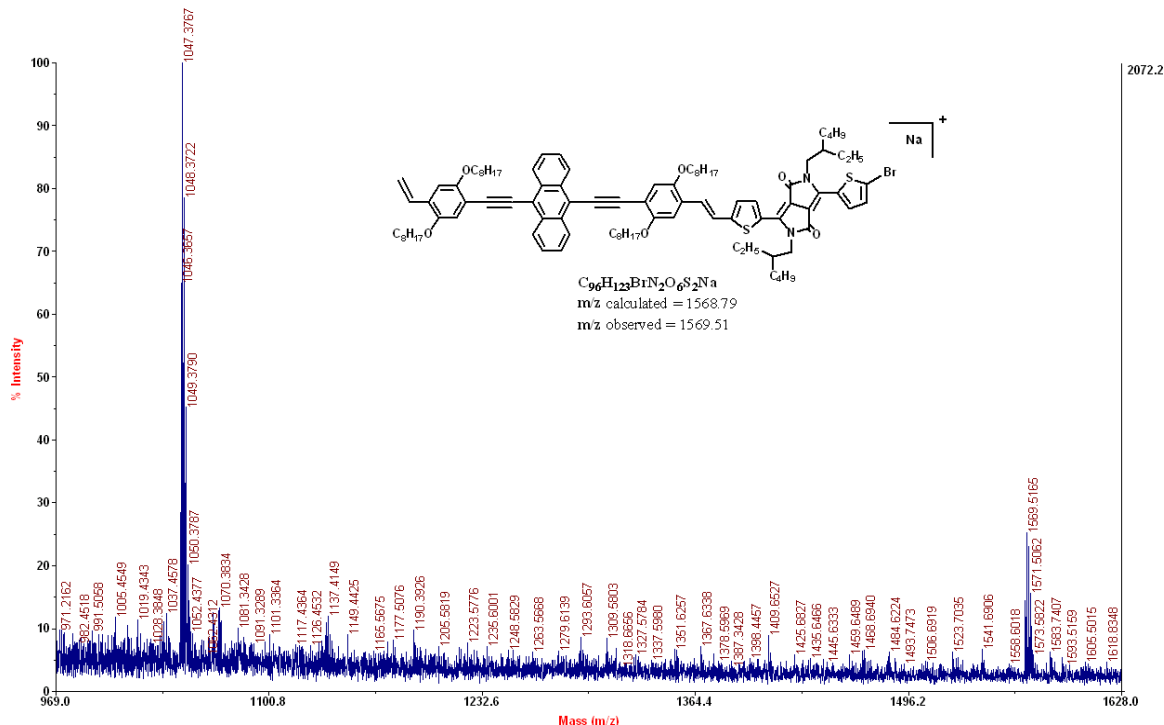


Figure 3b.4 MALDI-TOF spectrum of AnPPE-Th-DPP(EH).

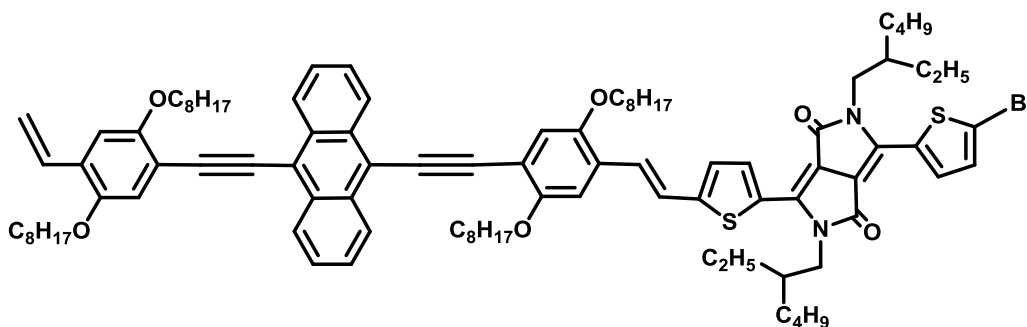


Figure 3b.5 Predicted structure of AnPPE-Th-DPP(EH).

3b.4.5 Photophysical Study

The photophysical data of donor, acceptor units and D-A small molecules was measured in chloroform/chlorobenzene solution as well as on thin films spin coated from chlorobenzene. The absorption spectra of compounds- AnPPE, DPP(EH) and D-A molecule- AnPPE-Th-DPP(EH) in dilute chloroform solution is depicted in **Figure 3b.6**. Donor unit- AnPPE and acceptor unit- DPP(EH) showed the wavelength at absorption

maximum (λ_a) at 502 and 563 nm, respectively. Both, donor unit and acceptor unit showed shoulder peak along with the main absorption peak at wavelengths 473 and 527 nm, respectively. The presence of shoulder peak is ascribed to the formation of aggregates in these molecules, in dilute solutions. On the other hand, the D-A molecule, AnPPE-Th-DPP(EH) exhibited wavelength at absorption maximum (λ_a) at 675 nm. The presence of the peak at 675 nm confirmed the formation donor-acceptor molecule.

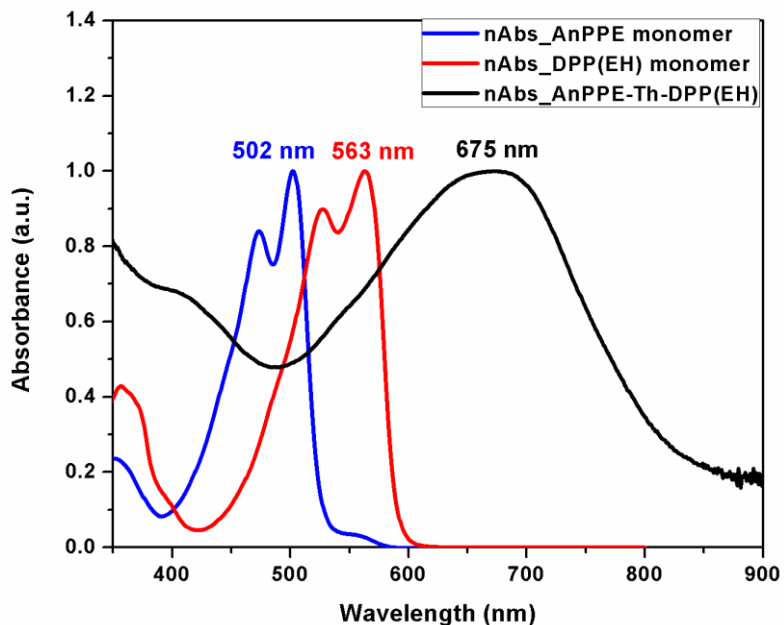


Figure 3b.6 The absorption spectra of AnPPE, DPP(EH) and AnPPE-Th-DPP(EH) in dilute chloroform solution.

Figure 3b.7 depicts the absorption spectra of compounds- AnPPE (RJ 15), BTDA and D-A molecule- AnPPE-Th-BTDA in dilute chlorobenzene solution. Donor unit AnPPE and acceptor unit BTDA showed the wavelength at absorption maximum (λ_a) at 502 and 461 nm, respectively. The D-A small molecule- AnPPE-Th-BTDA exhibited the wavelength at absorption maximum (λ_a) at 535 nm. Thus, presence of this band is a clear indication of formation of this molecule which otherwise cannot be confirmed by NMR, GPC or MALDI due to poor solubility of AnPPE-Th-BTDA in common organic solvents.

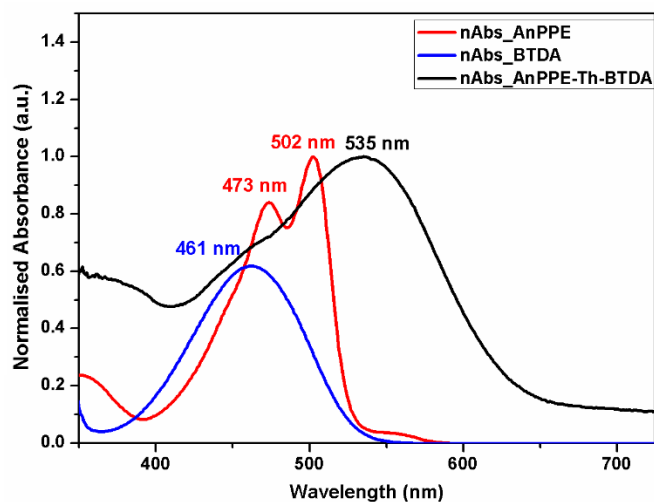


Figure 3b.7 Absorption spectra of AnPPE, BTDA and AnPPE-Th-BTDA in dilute chlorobenzene solution.

The photoluminescence spectra of AnPPE, DPP(EH) and D-A molecule- AnPPE-Th-DPP(EH) in dilute chloroform solution is presented in **Figure 3b.8**. The emission peaks for AnPPE and DPP(EH) were observed at 523 and 583 nm, respectively. The emission spectrum for AnPPE-Th-DPP(EH) didn't show any peak after 620 nm. The peak at 600 nm is due to detector response. This indicates complete quenching of PL spectra in AnPPE-Th-DPP(EH) molecule due to complete charge transfer from donor unit (AnPPE) to acceptor unit (DPP(EH)).

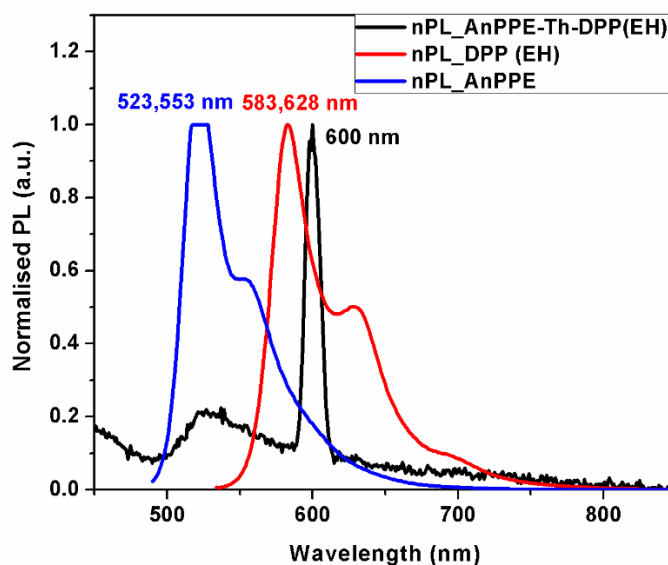


Figure 3b.8 The photoluminescence spectra of AnPPE, DPP(EH) and AnPPE-Th-DPP(EH) in dilute chloroform solution.

The photoluminescence spectra of AnPPE, BTDA and D-A molecule- AnPPE-Th-BTDA in dilute chlorobenzene solution is presented in **Figure 3b.9**. The emission peaks for AnPPE and BTDA were observed at 523 and 567 nm, respectively. The emission peak for AnPPE-Th-BTDA was observed at 643 nm.

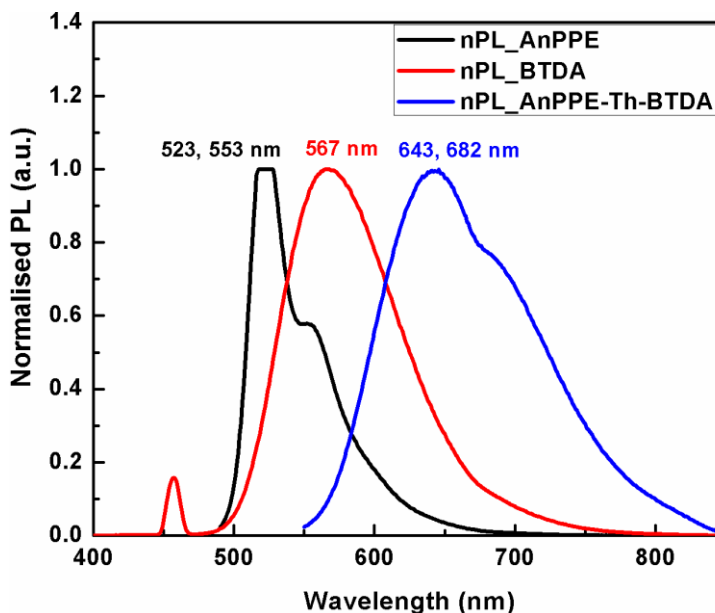


Figure 3b.9 The photoluminescence spectra of AnPPE, BTDA and AnPPE-Th-BTDA in dilute chlorobenzene solution

Table 3b.2 summarizes the photophysical data in chlorobenzene solutions which include the wavelength at absorption maximum (λ_a), the wavelength at the emission maximum (λ_f).

Table 3b.2 Photophysical data of D-A small molecules in solution

Small molecules	λ_a [nm]	λ_f [nm]
AnPPE-Th-DPP(EH)	675	-
AnPPE-Th-BTDA	535	643, 682 (sh)

3b.4.6 Electrochemical Study

Electrochemical experiments were performed on thin films of small molecules spin coated from chlorobenzene solutions under inert condition by using cyclic voltammetry technique (CV).³¹ The ionization potential (HOMO), and electron affinity (LUMO), were estimated from oxidation and reduction onset potentials on the basis of

the reference energy level of ferrocene (4.8 eV below the vacuum level) using the equation $(\text{HOMO}) = -(E_{\text{oxd}} + 4.8)$ eV, $(\text{HOMO}) = -(E_{\text{red}} + 4.8)$ eV where E_{oxd} and E_{red} are oxidation onset potential and reduction onset potential, respectively. The E_{oxd} and E_{red} values were evaluated from the first oxidation and reduction peaks of the cyclic voltammograms measured at a scan rates of 20 and 50 mV/s.

Cyclic voltammograms are shown in **Figure 3b.10**. Corresponding electronic data is summarized in **Table 3b.3**. The HOMO values for AnPPE-Th-DPP(EH) and AnPPE-Th-BTDA were found to be 5.11 and 5.10 eV, respectively. The LUMO values for AnPPE-Th-DPP(EH) and AnPPE-Th-BTDA were found to be 3.76 and 3.55 eV, respectively. The electrochemical band-gap energy, $E_{\text{g}}^{\text{elc}}$ for AnPPE-Th-DPP(EH) and AnPPE-Th-BTDA were found to be 1.35 and 1.55 eV.

Table 3b.3 Electrochemical data for small molecules films spin-coated from chlorobenzene

Small molecules	E_{oxd}	E_{red}	HOMO (eV)	LUMO (eV)	$E_{\text{g}}^{\text{elc}}$ (eV)
AnPPE-Th-DPP(EH)	0.31	-1.24	5.11	3.76	1.35
AnPPE-Th-BTDA	0.30	-1.25	5.10	3.55	1.55

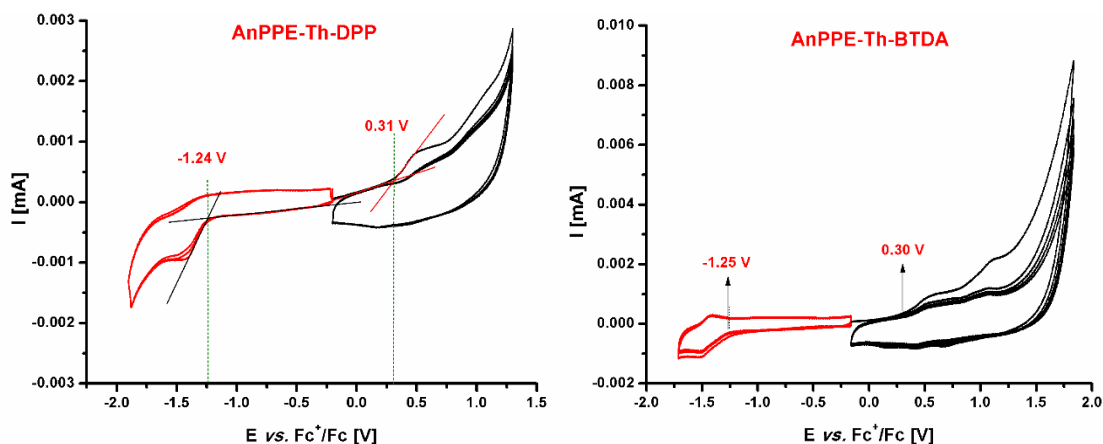


Figure 3b.10 Cyclic voltammograms of a) AnPPE-Th-DPP(EH) and, b) AnPPE-Th-BTDA

3b.4.7 Charge carrier mobility measurements:

Charge carrier mobility was measured in field effect transistor device prepared from AnPPE-Th-DPP(EH) by using the bottom gate and bottom contact device architecture.^{19,20} Organic Field effect transistor (OFET) devices were prepared using pre-fabricated bottom gate (SiO₂) and bottom contact (Au) silicon wafer substrates. In order to study the impact of thermal annealing, the devices were annealed at 100 °C under an argon atmosphere for 10 min and charge carrier mobility of annealed device was measured. The channel width and length were 10 mm and 5 μ, respectively. The small molecule was spun on top of the hexamethylenedisilazane (HMDS) modified substrates,^{21,22,32} and the device characterization was carried out inside the glovebox under argon atmosphere. The drain voltage (V_D) was varied between 0 and -100 V while holding constant negative gate voltages (V_G). The a) output characteristics and b) transfer characteristics of OFETs based on AnPPE-Th-DPP(EH) at room temperature and after thermal annealing at 100°C, are depicted in **Figure 3b.11** and **Figure 3b.12**, respectively. The output characteristics of AnPPE-Th-DPP(EH) showed well-defined linear and saturation regimes, indicating that AnPPE-Th-DPP(EH) is a hole transporter. The transfer characteristics curves were obtained by sweeping the V_G and holding the V_D at -100 V (determined from the output characteristics). The charge carrier mobility (μ) in the saturation regime was calculated using the following relationship $I_D = (\mu CW/2L)[(V_G - V_T)^2]$. The OFET parameters are summarized in **Table 3b.4**. In order to study the impact of thermal annealing, the devices were annealed at 100 °C under an argon atmosphere for 10 min. Charge carrier mobility (μ) of AnPPE-Th-DPP(TH) at room temperature was $1.2 \times 10^{-6} \text{ cm}^2 \text{ V}^{-1} \text{ s}^{-1}$. After thermal annealing at 100°C, the mobility increased to $4.19 \times 10^{-6} \text{ cm}^2 \text{ V}^{-1} \text{ s}^{-1}$. Thus, the thermal annealing had a significant impact on the efficiency of the devices as result of improved packing in the molecule for better charge transport.²²

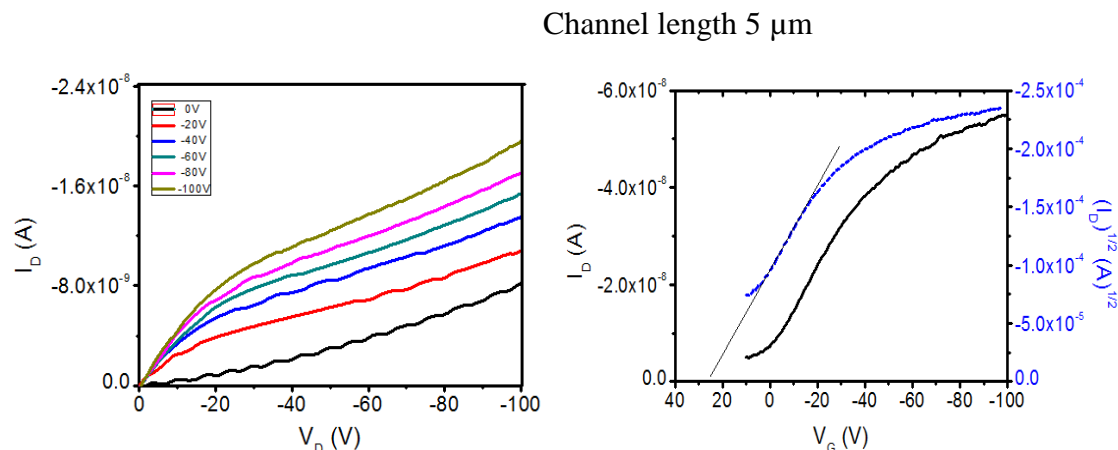


Figure 3b.11 Output and Transfer characteristics of OFETs based on AnPPE-Th-DPP(EH) at room temperature.

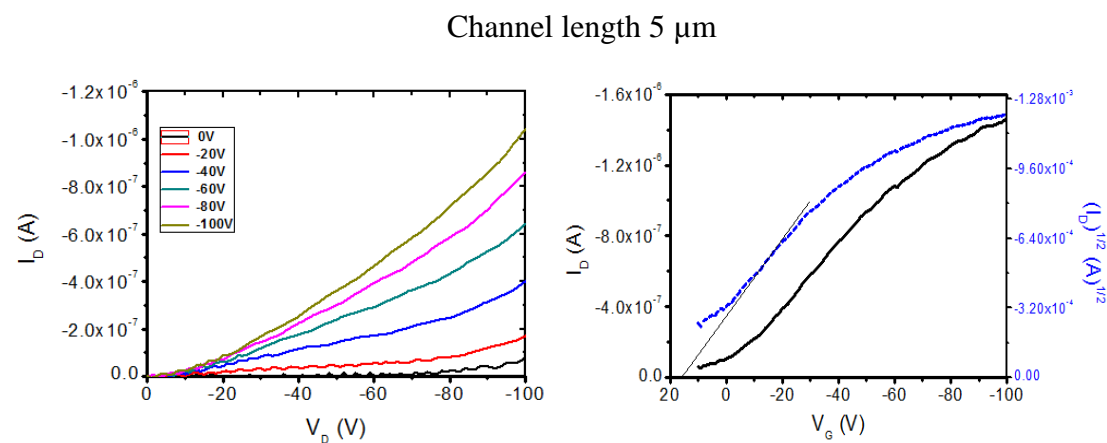


Figure 3b.12 Output and Transfer characteristics of OFETs based on AnPPE-Th-DPP(EH) after thermal annealing at 100°C.

Table 3b.4 The OFET parameters of device prepared from AnPPE-Th-DPP(EH)

Temperature (°C)	μ ($\text{cm}^2 \text{V}^{-1}\text{s}^{-1}$)	V_T (V)	$I_{\text{ON/OFF}}$
Room Temp.	1.2×10^{-6}	+10	1.29×10^3
100	4.19×10^{-6}	+15	2.04×10^2

3b.5 CONCLUSIONS

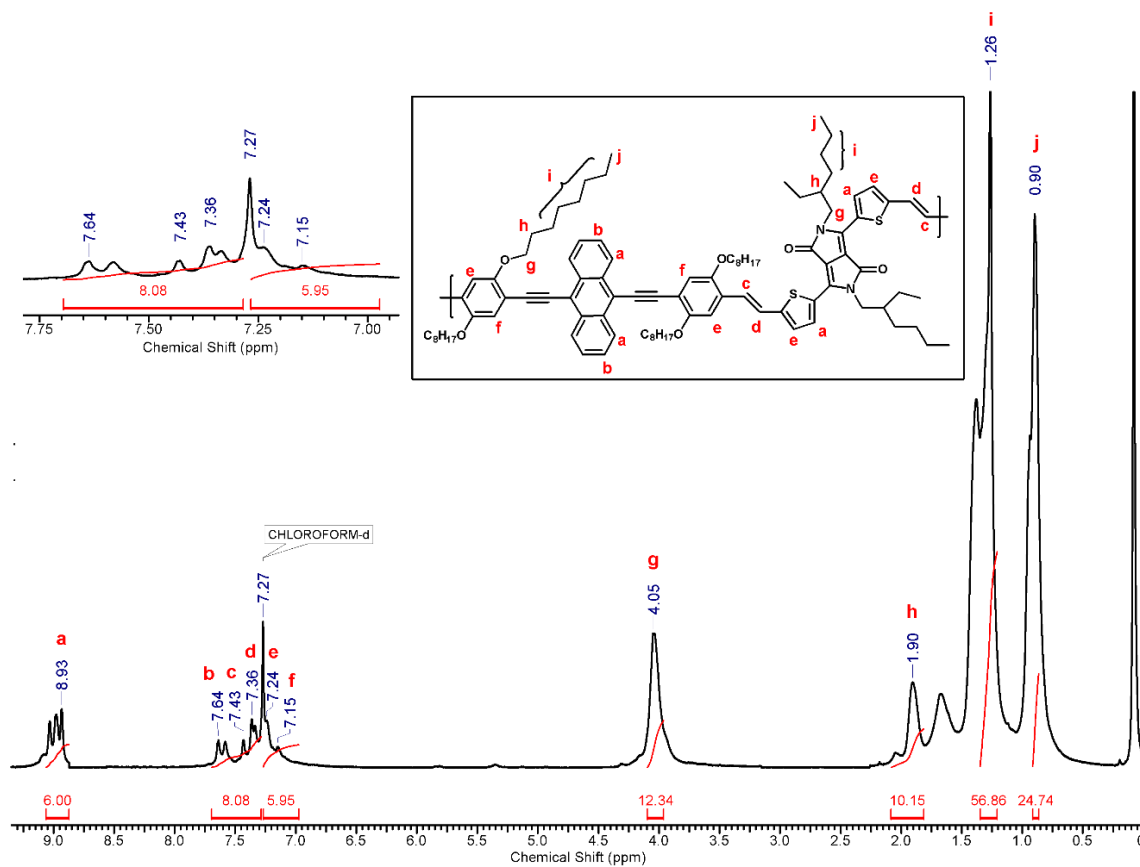
Low band-gap donor-acceptor small molecules namely- AnPPE-Th-DPP(EH) and AnPPE-Th-BTDA comprising anthracene containing (*p*-phenylene-ethynylene) (AnPPE) as a donor unit and either diketopyrrolopyrrole (DPP) or benzothiadizole (BTDA) as an acceptor unit were successfully synthesized by Pd-catalyzed Heck reaction. Polymers were not formed in both the cases. This may be attributed to inherent low reactivity of Heck reaction and partly to sterically crowded donor unit (AnPPE). AnPPE-Th-DPP(EH) was soluble in organic solvents such as chloroform, dichloromethane, dimethyl sulphoxide and chlorobenzene. AnPPE-Th-BTDA was partially soluble in dichloromethane and chlorobenzene at high temperature. The small molecules were characterized by ¹H-NMR and MALDI (TOF). UV-Vis spectra of AnPPE-Th-DPP(EH) and AnPPE-Th-BTDA showed wavelength of absorption maximum at 676 nm and 535 nm, respectively. Photoluminescence spectra of AnPPE-Th-DPP(EH) exhibited complete PL quenching indicating charge transfer from donor unit (AnPPE) to acceptor unit (DPP(EH)). Photoluminescence spectra of AnPPE-Th-BTDA showed emission maximum at 643 nm. Electrochemical band-gaps of AnPPE-Th-DPP(EH) and AnPPE-Th-BTDA were 1.35 and 1.55 eV, respectively. AnPPE-Th-DPP exhibited hole mobility value of $4.19 \times 10^{-6} \text{ cm}^2 \text{ V}^{-1} \text{ s}^{-1}$ in OFET devices.

REFERENCES

- 1 J. Chen and Y. Cao, *Acc. Chem. Res.*, 2009, **42**, 1709–1718.
- 2 Y. Li, *Acc. Chem. Res.*, 2012, **45**, 723–733.
- 3 S. Holliday, Y. Li and C. K. Luscombe, *Prog. Polym. Sci.*, 2017, **70**, 34–51.
- 4 H.-Y. Chen, J. Hou, S. Zhang, Y. Liang, G. Yang, Y. Yang, L. Yu, Y. Wu and G. Li, *Nat. Photonics*, 2009, **3**, 649–653.
- 5 J. M. Szarko, B. S. Rolczynski, S. J. Lou, T. Xu, J. Strzalka, T. J. Marks, L. Yu and L. X. Chen, *Adv. Funct. Mater.*, 2014, **24**, 10–26.
- 6 C. Liu, C. Yi, K. Wang, Y. Yang, R. S. Bhatta, M. Tsige, S. Xiao and X. Gong, *ACS Appl. Mater. Interfaces*, 2015, **7**, 4928–4935.
- 7 Y. Liu, J. Zhao, Z. Li, C. Mu, W. Ma, H. Hu, K. Jiang, H. Lin, H. Ade and H. Yan, *Nat. Commun.*, 2014, **5**, 5293.

- 8 W. Zhao, S. Li, H. Yao, S. Zhang, Y. Zhang, B. Yang and J. Hou, *J. Am. Chem. Soc.*, 2017, **139**, 7148–7151.
- 9 Z.-H. Zhou, T. Maruyama, T. Kanbara, T. Ikeda, K. Ichimura, T. Yamamoto and K. Tokuda, *J. Chem. Soc., Chem. Commun.*, 1991, 1210–1212.
- 10 K. Müllen and W. Pisula, *J. Am. Chem. Soc.*, 2015, **137**, 9503–9505.
- 11 Y. Qu, J. Hua and H. Tian, *Org. Lett.*, 2010, **12**, 3320–3323.
- 12 W. Li, K. H. Hendriks, W. S. C. Roelofs, Y. Kim, M. M. Wienk and R. A. J. Janssen, *Adv. Mater.*, 2013, **25**, 3182–3186.
- 13 C. B. Nielsen, M. Turbiez and I. McCulloch, *Adv. Mater.*, 2013, **25**, 1859–1880.
- 14 L. Ye, S. Zhang, W. Ma, B. Fan, X. Guo, Y. Huang, H. Ade and J. Hou, *Adv. Mater.*, 2012, **24**, 6335–6341.
- 15 Y.-C. Chen, C.-Y. Yu, Y.-L. Fan, L.-I. Hung, C.-P. Chen and C. Ting, *Chem. Commun.*, 2010, **46**, 6503–6505.
- 16 M. Zhang, Y. Gu, X. Guo, F. Liu, S. Zhang, L. Huo, T. P. Russell and J. Hou, *Adv. Mater.*, 2013, **25**, 4944–4949.
- 17 H. Zhou, L. Yang, A. C. Stuart, S. C. Price, S. Liu and W. You, *Angew. Chemie Int. Ed.*, 2011, **50**, 2995–2998.
- 18 D. D. Armarego, K. N., Perrin, in *Purification of Laboratory Chemicals*, Butterworth-Heinemann, Oxford, 4th Edition, Butterworth Heinemann, 1996.
- 19 D. Izuhara and T. M. Swager, *J. Am. Chem. Soc.*, 2009, **131**, 17724–17725.
- 20 A. Arulkashmir, R. Y. Mahale, S. S. Dharmapurikar, M. K. Jangid and K. Krishnamoorthy, *Polym. Chem.*, 2012, **3**, 1641.
- 21 S. H. Park, H. S. Lee, J.-D. Kim, D. W. Breiby, E. Kim, Y. D. Park, D. Y. Ryu, D. R. Lee and J. H. Cho, *J. Mater. Chem.*, 2011, **21**, 15580.
- 22 S. Hüttner, M. Sommer and M. Thelakkat, *Appl. Phys. Lett.*, 2008, **92**, 093302.
- 23 A. B. Tamayo, M. Tantiwiwat, B. Walker and T. Nguyen, *J. Phys. Chem. C*, 2008, **112**, 15543–15552.
- 24 L. Bürgi, M. Turbiez, R. Pfeiffer, F. Bienewald, H.-J. Kirner and C. Winnewisser, *Adv. Mater.*, 2008, **20**, 2217–2224.
- 25 H. Weyhardt and H. Plenio, *Organometallics*, 2008, **27**, 1479–1485.
- 26 L. Huo, J. Hou, H. Y. Chen, S. Zhang, Y. Jiang, T. L. Chen and Y. Yang,

- Macromolecules*, 2009, **42**, 6564–6571.
- 27 N. J. Whitcombe, K. K. Hii and S. E. Gibson, *Tetrahedron*, 2001, **57**, 7449–7476.
- 28 K. Liu, Y. Li and M. Yang, *J. Appl. Polym. Sci.*, 2009, **111**, 1976–1984.
- 29 J. H. Chi, C.-L. Lee, J.-J. Kim and J. C. Jung, *J. Appl. Polym. Sci.*, 2008, **108**, 914–922.
- 30 R. K. Ramchandani, M. P. Vinod, R. D. Wakharkar, V. R. Choudhary and A. Sudalai, *Chem. Commun.*, 1997, **29**, 2071–2072.
- 31 M. Namazian, C. Y. Lin and M. L. Coote, *J. Chem. Theory Comput.*, 2010, **6**, 2721–2725.
- 32 R. P. Ortiz, A. Facchetti and T. J. Marks, *Chem. Rev.*, 2010, **110**, 205–239.

Supporting Information**Figure SI 3b.1** $^1\text{H-NMR}$ spectrum of AnE-Th-DPP(EH) with zoomed aromatic region

CHAPTER 4

Bi(thienylene-vinylene)thiophene Containing PAE-PV: Modulation of Charge Carrier Mobility by Side Chain Engineering

4.1 INTRODUCTION

Soluble conjugated polymers have attracted broad academic and industrial interest as innovative semiconducting materials and are promising candidates for cost effective printed electronics owing to their unique combination of solution processability, excellent mechanical properties, and tunability of their electronic properties.^{1,2} It is well known that the nature, size, and position of the solubilising side chains attached to the conjugated backbone can have a dramatic effect not only on their processability from organic solvents but also on the electronic properties of conjugated polymers.^{3,4,5,6} Nowadays, two dimensional conjugated polymeric systems comprising the conjugated main chain and conjugated side chains are intensively studied. Since the first attempt by Li and coworkers,⁷ the two-dimensional conjugation concept has emerged as an attractive approach for the design of conjugated polymers with improved optoelectronic properties.⁸ Considerable research efforts are being made towards decorating best performing benzo[1,2-b:4,5-b']dithiophene (BDT) based polymers with varied conjugated side groups to achieve higher power conversion efficiencies.⁹⁻¹⁹ Recently, Hou *et al.* have also shown the modulating effect of the two-dimensional structure on reaching higher mobility in case of 2-alkylthienyl substituted benzo[1,2-b:4,5-b']dithiophene (BDT) based polymer, namely PBDT-TS1.²⁰

Previously, we systematically studied the effect of various alkoxy side-chains of different lengths and nature (linear or branched) on anthracene-containing poly(*p*-phenylene-ethynylene)-*alt*-poly(*p*-phenylene-vinylene) (PPE-PPV) copolymers^{3,21,22} and the strong dependence of the structural, optical, and electrical properties of the investigated polymer films on the lateral side-chains was demonstrated. In this chapter, four polymers with a two-dimensional conjugated system are considered. PPE-PPVs incorporating a bithienylene-vinylene thiophene group as a conjugated side-chain on the PPE unit (**BTE-PPVs**) and bearing octyloxy or 2-ethylhexyloxy side-chains on the BTE and PV parts were synthesized (Scheme 1), in order to investigate how their electronic properties can be modulated by simultaneous incorporation of conjugated as well as alkoxy side chains. In these polymers, the bithienylene-vinylene thiophene group extends the conjugation in the

lateral direction and an improved degree of the electronic interactions between the polymer chains is expected in the solid state, compared to a conventional linear conjugated structure.⁸ Thus, the conjugated lateral chain together with the octyloxy solubilising chains is expected to affect charge carrier mobility of the polymeric films under investigation. Indeed, the BTE-PV polymer containing the branched ethylhexyloxy chain in the BTE unit and the linear octyloxy chain in the PV unit exhibited a remarkable hole mobility of $2.2 \times 10^{-2} \text{ cm}^2 \text{ V}^{-1} \text{ s}^{-1}$ at a moderate applied electric field of $8 \times 10^4 \text{ V cm}^{-1}$.

4.2 EXPERIMENTAL

4.2.1 Materials:

Bromine, n-butyllithium solution (2.7 M in n-heptane), ethynyl trimethyl silane, bis(triphenylphosphine) palladium (II)dichloride ($\text{Pd}(\text{PPh}_3)_2\text{Cl}_2$), tetrakis(triphenylphosphine)palladium(0) ($\text{Pd}(\text{PPh}_3)_4$), copper iodide (CuI), diisopropyl amine, potassium *ter*-butoxide, 1-octyl bromide, 2-ethylhexyl bromide, 1-decyl bromide, 1-dodecyl bromide and 1-bromo-3,7-dimethyl octane (96%) (Aldrich Chemicals) were purchased and were used as received. Potassium hydroxide powder, paraformaldehyde, sodium bromide, potassium fluoride, glacial acetic acid, triethyl phosphite, benzyl bromide, hydroquinone and benzaldehyde (Merck) were purchased and were used as received.

N,N-Dimethylformamide (DMF), dimethyl sulphoxide (DMSO), diethyl ether, tetrahydrofuran (THF) and toluene (Aldrich Chemicals) were purchased and were dried and distilled according to standard procedures and stored under argon. Methanol, chloroform, n-hexane and ethyl acetate (Merck) were purchased and were used as received. If not otherwise specified, solvents or solution were degassed by bubbling with nitrogen 1 h prior to use.

4-Ethynyl-2,5-dioctyloxybenzaldehyde (**1a**), 4-ethynyl-2,5-di(2-ethyl)hexyloxybenzaldehyde (**1b**), 2,5-dioctyloxy-*p*-xylylene-bis(diethylphosphonate) (**4a**), and 2,5-bis((2-ethylhexyloxy)-*p*-xylylenebis(diethylphosphonate)) (**4b**) were synthesized as described in section **3a.3.1.1.5** of chapter 3a of this thesis. 2,5-Dibromo-3-((*E*)-2-(5-((*E*)-2-(5-dodecylthiophen-2-yl)vinyl)thiophen-2-yl)vinyl)thiophene (**2**)⁷ was synthesized according to the literature.

4.2.2 Characterisation and techniques

Different techniques were used for characterization of monomers and polymers and are listed below.

NMR Spectroscopy: ^1H and ^{13}C NMR spectra of monomers and polymers were recorded using a Bruker-AV spectrometer at operating frequency of 200 MHz, 400 MHz and 500 MHz in CDCl_3 or $\text{DMSO-}d_6$ with tetramethylsilane as an internal standard.

Gel permeation chromatography (GPC): Molecular weights and dispersity values of polymers were determined on Knauer Thermo-Finnigan make GPC using THF as an eluent at a flow rate of 1 mL min^{-1} at 25°C . Sample concentration was 2 mg mL^{-1} and narrow dispersity polystyrenes were used as calibration standards.

Thermogravimetric analysis (TGA): TGA was performed on a Mettler TA-300-thermal analyzer operating under nitrogen atmosphere. The samples were heated from 0 to 700°C with a heating rate of 10 K/min .

X-ray diffraction (XRD): XRD experiments were performed on PANalytical X'Pert diffractometer equipped with a copper anode ($\lambda_{\text{mean}} = 0.15418 \text{ nm}$) and a fast X'Celerator detector, with a step of 0.05° (2θ) and counting time of 120 sec/step . Polymer films prepared from chlorobenzene solutions (concentrations ranging between 18 and 33 g L^{-1} for the four polymers) were drop-cast on Mineral quartz 'zero background' (The Gem Dugout, State College, PA-USA), in order to strongly minimize its contribution to the total scattering. After deposition, the films were solvent-vapour annealed in chlorobenzene overnight. The films were directly investigated in reflection geometry.

Absorption and emission spectroscopy: The absorption spectra were recorded in dilute chloroform solutions ($5 \times 10^{-7} \text{ mol L}^{-1}$ per repeating unit) on a Perkin-Elmer Lambda 950 spectrophotometer. The absorption spectra were recorded on thin film spin coated from chlorobenzene solution ($8\text{-}14 \text{ g L}^{-1}$) on polished quartz substrates. The smooth and uniform films with a thickness of about 120 nm were tested and all of them behave in the same way. Quantum yields in solution were obtained by using an air-equilibrated $\text{Ru}(\text{bipy})_3\text{Cl}_2$ solution as the reference ($\Phi=0.28$).²³ The absorption and emission spectra were determined by using a Perkin Elmer Lambda 950 spectrophotometer and a Spex Fluorolog fluorometer, respectively. The same Spex Fluorolog fluorometer equipped with a custom-made integrating sphere system was employed for absolute measurements of the film emission

quantum yields. The estimated error for the quantum yield data is 20%. Photoluminescence lifetimes were determined with an IBH 5000F time-correlated single-photon counting device, by using a pulsed NanoLED excitation source at 465 nm. The analysis of the luminescence decay profiles was accomplished with the Decay Analysis Software DAS6 provided by the manufacturer. The estimated error on the lifetime is 10%. All measurements were performed at room temperature in ambient atmosphere in a single experimental session for each group of measurements in order to get rid of experimental errors which could affect comparison of the different polymer spectra, lifetimes and quantum yields.

Atomic Force Microscopy: The surface morphology of the samples was studied by Atomic Force Microscopy (AFM). The AFM images were obtained by means of a Digital Instruments Dimension 3100 microscope working in tapping mode. The samples were prepared by spin-coating from chlorobenzene solution.

4.2.3 Charge carrier mobility measurements by Time of Flight (TOF) experiments

Polymer films for Time of Flight experiments were drop-cast onto aluminium-coated glass substrates from chlorobenzene solutions (concentrations ranging between 18 and 33 g L⁻¹ for the four polymers). After the deposition, the films were solvent-vapour annealed (chlorobenzene) overnight. The device structure was completed with a vacuum-evaporated semi-transparent aluminium electrode (18 nm thick). The device area was 0.25 cm² and the film thicknesses were 4.7, 4.6, 10, and 11.4 μm for **BTE-PVaa**, **BTE-PVab**, **BTE-PVba**, and **BTE-PVbb**, respectively. A nitrogen laser ($\lambda = 337$ nm) with a pulse duration of 6-7 ns was used to photogenerate charge carriers in TOF experiments. A variable DC potential was applied to the samples and in order to ensure a uniform electric field inside the device, the total photo-generated charge was kept less than 0.1 CV (where C is the sample capacitance and V the applied potential) by attenuating the laser beam intensity with quartz neutral filters. The photocurrent was monitored across a variable load resistance by using a Tektronix TDS620A digital oscilloscope. TOF measurements were performed at room temperature and under dynamic vacuum (10⁻⁵ mbar).

4.2.4 Fabrication and Characterization of the Photovoltaic Cells

Solar cell device fabrication and characterization is similar to that described in section 3a.2.3 of chapter 3a except BTE-PV polymers were used as donor material.

4.3 SYNTHESIS

4.3.1 Synthesis of bi(thienylenevinylene)thiophene containing dialdehydes

4.3.1.1 2,5-Bis{[(2,5-dioctyloxy-4-formyl)phenyl]ethynyl}-3-(2-{5-[2-(5-dodecyl)thiophenyl] vinyl}thiophenyl)vinyl-thiophene (**3a**)

Into a 250 mL three-necked round bottom flask equipped with nitrogen gas inlet and a magnetic stir bar were added 4-ethynyl-2,5-dioctyloxybenzaldehyde (**1a**) (1.60 g, 2.56 mmol), 2,5-dibromo-3-((1-E)-2-(5-((2-(5-dodecylthiophen-2-yl)vinyl)thiophen-2-yl)vinyl)thiophene (**2**) (3.1 g, 8.02 mmol) and a mixture of toluene (100 mL) and diisopropylamine (40 mL). The reaction mixture was degassed for 1h in an argon atmosphere. Then, the catalysts Pd(PPh₃)₄ (332.8 mg, 0.28 mmol) and CuI (56 mg, 0.28 mmol) were added into the solution and the mixture was heated at 80 °C for 24 h in argon atmosphere. After cooling to room temperature, the precipitated diisopropylammonium bromide was filtered off and the solvent was distilled off under vacuum. The residue was purified by column chromatography on silica gel with toluene as an eluent to afford pure **3a** as a dark-red viscous liquid.

Yield: 1.74 g (56 %).

¹H-NMR (500 MHz, CDCl₃, δ/ppm): 10.47 (s, 2H, -CHO), 7.49-7.33 (multiple peaks, 4H, C_{phenyl}-H), 7.26-6.59 (multiple peaks, 9H, vinylic and thiophene protons), 4.07 (t, 8H, -O-CH₂-), 2.80, 2.72 (two triplets, 2H, -CH₂-CH₂-(CH₂)₉CH₃, first methylene of dodecyl chain which is directly attached to thiophene ring), 1.90-1.82 (m, 8H, -O-CH₂-CH₂-(CH₂)₅CH₃), 1.69-1.64 (m, 2H, -CH₂-CH₂-(CH₂)₉CH₃), 1.53-1.44 (m, 10H, -CH₂-CH₃), 1.29-1.18 (m, 48H, -CH₂-), 0.92-0.85 (t, 15H, -CH₃).

4.3.1.2 2,5-Bis{[(2,5-di(2-ethyl)hexyloxy-4-formyl)phenyl]ethynyl}-3-(2-{5-[2-(5-dodecyl)thiophenyl] vinyl}thiophenyl)vinyl-thiophene (**3b**)

The dialdehyde **3b** was synthesised using the same procedure as that given for **3a** but with **1a** (1.80 g, 4.68 mmol) and **2** (1.46 g, 2.32 mmol) as reactants and using Pd(PPh₃)₄ (107.6 mg, 0.092 mmol) and CuI (17.6 mg, 0.092 mmol) as catalysts. Pure **3b** was obtained as a dark red viscous liquid.

Yield: 1.80 g (63 %).

$^1\text{H-NMR}$ (500 MHz, CDCl_3 , δ/ppm): 10.47 (s, 2H, -CHO), 7.49-7.30 (multiple peaks, 4H, $\text{C}_{\text{phenyl-H}}$), 7.55-6.56 (multiple peaks, 9H, vinylic and thiophene protons), 3.97 (d, 8H, -O-CH₂-), 2.79 (t, 2H, -CH₂-CH₂-(CH₂)₉CH₃, first methylene of dodecyl chain which is directly attached to thiophene ring), 1.85-1.76 (m, 4H, -O-CH₂-CH₂-(CH₂)₅CH₃), 1.70-1.66 (m, 2H, -CH₂-CH₂-(CH₂)₉CH₃), 1.40-1.21 (m, 50H, -CH₂-), 0.95-0.82 (m, 27H, -CH₃).

4.3.2 Synthesis of bi(thienylenevinylene)thiophene containing PPE-PPV polymers

4.3.2.1 Synthesis of polymer BTE-PVab (General procedure)

Into a 250 mL three-necked round bottom flask equipped with nitrogen gas inlet and a magnetic stir bar were added 2,5-bis{[(2,5-dioctyloxy-4-formyl)phenyl]ethynyl}-3-(2-{5-[2-(5-dodecyl)thiophenyl]vinyl} thiophenyl)vinyl-thiophene (**3a**) (0.84 g, 0.675 mmol), 2,5-di(2-ethyl)hexyloxy-p-xylylenebis(diethylphosphonate) (**4b**) (0.44 g, 0.68 mmol) and 70 mL of dried toluene. The reaction mixture was vigorously stirred under argon atmosphere and then allowed to reflux. Potassium-*tert*-butoxide (0.62 g, 5.43 mmol) was added into the refluxing solution, which made the reaction to become successively darker and viscous. The reaction mixture was then heated at reflux for 3 h. Benzaldehyde (1 mL) was added for end-capping of the polymer and after 30 min the polymerisation was stopped. Reaction mixture was allowed to cool down and quenched with aqueous HCl. The organic phase was separated and extracted six times with distilled water (100 mL) until the aqueous phase became neutral (pH = 6-7). The organic layer was dried in Dean-Stark apparatus. The resulting toluene solution was filtered, concentrated and precipitated in cold methanol to get dark-brown coloured polymer. The polymer was then purified by Soxhlet extraction with methanol/diethylether mixture (1:1 v/v) for 3 h. The obtained sticky polymer was again dissolved in a small amount of toluene, precipitated in methanol, filtered and dried under vacuum to obtain dark-red colored polymer.

Yield: 0.735 g (69 %).

$^1\text{H-NMR}$ (500 MHz, CDCl_3 , δ/ppm): 7.60-6.61 (multiple peaks, 19H, $\text{C}_{\text{phenyl-H}}$, thiophene protons, vinylic protons in both the side chain and the polymer backbone), 4.17-3.88 (m, 12H, -O-CH₂-), 2.79 (t, 2H, -CH₂-CH₂-(CH₂)₉CH₃, first methylene of dodecyl chain which is directly attached to thiophene ring of the conjugated side chain), 1.94-1.76 (m, 10H, -O-CH₂-CH₂-(CH₂)₅CH₃ in octyl and -O-CH₂-CH₂(CH₂CH₃)(CH₂)₃CH₃ in 2-ethylhexyl side

chain), 1.70-1.66 (m, 2H, $-\text{CH}_2-\underline{\text{CH}}_2-(\text{CH}_2)_9\text{CH}_3$), 1.56-1.45 (m, 14H, $-\underline{\text{CH}}_2-\text{CH}_3$ of alkyl chains), 1.34-1.17 (m, 60H, $-\text{CH}_2-$), 0.95-0.80 (m, 27H, $-\text{CH}_3$).

GPC (PS standards): $M_w = 26,640$ g/mol, $M_n = 11,100$ g/mol, PDI = 2.4.

4.3.2.2 Synthesis of polymer BTE-PVaa

Polymer BTE-PVaa was synthesised using the same procedure as that given for BTE-PVab but by using 3a (1.05 g, 0.855 mmol), 4a (0.54 g, 0.86 mmol) and potassium-tert-butoxide (0.72 g, 6.42 mmol). BTE-PVaa was collected as a dark reddish brown solid. Yield: 0.81 g (61 %).

$^1\text{H-NMR}$ (500 MHz, CDCl_3 , δ/ppm): 7.65-6.61 (multiple peaks, 19H, $\text{C}_{\text{phenyl-H}}$, thiophene protons, vinylic protons in both the sidechain and the polymer backbone), 4.17-3.96 (t, 12H, $-\text{O}-\text{CH}_2$), 2.80-2.71 (t, 2H, $-\text{CH}_2-\text{CH}_2-(\text{CH}_2)_9\text{CH}_3$, first methylene of dodecyl chain which is directly attached to thiophene ring of the conjugated side chain), 1.93-1.83 (m, 12H, $-\text{O}-\text{CH}_2-\underline{\text{CH}}_2-(\text{CH}_2)_5\text{CH}_3$), 1.69-1.66 (m, 2H, $-\text{CH}_2-\underline{\text{CH}}_2-(\text{CH}_2)_9\text{CH}_3$), 1.58-1.54 (m, 14H, $-\underline{\text{CH}}_2-\text{CH}_3$), 1.34-1.24 (m, 64H, $-\text{CH}_2-$), 0.90-0.86 (m, 21H, $-\text{CH}_3$).

GPC (PS standards): $M_w = 47,800$ g/mol, $M_n = 26,700$ g/mol, PDI = 1.8.

4.3.2.3 Synthesis of polymer BTE-PVbb

Polymer BTE-PVbb was synthesised using the same procedure as that given for BTE-PVab but by using 3b (0.45 g, 0.38 mmol), 4b (0.24 g, 0.38 mmol) and potassium-tert-butoxide (0.17 g, 0.15 mmol). BTE-PVbb was collected as a dark brown solid. Yield: 0.285 g (49 %).

$^1\text{H-NMR}$ (500 MHz, CDCl_3 , δ/ppm): 7.65- 6.61 (multiple peaks, 19H, $\text{C}_{\text{phenyl-H}}$, thiophene protons, vinylic protons in both the sidechain and the polymer backbone), 4.11-3.77 (m, 12H, $-\text{O}-\text{CH}_2$), 2.79 (t, 2H, $-\text{CH}_2-$ directly attached to thiophene ring of the conjugated side chain), 1.91-1.77 (m, 6H, $-\text{O}-\text{CH}_2-\underline{\text{CH}}(\text{CH}_2\text{CH}_3)(\text{CH}_2)_3\text{CH}_3$), 1.69-1.66 (m, 2H, $-\text{CH}_2-\underline{\text{CH}}_2-(\text{CH}_2)_9\text{CH}_3$), 1.51-1.43 (m, 14H, $-\underline{\text{CH}}_2-\text{CH}_3$), 1.41-1.21 (m, 52H, $-\text{CH}_2-$), 1.00-0.75 (m, 39H, $-\text{CH}_3$).

GPC (PS standards): $M_w = 25,200$ g/mol, $M_n = 10,500$ g/mol, PDI = 2.4.

4.3.2.4 Synthesis of Polymer BTE-PVba

Polymer BTE-PVba was synthesised using the same procedure as that given for BTE-PVab but by using 3b (0.89 g, 0.72 mmol), 4a (0.45 g, 0.72 mmol) and potassium-tert-butoxide (0.63 g, 5.625 mmol). BTE-PVba was collected as a dark reddish brown solid

Yield: 0.42 g (40 %).

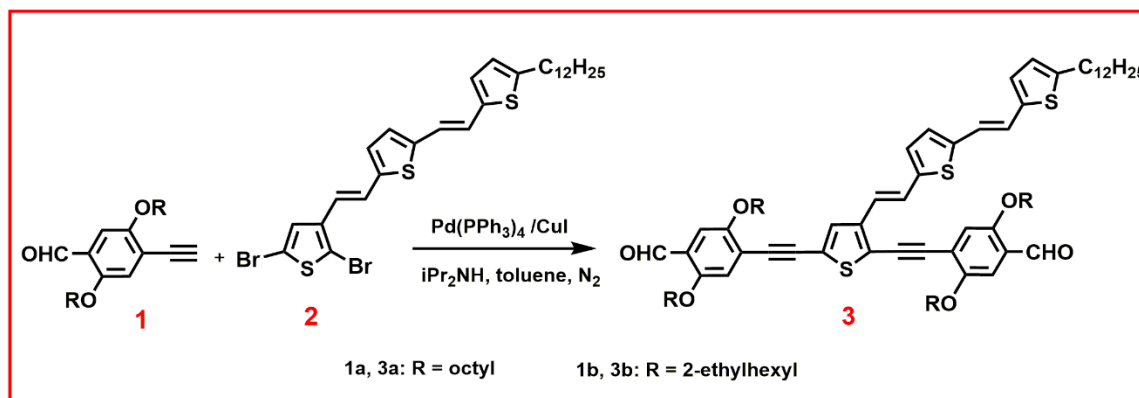
$^1\text{H-NMR}$ (500 MHz, CDCl_3 , δ/ppm): 7.65-6.64 (multiple peaks, 19H, $\text{C}_{\text{phenyl-H}}$, thiophene protons, vinylic protons in both the sidechain and the polymer backbone), 4.18-3.64 (m, 12H, $-\text{O}-\text{CH}_2$), 2.79 (t, 2H, $-\text{CH}_2-\text{CH}_2-(\text{CH}_2)_9\text{CH}_3$, first methylene of dodecyl chain which is directly attached to thiophene ring of the conjugated side chain), 1.90-1.78 (m, 8H, $-\text{O}-\text{CH}_2-\text{CH}_2-(\text{CH}_2)_5\text{CH}_3$ in octyl and $-\text{O}-\text{CH}_2-\text{CH}(\text{CH}_2\text{CH}_3)(\text{CH}_2)_3\text{CH}_3$ in 2-ethylhexyl side chain), 1.65-1.26 (multiple peaks, 72H, $-\text{CH}_2-$), 0.96-0.81 (m, 33H, $-\text{CH}_3$).

GPC (PS standards): $M_w = 12,390$ g/mol, $M_n = 5,900$ g/mol, PDI = 2.1.

4.4 RESULTS AND DISCUSSION

4.4.1 Synthesis of bi(thienylenevinylene)thiophene-containing dialdehydes

The two bi(thienylenevinylene)thiophene-containing dialdehydes (**3a** and **3b**) were obtained by Heck–Cassar–Sonogashira–Hagihara Pd-catalysed cross coupling reaction²⁴⁻²⁸ of either 4-ethynyl-2,5-dioctyloxybenzaldehyde (**1a**) or 4-ethynyl-2,5-di(2-ethyl)hexyloxy-benzaldehyde (**1b**) with 2,5-dibromo-3-((*E*)-2-(5-((*E*)-2-(5-dodecylthiophen-2-yl)vinyl)thiophen-2-yl)vinyl)thiophene (**2**)⁷ in the presence of $\text{Pd}(\text{PPh}_3)_4$ and CuI . The dialdehydes were purified by column chromatography on silica gel with toluene as an eluent. The chemical structures of all the intermediates were confirmed by $^1\text{H-NMR}$ spectroscopy.



Scheme 4.1 Synthesis of bi(thienylenevinylene)thiophene-containing dialdehydes (**3a** and **3b**)

$^1\text{H-NMR}$ spectrum of the dialdehyde **3a** is presented in **Figure 4.1**. The peak due to aldehyde group was observed at 10.47 δ ppm. Four aromatic protons on phenyl ring

appeared in the range 7.49-7.33 δ ppm. Appearance of nine aromatic protons on thiophene rings of main chain and side chain, in the range 7.26-6.59 δ ppm confirmed the incorporation of bithienylene vinylene group. The methylene protons, adjacent to oxygen, on octyloxy side chain were observed as a triplet at 4.07 δ ppm. The two protons on methylene group of dodecyl chain which is directly attached to thiophene ring appeared as two triplets at 2.80 and 2.72 δ ppm. The remaining methylene protons appeared in the range 1.90-1.18 δ ppm. The methyl protons appeared at 0.89 δ ppm.

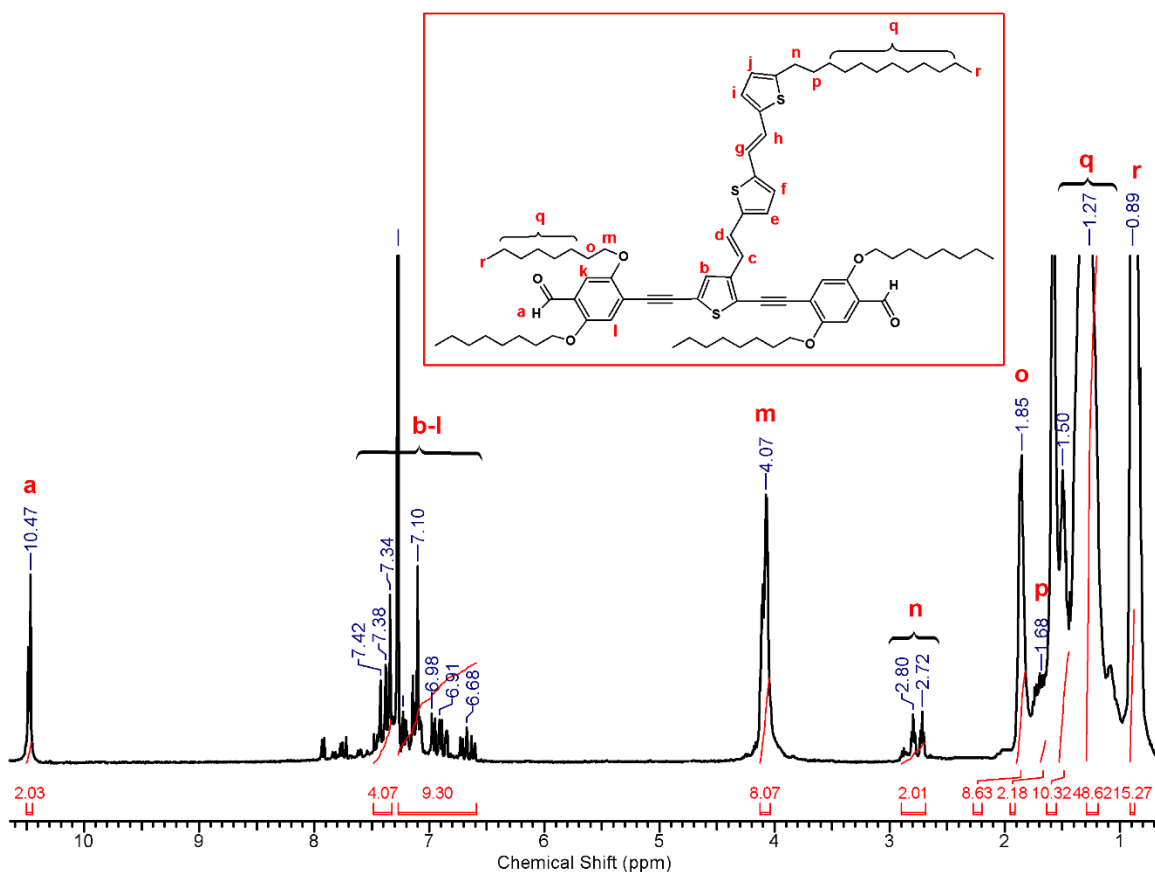


Figure 4.1 $^1\text{H-NMR}$ spectrum (CDCl_3) of 2,5-Bis[(2,5-dioctyloxy-4-formyl)phenyl]ethynyl}-3-(2-{5-[2-(5-dodecyl)thiophenyl]vinyl}thiophenyl)vinyl-thiophene (3a)

$^1\text{H-NMR}$ spectrum of the dialdehyde 3b is presented in **Figure 4.2**. Since the two dialdehydes differ only in side chains on phenyl ring, they have similar NMR spectrum except the integration of 'o' and 'p' type protons. Due to branched 2-ethylhexyl side chain on 3b, integration of 'o' protons is decreased and that of 'p' protons is increased in 3b.

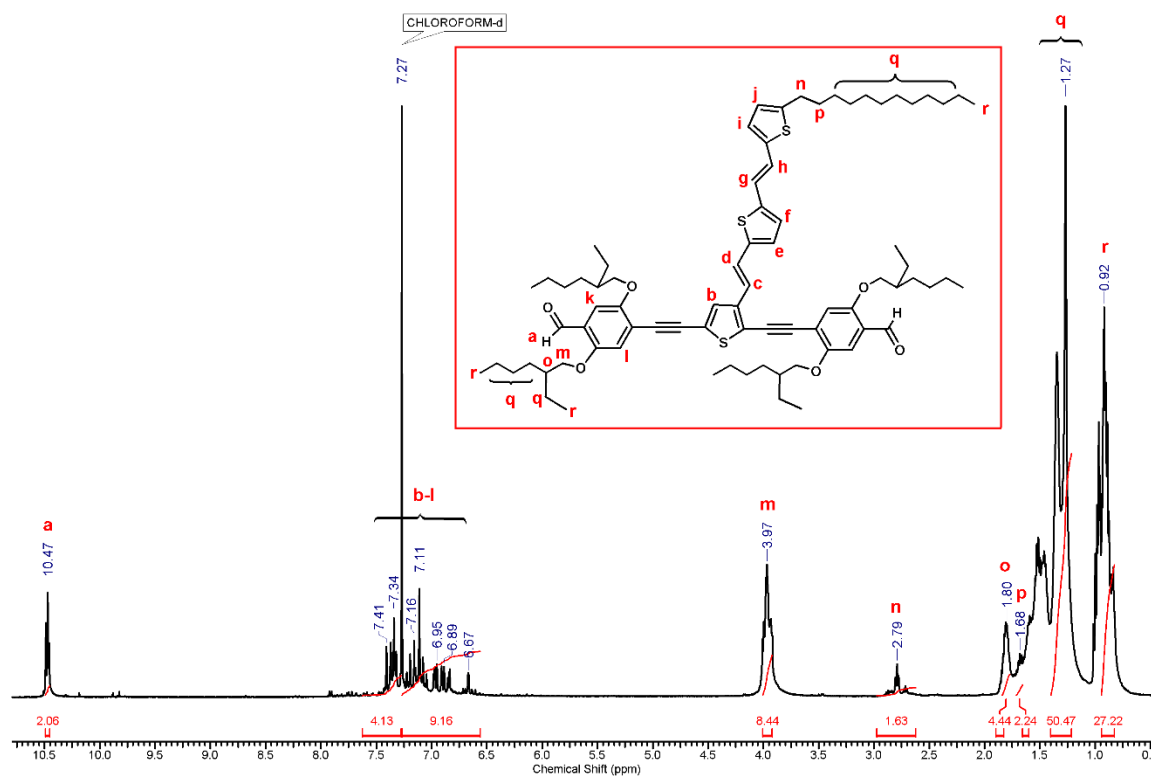
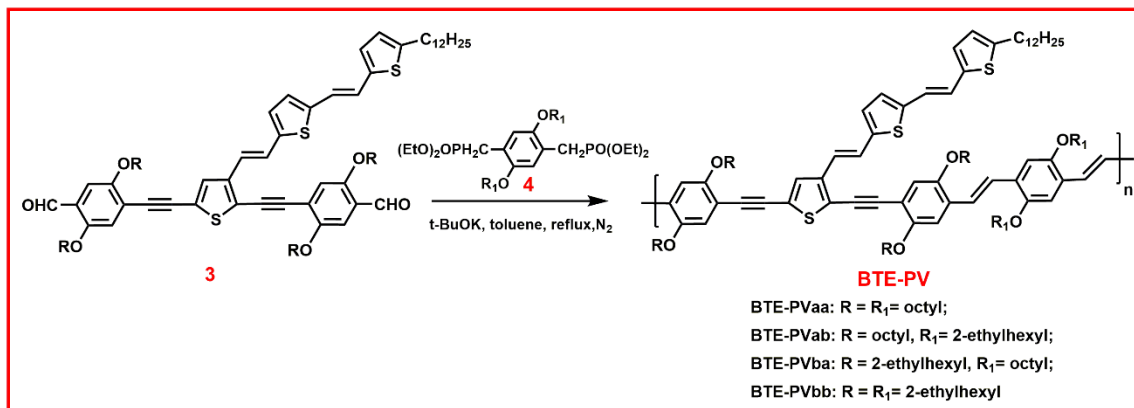


Figure 4.2 $^1\text{H-NMR}$ spectrum (CDCl_3) of 2,5-bis{[(2,5-di-ethylhexyloxy-4-formyl)phenyl]ethynyl}-3-(2-{5-[2-(5-dodecyl)thiophenyl]vinyl}thiophenyl)vinylthiophene (3b)

4.4.2 Synthesis of bi(thienylenevinylene)thiophene-containing PPE-PPV polymers

The bi(thienylenevinylene)thiophene-containing PPE-PPV polymers were synthesized by Horner-Wadsworth-Emmons olefination reaction of the didehydes (3a, 3b) with either 2,5-dioctyloxy-*p*-xylylene-bis(diethylphosphonate) (4a), or 2,5-bis((2-ethylhexyloxy)-*p*-xylylenebis(diethyl phosphonate) (4b) in the presence of potassium *tert*-butoxide.²⁹⁻³¹ The polymers were purified by Soxhlet extraction with methanol/diethyl ether mixture (1:1 v/v). The pure polymers were obtained in yields between 40 % and 69 %. The synthesis is depicted in **Scheme 4.2**.



Scheme 4.2 Synthesis of bi(thienylenevinylene)thiophene-containing polymers BTE-PVaa, BTE-PVab, BTE-PVba and BTE-PVbb

¹H-NMR spectrum of polymer BTE-PVab is presented in **Figure 4.3**. Disappearance of peak due to aldehyde group at around 10.47 δ ppm indicated complete consumption of monomeric dialdehydes (3a) during polymerization. The aromatic protons on phenyl, thiophene rings and vinylic protons on main as well as side chain of polymer were observed in the range of 7.60-6.61 δ ppm. The methylene protons on various side chains which are adjacent to oxygen, appeared in the range of 4.17-3.88 δ ppm. The two protons on methylene group of dodecyl chain which is directly attached to thiophene ring appeared as triplet at 2.79 δ ppm. The remaining methylene protons appeared in the range 1.94-1.17 δ ppm. The methyl protons appeared as triplet at 0.89 δ ppm.

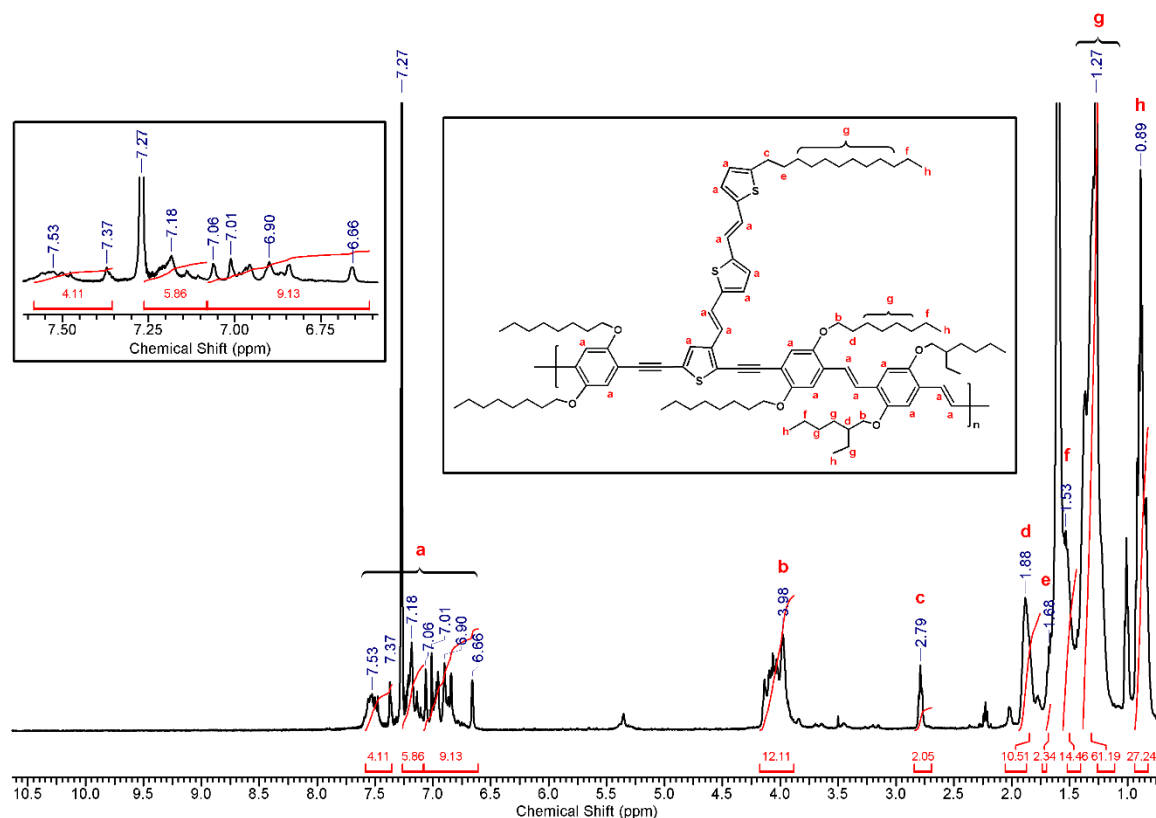


Figure 4.3 ¹H-NMR spectrum (CDCl₃) of the polymer BTE-PVab

Four bi(thienylenevinylene)thiophene-containing poly(*p*-phenylene-ethynylene)-alt-poly(*p*-phenylene-vinylene) (PPE-PPV) polymers denoted as AnE-PV were synthesized and characterized. The polymers differ in nature (linear/ branched) of the side chains on polymer backbone. All the polymers were found to be soluble in organic solvents such as chloroform, dichloromethane, tetrahydrofuran, toluene and chlorobenzene at room temperature.

Molecular weights of polymers were determined by gel permeation chromatography (GPC) in tetrahydrofuran using polystyrene as the standard. The data obtained from GPC and thermogravimetric analysis (TGA) is summarised in **Table 4.1**. Number average molecular weights were in the range 5.9- 26.7 kg/mol. Dispersities were in the range of 1.8– 2.4. **Figure SI 4.2** shows TGA curves for various polymers. TGA study revealed that the polymers are thermostable compounds. Thermal degradation under nitrogen at 10 % weight loss was recorded between 350 and 392 °C.

Table 4.1 Data obtained from GPC and TGA studies.

Polymers	M_n (kg/mol)^a	M_w (kg/mol)^b	Dispersity (M_w/M_n)	T_{10%}/°C^c
BTE-PVaa	26.7	47.80	1.8	392
BTE-PVab	11.1	26.64	2.4	363
BTE-PVbb	10.5	25.20	2.4	350
BTE-PVba	5.9	12.39	2.1	379

a: M_n= number-average molecular weight, b: M_w= weight-average molecular weight, c: T_{10%}=decomposition temperatures at 10% weight loss

4.4.3 Photophysical Study

The photophysical data of polymers was measured in chloroform solution as well as on thin films spin coated from chloroform solution. **Table 4.2** summarizes photophysical data of polymers in solution and on film, which include wavelength at absorption maximum (λ_a), the wavelength at the emission maximum, (λ_{em}), fluorescence quantum yield (Φ_ϕ) and lifetime (τ). The normalized absorption and emission spectra in dilute chloroform solution is depicted in **Figure 4.4**. In solutions, the polymers show absorption maxima between 445-450 nm and emission maxima between 445-450 nm. The Fluorescence quantum yield and lifetimes of the four polymers are very similar. This implies that, in solution, the polymer backbone organisation and conjugation is less affected by the nature of sidechains (branched/linear). The normalized absorption and emission spectra in film is presented in **Figure 4.5** which shows that the different solubilizing side-chains slightly affect the polymer aggregation in the films. Thin-film absorption spectra of polymers BTE-PVbb and BTE-PVba are slightly red shifted and broadened with respect to the solution ones, as a result of polymer–polymer interactions. For BTE-PVab and BTE-PVaa a broadening of the absorption band with a shoulder peak at around 540 nm, indicated a more effective interaction between polymer backbones. In particular, for BTE-PVaa a strong optical coupling of the polymer chains is effective, as

demonstrated by the large red shift of the emission band. Evidently, the linear octyloxy side-chains help the solid-state organization of polymer backbones. The quantum yields are similar for all polymers in thin films (Table 4.2) and are about 20 times lower than the solution values, while the luminescence lifetimes drop below 200 ps (the luminescence decay curves are reported in Fig. SI). Both effects are due to a faster nonradiative decay of the excited states in the films.

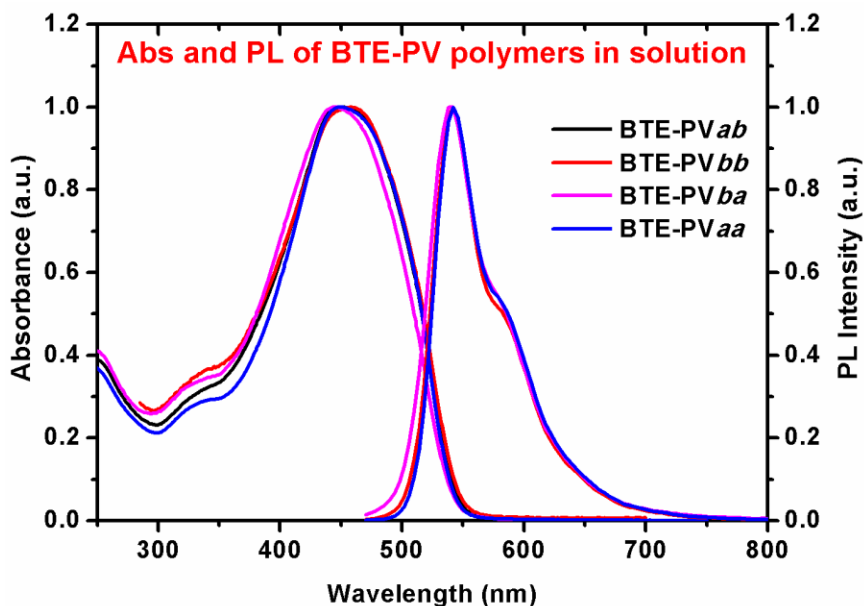


Figure 4.4 The absorption and emission spectra of AnE-PV polymers in dilute chloroform solution

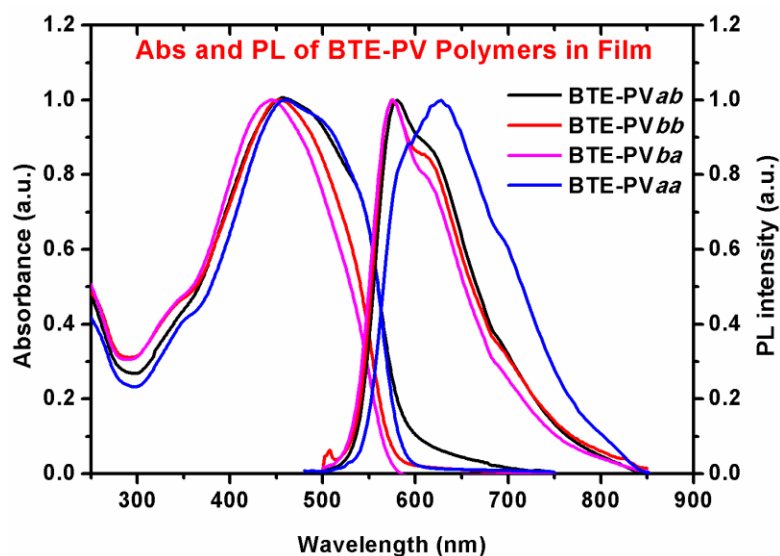


Figure 4.5 The absorption and emission spectra of AnE-PV polymers in thin films

Table 4.2. Photophysical data in dilute chloroform solution and thin film

	<i>Dilute solution</i>				<i>Thin film</i>			
	λ_{abs} (nm)	λ_{em} (nm)	Φ_{ϕ}	τ (ns)	λ_{abs} (nm)	λ_{em} (nm)	Φ_{ϕ}	τ (ns)
BTE-PV ab	450	542	0.28	0.9	460 (540 sh)	580 (610 sh)	0.019	0.2
BTE-PV bb	450	544	0.24	0.9	460	575 (610 sh)	0.010	≤ 0.2
BTE-PV ba	450	540	0.27	0.9	445	575 (610 sh)	0.015	≤ 0.2
BTE-PV aa	450	542	0.26	0.9	460 (540 sh)	630 (585 sh)	0.012	≤ 0.2

4.4.4 Charge carrier mobility measurements:

The drift mobility of charge carriers was studied as a function of the applied electric field (E) by using differential small-signal Time of Flight.³² The TOF experiments were performed on sandwich-type devices with the structure glass/Al/polymer/Al, with the top aluminium layer being semi-transparent for sample irradiation. The film deposition conditions for all polymers were kept same for better comparison of charge transport properties. The illuminated electrode was positively biased for holes and negatively biased for electrons. This class of conjugated polymers show an ambipolar behavior.³³ Typical photocurrent transients, for holes and electrons, are displayed in Figure S2 in a double-logarithmic representation and for a comparable applied electric field of about $8 \times 10^4 \text{ V cm}^{-1}$. The comparison of the signals of Figure S2 confirms the usual finding that transport of electrons is more dispersed than that of positive carriers in conjugated polymers,³⁴ due to trapping effects by impurities, acting as trapping states for negative carriers.³⁵ In the double-logarithmic plots, an inflection point was visible for electrons from which the transit time (t_{tr}) of charge carriers can be evaluated.³⁶ In the case of BTE-PV ba , it was not possible to detect the photocurrent signal for negative carriers, presumably because of very short transit times of electrons for this polymer.

The values of charge carrier mobility (μ) were calculated as a function of the applied electric field E through the well-known expression $\mu = d/\tau E$ where d is the

thickness of the polymer layer, and with the transit times extracted from the TOF signals by using the same method in all cases, that is from the inflection point observed in the double-logarithmic representation. The mobility data are compared in **Figure 4.6** which clearly shows the dramatic effect of lateral solubilising chains on charge carrier mobility, with mobility varying by orders of magnitude for the polymers under consideration. The drift mobility of positive carriers (μ_h) was found to range from $1.3 \times 10^{-5} \text{ cm}^2 \text{ V}^{-1} \text{ s}^{-1}$, for **BTE-PVaa**, to $2.2 \times 10^{-2} \text{ cm}^2 \text{ V}^{-1} \text{ s}^{-1}$, for **BTE-PVba**, at a comparable electric field of about $8 \times 10^4 \text{ V cm}^{-1}$. Similarly, the drift mobility of electrons (μ_e) shows a great variation by changing the solubilising side-chains.

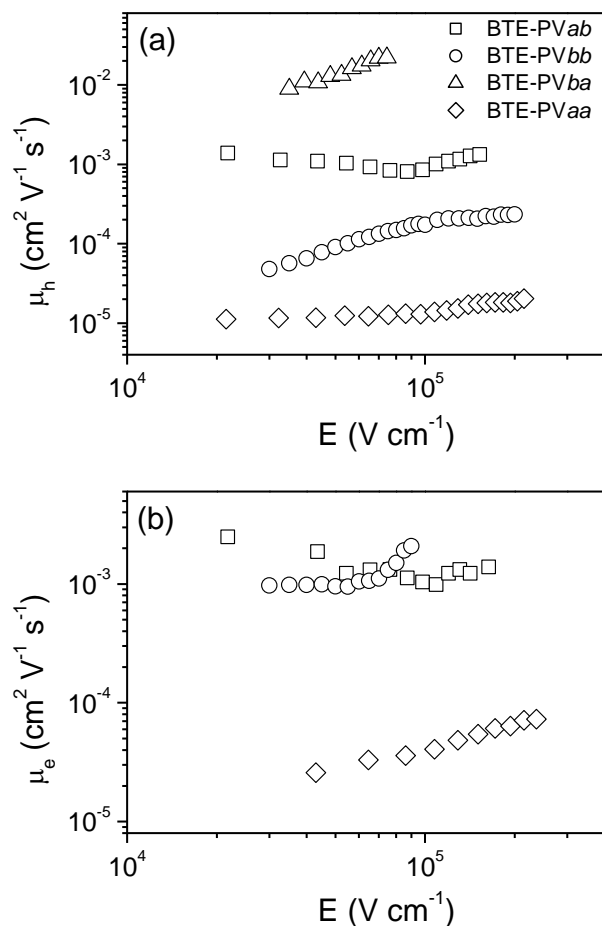


Figure 4.6 Hole mobility (a) and electron mobility (b) as a function of the square root of the electric field for: BTE-PVaa (diamonds); BTE-PVab (squares); BTE-PVba (triangles); BTE-PVbb (circles).

Table 4.3 Hole (μ_h) and electron (μ_e) mobilities of polymers for an electric field of 8×10^4 Vcm^{-1}

Polymers	μ_h ($\text{cm}^2\text{V}^{-1}\text{s}^{-1}$)	μ_e ($\text{cm}^2\text{V}^{-1}\text{s}^{-1}$)
BTE-PVaa	1.3×10^{-5}	3.6×10^{-5}
BTE-PVab	8.4×10^{-4}	1.3×10^{-3}
BTE-PVbb	1.4×10^{-4}	1.3×10^{-3}
BTE-PVba	2.2×10^{-2}	-

4.4.5 X-Ray Diffraction studies

The organization of polymer chains in solid state highly affects transport of charge carriers.^{37,38} So, X-ray diffraction studies were performed on polymer films in order to evaluate the effect of structural variations induced by the different side-chains. The polymer films were prepared under the same conditions used for TOF experiments. XRD patterns of the four samples are compared in **Figure 4.7**. All the samples show the typical pattern of a disordered solid. In more detail, the samples BTE-PVaa and BTE-PVab, richer in the linear octyloxy chains, show an asymmetric amorphous halo with intensity maximum at 2 theta of 22.7° (corresponding to 0.39 nm) while for BTE-PVbb and BTE-PVba, richer in the branched substituents, the symmetric halo is centred at about 20.8° (0.42 nm). It seems that the pattern shape of BTE-PVaa and BTE-PVab samples is affected by the tentative packing of the methylene units: indeed, the position of the two main peaks of polyethylene packing is 21.6° and 24.1° . The sample BTE-PVaa shows an additional very low intensity reflection at 3.91° (2.2 nm) which suggests an initial stage of ordering in the sample with all linear substituents. This result correlates with the broadening of the absorption spectrum observed for BTE-PVaa thin-film (Figure 4.5). Overall, the XRD patterns showed the complete amorphous features of all investigated films prepared under the same conditions used for TOF experiments. This indicated that the substantial variation observed for the drift mobility of charge carriers cannot be attributed to a significantly different organization of polymer chains in the solid state.

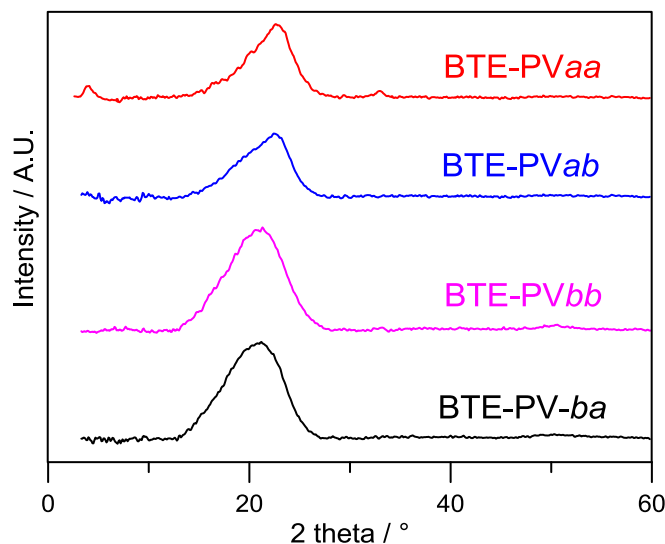


Figure 4.7 XRD patterns of polymer films drop-casted onto zero-background quartz substrate

Charge carrier mobility studies along with XRD studies suggests that the combination of linear and branched substituents (BTE-PVab) is favourable for charge transport properties of the investigated polymers, compared to the incorporation of only linear (BTE-PVaa) or only branched side-chains (BTE-PVbb). The BTE-PVs films have a common amorphous feature. However, the wide range of obtained mobility values could suggest that the mixed linear-branched approach could promote favourable intermolecular interactions for charge transport. The drift mobility of holes in BTE-PVba (bearing combination of linear and branched side chains), richer in branched substituents when compared to BTE-PVab, reaches values of $10^{-2} \text{ cm}^2 \text{ V}^{-1} \text{ s}^{-1}$ for a moderate applied electric field ($< 10^5 \text{ V}^{-1} \text{ cm}^{-1}$), which is indeed remarkable for the bulk mobility of an amorphous polymer film.

A high bulk mobility for holes could be advantageous for the electron-donor (D) in bulk heterojunction solar cells. Therefore, the photovoltaic behaviour of devices made of BTE-PVs as donor and PC₆₁BM as the electron acceptor (A) was investigated.

4.4.6 Photovoltaic studies

The bulk heterojunction solar cells, with a common device structure-ITO/PEDOT:PSS with LiF as hole-selective and Al as electron-selective contacts, were

used. The weight ratio between the conjugated polymer and PC₆₁BM in the photoactive blends was varied between 1:1 (1:0.7 for BTE-PV*ab*) and 1:4, in order to achieve an optimal active layer morphology enabling efficient charge generation and balanced charge transport. **Figure 4.8** shows Atomic Force Microscopy (AFM) images obtained for BTE-PV*ab*: PC₆₁BM blends prepared with 1:1, 1:2, 1:3 and 1:4 D/A weight ratios. The most homogeneous films were obtained for the blends with the lowest PC₆₁BM loading (1:1 and 1:0.7, the latter not shown). The increase of fullerene concentration in the blends resulted in the appearance of round-shaped features corresponding, most probably, to clusters of PC₆₁BM segregated from the polymer phase, similar to those reported for MDMO-PPV: PC₆₁BM blends.^{39,40} Those round-shaped clusters were found to be 150-200 nm in size in BTE-PV*ab*: PC₆₁BM blends prepared with 1:2 donor/acceptor ratio and further increased by increasing the acceptor concentration (300-400 nm for 1:3 and 400-600 nm for 1:4 D/A ratio). Thus, it points out that these clusters are mainly composed of the fullerene derivative. Similar surface morphology was also observed for blends made with BTE-PV*aa*, BTE-PV*bb* and BTE-PV*ba* donors. The AFM images obtained for BTE-PV*ba*: PC₆₁BM blends are shown in **Figure SI 4.5**.

The blend morphology exhibited by the investigated blends is not optimal for achieving an efficient generation of free charge carriers. Indeed, charge generation in bulk heterojunction solar cells occurs at the interface between the donor and acceptor components of the blend and photogenerated excitons have to reach by diffusion to the D/A interface, in order that their dissociation can take place before their radiative or non-radiative recombination. Because of the short exciton diffusion length in organic semiconductors (20 nm, typically)^{41,42,43} a nanoscale phase separation between the two components is required for efficient charge carrier generation. Therefore, the AFM investigation could suggest that a high generation rate of free charge carriers cannot be expected for the BTE-PV: PC₆₁BM blends investigated here, negatively affecting the short-circuit current density (J_{SC}) of the related cells.

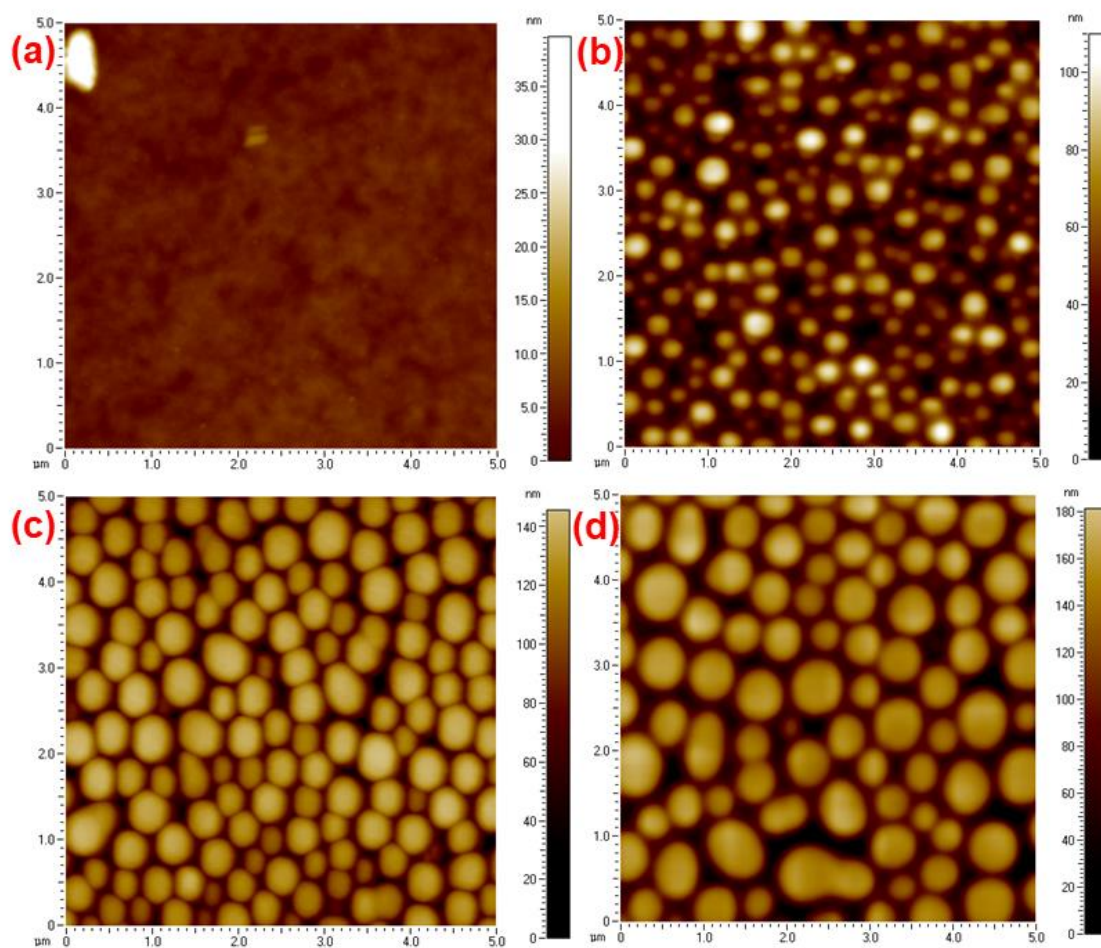


Figure 4.8 AFM height images ($5\ \mu\text{m} \times 5\ \mu\text{m}$) of BTE-PVab: PC₆₁BM blends prepared in 1:1 (a), 1:2 (b), 1:3 (c) and 1:4 (d) w/w D/A ratios.

Figure 4.9 depicts the current density-voltage (J - V) curves of the solar cells based on polymer:PC₆₁BM active layers. A solar simulator (AM1.5, class A) was used for illumination. The current density-voltage (J - V) curves and external quantum efficiency (EQE) spectra also support the detrimental effect of unsuitable morphology on efficient free charge generation, resulting in moderate values for J_{SC} , ranging between 1.5 and 4.3 mA cm^{-2} , as shown by the photovoltaic parameters extracted from the J - V characteristics collected in **Table 4.4**. The maximum power conversion efficiency was obtained for polymer BTE-PVab ($\eta = 2.1\%$) having linear octyloxy side-chains on the BTE part.

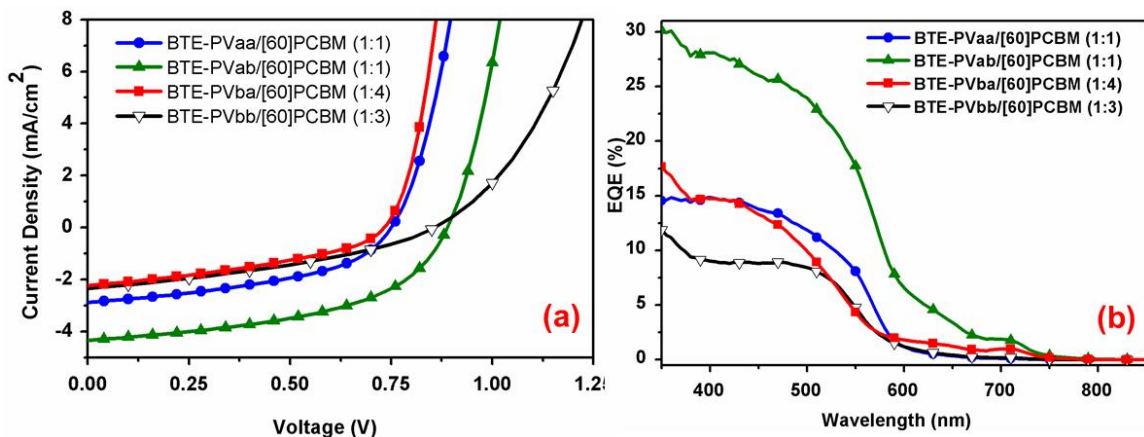


Figure 4.9 (a) J - V curves for the best performing solar cells obtained under simulated AM1.5 illumination and (b) corresponding EQE spectra.

Table 4.4 Photovoltaic parameters of solar cells made of BTE-PVs as donors and PC₆₁BM as acceptor: short-circuit current-density (J_{sc}), open-circuit voltage (V_{oc}), fill factor (FF), power conversion efficiency (η).

	D/A w/w ratio	J_{sc} (mA cm ⁻²)	V_{oc} (mV)	FF (%)	η (%)
BTE-PVaa	1:1	2.9	740	46	1.0
BTE-PVab	1:0.7	2.6	900	29	0.7
	1:1	4.3	880	55	2.1
	1:2	3.4	880	50	1.5
	1:3	2.6	900	40	1.0
	1:4	2.8	900	39	1.0
BTE-PVba	1:1	1.8	740	31	0.4
	1:2	1.5	780	34	0.4
	1:3	1.6	700	34	0.4
	1:4	2.4	740	38	0.7
BTE-PVbb	1:1	2.0	850	30	0.5
	1:2	1.8	850	29	0.4
	1:3	2.3	900	34	0.7
	1:4	2.0	900	33	0.6

The analysis of the data reported in **Table 4.3** and **Table 4.4** reveals that a correlation between hole mobility of pristine polymers and the photovoltaic performance of the cells cannot be established. This is a result of the unsuitable morphology of the photoactive blends which hampered the photovoltaic performance. Indeed, in addition to the poor generation of charge carriers, the moderate values of fill factor (*FF*) achieved in most cases may indicate a significant charge-carrier recombination loss, due to an improper formation of de-mixed donor and acceptor pathways for efficient charge transport and extraction. Probably, the performance of BTE-PVs in photovoltaic cells is somehow limited by supramolecular interactions between the polymers and fullerene, not leading to an appropriate miscibility of the two components. Thus, these photovoltaic results confirm once again that the morphology of the blend plays a pivotal role for the performance of bulk-heterojunction solar cells. Nevertheless, the inspection of the data presented in **Table 4.4** could suggest that cells made of BTE-PV*aa* and BTE-PV*ab*, possessing linear octyloxy side-chains on the BTE part, perform better than other polymers. This behaviour is in correlation with the results obtained for solar cells made with a series of AnE-PVs (Chapter 3a of this thesis) as donors,⁹ for which higher power conversion efficiencies were observed for polymers bearing linear octyloxy side-chains attached to the AnE part, compared to those comprising 2-ethylhexyloxy chains in the same position.

4.5 CONCLUSIONS

The four side-chain conjugated polymers, differing in the nature of solubilising side chains octyloxy (linear) and 2-ethylhexyloxy (branched) chains on the PPE and PPV units were synthesised and characterised. The polymers exhibited very different charge transport properties, investigated by TOF technique. The bulk hole mobility at a field of about 8×10^4 V cm⁻¹ ranged from 1.3×10^{-5} cm² V⁻¹ s⁻¹ for BTE-PV*aa*, substituted with solely linear chains, to the outstanding value of 2.2×10^{-2} cm² V⁻¹ s⁻¹ for BTE-PV*ba*, with branched and linear solubilising chains. The XRD study on thick films showed no difference in the structure of the polymer films. The XRD patterns indicated a completely amorphous feature of polymer films. Though the thin film absorption spectra suggested a moderate organisation for the polymers containing linear octyloxy chains, (BTE-PV*ab* and BTE-PV*aa*), no obvious evidence of ordering has appeared in the XRD spectra of thicker films.

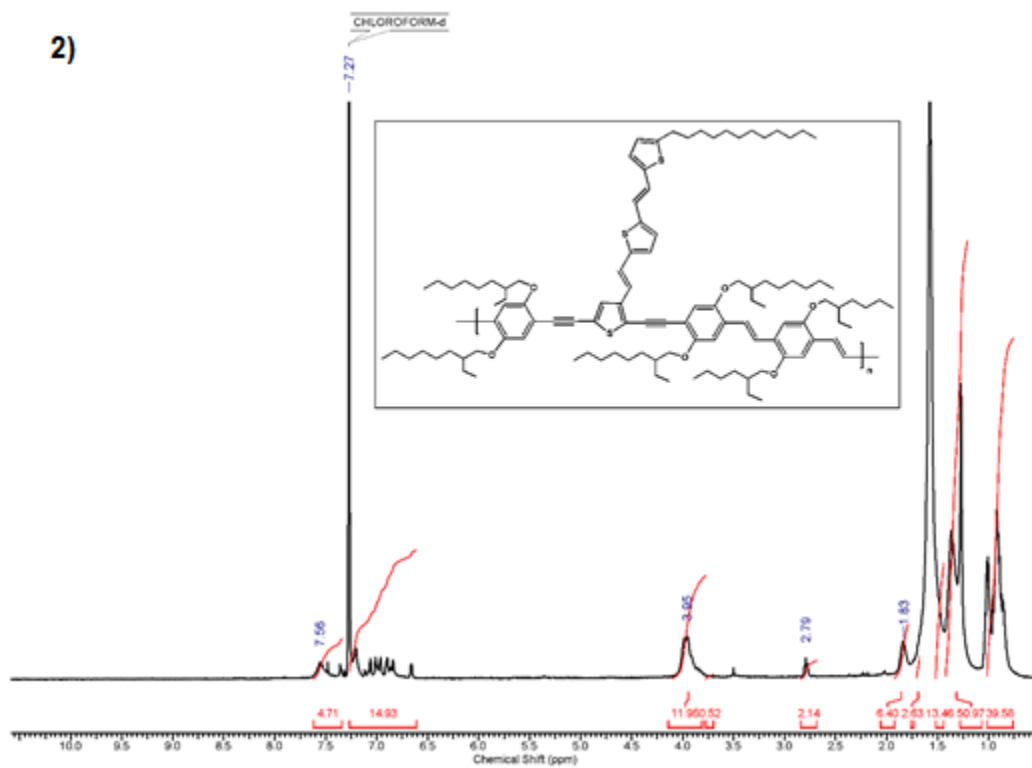
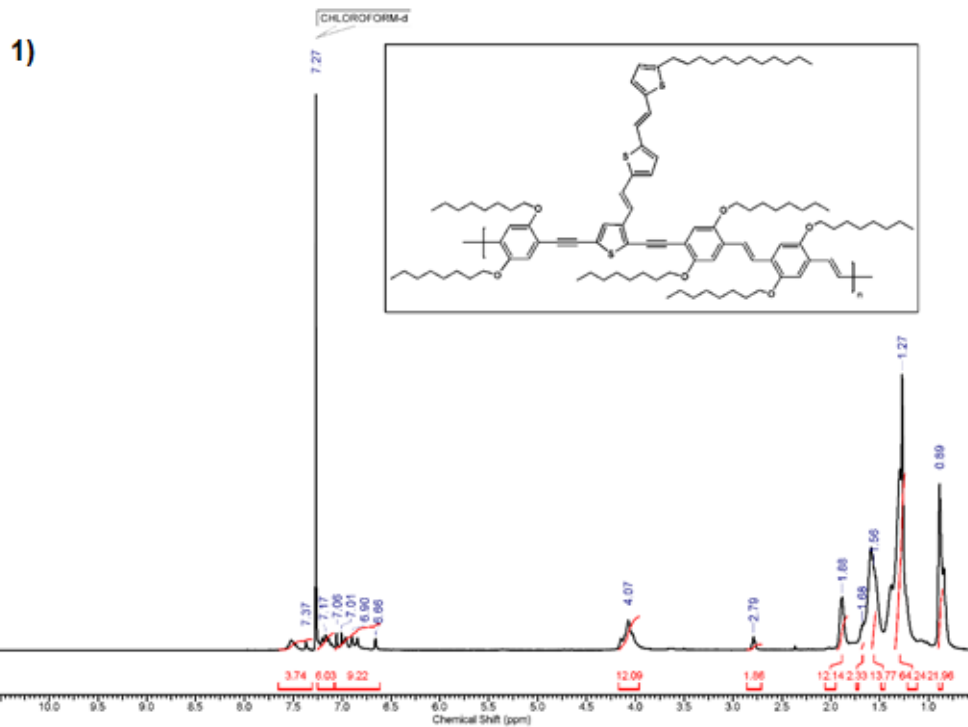
Given the similarity of the structural properties of the polymer films, the remarkable difference of mobility values, spanning over three orders of magnitude, can be mainly attributed to the chemical structure of the polymers. The combination of linear and branched chains was found to be favorable for charge transport properties of the investigated polymers, compared to the incorporation of only linear or branched side-chains, similar to the behaviour already reported for AnE-PV copolymers. Nevertheless, the bulk heterojunction solar cells made with BTE-PV*ba* as donor and PC₆₀BM as acceptor did not take advantage of their remarkable hole mobility, because of an unfavourable morphology of the blends. The maximum power conversion efficiency was obtained for polymer BTE-PV*ab* ($\eta = 2.1\%$) having linear octyloxy side-chains on the BTE part.

REFERENCES

1. D. Gamota, P. Brazis, K. Kalyanasundaram, and J. Zhang, *Printed Organic and Molecular Electronic*; Springer; Kluwer Academic, Norwell, 2004.
2. A. Heeger, *Chem. Soc. Rev.*, 2010, **39**, 2354-2371.
3. D. A. M. Egbe, B. Carbonnier, E. Birckner and U.-W. Grummt, *Prog. Polym. Sci.*, 2009, **34**, 1023-1067.
4. S. Lee, H. Cho, K. Cho and Y. Park, *J. Phys. Chem. C.*, 2013, **117**, 11764-11769.
5. T. Lei, J.-Y. Wang and J. Pei, *Chem. Mater.*, 2014, **26**, 594-603.
6. J. Mei and Z. Bao, *Chem. Mater.*, 2014, **26**, 604-615.
7. J. Hou, Z. Tan, Y. Yan, Y. He, C. Yang, Y. Li, *J. Am. Chem. Soc.* 2006, **128**, 4911-4916.
8. Y. Li, *Acc. Chem. Res.*, 2012, **45**, 723-733.
9. F. Huang, K. Chen, H. Yip, S. Hau, O. Acton, Y. Zhang, J. Luo, A. K. Y. Jen, *J. Am. Chem. Soc.*, 2009, **131**, 13886-13887.
10. Q. Peng, X. Liu, D. Su, G. Fu, J. Xu, and L. Dai, *Adv. Mater.*, 2011, **23**, 4554-4558.
11. E. Zhou, J. Cong, K. Hashimoto and K. Tajima, *Energy Environ. Sci.*, 2012, **5**, 9756-9759.
12. R. Kularatne, P. Sista, H. Nguyen, M. Bhatt, M. Biewer and M. Stefan, *Macromolecules*, 2012, **45**, 7855-7862.
13. S. Liao, H.-J. Jhuo, Y. Cheng, and S. Chen, *Adv. Mater.*, 2013, **25**, 4766-4771.

14. L. Ye, S. Zhang, L. Huo, M. Zhang and J. Hou, *Acc. Chem. Res.*, 2014, **47**, 1595-1603.
15. J. Lee, J.-H. Kim, B. Moon, H. G. Kim, M. Kim, J. Shin, H. Hwang and K. Cho, *Macromolecules*, 2015, **48**, 1723–1735.
16. G. Li, Z. Lu, C. Li and Z. Bo, *Polym. Chem.*, 2015, **6**, 1613-1618.
17. M. Wang, D. Ma, K. Shi, S. Shi, S. Chen, C. Huang, Z. Qiao, Z.G. Zhang, Y. Li, X. Li and H. Wang, *J. Mater. Chem. A*, 2015, **3**, 2802–2814.
18. J. Yuan and W. Ma, *J. Mater. Chem. A*, 2015, **3**, 7077–7085.
19. H. Wu, B. Zhao, W. Wang, Z. Guo, W. Wei, Z. An, C. Gao, H. Chen, B. Xiao, Y. Xie, H. Wu and Y. Cao, *J. Mater. Chem. A*, 2015, **3**, 18115-18126.
20. L. Ye, S. Zhang, W. Zhao, H. Yao and J. Hou, *Chem. Mater.*, 2014, **26**, 3603–3605
21. D. A. M. Egbe, S. Türk, S. Rathgeber, F. Kuehnlenz, R. Jadhav, A. Wild, E. Birckner, G. Adam, A. Pivrikas, V. Cimrova, G. Knör, N. S. Sariciftci and H. Hoppe, *Macromolecules*, 2010, **43**, 1261-1269.
22. F. Tinti, F. Sabir, M. Gazzano, S. Righi, Ö. Usluer, C. Ulbricht, T. Yohannes, D. A. M. Egbe and N. Camaioni, *Macromol. Chem. Phys.*, 2014, **215**, 452-457.
23. M. Montalti, A. Credi, L. Prodi and T. Gandolfi, *Handbook of Photochemistry*, 3rd edn., CRC Press, Taylor & Francis: Boca Raton, 2006.
24. Dieck, H. A.; Heck, F. H. *J. Org. Chem.* 1975, **93**, 259.
25. Tohda, Y.; Sonogashira, K.; Hagihara, N. *Tetrahedron Lett.* 1975, **50**, 4467.
26. Yamamoto, T.; Yamamoto, A. *Bull. Chem. Soc. Jpn.* 1984, **57**, 752.
27. Yamamoto, T. *Bull. Chem. Soc. Jpn.* 1999, **72**, 621.
28. Bunz, U. H. F. *Chem. Rev.* 2000, **100**, 1605.
29. H.-H. Hörhold, J. Opfermann, *Makromol. Chem.* 1970, **131**, 105;
30. H.-H. Hörhold, H. Wildner; *Chem. Abstr.* 1967, **66**, 105346.
31. H.-H. Hörhold, M. Helbig, *Makromol. Chem., Macromol. Symp.* 1987, **12**, 229.
32. P. Borsenberger and D. Weiss, in *Organic Photoreceptors for Xerography*, Marcel Dekker, New York, 1998.
33. N. Camaioni, F. Tinti, A. Esposti, S. Righi, Ö. Usluer, S. Boudiba and D. A. M. Egbe, *Appl. Phys. Lett.*, 2012, **101**, 053302.
34. A. Campbell, D.D.C. Bradley and H. Antoniadis, *Appl. Phys. Lett.*, 2001, **79**, 2133

- 2135.
35. A. Campbell, D.D.C. Bradley and D. Lidzey *J. Appl. Phys.*, 1997, **82**, 6326-6342.
 36. H. Scher and E. Montroll, *Phys. Rev. B*, 1975, **12**, 2455-2477.
 37. R. Kline and M. McGehee, *J. Macromol. Sci., Part C: Polym. Rev.*, 2006, **46**, 27-45.
 38. Y. Olivier, D. Niedzialek, V. Lemaur, W. Pisula, K. Müllen, U. Koldemir, J. Reynolds, R. Lazzaroni, J. Cornil and D. Beljonne, *Adv. Mater.*, 2014, **26**, 2119-2136.
 39. Hoppe, H.; Niggemann, M.; Winder, C.; Kraut, J.; Hiesgen, R.; Hinsch, A.; Meissner, D.; Sariciftci, N. S. *Adv. Funct. Mater.* 2004, **14**, 1005.
 40. Hoppe, H.; Glatzel, T.; Niggemann, M.; Hinsch, A.; Lux-Steiner, M. C.; Sariciftci, N.S. *Nano Lett.* 2005, **5**, 269.
 41. Theander, M.; Yartsev, A.; Zigmantas D.; Sundstrom V.; Mammo W.; Andersson M. R.; Inganas O. *Phys. Rev. B* 2000, **61**, 12957.
 42. Markov, D. E.; Tanase, C.; Blom, P. W. M.; Wildeman, J. *Phys. Rev. B* 2005, **72**, 045217.
 43. Markov, D. E.; Amsterdam, E.; Blom, P. W. M.; Sieval, A. B.; Hummelen, J. C. *J. Phys. Chem. A* 2005, **109**, 5266.

Supporting Information

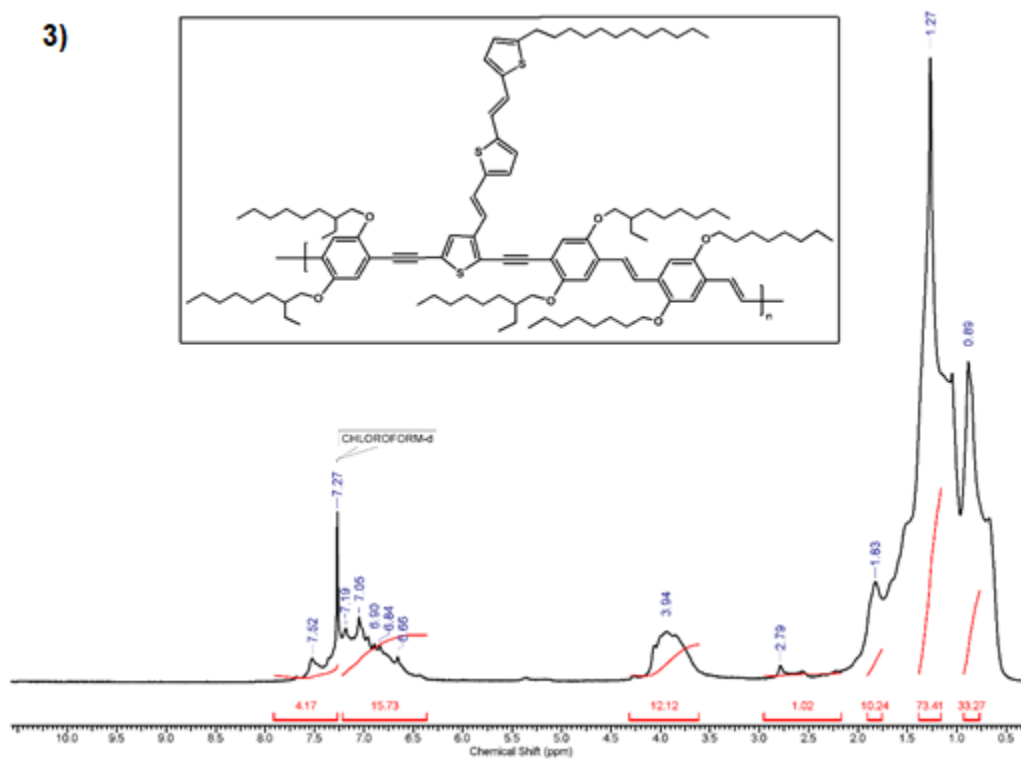


Figure SI 4.1 $^1\text{H-NMR}$ spectrum (CDCl_3) of polymers- 1) BTE-PV aa , 2) BTE-PV bb and 3) BTE-PV ba

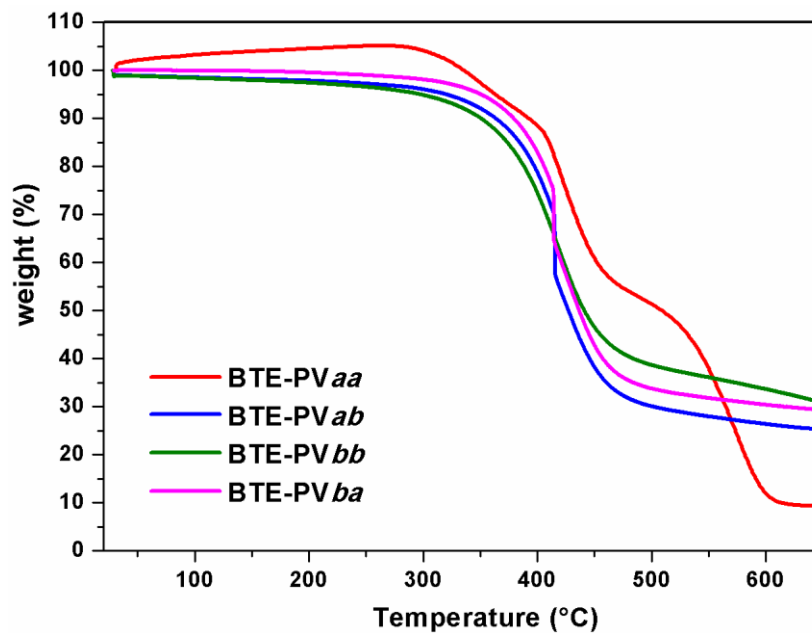


Figure SI 4.2 TG curves of BTE-PV polymers

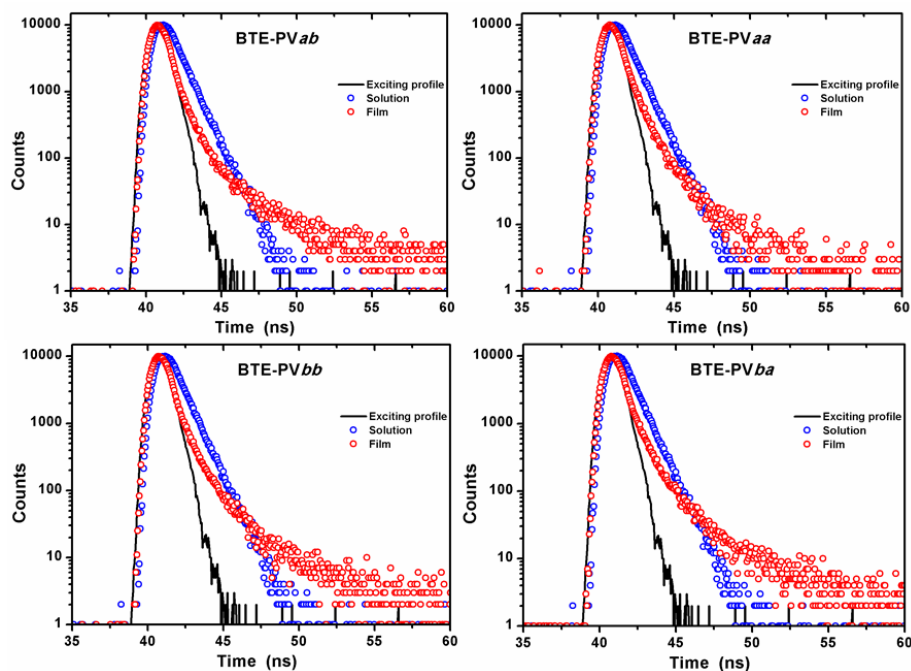


Figure SI 4.3 Luminescence decay curves in dilute chloroform solution and thin film

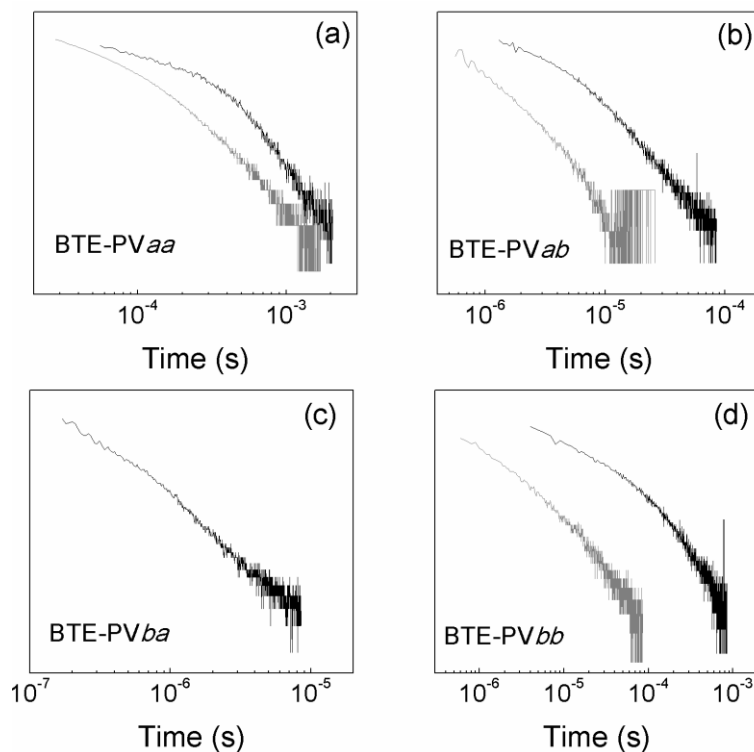


Figure SI 4.4 Typical TOF signals for positive (black lines) and negative charge carriers (gray lines) in log-log scales: BTE-PVaa (a); BTE-PVab (b); BTE-PVba (c); BTE-PVbb (d). Applied electric field of about $8 \times 10^4 \text{ V cm}^{-1}$

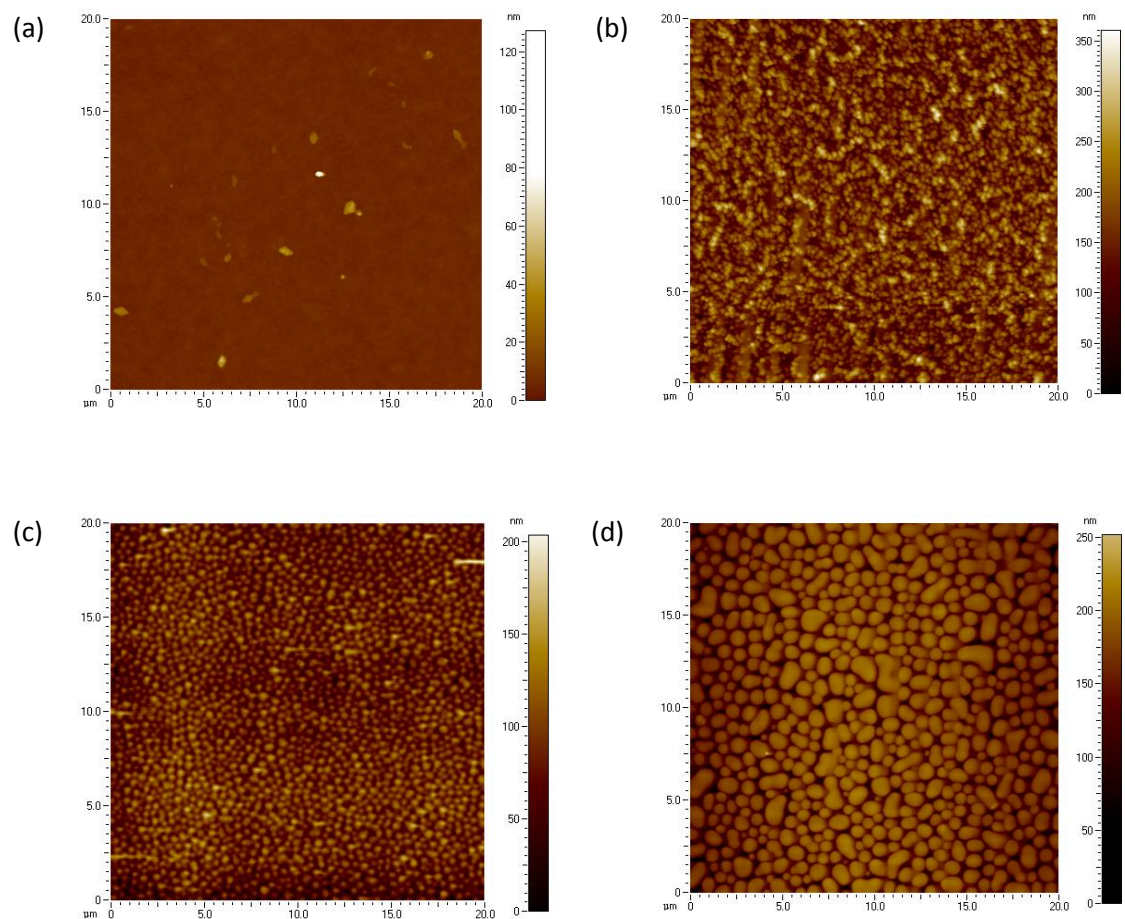


Figure SI 4.5 AFM height images (20 μm x 20 μm) of BTE-PVba: PC₆₁BM blends prepared in 1:1 (a), 1:2 (b), 1:3 (c) and 1:4 (d) w/w D/A ratios

CHAPTER 5

Benzo[1,2-c:4,5-c']dithiophene-4,8-dione Containing Copolymers and Terpolymers: Implications of Active Layer Morphology on Photovoltaic Performance

5.1 INTRODUCTION

Solution processable polymer solar cells (PSCs) have emerged as potential candidates for commercialization of solar cell technology due to their advantages such as large area production, flexibility, light weight and cost effectiveness. The power conversion efficiency (PCE) of PSCs has been rapidly improved over the past few years and approached 14 % in single junction solar cells.¹⁻⁴ Donor-Acceptor (D-A) copolymers were successfully employed as a donor material in an active layer in the bulk heterojunction construct of solar cells. The judicious choice of electron-donating (D) and electron-accepting (A) units for the construction of new donor polymers is imperative to get efficient systems. The design criteria for new D-A polymers for their practical applications are as follows- i) good solubility in common organic solvents for solution processability, ii) strong and broad absorption in visible and near IR region to match the solar spectrum, iii) proper highest occupied molecular orbital (HOMO) and lowest unoccupied molecular orbital (LUMO) energy levels to achieve higher open circuit voltage (V_{oc}), also efficient exciton dissociation into free charge carriers to achieve high short-circuit current (J_{sc}); iv) high and balanced charge carrier mobility, to ensure efficient charge transport; and v) controlled morphology with nanoscale phase separation between donor- and acceptor-domains to afford bicontinuous interpenetrating networks in active layer for better charge separation and charge transport. Indeed, some of the polymers possessing above mentioned properties have shown remarkable photovoltaic performance.⁵⁻¹² Albeit, most of the D-A copolymers with low band gap energy absorb strongly in near IR region but they show poor absorption in visible region. Thus, they lack broad absorption covering entire solar spectrum and result in poor J_{sc} values. Also, incorporation of solubilizing side chains on D and A units, sometimes adversely affect molecular packing leading to diminished charge transport and hence the lower photovoltaic performance. Moreover, designing and synthesizing novel structures of D and A units for new, more efficient D-A copolymers has now become limited and non-economic.¹³ Because of these limitations, there is a need to search new approaches in the design of polymers so as to further improve the photovoltaic performance of PSCs.

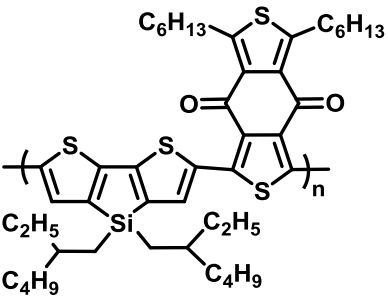
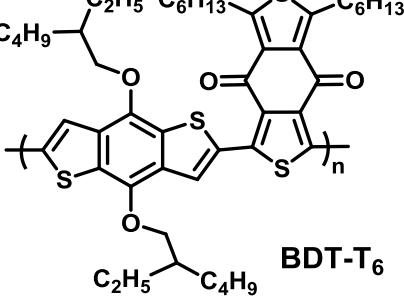
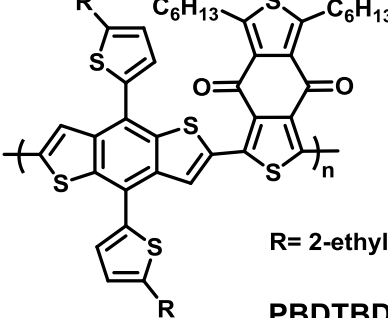
In this regard, terpolymers, which consist of three different units in the polymer backbone, are promising candidates. The incorporation of a third component (donor D or

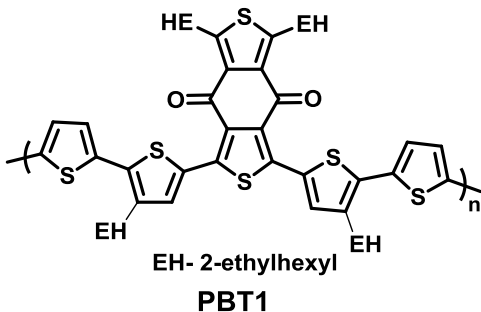
acceptor A) into D–A copolymers affords either D–A–A or D–D–A type terpolymeric system.^{14–17} With added new D or A unit, there exists a possibility of tuning solar absorption, solubility, HOMO-LUMO energy levels and π - π stacking of terpolymers^{16–21} In general, terpolymers show a broader absorption range compared to their corresponding D–A copolymers. The extended light absorption favours more photon harvesting, resulting in more exciton generation which mainly contribute to high photocurrent.^{18,19} Interestingly, side chains on the new D or A unit, apart from enhancing solubility, also play important role in manipulating π - π stacking and thus the molecular packing.^{20–22} Further, in random terpolymers, the ratio of monomers can be carefully optimised to get large current densities²³ and desired crystallinity with superior performance in PSCs.²⁴ Therefore, the design of terpolymers based on knowledge of existing promising D–A copolymers, is found to be attractive strategy for tailoring polymers with superior opto-electronic properties by proper selection of the third component.

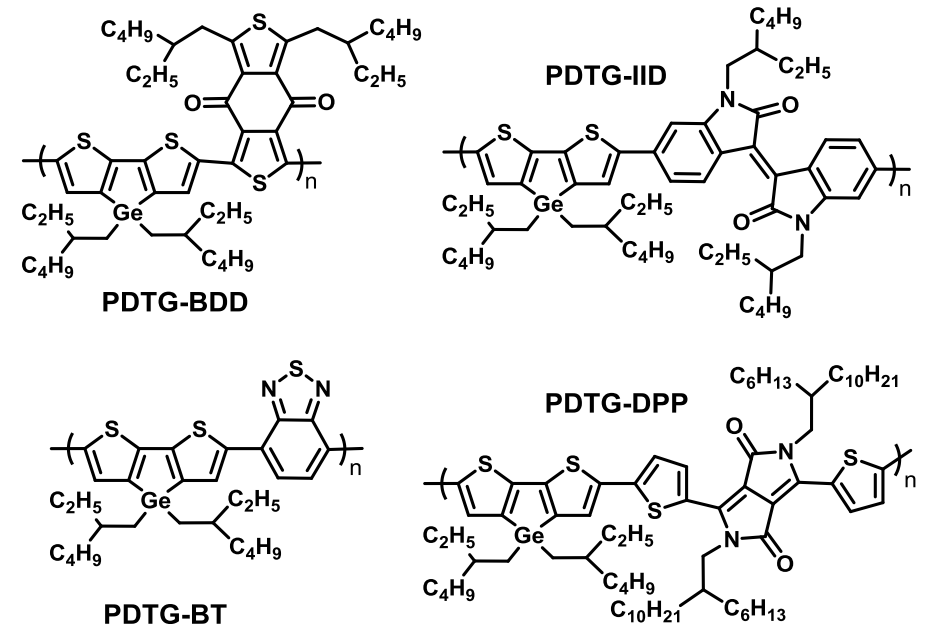
Recently, Ie et al designed and synthesised new acceptor unit namely- 1,3-dibromo-5,7-dihexyl-4H,8H-benzo[1,2-c:4,5-c']dithiophene-4,8-dione.²⁵ Later, Qian et al modified this unit by changing the alkyl groups from hexyl to 2-ethylhexyl to synthesize new acceptor-1,3-bis(thiophen-2-yl)-5,7-bis(2-ethylhexyl)benzo-[1,2-c:4,5c']dithiophene-4,8-dione (BDD)²⁶. Since then, several BDD-based D–A copolymers as donor materials in combination with PCBM and non-fullerene acceptors, with impressive photovoltaic performance were developed.

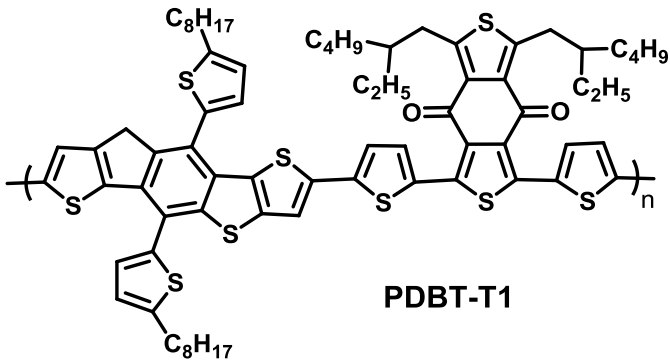
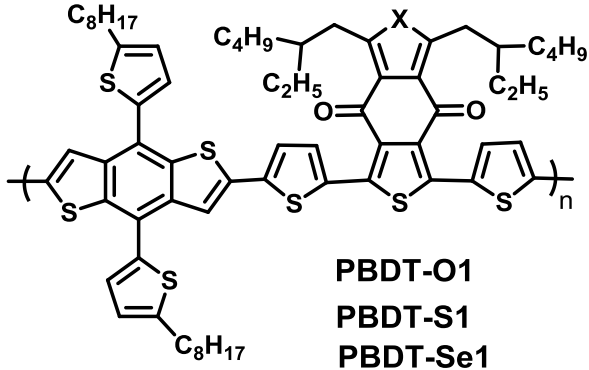
Table 5.1 summarises BDD-based copolymers reported in the literature.

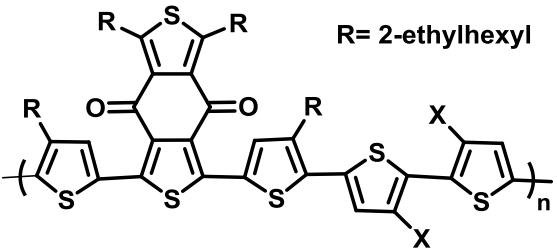
Table 5.1 BDD-based copolymers reported in the literature

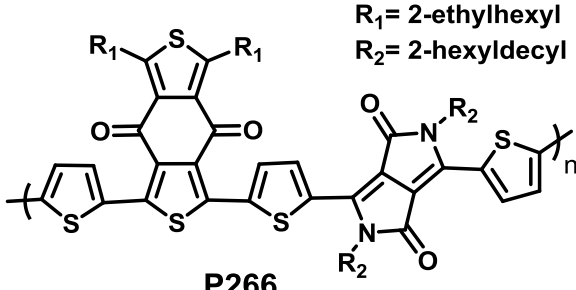
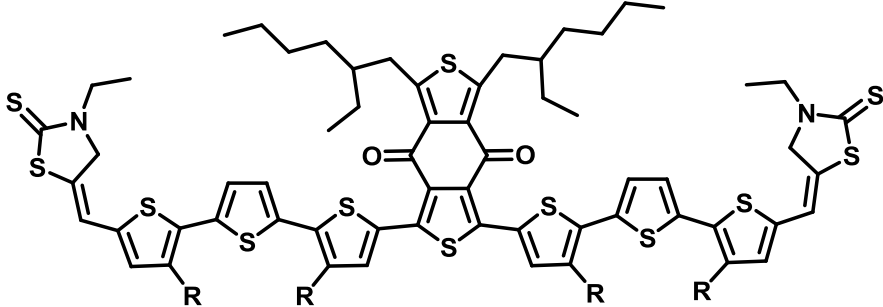
Sr. No.	1,3-bis(thiophen-2-yl)-5,7-bis(2-ethylhexyl)benzo-[1,2-c:4,5c']dithiophene -4,8-dione (BDD) based copolymers	Ref. No.
1	<div style="display: flex; justify-content: space-around; align-items: center;"> <div style="text-align: center;">  <p>DTS-T₆</p> </div> <div style="text-align: center;">  <p>BDT-T₆</p> </div> </div> <p>Two donor-acceptor type copolymers namely- DTS-T₆ and BDT-T₆ containing dioxocycloalkene-annelated thiophenes as electron-accepting units were designed and synthesized and applied as p-type organic semiconducting materials in organic photovoltaics. These copolymers possessed low optical band gaps (1.63-1.92 eV) and low-lying HOMO energy levels (-5.41 to -5.33 eV). Organic field-effect transistor measurements showed that these copolymers had hole-transporting characteristics with mobilities in the order of 10⁻⁷-10⁻⁴ cm² V⁻¹ s⁻¹. The solar cell devices fabricated using these materials as donor with fullerene derivatives as acceptors exhibited power conversion efficiencies of up to 4.87 % (V_{oc}= 0.90 V, J_{sc}= 11.46 mA cm⁻² and FF= 0.48).</p>	25
2	<div style="text-align: center;">  <p>R= 2-ethylhexyl PBDBTDD</p> </div>	26

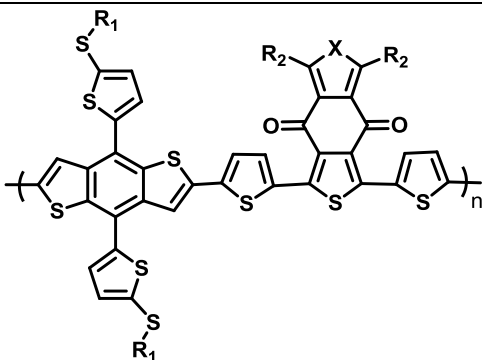
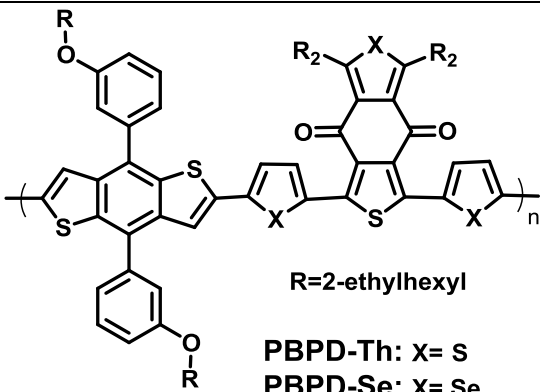
	<p>In 2012, Qian et al designed and synthesized a new polymer PBDBTDD and applied it as a donor material in polymer solar cells. A power conversion efficiency of 6.67 % was obtained from the PBDBTDD:PC₆₁BM-based devices, which is a remarkable result for the PSCs using PC₆₁BM as electron acceptor. The PBDBTDD/PC₆₁BM-based device exhibited a narrow absorption band and excellent quantum efficiency. In solution, PBDBTDD showed a strong aggregation effect, and the study indicated that the temperature used in solution preparation has minor influence on molecular orientation and crystallinity of the D/A blend, but it has strong effect on forming proper domain size in the blend. This study established a good correlation between morphology of blend films and the processing temperature of blend solution. Thus, this is an interesting and feasible approach to modulate domain size without changing crystallinity of the blend films in PSCs.</p>	
3	<div style="text-align: center;">  <p>PBT1</p> </div> <p>Qian et al, in 2013, designed and synthesized a new polymer PBT1 and used it as a donor component in polymer solar cells and recorded an efficiency of 6.88 % with a 75 nm active layer. This work emphasises the use of molecular structure as a tool to realize optimal photovoltaic performance with high polymer content. This enables the efficient photo-absorption in very thin films.</p>	27

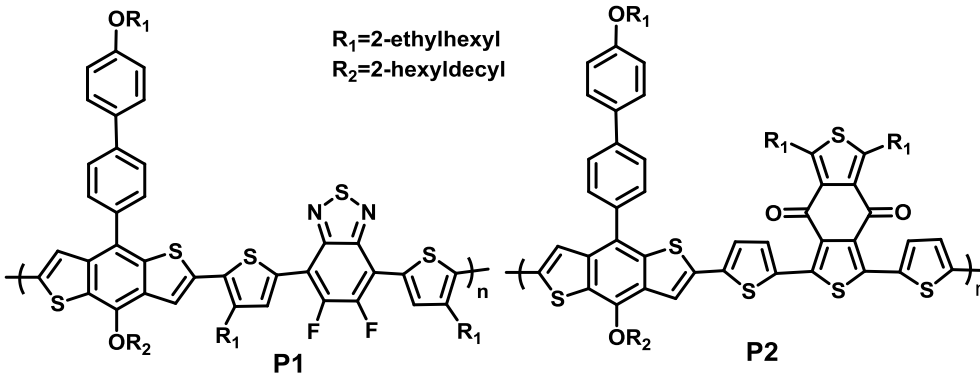
4	 <p data-bbox="292 861 1218 1596">Wang et al in 2014, synthesised four conjugated polymers based on dithienogermole (DTG) units, namely- PDTG-BDD, PDTG-IID, PDTG-BT, and PDTG-DPP and investigated their photovoltaic properties with respect to the varied backbone structure. The results showed that the device fabricated using PDTG-BDD exhibited a PCE of 6.3 % with a high Voc of 0.935 V, a FF of 65.0 %, and a Jsc of 10.3 mA/cm², which is the highest one in these four polymers while the devices fabricated using PDTG-DPP showed a very low Jsc of 3.19 mA/cm² due to the unfavorable morphologies of the polymer:PC₇₁BM blend. Overall, the comparisons among these four polymers provide fundamental information for understanding the correlations among molecular structures and photovoltaic properties of the DTG-based polymers, and how to control or modulate the band-gap, molecular energy levels, and morphologies of the DTG-polymers to fully explore their potential as photovoltaic materials.</p>	28
---	--	----

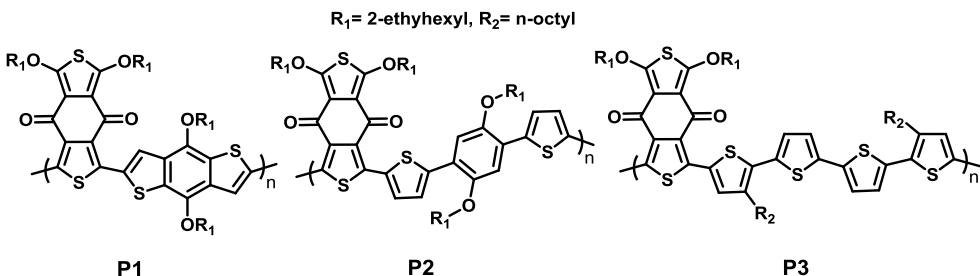
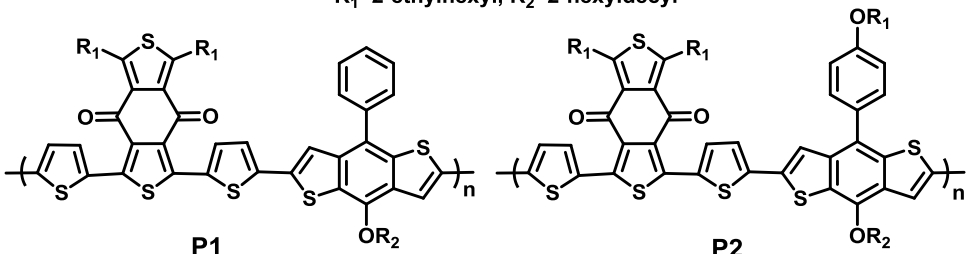
5	 <p style="text-align: center;">PDBT-T1</p> <p>Huo et al in 2015, synthesised a novel WBG copolymer, PDBT-T1 comprising of an electron-rich DTBDT subunit and a strong electron-deficient 1,3-bis(5-bromothiophen-2-yl)-5,7-bis(2-ethylhexyl) -4H,8H-benzo[1,2-c:4,5-c']dithiophene-4,8-dione (T1) subunit. The polymer has a highly rigid backbone since both DTBDT and T1 subunits are rigid and planar. Single-junction organic solar cells based on PDBT-T1 as the donor and PC₇₀BM) as the acceptor exhibited a high PCE of 8.3 % for cells without any solvent additives and post-annealing treatments. When 1,8-diiodooctane (DIO) was used as the solvent additive, the PCE can be further improved to 9.7 %, with a high fill factor (<i>FF</i>) of 75 %.</p>	9
6	 <p style="text-align: center;">PBBDT-O1 PBBDT-S1 PBBDT-Se1</p> <p>Three wide band-gap copolymers, PBBDT-O1, PBBDT-S1 and PBBDT-Se were designed and synthesised by Huang et al in 2016 by incorporating benzodithiophene (BDT) as donor unit and benzothienothioindione (BTTDO) as an acceptor unit. The effects of heteroatoms on the thermal stability, absorption spectra, energy level, charge carrier mobility, and photovoltaic properties of these copolymers were studied. The results</p>	29

	<p>indicated that upon increasing the size of the heteroatoms, the maximum absorption peaks were red-shifted and the optical band-gap decreased. Among the three polymers, PBDT-S1 achieved the best photovoltaic performance, with a high power conversion efficiency (PCE) of 9.0 %, (V_{oc} = 0.91 V, J_{sc} = 12.99 mA cm², and FF = 74.9 %).</p>	
7	<div style="text-align: center;">  <p>R= 2-ethylhexyl</p> <p>X= H PBDD4T = F PBDD4T-2F</p> </div> <p>Zhang et-al in 2016, synthesized two copolymers- a polythiophene derivative (PBDD4T) and fluorinated derivative of PBDD4T (PBDD4T-2F). PBDD4T-2F was synthesised to increase the rotational barrier and hence stabilize its backbone conformation by introducing fluorine into the β- and β'-position of the α-linked bithiophene segments. It was demonstrated that BDD4T-2F has a more stable backbone conformation than PBDD4T due to fluorination. Comparatively, PBDD4T-2F shows stronger aggregation effect in solution state and more compact π-π stacking in solid thin film and also possesses deeper HOMO level. Taking advantage of these properties, PBDD4T-2F-based device showed a power conversion efficiency (PCE) of 9.04 %, when blended with PC₇₁BM; of 8.69 %, when blended with ITIC and of 10.12 %, in the tandem cell, in which the blend of PBDD4T-2F:PC₆₁BM was used for making the front subcell, These results indicated that the fluorination is an effective method to enhance interchain π-π interaction for the polythiophene and especially for the fullerene-free device based on ITIC.</p>	30

8	<div style="text-align: center;">  <p>P266</p> <p>$R_1 = 2\text{-ethylhexyl}$ $R_2 = 2\text{-hexyldecyl}$</p> </div> <p>Zhang et al synthesised a conjugated polymer (P266) using diketopyrrolopyrrole (DPP) and benzo[1,2-c:4,5-c']dithiophene-4,8-dione (BDD) units as the backbone framework. The new polymer exhibited a narrow optical band-gap and strong aggregation behaviour in the solution state. The result showed that by dissolving the donor and acceptor in different solvents and then mixing them before film casting, better performing solar cell devices and distinct film morphology could be achieved, rather than by dissolution in one solvent. A high efficiency of 9.18 % was obtained using PC₇₁BM as an acceptor. This study demonstrated the importance of manipulating the aggregation state in bulk heterojunction solar cell fabrication and revealed the influence of polymer-fullerene interplay on the blend film morphology.</p>	31
9	<div style="text-align: center;">  <p>DR3TBDD</p> <p>$R = n\text{-octyl}$</p> </div> <p>A small molecule named DR3TBDD, using 1,3-bis(4-(2-ethylhexyl)-thiophen-2-yl)-5,7-bis(2-ethylhexyl)benzo[1,2-c:4,5-c']-dithiophene-4,8-dione (BDD) with strong electron-withdrawing ability and a large planar structure as the central core was synthesised by Zhang et al in 2017. The HOMO energy level for DR3TBDD is -5.12 eV, which is deeper than most</p>	32

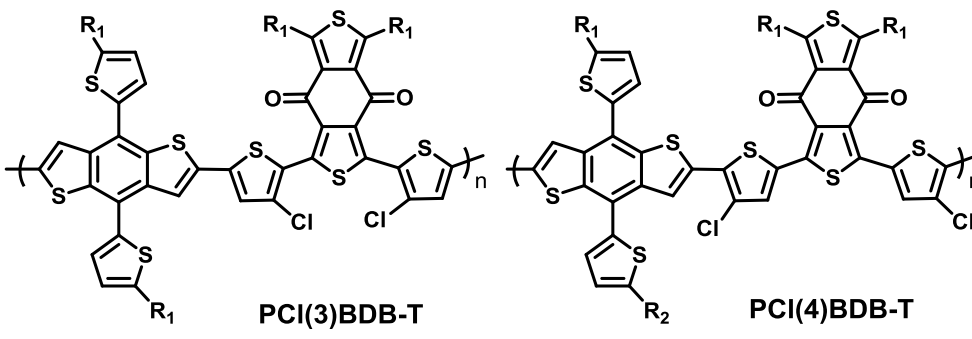
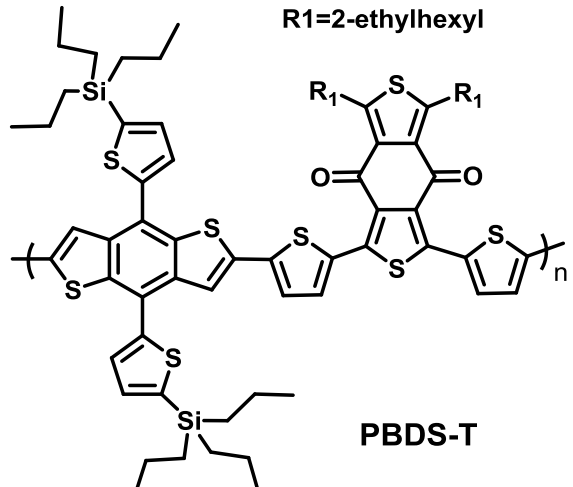
	<p>of the high efficiency small molecules. The optimal solar cell devices based on DR3TBDD: PC₇₁BM as the active layer exhibited a PCE of 9.53 %, (V_{oc} = 0.97 V, J_{sc} = 14.77 mA cm⁻², and FF = 66.9 %. This V_{oc} value is one of the highest values among high performance small molecular-OPVs and also significantly higher than most of the polymeric OPVs.</p>									
10	 <table style="margin-left: auto; margin-right: auto;"> <thead> <tr> <th style="text-align: center;">R1</th> <th style="text-align: center;">R2</th> </tr> </thead> <tbody> <tr> <td>PBT1-MP: 2-methoxypropyl</td> <td>2-hexyldecyl</td> </tr> <tr> <td>PBT1-EH: 2-ethylhexyl</td> <td>2-butyloctyl</td> </tr> <tr> <td>PBT1-BO: 2-butyloctyl</td> <td>2-ethylhexyl</td> </tr> </tbody> </table> <p>Liu et-al in 2017 synthesised three wide band-gap polymers (PBT1-MP, PBT1-EH, and PBT1-BO) having the same polymeric backbones but differing in alkyl chains on benzodithiophene (BDT) unit and on benzodithiophene-4,8-dione (BDTDO) unit. The result showed that PBT1-EH with the moderate bulky side chains exhibited the best photovoltaic performance. PBT1-EH-based solar cells when paired with PC₇₁BM, showed a high PCE of 10.3 %, A high PCE of 10.6 % was achieved with non-fullerene acceptor (ITIC-Th). The results suggested that the alkyl side-chain engineering is an effective strategy to tune the optoelectronic properties of WBG polymers.</p>	R1	R2	PBT1-MP: 2-methoxypropyl	2-hexyldecyl	PBT1-EH: 2-ethylhexyl	2-butyloctyl	PBT1-BO: 2-butyloctyl	2-ethylhexyl	33
R1	R2									
PBT1-MP: 2-methoxypropyl	2-hexyldecyl									
PBT1-EH: 2-ethylhexyl	2-butyloctyl									
PBT1-BO: 2-butyloctyl	2-ethylhexyl									
11	 <p style="text-align: center;">R=2-ethylhexyl</p> <table style="margin-left: auto; margin-right: auto;"> <tbody> <tr> <td>PBPD-Th: X= S</td> </tr> <tr> <td>PBPD-Se: X= Se</td> </tr> </tbody> </table>	PBPD-Th: X= S	PBPD-Se: X= Se	34						
PBPD-Th: X= S										
PBPD-Se: X= Se										

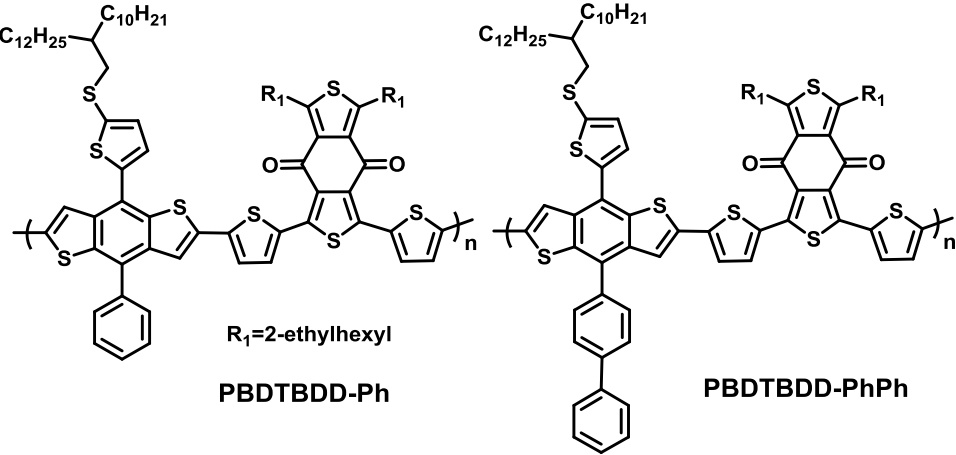
	<p>Xu et al in 2017, synthesised two copolymers, namely PBPD-Th and PBPD-Se based on m-alkoxyphenyl substituted benzodithiophene (BDT-m-OP) as donor unit and benzo[1,2-c:4,5-c']dithiophene-4,8-dione (BDD) as acceptor unit, in which thiophene and selenophene units were used as π-conjugated spacer, respectively. Selenium was incorporated into the polymer to broaden the absorption spectrum and enhance the charge transport properties. Compared with PBPD-Th, PBPD-Se exhibited extended absorption spectrum and an enhanced hole mobility. The PBPD-Se:PC₇₁BM-based solar cells exhibited a significantly improved PCE of 9.8 %, (J_{sc} =14.9 mA cm⁻², V_{oc} =0.90 V). These results indicated that the rational selection of π-conjugated spacer in the D-A copolymer is very important to achieve high efficiency PSCs.</p>	
12	<div style="text-align: center;">  <p style="text-align: center;">$R_1=2\text{-ethylhexyl}$ $R_2=2\text{-hexyldecyl}$</p> </div> <p>Zhu et al designed a new asymmetric monomer asy-BDTBP with an alkoxy group as the 1D (1-dimensional) and an alkoxybiphenyl as the 2D (2-dimensional) substituted group. Medium band-gap donor-acceptor conjugated polymer P1 was synthesized with asy-BDTBP and 4,7-di(4-(2-ethylhexyl)-2-thienyl)-5,6-difluoro-2,1,3-benzothiadiazole (DTffBT) as the donor and acceptor unit, respectively. P1 when blended with PC₇₁BM exhibited an enhanced power conversion efficiency (PCE) of 8.45 % (V_{oc} =0.838 V, J_{sc} =14.35 mA cm⁻² and FF= 70.27 %) compared to the reported symmetric analogue PBDTBP-DTffBT (6.70 %). However, P1 coupled with a classical non-fullerene acceptor ITIC revealed a relatively poor</p>	35

	<p>efficiency of 6.35 % due to non-complementarity of absorption spectra. To overcome this problem, a wide band-gap D–A polymer P2 was synthesized with a weak electron-withdrawing group benzo[1,2-c:4,5-c0]dithiophene-4,8-dione (BDD) instead of DTffBT as the acceptor unit. As a result, P2 possessed a complementary absorption spectrum with ITIC, and exhibited an excellent photovoltaic performance. The optimal efficiency boosted to 10.04 % ($V_{OC} = 0.873$ V, $J_{sc} = 7.60$ mA cm⁻² and $FF = 65.37$ %). This work demonstrates the potential of asymmetric BDTs for high efficiency PSCs.</p>	
13	<p style="text-align: center;">$R_1 = 2\text{-ethylhexyl}, R_2 = n\text{-octyl}$</p>  <p style="text-align: center;">P1 P2 P3</p> <p>Bohra et al in 2018 reported a “greener” synthetic route of direct arylation polymerization for series of wide band-gap D–A copolymers with a common acceptor building block of BDTD (P1, P2 and P3). The structure– property relationship in these polymers was studied. The device performances of these polymers in both thin-film field-effect transistors and organic BHJ solar cells involving the BDTD-based polymers as the electron donors and fullerene derivatives as the electron acceptors were investigated. Polymer P3 showed maximum PCE of 3.5 %.</p>	36
14	<p style="text-align: center;">$R_1 = 2\text{-ethylhexyl}, R_2 = 2\text{-hexyldecyl}$</p>  <p style="text-align: center;">P1 P2</p>	37

<p>Li et al reported two wide band-gap donor–acceptor (D–A) photovoltaic polymers based on asymmetric benzodithiophene units with a bare phenyl or alkoxy chain modified phenyl group as one of the substitutions. Both the polymers have almost identical optical bandgaps. P2 (with a side chain in the phenyl group) revealed slightly red-shifted film absorption spectra compared to polymer P1 (with the bare phenyl group), which is partly attributed to the better molecular conformations and intermolecular interactions. The results demonstrated that P2 based solar cells, both - fullerene and non-fullerene exhibited superior photovoltaic performance over that of P1. This was mainly attributed to the more favourable heterojunction morphologies and more balanced charge transport. P2 based PSCs with PC₇₁BM as the acceptor demonstrate an enhanced efficiency (8.58 %) compared to that of P1 (7.04 %). It was proved that low boiling point toluene can be used as an effective additive to optimize the photovoltaic performance of fullerene-free polymer solar cells. The best efficiency of the P2/ITIC based devices reached over 9 % ($V_{OC} = 0.90$ V, $J_{sc} = 16.70$ mA cm⁻², and $FF = 0.603$).</p>	
---	--

15	<div style="text-align: center;"> <p style="text-align: center;">PzNDT-T-BDD</p> <p style="text-align: center;">PzNDT-TT-BDD</p> <p style="text-align: center;">PzNDTP-T-BDD</p> <p style="text-align: center;">R = 2-ethylhexyl</p> </div>	38
<p>Jian et al, in 2018 designed and synthesised three copolymers based on zigzag naphthodithiophene (zNDT) with different aromatic rings as π bridges and different core side substitutions (PzNDT-T-BDD, PzNDT-TT-BDD, and PzNDTP-T-BDD, respectively). The 2D conjugation structure and molecular planarity of the polymers can be effectively altered through the modification of conjugated side chains and π-bridges. When blended with the non-fullerene acceptor (2,2'-[(4,4,9,9-tetrahexyl-4,9-dihydro-sindaceno[1,2-b:5,6-b']dithiophene-2,7-diyl)bis[methyldiyne(3-oxo-1H-indene-2,1(3H)-diylidene)]]bis-propanedinitrile) (IDIC), PzNDT-T-BDD exhibits the highest power conversion efficiency (PCE) of 9.72 % among the three polymers. This result can be attributed to its superior crystallinity and more obvious face-on orientation in blend film. PzNDT-TT-BDD and PzNDTP-T-BDD exhibited PCE values of 8.20 % and 4.62 %, respectively. The result suggested that the modification of conjugated side chains and π-bridges, is an effective strategy for designing NDT-based polymers with high photovoltaic performance.</p>		

16	<p style="text-align: center;">$R_1=2\text{-ethylhexyl}, R_2=3\text{-butylonyl}$</p>  <p style="text-align: center;">PCI(3)BDB-T PCI(4)BDB-T</p> <p>Chlorinated conjugated polymers are important candidates for highly efficient polymer solar cells since they can be prepared from low-cost raw materials by simple and high-yield synthetic routes. However, the study of the structure–property relationship of chlorinated polymers is lagging. Wu et al in 2018, synthesised two chlorinated conjugated polymers, PCI(3)BDB-T and PCI(4)BDB-T and they were used to fabricate PSCs with the non-fullerene acceptor (IT-4F). The PCI(3)BDB-T:IT-4F-based device exhibited a negligible power conversion efficiency of 0.18 %, while the PCI(4)BDBT:IT-4F-based device showed an outstanding PCE of 12.33 %. Thus, these results provided new insight for the rational design of new chlorinated polymer donors for further improving the photovoltaic efficiencies of PSCs.</p>	39
17	<p style="text-align: center;">$R_1=2\text{-ethylhexyl}$</p>  <p style="text-align: center;">PBDS-T</p>	40

	<p>A new alkylsilyl functionalized copolymer donor PBDS-T with low-lying energy levels was designed and synthesised by Huang et al in 2018 for efficient PSCs. By monitoring the photoluminescence quenching of the bulk and bilayer heterojunctions, small driving forces, ΔE_{HOMO} of 0.15 eV and ΔE_{LUMO} of 0.22 eV were found. These parameters were observed to correlate with the crystalline PBDS-T and the optimal morphology in PBDS-T:ITIC. The results showed that simultaneous improvement of V_{OC}, J_{sc} and small E_{loss} boosted the PCE over 11 %, which is one of the highest values for annealing-free device. These results throw a light on precise design of a light-harvesting system with small driving force to simultaneously improve the V_{OC} and J_{sc} for highly efficient PSCs.</p>	
18	 <p>Two wide-bandgap polymers (PBDTBDD-Ph and PBDTBDD-PhPh) with different aggregation degrees and fused-ring electron acceptors (ITIC-4T, ITIC-3T and ITIC-2T) with different sizes were synthesized by Zhu et al very recently. The results demonstrated that weakly aggregated donor polymers and small-sized FREAs in appropriate degrees can match well with each other to achieve high power conversion efficiencies (PCEs). Small-sized FREAs can be embedded more easily into the interspace of weakly aggregated polymer chains. As a result, an NF-PSC device based on weakly aggregated polymer PBDTBDD-Ph and small-sized ITIC-3T yielded over 11 % PCE. The work found to be useful in the design the donor</p>	41

polymers and fused-ring electron acceptors (FREAs) for high-performance non-fullerene polymer solar cells (NF-PSCs).	
--	--

Recently, Sun et. al reported two BDD-based terpolymers constituting bithiophene (BT) as donor unit and BDD as acceptor unit. Thieno[3,2-b]thiophene (TT) and thiazolo[5,4-d]thiazole (TTz) were used as the third component to form D-D-A and D-A-A terpolymeric system, respectively.²⁴ It was shown that, D-A-A-based solar cells showed a high PCE of 8.1 % ($FF=0.74$), which is much higher than those of D-D-A-based devices (PCE =3.4 %, $FF=0.55$). The high performance was mainly ascribed to the efficient charge carrier transport in the active layer of solar cell device, high crystallinity of D-A-A, and high domain purity. Their research along with that of several other research groups suggest that conjugated terpolymers with one donor and two acceptor units is an effective strategy for designing high-performance solar cell materials.⁴²⁻⁴⁸ Moreover, few other research groups have proved that BDD based terpolymers are promising systems to study, for their applications in photovoltaics.^{22,49-52}

Inspired from this literature back ground, we have synthesized 1,3-bis(5-bromothiophen-2-yl)-5,7-bis(2-ethylhexyl)-benzo[1,2-c:4,5-c']dithiophene-4,8-dione (BDD) based copolymers and terpolymers. All the monomers have complementary absorption in visible region, so that the terpolymers could cover entire visible and near IR region. The terpolymers showed broader absorption and higher solubility in organic solvents as compared to copolymers. The influence of active layer (polymer:PCBM) morphology on photovoltaic behaviour was investigated.

5.2 EXPERIMENTAL

5.2.1 Materials:

Thiophene, bromine, n-butyllithium solution (2 M in cyclohexane), 2-ethylhexyl bromide, 2-ethyl hexanoic acid, 2-hexyl-1-bromodecane, thiophene-3-carboxylic acid, 1-octyl bromide, thiophene-3,4-dicarboxylic acid, trimethyl(thiophen-2-yl)stannane, 5,5'-bis(trimethylstannyl)-2,2'-bithiophene, tetrabutyl ammonium bromide, aluminium chloride ($AlCl_3$), lithium aluminium hydride, tetrakis(triphenylphosphine)palladium(0) ($Pd(PPh_3)_4$), copper iodide (CuI), diisopropyl amine and potassium tertiary-butoxide

(Aldrich Chemicals) were used as received. Cyclopentadithiophene (TCI Chemicals) was used as received. Sodium bisulphate, glacial acetic acid, oxalyl chloride and N-bromosuccinimide (NBS) (Merck) were used as received.

N,N-Dimethylformamide (DMF), dimethyl sulphoxide (DMSO), diethyl ether, tetrahydrofuran (THF) and toluene (Aldrich Chemicals) were purchased and were dried and distilled according to standard procedures⁵³ and stored under argon. Methanol, chloroform, dichloromethane, n-hexane and ethyl acetate (Merck) were purchased and were used as received. If not otherwise specified, solvents or solution were degassed by bubbling with argon for 1 h prior to use.

5.2.2 Characterisation and techniques

Different techniques were used for characterization of monomers and polymers and are listed below.

NMR Spectroscopy: ¹H and ¹³C NMR spectra of monomers and polymers were recorded using a Bruker-AV spectrometer at operating frequency of 200 MHz, 400 MHz or 500 MHz in CDCl₃ or DMSO-*d*₆ with tetramethylsilane as an internal standard.

Gel permeation chromatography (GPC): Molecular weights and dispersity values of polymers were determined on Thermo-Finnigan make gel-permeation chromatography (GPC) using tetrahydrofuran as an eluent at a flow rate of 1 mL min⁻¹ at 25 °C. Sample concentration was 2 mg mL⁻¹ and narrow dispersity polystyrenes were used as calibration standards.

Differential scanning calorimetry (DSC): DSC measurements were carried out on a Mettler DSC 30 with a cell purged with nitrogen. Calibration for temperature and enthalpy changes was performed using an Indium standard. The temperature was varied between 0 and 250°C with a heating/cooling rate of 10 K/min. In total two heating-cooling cycles were performed on each sample.

Thermogravimetric analysis (TGA): TGA was performed on a Mettler TA-300-thermal analyzer operating under nitrogen atmosphere. The samples were heated from 0 to 400°C with a heating rate of 10 K/min.

Absorption and emission spectroscopy: The absorption spectra were recorded in dilute chloroform solution ($c \approx 10^{-6}$ mol l⁻¹) on a Perkin–Elmer UV/VIS-NIR Spectrometer Lambda 19. The absorption spectra of thin films spin coated from chlorobenzene solution

were recorded on Varian UV/Vis spectrophotometer and the corresponding emission spectra were recorded on a home-built photoluminescence setup. Thin films were spin coated on glass substrates using chlorobenzene solutions (0.6-0.8 wt %).

Cyclic voltammetry (CV): CV was performed with a PA4 polarographic analyzer (Laboratory Instruments, Prague, CZ) with a three-electrode cell. Platinum (Pt) wire electrodes were used both as working and counter electrodes, and a non-aqueous Ag/Ag⁺ electrode (Ag in 0.1 M AgNO₃ solution) was used as the reference electrode. CV measurements were made in solutions of 0.1 M tetrabutylammonium hexafluorophosphate (TBAPF₆) in acetonitrile under nitrogen atmosphere. Typical scan rates were 20, 50 and 100 mVs⁻¹, respectively. Polymer thin films were prepared onto Pt wire electrodes from chlorobenzene solution. All measurements and film preparations were performed in a nitrogen atmosphere in a glove box.

Atomic Force Microscopy: The surface morphology of the samples was studied by Atomic Force Microscopy (AFM). The AFM images were obtained by means of a Digital Instruments Dimension 3100 microscope working in tapping mode. The samples were prepared by spin-coating from chlorobenzene solution.

5.2.3 Fabrication and Characterization of the Photovoltaic Cells

Anthracene containing poly(-p-arylene-ethynylene)-alt-poly(-p-arylene-vinylene) (AnE-PV) as donor and phenyl C70 butyric acid methyl ester (PC₇₀BM, Solenne 99.5%) as an acceptor were used. AnE-PV was blended with PC₇₀BM in chlorobenzene and stirred at 40 °C for 24-48 h. The donor: acceptor (D: A) ratio was varied from 1:1 to 1:2 (w/w) and total concentrations of (D+A) in chlorobenzene solution was ~10 mg/mL. Indium tin oxide (ITO) coated glass (Merck KgaA, Darmstadt) was used as substrate for device fabrication. A part of ITO layer on glass was etched using aqua regia for selective contacting of back electrode. These glass substrates were thoroughly cleaned by subjecting them to ultrasonication in soap, deionized water, acetone and in isopropyl alcohol. The substrates were then dried for several hours in an oven at 120 °C. A hole transporting layer-PEDOT:PSS (Baytron/Clevios PH H.C. Starck) was spin coated at 3000 rpm for 60 sec. Then the photoactive layer was spin coated with polymer: PC₇₀BM blend solution at 4000 rpm for 60 sec. The final thickness of each active layer film was 100~110 nm. Finally, aluminum (~100 nm) was thermally deposited under high vacuum (~10⁻⁷ torr). The active

area of solar cells was 0.5 cm² for all the devices. The photovoltaic performance of the devices was measured using a solar spectrum simulator with an air-mass (AM) 1.5 G filter. The intensity of the solar simulator was carefully calibrated using an AIST-certified silicon photodiode. The current-voltage behavior was measured using a Keithley 2400 SMU.

5.3 SYNTHESIS

5.3.1 Synthesis of 1,3-bis(5-bromothiophen-2-yl)-5,7-bis(2-ethylhexyl)-benzo[1,2-c:4,5-c']dithiophene-4,8-dione (BDD monomer)

5.3.1.1 Synthesis of 2-(2-ethylhexyl)thiophene (1)

Into a 250 mL three-necked round bottom flask equipped with a nitrogen gas inlet and a magnetic stirrer added thiophene (7.0 g, 83 mmol) and of dry THF (50 mL) under nitrogen atmosphere. The solution was cooled to -40°C and 46 mL of n-butyllithium (91.5 mmol, 2 M in cyclohexane) was added dropwise. After being stirred at -40°C for 1 h, 16.27 mL of 2-ethylhexyl bromide (91.5 mmol) was added dropwise and the mixture was warmed up to room temperature and stirred overnight. The mixture was quenched by 100 mL of cold water and extracted with hexane (3x100 mL). The organic extracts were dried over anhydrous Na₂SO₄, filtered and concentrated by evaporation in vacuo. The residue was purified by vacuum distillation (92°C, 2.0 mbar) to afford a colourless oil.

Yield: 5.95 g (58%).

¹H-NMR (200 MHz, CDCl₃, δ/ppm): 7.11 (d, 1H), 6.93 (dd, 1H), 6.78 (d, 1H), 2.76 (d, 2H), 1.65-1.45 (m, 3H), 1.34-1.26 (m, 6H), 0.94-0.85 (t, 6H).

5.3.1.2 Synthesis of 2-ethyl-1-(5-(2-ethylhexyl)thiophen-2-yl)hexan-1-one (2)

Into a 100 mL single-necked round bottom flask equipped with nitrogen gas balloon and a magnetic stir bar was added 2-ethyl hexanoic acid (3.1 g, 21.5 mmol) and the reaction mixture was cooled to 0°C. Oxalyl chloride (2.5 mL, 29.0 mmol) and DMF (0.1 mL) were added into it. Reaction mixture was stirred at room temperature overnight. Then, excess oxalyl chloride was distilled off, the residue was cooled and AlCl₃ (3.87 g, 29.0 mmol) was added into it at 0°C. 2-(2-Ethylhexyl)thiophene (3.84 g, 19.5 mmol) dissolved in dichloromethane (40 mL) was added into the reaction mixture and stirred overnight at room temperature. Reaction was quenched by addition of 1 M HCL (40 mL) and extracted with dichloromethane (3x100 mL). Dichloromethane extracts were washed with water, dried on

Na₂SO₄ and concentrated by evaporation in vacuo. The purification was carried out by column chromatography on silica gel eluting with 30 % dichloromethane in petroleum ether to obtain pure 2 as a brown liquid.

Yield: 2.0 g (76%).

¹H-NMR (200 MHz, CDCl₃, δ/ppm): 7.55 (d, 1H, thiophene hydrogen near to C=O group), 6.80 (d, 1H, thiophene 'H'), 3.08 (m, 1H, -OH of keto-enol tautomer), 2.77 (d, 2H, -CH₂ of ethylhexyl chain), 2.15 (m, ¹H, -CH at branch position of 2-ethylhexyloxy chain), 1.85-1.45 (m, 7H, -CH and -CH₂ of side chains), 1.28 (m, 10H, -CH₂), 0.89 (t, 12H, -CH₃).

¹³C-NMR (200 MHz, CDCl₃, δ/ppm): 197.52, 154.81, 143.52, 131.99 (CH), 126.73 (CH), 49.76 (CH), 41.65 (CH), 34.97 (CH₂), 32.62 (CH₂), 32.52 (CH₂), 30.11 (CH₂), 29.06 (CH₂), 26.23 (CH₂), 25.80 (CH₂), 23.17 (CH₂), 23.12 (CH₂), 14.32 (CH₃), 14.16 (CH₃), 12.37 (CH₃), 11.01 (CH₃).

5.3.1.3 Synthesis of 2,5-bis(2-ethylhexyl)thiophene (3)

LiAlH₄ (3.88 g, 102.3 mmol) and AlCl₃ (13.6 g, 102.3 mmol) were taken in two different 100 mL single necked round bottom flasks and dissolved separately in 60 mL dry ether under argon protection at 0 °C and then the solutions were combined, portion wise. Afterwards, solution of 2 (5.5 g, 17.04 mmol) in dry ether (60 mL) was added via syringe to the mixture at 0°C. The reaction mixture was allowed to attain room temperature and stirred for 5 h. Then, to quench the reaction, ether (1 mL) and 2M HCl (20 mL) were added carefully. The organic phase was extracted with ether, washed with water and dried over Na₂SO₄. The pure product was obtained as an orange liquid after column chromatography on silica gel (40 % dichloromethane in petroleum ether).

Yield: 4.5 g (85 %).

¹H-NMR (200 MHz, CDCl₃, δ/ppm): 6.56 (s, 2H, thiophene protons), 2.69 (d, 4H, -CH₂- attached to thiophene ring), 1.57 (m, 2H, -CH- at branch position of ethylhexyl chain), 1.37-1.26 (m, 16H, -CH₂-), 0.94-0.86 (t, 12H).

¹³C-NMR (200 MHz, CDCl₃, δ/ppm): 141.92 (CH), 124.32 (CH) 41.38 (CH), 34.16 (CH₂), 32.40(CH₂), 28.91 (CH₂), 25.59 (CH₂), 23.01 (CH₂), 14.09 (CH₃), 10.84 (CH₃).

5.3.1.4 Synthesis of 2,5-dibromothiophene-3,4-dicarboxylic acid (4)

Into a 250 mL single-necked round bottom flask equipped with an addition funnel and a magnetic stir bar were added thiophene-3,4-dicarboxylic acid (10 g, 58.2 mmol) and

glacial acetic acid (100 mL). Bromine (18 mL, 348 mmol) was added dropwise into the solution and the mixture was stirred overnight. Aqueous sodium bisulphate solution was added until the reddish colour disappeared. The mixture was cooled, filtered and washed with 100 mL water. Drying of the precipitate afforded 2,5-dibromothiophene-3,4-dicarboxylic acid as a grey coloured solid.

Yield: 16.20 g (84.6%).

$^1\text{H-NMR}$ (200 MHz, Acetone- d_6 , δ /ppm): broad 5-7 δ (-COOH protons)

$^{13}\text{C NMR}$ (200 MHz, Acetone- d_6 , δ /ppm): 162.14, 135.41, 114.92.

5.3.1.5 Synthesis of 1,3-dibromo-5,7-bis(2-ethylhexyl)-4H,8H-benzo[1,2-c:4,5-c']dithiophene-4,8-dione (5)

Into a 100 mL single necked round bottom flask fitted with a nitrogen gas balloon were added compound **4** (1.50 g, 4.53 mmol), DMF (1 drop) and dry dichloromethane (5 mL). Oxalyl chloride (2.5 mL, 27.2 mmol) was slowly added into the mixture and was stirred overnight at room temperature. The solvent was removed under vacuum to obtain crude 2,5-dibromothiophene-3,4-dicarbonyl dichloride, which was used for next step without further purification. To a stirred solution of 2,5-dibromothiophene-3,4-dicarbonyl dichloride and 2,5-bis(2-ethylhexyl)thiophene (1.4 g, 4.53 mmol) in 20 mL dry dichloromethane, AlCl_3 (2.41 g, 18.12 mmol) was added in small portions at 0 °C. The mixture was allowed to stir at 0°C for 30 min, then at room temperature for 3 h. The reaction mixture was poured into a mixture of ice water (100 mL) and 1 M hydrochloric acid and extracted with dichloromethane (3x100 mL). The organic layer was washed with brine water, dried over Na_2SO_4 , and the solvent was removed under vacuum. The crude product was purified through silica gel column with petroleum ether/dichloromethane (5:1, v/v) to give a yellow solid.

Yield: 0.95 g (34 %).

$^1\text{H-NMR}$ (200 MHz, CDCl_3 , δ /ppm): 3.33 (d, 4H, $-\text{CH}_2-$ attached to thiophene ring), 1.77 (m, 2H, $-\text{CH}-$ at branch position of 2-ethylhexyl chain), 1.43-1.25 (m, 16H, $-\text{CH}_2-$), 0.94-0.85 (m, 12H, $-\text{CH}_3$).

$^{13}\text{C-NMR}$ (200 MHz, CDCl_3 , δ /ppm): 175.44, 155.19, 134.78, 132.76, 119.38, 41.13 (CH), 33.92 (CH_2), 32.59 (CH_2), 28.68 (CH_2), 25.90 (CH_2), 22.98 (CH_2), 14.07 (CH_3), 10.77 (CH_3).

5.3.1.6 Synthesis of 1,3-bis(2-ethylhexyl)-5,7-di(thiophen-2-yl)benzo[1,2-c:4,5-c']-dithiophene-4,8-dione (6)

In a 100 mL Schlenk tube equipped with a nitrogen gas inlet and a magnetic stir bar were added compound 5 (415 mg, 689 μmol), trimethyl(thiophen-2-yl)stannane (771 mg, 2.068 μmol) and toluene (40 mL). The reaction mixture was purged with nitrogen for 15 min. Then, $\text{Pd}(\text{PPh}_3)_4$ (40 mg) was added to the reaction mixture and was refluxed in nitrogen atmosphere for 12 h. After the removal of the solvent under reduced pressure, the residue was purified by column chromatography on a silica gel column with petroleum ether/dichloromethane (5:1 by v/v) to give a yellow solid.

Yield: 400 mg (95.4%).

$^1\text{H-NMR}$ (200 MHz, CDCl_3 , δ/ppm): 7.74 (d, 2H), 7.50 (d, 2H), 7.13 (t, 2H) (thiophene protons), 3.30 (d, 4H), 1.77 (m, 2H), 1.42–1.24 (m, 16H), 0.98–0.86 (m, 12H).

$^{13}\text{C-NMR}$ (200 MHz, CDCl_3 , δ/ppm): 180.05, 153.5, 142.41, 133.4, 130.5, 129.27, 127.17, 124.51, 123.83, 41.26, 33.62, 32.74, 28.80, 25.99, 14.12, 10.82.

5.3.1.7 Synthesis of 1,3-bis(5-bromothiophen-2-yl)-5,7-bis(2-ethylhexyl)-benzo[1,2-c:4,5-c']dithiophene-4,8-dione (BDD monomer)

Into 100 mL single necked round bottom flask equipped with a reflux condenser, were added compound 6 (0.476 μmol , 290 mg) and DMF (9 mL). After the solid dissolved completely, N-bromosuccinimide (NBS) (0.952 μmol , 180 mg) was added in one portion. The reaction mixture was heated at 60°C for 3 h. Then, water (50 mL) was added into the mixture, and it was extracted with CHCl_3 (3X100 mL). The organic layer was washed with brine water and dried over anhydrous sodium sulphate. The solvent was removed under reduced pressure; the residue was purified by column chromatography on silica gel with petroleum ether/ethyl acetate (30:1 v/v) to give a red solid.

Yield: 256.7 mg (70.4%).

$^1\text{H-NMR}$ (200 MHz, CDCl_3 , δ/ppm): 7.45 (d, 2H, thiophene C₃ protons), 7.08 (d, 2H, thiophene C₄ protons), 3.31 (m, 4H), 1.76 (m, 2H), 1.45–1.30 (m, 16H), 0.98–0.87 (m, 12H).

$^{13}\text{C-NMR}$ (200 MHz, CDCl_3 , δ/ppm): 177.55, 154.08, 141.41, 134.64, 132.67, 132.12, 130.33, 129.75, 118.05, 41.22, 33.66, 32.79, 28.86, 26.01, 23.02, 14.18, 10.85.

5.3.2 Synthesis of 3,6-bis(5-bromothiophen-2-yl)-2,5-bis(2-hexyldecyl)-2,5-dihydropyrrolo[3,4-c]pyrrole-1,4-dione (DPP(HD) monomer)

Precursor- 3,6-Di(thiophen-2-yl)-2,5-dihydropyrrolo[3,4-c]pyrrole-1,4-dione was synthesised as described in section 3b.3.2.1 of this thesis.

5.3.2.1 Synthesis of 2,5-bis(2-hexyldecyl)-3,6-di(thiophen-2-yl)-2,5-dihydropyrrolo[3,4-c]pyrrole-1,4-dione (7)

The compound 7 was synthesized by reaction of 3,6-di(thiophen-2-yl)-2,5-dihydropyrrolo[3,4-c]pyrrole-1,4-dione (3 g, 9.98 mmol) with 2-hexyl-1-bromodecane (12.14 g, 39.9 mmol) according to the procedure described in section 3b.3.2.2 of the thesis. The crude product was purified by column chromatography using hexane-dichloromethane (7:3, v/v) mixture to obtain purple coloured solid.

Yield: 2.84 g (38%).

¹H-NMR (400 MHz, CDCl₃, δ/ppm): 8.87 (2 H, d, thiophene C₅ protons), 7.62 (2 H, d, thiophene C₃ protons), 7.26 (2 H, t, thiophene C₄ protons), 4.01 (4 H, d, -CH₂- of hexyldecyl chain), 1.90 (2 H, m, -CH- at branch position of hexyldecyl chain), 1.43 – 1.09 (48 H, m, -CH₂-), 0.85 (12 H, m, -CH₃).

5.3.2.2 Synthesis of 3,6-bis(5-bromothiophen-2-yl)-2,5-bis(2-hexyldecyl)pyrrolo[3,4-c]pyrrole-1,4(2H,5H)-dione (DPP(HD) monomer)

The DPP(HD) monomer was synthesized by reaction of 2,5-bis(2-hexyldecyl)-3,6-di(thiophen-2-yl)-2,5-dihydropyrrolo[3,4-c]pyrrole-1,4-dione (2) (1 g, 1.1 mmol) with N-bromosuccinimide (432 mg, 2.5 mmol) according to the procedure described in section 3b.3.2.3 of the thesis. The crude product was purified by column chromatography using hexane- dichloromethane (3:7, v/v) mixture to obtain purple coloured product.

Yield: 0.68 g (56 %)

¹H-NMR (400 MHz, CDCl₃, δ/ppm): 8.63 (2H, d, thiophene C₃ protons), 7.22 (2H, d, thiophene C₄ protons), 3.90 (4H, d), 1.88 (2H, s), 1.35 – 1.02 (48H, m), 0.86 (12H, t).

5.3.3 Synthesis of 2,6-bis(trimethyltin)-4,8-bis(2-ethylhexyl)benzo[1,2-b:4,5-b']dithiophene (BDT monomer)

5.3.3.1 Synthesis of thiophene-3-carbonyl chloride (8)

Into a 100 mL single necked round bottom flask fitted with a nitrogen gas balloon were added thiophene-3-carboxylic acid (19.2 g, 0.15 mol) and 30 mL of DCM. The

reaction mixture was cooled in an ice-bath, and then oxalyl chloride (38.1 g, 0.3 mol) was added in one portion. The reaction mixture was stirred overnight at room temperature. The resulting clear solution was concentrated under reduced pressure to obtain the product as colorless solid. It was dissolved into dichloromethane (100 mL) and used for the next step.

5.3.3.2 Synthesis of N,N-diethylthiophene-3-carboxamide (9)

Into a 100 mL single necked round bottom flask equipped with a magnetic stir bar were added 62.5 mL of diethylamine (21.9 g, 0.3 mol) and dichloromethane (50 mL) and the solution was cooled by ice-bath. The solution of thiophene-3-carbonyl chloride was added slowly into the reaction mixture. The ice bath was removed after the addition, and the reaction mixture was stirred at room temperature for 30 min. Then, the reaction mixture was washed with water, and the organic layer was dried over Na₂SO₄. After removing solvent, the crude product was purified by vacuum distillation. The pure product was obtained as a yellow viscous liquid.

Yield: 23.5 g (86 %).

¹H-NMR (200 MHz, CDCl₃, δ/ppm): 7.54 (s, 1H, proton on C₂ carbon of thiophene ring), 7.39 (d, 1H, proton on C₄ carbon of thiophene ring), 7.26 (d, 1H, proton on C₅ carbon of thiophene ring), 3.41 (m, 4H, -CH₂- attached to nitrogen atom of amide group), 1.19 (t, 6H, -CH₃).

5.3.3.3 Synthesis of 4,8-dihydrobenzo[1,2-b:4,5-b']dithiophen-4,8-dione (10)

Into a 250 mL single-necked round bottom flask equipped with a nitrogen gas inlet and a magnetic stir bar were added compound 2 (0.1 mol, 18.3 g) and tetrahydrofuran (100 mL) and the solution was degassed for 30 min. After degassing, the solution was cooled by an ice-water bath, and n-butyllithium (0.2 mol, 2 M cyclohexane) was added into the reaction mixture dropwise over a period of 30 min. After stirring at room temperature for 1h, the reaction mixture was poured into ice water (200 mL) and stirred overnight. The mixture was filtrated and the yellow precipitate was washed by 100 mL of water, then with methanol, and finally with hexane. The product was obtained as a yellow powder.

Yield: 17.5 g (78 %)

¹H-NMR (200 MHz, CDCl₃, δ/ppm): 7.75 (d, 2 H, proton near to thiophene atom on fused thiophene ring), 7.95 (d, 2 H, proton on fused thiophene ring).

¹³C-NMR (200 MHz, CDCl₃, δ/ppm): 174.50, 144.90, 142.82, 133.60, 126.60.

5.3.3.4 Synthesis of 4,8-bis((2-ethylhexyl)oxy)benzo[1,2-b:4,5-b']dithiophene (11)

Into a 250 mL single-necked round bottom flask equipped with a reflux condenser and a magnetic stir bar were added compound 3 (5.0 g, 22.7 mmol), zinc powder (3.25 g, 50 mmol) and water (60 mL) and stirred for 15 min. After addition of 15 g of NaOH, the mixture was refluxed for 1 h. Then, 2-ethylhexyl bromide (17 g, 68 mmol) and a catalytic amount of tetrabutylammonium bromide were added into the reaction mixture. After refluxing for 6 h, the reaction mixture was poured into cold water and extracted with diethyl ether (3X200 mL). The ether layer was dried over anhydrous Na₂SO₄. After removing solvent, the crude product was purified by recrystallization from ethanol to yield colourless sticky solid.

Yield: 8.24 g (82 %).

¹H-NMR (200 MHz, CDCl₃, δ/ppm): 7.48 (d, 2H), 7.39 (d, 2H), 4.20 (t, 4H, -CH₂-on ethylhexyl chain), 1.87(m, 4H, -CH- at branch position), 1.53 (m, 4H, -CH₂-), 1.67-1.30 (m, 16H, -CH₂-), 1.05-0.90 (m, 12H, -CH₃).

5.3.3.5 Synthesis of 2,6-dibromo-4,8-bis(2-ethylhexyl)benzo[1,2-b:4,5-b']dithiophene (12)

Into a 250 mL single-necked round bottom flask equipped with an addition funnel and a magnetic stir bar were added compound 4 (5.0 g, 11.2 mmol) and dichloromethane (50 mL). The solution was cooled by keeping the flask in an ice-bath. The solution of bromine (3.58 g, 22.4 mmol) in dichloromethane (60 mL) was slowly added into the flask at 0°C, and then the reaction mixture was stirred overnight at room temperature. The reaction mixture was concentrated under reduced pressure and the residue was recrystallized with hexane to obtain desired product as a pale-yellow sticky solid.

Yield: 5.38 g (89 %)

¹H-NMR (200 MHz, CDCl₃, δ/ppm): 7.43 (s, 2H), 4.17 (d, 4H), 1.85 (m, 4H), 1.54-1.27 (m, 16H), 1.04-0.89 (m, 12H).

5.3.3.6 Synthesis of 2,6-bis(trimethyltin)-4,8-bis(2-ethylhexyl)benzo[1,2-b:4,5-b']dithiophene (BDT monomer)

Into a 250 mL three-necked round bottom flask equipped with a nitrogen gas inlet and a magnetic stir bar were added compound 12 (5.0 g, 8.3 mmol) and THF (100 mL). The solution was degassed for 30 min and then cooled to -78 °C by a liquid nitrogen-

acetone bath. Into the reaction mixture, *n*-butyllithium (9 mL, 18.3 mmol, 2 M in cyclohexane) was added dropwise and stirred at -78 °C for 1 h. Trimethyltin chloride (19 mL, 19 mmol, 1 M in THF) was added. After stirring at room temperature for 2 h, the reaction mixture was poured into cold water and extracted with diethylether (3X200 mL). The organic layer was washed with water and dried over anhydrous Na₂SO₄. The solvents were removed under vacuum and the residue was recrystallized from ethanol. The pure product was obtained as colourless crystalline solid.

Yield: 6.48 g (75 %)

¹H-NMR (200 MHz, CDCl₃, δ/ppm): 7.52 (s, 2H), 4.19 (t, 4H), 1.80 (m, 2H), 1.64 (m, 4H), 1.49-0.65 (multiple peaks, 24H), 0.45 (t, 18H).

¹³C-NMR (200 MHz, CDCl₃, δ/ppm): 143.25, 140.37, 132.89, 127.97, 75.63, 40.66, 30.53, 29.23, 23.89, 23.16, 14.17, 11.34, 8.37.

5.3.4 Synthesis of (4,4-bis(2-ethylhexyl)-4H-cyclopenta[2,1-b:3,4-b']dithiophene-2,6-diyl)bis(trimethylstannane) (CPDT monomer)

5.3.4.1 Synthesis of 4,4-bis(2-ethylhexyl)-4H-cyclopenta[2,1-b:3,4-b']dithiophene (13)

Into a 150 mL single-necked round bottom flask equipped with nitrogen gas inlet and a magnetic stir bar were added cyclopentadithiophene (CPDT) (3.0 g, 16.8 mmol), 2-ethylhexyl bromide (6.45 g, 33.4 mmol), potassium iodide (75 mg) and dimethyl sulfoxide (75 mL). The mixture was degassed for 15 minutes and cooled in an ice bath. Into it, powdered potassium hydroxide (3.0 g) was added portion wise. The reaction mixture was stirred vigorously overnight at room temperature. After cooling in an ice bath, water (75 mL) was added. The organic phase was extracted with diethyl ether; washed with water, brine water and dried on sodium sulphate. The extracts were concentrated under vacuum and purified by column chromatography on silica using hexane as an eluent to remove monoalkylated product and unreacted ethylhexyl bromide. The product was obtained as a yellow coloured oily liquid.

Yield: 5.76 g (85%).

¹H-NMR (200 MHz, CDCl₃, δ/ppm): 7.11 (d, 2H), 6.94 (m, 2H), 1.95–1.80 (m, 4H), 1.0–0.6 (m, 30H).

¹³C-NMR (200 MHz, CDCl₃, δ/ppm): 157.56, 136.76, 123.93, 122.29, 53.20, 43.20, 34.95, 34.10, 28.55, 27.23, 22.73, 14.07, 10.63.

5.3.4.2 Synthesis of (4,4-bis(2-ethylhexyl)-4H-cyclopenta[2,1-b:3,4-b']dithiophene-2,6-diyl)bis(trimethylstannane) (CPDT monomer)

Into a 250 mL single-necked round bottom flask equipped with a nitrogen gas inlet and a magnetic stir bar were added compound 13 (0.82 g, 2 mmol) and dry THF (160 mL). The reaction mixture was degassed with nitrogen for 30 min. The addition of n-BuLi and trimethyltin chloride was performed sequentially in two portions. First portion of n-BuLi (2 M in cyclohexane, 1.50 mL, 3.0 mmol) was added dropwise at -78°C , and allowed to stir at -78°C for 1 h. Subsequently, the mixture was allowed to warm to room temperature and stirred for 30 min. After stirring, the first portion of 1 M trimethyltin chloride in THF (2.11 mL, 2.11 mmol) was added at -78°C , and stirred for 1 h. Then, the second portion of n-BuLi (2 M in cyclohexane, 1.50 mL, 3.0 mmol) was added, and stirred at -78°C for 1 h. Again, the mixture was allowed to warm to room temperature and stirred for 30 min. After stirring, the second portion of 1 M trimethyltin chloride in THF (2.11 mL, 2.11 mmol) was added at -78°C , and stirred overnight at room temperature. The reaction mixture was extracted with hexane, purified by column chromatography on silica using hexane-methanol (1:4, v/v) solvent mixture as an eluent. The pure product was obtained as a yellow liquid.

Yield: 0.72 g (98.6 %).

$^1\text{H-NMR}$ (200 MHz, CDCl_3 , δ/ppm): 6.95 (m, 2H, aromatic proton), 1.95–1.75 (m, 4H, $-\text{CH}_2-$ proton near to fused aromatic ring), 1.28 (m, 2H, $-\text{CH}-$ at branch position of ethylhexyl chain) 1.10–0.90 (m, 16H, $-\text{CH}_2-$ proton on sidechain), 0.75 (m, 6H, $-\text{CH}_3$ proton on ethyl chain), 0.59 (t, 6H, $-\text{CH}_3$ proton on hexyl chain), 0.45–0.12 (t, 18H, $-\text{CH}_3$ proton on Sn atom).

5.3.5 Synthesis of copolymers and terpolymers

5.3.5.1 Synthesis of CPDT-BDD copolymer: Typical procedure

Into a 50 mL Schlenk tube equipped with a nitrogen gas inlet and a magnetic stir bar were added BDD monomer (230 mg, 0.30 mmol), CPDT monomer (219 mg, 0.30 mmol) and 10 mL of dry toluene. The reaction mixture was purged with nitrogen for 30 min. after which tris(dibenzylideneacetone)dipalladium(0) ($\text{Pd}_2(\text{dba})_3$) (10.99 mg, 0.012 mmol) and tri(o-tolyl)phosphine ($\text{P}(\text{o-tolyl})_3$) (14.61 mg, 0.048 mmol) were added into the

solution. The reaction mixture was again purged with nitrogen for 30 min and was stirred at 100°C for 12 h. Upon cooling to room temperature, the reaction mixture was added dropwise into methanol (100 mL). The precipitate was filtered, dried and further purified by Soxhlet extraction with methanol, hexane, chloroform, respectively for 48 h each. The chloroform fraction was concentrated and added dropwise into methanol. Subsequently, the precipitate was collected and dried under vacuum overnight to obtain polymer as a black solid.

Yield: 295 mg (88 %).

¹H-NMR (200 MHz, CDCl₃, δ/ppm): 7.77, 7.21, 7.06 (6H, aromatic protons), 3.37 (4H, d, -CH₂- protons of ethylhexyl chain on BDD unit which are near to fused thiophene ring), 1.95 (4H, d, -CH₂- protons of ethylhexyl chain on CPDT unit which are near to fused thiophene ring), 1.81 (4H, m, methine proton at branch position of ethyl hexyl chain) 1.1-0.67 (56H, m, -CH₂- and -CH₃).

5.3.5.2 Synthesis of BT-BDD copolymer

The BT-BDD copolymer was synthesised by following the procedure described in section 5.3.5.1. 5,5'-Bis(trimethylstannyl)-2,2'-bithiophene (103.2 mg, 0.21 mmol) was reacted with BDD monomer (161 mg, 0.21 mmol) in presence of Pd₂(dba)₃ (7.69 mg, 0.008 mmol) and P(o-tolyl)₃ (10.23 mg, 0.034 mmol) to yield BT-BDD copolymer as a brown solid.

Yield: 112 mg (71 %).

¹H-NMR (200 MHz, CDCl₃, δ/ppm): 7.50-7.30 (4H, thiophene protons of BDD unit), 7.20-7.09 (4H, thiophene protons of bithiophene unit), 2.48 (4H, d, -CH₂- protons of ethylhexyl chain on BDD unit which are near to fused ring), 1.87-0.68 (30H, m, methine, -CH₂- and -CH₃ of ethylhexyl chain).

5.3.5.3 Synthesis of BDT-DPP(EH)-BDD terpolymer: Typical procedure

Into a 50 mL Schlenk tube equipped with a nitrogen gas inlet and a magnetic stir bar were added BDD monomer (110 mg, 0.14 mmol), DPP(EH) monomer (97.93 mg, 0.14 mmol), BDT monomer (221.6 mg, 0.29 mmol) and dry toluene (10 mL). The reaction mixture was purged with nitrogen for half hour, and then tris(dibenzylideneacetone)dipalladium(0) (Pd₂(dba)₃) (10.25 mg, 0.011 mmol) and tri(o-tolyl)phosphine (P(o-tolyl)₃) (13.62 mg, 0.045 mmol) was added into the solution. The

reaction mixture was again purged with nitrogen for half hour and was stirred at 100°C for 12 hours. The reaction mixture started thickening within 3 h of polymerisation. Upon cooling to room temperature, the reaction mixture was added dropwise to 100 mL of methanol. The precipitate was filtered, dried and further purified by Soxhlet extraction with methanol, hexane, chloroform respectively for 48 h each. The chloroform fraction was concentrated and added dropwise into methanol. Subsequently, the precipitate was collected and dried under vacuum overnight to obtain polymer as an indigo coloured solid. Yield: 411.7 mg (71 %).

¹H-NMR (400 MHz, TCE-d₂, 80°C, δ/ppm): 7.95-7.65 (4H, thiophene protons of DPP unit), 7.63-6.95 (8H, thiophene protons of BT and BDD units), 4.31 (12H, m, -CH₂- protons attached to oxygen or nitrogen atoms on sidechains of BDT and DPP unit) 3.39 (4H, d, -CH₂- protons of ethylhexyl chain on BDD unit which are near to fused ring), 1.93 (8H, m, methine at branch position of ethylhexyl chain), 1.43-1.20 (64H, -CH₂- protons of sidechains), 0.97-0.75 (48H, -CH₃ protons of sidechains).

5.3.5.4 Synthesis of BDT-DPP(HD)-BDD terpolymer

BDT-DPP(HD)-BDD terpolymer was synthesised by following the procedure described in section 5.3.5.3. 2,6-bis(trimethyltin)-4,8-bis(2-ethylhexyl)benzo[1,2-b:4,5-b']dithiophene (BDT monomer) (200 mg, 0.259 mmol) reacted with DPP monomer (117.4 mg, 0.129 mmol) and BDD monomer (99.27 mg, 0.129 mmol) in presence of Pd₂(dba)₃ (9.5 mg, 0.010 mmol) and P(o-tolyl)₃ (12.66 mg, 0.042 mmol) to yield BDT-DPP(HD)-BDD copolymer as an indigo coloured solid.

Yield: 471 mg (82 %).

¹H-NMR (400 MHz, TCE-d₂, 80°C, δ/ppm): 8.05-7.63 (4H, thiophene protons of DPP unit), 7.60-6.72 (8H, thiophene protons of BT and BDD units), 4.33 (12H, m, -CH₂- protons attached to oxygen or nitrogen atoms on sidechains of BDT and DPP unit) 3.42 (4H, d, -CH₂- protons of ethylhexyl chain on BDD unit which are near to fused ring), 1.93 (8H, m, methine at branch position of ethylhexyl chain), 1.40-1.30 (96H, -CH₂- protons of sidechains), 0.95-0.89 (48H, -CH₃ protons of sidechains).

5.3.5.5 Synthesis of BT-DPP(EH)-BDD terpolymer

BT-DPP(EH)-BDD terpolymer was synthesised by following the procedure described in section 5.3.5.3. 5,5'-Bis(trimethylstannyl)-2,2'-bithiophene (BT monomer)

(128 mg, 0.259 mmol) reacted with DPP monomer (89.02 mg, 0.130 mmol) and BDD monomer (100 mg, 0.130 mmol) in presence of $\text{Pd}_2(\text{dba})_3$ (9.5 mg, 0.010 mmol) and $\text{P}(\text{o-tolyl})_3$ (12.66 mg, 0.042 mmol) to yield BT-DPP(EH)-BDD copolymer as a black solid.

Yield: 304 mg (80 %).

$^1\text{H-NMR}$ (400 MHz, CDCl_3 , δ/ppm): 9.15-7.28 and 7.25-5.31 (16H, m, all aromatic protons), 3.94 (4H, m, $-\text{CH}_2-$ protons attached to nitrogen atoms on sidechains of DPP unit), 3.32 (4H, d, $-\text{CH}_2-$ protons of ethylhexyl chain on BDD unit which are near to fused ring), 1.80 (4H, m, methine at branch position of ethylhexyl chain), 1.50-1.20 (32H, $-\text{CH}_2-$ protons of sidechains), 1.06-0.76 (24H, $-\text{CH}_3$ protons of sidechains).

5.3.5.6 Synthesis of BT-DPP(HD)-BDD terpolymer

BT-DPP(HD)-BDD terpolymer was synthesised by following the procedure described in section 5.3.5.3. 5,5'-Bis(trimethylstannyl)-2,2'-bithiophene (BT monomer) (134.72 mg, 0.274 mmol) reacted with DPP monomer (124.2 mg, 0.137 mmol) and BDD monomer (105.04 mg, 0.137 mmol) in presence of $\text{Pd}_2(\text{dba})_3$ (10.04 mg, 0.011 mmol) and $\text{P}(\text{o-tolyl})_3$ (13.34 mg, 0.044 mmol) to yield BT-DPP(HD)-BDD copolymer as a black solid.

Yield: 227 mg (49.9 %).

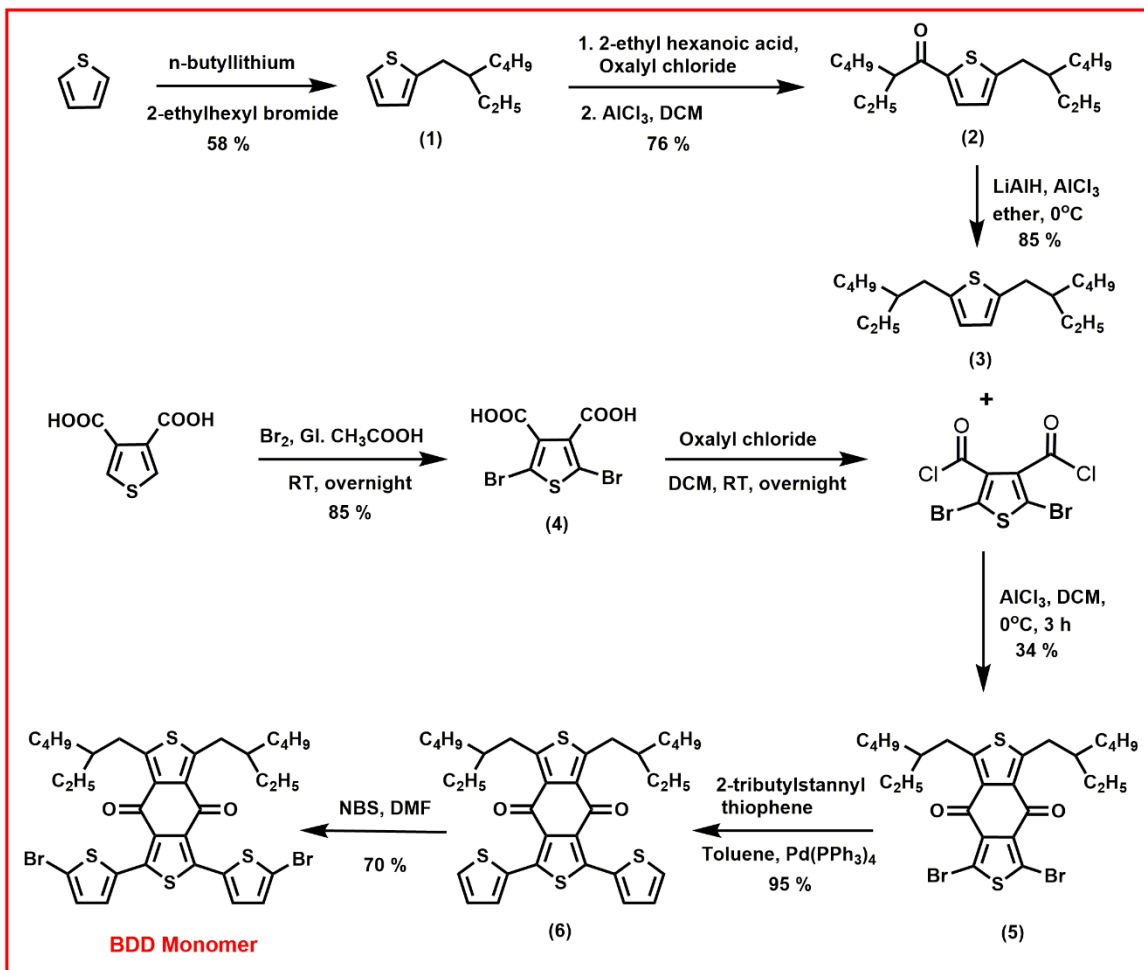
$^1\text{H-NMR}$ (400 MHz, TCE-d_2 , 80°C , δ/ppm): 9.10-6.45 (16H, m, all aromatic protons), 4.07 (4H, m, $-\text{CH}_2-$ protons attached to nitrogen atoms on sidechains of DPP unit), 3.41 (4H, d, $-\text{CH}_2-$ protons of ethylhexyl chain on BDD unit which are near to fused ring), 1.87 (4H, m, methine at branch position of ethylhexyl chain), 1.37-1.25 (64H, $-\text{CH}_2-$ protons of sidechains), 0.95-0.87 (24H, $-\text{CH}_3$ protons of sidechains).

5.4 RESULTS AND DISCUSSION

5.4.1 Synthesis of 1,3-bis(5-bromothiophen-2-yl)-5,7-bis(2-ethylhexyl)-benzo[1,2-c:4,5-c']dithiophene-4,8-dione (**BDD monomer**)

The seven-step route for the synthesis of BDD monomer starting from thiophene is depicted in **Scheme 5.1**. In one scheme, 2,5-bis(2-ethylhexyl)thiophene (3) was synthesised in a step-wise manner from thiophene. Thiophene was first monoalkylated with 2-ethylhexyl bromide in presence of n-butyl lithium to form 2-(2-Ethylhexyl)thiophene (1). Friedel-Crafts acylation of compound 1 with 2-ethylhexanoyl

chloride in presence of Lewis acid, AlCl_3 , afforded compound 2-ethyl-1-(5-(2-ethylhexyl)thiophen-2-yl)hexan-1-one (2). Compound 2 on reduction with lithium aluminium hydride yielded the dialkylated compound - 2,5-bis(2-ethylhexyl)thiophene (3). In another scheme, thiophene-3,4-dicarboxylic acid was first brominated to produce 2,5-dibromothiophene-3,4-dicarboxylic acid (4). Compound 4 was then reacted with oxalyl chloride to produce corresponding acid chloride- 2,5-dibromothiophene-3,4-dicarbonyl dichloride which underwent Friedel-Crafts acylation with 2,5-bis(2-ethylhexyl)thiophene (3) to produce 1,3-dibromo-5,7-bis(2-ethylhexyl)-4H,8H-benzo[1,2-c:4,5-c']dithiophene-4,8-dione (5). Compound 5 reacted with trimethyl(thiophen-2-yl)stannane in presence of catalyst $\text{Pd}(\text{PPh}_3)_4$ to synthesise 1,3-bis(2-ethylhexyl)-5,7-di(thiophen-2-yl)benzo[1,2-c:4,5-c']-dithiophene-4,8-dione (6) which on bromination using N-bromosuccinimide afforded the desired monomer 1,3-bis(5-bromothiophen-2-yl)-5,7-bis(2-ethylhexyl)-benzo[1,2-c:4,5-c']dithiophene-4,8-dione (BDD monomer). The chemical structures of all the intermediates were confirmed by ^1H and ^{13}C NMR spectroscopy. (Data provided in the supporting information)



Scheme 5.1 Synthesis of 1,3-bis(5-bromothiophen-2-yl)-5,7-bis(2-ethylhexyl)-benzo[1,2-c:4,5-c']dithiophene-4,8-dione (BDD monomer)

$^1\text{H-NMR}$ spectrum of BDD monomer is presented in **Figure 5.1**. The protons on C_3 and C_4 carbon atoms of thiophene ring appeared as doublets at 7.45 and 7.08 δ ppm, respectively. The methylene protons on ethylhexyl side chain which are directly attached to thiophene ring were observed as a doublet at 3.31 δ ppm. The proton at branch position of ethylhexyl side chain was observed as a multiplet in the range 1.84–1.72 δ ppm. The remaining methylene protons on ethylhexyl side chain observed in the range 1.45–1.30 δ ppm. The methyl protons appeared as multiplet in the range 0.98–0.87 δ ppm.

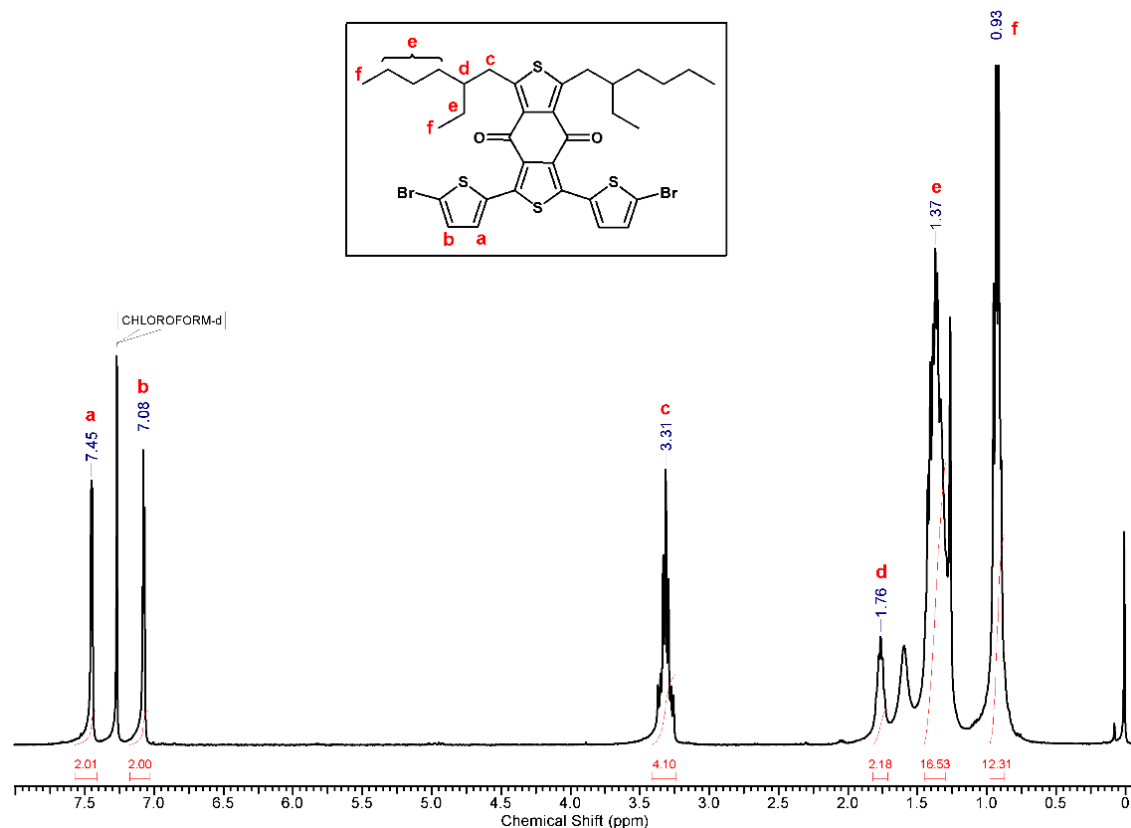


Figure 5.1 $^1\text{H-NMR}$ spectrum (CDCl_3) of 1,3-bis(5-bromothiophen-2-yl)-5,7-bis(2-ethylhexyl)-benzo[1,2-c:4,5-c']dithiophene-4,8-dione (BDD monomer)

$^{13}\text{C-NMR}$ spectrum of BDD monomer is presented in **Figure 5.2**. The carbonyl carbon appeared at 177.55 δ ppm. The remaining carbons on fused BDD unit and thiophene rings were observed in the range 154.08-118.05 δ ppm. The tertiary carbon at branch position of ethylhexyl side chain appeared at 41.22 δ ppm. The methylene carbon on side chain which is directly attached to thiophene ring were observed at 33.66 δ ppm. The remaining methylene carbons on ethylhexyl side chain appeared in the range 32.79- 23.02 δ ppm. The methyl carbons on hexyl chain and ethyl chain appeared at 14.18 and 10.85 δ ppm, respectively.

$^{13}\text{C-DEPT}$ NMR spectrum of BDD monomer is presented in supporting information in **Figure SI 5.11**.

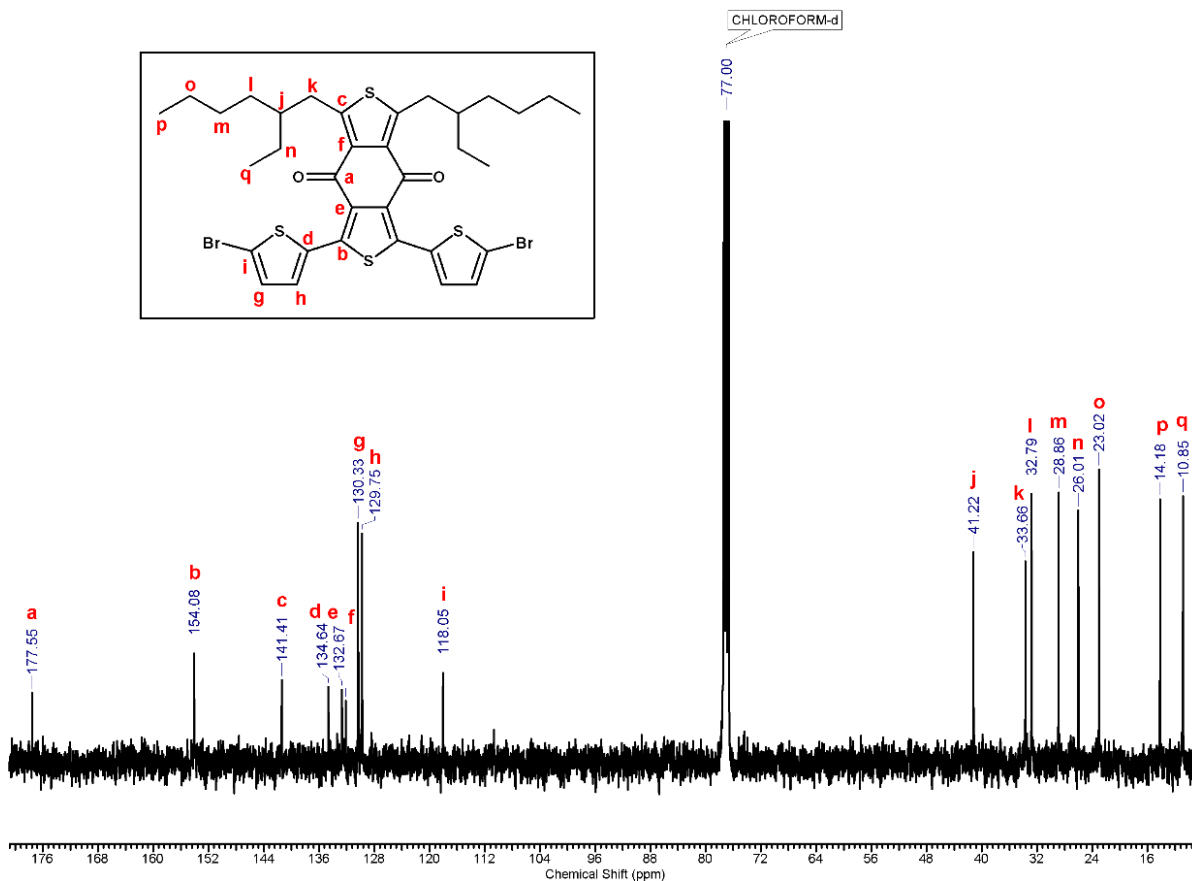
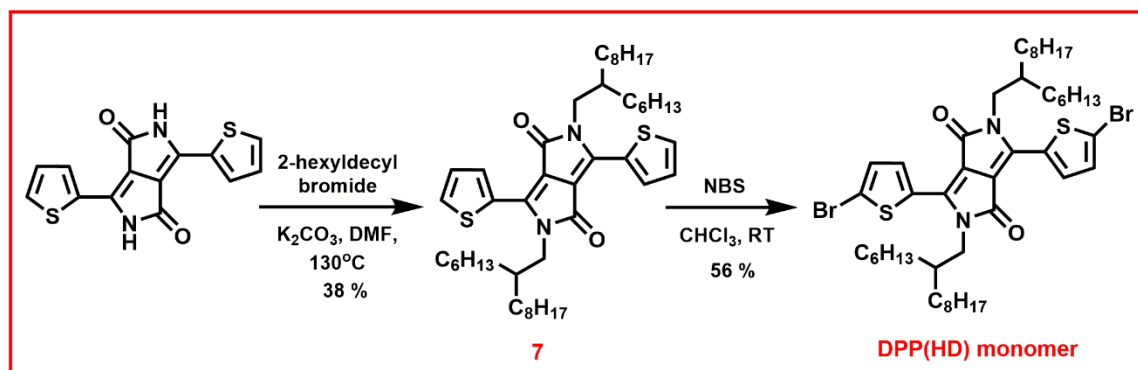


Figure 5.2 ¹³C-NMR spectrum (CDCl₃) of 1,3-bis(5-bromothiophen-2-yl)-5,7-bis(2-hexyldecyl)-benzo[1,2-c:4,5-c']dithiophene-4,8-dione (BDD monomer)

5.4.2 Synthesis of 3,6-bis(5-bromothiophen-2-yl)-2,5-bis(2-hexyldecyl)pyrrolo[3,4-c]pyrrole-1,4(2H,5H)-dione (DPP(HD) monomer)

The synthesis of 3,6-bis(5-bromothiophen-2-yl)-2,5-bis(2-hexyldecyl)pyrrolo[3,4-c]pyrrole-1,4(2H,5H)-dione DPP(HD) monomer is depicted in **Scheme 5.2**. 3,6-Di(thiophen-2-yl)-2,5-dihydropyrrolo[3,4-c]pyrrole-1,4-dione was N-alkylated using 2-hexyldecyl bromide and potassium carbonate to yield 2,5-bis(2-hexyldecyl)-3,6-di(thiophen-2-yl)-2,5-dihydropyrrolo[3,4-c]pyrrole-1,4-dione (7). The subsequent bromination of N-alkylated derivative 7 with N-bromosuccinimide in chloroform afforded the desired product- DPP(EH) monomer.



Scheme 5.2 Synthesis of 3,6-bis(5-bromothiophen-2-yl)-2,5-bis(2-hexyldecyl)pyrrolo[3,4-c]pyrrole-1,4(2H,5H)-dione (DPP(HD) monomer)

1H -NMR spectrum of DPP(HD) monomer is presented in **Figure 5.3a**. The protons on thiophene ring were appeared in the range 139.35-107.97 δ ppm. The methylene protons on hexyldecyl side chain which are adjacent to nitrogen atom of lactum ring, were observed as a doublet at 3.90 δ ppm. The proton at branch position of hexyldecyl side chain was observed as multiplet at 1.88 δ ppm. The remaining methylene protons on hexyldecyl side chain were observed in the range 1.35- 1.02 δ ppm. The peak due to methyl protons was appeared as triplet at 0.86 δ ppm.

^{13}C -NMR spectrum of DPP(HD) monomer is presented in **Figure 5.3b**. The carbonyl carbon appeared at 161.33 δ ppm. The remaining carbons on DPP unit and thiophene rings were observed in the range 139.35-107.97 δ ppm. The methylene carbon on side chain which is directly attached to the nitrogen atom of DPP unit resonated at 46.30 δ ppm. The tertiary carbon at branch position of ethylhexyl side chain appeared at 37.72 δ ppm. The remaining methylene carbons on ethylhexyl side chain appeared in the range 31.85- 22.64 δ ppm. The methyl carbon on side chain appeared at 14.08 δ ppm.

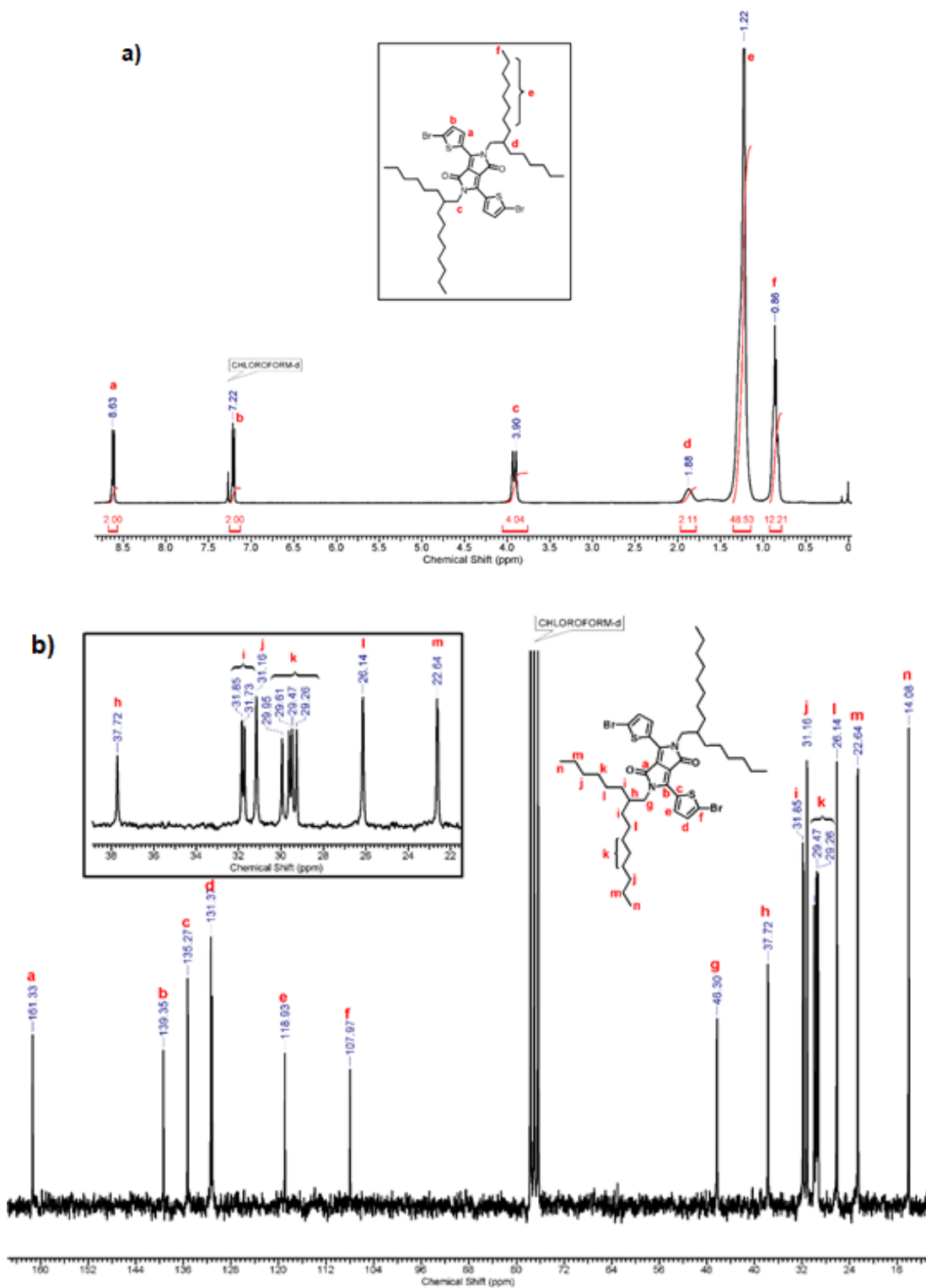
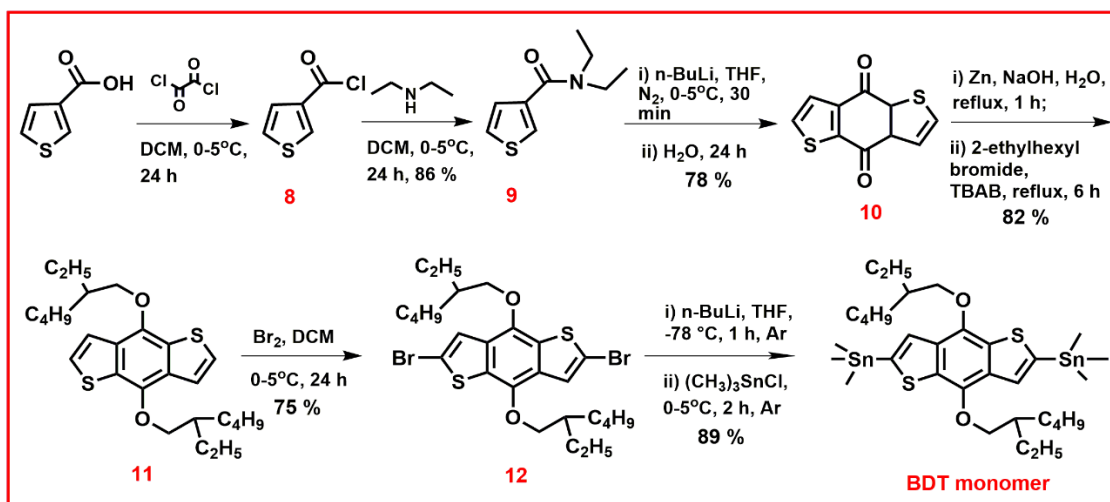


Figure 5.3 a) ^1H -NMR and b) ^{13}C -NMR spectrum (CDCl_3) of 3,6-bis(5-bromothiophen-2-yl)-2,5-bis(2-hexyldecyl)pyrrolo[3,4-c]pyrrole-1,4(2H,5H)-dione (DPP(HD) monomer)

5.4.3 Synthesis of 2,6-bis(trimethyltin)-4,8-bis(2-ethylhexyl)benzo[1,2-b:4,5-b']dithiophene (BDT monomer)

The six-step route for the synthesis of 2,6-bis(trimethyltin)-4,8-bis(2-ethylhexyl)benzo[1,2-b:4,5-b']dithiophene (BDT monomer) from thiophene-3-carboxylic acid is depicted in **Scheme 5.3**. Thiophene-3-carboxylic acid was reacted with oxalyl chloride to form thiophene-3-carbonyl chloride (8) which was reacted *in situ* with diethyl amine to produce N,N-diethylthiophene-3-carboxamide, (9). Compound-9 on reaction with *n*-butyllithium in cyclohexane at 0°C afforded the compound- benzo[1,2-*b*:4,5-*b'*]dithiophene-4,8-dione, (10). Further, compound-10 was first reduced by zinc dust in aqueous sodium hydroxide solution and then alkylated with 2-ethylhexyl bromide in presence of a catalytic amount of tetrabutylammonium bromide to yield 4,8-bis((2-ethylhexyl)oxy)benzo[1,2-*b*:4,5-*b'*]dithiophene (11). Compound-11 was brominated with bromine, to produce 2,6-dibromo-4,8-bis(2-ethylhexyl)benzo[1,2-*b*:4,5-*b'*]dithiophene (12) which was further stannylated using trimethyltin chloride in THF to obtain the product, 2,6-bis(trimethyltin)-4,8-bis(2-ethylhexyl)benzo[1,2-*b*:4,5-*b'*]dithiophene (BDT monomer) in 75% yield. The chemical structures of all the intermediates were confirmed by ¹H and ¹³C NMR spectroscopy. (Data provided in the supporting information).



Scheme 5.3 Synthesis of 2,6-bis(trimethyltin)-4,8-bis(2-ethylhexyl)benzo[1,2-*b*:4,5-*b'*]dithiophene (BDT monomer)

¹H-NMR spectrum of BDT monomer is presented in **Figure 5.4**. The aromatic proton appeared as a singlet at 7.52 δ ppm. The four methylene protons of side chains

which are directly attached to oxygen atom observed at 4.19 δ ppm. The proton at branch position of ethylhexyl chain appeared at 1.80 δ ppm. The remaining methylene protons and methyl protons resonated in the range 1.49-0.65 δ ppm. The methyl protons attached to tin (Sn) atom resonated in the range 0.63-0.19 δ ppm.

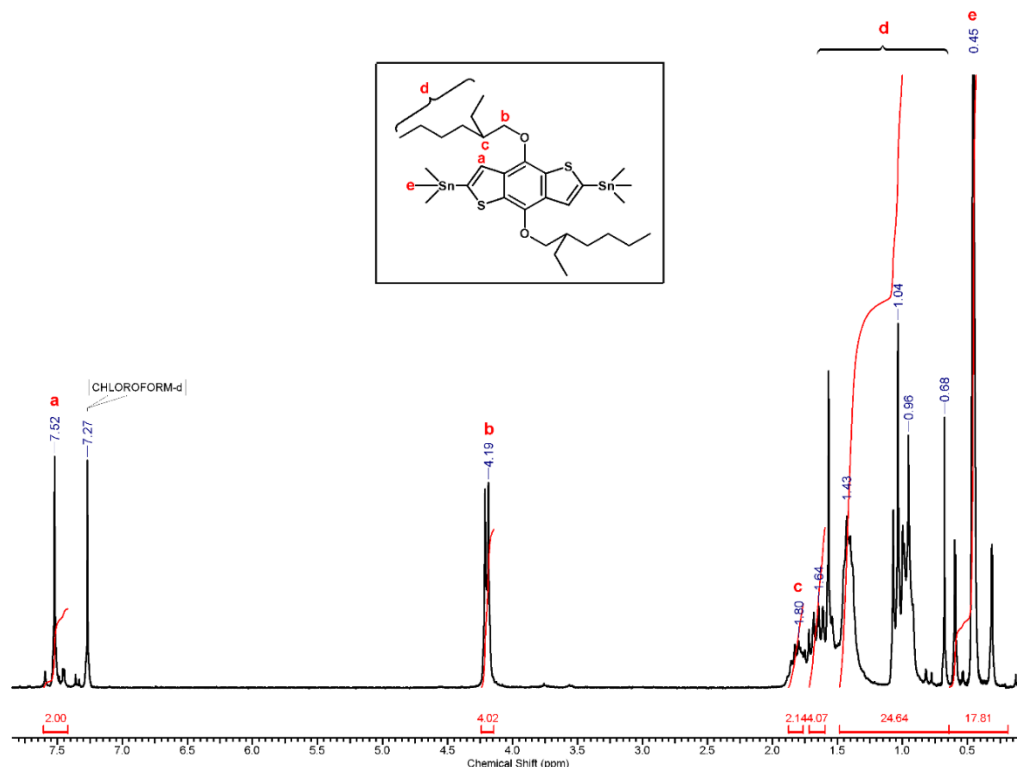
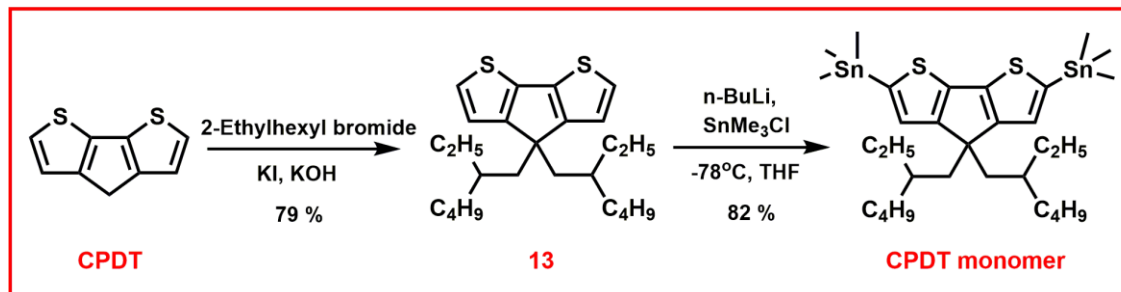


Figure 5.4 $^1\text{H-NMR}$ spectrum (CDCl_3) of 2,6-bis(trimethyltin)-4,8-bis(2-ethylhexyl)benzo[1,2-b:4,5-b']dithiophene

5.4.4 Synthesis of (4,4-bis(2-ethylhexyl)-4H-cyclopenta[2,1-b:3,4-b']dithiophene-2,6-diyl)bis(trimethylstannane) (CPDT monomer)

The synthesis of (4,4-bis(2-ethylhexyl)-4H-cyclopenta[2,1-b:3,4-b']dithiophene-2,6-diyl)bis(trimethylstannane) (CPDT monomer) from 4H-cyclopenta[2,1-b:3,4-b']dithiophene (CPDT) is depicted in **Scheme 5.4**. CPDT was reacted with 2-ethylhexyl bromide in presence of potassium hydroxide and potassium iodide to form alkylated derivative 4,4-bis(2-ethylhexyl)-4H-cyclopenta[2,1-b:3,4-b']dithiophene (13). Compound 13 was then reacted with n-butyl lithium and trimethyl tin chloride to afford desired product, CPDT monomer in 82 % yield. The chemical structure of alkylated CPDT (compound 13) was confirmed by ^1H and ^{13}C NMR spectroscopy (supporting information).



Scheme 5.4. Synthesis of (4,4-bis(2-ethylhexyl)-4H-cyclopenta[2,1-b:3,4-b']dithiophene-2,6-diyl)bis(trimethylstannane) (CPDT monomer)

$^1\text{H-NMR}$ spectrum of CPDT monomer is presented in **Figure 5.5**. Aromatic proton appeared as a singlet at 6.9 δ ppm. Methylene protons which are near to fused aromatic ring observed at 1.85 δ ppm. The proton at branch position of ethylhexyl chain appeared at 1.28 δ ppm. The remaining methylene protons resonated in the range 1.10-0.90 δ ppm. The methyl protons on hexyl chain and ethyl chain appeared at 0.75 and 0.59 δ ppm, respectively. The methyl protons attached to tin (Sn) atom resonated in the range 0.45-0.12 δ ppm.

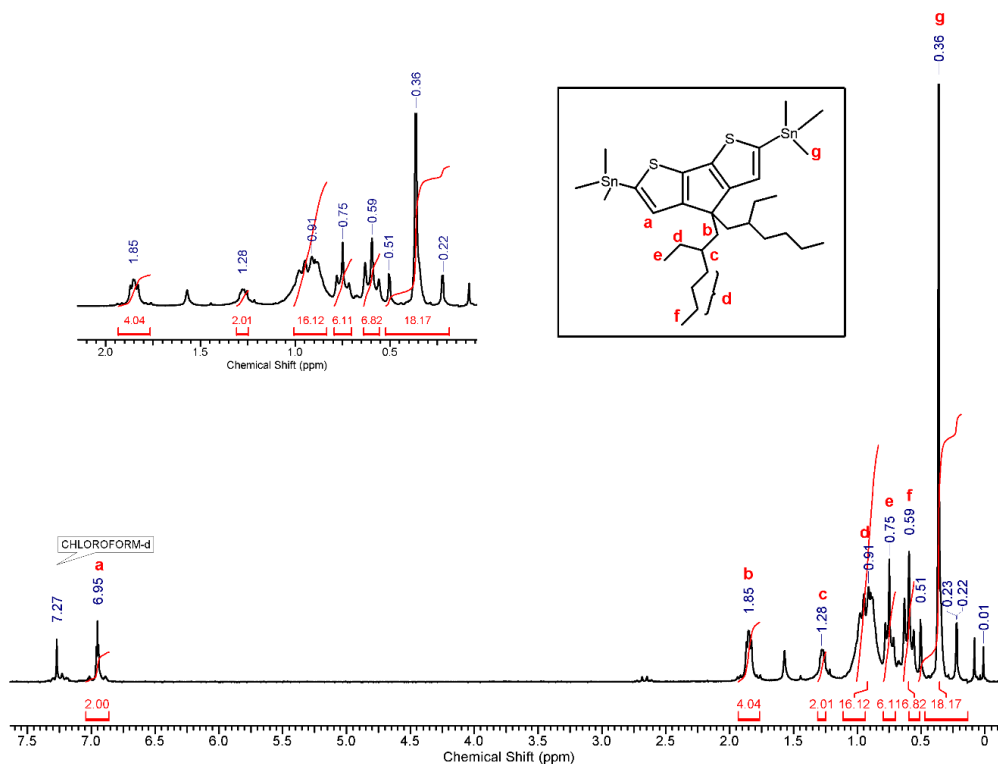
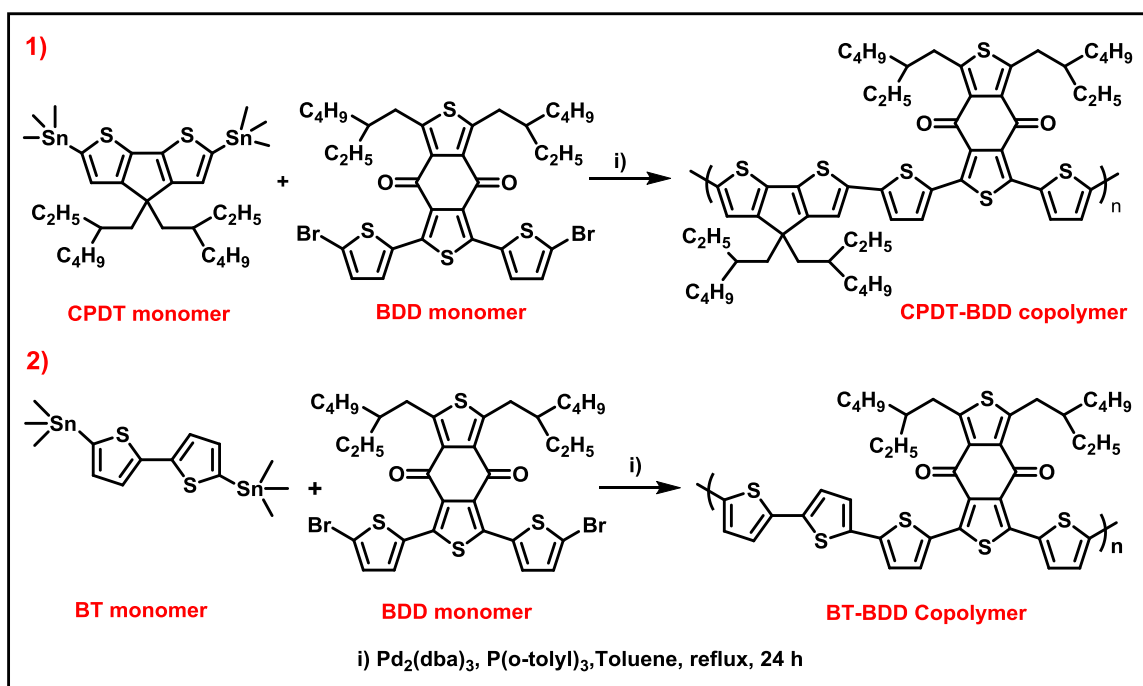


Figure 5.5 $^1\text{H-NMR}$ spectrum (CDCl_3) of (4,4-bis(2-ethylhexyl)-4H-cyclopenta[2,1-b:3,4-b']dithiophene-2,6-diyl)bis(trimethylstannane) (CPDT monomer)

5.4.5 Synthesis of BDD based copolymers

Two copolymers comprising either cyclopenta[2,1-b:3,4-b']dithiophene (CPDT) or bithiophene as donor unit and benzo[1,2-c:4,5-c']dithiophene-4,8-dione (BDD) as an acceptor unit were synthesised. The synthesis of copolymers is depicted in **Scheme 5.5**. The Stille coupling reactions between distannylated compounds (CPDT monomer and BT monomer) and brominated compound (BDD monomer) in the presence of catalyst $\text{Pd}_2(\text{dba})_3$ and ligand $\text{P}(\text{o-tolyl})_3$ in toluene at $100\text{ }^\circ\text{C}$ for 24 h gave the target copolymers-CPDT-BDD and BT-BDD. The copolymers were purified by sequential Soxhlet extraction with methanol, hexane, chloroform, to remove catalysts and low molecular-weight compounds. The CPDT-BDD and BT-BDD were obtained in 60 and 45 % overall yield, respectively.



Scheme 5.5 Synthesis of BDD based copolymers- 1) CPDT-BDD and 2) BT-BDD

$^1\text{H-NMR}$ spectrum of polymer CPBT-BDD is presented in **Figure 5.6**. The protons on thiophene rings of BDD appeared in the range of $8.05\text{-}7.30\text{ }\delta$ ppm. Aromatic protons on CPDT unit was observed in the range of $7.23\text{-}6.98\text{ }\delta$ ppm. The peak at $3.37\text{ }\delta$ ppm was appeared for four methylene protons on side chain on BDD which are near to fused ring. The peak at $1.95\text{ }\delta$ ppm was observed for four methylene protons on side chain on CPDT

unit which are near to fused ring. The four methine proton at branch position of ethylhexyl chain resonated at 1.81 δ ppm. The remaining methylene and methyl protons of side chains appeared in the range of 1.1-0.67 δ ppm.

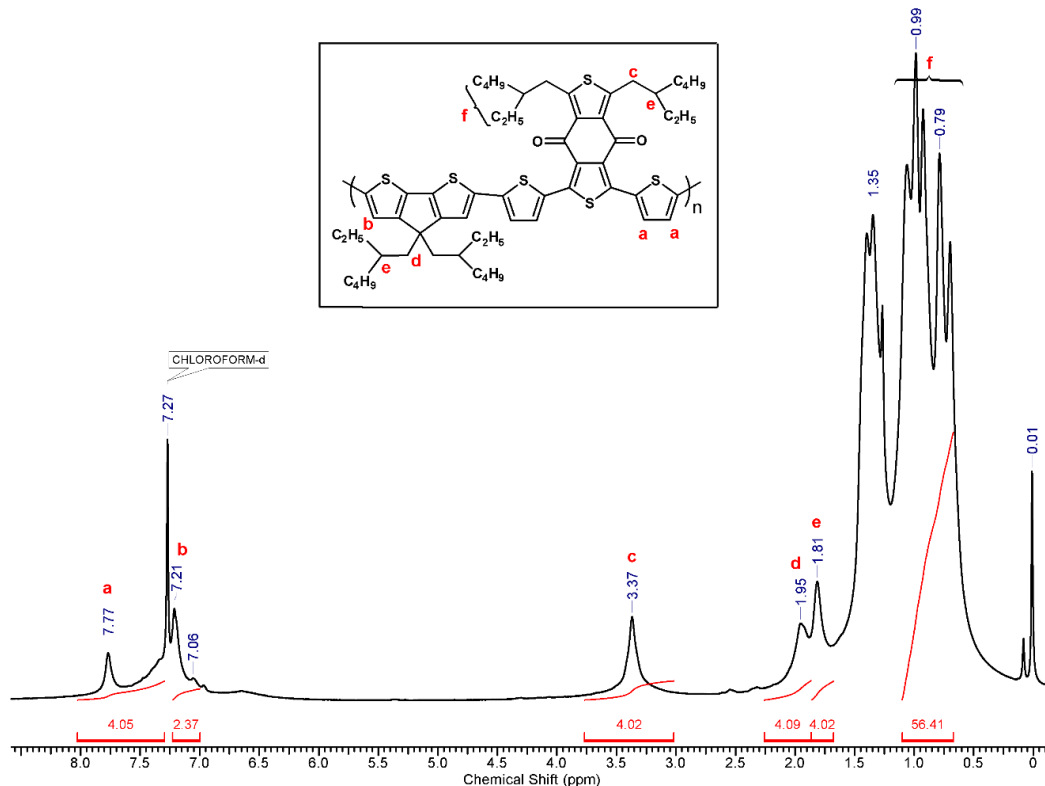


Figure 5.6 $^1\text{H-NMR}$ spectrum (CDCl_3) of copolymer CPDT-BDD

$^1\text{H-NMR}$ spectrum of polymer BT-BDD is presented in **Figure 5.7**. The protons on thiophene rings of BDD appeared in the range of 7.50-7.30 δ ppm while those on the bithiophene ring observed in the range of 7.20-7.09 δ ppm. The peak at 2.48 δ ppm was observed for four methylene protons on side chain which are near to fused ring. The remaining methylene, methyl protons of side chain located in the range of 1.87-0.68 δ ppm.

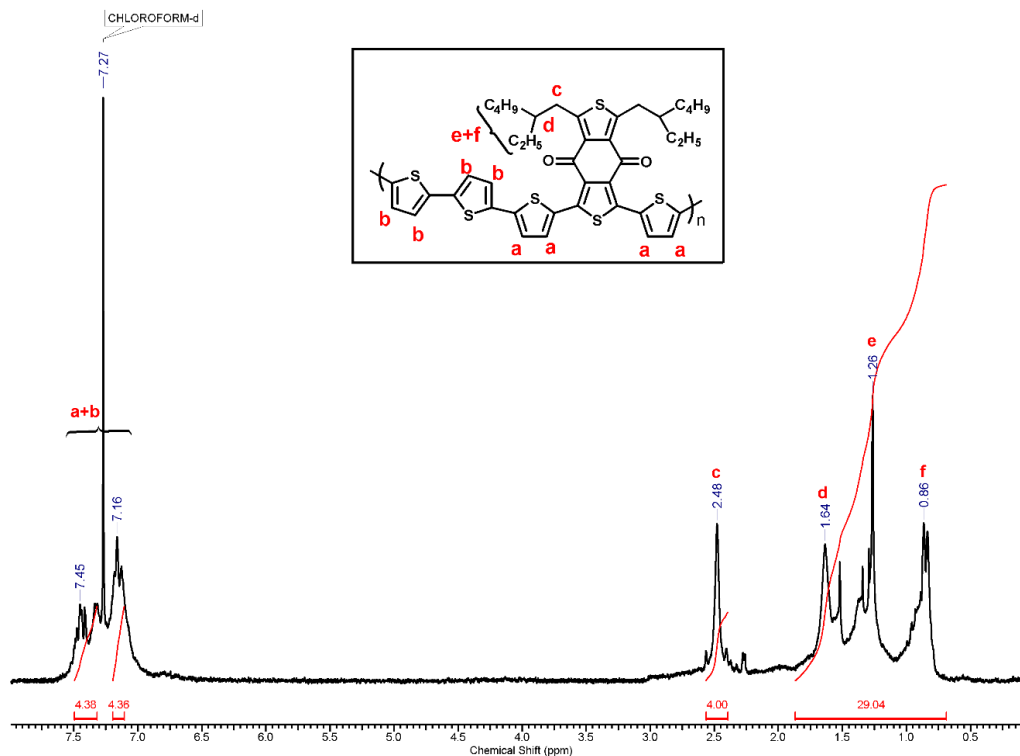


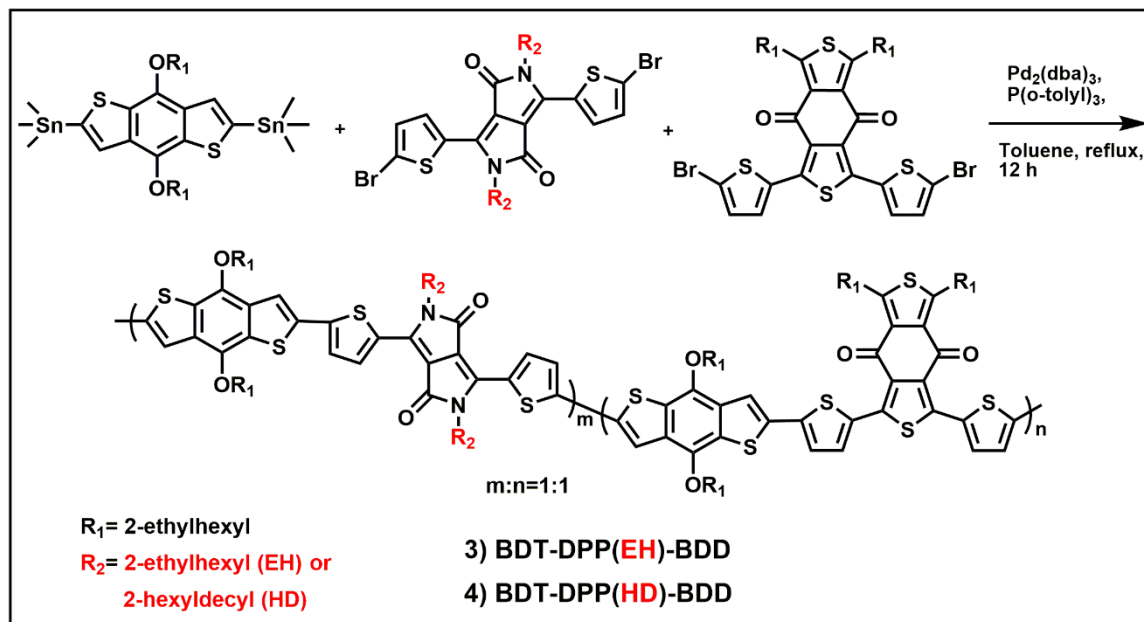
Figure 5.7 ¹H-NMR spectrum (CDCl₃) of copolymer BT-BDD

5.4.6 Synthesis of BDD based random terpolymers

5.4.6.1 Synthesis of BDD based random terpolymers comprising benzo[1,2-b:4,5-b']dithiophene (BDT) as donor unit

Two random terpolymers comprising benzo[1,2-b:4,5-b']dithiophene (BDT) as donor unit and diketopyrrolo[3,4-c]pyrrole-1,4-dione (DPP), benzo[1,2-c:4,5-c']dithiophene-4,8-dione (BDD) as acceptor units were synthesised. The two terpolymers differ only in the length of side chain of DPP unit. Terpolymers, BDT-DPP(EH)-BDD and BDT-DPP(HD)-BDD possess ethylhexyl and hexyldecyl side chains on DPP unit respectively, remaining structure being the same. The synthesis of terpolymers is depicted in **Scheme 5.6**. The Stille coupling reactions between distannylated compound (BDT monomer) and brominated compounds (DPP monomer, BDD monomer) in the presence of catalyst Pd₂(dba)₃ and ligand P(o-tolyl)₃ in toluene at 100 °C for 12 h gave the target terpolymers- BDT-DPP(EH)-BDD and BDT-DPP(HD)-BDD. The copolymers were purified by sequential Soxhlet extraction with methanol, hexane and chloroform, to remove

catalysts and low molecular-weight compounds. The BDT-DPP(EH)-BDD and BDT-DPP(HD)-BDD were obtained in 60 % and 42 % yield, respectively.



Scheme 5.6 Synthesis of BDD based random terpolymers comprising BDT as donor unit- 3) BDT-DPP(EH)-BDD and 4) BDT-DPP(HD)-BDD

$^1\text{H-NMR}$ spectrum of terpolymer BDT-DPP(EH)-BDD is presented in **Figure 5.8**. The aromatic protons of DPP ring appeared in the range of 7.95-7.65 δ ppm. The remaining aromatic protons on BDD and BDT ring observed in the range of 7.63-6.95 δ ppm. The peak at 4.31 δ ppm was appeared for twelve methylene protons (attached to oxygen or nitrogen atom) on sidechains on BDT and DPP unit. The peak at 3.39 δ ppm was appeared for four methylene protons on sidechain of BDD unit which are near to fused ring. Eight methine protons at branch position of ethylhexyl chain resonated at 1.93 δ ppm. The remaining methylene and methyl protons of side chains appeared in the range of 1.43-1.20 and 0.97-0.75 δ ppm, respectively.

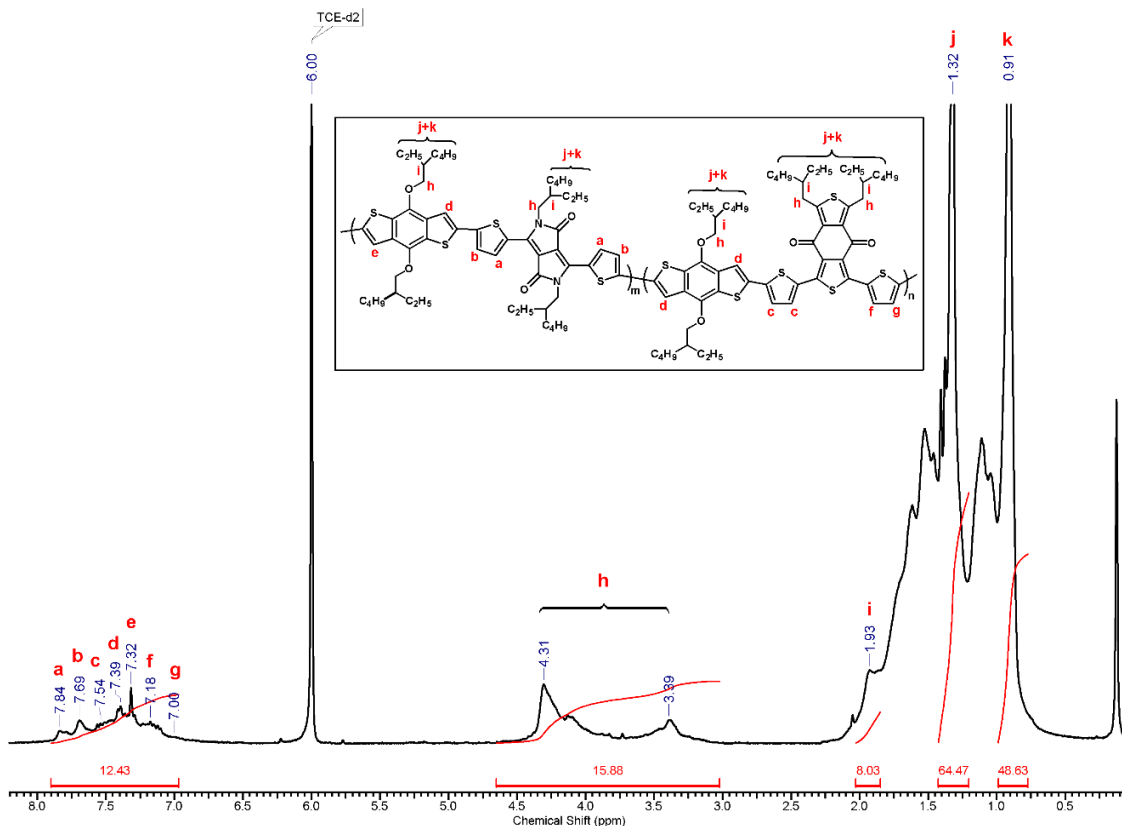


Figure 5.8 ¹H-NMR spectrum (TCE-d₂) of terpolymer BDT-DPP(EH)-BDD

¹H-NMR spectrum of terpolymer BDT-DPP(HD)-BDD is presented in **Figure 5.9**. The aromatic protons of DPP ring appeared in the range of 8.05-7.63 δ ppm. The remaining aromatic protons on BDD and BDT ring observed in the range of 7.60-6.72 δ ppm. The peak at 4.33 δ ppm was appeared for twelve methylene protons (attached to oxygen or nitrogen atom) on side chains on BDT and DPP unit. The peak at 3.42 δ ppm was appeared for four methylene protons on side chain of BDD unit which are near to fused ring. Eight methine protons at branch position of ethylhexyl chain resonated at 1.96 δ ppm. The remaining methylene and methyl protons of side chains appeared in the range of 1.40-1.30 and 0.95-0.89 δ ppm, respectively.

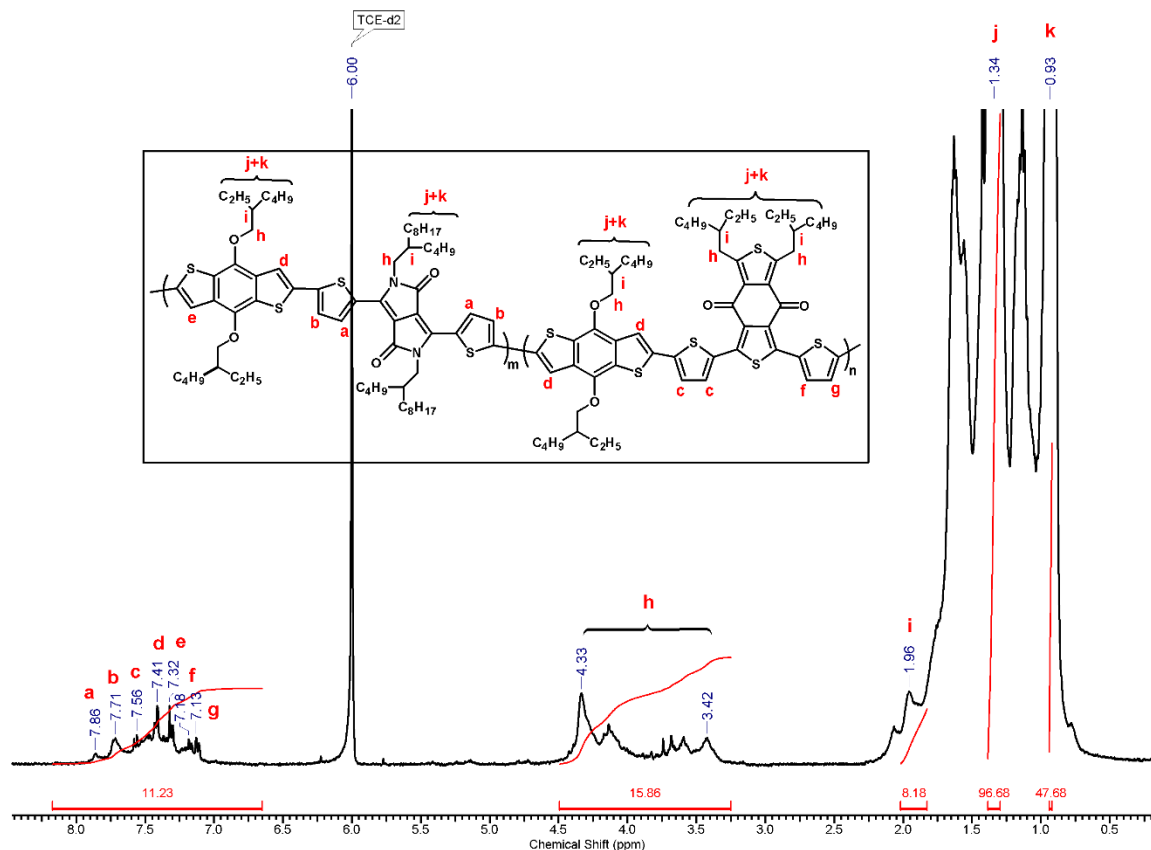
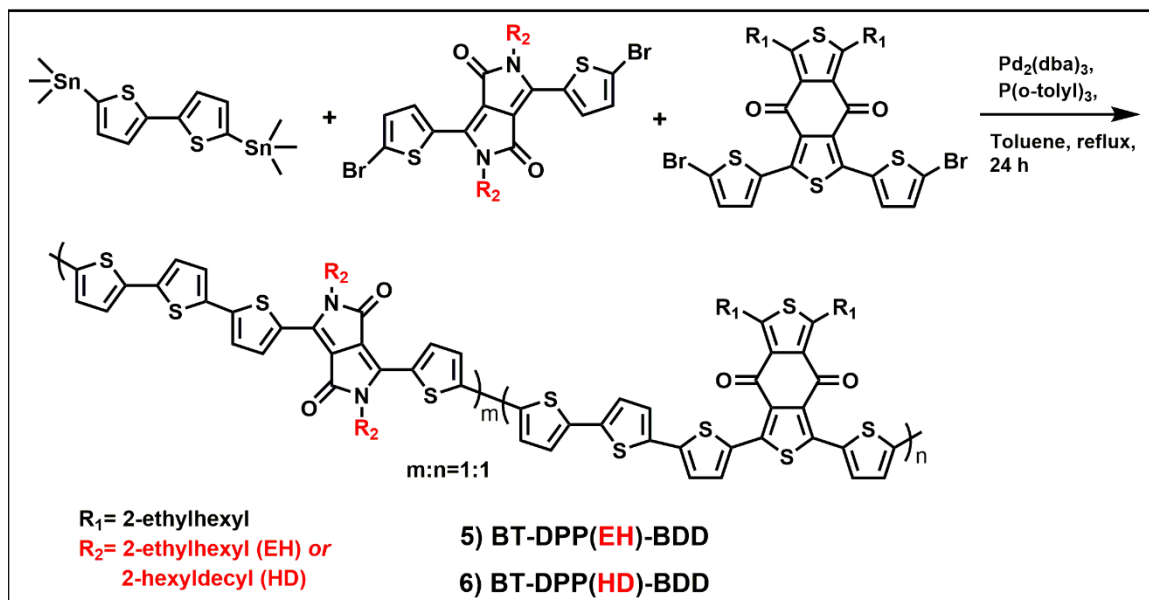


Figure 5.9 $^1\text{H-NMR}$ spectrum (TCE- d_2) of terpolymer BDT-DPP(HD)-BDD

5.4.6.2 Synthesis of BDD based random terpolymers comprising bithiophene (BT) as donor unit

Two random terpolymers comprising bithiophene (BT) as donor unit and diketopyrrolo[3,4-c]pyrrole-1,4-dione (DPP), benzo[1,2-c:4,5-c']dithiophene-4,8-dione (BDD) as acceptor units were synthesised. The two terpolymers differ only in the length of side chain of DPP unit. Terpolymers, BT-DPP(EH)-BDD and BT-DPP(HD)-BDD possess ethylhexyl and hexyldecyl side chains on DPP unit respectively, remaining structure being the same. The synthesis of terpolymers is depicted in **Scheme 5.7**. The Stille coupling reactions between distannylated compound (BT monomer) and brominated compounds (DPP monomer, BDD monomer) in the presence of catalyst $\text{Pd}_2(\text{dba})_3$ and ligand $\text{P}(\text{o-tolyl})_3$ in toluene at 100°C for 24 h gave the target terpolymers- BT-DPP(EH)-BDD and BT-DPP(HD)-BDD. The copolymers were purified by sequential Soxhlet extraction with methanol, hexane and chloroform, to remove catalysts and low molecular-

weight compounds. The BT-DPP(EH)-BDD and BT-DPP(HD)-BDD were obtained in 74 % and 50 % overall yield, respectively.



Scheme 5.7 Synthesis of BDD based random terpolymers comprising BT as donor unit- 5) BT-DPP(EH)-BDD and 6) BT-DPP(HD)-BDD

$^1\text{H-NMR}$ spectrum of terpolymer BT-DPP(EH)-BDD is presented in **Figure 5.10**. The various aromatic protons appeared in the range of 9.15-7.28 and 7.25-5.31 δ ppm. The peaks at 3.94 δ ppm was observed for four methylene protons on side chains of DPP ring which are attached to nitrogen atom. The peak at 3.32 δ ppm was appeared for four methylene protons on side chains of BDD which are near to fused ring. The four methine protons at branch position of ethylhexyl chain resonated at 1.80 δ ppm. The remaining methylene and methyl protons of side chains appeared in the range of 1.50-1.20 and 1.06-0.76 δ ppm, respectively.

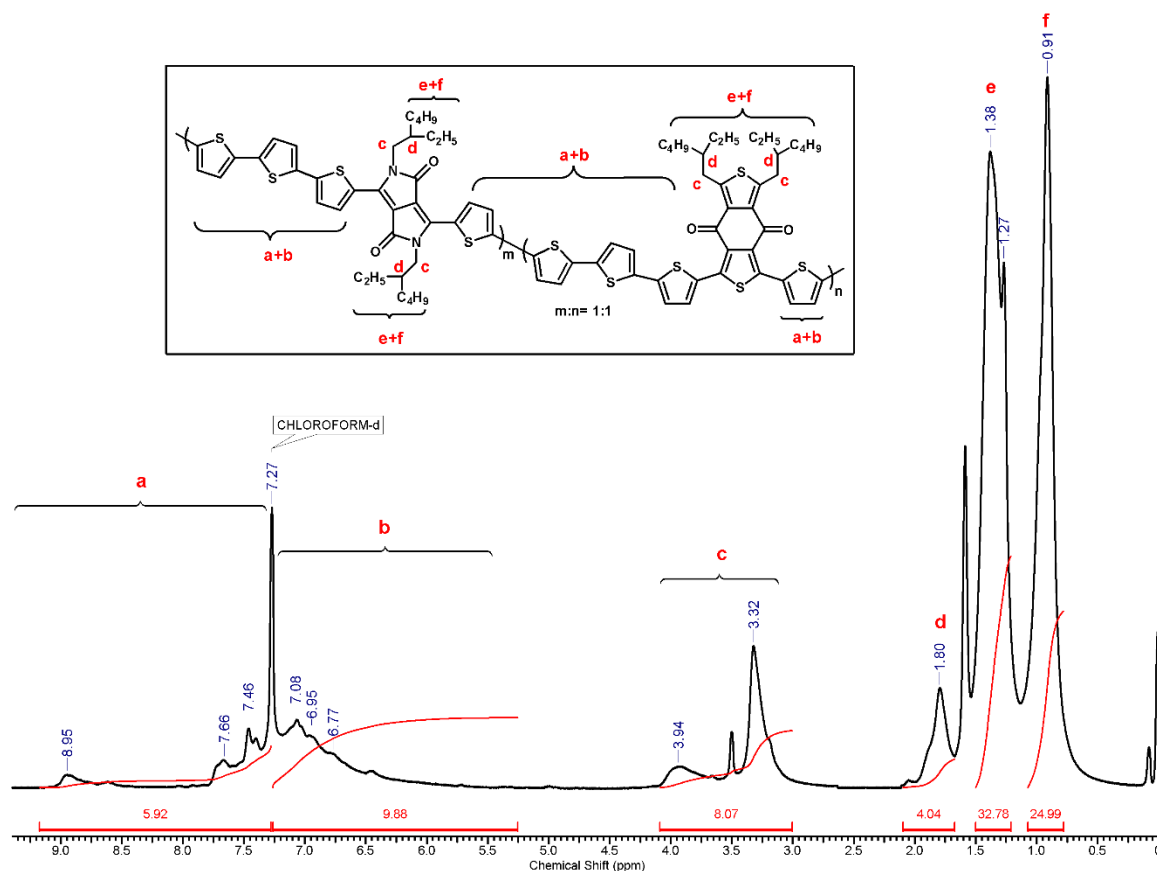


Figure 5.10 $^1\text{H-NMR}$ spectrum (CDCl_3) of terpolymer BT-DPP(EH)-BDD

$^1\text{H-NMR}$ spectrum of terpolymer BT-DPP(HD)-BDD is presented in **Figure 5.11**. The various aromatic protons appeared in the range of 9.10-6.45 δ ppm. The peak for four methylene protons on side chains of DPP ring which are attached to nitrogen atom observed at 4.07 δ ppm. The peak at 3.41 δ ppm was appeared for four methylene protons on sidechains of BDD which are near to fused ring. The four methine protons at branch position of ethylhexyl chain resonated at 1.87 δ ppm. The remaining methylene and methyl protons of side chains appeared in the range of 1.37-1.25 and 0.95-0.87 δ ppm, respectively.

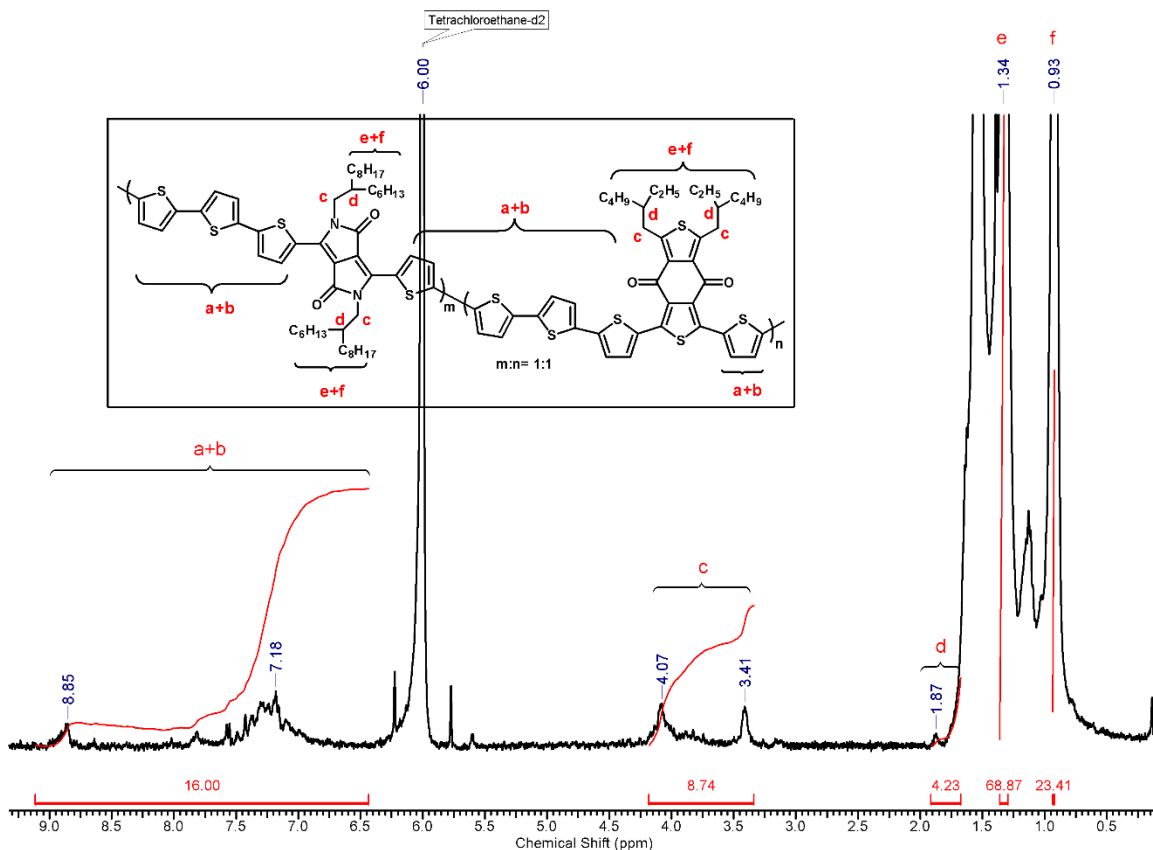


Figure 5.11 $^1\text{H-NMR}$ spectrum (TCE- d_2) of terpolymer BT-DPP(HD)-BDD

Two D-A copolymers and four D-A-A terpolymers comprising benzo[1,2-c:4,5-c']dithiophene-4,8-dione BDD as acceptor unit (A) were synthesized. Three different donor units, namely- cyclopenta[2,1-b:3,4-b']dithiophene, bithiophene (BT) and benzo[1,2-b:4,5-b']dithiophene (BDT) were used. Either 2,5-bis(2-ethylhexyl)pyrrolo[3,4-c]pyrrole-1,4(2H,5H)-dione (DPP (EH)) or 2,5-bis(2-hexyldecyl)pyrrolo[3,4-c]pyrrole-1,4(2H,5H)-dione (DPP (HD)) was used as second acceptor unit in terpolymeric systems. Copolymers were soluble in organic solvents such as chloroform, dichloromethane, tetrahydrofuran, toluene and chlorobenzene at room temperature. Terpolymers were soluble in organic solvents such as chloroform, tetrahydrofuran, toluene and chlorobenzene at higher temperatures (70°C). Polymers were obtained with the yields in the range of 50 % to 88 %.

Molecular weights of polymers were determined by gel permeation chromatography (GPC) in THF using polystyrene as the standard. The data obtained from GPC and thermogravimetric analysis (TGA) is summarised in **Table 5.1**. Number average

molecular weights were in the range 1.70- 28.66 kg/mol. Dispersities were in the range of 2.80– 1.52. TG curves for various polymers are shown in **Figure SI 5.16**. Thermal degradation under nitrogen at 10 % weight loss was started between 285 and 411 °C for various polymers.

Table 5.2 Data obtained from GPC and TGA studies.

Polymers	M _n (kg/mol) ^a	M _w (kg/mol) ^b	Dispersity (M _w /M _n)	T _{10%} /°C ^c
CPDT-BDD*	28.66	79.58	2.80	-
BT-BDD	1.70	2.59	1.52	410
BT-DPP(EH)-BDD	2.70	5.22	1.94	411
BT-DPP(HD)-BDD	3.50	8.17	2.41	310
BDT-DPP(EH)-BDD	9.01	15.83	1.76	352
BDT-DPP(HD)-BDD	16.10	45.81	2.84	285

a: M_n= number-average molecular weight, b: M_w= weight-average molecular weight, c: T_{10%}=decomposition temperatures at 10% weight loss.

* for this polymer molecular weight was determined on Agilent Technologies GPC220 HT using 1,2,4-trichlorobenzene as an eluent at a flow rate of 1 mL min⁻¹ at 140°C. Sample concentration was 2 mg mL⁻¹ and PS Easivial PS-M was used as calibration standards.

5.4.7 Photophysical Study

The photophysical data of copolymers and terpolymers was measured in chloroform solution as well as on thin films spin coated from chlorobenzene. **Table 5.2** summarizes photophysical data which include wavelength at absorption maximum (λ_a), wavelength at emission maximum (λ_f), wavelength at which absorbance starts to increase rapidly, on the lower energy side (λ_{onset}), the optical band gap energy (E_g^{opt}) calculated using $1240/\lambda_{onset}$,

The absorption and photoluminescence spectra of copolymer and terpolymers comprising bithiophene as donor unit, in dilute chloroform solution is depicted in **Figure 5.12**.

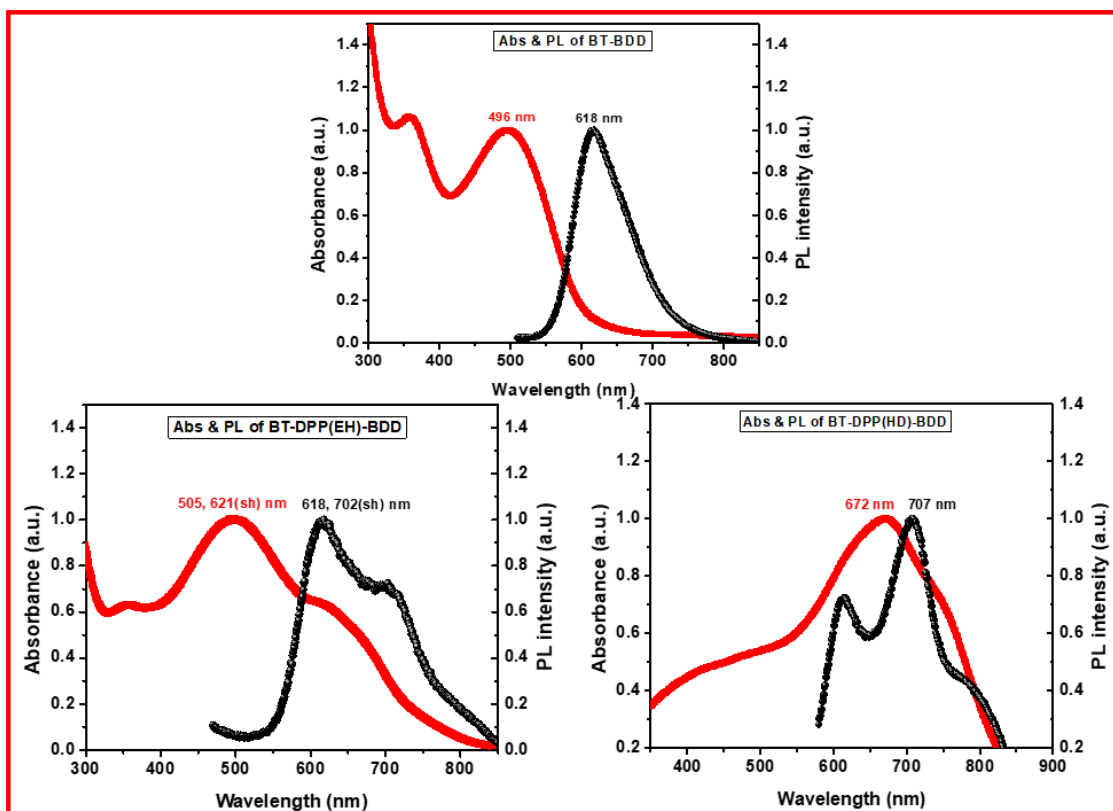


Figure 5.12 The absorption and photoluminescence spectra of copolymer and terpolymers comprising bithiophene (BT) as donor unit in dilute chloroform solution

In solution, bithiophene containing copolymer (BT-BDD) shows absorption and emission maximum at 496 nm and 618 nm, respectively. The terpolymer bearing ethylhexyl chain on DPP (BT-DPP(EH)-BDD), exhibits absorption and emission maximums at 505 and 618 nm, along with shoulder peaks at 621 and 702 nm, respectively. The shoulder peak in absorption spectrum of terpolymer BT-DPP(EH)-BDD may be due to intramolecular charge transfer (ICT). Apart from this, absorption spectra of terpolymer bearing hexyldecyl chain on DPP (BT-DPP(HD)-BDD), is red shifted by 167 nm as compared to that for BT-DPP(EH)-BDD. This may be due to increased molecular weight of this terpolymer due to enhanced solubility of the polymer in reaction mixture as a result of incorporation of longer side chains (hexyldecyl) on DPP ring.

The absorption and photoluminescence spectra of terpolymers comprising benzo[1,2-b:4,5-b']dithiophene (BDT) as donor unit in dilute chloroform solution is exhibited in **Figure 5.13**.

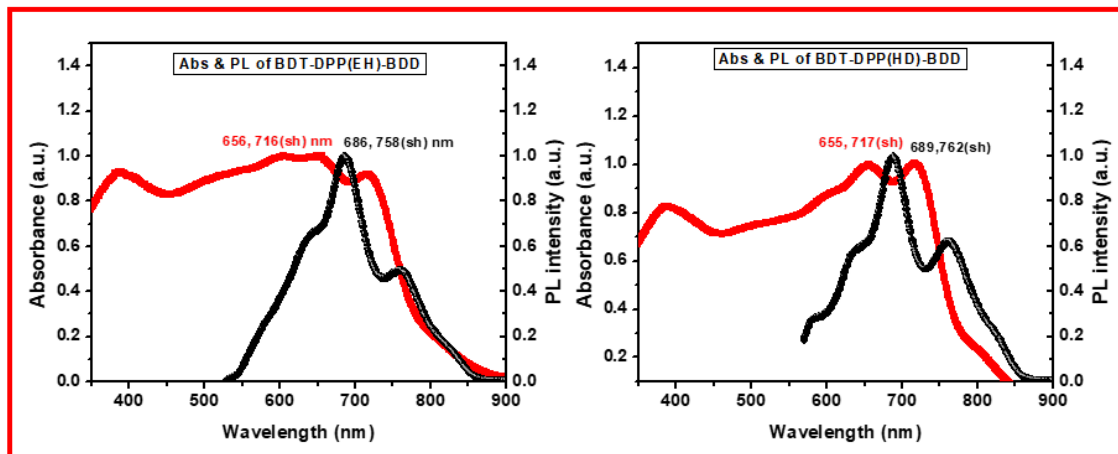


Figure 5.13 The absorption and photoluminescence spectra of terpolymers comprising benzo[1,2-b:4,5-b']dithiophene (BDT) as donor unit in dilute chloroform solution

Absorption and emission spectra of terpolymers- BDT-DPP(EH)-BDD and BDT-DPP(HD)-BDD, in solution were almost identical. These polymers show absorption maximum at about 656 nm with shoulder peak at 716 nm while emission maximum at about 686 nm with shoulder peak at about 758 nm.

The absorption and photoluminescence spectra of thin films of copolymer and terpolymers comprising bithiophene as donor unit, spin coated from chlorobenzene solution is depicted in **Figure 5.14**.

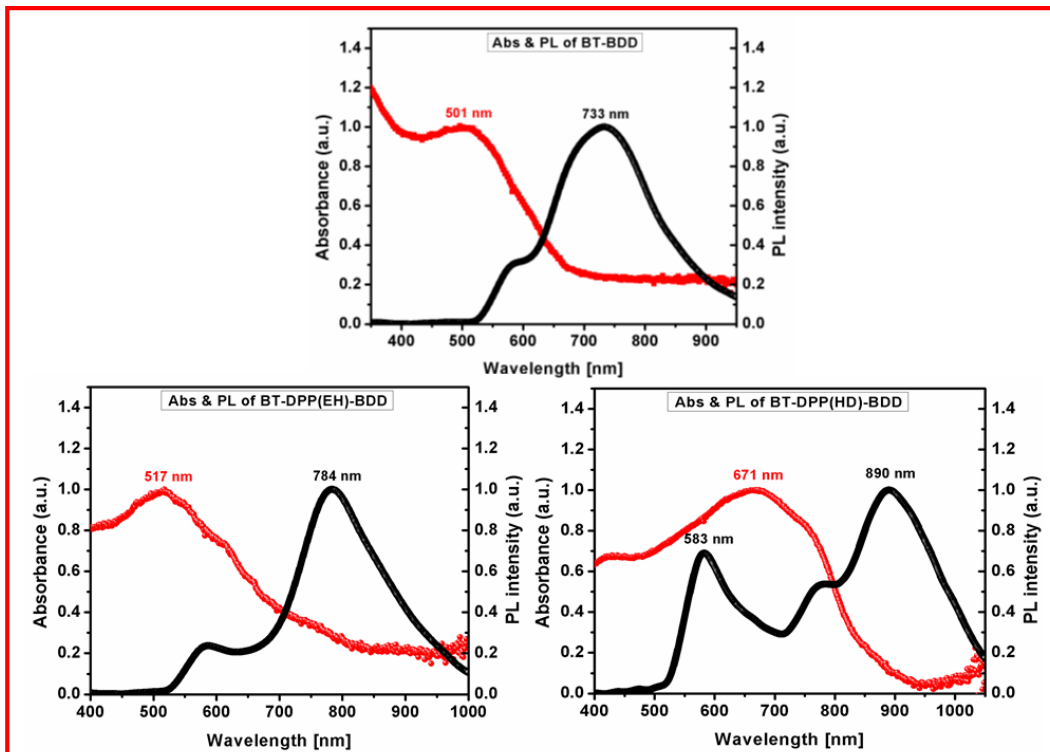


Figure 5.14 The absorption and photoluminescence spectra of thin films of copolymer and terpolymers solution comprising bithiophene (BT) as donor unit, spin coated from their chlorobenzene solution.

The absorption and photoluminescence spectra of thin films of terpolymers comprising BDT as donor unit, spin coated from chlorobenzene solution is depicted in **Figure 5.15**.

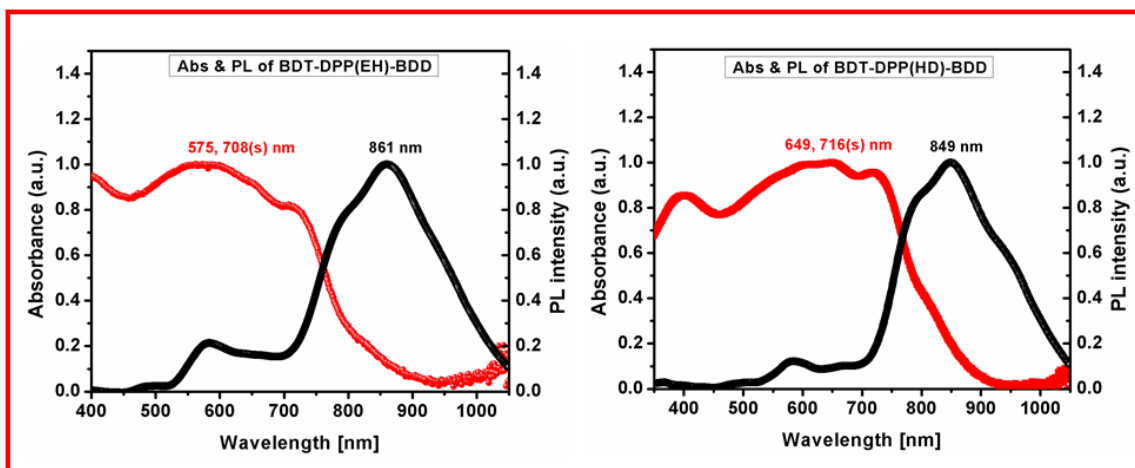


Figure 5.15 The absorption and photoluminescence spectra of thin films of terpolymers comprising BDT as donor unit, spin coated from chlorobenzene solution

The absorption maxima of various polymers in thin films were slightly red-shifted compared to that in solution. Also, there is broadening of the absorption spectra in films due to enhanced planarization of the molecules in films. These polymers are characterized by large Stoke's shift. Especially, stokes shift for thin films of terpolymers **BDT-DPP(EH)-BDD** and **BDT-DPP(HD)-BDD** is very high (153 and 133 nm, respectively). In case of these polymers, incorporation of planer BDT unit in the backbone of terpolymers, enhances planarization of polymer chains in solid state, facilitating stronger intermolecular interaction in terpolymer films, resulting in larger stokes shift. The optical band gap energies (calculated from onset of absorption, λ_{onset} in the film state) of all the polymers were found to be between 1.44 and 1.71 eV.

Table 5.3 Photophysical data of BDD based polymers in solution and on thin films

Polymers	λ_a [nm]	λ_f [nm]	λ_{onset} [nm]	E_g^{opt} [eV]
CPDT-BDD ^{a)}	625	-	728	1.70
BT-BDD	496	618	725	1.71
BT-BDD ^{a)}	501	733		
BT-DPP(EH)-BDD	505, 621(s)	618, 702(s)	814	1.52
BT-DPP(EH)-BDD ^{a)}	517	784		
BT-DPP(HD)-BDD	672	707	861	1.44
BT-DPP(HD)-BDD ^{a)}	671	890, 583		
BDT-DPP(EH)-BDD	656, 716(s)	686, 758(s)	832	1.49
BDT-DPP(EH)-BDD ^{a)}	575, 708(s)	861		
BDT-DPP(HD)-BDD	655, 717(s)	689, 762(s)	840	1.48
BDT-DPP(HD)-BDD ^{a)}	649, 716(s)	849		

Thin film spin coated from ^{a)} chloroform solution

The absorption and photoluminescence spectra of the pristine polymer films (red and black circles respectively) of all polymers and of the corresponding polymer-PC₇₀BM blend films (weight ratio 1:1) (blue and brown circles, respectively) is depicted in **Figure 5.16**. The films were spin-coated from chlorobenzene. It was observed that, there is a

quenching of photoluminescence in the blend due to photoinduced charge transfer from the polymer to PC₇₀BM except the polymers BT-DPP(HD)-BDD and BDT-DPP(HD)-BDD.

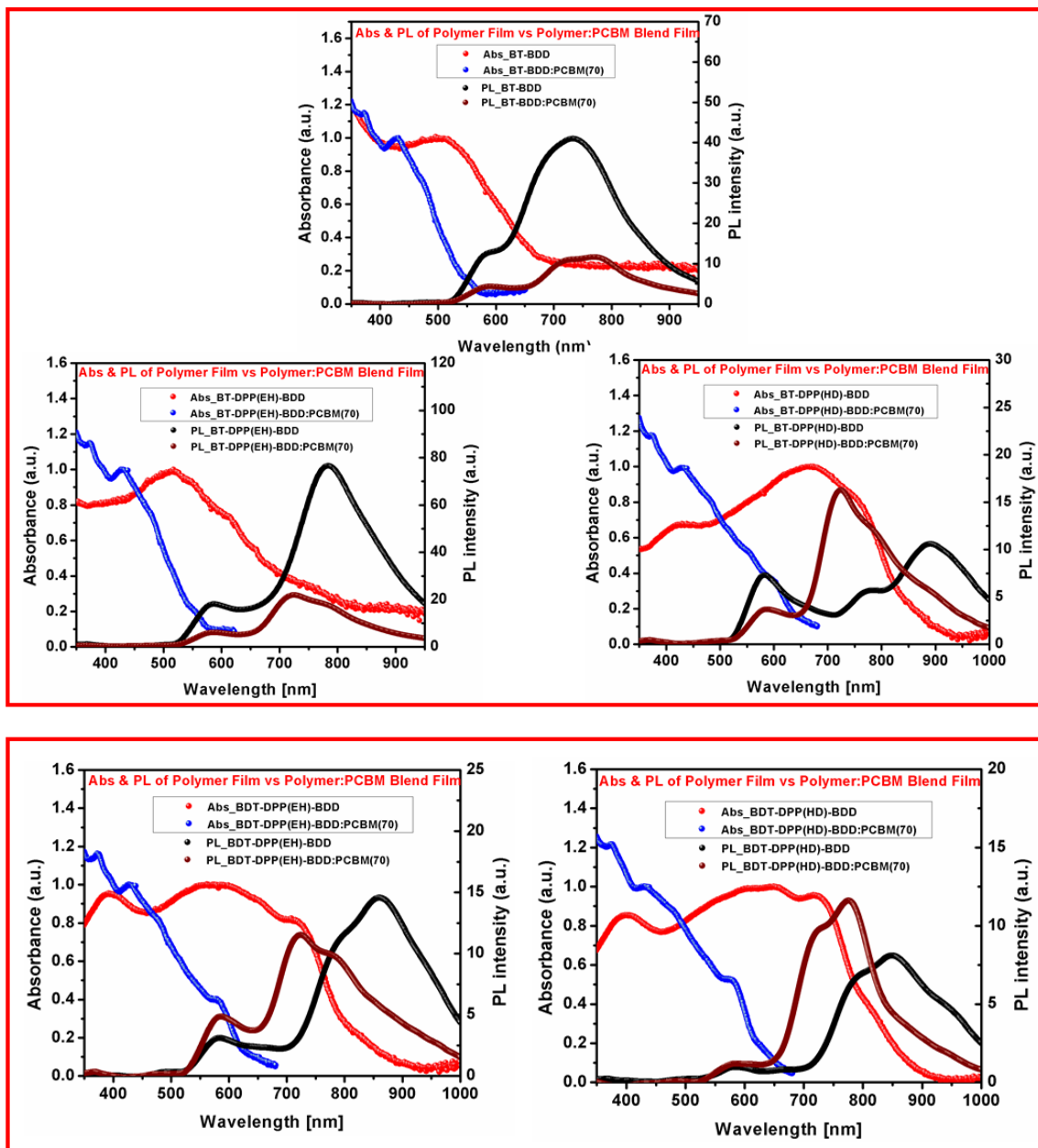


Figure 5.16 Thin film absorption and photoluminescence spectra of polymers and their 1:1 blends with PC₇₀BM

The absorption spectra of BDT-DPP(EH)-BDD exhibited a shoulder at around 716 nm, which is ascribed to the formation of aggregates, in dilute solution. This aggregate formation was confirmed by recording temperature-dependent absorption spectra of BDT-

DPP(EH)-BDD in chlorobenzene (**Figure 5.17**). Upon increasing the temperature from 20 to 60 °C, the shoulder band gradually disappeared with simultaneous blue shift of the absorption peak from 716 to 708 nm. Similarly, the terpolymer BDT-DPP(HD)-BDD also exhibited temperature dependent aggregation behaviour and blue shift of the absorption peak from 717 to 709 nm upon heating from 20 to 60 °C. This study proved that the heating and cooling process facilitates backbone planarization and stronger intermolecular interactions (aggregate formation) in polymer solution. Thus, this heating and cooling process might be useful to induce preorganization of polymers, before the spin-coating step, during device preparation.

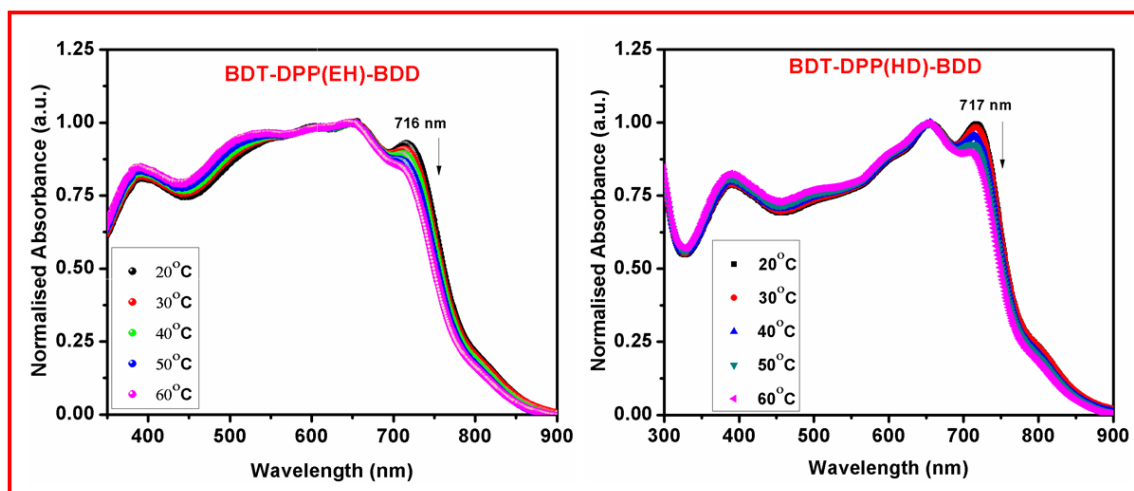


Figure 5.17 The temperature dependent absorption spectrum of BDT-DPP(EH)-BDD and BDT-DPP(HD)-BDD in chlorobenzene solution

5.4.8 Electrochemical Study

Electrochemical experiments were performed on thin polymer films drop coated from chlorobenzene solutions under inert condition by using cyclic voltammetry technique (CV). The HOMO and LUMO energy levels were estimated from oxidation and reduction onset potentials on the basis of the reference energy level of ferrocene (4.8 eV below the vacuum level) using the equations, $E_{\text{HOMO}} = -(E_{\text{onset, ox}} + 4.8)$ eV and $E_{\text{LUMO}} = -(E_{\text{onset, red}} + 4.8)$ eV. The CV curves are shown in the Supporting Information (Figure) and the electronic data are summarized in **Table 5.3** (values for $E_{\text{g}}^{\text{opt}}$ were included from **Table 5.2** for comparison).

Table 5.4 Electrochemical data for polymer films spin-coated from chlorobenzene solution

Polymers	HOMO (eV)	LUMO (eV)	E_g^{elc} (eV)	E_g^{opt} (eV)
CPDT-BDD	-4.99	-3.48	1.51	1.70
BT-BDD	-5.09	-3.50	1.59	1.71
BT-DPP(EH)-BDD	-5.05	-3.53	1.52	1.52
BT-DPP(HD)-BDD	-5.15	-3.49	1.66	1.44
BDT-DPP(EH)-BDD	-5.07	-3.51	1.56	1.49
BDT-DPP(HD)-BDD	-5.13	-3.55	1.58	1.48

The electrochemical band gap energy, E_g^{elc} for all polymers was found in the range 1.51-1.66 eV. The difference, between E_g^{opt} and E_g^{elc} , may be related, along with other reasons, to the differences in thin film preparation during the optical and electrochemical process, resulting in differences in thin film thicknesses and backbone coplanarity.

5.4.9 Photovoltaic Studies

Photovoltaic devices based on polymer:PCBM active layers with weight ratios of 1:1 were prepared and optimized by variation of solution concentration and film thickness. Influence of additive (DIO) was also studied. Two polymers among the series – copolymer CPDT-BDD and terpolymer BDT-DPP(EH)-BDD exhibited solar cell device performance. For CPDT-BDD polymer, solar cells were prepared by the both the configurations: conventional (glass substrate/ ITO/PEDOT:PSS/active layer/Mg/Al) and inverted (glass substrate/ ITO/ZnO/active layer/MoO₃/Al). **Figure 5.18** depicted the current-voltage (*J-V*) curves of the solar cells based on polymer: PC₇₀BM (1:1) active layers. A solar simulator (AM1.5, class A) was used for illumination.

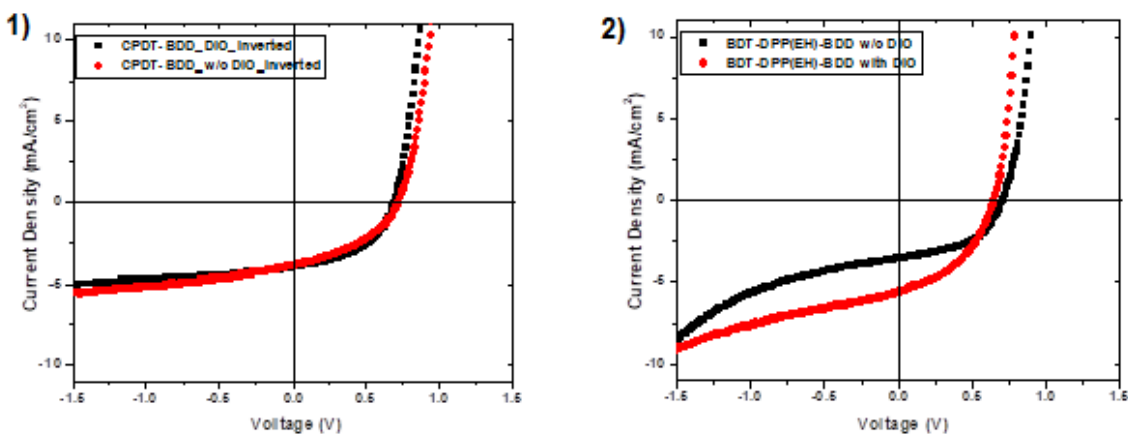


Figure 5.18 J - V curves of solar cells incorporating polymer: PC₇₀BM active layers of 1) CPDT-BDD 2) BDT-DPP(EH)-BDD

In **Table 5.4**, are summarized the photovoltaic parameters obtained from current density-voltage (J - V) measurements for polymer: PCBM blends. These include the short circuit current, (J_{SC}) the open circuit voltage (V_{OC}), the fill factor (FF), the series and parallel resistance (R_S and R_p). In general, solar cells with active layers having higher fullerene contents yielded higher power conversion efficiencies (η). CPDT-BDD polymer exhibited highest power conversion efficiency (η) of 1.63 %, in inverted device architecture, without DIO. Terpolymer BDT-DPP(EH)-BDD showed power conversion efficiency of 1.57 % in conventional device architecture, in presence of DIO. Other copolymers and terpolymers exhibited negligible photovoltaic performance.

Table 5.5 Photovoltaic parameters for polymer solar cells

Polymer	Additive	J_{sc} (mA/cm ²)	V_{oc} (mV)	FF (%)	PCE (%)	R_s (Ohm)	R_p (Ohm)
CPDT-BDD conventional	-	4.726	675	43	1.39	5	1073
CPDT-BDD Inverted	-	4.533	766	47	1.63	8	1541
BDT- DPP(EH)-BDD	DIO	5.629	646	43	1.57	7	789

In case of BDD based terpolymers, superior photovoltaic properties were expected from polymer BDT-DPP(HD)-BDD as compared to BDT-DPP(EH)-BDD, since the

former one has longer solubilizing side chains and higher molecular weight. Absorption spectrum of the polymer BDT-DPP(HD)-BDD was also redshifted by 167 nm than that of polymer BDT-DPP(EH)-BDD. In spite of this, the polymer BDT-DPP(HD)-BDD showed inferior photovoltaic performance which can be explained by Atomic force microscopy studies and photoluminescence studies. The AFM topography images of polymer:PC₇₀BM blend is shown in **Figure 5.19**. It was observed that the blend film of polymer BDT-DPP(EH)-BDD has much smooth surface than the blend film of polymer BDT-DPP(HD)-BDD. In fact, the polymer BDT-DPP(HD)-BDD is phase separating in the blend film to form bead like structures. This unfavorable morphology limits the exciton dissociation due to the reduced donor acceptor interfacial area and hence the inferior photovoltaic performance. The longer hexyl decyl sidechains on DPP unit might be causing steric hindrance and disturbing the planarity of polymer BDT-DPP(HD)-BDD. Such a phenomenon was also observed by Lee et al.⁵⁴ The PL spectrum of this polymer:PCBM blend didn't show quenching of photoluminescence (as a result of energy transfer from polymer to PC₇₀BM) which further supported the observed results.

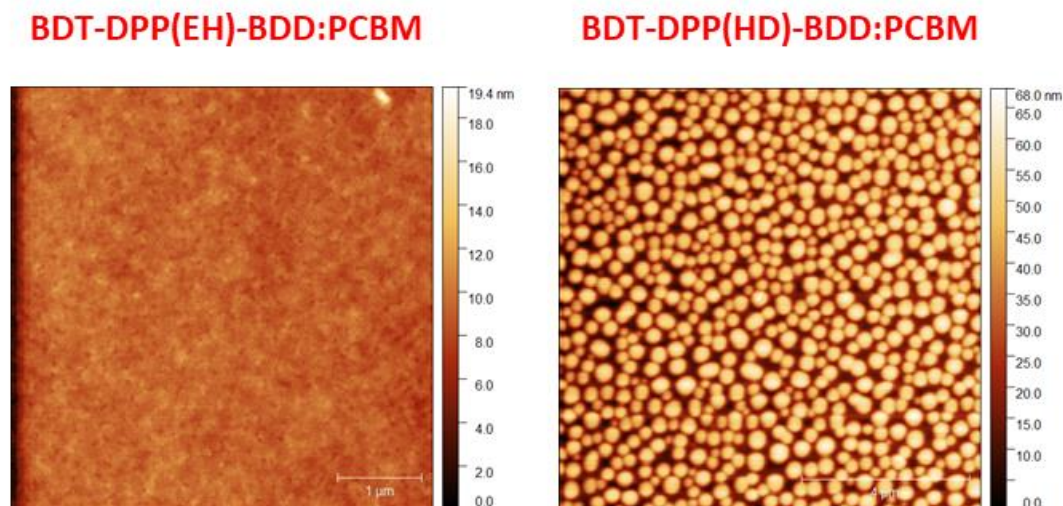


Figure 5.19 AFM image of active layer (polymer:PC₇₀BM blend film) of polymer BDT-DPP(EH)-BDD and BDT-DPP(HD)-BDD.

5.5 CONCLUSIONS

In summary, two copolymers and four terpolymers comprising cyclopentadithiophene (CPDT), bithiophene (BT), benzo[1,2-b:4,5-b']dithiophene (BDT)

as electron donor units and diketopyrrolopyrrole (DPP), benzo[1,2-c:4,5-c']dithiophene-4,8-dione (BDD) as electron acceptor units were synthesized and characterized by ^1H and ^{13}C -NMR spectroscopy. Terpolymers showed much broader absorption in visible and near IR region of light spectrum and improved solubility in common solvents as compared to copolymers comprising same electron donor and electron acceptor units. Terpolymers BDT-DPP(EH)-BDD and BDT-DPP(HD)-BDD exhibited temperature dependent UV-Vis absorption spectra indicating presence of aggregates. This property can be utilized to manipulate morphology of active layer in the fabrication of solar cell devices. The two polymers -CPDT-BDD and BDT-DPP(EH)-BDD were used as donor material with PC₇₀BM to evaluate their performance in bulk heterojunction solar cells. CPDT-BDD polymer showed maximum power conversion efficiency of 1.63 % and 1.39 % in inverted and conventional device architecture, respectively. The terpolymer BDT-DPP(EH)-BDD exhibited $\eta=1.57$ % in conventional device. The terpolymer BDT-DPP(HD)-BDD showed negligible solar cell performance as compared to polymer BDT-DPP(EH)-BDD which is attributed to the longer side chains on this polymer causing steric hindrance and thus the unsuitable morphology in polymer:PC₇₀BM blend film used as active layer in device fabrication process. The results were confirmed by atomic force microscopy studies and photoluminescence studies.

REFERENCES

- 1 S. Zhang, Y. Qin, J. Zhu and J. Hou, *Adv. Mater.*, 2018, **30**, 1800868.
- 2 R. Geng, X. Song, H. Feng, J. Yu, M. Zhang, N. Gasparini, Z. Zhang, F. Liu, D. Baran and W. Tang, *ACS Energy Lett.*, 2019, **4**, 763–770.
- 3 S. Li, L. Ye, W. Zhao, H. Yan, B. Yang, D. Liu, W. Li, H. Ade and J. Hou, *J. Am. Chem. Soc.*, 2018, **140**, 7159–7167.
- 4 Z. Xiao, X. Jia and L. Ding, *Sci. Bull.*, 2017, **62**, 1562–1564.
- 5 C. Duan, A. Furlan, J. J. van Franeker, R. E. M. Willems, M. M. Wienk and R. A. J. Janssen, *Adv. Mater.*, 2015, **27**, 4461–4468.
- 6 Y. Jin, Z. Chen, S. Dong, N. Zheng, L. Ying, X.-F. Jiang, F. Liu, F. Huang and Y. Cao, *Adv. Mater.*, 2016, **28**, 9811–9818.
- 7 D. Liu, Q. Zhu, C. Gu, J. Wang, M. Qiu, W. Chen, X. Bao, M. Sun and R. Yang,

- Adv. Mater.*, 2016, **28**, 8490–8498.
- 8 H. Hu, K. Jiang, G. Yang, J. Liu, Z. Li, H. Lin, Y. Liu, J. Zhao, J. Zhang, F. Huang, Y. Qu, W. Ma and H. Yan, *J. Am. Chem. Soc.*, 2015, **137**, 14149–14157.
- 9 L. Huo, T. Liu, X. Sun, Y. Cai, A. J. Heeger and Y. Sun, *Adv. Mater.*, 2015, **27**, 2938–2944.
- 10 Z. Ma, D. Dang, Z. Tang, D. Gedefaw, J. Bergqvist, W. Zhu, W. Mammo, M. R. Andersson, O. Inganäs, F. Zhang and E. Wang, *Adv. Energy Mater.*, 2014, **4**, 1301455.
- 11 Y. Liu, J. Zhao, Z. Li, C. Mu, W. Ma, H. Hu, K. Jiang, H. Lin, H. Ade and H. Yan, *Nat. Commun.*, 2014, **5**, 5293.
- 12 D. Dang, W. Chen, S. Himmelberger, Q. Tao, A. Lundin, R. Yang, W. Zhu, A. Salleo, C. Müller and E. Wang, *Adv. Energy Mater.*, 2014, **4**, 1400680.
- 13 D. Dang, D. Yu and E. Wang, *Adv. Mater.*, 2019, **31**, 1807019.
- 14 X. Huang, G. Zhang, C. Zhou, L. Liu, Y. Jin, S. Liu, L. Ying, F. Huang and Y. Cao, *Polym. Chem.*, 2015, **6**, 4154–4161.
- 15 D. Dang, W. Chen, R. Yang, W. Zhu, W. Mammo and E. Wang, *Chem. Commun.*, 2013, **49**, 9335.
- 16 T. Qin, W. Zajaczkowski, W. Pisula, M. Baumgarten, M. Chen, M. Gao, G. Wilson, C. D. Easton, K. Müllen and S. E. Watkins, *J. Am. Chem. Soc.*, 2014, **136**, 6049–6055.
- 17 J. Zhou, S. Xie, E. F. Amond and M. L. Becker, *Macromolecules*, 2013, **46**, 3391–3394.
- 18 Q. Tao, Y. Xia, X. Xu, S. Hedström, O. Bäcke, D. I. James, P. Persson, E. Olsson, O. Inganäs, L. Hou, W. Zhu and E. Wang, *Macromolecules*, 2015, **48**, 1009–1016.
- 19 B. Fan, X. Xue, X. Meng, X. Sun, L. Huo, W. Ma and Y. Sun, *J. Mater. Chem. A*, 2016, **4**, 13930–13937.
- 20 L. Fang, Y. Zhou, Y.-X. Yao, Y. Diao, W.-Y. Lee, A. L. Appleton, R. Allen, J. Reinspach, S. C. B. Mannsfeld and Z. Bao, *Chem. Mater.*, 2013, **25**, 4874–4880.
- 21 W.-H. Chang, J. Gao, L. Dou, C.-C. Chen, Y. Liu and Y. Yang, *Adv. Energy Mater.*, 2014, **4**, 1300864.
- 22 L. Huo, X. Xue, T. Liu, W. Xiong, F. Qi, B. Fan, D. Xie, F. Liu, C. Yang and Y.

- Sun, *Chem. Mater.*, 2018, **30**, 3294–3300.
- 23 B. Burkhart, P. P. Khlyabich and B. C. Thompson, *ACS Macro Lett.*, 2012, **1**, 660–666.
- 24 K.-H. Kim, S. Park, H. Yu, H. Kang, I. Song, J. H. Oh and B. J. Kim, *Chem. Mater.*, 2014, **26**, 6963–6970.
- 25 Y. Ie, J. Huang, Y. Uetani, M. Karakawa and Y. Aso, *Macromolecules*, 2012, **45**, 4564–4571.
- 26 D. Qian, L. Ye, M. Zhang, Y. Liang, L. Li, Y. Huang, X. Guo, S. Zhang, Z. Tan and J. Hou, *Macromolecules*, 2012, **45**, 9611–9617.
- 27 D. Qian, W. Ma, Z. Li, X. Guo, S. Zhang, L. Ye, H. Ade, Z. Tan and J. Hou, *J. Am. Chem. Soc.*, 2013, **135**, 8464–8467.
- 28 Q. Wang, S. Zhang, L. Ye, Y. Cui, H. Fan and J. Hou, *Macromolecules*, 2014, **47**, 5558–5565.
- 29 X. Huang, K. Weng, L. Huo, B. Fan, C. Yang, X. Sun and Y. Sun, *J. Mater. Chem. C*, 2016, **4**, 9052–9059.
- 30 S. Zhang, Y. Qin, M. A. Uddin, B. Jang, W. Zhao, D. Liu, H. Y. Woo and J. Hou, *Macromolecules*, 2016, **49**, 2993–3000.
- 31 H. Zhang, S. Zhang, K. Gao, F. Liu, H. Yao, B. Yang, C. He, T. P. Russell and J. Hou, *J. Mater. Chem. A*, 2017, **5**, 10416–10423.
- 32 H. Zhang, Y. Liu, Y. Sun, M. Li, B. Kan, X. Ke, Q. Zhang, X. Wan and Y. Chen, *Chem. Commun.*, 2017, **53**, 451–454.
- 33 T. Liu, X. Pan, X. Meng, Y. Liu, D. Wei, W. Ma, L. Huo, X. Sun, T. H. Lee, M. Huang, H. Choi, J. Y. Kim, W. C. H. Choy and Y. Sun, *Adv. Mater.*, 2017, **29**, 1604251.
- 34 Z. Xu, Q. Fan, X. Meng, X. Guo, W. Su, W. Ma, M. Zhang and Y. Li, *Chem. Mater.*, 2017, **29**, 4811–4818.
- 35 T. Zhu, D. Liu, K. Zhang, Y. Li, Z. Liu, X. Gao, X. Bao, M. Sun and R. Yang, *J. Mater. Chem. A*, 2018, **6**, 948–956.
- 36 H. Bohra, H. Chen, Y. Peng, A. Efrem, F. He and M. Wang, *J. Polym. Sci. Part A Polym. Chem.*, 2018, **56**, 2554–2564.
- 37 Y. Li, L. Duan, D. Liu, W. Chen, X. Bao, H. Zhen, H. Liu and R. Yang, *J. Mater.*

- Chem. C*, 2018, **6**, 2806–2813.
- 38 Z. Jiang, H. Li, Z. Wang, J. Zhang, Y. Zhang, K. Lu and Z. Wei, *Macromol. Rapid Commun.*, 2018, **39**, 1700872.
- 39 Y. Wu, C. An, L. Shi, L. Yang, Y. Qin, N. Liang, C. He, Z. Wang and J. Hou, *Angew. Chemie Int. Ed.*, 2018, **57**, 12911–12915.
- 40 B. Huang, L. Chen, X. Jin, D. Chen, Y. An, Q. Xie, Y. Tan, H. Lei and Y. Chen, *Adv. Funct. Mater.*, 2018, **28**, 1800606.
- 41 Q. Zhu, D. Liu, Z. Lu, C. Gu, K. Zhang, X. Bao, Q. Li and R. Yang, *J. Mater. Chem. A*, 2019, **7**, 4823–4828.
- 42 T. E. Kang, H.-H. Cho, H. jun Kim, W. Lee, H. Kang and B. J. Kim, *Macromolecules*, 2013, **46**, 6806–6813.
- 43 J. W. Lee, H. Ahn and W. H. Jo, *Macromolecules*, 2015, **48**, 7836–7842.
- 44 Z. Li, Z. Wang, W. Liu, Y. Cui, H. Wang, F. Shi and Y. Hao, *J. Mater. Sci.*, 2015, **50**, 5363–5370.
- 45 Q. Fan, Y. Liu, M. Xiao, W. Su, H. Gao, J. Chen, H. Tan, Y. Wang, R. Yang and W. Zhu, *J. Mater. Chem. C*, 2015, **3**, 6240–6248.
- 46 P. Qi, Z. Wang, Z. Liu, S. Yang, Y. Yang, J. Yao, G. Zhang and D. Zhang, *Polym. Chem.*, 2016, **7**, 3838–3847.
- 47 M. L. Keshtov, A. R. Khokhlov, S. A. Kuklin, F. C. Chen, A. Y. Nikolaev, E. N. Koukaras and G. D. Sharma, *Polym. Chem.*, 2016, **7**, 4025–4035.
- 48 H. J. Kim, G. E. Park, D. H. Lee, M. J. Cho and D. H. Choi, *Org. Electron. physics, Mater. Appl.*, 2016, **38**, 256–263.
- 49 X. Pan, W. Xiong, T. Liu, X. Sun, L. Huo, D. Wei, M. Yu, M. Han and Y. Sun, *J. Mater. Chem. C*, 2017, **5**, 4471–4479.
- 50 M. Jeong, S. Chen, S. M. Lee, Z. Wang, Y. Yang, Z.-G. Zhang, C. Zhang, M. Xiao, Y. Li and C. Yang, *Adv. Energy Mater.*, 2018, **8**, 1702166.
- 51 M. H. Hoang, G. E. Park, S. Choi, C. G. Park, S. H. Park, T. Van Nguyen, S. Kim, K. Kwak, M. J. Cho and D. H. Choi, *J. Mater. Chem. C*, 2019, **7**, 111–118.
- 52 Z. Li, K. Weng, A. Chen, X. Sun, D. Wei, M. Yu, L. Huo and Y. Sun, *Macromol. Rapid Commun.*, 2018, **39**, 1700547.
- 53 D. D. Armarego, K. N., Perrin, in *Purification of Laboratory Chemicals*,

Butterworth-Heinemann, Oxford, 4th Edition, Butterworth Heinemann, 1996.

- 54 Y.-S. Lee, J. Y. Lee, S.-M. Bang, B. Lim, J. Lee and S.-I. Na, *J. Mater. Chem. A*, 2016, **4**, 11439–11445.

Supporting Information

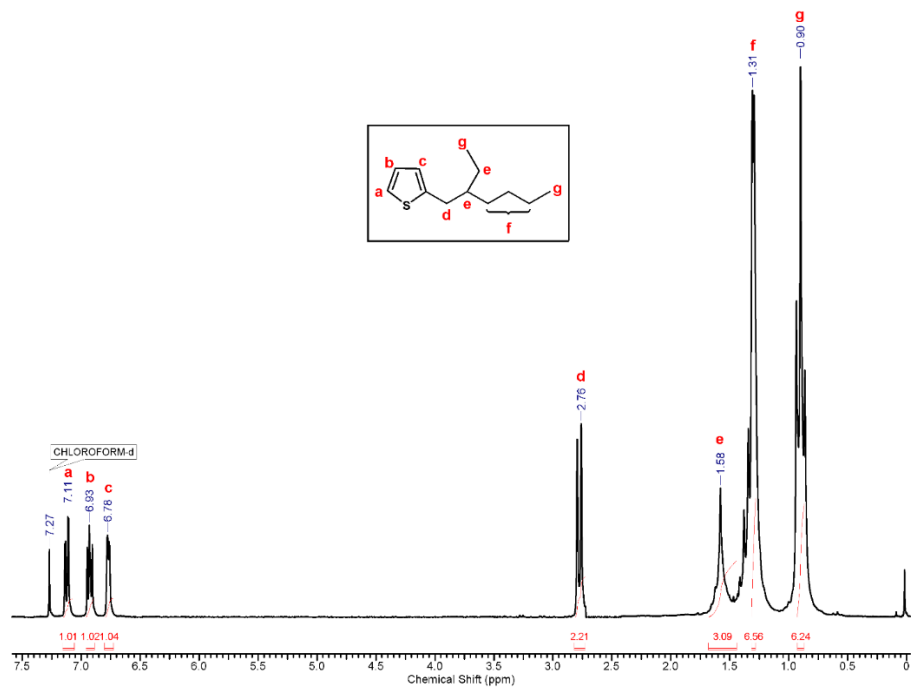


Figure SI 5.1 ¹H-NMR spectrum (CDCl₃) of 2-(2-ethylhexyl)thiophene (1)

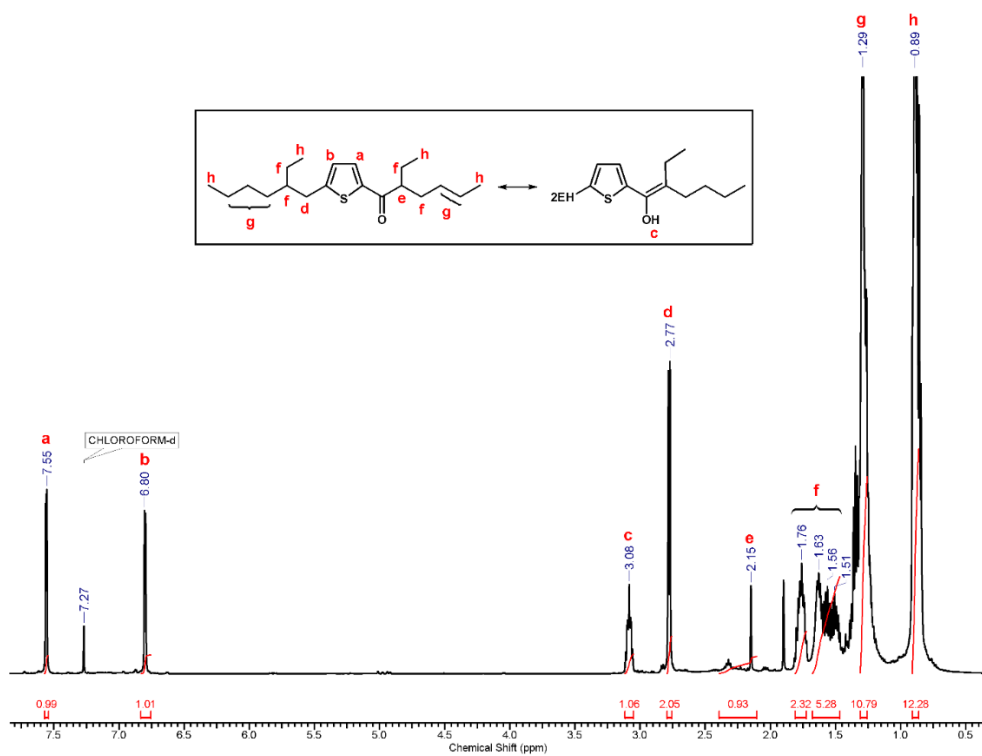


Figure SI 5.2 ¹H-NMR spectrum (CDCl₃) of 2-ethyl-1-(5-(2-ethylhexyl)thiophen-2-yl)hexan-1-one (2)

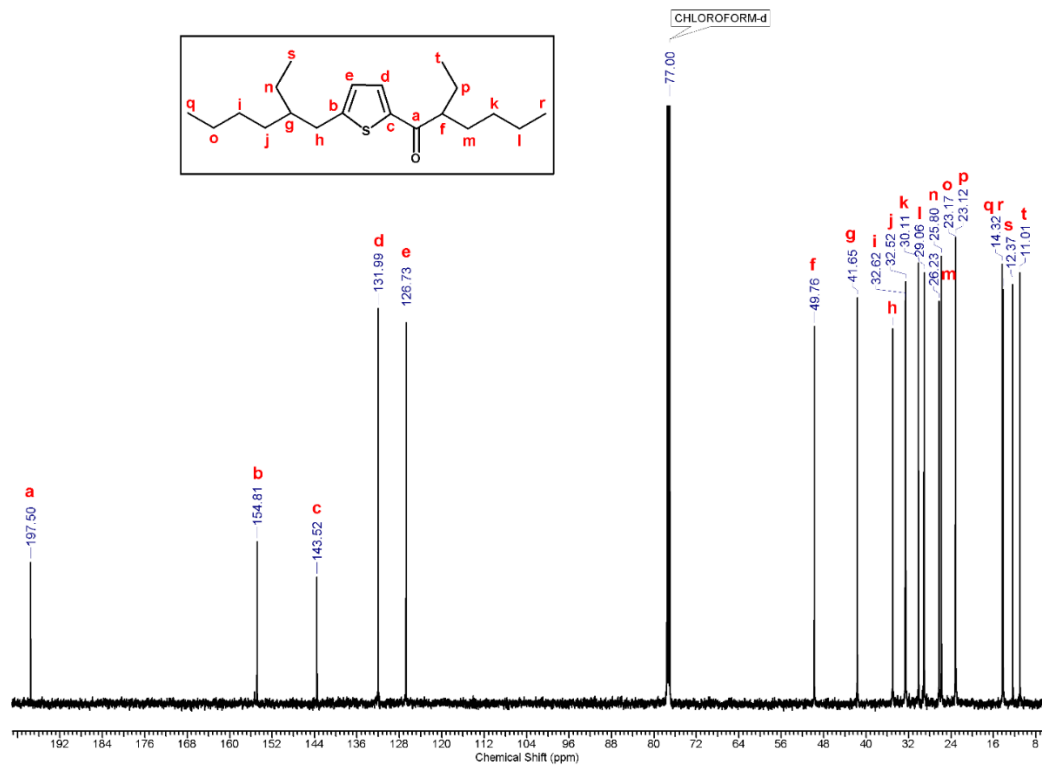


Figure SI 5.3 ^{13}C -NMR spectrum (CDCl₃) of 2-ethyl-1-(5-(2-ethylhexyl)thiophen-2-yl)hexan-1-one (2)

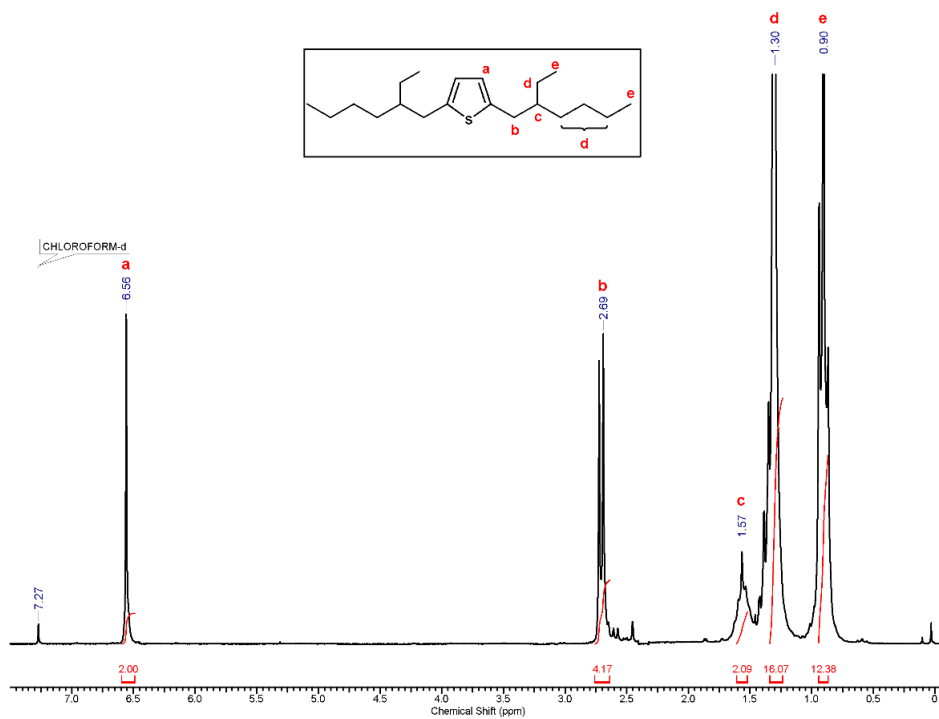


Figure SI 5.4 ^1H -NMR spectrum (CDCl₃) of 2,5-bis(2-ethylhexyl)thiophene (3)

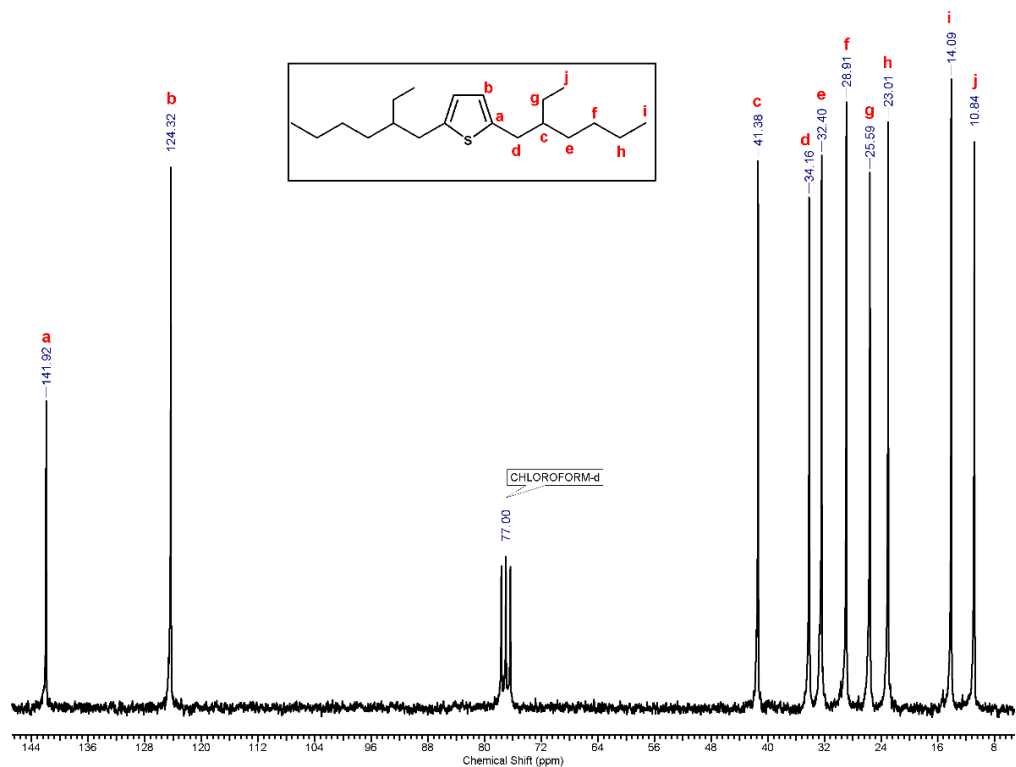


Figure SI 5.5 ^{13}C -NMR spectrum (CDCl₃) of 2,5-bis(2-ethylhexyl)thiophene (3)

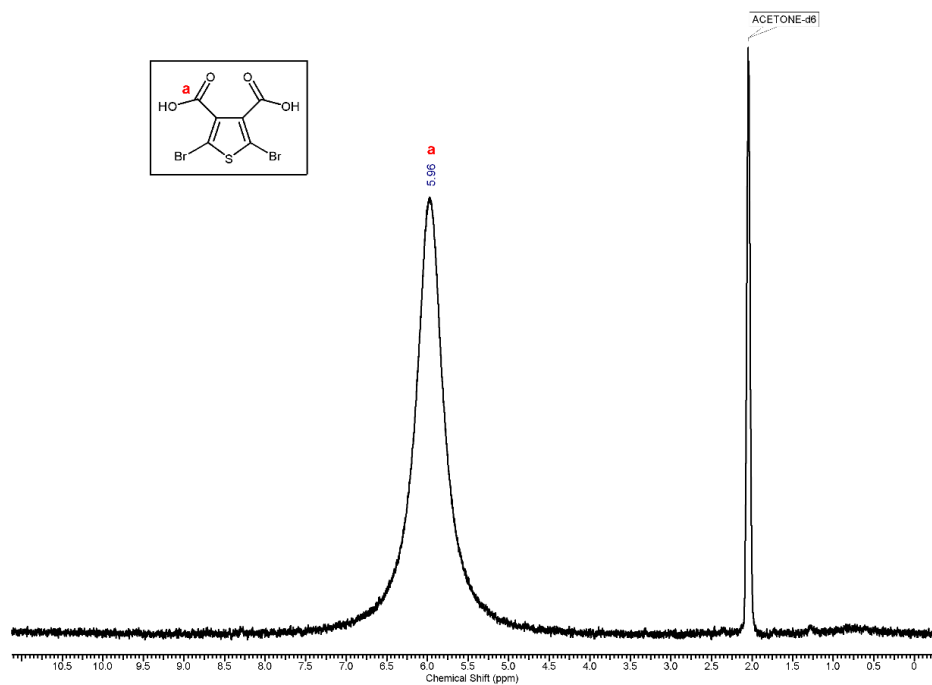


Figure SI 5.6 ^1H -NMR spectrum (Acetone-d₆) of 2,5-dibromothiophene-3,4-dicarboxylic acid (4)

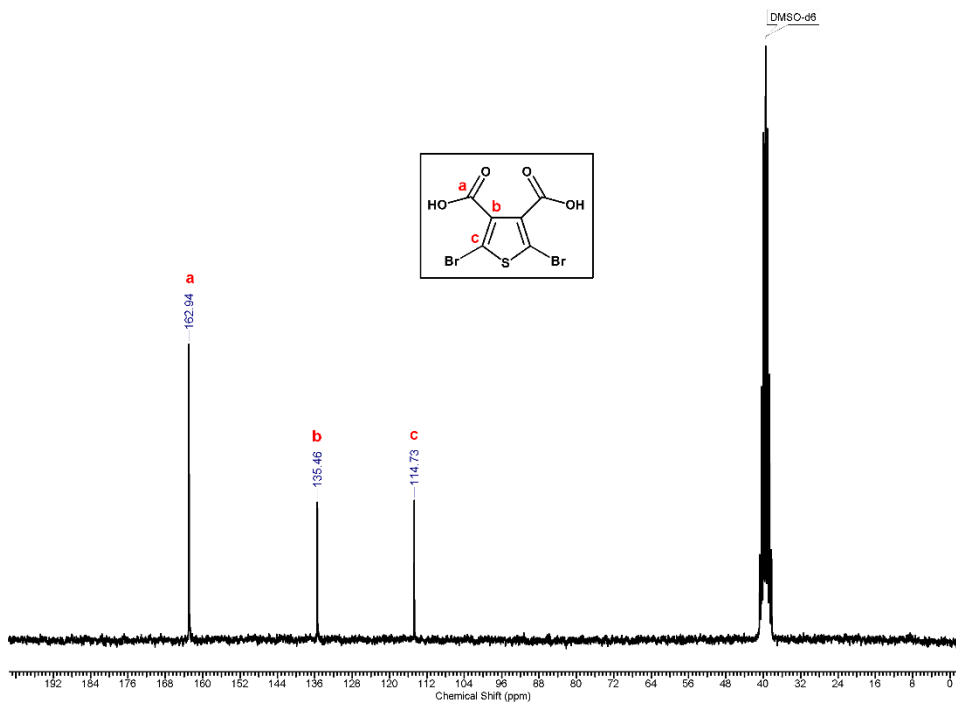


Figure SI 5.7 ¹³C-NMR spectrum (Acetone-d₆) of 2,5-dibromothiophene-3,4-dicarboxylic acid (4)

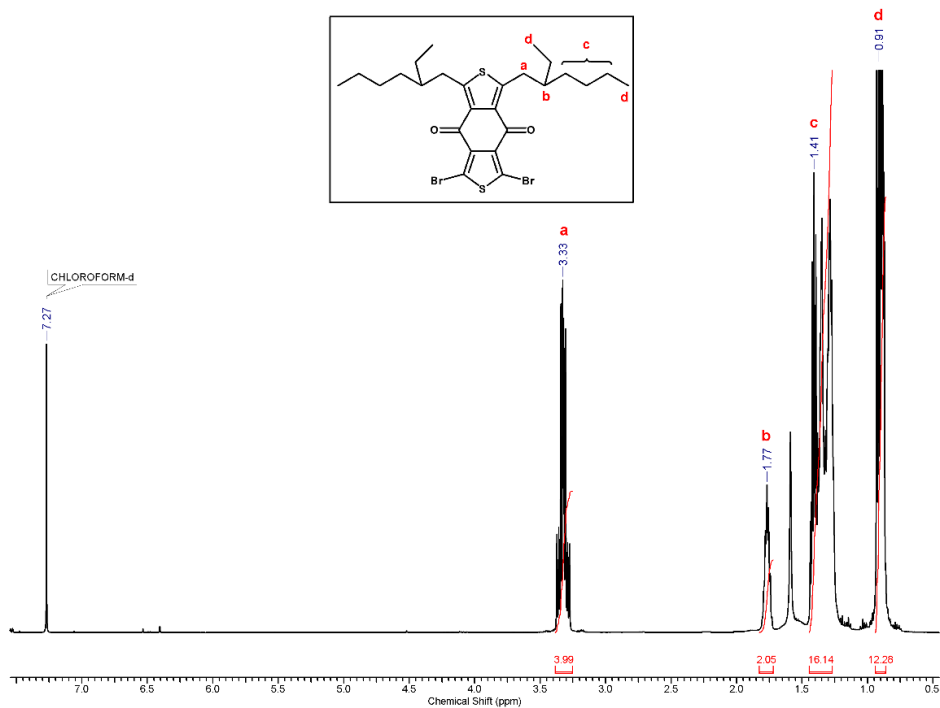


Figure SI 5.8 ¹H-NMR spectrum (CDCl₃) of 1,3-dibromo-5,7-bis(2-ethylhexyl)-4H,8H-benzo[1,2-c:4,5-c']dithiophene-4,8-dione (5)

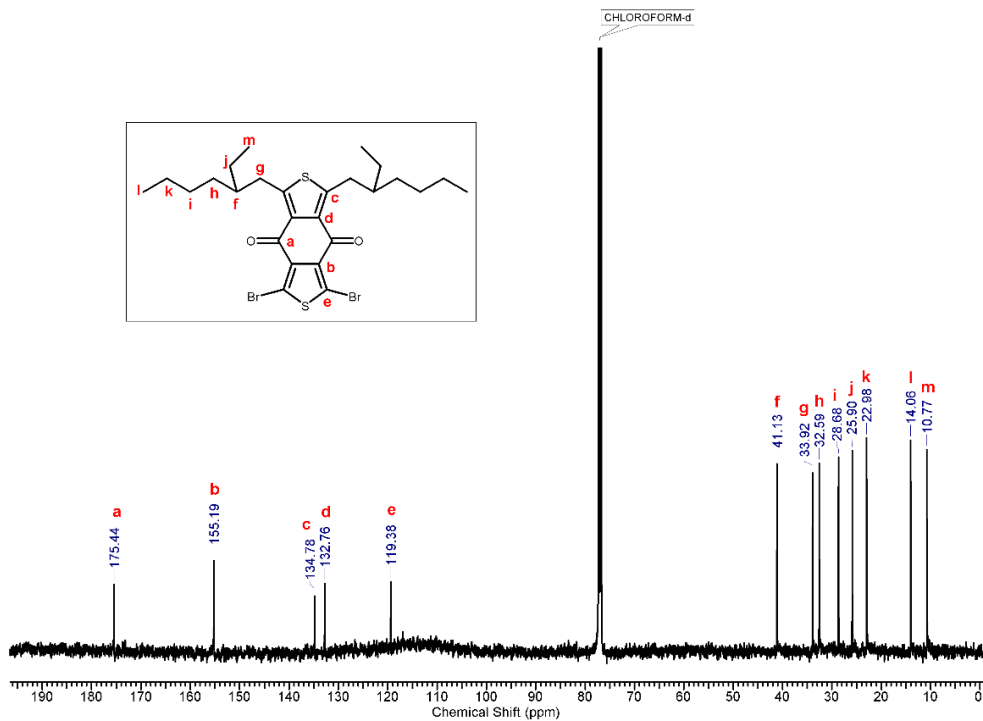


Figure SI 5.9 ¹³C-NMR spectrum (CDCl₃) of 1,3-dibromo-5,7-bis(2-ethylhexyl)-4H,8H-benzo[1,2-c:4,5-c']dithiophene-4,8-dione (5)

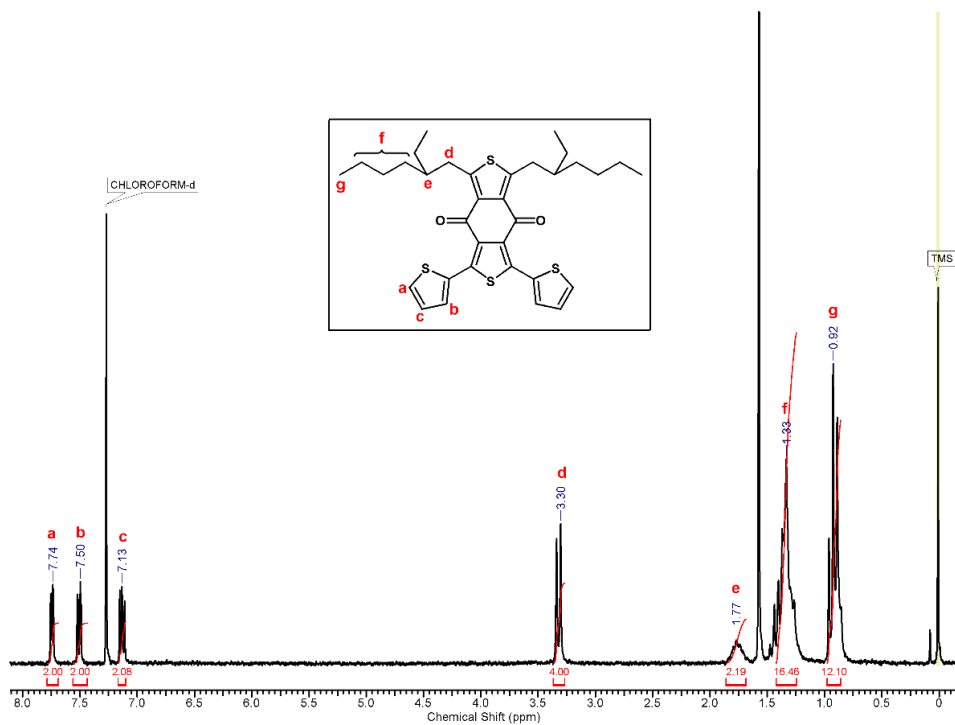


Figure SI 5.10 ¹H-NMR spectrum (CDCl₃) of 1,3-bis(2-ethylhexyl)-5,7-di(thiophen-2-yl)benzo[1,2-c:4,5-c']dithiophene-4,8-dione (6)

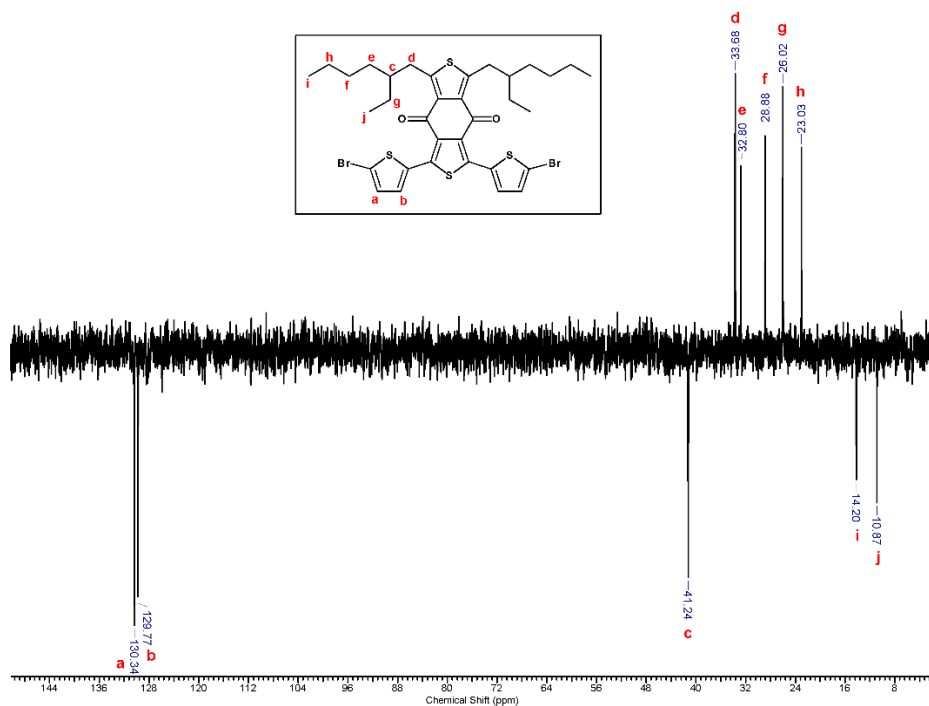


Figure SI 5.11 ^{13}C -DEPT-NMR spectrum (CDCl₃) of 1,3-bis(5-bromothiophen-2-yl)-5,7-bis(2-ethylhexyl)-benzo[1,2-c:4,5-c']dithiophene-4,8-dione (BDD monomer)

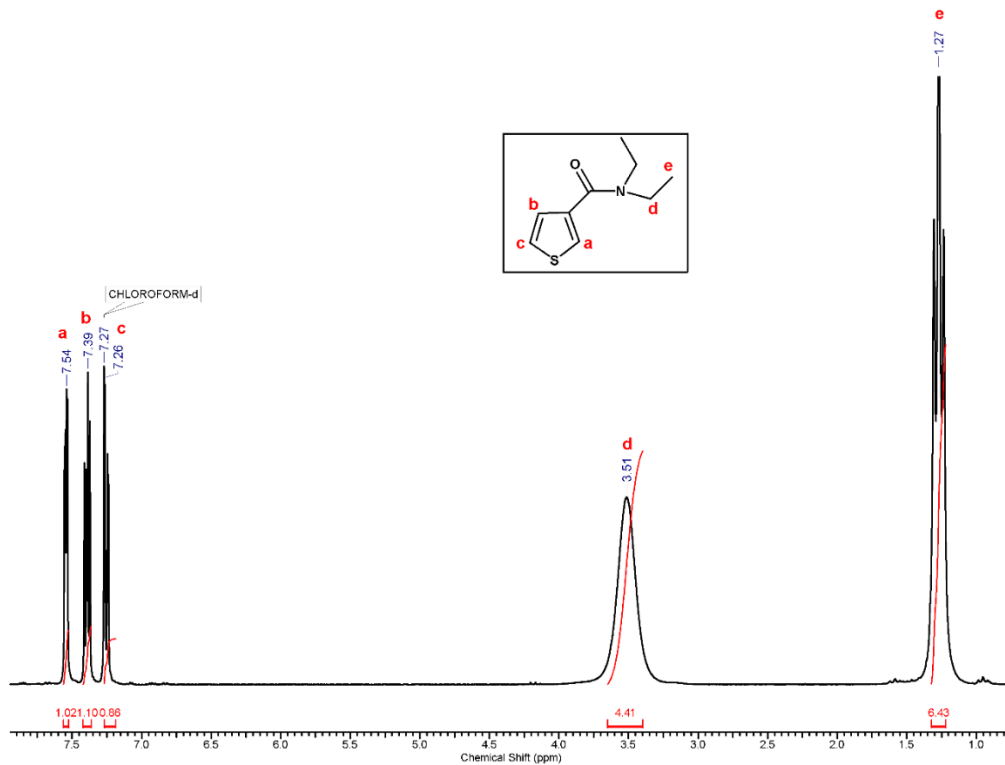
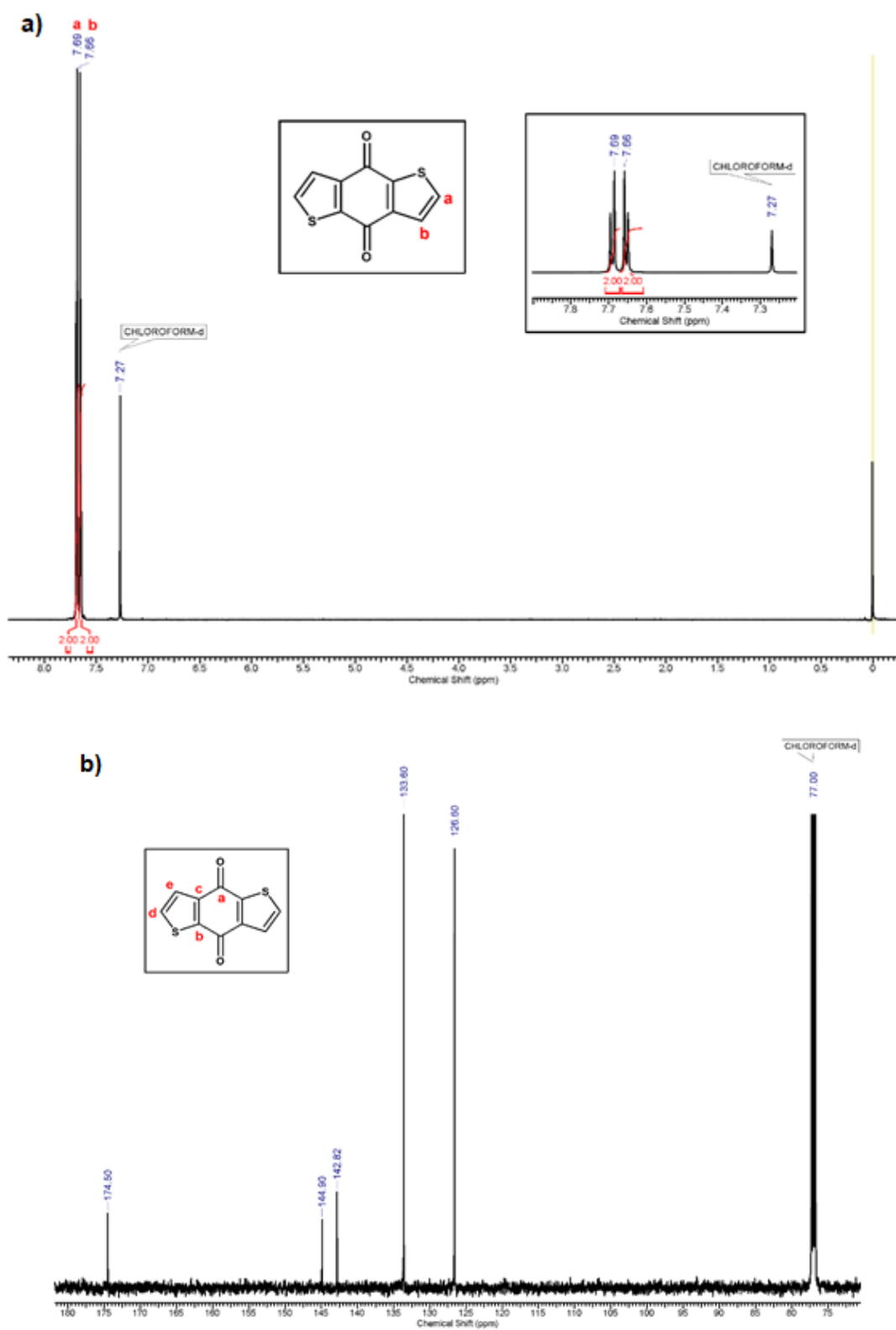


Figure SI 5.12 ^1H -NMR spectrum (CDCl₃) of N,N-diethylthiophene-3-carboxamide (9)



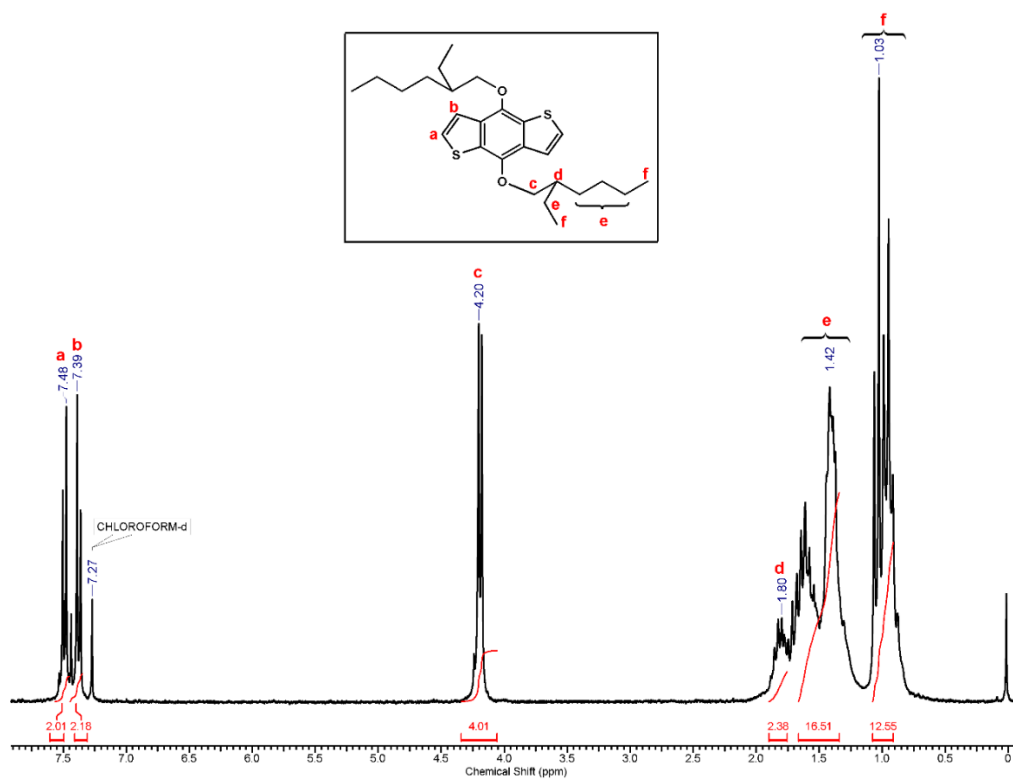


Figure SI 5.14 ¹H-NMR spectrum (CDCl₃) of 4,8-bis((2-ethylhexyl)oxy)benzo[1,2-b:4,5-b']dithiophene (11).

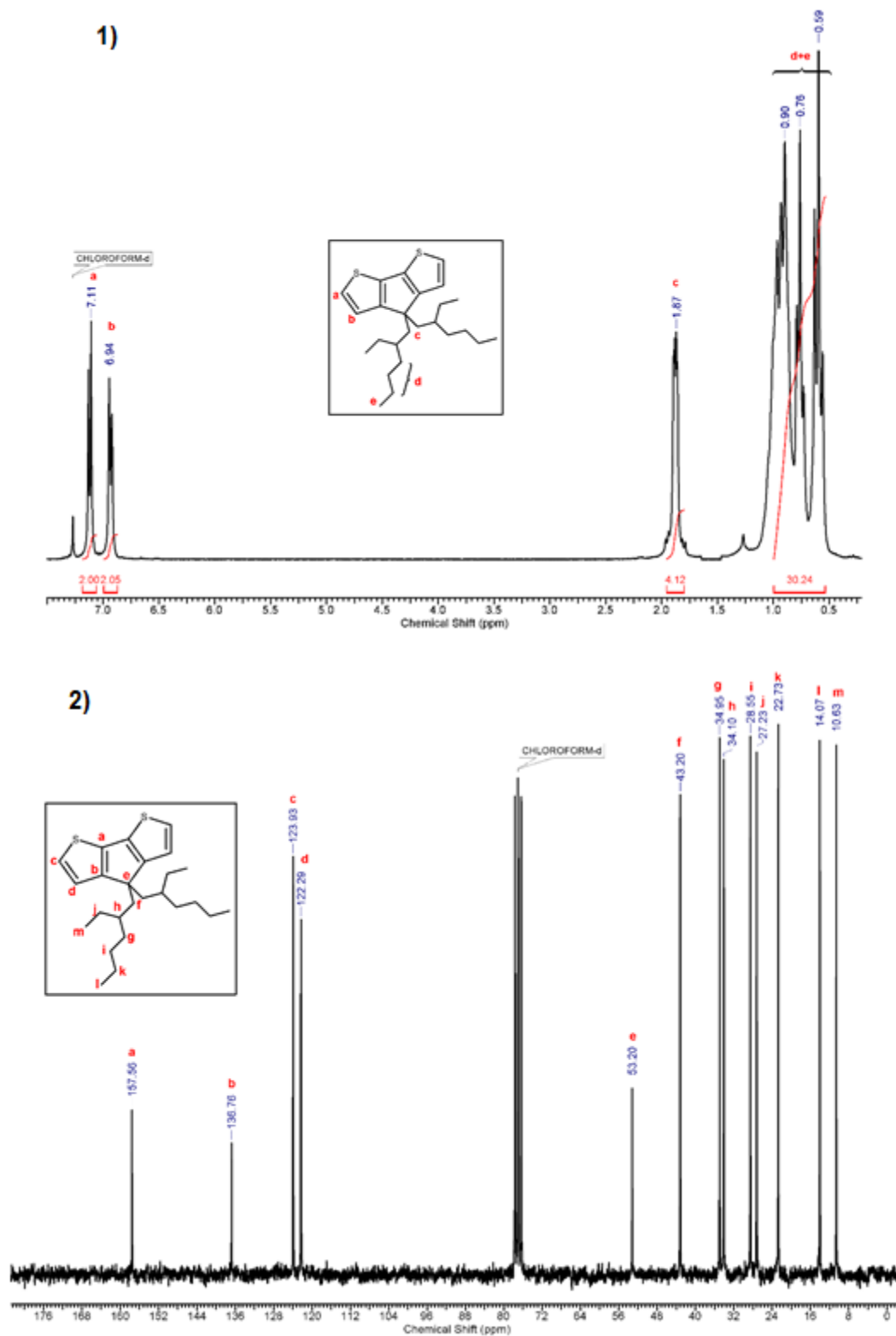


Figure SI 5.15 1) ^1H -NMR spectrum and 2) ^{13}C -NMR spectrum (CDCl_3) of 4,4-bis(2-ethylhexyl)-4H-cyclopenta[2,1-b:3,4-b']dithiophene (13)

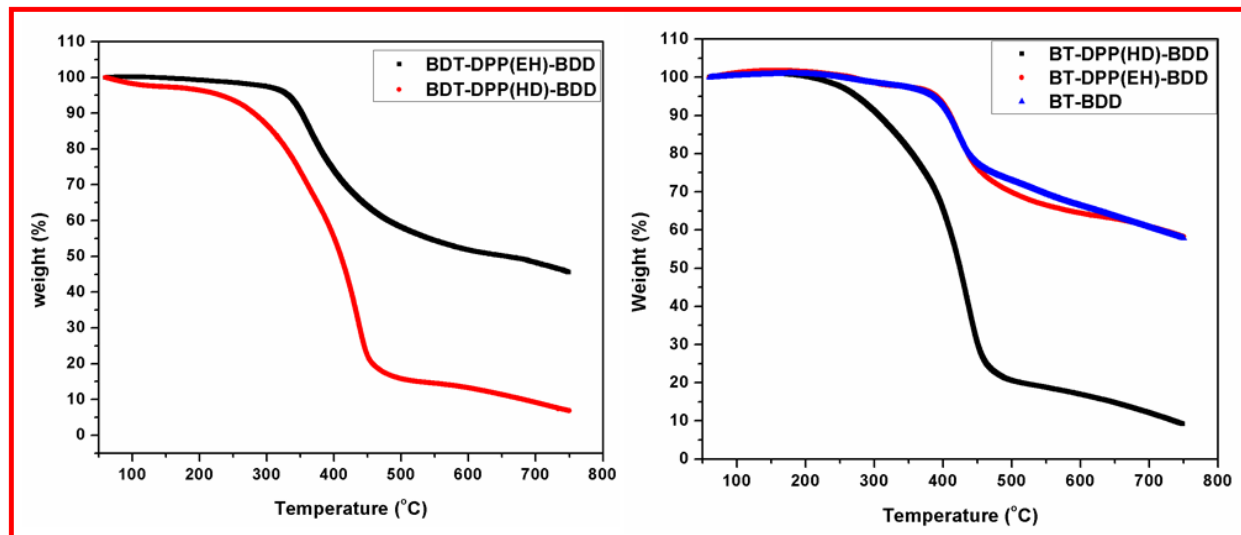


Figure SI 5.16 TG curves of BDD based copolymers and terpolymers

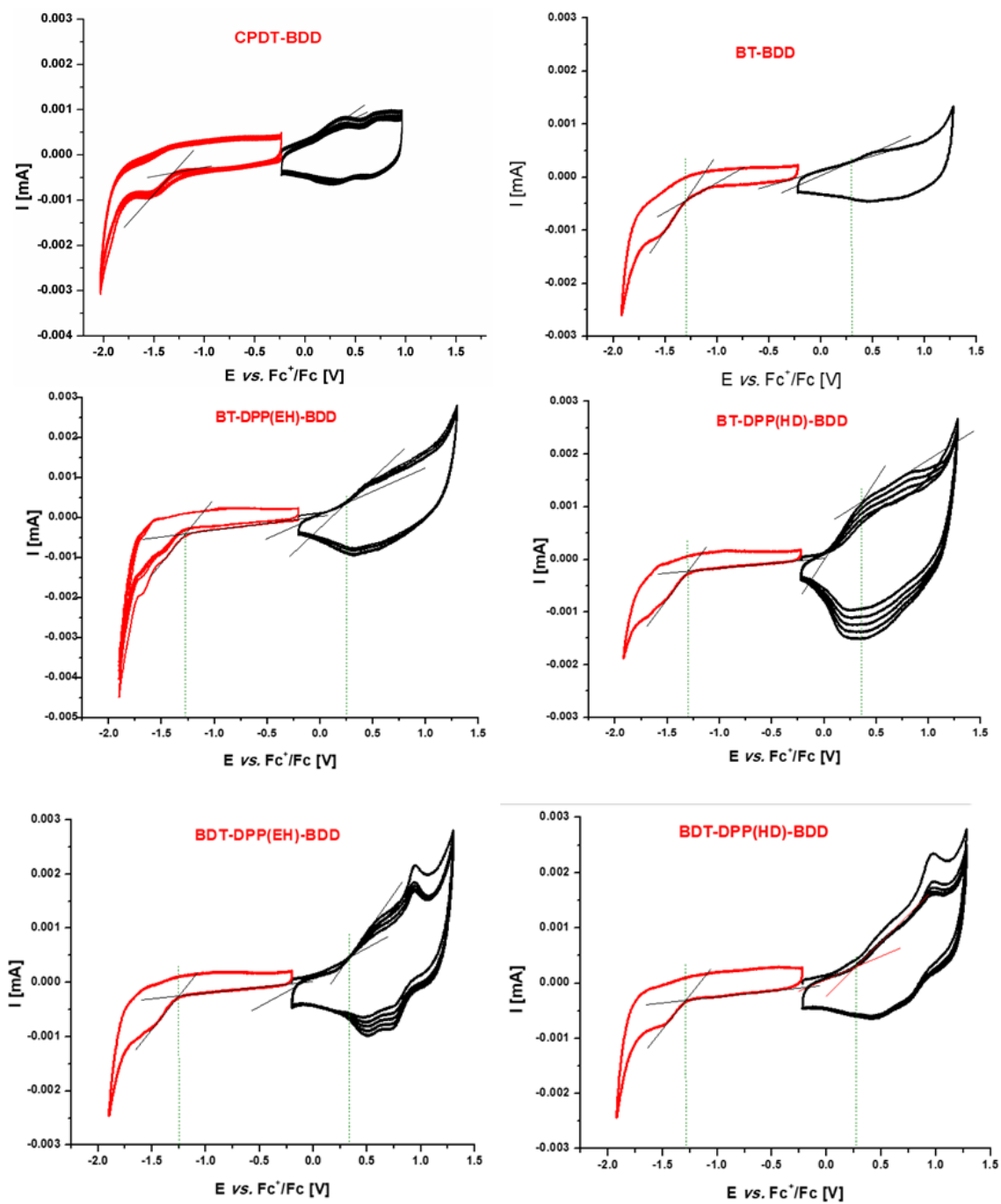


Figure SI 5.17 CV curves for BDD based copolymers and terpolymers.

CHAPTER 6

DPP-Based Spacer Polymers Functionalized with Urethane Linker Containing Alkyl Side chains: Study of Self-assembly Behavior

6.1 INTRODUCTION

Conjugated polymers have been potentially used in large area, flexible and low cost electronic devices that are processable by printing technologies, due to their solution processability and superior mechanical properties.¹⁻³ In the past, a variety of new design motifs for the synthesis of conjugated polymers have been developed to meet the requirements for solution-processable optoelectronic devices such as organic field effect transistors (OFETs), organic light emitting diodes (OLEDs) and organic solar cells (OSCs). In general, charge carrier mobility of polymer FETs is low due to the poor packing of the polymeric material. One of the important approaches to solve this problem is to improve the intermolecular interactions between neighbouring molecules by enhancing their molecular orbital overlapping. This can be achieved by incorporating fused aromatic moieties such as diketopyrrolopyrrole and thieno[3,2-*b*]-thiophene which provide large orbital overlapping area useful for charge carrier transport. Another approach is to develop alternating donor- acceptor (D-A) copolymers, as these polymers exhibit small π - π stacking distance (thus, strong intermolecular interactions) due to attractive forces between donor and acceptor units and hence the enhanced charge carrier mobility.⁴ In spite of these tremendous efforts, simultaneous improvement of charge carrier mobility along with air and operational stability of device remains a big challenge in the development of organic electronics.

In recent years, the focus of research from synthetic point of view is changed from designing novel structures of conjugated material to the chemical modification of the existing materials to achieve desired physical properties.⁵ The development in the structure of alkyl side chains is crucial in this regard as they are no longer considered as only solubilizing groups but attractive functional groups which severely influence the physical properties of polymeric semiconductors. Several studies have demonstrated that the alkyl chains influence the interchain packing and backbone conformation which in turn affect thin-film microstructure and charge transport. Long and branched alkyl side chains, on one hand, provide better solubility and thus increase processability, but on other hand reduce effective molecular packing and thus charge carrier mobilities in OFETs.^{6,7} On the contrary, short and linear alkyl side chains increase π - π interactions and crystallinity,

usually resulting in enhanced charge carrier mobilities but at the expense of material processability.^{8,9} Moving the branching point of alkyl chain away from the conjugated backbone has been found to be effective strategy for enhancing the charge carrier mobility for isoindigo and DPP-based conjugated polymer.¹⁰⁻¹³ By using similar strategy an outstanding value of $12.04 \text{ cm}^2 \text{ V}^{-1} \text{ s}^{-1}$ of charge carrier mobility was obtained for DPP based copolymer in which branching point of alkyl side chain was moved six carbon away from the main conjugated backbone.⁷

Yet another strategy for rational design of conjugated polymers with improved electronic properties includes incorporation of non-covalent interactions apart from usual π - π and hydrogen bonding interactions. These non-covalent interactions comprise interactions between sulfur-oxygen, sulfur-nitrogen, fluorine-hydrogen, nitrogen-hydrogen, etc.¹⁴⁻¹⁶ These interactions create intramolecular conformational locks which help in improving polymer backbone planarity, π -delocalization and thus charge carrier mobility in OFETs. Hydrogen bonds have also known to influence polymer self-assembly and the solid-state morphology of conjugated materials.¹⁷⁻²⁶ Recently, Zhang et al. reported DPP-quarterthiophene conjugated polymers in which part of branching alkyl chains were replaced by urea containing alkyl chains.²⁷ Incorporation of urea groups in the side chains promoted hydrogen bonding and induced inter-chain interactions in the polymer resulting in improved photovoltaic performance (Power Conversion Efficiency = 6.8 %) in solar cell devices and an outstanding value of hole mobility ($13.1 \text{ cm}^2 \text{ s}^{-1} \text{ V}^{-1}$) in Field Effect Transistor (FET) devices. The same research group further synthesized new thiazole-flanked DPP-based polymers with urea containing linear side-chains.²⁸ Ambipolar semiconducting properties of thin films of these polymers, including the hole and electron mobilities (μ_h and μ_e) and current on/off ratios were enhanced compared to those of the polymer without urea groups. In 2018, Rondeau-Gagné et al. synthesized DPP based conjugated polymers with amide group containing alkyl side chains.²⁹ They showed that the intermolecular hydrogen bonds formed between adjacent amide moieties directly affected the lamellar packing of the polymer and aggregation, without affecting the π -conjugation. The charge carrier mobility in organic field-effect transistor (OFET) devices using these materials achieved a maximum value of $2.46 \text{ cm}^2 \text{ s}^{-1} \text{ V}^{-1}$ for 5 mol % of amide containing polymer. They further demonstrated that introduction of hydrogen bonding

influenced the mechanical properties of this class of DPP-polymers, by promoting their stretching ability, reducing the elastic modulus of the polymers and facilitating the molecular alignment after stretch. The resulting polymers with 10% hydrogen bonding side chains showed a maximum stretchability of 75% elongation, without the appearance of nanoscale cracks.³⁰

Apart from numerous efforts for enhancing charge carrier mobility and mechanical strength of the photoactive blend film comprising polymeric donor and PCBM acceptor, improving long term morphological stability of BHJ film is one of major challenges in the photovoltaics. The inherent thermodynamic immiscibility of the donor and acceptor phases promotes phase separation and thus decreases device performance. Crystallization of donor phase is found to be another driving force for blend separation. Various strategies such as, volatile additives like diiodooctane,³¹ non-volatile nucleation promoters,³² or insulating polymers³³ have been employed to address the issue. But these approaches were not effective to offer control over donor crystallization or the stability of blend morphology. Introduction of a “flexible linker” or “conjugation break spacer” in which well-defined conjugated segments are covalently linked with flexible aliphatic chains in a polymer, was found to be an interesting approach to circumvent above mentioned problems.^{34–36} Nonetheless, this strategy is already known to modulate molecular arrangement in solid state and resulting opto-electronic properties of small organic materials.^{37–39} and poly phenylene-vinylene (PPV) based polymers.⁴⁰ The incorporation of flexible aliphatic linkers/spacers in the conjugated backbone provides unique control over solution processability of semiconducting polymers,^{41,42} morphology,⁴³ thermal stability,^{44,45} and mechanical properties^{46–48} of solution processed polymer thin films without negatively affecting charge transport properties. The superior mechanical properties of this class of conjugated systems possessing flexible linkers in their backbone make them potential candidates for stretchable electronics applications.^{47,49,50}

Inspired by these approaches, herein, we propose a method to enhance the charge mobility of semiconducting polymers through the simultaneous incorporation of intermolecular hydrogen bonding and flexible linker/spacer in the backbone. Towards that objective, we designed and synthesized DPP-based semiconducting copolymers incorporating a flexible spacer unit containing four carbon atom chain in the backbone and

urethane linker containing aliphatic side chains. The urethane linker containing aliphatic side chains enable intermolecular hydrogen bonding in the polymer and the spacer unit is proposed to control the crystallisation/self-assembly induced by the H-bonding in the thin films. Thus, the combination of two approaches may affect supramolecular interactions which can modify the thin film morphology and potentially affect the charge transport in solid state.

6.2 EXPERIMENTAL

6.2.1 Materials:

Bromine, 2-octyl-1-dodecanol, triphenylphosphine, imidazole, iodine, 3,6-bis(thiophen-2-yl)-2H,5H-pyrrolo[3,4-c]pyrrole-1,4-dione, 11-bromoundecanoic acid, sodium azide, thiophene, 1,4-dibromobutane, n-BuLi (2.5 M in n-hexane), tris(dibenzylideneacetone)dipalladium(0) ($\text{Pd}_2(\text{dba})_3$) and tri(*o*-tolyl)₃, phosphine (P(*o*-tolyl)) (97%) (Aldrich Chemicals) were used as received. Anhydrous potassium carbonate, triethylamine, ethyl chloroformate and N-bromosuccinimide (Merck) were purchased and were used as received.

N,N-Dimethylformamide (DMF), dimethyl sulphoxide (DMSO), diethyl ether, tetrahydrofuran (THF) and toluene (Aldrich Chemicals) were dried and distilled according to standard procedures and stored under argon. Methanol, chloroform, n-hexane, and ethyl acetate (Merck) were purchased and were used as received. If not otherwise specified, solvents or solution were degassed by bubbling with nitrogen 1 h prior to use.

11-Bromoundecanoyl azide (compound 1) was synthesised from 11-bromoundecanoic acid using triethylamine, ethyl chloroformate and sodium azide by following literature protocol⁵¹ and used in the synthesis of compound 2.

6.2.2 Characterisation and techniques

Different techniques were used for characterization of monomers and polymers. They are listed below.

NMR Spectroscopy: ¹H and ¹³C NMR spectra of monomers and polymers were recorded using a Bruker-AV spectrometer at operating frequency of 200 MHz, 400 MHz and 500 MHz in CDCl₃ or DMSO-*d*₆ with tetramethylsilane as an internal standard.

Gel permeation chromatography (GPC): Molecular weights and dispersity values of polymers were determined on Thermo-Finnigan make gel-permeation chromatography (GPC) using THF as an eluent at a flow rate of 1 mL min⁻¹ at 25 °C. Sample concentration was 2 mg mL⁻¹ and narrow dispersity polystyrenes were used as calibration standards.

Thermogravimetric analysis (TGA): TGA was performed on a Mettler TA-300-thermal analyzer operating under nitrogen atmosphere. The samples were heated from 0 to 700 °C at a heating rate of 10 K/min.

Absorption spectroscopy: The absorption spectra were recorded in dilute chloroform solutions (5×10^{-7} mol L⁻¹ per repeating unit) on a Perkin-Elmer Lambda 950 spectrophotometer. The absorption spectra were recorded on thin films spin-coated from chloroform and methylcyclohexane solution on glass substrates. The smooth and uniform films with a thickness of about 100 nm were tested.

Cyclic Voltammetry: Cyclic voltammetry measurements were performed on Solartron electrochemical station (METEK, Versa STAT3) with a three-electrode cell in a 0.1 M tetra-n butylammonium hexafluorophosphate (n-Bu₄NPF₆) solution in acetonitrile at a scan rate of 100 mV/s at room temperature. Ag/Ag⁺ (0.01M AgNO₃ in acetonitrile) electrode, a platinum wire, and a polymer-coated platinum electrode were used as the reference electrode; counter electrode, and working electrode, respectively. The Ag/Ag⁺ reference electrode was calibrated using a ferrocene/ferrocenium redox couple as an internal standard, whose oxidation potential is set at -4.8 eV with respect to zero vacuum level. The HOMO energy levels were obtained from the equation HOMO (eV) = LUMO - $E_{g \text{ opt}}$. The LUMO levels of the polymers were obtained from the equation LUMO (eV) = -4.8 - ($E_{1/2 \text{ red first}} - E_{1/2 \text{ ox Fc/Fc}^+}$).

6.3 SYNTHESIS

6.3.1 Synthesis of 3,6-bis(5-bromothiophen-2-yl)-2,5-bis(2-octyldodecyl)-2,5-dihydropyrrolo[3,4-c]pyrrole-1,4-dione (**DPP(OD) monomer**)

A precursor compound, namely- 3,6-di(thiophen-2-yl)-2,5-dihydropyrrolo[3,4-c]pyrrole-1,4-dione was synthesised as described in section 3b.3.2.1 of this thesis.

6.3.1.1 Synthesis of 9-(iodomethyl) nonadecane

Into a 250 mL two-necked round bottom flask equipped with a nitrogen gas inlet and a magnetic stir bar were added 2-octyl-1-dodecanol (10.0 g, 33.6 mmol), triphenylphosphine (10.55 g, 40.3 mmol), imidazole (2.74 g, 40.25 mmol) and 50 mL of dichloromethane at 0°C. The solution was stirred for 20 min. Iodine (10.16 g, 40.25 mmol) was added to the solution with continuous stirring at 0°C. The reaction mixture was allowed to warm to room temperature over 2 h. Then, 10 mL of sat. Na₂SO₃ solution was added. The organic layer was separated, concentrated on rotavapor and 50 mL hexane was added. The resulting mixture was washed with water, brine solution and passed through a silica gel plug, and dried over Na₂SO₄. The hexane solution was concentrated under reduced pressure and dried under vacuum to give light yellow color oil.

Yield: 11.3 g (93%).

¹H-NMR (400 MHz, CDCl₃, δ/ppm): 3.01 (2 H, d, methylene group attached to I atom), 1.53 (1 H, m, hydrogen at branch position), 1.48–1.45 (32 H, m, -CH₂-), 0.89 (t, 6H, -CH₃).

¹³C-NMR (400 MHz, CDCl₃, δ/ppm): 39.2, 35.9, 31.9, 29.9, 29.3, 29.6, 27.7, 26.2, 14.1, 13.2.

6.3.1.2 Synthesis of 2,5-bis(2-octyldodecyl)-3,6-di(thiophen-2-yl)-2,5-dihydropyrrolo[3,4-c]pyrrole-1,4-dione

Into a 250 mL two-necked round bottom flask equipped with an argon gas inlet, a magnetic stir bar and an addition funnel were added, 3,6-bis(thiophen-2-yl)-2H,5H-pyrrolo[3,4-c]pyrrole-1,4-dione (2.5 g, 8.35 mmol), anhydrous potassium carbonate (4.6 g, 33.3 mmol) and 150 mL anhydrous N,N-dimethylformamide at 120°C for 1 h. 9-(Iodomethyl) nonadecane (10.21 g, 25.0 mmol) was then added drop wise and the reaction mixture was stirred at 120°C for 24 h. The reaction mixture was allowed to cool and then poured into ice water and stirred for 1 h. The mixture was filtered and the solid product was extracted with dichloromethane. The organic layer was washed with water and dried over anhydrous Na₂SO₄. Removal of the solvent afforded the crude product which was further purified by column chromatography on silica gel using hexane: dichloromethane (7:3, v/v) mixture as an eluent to get desired product as a dark red solid.

Yield: 3.2 g (45%).

$^1\text{H-NMR}$ (400 MHz, CDCl_3 , δ/ppm): 8.88 (2H, dd, thiophene C_5 proton), 7.62 (2H, dd, thiophene C_3 proton), 7.27 (2H, t, thiophene C_4 proton), 4.03(4H, d, $-\text{CH}_2-$ group attached to 'N' atom of lactum ring), 1.22–1.30 (66H, m, $-\text{CH}-$ and $-\text{CH}_2-$ of sidechain), 0.88 (12H, m, $-\text{CH}_3$).

6.3.1.3 Synthesis of 3,6-bis(5-bromothiophen-2-yl)-2,5-bis(2-octyldodecyl)pyrrolo [3,4-c]pyrrole-1,4(2H,5H)-dione (DPP(OD) monomer)

Into a 250 mL two-necked round bottom flask equipped with a nitrogen gas inlet, an addition funnel and a magnetic stir bar were added 2,5-bis(2-octyldodecyl)-3,6-di(thiophen-2-yl)-2,5-dihydropyrrolo[3,4-c]pyrrole-1,4-dione (3 g, 3.48 mmol), chloroform (50 mL) and reaction mixture was protected from light. After the reaction mixture was stirred in an ice bath at 0°C for 20 min, chloroform solution (20 mL) of bromine (0.696 g, 8.7 mmol) was added drop wise into the reaction mixture. The solution was stirred at room temperature for 48 h. The obtained crude product was extracted with chloroform (50 mLx3), washed with water (50 mLx3), and dried over anhydrous Na_2SO_4 . Volatile components were removed under reduced pressure and product was purified by column chromatography on silica gel using hexane: dichloromethane (7:3, v/v) mixture as an eluent to get the product as dark purple red solid.

Yield: 2.5 g, (70 %)

$^1\text{H-NMR}$ (400 MHz, CDCl_3 , δ/ppm): 8.90 (2H, d, thiophene C_3 proton), 7.22 (2H, d, thiophene C_4 proton), 3.93(4H, d, $-\text{CH}_2-$ group attached to 'N' atom of lactam ring) 1.22–1.29 (66H, m, $-\text{CH}-$ and $-\text{CH}_2-$ of sidechain), 0.88 (12H, m, $-\text{CH}_3$).

$^{13}\text{C-NMR}$ (400 MHz, CDCl_3 , δ/ppm): 161.6, 139.6, 135.5, 131.6, 119.2, 46.6, 38.8, 32.2, 31.4, 30.2, 29.9, 29.8, 29.6, 26.9, 22.9, 14.4.

6.3.2 Synthesis of DPP monomer with urethane linkage containing side chain (DPP_{urethane} monomer)

6.3.2.1 Synthesis of 2-octyldodecyl (10-bromodecyl)carbamate (urethane linkage containing side chain) (compound 2)

Into a 250 mL two-necked round bottom flask equipped with a nitrogen gas inlet, an addition funnel and a magnetic stir bar were added 11-bromoundecanoyl azide (5 g, 17 mmol) and anhydrous toluene (50 ml). The reaction mixture was heated at 70°C for 1 hour. A solution of 2-octyldodecan-1-ol (5.1 g, 17 mmol) in toluene (20 mL) was added drop-

wise for 15 min. into the mixture. The resulting solution was heated at same temperature for 12 h. The solution was poured into the water and extracted with diethyl ether (100 mL x3). The organic layer was washed with brine (100 mLx2) and dried over Na₂SO₄. The product was purified using column chromatography on silica gel using ethyl acetate: pet ether (1:4, v/v) mixture as an eluent to obtain viscous oil.

Yield: 8.7 g, (90 %)

¹H-NMR (400 MHz, CDCl₃, δ/ppm): 4.62 (1H, s, hydrogen attached to nitrogen atom), 3.96 (2H, d, -CH₂- attached to oxygen atom), 3.41 (2H, d, -CH₂ attached to bromine atom), 3.16 (2H, d, -CH₂- attached to nitrogen atom), 1.92-1.54 (5H, m), 1.44-1.2 (44H, m, -CH₂- of aliphatic chain), 0.89 (6H, t, -CH₃).

¹³C-NMR (400 MHz, CDCl₃, δ/ppm): 156.94, 77.32, 77.20, 77.00, 76.68, 67.61, 40.97, 37.63, 34.00, 32.80, 31.91, 31.90, 31.21, 30.92, 29.99, 29.66, 29.64, 29.61, 29.56, 29.41, 29.35, 29.32, 29.23, 28.72, 28.14, 26.88, 26.72, 22.68, 14.11.

6.3.2.2 Synthesis of DPP_{urethane} (compound 3)

Into a 100 mL two-necked round bottom flask equipped with an argon gas inlet, an addition funnel and a magnetic stir bar were charged K₂CO₃ (0.15 g, 8.3 mmol) and 20 mL anhydrous DMF. 3,6-Bis(thiophen-2-yl)-2H,5H-pyrrolo[3,4-c]pyrrole-1,4-dione (1 g, 3 mmol) was added into the mixture and the solution was heated at 100°C for 1 h under argon atmosphere. The solution of compound 2 (4.5 g, 8.3 mmol) in anhydrous DMF was added to the reaction mixture slowly. The resulting solution was heated at 100 °C for 24 h. The reaction mixture was allowed to cool and then added in water, extracted with DCM. The organic layer was washed with brine three times and dried over Na₂SO₄. The product was purified using column chromatography on silica gel using hexane: DCM (1:1, v/v) mixture as an eluent to get red solid.

Yield: 1.86 g, (65%)

¹H-NMR (400 MHz, CDCl₃, δ/ppm): 8.93 (d, 2H, thiophene C₅ proton), 7.64 (d, 2H, thiophene C₃ proton), 7.29 (m, 2H, thiophene C₄ proton), 4.63 (s, 2H, -N-H proton of urethane group), 4.07 (m, 4H, -CH₂- group attached to oxygen of urethane group), 3.95 (d, 4H, -CH₂- group attached to nitrogen atom of lactam ring), 3.15 (m, 4H, -CH₂- group attached to nitrogen atom of urethane group), 1.75 (m, 2H, -CH- at branch position), 1.64

(m, 4H, -CH₂- group on middle decyl chain), 1.48 (m, 4H, -CH₂- group on middle decyl chain), 1.26 (m, 88H, -CH₂- group on middle decyl chain and octyldecyl chain), 0.88 (t, 12H, -CH₃).

¹³C-NMR (400 MHz, CDCl₃, δ/ppm): 161.34, 156.93, 139.99, 135.25, 130.66, 129.74, 128.59, 107.65, 67.57, 42.18, 40.98, 37.61, 31.89, 31.18, 29.97, 29.62, 29.33, 29.22, 26.71, 22.66, 14.10. (**Figure SI 6.2**)

6.3.2.3 Synthesis of DPP_{urethane} monomer (compound 4)

Into a 100 mL two-necked round bottom flask equipped with an argon gas inlet and magnetic stir bar were charged the compound 3 (1.86 g, 0.006 mol) and chloroform (30 mL). The solution was protected from light. NBS (2.76 g, 0.0155 moles) was then added to the reaction mixture in three portions, and the reaction mixture was allowed to stir for 24 h. Then, the mixture was poured into water and extracted with dichloromethane (50 mLx3). The organic layer was washed with brine and dried over Na₂SO₄. The product was purified using column chromatography on silica gel using dichloromethane as an eluent to get red solid.

Yield: 1.65 g, (75%)

¹H-NMR (400 MHz, CDCl₃, δ/ppm): 8.68 (d, 2H, thiophene C₃ proton), 7.25 (d, 2H, thiophene C₄ proton), 4.63 (broad singlet, 2H, -N-H proton of urethane group), 3.98 (m, 8H, -CH₂- group attached to oxygen of urethane group and -CH₂- group attached to nitrogen atom of lactam ring), 3.15 (t, 4H, CH₂- group attached to nitrogen atom of urethane group), 1.72 (m, 2H, -CH- at branch position of octyldodecyl chain), 1.48 (m, 4H, -CH₂- group on middle decyl chain), 1.41 (m, 4H, -CH₂- group on middle decyl chain), 1.91-1.85 (d, 88H, -CH₂- group on middle decyl chain and octyldecyl chain), 0.88 (t, 12H, -CH₃).

¹³C-NMR (400 MHz, CDCl₃, δ/ppm): 161.02, 156.95, 138.99, 135.38, 131.66, 131.09, 119.17, 107.79, 67.63, 42.27, 40.97, 37.65, 31.93, 31.23, 30.01, 29.96, 29.68, 29.66, 29.63, 29.59, 29.44, 29.39, 29.37, 29.34, 29.27, 29.14, 26.80, 26.75, 22.70, 14.13. (**Figure SI 6.3**)

6.3.3 Synthesis of 1,4-bis(5-(trimethylstannyl)thiophen-2-yl)butane (spacer monomer)

6.3.3.1 Synthesis of 1,4-di(thiophen-2-yl)butane

Into a 100 mL two-necked round bottom flask equipped with an argon gas inlet and a magnetic stir bar were added thiophene (5.0 g, 59.6 mmol), anhydrous THF (30 mL) and the mixture is cooled to -78 °C. The solution of n-BuLi (44.9 mmol, 2.5 M) in n-hexane was added drop-wise and kept stirring for 1 h at 0 °C. Then, 1,4-dibromobutane (3.0 g, 15 mmol) was added into the reaction mixture. The reaction mixture was stirred overnight at room temperature and was poured into water and then extracted with hexane. The combined organic layers were dried over Na₂SO₄ and concentrated under reduced pressure. The crude product was purified by column chromatography on silica gel using hexane as an eluent. The product was obtained as a colorless solid.

Yield: 1.96 g, (63 %)

¹H-NMR (200 MHz, CDCl₃, δ/ppm): 7.11 (dd, 2H), 6.94 (dd, 2H), 6.8 (d, 2H), 2.88 (t, 4H), 1.78 (m, 4H). (**Figure SI 6.1**)

6.3.3.2 Synthesis of 1,4-bis(5-(trimethylstannyl)thiophen-2-yl)butane (spacer monomer)

Into a 100 mL two-necked round bottom flask equipped with an argon gas inlet and a magnetic stir bar were added 1,4-di(thiophen-2-yl)butane (2.0 g, 8.9 mmol), 50 mL of THF and the solution was cooled to -78 °C. The solution of n-BuLi (2.5 M, 22 mmol) in hexane was slowly added dropwise to the solution. The reaction was maintained at -78 °C for 30 min, and warmed up to 25 °C for another 30 min. Then the solution was cooled to -78 °C again, and trimethyltin chloride (1 M, 22 mL, 22 mmol) was added dropwise through a syringe. The mixture was slowly warmed up to room temperature and stirred overnight. The solvent was evaporated and the residue was dissolved in diethyl ether and washed with water. The combined organic layers were dried over Na₂SO₄, kept on activated carbon and concentrated under reduced pressure. The crude product was purified by recrystallization from ethanol to give white solid.

Yield: 3.5 g, (68 %)

¹H-NMR (200 MHz, CDCl₃, δ/ppm): 7.02 (d, 2H), 6.90 (d, 2H), 2.91 (t, 4H), 1.77 (m, 2H), 0.35 (m, 18H).

¹³C-NMR (200 MHz, CDCl₃, δ/ppm): 135.52, 134.97, 126.17, 125.80, 33.95, 29.60, -7.81.

6.3.4 Synthesis of spacer polymers

6.3.4.1 Synthesis of DPP_{urethane} spacer polymer: Typical procedure

Into 50 mL Schlenk tube equipped with an argon gas inlet and a magnetic stir bar were added DPP_{urethane} monomer (300 mg, 0.21 mmol), 1,4-bis(5-(trimethylstannyl)thiophen-2-yl)butane (116 mg, 0.21 mmol) and dry toluene (10 mL). The reaction mixture was purged with argon for half hour, and then tris(dibenzylideneacetone)dipalladium(0) (Pd₂(dba)₃) (9.61 mg, 0.011 mmol) and tri(o-tolyl)phosphine (P(o-tolyl)₃) (5.11 mg, 0.017 mmol) was added into the solution. The reaction mixture was again purged with nitrogen for half an hour and was stirred at 100°C for 90 min. Upon cooling to room temperature, the reaction mixture was added dropwise to methanol (100 mL). The precipitated polymer was filtered, dried and further purified by Soxhlet extraction with methanol, hexane, acetone and chloroform to remove catalytic impurity and oligomers. The chloroform fraction containing high molecular weight polymer was concentrated and added dropwise into methanol. Subsequently, the precipitate was collected and dried under vacuum overnight to obtain target polymer as a dark black solid.

Yield: 220 mg (69 %).

¹H-NMR (400 MHz, CDCl₃, δ/ppm): 8.89 (m, 2H, proton on thiophene ring attached to DPP unit), 7.23-6.41 (multiple peaks, 6H, protons on various thiophene rings), 4.67 (broad singlet, 2H, N-H proton of urethane group), 3.95 (m, 8H, methylene protons attached to oxygen atom of urethane group and protons attached to nitrogen atom of DPP ring), 3.15 (t, 4H, methylene protons attached to N-H of urethane group), 2.85 (t, 4H, methylene protons of butane chain (spacer unit)), 1.76 (6H, methyne protons at branch position of octyldodecyl chain and methylene protons of spacer unit), 1.40-1.15 (m, 96H, methylene protons of octyldodecyl chain), 0.88 (m, 12H, methyl protons)

GPC (PS standards): *M_w* = 25.0 kg/mol, *M_n* = 18.2 kg/mol, PDI = 1.38.

6.3.4.2 Synthesis of DPP_{alkyl} spacer polymer (DPP_{alkyl}-Th-C₄-Th polymer)

The DPP_{alkyl} spacer polymer was synthesised by following the procedure described in section 6.3.4.1. DPP_{alkyl} monomer (300 mg, 0.28 mmol), reacted with spacer monomer (152 mg, 0.28 mmol) in presence of Pd₂(dba)₃ (12.82 mg, 0.014 mmol) and P(o-tolyl)₃ (6.82mg, 0.022 mmol) to yield DPP_{alkyl} spacer polymer as a black solid.

Yield: 232.5 mg (73 %).

$^1\text{H-NMR}$ (400 MHz, CDCl_3 , δ/ppm): 8.90 (m, 2H, proton on thiophene ring attached to DPP unit), 7.53 (m, 2H, proton on thiophene ring attached to butane chain i.e. spacer unit, in the conjugated backbone), 7.23-6.70 (multiple peaks, 2H, protons on various thiophene rings), 6.75 (m, 2H proton on thiophene ring attached to spacer unit), 4.02 (d, 4H, methylene protons directly attached to nitrogen atom of DPP), 2.87 (t, 4H, methylene protons of butane chain), 1.97 (2H, methylene protons at branch position of octyldodecyl chain), 1.81 (m, 4H, methylene protons of butane chain), 1.35-1.12 (m, 64H, methylene protons of octyldodecyl chain), 0.85 (m, 12H, methyl protons)

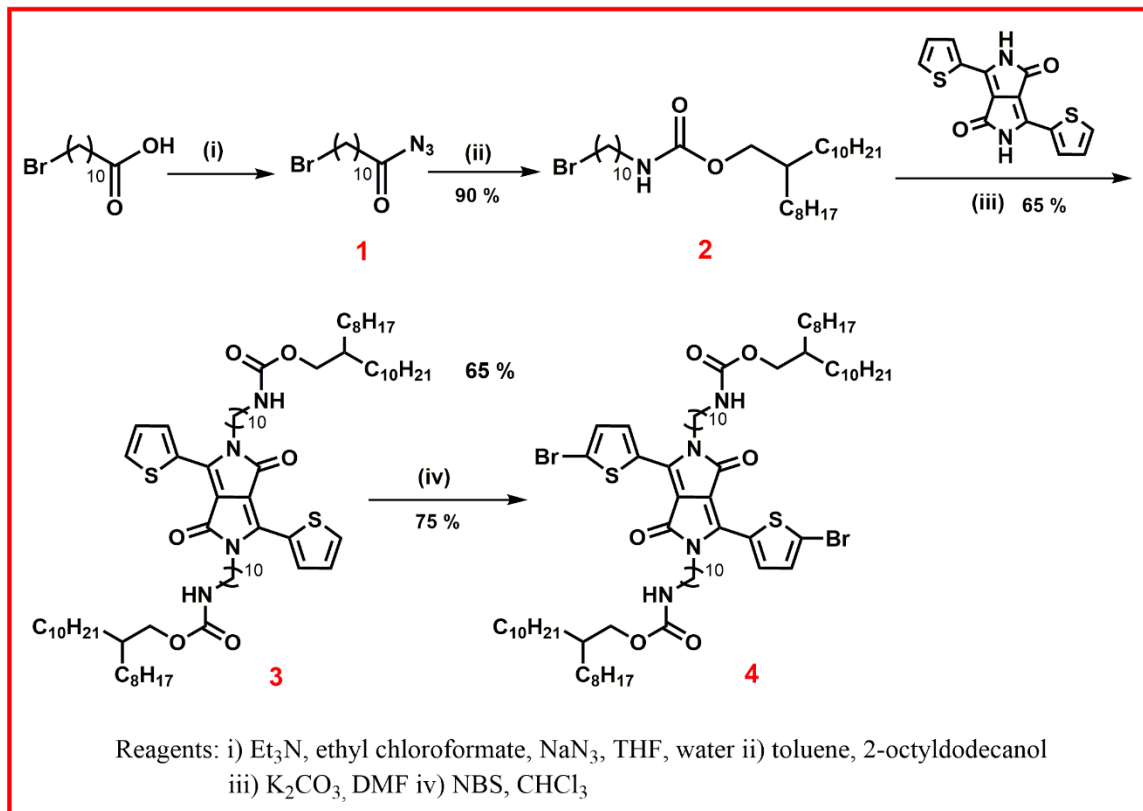
GPC (PS standards): $M_w = 47.1 \text{ kg/mol}$, $M_n = 23.8 \text{ kg/mol}$, PDI = 1.98.

6.4 RESULTS AND DISCUSSION:

6.4.1 Synthesis of spacer polymers

6.4.1.1 Synthesis of DPP_{urethane} monomer

Synthesis of DPP_{urethane} monomer is outlined in **Scheme 6.1**. The first step in the synthesis of DPP_{urethane} monomer is the synthesis of urethane containing side chain (2-octyldodecyl (10-bromodecyl)carbamate i.e. compound 2) by Curtius reaction. 11-Bromoundecanoic acid was reacted with ethyl chloroformate in the presence of triethylamine to form in situ carboxylic carbonic anhydride, which then reacted with sodium azide to obtain 11-bromoundecanoyl azide (compound 1). The corresponding isocyanate of compound 1 was synthesized by gentle heating, which was converted to compound 2 by reaction with octyl dodecanol, in the yield 90 %. In the second step, DPP was alkylated with compound 2 in the presence of K_2CO_3 , to obtain DPP_{urethane} (compound 3). The final DPP_{urethane} monomer (compound 4) was obtained by bromination of compound 3 using NBS in overall yield of 55 %.



Scheme 6.1 Synthetic scheme of DPP_{urethane} monomer (4).

¹H-NMR spectrum of urethane containing side chain i.e. 2-octyldodecyl (10-bromodecyl)carbamate (compound 2) is presented in **Figure 6.1**. The presence of urethane group was confirmed by the singlet at 4.62 δ ppm due to N-H proton. The methylene protons attached to oxygen atom of urethane group were observed at 3.96 δ ppm. The methylene protons attached to bromine atom appeared at 3.41 δ ppm. The methylene protons attached to nitrogen atom of urethane group were observed at 3.16 δ ppm. The multiple peaks in the range of 1.92-1.54 δ ppm were observed due to the protons at branch position of octyldodecyl side chains and methylene protons decyl chain. The remaining methylene protons on side chains and on aliphatic chain appeared in the range 1.44-1.20 δ ppm. The methyl protons on side chains were observed at 0.89 δ ppm as a triplet.

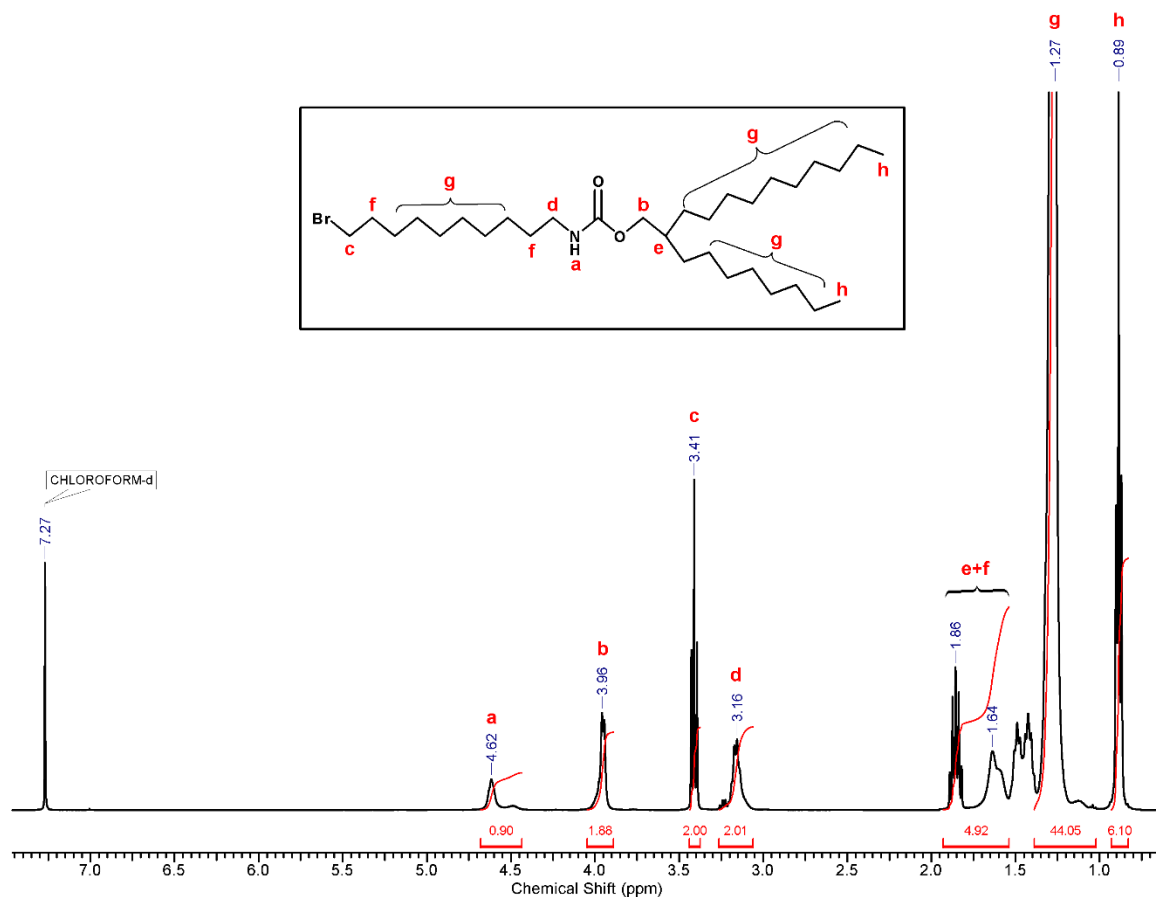


Figure 6.1 $^1\text{H-NMR}$ spectrum (CDCl_3) of 2-octyldodecyl (10-bromodecyl)carbamate (urethane linkage containing side chain) (2).

$^1\text{H-NMR}$ spectrum of the DPPurethane 3 is presented in **Figure 6.2**. The appearance of three peaks in the aromatic region at 8.93, 7.64, and 7.29 δ ppm, confirmed the presence of DPP ring. The incorporation of urethane group was confirmed by the presence of singlet at 4.63 δ ppm due to N-H proton. The methylene protons attached to oxygen atom of urethane group were observed at 4.07 δ ppm. The methylene protons attached to nitrogen atom of lactam ring appeared at 3.95 δ ppm. The methylene protons attached to nitrogen atom of urethane group were observed at 3.15 δ ppm. The proton at branch position of octyldodecyl side chains was observed as multiplet at 1.75 δ ppm. The remaining methylene protons on side chains and on aliphatic spacer chain appeared in the range 1.69-1.13 δ ppm. The methyl protons on side chains were observed at 0.88 δ ppm as a triplet.

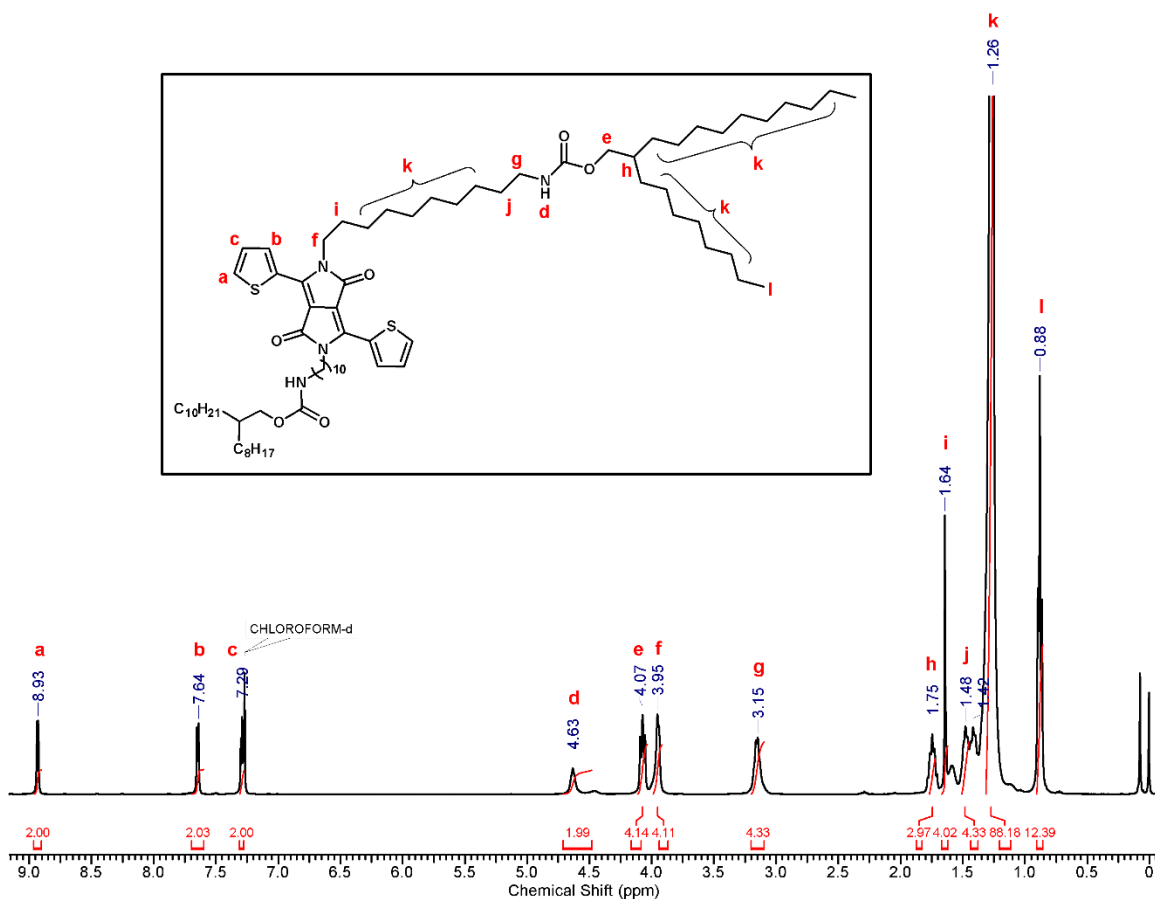


Figure 6.2 $^1\text{H-NMR}$ spectrum (CDCl_3) of $\text{DPP}_{\text{urethane}}$ (3).

$^1\text{H-NMR}$ spectrum of the $\text{DPP}_{\text{urethane}}$ Monomer 4 is presented in **Figure 6.3**. The one aromatic proton of each thiophene ring was replaced by bromine. So, the aromatic region showed two peaks at 8.68 and 7.25 δ ppm due to remaining two protons on each thiophene ring. The N-H proton of urethane group appeared as singlet, at 4.63 δ ppm. The methylene protons attached to oxygen atom of urethane group and those attached to nitrogen atom of lactam ring appeared as multiplet in the range 4.19-3.85 δ ppm. The methylene protons attached to nitrogen atom of urethane group were observed at 3.15 δ ppm. The aliphatic region of NMR spectrum of $\text{DPP}_{\text{urethane}}$ monomer exhibited similar peaks as that of NMR spectrum of $\text{DPP}_{\text{urethane}}$, since aliphatic region is not affected by bromination.

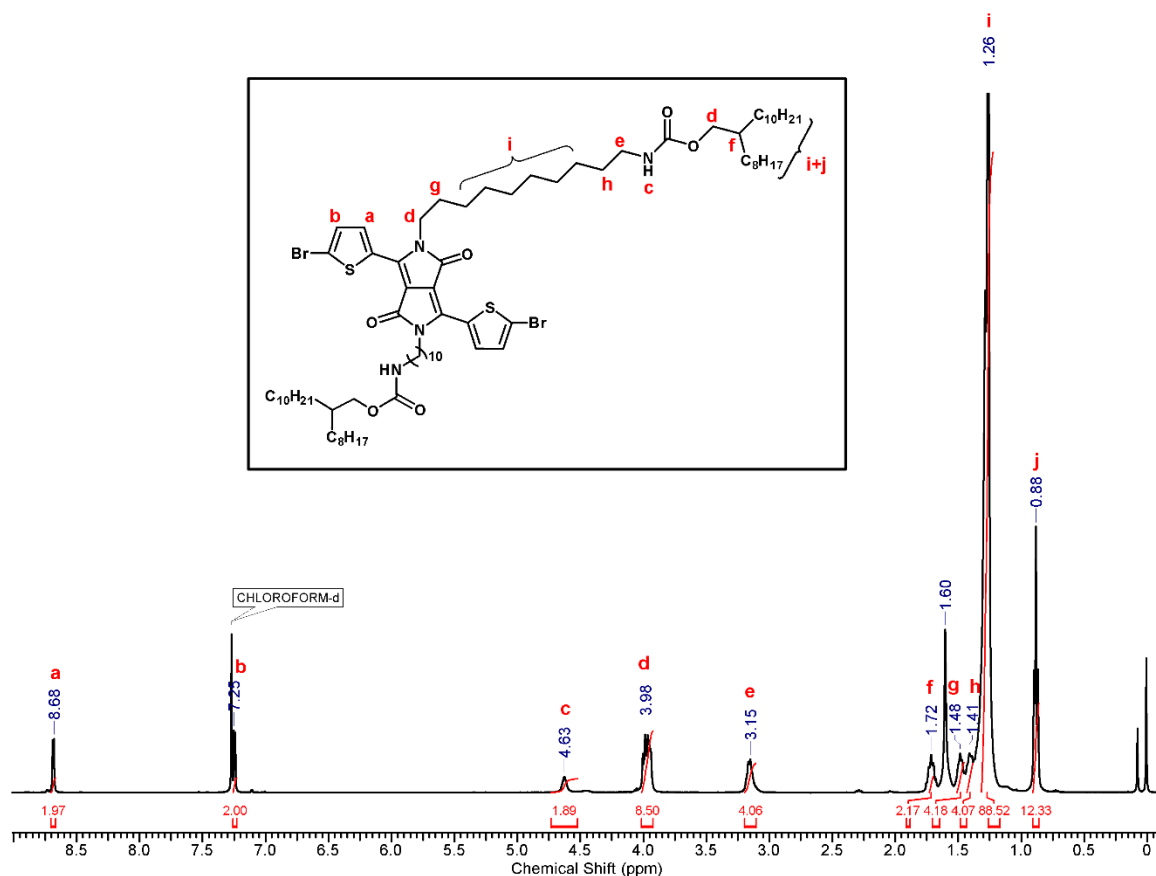
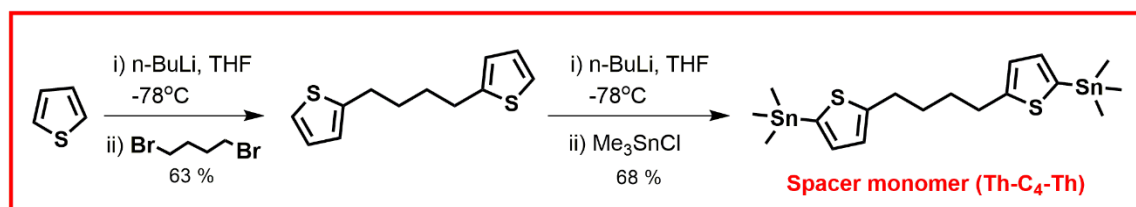


Figure 6.3 $^1\text{H-NMR}$ spectrum (CDCl_3) of $\text{DPP}_{\text{urethane}}$ monomer (4).

6.4.1.2 Synthesis of 1,4-bis(5-(trimethylstannyl)thiophen-2-yl)butane (spacer monomer)

1,4-Di(thiophen-2-yl)butane was synthesised by reaction of thiophene with 1,4-dibromobenzene in presence of *n*-butyl lithium at 0°C . The final spacer monomer was synthesised by reaction of 1,4-di(thiophen-2-yl)butane with trimethyltin chloride in presence of *n*-butyl lithium at -78°C in 42 % overall yield.



Scheme 6.2 Synthesis of 1,4-bis(5-(trimethylstannyl)thiophen-2-yl)butane (spacer monomer).

$^1\text{H-NMR}$ spectrum (CDCl_3) of 1,4-bis(5-(trimethylstannyl)thiophen-2-yl)butane (spacer monomer) is depicted in **Figure 6.4**. The protons on thiophene rings were observed at 7.02 and 6.90 δ ppm, respectively. The triplet at 2.91 δ ppm was observed for protons on the methylene group attached to thiophene ring. The remaining methylene protons were observed at 1.77 δ ppm. The triplet at 0.35 δ ppm was appeared due to methyl group attached to tin atom.

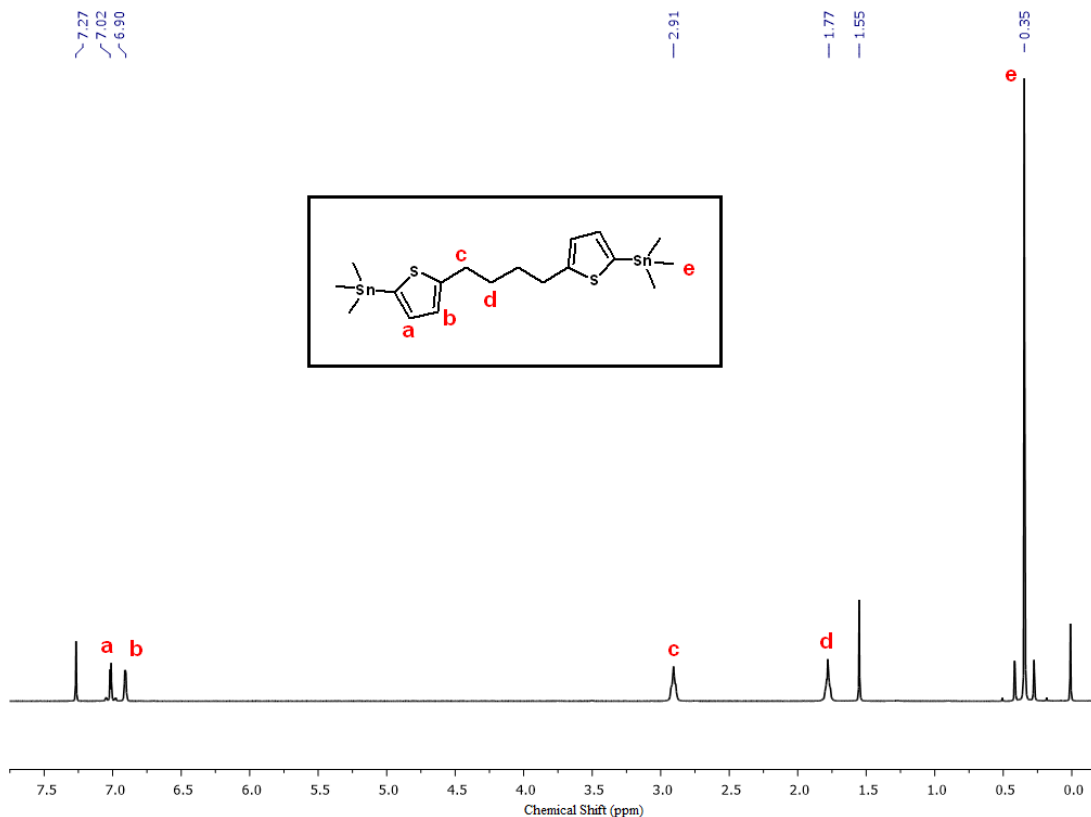
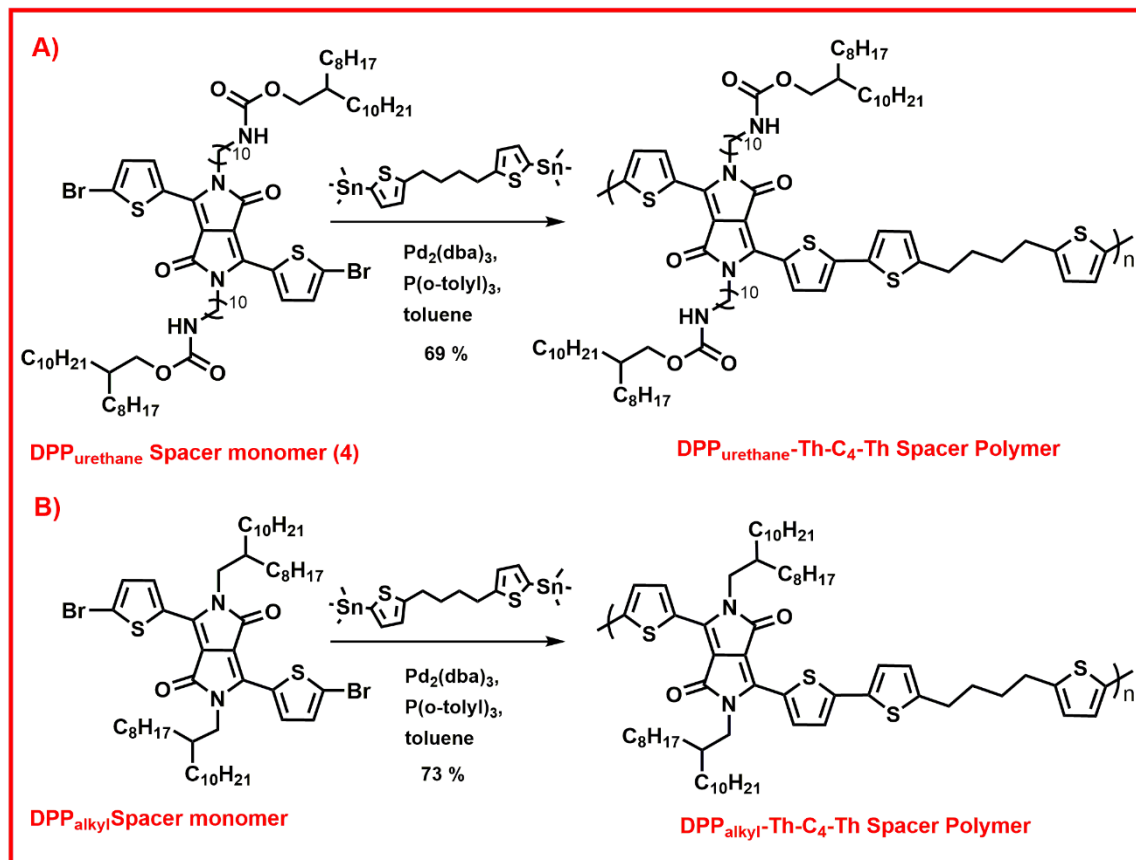


Figure 6.4 $^1\text{H-NMR}$ spectrum (CDCl_3) of 1,4-bis(5-(trimethylstannyl)thiophen-2-yl)butane (spacer monomer).

6.4.1.3 Synthesis of polymers- $\text{DPP}_{\text{urethane}}\text{-Th-C}_4\text{-Th}$ polymer and $\text{DPP}_{\text{alkyl}}\text{-Th-C}_4\text{-Th}$ polymer

Synthesis of the polymers is depicted in **Scheme 6.3**. $\text{DPP}_{\text{urethane}}$ monomer and $\text{DPP}_{\text{alkyl}}$ monomer were polymerized with 1,4-bis(5-(trimethylstannyl)thiophen-2-yl)butane (spacer monomer) under Stille coupling protocol (in presence of $\text{Pd}_2(\text{dba})_3$ as catalyst and $\text{P}(\text{o-tolyl})_3$ as ligand) to obtain $\text{PDPP}_{\text{urethane}}\text{-Th-C}_4\text{-Th}$ polymer, $\text{DPP}_{\text{alkyl}}\text{-Th-C}_4\text{-Th}$ polymer, respectively. The polymerization time was restricted to 3 h to achieve

soluble polymers. All the polymers are soluble in chloroform, chlorobenzene, 1, 1, 2, 2 tetrachloroethane and toluene. The molecular weights of DPP_{urethane}-Th-C₄-Th polymer and DPP_{alkyl}-Th-C₄-Th polymer were measured using GPC by using chloroform as eluent and polystyrene standard. The structures of all polymers were confirmed by ¹H-NMR.



Scheme 6.3 Synthesis of spacer polymers A) DPP_{urethane}-Th-C₄-Th polymer B) DPP_{alkyl}-Th-C₄-Th polymer.

¹H-NMR spectrum of the DPP_{urethane}-Th-C₄-Th polymer is presented in **Figure 6.5**. The peaks at 4.67 δ ppm (due to N-H proton) and at 2.85 δ ppm (due to proton on spacer unit) are the characteristic peaks of DPP_{urethane} and spacer unit, respectively. The appearance of these two peaks confirmed the incorporation of spacer unit in the conjugated backbone and hence the polymer formation. The proton on thiophene ring which is attached to DPP unit was observed as multiplet at 8.89 δ ppm. The remaining protons on thiophene rings were observed in the range 7.23-6.41 δ ppm. The broad singlet at 4.67 δ ppm was observed for N-H proton. The multiple peaks in the range 4.22-3.84 δ ppm correspond to

methylene protons attached to nitrogen atom of DPP group and those attached to oxygen atom of urethane group. The methylene protons attached to N-H of urethane group appeared as a triplet at 3.15 δ ppm. The methylene protons of spacer unit were observed at 2.85 δ ppm. The methylene protons of spacer chain and the methine protons at branch position of octyldodecyl chain appeared at 1.76 δ ppm. The remaining methylene protons of octyldodecyl chain were observed in the range 1.40-1.15 δ ppm. The twelve methyl protons were observed as triplet at 0.88 δ ppm.

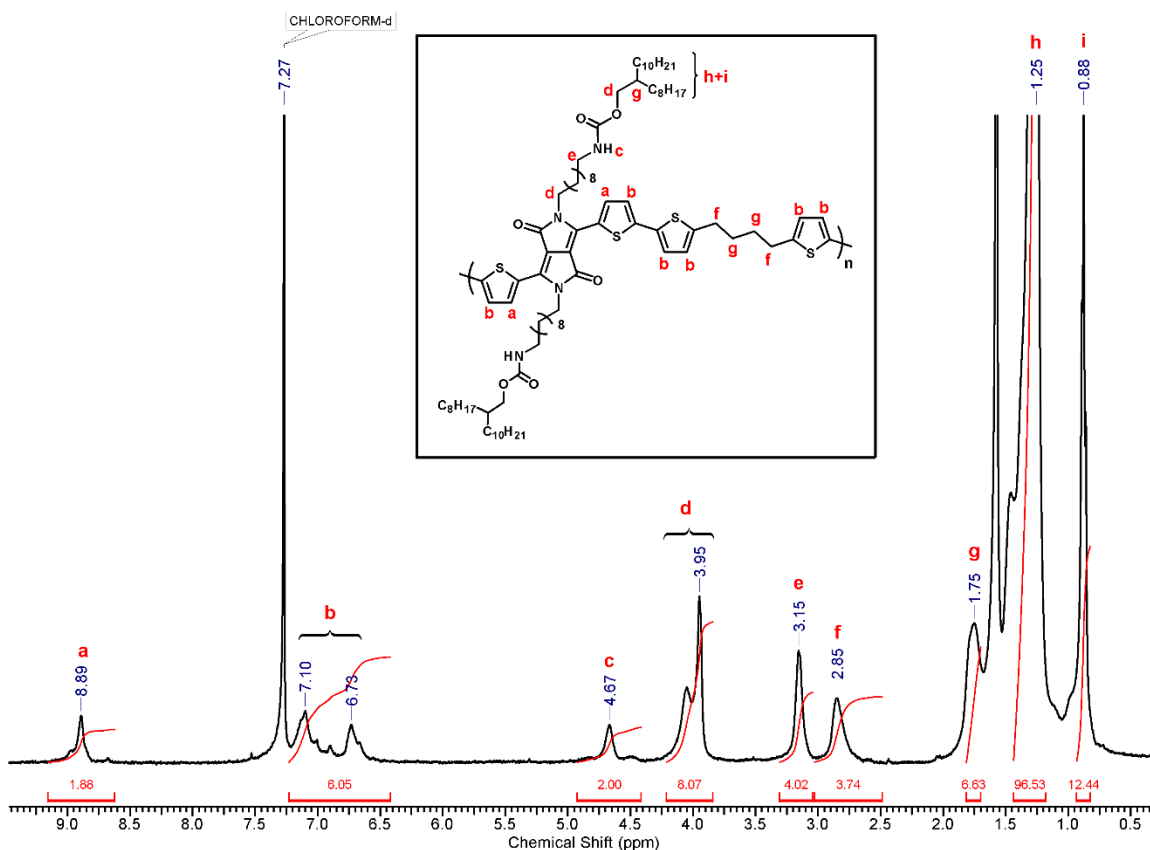


Figure 6.5 $^1\text{H-NMR}$ spectrum (CDCl_3) of $\text{DPP}_{\text{urethane-Th-C}_4\text{-Th}}$ polymer.

$^1\text{H-NMR}$ spectrum of the $\text{DPP}_{\text{alkyl-Th-C}_4\text{-Th}}$ polymer is presented in **Figure 6.6**. The appearance of peaks at 2.87 and 1.81 δ ppm confirmed the incorporation of spacer unit in the conjugated backbone and hence the formation of polymer. The proton on thiophene ring which is attached to DPP unit was observed as multiplet at 8.90 δ ppm. The protons on thiophene ring which is attached to spacer unit, were appeared at 7.53 δ ppm and 6.75 δ ppm. The remaining protons on various thiophene rings were observed in the range 7.23-6.70 δ ppm. The peak at 4.02 δ ppm corresponds to methylene protons directly attached to

nitrogen atom of DPP. The methylene protons of spacer unit were observed at 2.87 and 1.18 δ ppm as triplet and multiplet, respectively. The peak at 1.97 δ ppm was due to methine protons at branch position of octyldodecyl chain. The remaining methylene protons of octyldodecyl chain were observed in the range 1.35-1.12 δ ppm. The methyl protons were observed as triplet at 0.85 δ ppm.

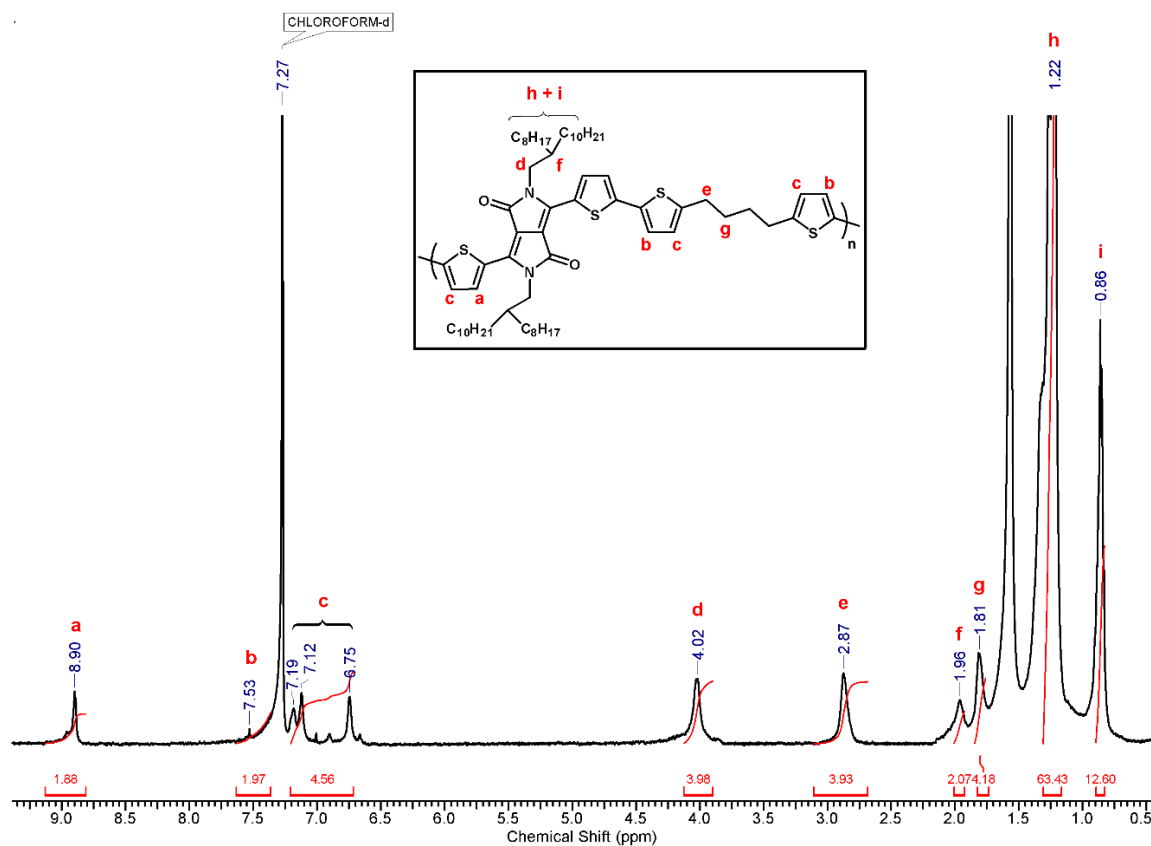


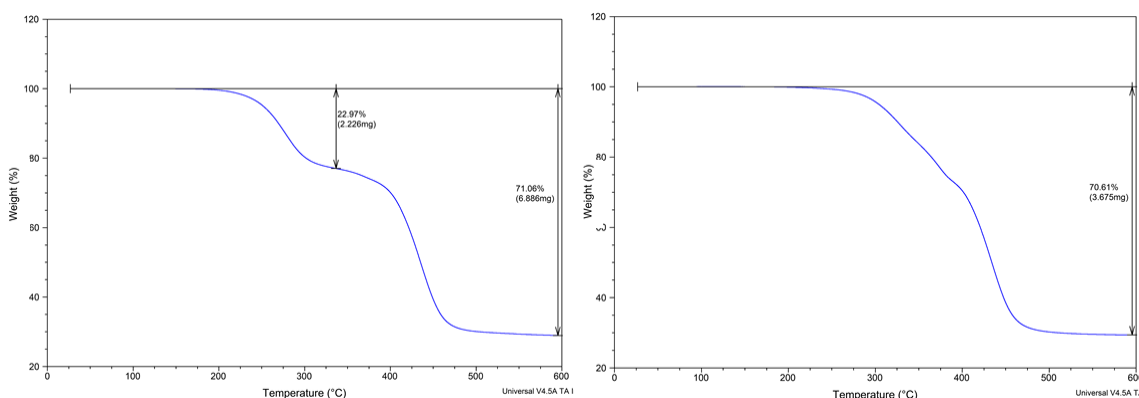
Figure 6.6 ¹H-NMR spectrum (CDCl₃) of DPP_{alkyl}-Th-C₄-Th polymer.

The data obtained from gel permeation chromatography (GPC) and thermogravimetric analysis (TGA) is summarised in **Table 6.1**. Number average molecular weights of DPP_{urethane}-Th-C₄-Th polymer and DPP_{alkyl}-Th-C₄-Th polymer are found to be 18.2 and 23.8 kg/mol with dispersities 1.4 and 2.0, respectively. **Figure 6.7** shows TGA curves for the spacer polymers. TGA curve for DPP_{urethane}-Th-C₄-Th polymer exhibited two stage degradation profile. This may be because the urethane containing side chains would degrade first and then the polymer backbone. Temperature at 10 % weight loss was recorded at 325°C for DPP_{alkyl}-Th-C₄-Th polymer.

Table 6.1 Data obtained from GPC and TGA studies.

Polymers	M _n (kg/mol) ^a	M _w (kg/mol) ^b	Dispersity (M _w /M _n)	T _{10%} /°C ^c
DPP _{urethane} -Th-C ₄ -Th	18.2	25.0	1.38	-
DPP _{alkyl} -Th-C ₄ -Th	23.8	47.2	1.98	325

a: M_n= number-average molecular weight, b: M_w= weight-average molecular weight, c: T_{10%}=decomposition temperatures at 10% weight loss

**Figure 6.7** TG curves for the spacer polymers.

Variable temperature ¹H-NMR spectrum of DPP_{urethane}-Th-C₄-Th polymer is presented in **Figure 6.8**. ¹H-NMR spectra of DPP_{urethane}-Th-C₄-Th polymer in 1,1,2,2-tetrachloroethane-d₂ (TCE-d₂) at different temperatures, were examined to confirm the formation of interchain H-bonding. ¹H-NMR signal corresponding to urethane groups in DPP_{urethane} spacer polymer was found at 4.71 ppm at 23°C. The signal showed an upfield shift to 4.63, 4.59 and 4.56 ppm at 50°C, 70°C and 90°C, respectively. This observation agrees with the interchain hydrogen-bonding formation of urethane groups. Thus, this variable temperature ¹H-NMR data provides the evidence for the interchain hydrogen-bonding formation of urethane groups.

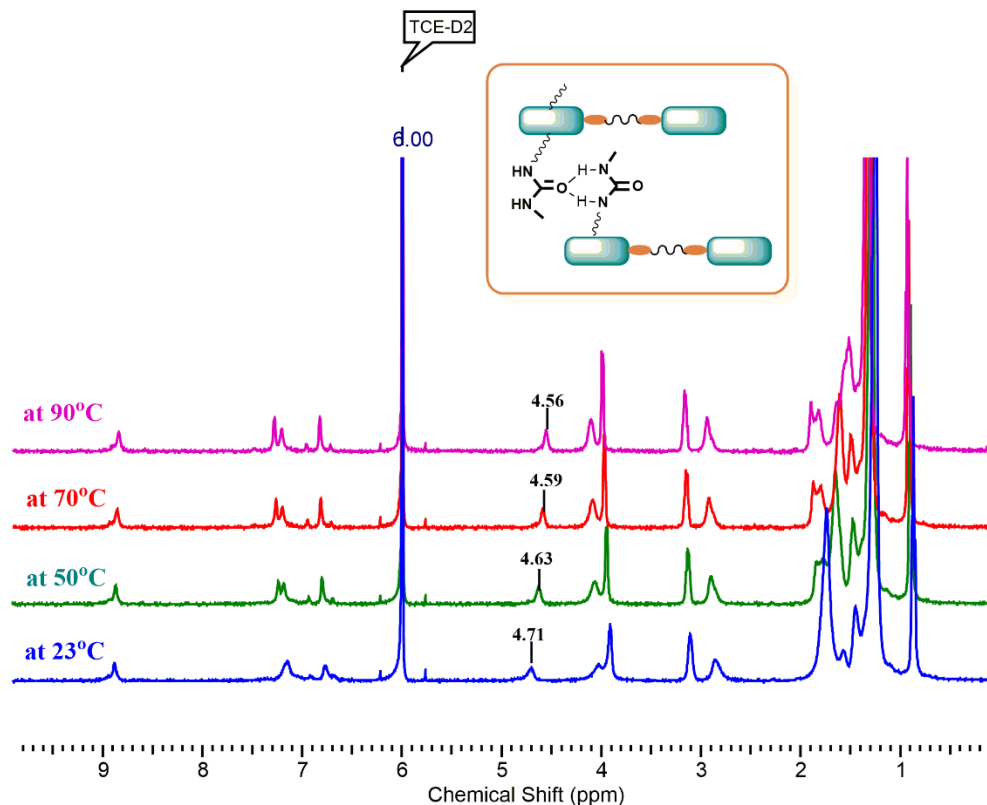


Figure 6.8 Variable temperature $^1\text{H-NMR}$ spectrum of $\text{DPP}_{\text{urethane-Th-C}_4\text{-Th}}$ polymer.

6.4.2 Optical and Electrochemical studies:

HOMO and LUMO energy levels of $\text{PDPP}_{\text{urethane-Th-C}_4\text{-Th}}$ and $\text{PDPP}_{\text{alkyl-Th-C}_4\text{-Th}}$ were estimated from the respective onset oxidation and reduction potentials on the basis of their thin-film cyclic voltammogram as shown in **Figure 6.9**. As listed in **Table 6.2**, the HOMO energy of $\text{PDPP}_{\text{urethane-Th-C}_4\text{-Th}}$ and $\text{PDPP}_{\text{alkyl-Th-C}_4\text{-Th}}$ were -5.45 eV and -5.40 eV respectively.

The absorption spectra of polymers were measured in chloroform and methyl cyclohexane solution as well as on thin films spin coated from chloroform and methyl cyclohexane solution. **Table 6.2** summarizes photophysical and electrochemical data of polymers. **Figure 6.10** depicts the normalized absorption in dilute chloroform and methylcyclohexane solution. In solutions, the polymers show absorption maxima between 550-680 nm. In general, absorption spectra of polymers in methyl cyclohexane solution were red shifted as compared to those in chloroform solution. The absorption spectra of both the polymers in chloroform solution as well as that of $\text{DPP}_{\text{alkyl-Th-C}_4\text{-Th}}$ in methyl

cyclohexane solution, showed a shoulder peak indicating presence of more effective interaction between polymer backbones of these polymers. **Figure 6.11** depicts the normalized absorption spectra on films, spin coated from their dilute chloroform and methylcyclohexane solution. In films, the polymers show absorption maxima between 600-690 nm. Thin-film absorption spectra of both the polymers are slightly red shifted and broadened with respect to the solution ones, as a result of polymer–polymer/ intermolecular interactions. A broad absorption around 800 nm in the DPP_{urethane}-Th-C4-Th thin film from methyl cyclohexane solution, indicated the presence of strong excitonic interactions and the formation of π -stacks.³⁶ Thus, optical data of also confirmed the presence of self-assembly in this polymer as already evidenced through variable temperature ¹H-NMR study as described in above section.

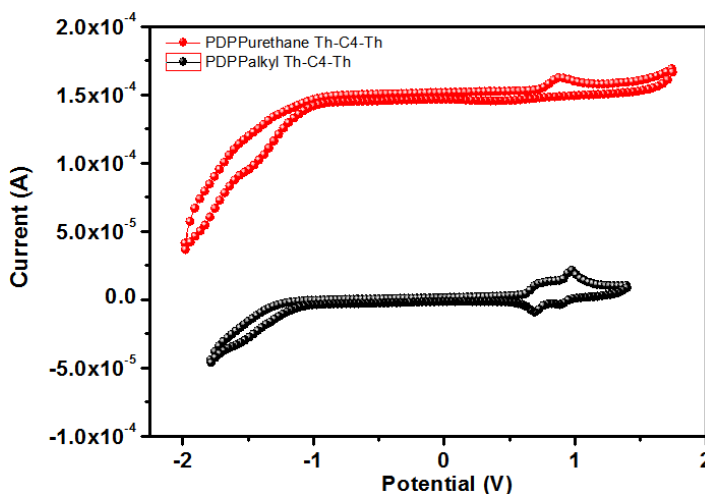


Figure 6.9 Thin-film cyclic voltammogram of spacer polymers.

Table 6.2 Photophysical and electrochemical data of polymers.

Polymer	E _{ox}	E _{red}	HOMO	LUMO	λ _{max} (nm) solution		λ _{max} (nm) film	
					CHCl ₃	MCH	CHCl ₃	MCH
DPP _{urethane} -Th-C ₄ -Th	0.65	-1.0	-5.45	-3.80	593, 631(s)	640	666	648
DPP _{alkyl} -Th-C ₄ -Th	0.60	-1.1	-5.40	-3.70	628, 590 (s)	629, 670 (s)	666, 615(s)	679, 629 (s)

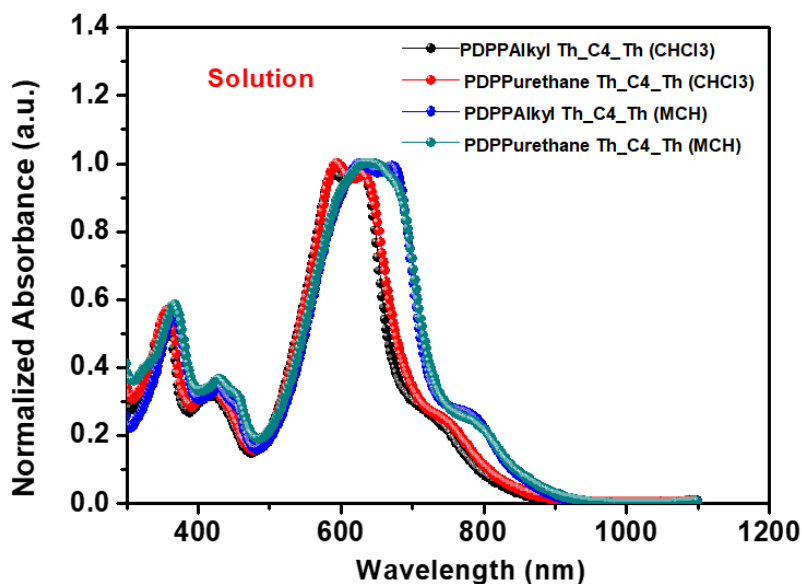


Figure 6.10 The absorption spectra of spacer polymers in dilute chloroform (CHCl_3) solution and dilute methylcyclohexane (MCH) solution.

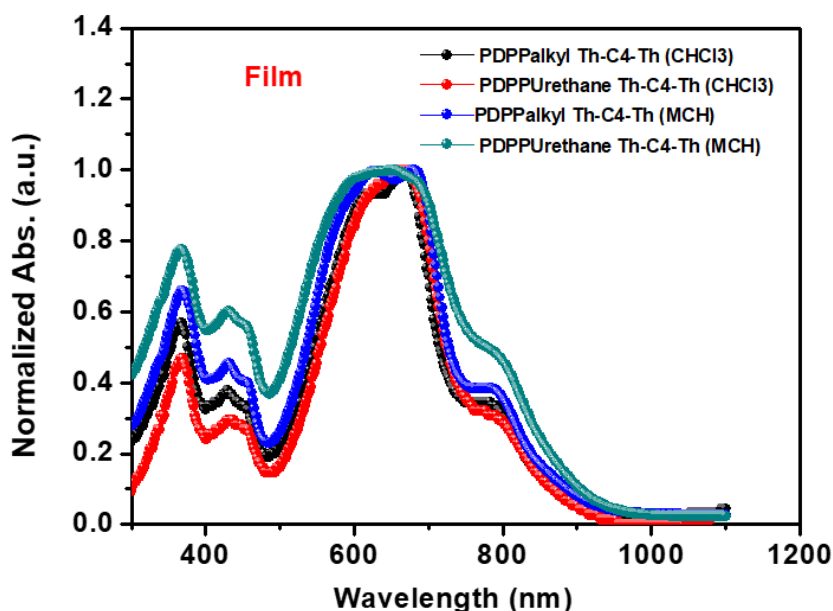


Figure 6.11 The absorption and emission spectra of spacer polymers on thin films prepared from their dilute chloroform and methylcyclohexane (MCH) solution.

6.4.3 Self-assembly in methyl cyclohexane

Figure 6.12 depicts $^1\text{H-NMR}$ of spacer polymers in tetrachloroethane- d_2 at room temperature (RT) and at 80°C . **Figure 6.13** depicts $^1\text{H-NMR}$ of spacer polymers in cyclohexane- d_{12} at RT and at 80°C .

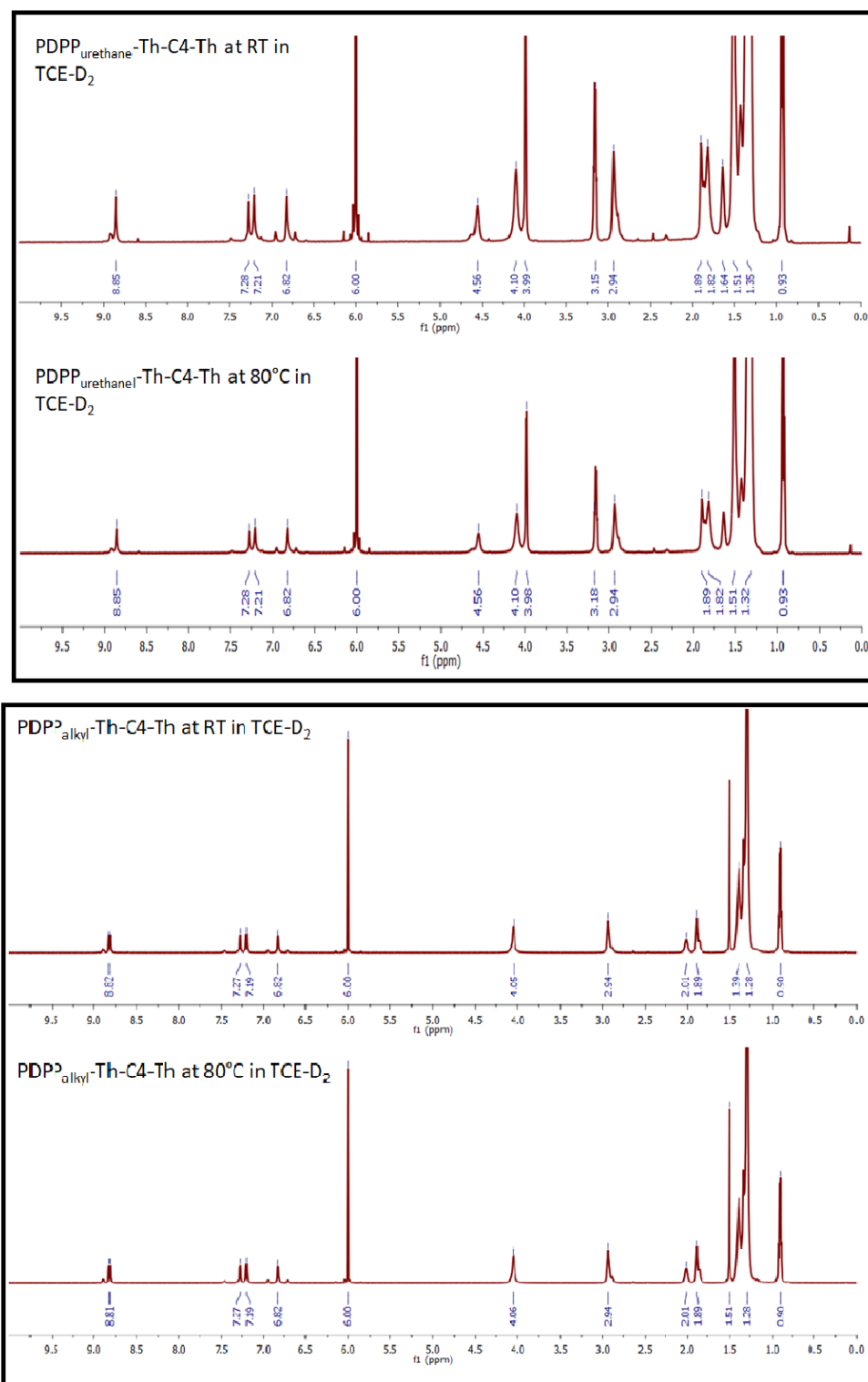


Figure 6.12 ¹H-NMR spectra of spacer polymers in tetrachloroethane-D₂ at RT and at 80°C.

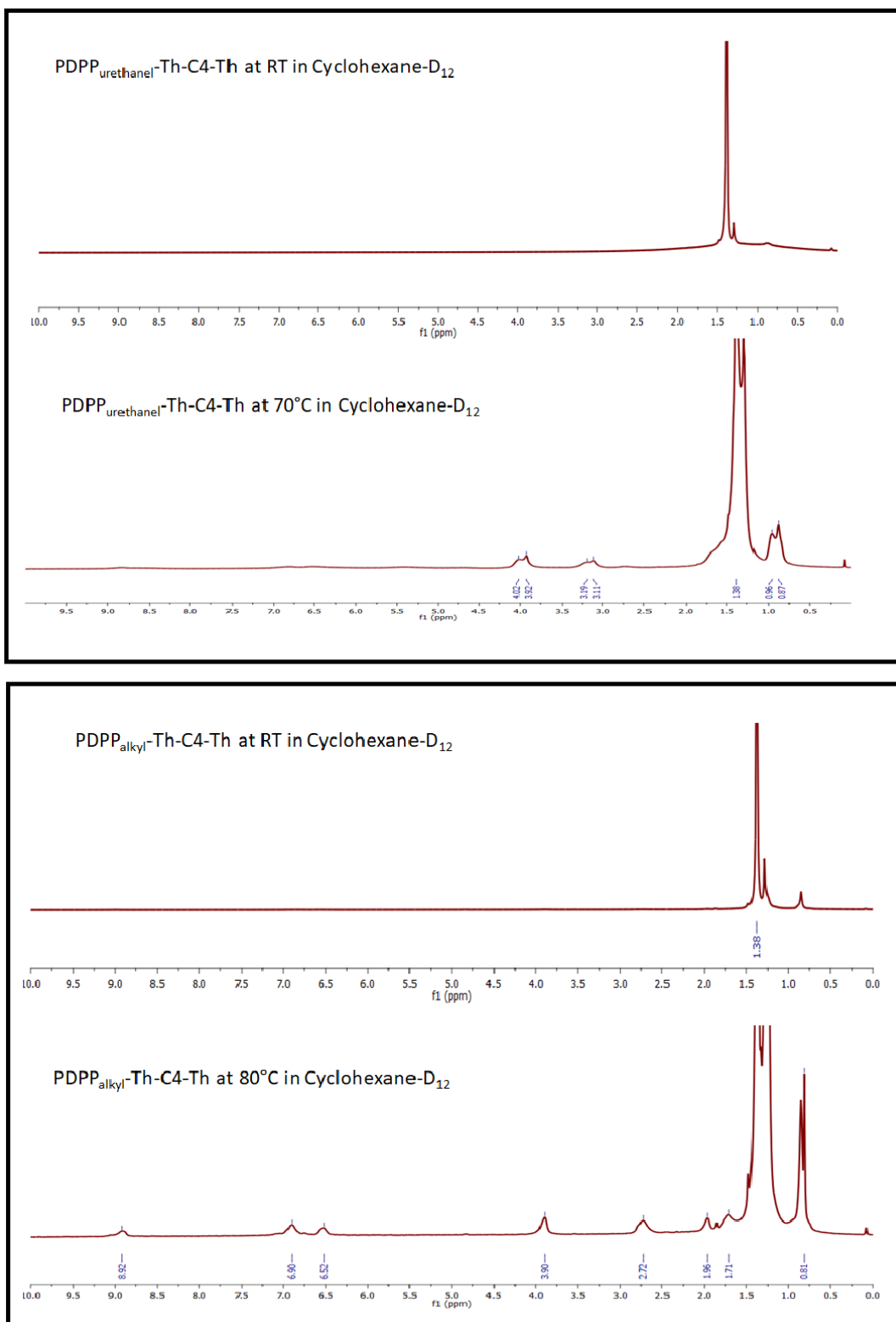


Figure 6.13 $^1\text{H-NMR}$ spectra of spacer polymers in cyclohexane- D_{12} at RT and at 80°C .

^1H -NMR spectra shown above (**Figure 6.12**) evidenced that the $\text{DPP}_{\text{urethane}}\text{-Th-C}_4\text{-Th}$ polymer was well solvated in tetrachloroethane and showed all the chemical shifts corresponding to the polymer structure. The same observation holds true for alkyl side chain counterpart i.e. $\text{PDPP}_{\text{alkyl}}\text{-Th-C}_4\text{-Th}$. Thus, both the polymers were well solvated in tetrachloroethane- d_2 . On contrary, the ^1H -NMR spectra of both the polymers in cyclohexane- d_{12} (**Figure 6.13**) didn't show any peak at room temperature but at higher temperature the peak intensity was increased slightly, additionally, the peak broadening was also observed. These results suggest that polymers were self-assembled in methylcyclohexane and cyclohexane. Thus, this study was also in agreement with the formation of self-assembled structures in these polymers as demonstrated by variable temperature NMR and UV. This property would have influence on charge carrier mobility in OFET devices.

6.5 CONCLUSIONS

Two DPP-based spacer polymers functionalized with urethane linker containing alkyl side chains namely- $\text{DPP}_{\text{urethane}}\text{-Th-C}_4\text{-Th}$ and $\text{PDPP}_{\text{alkyl}}\text{-Th-C}_4\text{-Th}$ were synthesized and characterized by ^1H -NMR, ^{13}C -NMR and UV spectroscopy. The incorporation of the spacer units reduced the backbone conjugation and improved the solubility in various solvents. Both the polymers were soluble in CHCl_3 and tetrachloroethane at room temperature and at 80°C . But in cyclohexane or in methylcyclohexane, they formed self-assembly at room temperature, which was confirmed by high temperature ^1H -NMR spectroscopy in cyclohexane- D_{12} and UV-Vis absorption spectroscopy. Variable temperature ^1H -NMR spectra demonstrated the presence of hydrogen bonding and self-assembled behavior in these polymers. It would be interesting to study the influence of polymer self-assembly on charge carrier mobility in OFET device. In the present work, this study could not be taken up due to lack of device fabrication facilities.

REFERENCES

- 1 H. Yan, Z. Chen, Y. Zheng, C. Newman, J. R. Quinn, F. Dötz, M. Kastler and A. Facchetti, *Nature*, 2009, **457**, 679–686.
- 2 H. Sirringhaus, *Science*, 1998, **280**, 1741–1744.

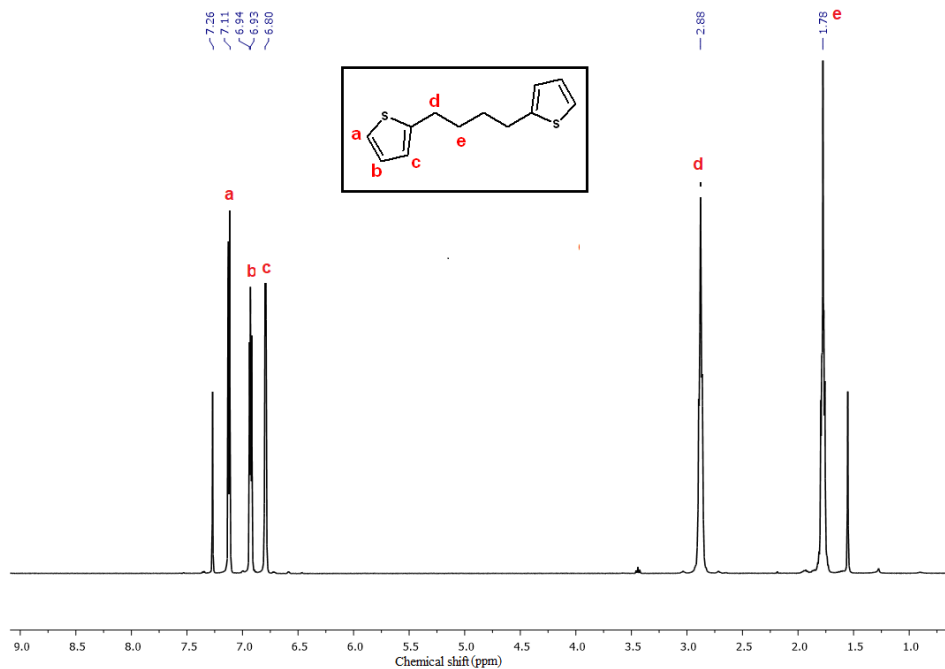
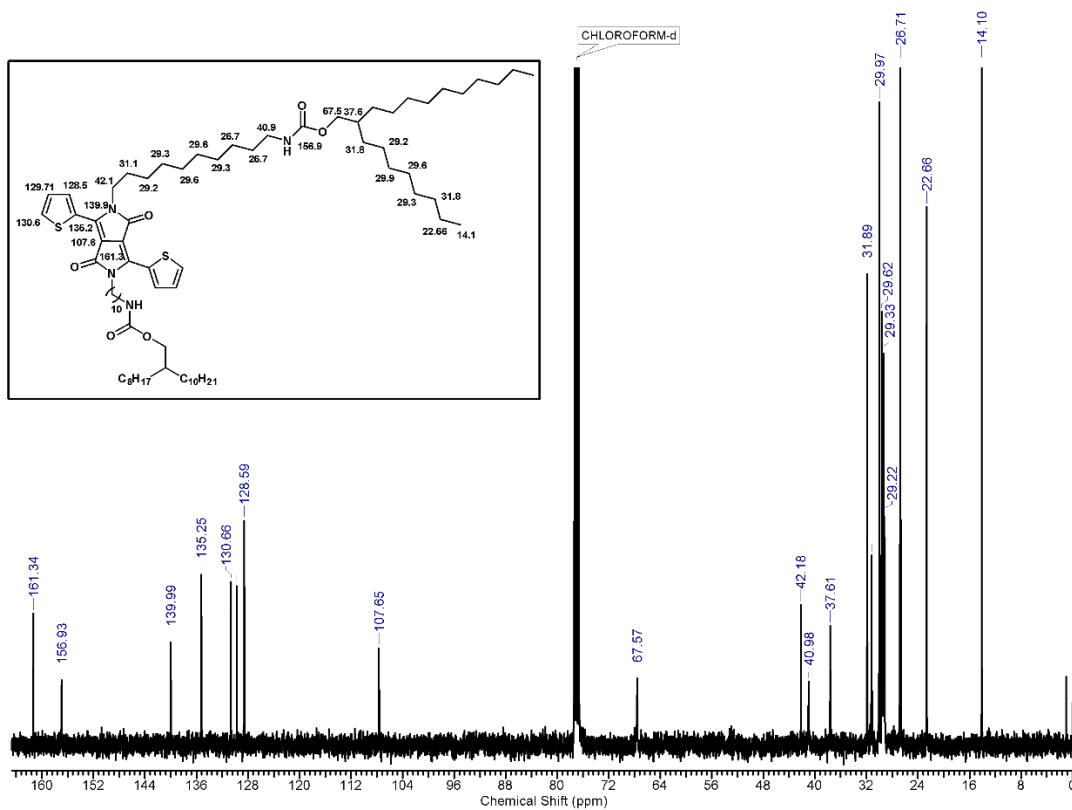
- 3 E. P. Woo, H. Sirringhaus, M. Inbasekaran, R. H. Friend, T. Kawase, T. Shimoda and W. Wu, *Science*, 2000, **290**, 2123–2126.
- 4 H. Chen, Y. Guo, G. Yu, Y. Zhao, J. Zhang, D. Gao, H. Liu and Y. Liu, *Adv. Mater.*, 2012, **24**, 4618–4622.
- 5 B. C. Schroeder, T. Kurosawa, T. Fu, Y. Chiu, J. Mun, G. N. Wang, X. Gu, L. Shaw, J. W. E. Kneller, T. Kreouzis, M. F. Toney and Z. Bao, *Adv. Funct. Mater.*, 2017, **27**, 1701973.
- 6 F. Hinkel, T. Marszalek, W. Zajaczkowski, S. R. Puniredd, M. Baumgarten, W. Pisula and K. Müllen, *Chem. Mater.*, 2014, **26**, 4844–4848.
- 7 I. Kang, H.-J. Yun, D. S. Chung, S.-K. Kwon and Y.-H. Kim, *J. Am. Chem. Soc.*, 2013, **135**, 14896–14899.
- 8 J. Lee, J. W. Chung, J. Jang, D. H. Kim, J. Il Park, E. Lee, B. L. Lee, J. Y. Kim, J. Y. Jung, J. S. Park, B. Koo, Y. W. Jin and D. H. Kim, *Chem. Mater.*, 2013, **25**, 1927–1934.
- 9 Z. Fei, P. Pattanasattayavong, Y. Han, B. C. Schroeder, F. Yan, R. J. Kline, T. D. Anthopoulos and M. Heaney, *J. Am. Chem. Soc.*, 2014, **136**, 15154–15157.
- 10 F. Zhang, Y. Hu, T. Schuettfort, C. A. Di, X. Gao, C. R. McNeill, L. Thomsen, S. C. B. Mannsfeld, W. Yuan, H. Sirringhaus and D. Zhu, *J. Am. Chem. Soc.*, 2013, **135**, 2338–2349.
- 11 T. Lei, J. H. Dou and J. Pei, *Adv. Mater.*, 2012, **24**, 6457–6461.
- 12 A.-R. Han, G. K. Dutta, J. Lee, H. R. Lee, S. M. Lee, H. Ahn, T. J. Shin, J. H. Oh and C. Yang, *Adv. Funct. Mater.*, 2015, **25**, 247–254.
- 13 I. Meager, R. S. Ashraf, S. Mollinger, B. C. Schroeder, H. Bronstein, D. Beatrup, M. S. Vezie, T. Kirchartz, A. Salleo, J. Nelson and I. McCulloch, *J. Am. Chem. Soc.*, 2013, **135**, 11537–11540.
- 14 N. E. Jackson, B. M. Savoie, K. L. Kohlstedt, M. Olvera De La Cruz, G. C. Schatz, L. X. Chen and M. A. Ratner, *J. Am. Chem. Soc.*, 2013, **135**, 10475–10483.
- 15 Y. Cheng, Y. Qi, Y. Tang, C. Zheng, Y. Wan, W. Huang and R. Chen, *J. Phys. Chem. Lett.*, 2016, **7**, 3609–3615.
- 16 M. E. Ziffer, S. B. Jo, Y. Liu, H. Zhong, J. C. Mohammed, J. S. Harrison, A. K.-Y. Jen and D. S. Ginger, *J. Phys. Chem. C*, 2018, **122**, 18860–18869.

- 17 A. P. H. J. Schenning and E. W. Meijer, *Chem. Commun.*, 2005, 3245.
- 18 S.-L. Hsu, C.-M. Chen, Y.-H. Cheng and K.-H. Wei, *J. Polym. Sci. Part A Polym. Chem.*, 2011, **49**, 603–611.
- 19 F. Li, K. G. Yager, N. M. Dawson, J. Yang, K. J. Malloy and Y. Qin, *Macromolecules*, 2013, **46**, 9021–9031.
- 20 S. J. Ananthakrishnan, B. S. Kumar, N. Somanathan and A. B. Mandal, *RSC Adv.*, 2013, **3**, 8331.
- 21 J. Huang, B. Peng, W. Wang, H. Ji, L. Li, K. Xi, W. Lai, X. Zhang and X. Jia, *Adv. Funct. Mater.*, 2016, **26**, 1646–1655.
- 22 F. Li, K. G. Yager, N. M. Dawson, Y. Jiang, K. J. Malloy and Y. Qin, *Polym. Chem.*, 2015, **6**, 721–731.
- 23 Y. Lin, J. A. Lim, Q. Wei, S. C. B. Mannsfeld, A. L. Briseno and J. J. Watkins, *Chem. Mater.*, 2012, **24**, 622–632.
- 24 C. Liu, S. Dong, P. Cai, P. Liu, S. Liu, J. Chen, F. Liu, L. Ying, T. P. Russell, F. Huang and Y. Cao, *ACS Appl. Mater. Interfaces*, 2015, **7**, 9038–9051.
- 25 B. Adhikari, X. Lin, M. Yamauchi, H. Ouchi, K. Aratsu and S. Yagai, *Chem. Commun.*, 2017, **53**, 9663–9683.
- 26 H. Cui, X. Chen, Y. Wang, D. Wei, F. Qiu and J. Peng, *Soft Matter*, 2018, **14**, 5906–5912.
- 27 J. Yao, C. Yu, Z. Liu, H. Luo, Y. Yang, G. Zhang and D. Zhang, *J. Am. Chem. Soc.*, 2016, **138**, 173–185.
- 28 J. Ma, Z. Liu, J. Yao, Z. Wang, G. Zhang, X. Zhang and D. Zhang, *Macromolecules*, 2018, **51**, 6003–6010.
- 29 M. U. Ocheje, B. P. Charron, Y. H. Cheng, C. H. Chuang, A. Soldera, Y. C. Chiu and S. Rondeau-Gagné, *Macromolecules*, 2018, **51**, 1336–1344.
- 30 M. U. Ocheje, M. Selivanova, S. Zhang, T. H. Van Nguyen, B. P. Charron, C. Chuang, Y. Cheng, B. Billet, S. Noori, Y. Chiu, X. Gu and S. Rondeau-Gagné, *Polym. Chem.*, 2018, **9**, 5531–5542.
- 31 Y. Sun, G. C. Welch, W. L. Leong, C. J. Takacs, G. C. Bazan and A. J. Heeger, *Nat. Mater.*, 2012, **11**, 44–48.
- 32 N. D. Treat, J. A. N. Malik, J. A. Nekuda Malik, O. Reid, L. Yu, C. G. Shuttle, G.

- Rumbles, C. J. Hawker, M. L. Chabynec, P. Smith and N. Stingelin, *Nat. Mater.*, 2013, **12**, 628–633.
- 33 Y. Huang, W. Wen, S. Mukherjee, H. Ade, E. J. Kramer and G. C. Bazan, *Adv. Mater.*, 2014, 26, 4168–4172.
- 34 H. J. Li, J. T. Wang, C. Y. Mei and W. S. Li, *Chem. Commun.*, 2014, **50**, 7720–7722.
- 35 A. Gasperini, S. Bivaud and K. Sivula, *Chem. Sci.*, 2014, **5**, 4922–4927.
- 36 Y. Zhao, X. Zhao, Y. Zang, C. A. Di, Y. Diao and J. Mei, *Macromolecules*, 2015, **48**, 2048–2053.
- 37 Z. Liang, R. A. Cormier, A. M. Nardes and B. A. Gregg, *Synth. Met.*, 2011, **161**, 1014–1021.
- 38 L. Ding, H. Bin Li, T. Lei, H. Z. Ying, R. B. Wang, Y. Zhou, Z. M. Su and J. Pei, *Chem. Mater.*, 2012, **24**, 1944–1949.
- 39 X. Lin, M. Hirono, T. Seki, H. Kurata, T. Karatsu, A. Kitamura, D. Kuzuhara, H. Yamada, T. Ohba, A. Saeki, S. Seki and S. Yagai, *Chem. - A Eur. J.*, 2013, **19**, 6561–6565.
- 40 X. Zhu, M. C. Traub, D. A. Vanden Bout and K. N. Plunkett, *Macromolecules*, 2012, **45**, 5051–5057.
- 41 G. J. N. Wang, F. Molina-Lopez, H. Zhang, J. Xu, H. C. Wu, J. Lopez, L. Shaw, J. Mun, Q. Zhang, S. Wang, A. Ehrlich and Z. Bao, *Macromolecules*, 2018, **51**, 4976–4985.
- 42 Y. Zhao, X. Zhao, M. Roders, G. Qu, Y. Diao, A. L. Ayzner and J. Mei, *Chem. Mater.*, 2015, **27**, 7164–7170.
- 43 W. J. Xiao, J. Wang, H. J. Li, L. Liang, X. Xiang, X. Q. Chen, J. Li, Z. Lu and W. S. Li, *RSC Adv.*, 2018, **8**, 23546–23554.
- 44 A. Gasperini, X. A. Jeanbourquin, A. Rahmanudin, X. Yu and K. Sivula, *Adv. Mater.*, 2015, **27**, 5541–5546.
- 45 X. A. Jeanbourquin, A. Rahmanudin, A. Gasperini, E. Ripaud, X. Yu, M. Johnson, N. Guijarro and K. Sivula, *J. Mater. Chem. A*, 2017, **5**, 10526–10536.
- 46 J. Mun, G. J. N. Wang, J. Y. Oh, T. Katsumata, F. L. Lee, J. Kang, H. C. Wu, F. Lissel, S. Rondeau-Gagné, J. B. H. Tok and Z. Bao, *Adv. Funct. Mater.*, 2018, **28**,

- 1–10.
- 47 B. C. Schroeder, Y. C. Chiu, X. Gu, Y. Zhou, J. Xu, J. Lopez, C. Lu, M. F. Toney and Z. Bao, *Adv. Electron. Mater.*, 2016, **2**, 1600104-1600114.
- 48 E. L. Melenbrink, K. M. Hilby, K. Choudhary, S. Samal, N. Kazerouni, J. L. McConn, D. J. Lipomi and B. C. Thompson, *ACS Appl. Polym. Mater.*, 2019, **1**, 1107–1117.
- 49 E. L. Melenbrink, K. M. Hilby, M. A. Alkhadra, S. Samal, D. J. Lipomi and B. C. Thompson, *ACS Appl. Mater. Interfaces*, 2018, **10**, 32426–32434.
- 50 Y.-C. Chiang, H.-C. Wu, H.-F. Wen, C.-C. Hung, C.-W. Hong, C.-C. Kuo, T. Higashihara and W.-C. Chen, *Macromolecules*, 2019, **52**, 4396-4404.
- 51 T. Lebarbé, A. S. More, P. S. Sane, E. Grau, C. Alfos and H. Cramail, *Macromol. Rapid Commun.*, 2014, **35**, 479–483.

Supporting Information

Figure SI 6.1 $^1\text{H-NMR}$ spectrum (CDCl₃) of 1,4-di(thiophen-2-yl)butaneFigure SI 6.2 $^{13}\text{C-NMR}$ spectrum (CDCl₃) of DPP_{urethane}

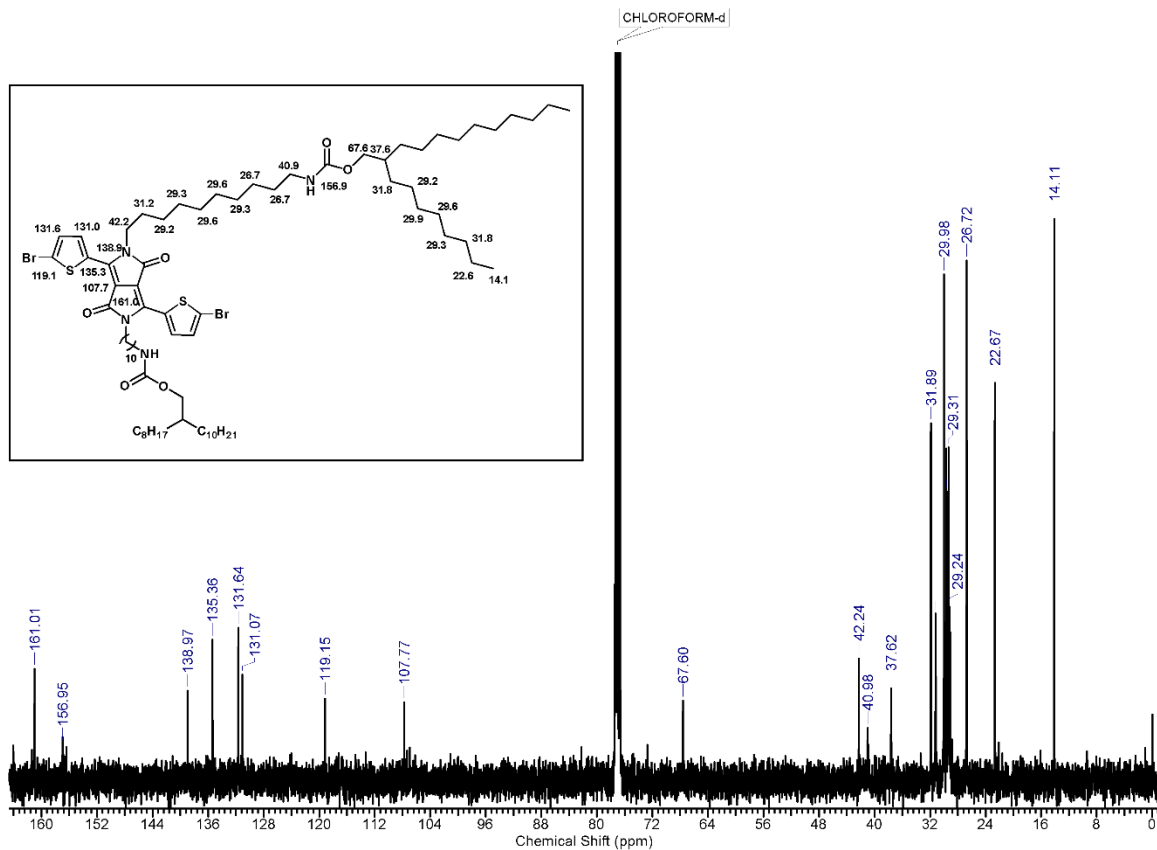


Figure SI 6.3 ^{13}C -NMR spectrum (CDCl₃) of DPPurethane monomer

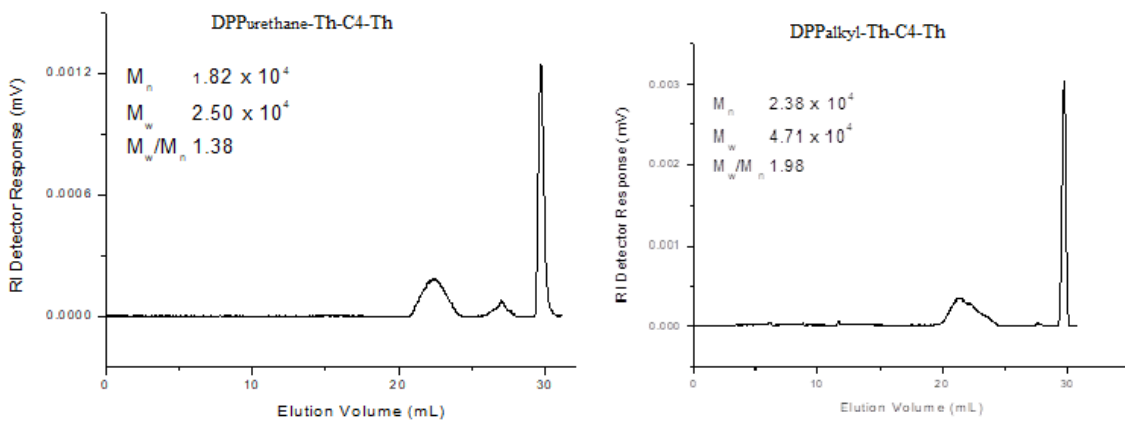


Figure SI 6.4 GPC traces for spacer polymers

CHAPTER 7

Summary and Conclusions

7.1 SUMMARY AND CONCLUSIONS

The overall objective of the work was to design and synthesize new solution processable π -conjugated materials (small molecules/polymers) for photovoltaic applications and to derive structure-property relationship with respect to their optoelectronics properties.

Poly(*p*-arylene-ethynylene)-*alt*-poly(*p*-arylene-vinylene)s (PAE-PAVs) constitute an important class of conjugated polymers which exhibit interesting properties like low-lying LUMO levels, higher molar extinction coefficients, and especially higher fluorescence quantum yields and have been successfully utilised as donor material in the active layer of the optoelectronic devices like OLEDs and OSCs. Introduction of anthracene group in PAE-PAV system resulted in lowering of the band-gap of the polymer. With an objective to tune the π - π stacking distance of PAE-PAV polymers, alkoxy side chains of different nature (linear/branched) and length were appended onto polymer backbone with an anticipation that it would result in favorable nanoscale morphology of polymer:PCBM blend in optoelectronic devices. Five anthracene-containing PPE-PPV polymers bearing different side chains lengths and nature were synthesized and characterized by $^1\text{H-NMR}$ and $^{13}\text{C-NMR}$ spectroscopy. Polymers were obtained with number average molecular weights in the range 15.8- 47.5 kg/mol. Polymer with octyloxy substitution close to the AnE units (AnE-PV ab , - ad) arranged in a stacked structure. Whereas asymmetric (AnE-PV cc) or branched side chain substitution (AnE-PV bb , - ba) near the AnE unit yielded less organized or even amorphous polymers. Polymers with strong tendency of stacking exhibited well resolved thin film absorption peaks in UV-Vis spectra. Polymers with less or no intrinsic stacking ability exhibited featureless absorption peaks. Polymers (AnE-PV bb , - ba , - cc) exhibited higher hole mobilities as compared to polymers (AnE-PV ab , - ad) but they exhibited poor photovoltaic performance as a result of insufficient donor-acceptor phase separation in their blends with PCBM which hindered efficient charge separation. On the other hand, the polymers (AnE-PV ab , - ad) having inclination to stack, exhibited stronger phase separation and better photovoltaic performance. Among the series of synthesized polymers, the best photovoltaic performance ($\eta = 3.14\%$) was achieved for polymer AnE-PV ab , which exhibited stacking ability. Thus, it was concluded that the alkoxy

chains appended onto the polymer backbone, not only improved polymer solubility, but also played a significant role in controlling active layer nanomorphology and hence the solar cell performance. Thus, a correlation between the ability to form π - π -stacking, the absorption behavior, the charge carrier mobility, the active layer nanoscale morphology, and the photovoltaic performance was established in anthracene-containing PAE-PAV polymers.

It is generally recognized that donor-acceptor (D-A) type of low band-gap materials are promising candidates as an active layer material in optoelectronic devices. Taking a clue from this, a new anthracene containing PPE compound; viz. 9,10-bis((2,5-bis(octyloxy)-4-vinylphenyl)ethynyl)anthracene (AnPPE) was synthesised. AnPPE was reacted with two different acceptor units namely, DPP and BTDA by Pd-catalyzed Heck reaction to form two new D-A small molecules namely- AnPPE-Th-DPP(EH) and AnPPE-Th-BTDA. The small molecules were characterized by $^1\text{H-NMR}$, HRMS and MALDI (TOF). AnPPE-Th-DPP(EH) was soluble in organic solvents such as chloroform, dichloromethane, dimethyl sulphoxide and chlorobenzene. AnPPE-Th-BTDA was partially soluble in dichloromethane, and chlorobenzene at higher temperature. UV-Vis spectra of AnPPE-Th-DPP(EH) and AnPPE-Th-BTDA showed wavelength of absorption maxima at 676 nm and 535 nm, respectively. Optical band gap energy for AnPPE-Th-DPP(EH) was found to be 1.47 eV. Photoluminescence spectrum of AnPPE-Th-BTDA showed emission maximum at 643 nm. Electrochemical band-gap values of AnPPE-Th-DPP(EH) and AnPPE-Th-BTDA were 1.35 and 1.55 eV, respectively. OFET devices fabricated using AnPPE-Th-DPP molecule showed hole mobility value of $4.19 \times 10^{-6} \text{ cm}^2 \text{ V}^{-1} \text{ s}^{-1}$.

The introduction of a conjugated side chain on main donor-acceptor conjugated backbone is considered to be an effective approach for enhancing photovoltaic performance by broadening the absorption in visible to near IR region and by improving short circuit current density (J_{sc}). Towards this end, PPE-PPV polymers incorporating a bithienylene-vinylene thiophene group as a conjugated side chain on the PPE unit (BTE-PPVs) were synthesised. The polymers differ in the nature of solubilizing side chains, viz octyloxy (linear) or 2-ethylhexyloxy (branched) chains on the PPE and PPV units. Polymers were characterized by $^1\text{H-NMR}$ and $^{13}\text{C-NMR}$ spectroscopy. Polymers were

obtained with number average molecular weights in the range 5.9- 26.7 kg/mol. XRD study on films indicated a completely amorphous feature of polymer films. Even though the thin film absorption spectra for the polymers containing linear octyloxy chains, (BTE-PV ab and BTE-PV aa), suggested the presence of a moderate organization in the polymers, no obvious evidence of ordering (π - π stacking) appeared in the XRD study of films. Time of flight technique was used to study charge carrier mobility. Polymers exhibited very different charge transport properties. The bulk hole mobility at a field of about 8×10^4 V cm $^{-1}$ ranged from 1.3×10^{-5} cm 2 V $^{-1}$ s $^{-1}$ for BTE-PV aa , substituted with solely linear chains, to the outstanding value of 2.2×10^{-2} cm 2 V $^{-1}$ s $^{-1}$ for BTE-PV ba , with branched and linear solubilizing chains. This remarkable difference of mobility values (order of three), is mainly attributed to the chemical structure of the polymers. The combination of linear and branched chains was found to be favorable for charge transport properties of the investigated polymers, compared to the incorporation of only linear or branched side-chains. The bulk heterojunction solar cells were fabricated with BTE-PV as donors and PC $_{60}$ BM as acceptor. The highest photovoltaic performance ($\eta = 2.1$ %) was observed for polymer BTE-PV ab . Polymer BTE-PV ba exhibiting highest hole mobility showed poor photovoltaic performance because of an unfavorable morphology of the blends.

Recently, terpolymers comprising three different components in the polymer backbone have emerged as a new design strategy for conjugated polymers. These polymers are known to exhibit improved solubility, solar absorption and photocurrent. With added new D or A unit, tuning of HOMO-LUMO energy levels and π - π stacking in terpolymers is possible. In this context, a new molecule-1,3-dibromo-5,7-dihexyl-4H,8H-benzo[1,2-c:4,5-c']dithiophene-4,8-dione (BDD) was incorporated as second acceptor in the synthesis of terpolymers. Two copolymers and four terpolymers comprising cyclopentadithiophene (CPDT), bithiophene (BT), benzo[1,2-b:4,5-b']dithiophene (BDT) as electron donor units and diketopyrrolopyrrole (DPP), benzo[1,2-c:4,5-c']dithiophene-4,8-dione (BDD) as electron acceptor units were synthesized and characterized by ^1H and ^{13}C -NMR spectroscopy. Terpolymers showed much broader absorption in visible and near IR region of light spectrum and improved solubility in organic solvents such as chloroform, dichloromethane, dimethyl sulphoxide and chlorobenzene as compared to

copolymers comprising same electron donor and electron acceptor units. Terpolymers- BDT-DPP(EH)-BDD and BDT-DPP(HD)-BDD, exhibited temperature dependent UV-Vis absorption spectra which indicated presence of aggregates in these polymers. This property can be utilized to manipulate morphology of active layer in the fabrication of solar cell devices. Bulk heterojunction solar cells were fabricated using two polymers- CPDT-BDD and BDT-DPP(EH)-BDD as donor material with PC₇₀BM acceptor. CPDT-BDD polymer showed maximum power conversion efficiency of 1.63 % and 1.39 % in inverted and conventional device architecture, respectively. The terpolymer BDT-DPP(EH)-BDD exhibited $\eta=1.57$ % in conventional device. The terpolymer BDT-DPP(HD)-BDD showed negligible solar cell performance as compared to polymer BDT-DPP(EH)-BDD which is attributed to the longer side chains on this polymer causing steric hindrance and thus the unsuitable morphology in polymer: PC₇₀BM blend film used as active layer during device fabrication.

Hydrogen bonds have also known to influence polymer self-assembly and the solid-state morphology of conjugated materials. It was found that the intermolecular hydrogen bonds formed between adjacent moieties directly affect the lamellar packing of the polymer and aggregation, without affecting the π -conjugation. With certain DPP-based polymers incorporating hydrogen-bonding sites, it is possible to achieve excellent mechanical properties such as enhanced stretching ability and reduction in elastic modulus of the polymers for stretchable electronics applications. Another exciting approach to improve long term morphological stability of BHJ film by reducing donor crystallization, is the incorporation of flexible aliphatic linkers/spacers in the conjugated backbone without negatively affecting charge transport properties. Taking a clue from these strategies, two DPP-based semiconducting copolymers incorporating a flexible spacer unit (containing four carbon atom chain) in the conjugated backbone and urethane-linker containing alkyl side chains were synthesized. The urethane-containing aliphatic side chains enable intermolecular hydrogen bonding in the polymer and the spacer unit is proposed to control the crystallization/self-assembly induced by the hydrogen-bonding in the thin films. The two spacer polymers, namely- DPP_{urethane}-Th-C4-Th and DPP_{alkyl}-Th-C4-Th were characterized by ¹H-NMR, ¹³C-NMR and UV-Vis spectroscopy. The incorporation of the spacer units reduced the backbone conjugation and improved the

solubility in solvents such as chloroform, dichloromethane, dimethyl sulphoxide, etc. Variable temperature $^1\text{H-NMR}$ spectra demonstrated the presence of hydrogen bonding and self-assembled behavior in the $\text{DPP}_{\text{urethane}}\text{-Th-C4-Th}$ polymer. Both the polymers were soluble in CHCl_3 and tetrachloroethane at room temperature and at 80°C . But in cyclohexane or in methylcyclohexane (MCH), they formed self-assembly at room temperature, which was confirmed by high temperature $^1\text{H-NMR}$ spectroscopy in cyclohexane- D_{12} and UV-Vis absorption spectroscopy. These supramolecular interactions have been known to modify the thin film morphology and potentially affect the charge transport in the solid state. Based on these results, the synthesized polymers could find potential application as active layer in OFET devices. However, the evaluation couldn't be carried out due to lack of device fabrication facility at this point of time.

7.2 FUTURE PERSPECTIVES

The work embodied in the thesis was focused on design and synthesis of new solution-processable π -conjugated small molecules and polymers with improved photovoltaic properties and has opened many new avenues for the future work.

1. In case of terpolymers, the percentage of co-monomers in a terpolymer could be varied. The optimum composition of monomers would lead to the terpolymeric system with optimized thin film morphology for enhanced photophysical and photovoltaic properties.
2. The terpolymers can be further evaluated for their solar cell performance with non-fullerene acceptors such as ITIC (2,2'-[[6,6,12,12-tetrakis(4-hexylphenyl)-6,12 dihydrodithieno[2,3-*d'*:2',3'-*d'*]-s-indaceno[1,2-*b*:5,6-*b'*]dithiophene-2,8 diyl]bis[methyldiylidene(3-oxo-1*H*-indene2,1(3*H*)-diylidene)]bis[propanedinitrile]) to achieve higher efficiency values in solar cell devices.
3. The spacer polymers exhibited self-assembled behavior in solution. It would be interesting to study, as how to transfer this self-assembly in solid state/films.
4. There is a scope to vary the percentage of urethane linkage in the spacer polymers and to study its influence on solid state self-assembly.

5. It would be worthwhile to investigate the spacer polymers for the charge carrier mobility studies in OFET devices. The influence of these supramolecular forces on charge transport in OFET devices would be interesting to study.
6. Anthracene containing PPE-PPV polymers are highly fluorescent materials. It would be worth to evaluate them for sensor applications.

Synopsis of the Thesis Entitled “New π -Conjugated Materials for Optoelectronic Applications”

Chapter 1: Introduction

Replacing the fossil fuels by renewable energy sources is essential to solve the non-avoidable future energy problems of our society. In addition, they contribute to the protection of our fragile environment. Photovoltaics are of great importance in this context. Organic Photovoltaics (OPVs) has recently gained significant attention due to the possibility of processing organic semiconductors (conjugated polymers or small molecules) from solution at low temperature and for large area devices with lower cost. Moreover, organic semiconductors can be deposited on various substrates including flexible plastic substrates which open up the way for their applications in products with lower cost, flexibility and lighter weight. In addition, the structural versatility of organic semiconductors allows the incorporation of functionalities by molecular design, which is the most attractive feature of OPV. Thus, OPV technology can be considered as a promising alternative to current silicon technology for potential applications in optoelectronics.^{1d,1e}

OPV devices (also known as Organic Solar Cell (OSC) or Polymer Solar Cell (PSC)) generate electrical power by converting solar radiations into electricity by means of organic semiconductors. Organic semiconductors can be classified into two broad categories, namely small molecules and conjugated polymers, both of which possess π -conjugation, enabling optical absorption and proper charge transport. These semiconductors are used as an active material in single layer OSC^{4a-4i}, donor materials in Bilayer and Bulk Heterojunction (BHJ) OSC^{2a-2d} and non-fullerene acceptor.³ Conjugated polymers, on one hand, have advantages over small molecular semiconductors such as isotropic transport characteristics, solution processability, control on structural and morphological characteristics of the film and robust mechanical properties for roll-to-roll fabrication on flexible substrates. On the other hand, small-molecule semiconductors exhibit properties such as well-defined molecular structure, defined molecular weight, and high purity without batch- to -batch variations which are hard to achieve for polymers.

Chapter 2: Scope and Objectives

The last two decades have been marked by intensive research in the field of OPVs.^{1a-1e} A number of interesting conjugated polymeric materials, exhibiting band gap energies around and below 2 eV have been synthesized for organic solar cell applications.^{5a-5d} High power conversion efficiencies have been reported by various research groups using various conjugated polymers as donor material in conjunction with fullerene derivatives (PC₆₁BM or PC₇₁BM) as acceptors in a bulk hetero-junction construct.^{6a-6e}

Realization of high-performance polymer solar cells (PSCs) requires efficient harvesting of the solar energy which can be achieved by-

1. Optimizing the energy gap and film absorption coefficient of conjugated polymers.
2. Designing the conjugated polymers with strong and broad absorption covering entire solar radiation range.
3. Improving the active layer morphology to provide extended donor-acceptor interfaces facilitating exciton diffusion and charge transfer.

Theoretically, the ideal band gap of conjugated polymers for PSCs should be around 1.5 eV.^{7a-7c} However, the most studied conjugated polymers, such as polythiophenes (PTs) and poly(phenylene vinylene)s (PPVs),^{8a,8b} exhibit optical band gap energies larger than or around 2.0 eV and therefore can harvest only visible light. This mismatch of the absorption to the solar spectrum significantly limits the device performance of PSCs. Therefore, development of NIR-absorbing or low band gap polymers is very important. One of the strategies for lowering the band gap energy is to design push-pull conjugated polymer (D-A conjugated polymer). Such polymers have been demonstrated to be highly efficient donor materials in BHJ-PSCs because their light harvesting abilities and energy levels can be well tuned by controlling the photo-induced intramolecular charge transfer (ICT) from donor to acceptor units. Therefore, different building units have significant influence on the final photovoltaic properties of the resulting polymers.^{4a,4i,9a-9d}

Yet another approach for improving the absorption of solar spectrum is to design two-dimensionally conjugated polymers. Such polymers have strong and broad absorption covering UV as well as visible portion of solar spectrum.^{10a,10b} Li et al. synthesized bi-

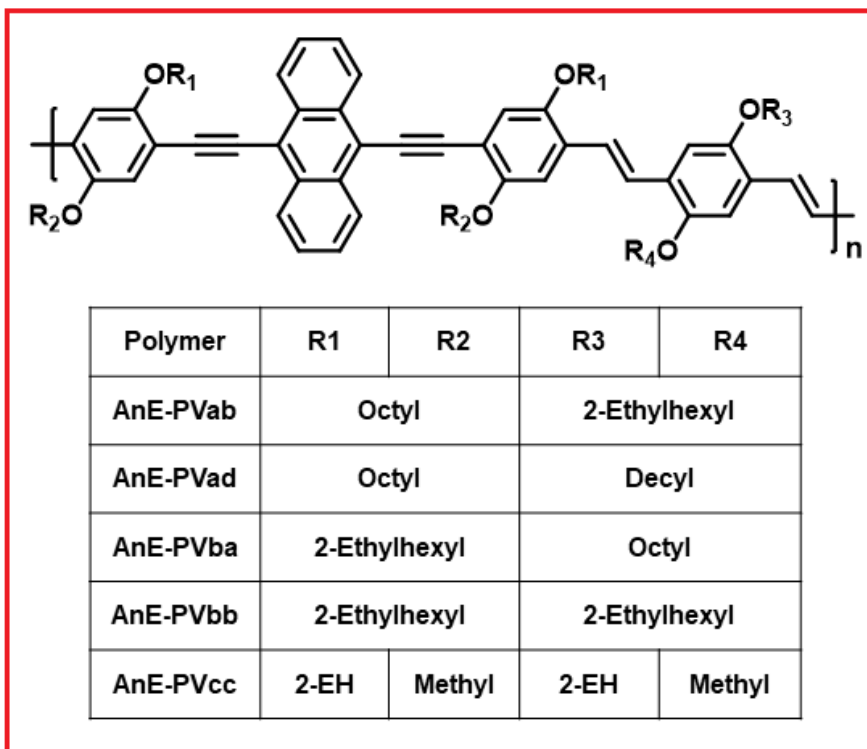
(thienylenevinylene) substituted polythiophenes (biTV-PTs) which possess a broad and strong absorption band in the region 350 to 650 nm. The best performing polymer showed the maximum power conversion efficiency of 3.18 % which is 38 % increase in comparison with that of the devices based on P3HT under the same experimental conditions.^{10a} Subsequently, few other two-dimensionally conjugated polymers have been designed and were found to exhibit excellent performance as donor material in BHJ solar cells.^{10c-e}

The aim of the research work was to design and synthesise polymers with enhanced solar absorption by appropriate band gap engineering which would find applications as active layer material in optoelectronic devices such as organic solar cells, organic field effect transistors, etc. Another objective of the present work was to utilise non-covalent interactions to guide polymer self-assembly and influence the solid-state morphology of the conjugated polymers.

The following specific objectives were pursued in the research work-

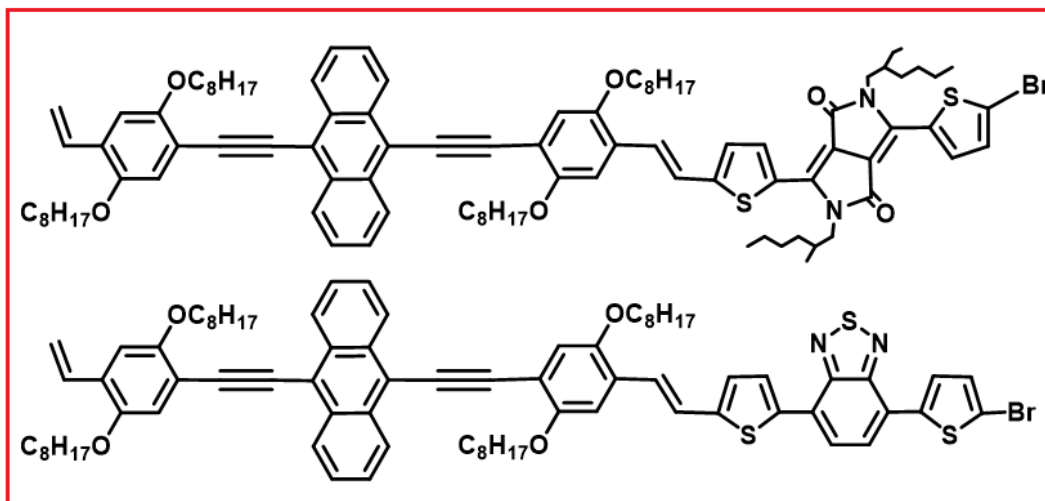
1. Synthesis of low band gap polymers with high absorption coefficient, study of structure-property relationship and evaluation of their performance as donor material in BHJ solar cells.
2. Synthesis of two-dimensionally conjugated polymers for strong and broad absorption in solar spectrum and evaluation of their performance as donor material in BHJ solar cells.
3. Synthesis of terpolymers comprising three different units in the polymer backbone rendering broad absorption, deep energy levels, high mobility and good solubility and to evaluate their performance in BHJ solar cells.
4. The side chain engineering by introduction of urethane linkage (hydrogen-bonding sites) on DPP-based polymers, simultaneously incorporating non-conjugated spacer in the polymer backbone to afford self-assembled polymers and study their solid-state morphology.

Chapter 3- Part a: Anthracene Containing PAE-PV Polymers: Influence of π - π Stacking Distance on the Morphology and Performance of Solar Cells



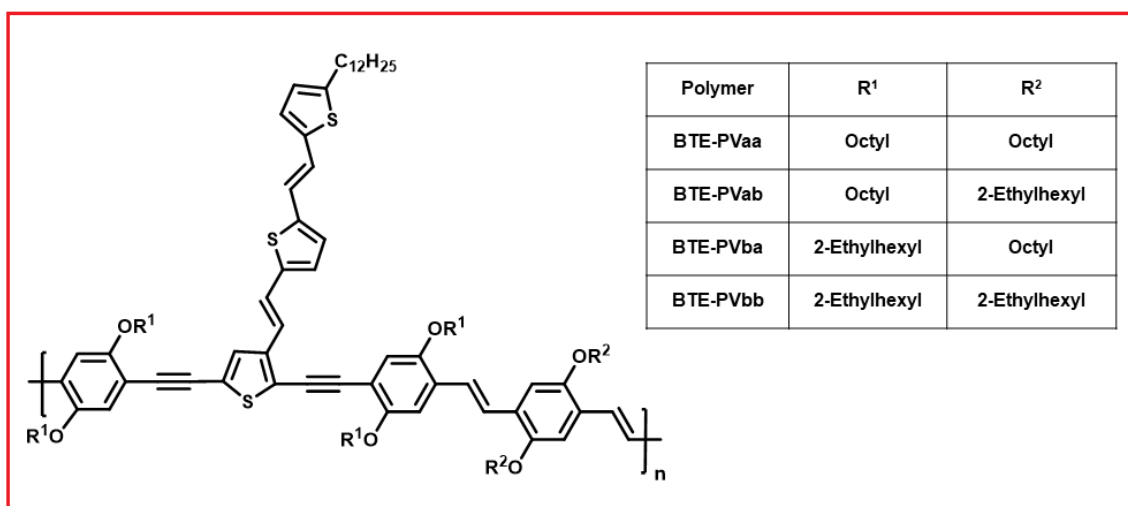
Anthracene containing PAE-PV copolymers were successfully synthesized and their side chains were systematically varied between linear, branched and asymmetric substitution. Photophysical and electrochemical characterization were performed; typical band-gap energies were 2 eV (optical) and 1.8 eV (electrochemical), respectively. Structure investigation in the bulk and in filaments yielded information about crystallinity and order with respect to the interlayer distance and the π - π stacking distance. Polymers with linear side chains on PAE unit showed improved ordering during and after annealing at 80-100°C. Relatively high open circuit voltage values (0.9 V) were achieved due to the lower LUMO levels of the polymers. Solar cell efficiency up to 3.1 % was achieved.

Chapter 3- Part b: Donor-Acceptor Low Band Gap Small Molecule Containing Anthracene Based Donor Unit and Diketopyrrolopyrrole, Benzothiadazole as Acceptor Units



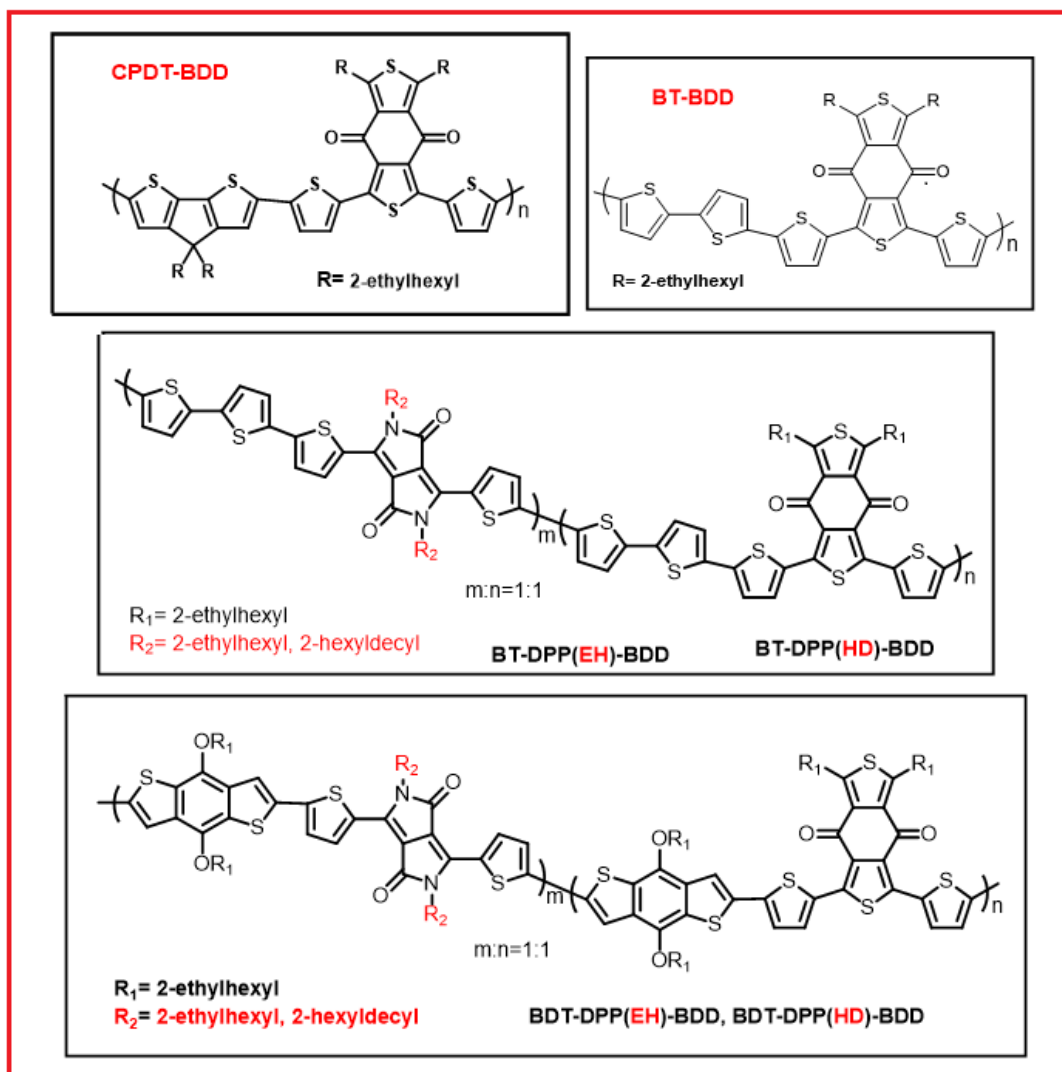
Two low band gap donor-acceptor small molecules comprising anthracene containing (*p*-phenylene ethynylene) (AnPPE) as a donor unit; and diketopyrrolopyrrole (DPP) or benzothiadiazole (BTDA) as acceptor units respectively were successfully synthesized by Pd-catalyzed Heck reaction. The small molecules were characterized by $^1\text{H-NMR}$ and UV-Vis spectroscopy. UV-Visible absorption spectrum of AnE-PV-DPP and AnE-PV-BTDA showed absorption maxima at 676 nm and 535 nm, respectively. Electrochemical band-gap energies of AnE-PV-DPP and AnE-PV-BTDA were 1.29 eV and 1.55 eV, respectively. AnE-PV-DPP showed hole mobility value of $4.19 \times 10^{-6} \text{ cm}^2 \text{ V}^{-1} \text{ s}^{-1}$ in OFET devices.

Chapter 4: Bi(thienylene-vinylene)thiophene Containing PAE-PV: Modulation of Charge Carrier Mobility by Side Chain Engineering



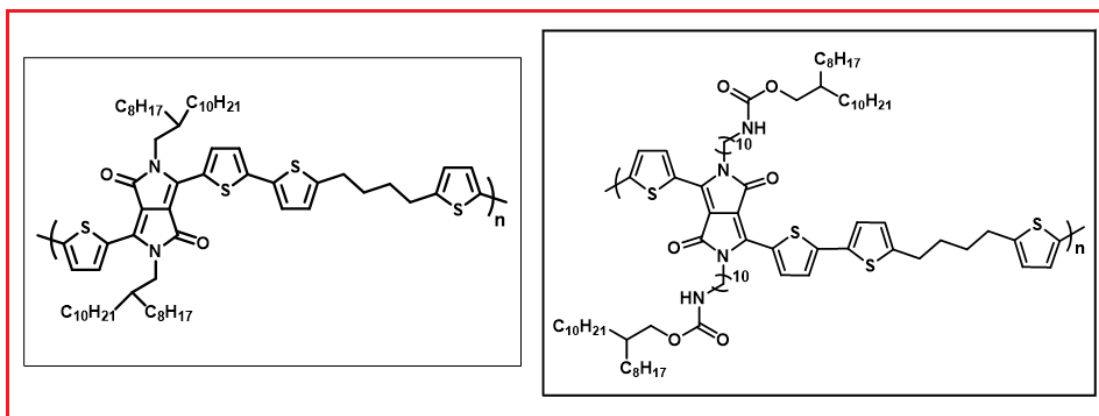
Four bi(thienylene-vinylene)thiophene based PAE-PV polymers bearing different side chain nature (linear/branched) were synthesised and characterised. The drift mobility of holes in BTE-PV ba , reached a value of $10^{-2} \text{ cm}^2 \text{ V}^{-1} \text{ s}^{-1}$ which is quite attractive. Polymers having linear side chains (BTE-PV aa , BTE-PV ab) at BTE unit showed higher efficiencies in solar cells. The highest efficiency was obtained for polymer BTE-PV ab bearing linear side chains at PAE unit and branched side chain at PV unit. This result correlated well with previous results reported for AnE-PPV polymers.¹¹

Chapter 5: Benzo[1,2-c:4,5-c']dithiophene-4,8-dione Containing Copolymers and Terpolymers: Implications of Active Layer Morphology on Photovoltaic Performance



Two copolymers and four terpolymers comprising cyclopentadithiophene (CPDT), bithiophene (BT), benzo[1,2-b:4,5-b']dithiophene (BDT) as electron donor units and diketopyrrolopyrrole (DPP), benzo[1,2-c:4,5-c']dithiophene-4,8-dione (BDD) as electron acceptor units were synthesized and characterized by ^1H and ^{13}C -NMR spectroscopy. Terpolymers showed much broader absorption in visible and near IR region of light spectrum and improved solubility in organic solvents as compared to copolymers. CPDT-BDD copolymer was used as donor material in active layer of bulk hetero-junction solar cells. It showed maximum power conversion efficiency of 1.63 % and 1.39 % in inverted and conventional device architecture, respectively. Terpolymers BDT-DPP(EH)-BDD and BDT-DPP(HD)-BDD exhibited temperature dependent UV-Vis absorption spectra, which indicated tendency to form aggregates in these polymers. This property can be utilized to manipulate morphology of active layer in the fabrication of solar cell devices.

Chapter 6: DPP-Based Spacer Polymers Functionalized with Urethane Linker Containing Alkyl Side chains: Study of Self-assembly Behaviour



Diketopyrrolopyrrole (DPP) based polymers with either long alkyl chain or urethane linkage containing alkyl chain on DPP unit (namely PDPP-alkyl-Th-C4-Th and PDPP-urethane-Th-C4-Th) were synthesized and characterized by ^1H and ^{13}C -NMR spectroscopy. These polymers were completely soluble in chloroform but insoluble in cyclohexane and methyl cyclohexane at room temperature. At higher temperature (80°C), they were found to dissolve in both the solvents as confirmed by ^1H -NMR spectroscopy. This indicated that the polymers form self-assembly in cyclohexane or methyl cyclohexane at room temperature. These supramolecular interactions have been known to modify the

thin film morphology and potentially affect the charge transport in the solid state.¹² It would be interesting to study the influence of polymer self-assembly on charge carrier mobility in OFET. In the present work, this study could not be taken up due to lack of device fabrication facilities.

REFERENCES

1. (a) M. Granstrom, K. Petritsch, A. C. Arias, A. Lux, M. R. Andersson and R. H. Friend, *Nature*, 1998, 395, 257. (b) P. Schilinsky, C. Waldauf and C. J. Brabec, *Appl. Phys. Lett.*, 2002, 81, 3885. (c) J. S. Kim, Y. Lee, J. H. Lee, J. H. Park, J. K. Kim and K. Cho, *Adv. Mater.*, 2010, 22, 1355. (d) J.-L. Bredas and J. R. Durrant, *Acc. Chem. Res.*, 2009, 42, 1689–1690. (e) R. Li, W. Hu, Y. Liu and D. Zhu, *Acc. Chem. Res.*, 2010, 43, 529–540.
2. (a) J. Roncali, *Acc. Chem. Res.*, 2009, 42, 1719. (b) B. Walker, C. Kim and T.-Q. Nguyen, *Chem. Mater.*, 2011, 23, 470. (c) A. W. Hains, Z. Liang, M. A. Woodhouse and B. A. Gregg, *Chem. Rev.*, 2010, 110, 6689. (d) F. Wuerthner and K. Meerholz, *Chem.–Eur. J.*, 2010, 16, 9366.
3. P. Sonar, J. P. Fong Lim and K. L. Chan, *Energy Environ. Sci.*, 2011, 4, 1558.
4. (a) Y.-J. Cheng, S.-H. Yang and C.-S. Hsu, *Chem. Rev.*, 2009, 109, 5868. (b) X. Zhao and X. Zhan, *Chem. Soc. Rev.*, 2011, 40, 3728. (c) J. Chen and Y. Cao, *Acc. Chem. Res.*, 2009, 42, 1709. (d) S. Guenes, H. Neugebauer and N. S. Sariciftci, *Chem. Rev.*, 2007, 107, 1324. (e) J. Roncali, *Chem. Soc. Rev.*, 2005, 34, 483. (f) C. J. Brabec, S. Gowrisanker, J. J. M. Halls, D. Laird, S. Jia and S. P. Williams, *Adv. Mater.*, 2010, 22, 3839. (g) Andersson, *Adv. Mater.*, 2010, 22, E100. (h) C. Li, M. Liu, N. G. Pschirer, M. Baumgarten and K. Mullen, *Chem. Rev.*, 2010, 110, 6817. (i) N. Blouin and M. Leclerc, *Acc. Chem. Res.*, 2008, 41, 1110.
5. (a) D. Muehlbacher, M. Scharber, M. Morana, Z. Zhu, D. Waller, R. Gaudiana and C. Brabec, *Adv. Mater.*, 2006, 18, 2884. (b) K.-H. Ong, S.-L. Lim, H.-S. Tan, H.-K. Wong, J. Li, Z. Ma, L. C. H. Moh, S.-H. Lim, J. C. de Mello and Z.-K. Chen, *Adv. Mater.*, 2011, 23, 1409. (c) K. Reichenbacher, H. I. Suss and J. Hulliger, *Chem. Soc. Rev.* 2005, 34, 22. (d) T.-Y. Chu, J. Lu, S. Beaupre', Y. Zhang, J.-R. Pouliot, S. Wakim, J. Zhou, M. Leclerc, Z. Li, J. Ding and Y. Tao, *J. Am. Chem. Soc.*, 2011, 133, 4250.

6. (a) H. Zhou, L. Yang, A. C. Stuart, S. C. Price, S. Liu and W. You, *Angew. Chem., Int. Ed.*, 2011, 50, 2995. (b) Y. Zou, A. Najari, P. Berrouard, S. Beaupre', B. Re'da Ai'ch, Y. Tao and M. Leclerc, *J. Am. Chem. Soc.*, 2010, 132, 5330. (c) C. Piliago, T. W. Holcombe, J. D. Douglas, C. H. Woo, P. M. Beaujuge and J. M. J. Fre'chet, *J. Am. Chem. Soc.*, 2010,132, 7595. (d) J. C. Bijleveld, A. P. Zoombelt, S. G. J. Mathijssen, M. M. Wienk, M. Turbiez, D. M. de Leeuw and R. A. J. Janssen, *J. Am. Chem. Soc.*, 2009, 131, 16616. (e) Y. Liang, Z. Xu, J. Xia, S.-T. Tsai, Y. Wu, G. Li, C. Ray and Yu, *Adv. Mater.*, 2010, 22, E135.
7. (a) M. C. Scharber, D. Muhlbacher, M. Koppe, P. Denk, C. Waldauf, A. J. Heeger, C. J. Brabec, *Adv. Mater.* 2006, 18, 789. (b) E. Bundgaard, F. C. Krebs, *Macromolecules* 2006, 39, 2823. (c) M. H. Petersen, O. Hagemann, K. T. Nielsen, M. Jørgensen, F. C. Krebs, *Sol. Energy Mater. Sol. Cells* 2007, 91, 996.
8. (a) M. M. Wienk, J. M. Kroon, W. J. H. Verhees, J. Knol, J. C. Hummelen, P. A. van Hal, R.A.J. Janssen, *Angew. Chem., Int. Ed.* 2003, 42, 3371. (b) S. E. Shaheen, C. J. Brabec, N. S. Sariciftci, F. Padinger, T. Fromherz, J. C. Hummelen, *Appl. Phys. Lett.* 2001, 78, 841.
9. (a) J. Chen and Y. Cao, *Acc. Chem. Res.*, 2009, 42, 1709. (b) X. Zhan and D. Zhu, *Polym. Chem.*, 2010, 1, 409. (c) P.-L. T. Boudreault, A. Najari and M. Leclerc, *Chem. Mater.*, 2011, 23, 456. (d) C. L. Chochos and S. A. Choulis, *Prog. Polym. Sci.*, 2011, 36, 1326. e) P. M. Beaujuge and J. M. J. Frechet, *J. Am. Chem. Soc.* 2011, 133, 20009.
10. (a) J. Hou, Z. Tan, Y. Yan, Y. He, C. Yang, and Y. Li, *J. Am. Chem. Soc.* 2006, 128, 4911. (b) Y. Li and Y. Zou, *Adv. Mater.* 2008, 20, 2952. (c) L. Huo, S. Zhang, X. Guo, F. Xu, Y. Li, and J. Hou, *Angew. Chem. Int. Ed.* 2011, 50, 9697. (d) R. Duan, L. Ye, X. Guo, Y. Huang, P. Wang, S. Zhang, J. Zhang, L. Huo, and J. Hou, *Macromolecules* 2012, 45, 3032. (e) S. Shen, P. Jiang, C. He, J. Zhang, P. Shen, Y. Zhang, Y. Yi, Z. Zhang, Z. Li, and Y. Li, *Chem. Mater.* 2013, 25, 2274.
11. D. A. M. Egbe, S. Turk, S. Rathgeber, F. Kuhnlenz, R. Jadhav, A. Wild, E. Birckner, G. Adam, A. Pivrikas, V. Cimrova, G. Knoer, N. S. Sariciftci, and H. Hoppe, *Macromolecules* 2010, 43, 1261.
12. J. Yao, C. Yu, Z. Liu, H. Luo, Y. Yang, G. Zhang and D. Zhang, *J. Am. Chem. Soc.* 2016,138,173.

List of Publications

1. **Rupali Jadhav**, Stephan Türk, Florian Kühnlenz, Vera Cimrova, Silke Rathgeber, Daniel A. M. Egbe, and Harald Hoppe, “*Anthracene-containing PPE-PPV copolymers: Effect of side chain nature and length on photophysical and photovoltaic properties*” **Phys. Stat. Solidi A**, 2009, **206**, 2695-2699.
2. Daniel A. M. Egbe, Stephan Türk, Silke Rathgeber, Florian Kühnlenz, **Rupali Jadhav**, Andreas Wild, Eckhard Birckner, Getachew Adam, Almantas Pivrikas, Vera Cimrova, Guenter Knoer, Niyazi S. Sariciftci, and Harald Hoppe, “*Anthracene based conjugated polymers: Correlation between π - π stacking ability, photophysical properties, charge carrier mobility and photovoltaic performance*” **Macromolecules**, 2010, **43**, 1261-1269.
3. Christian Kästner, Diana K. Susarova, **Rupali Jadhav**, Christoph Ulbricht, Daniel A. M. Egbe, Silke Rathgeber, Pavel A. Troshin and Harald Hoppe, “*Morphology evaluation of a polymer–fullerene bulk heterojunction ensemble generated by the fullerene derivatization*” **J. Mater. Chem.**, 2012, **22**, 15987-15997.
4. **Rupali R. Jadhav**, Nadia Camaioni, Kerstin Oppelt, Francesca Tinti, Massimo Gazzano, Valeria Fattori, Prakash P. Wadgaonkar, Silke Rathgeber, Harald Hoppe and Daniel A. M. Egbe, “*Modulation of charge carrier mobility by side-chain engineering of bi(thienylene vinylene)thiophene containing PPE–PPVs*” **RSC Adv.**, 2016, **6**, 51642-51648.
5. **Rupali Jadhav**, Shahidul Alam, Nitin Valsange, Daniel A. M. Egbe, Harald Hoppe and Prakash Wadgaonkar, “*Benzo[1,2-c:4,5-c']dithiophene-4,8-dione Containing Copolymers and Terpolymers: implications of active layer morphology on photovoltaic performance*” (Manuscript under preparation)
6. **Rupali Jadhav**, Satej Dharmapurikar, and Prakash Wadgaonkar, “*DPP-based spacer polymers functionalized with urethane linker containing alkyl side chains: influence of polymer self-assembly on organic field effect transistors performance*” (Manuscript under preparation)